UV Exposure of Multipotent Dermal Stem Cells as Potential Target Cells for the Development of UV-induced Malignant Melanoma

Dissertation

to obtain the academic degree of
Doctor rerum naturalium (Dr. rer. nat.)

at the Department of Biology
Faculty of Mathematics, Informatics and Natural Sciences
University of Hamburg

Submitted by
Christin Starzonek
from Hamburg, Germany

Hamburg 2024

This work was carried out externally at the Department of Molecular Cell Biology, Elbe Clinics Stade-Buxtehude from January 2019 to December 2023 under the supervision of Dr. Beate Volkmer and Dr. Rüdiger Greinert. The work was supervised by Prof. Dr. Udo Schumacher at the Institute of Anatomy and Experimental Morphology, University Medical Center Hamburg-Eppendorf, and by Prof. Dr. Julia Kehr at the Institute of Plant Science and Microbiology, University of Hamburg.

Approved by the Department of Biology, Faculty of Mathematics, Informatics and Natural Sciences at the University of Hamburg

First evaluator of the dissertation:	Prof. Dr. Udo Schumacher
Second evaluator of the dissertation:	Prof. Dr. Julia Kehr
Examination commission:	Prof. Dr. Tobias Lenz
	Prof. Dr. Julia Kehr
	Dr. Beate Volkmer
Date of oral defense:	June 14, 2024

To my family…

Table of Contents

List of Figures ..... **V**

List of Tables ..... **VII**

List of Abbreviations ..... **IX**

Preliminary Remarks / Publications ..... **XVI**

Abstract ..... **XVII**

Zusammenfassung ..... **XIX**

1 Introduction **1**

1.1 Structure of Human Skin 1

1.1.1 Epidermis 2

1.1.1.1 Melanocytes 2

1.1.1.2 Differentiation into Melanocytes 4

1.1.1.3 Regulation of Melanocytes 7

1.1.2 Dermis 9

1.1.3 Subcutaneous Tissue 10

1.2 Stem Cells 10

1.2.1 Potency of Stem Cells 12

1.2.2 Types of Stem Cells in The Skin 15

1.2.3 Dermal Stem Cells 17

1.3 UV Radiation 20

1.3.1 Physical Principles of UV Radiation 21

1.3.2 Solar UV Radiation 23

1.3.3 Penetration Depth of UV Radiation into Human Skin 23

1.3.4 Biological Effects of UV Radiation (on The Skin) 25

1.3.5 UV-Induced DNA Lesions 25

1.4 DNA Damage Response 28

1.4.1 DNA Damage Checkpoints 30

1.4.2 Cell Cycle Arrest 31

1.4.3 DNA Repair 32

1.4.4 Apoptosis 34

1.4.5 Transcriptional, Post-Translational, and Epigenetic Regulation 35

1.5 Skin Cancer 38

1.5.1 Non-Melanoma Skin Cancer 40

1.5.2 Malignant Melanoma 41

1.5.2.1 Melanomagenesis 42

1.5.2.2 Epigenetic Dysregulation in Melanoma 45

1.5.2.3 Cell of Origin 49

2 Aim of This Work 54

3 Materials 56
3.1 Devices 56
3.2 Consumables 57
3.3 Reagents 58
3.4 Buffers and Solutions 60
3.5 Culture Media 62
3.6 Kits 63
3.7 Antibodies 64
3.7.1 Primary Antibodies 64
3.7.2 Secondary Antibodies 64
3.8 mRNA Primers for qPCR Expression Analysis 65
3.8.1 Primer Sequences 65
3.8.2 Internet Addresses for Primer Design 65
3.9 MicroRNA Panel 66
3.10 Software 66
3.11 Cell Strains 67
3.11.1 Primary DSCs, Fibroblasts, Melanocytes, and Keratinocytes 67
3.11.2 Melanoma Cells 67

4 Methods 68
4.1 Cell Culture 68
4.1.1 Isolation of Cells 68
4.1.2 Dissociation of Dermal Spheres 69
4.1.3 Coating with Basement Membrane Extract for DSCs 70
4.1.4 Splitting of Cells 70
4.1.5 Freezing of Cells 71
4.1.6 Thawing of Cells 71
4.2 Enrichment of DSCs 71
4.2.1 Geneticin Treatment 72
4.2.2 Selective Detachment 72
4.2.3 Immunomagnetic Separation 72
4.2.3.1 EasySep™ Column-Free Separation 73
4.2.3.2 MACS® Automatic Column-Based Separation 75
4.3 UV Irradiation 77
4.3.1 Irradiation Device 77
4.3.2 Cell Preparation for Irradiation 79
4.3.3 Irradiation of Cells 79
4.4 Differentiation of DSCs into Melanocytes 81
4.4.1 Differentiation for Characterization 81
4.4.2 Differentiation after UV Irradiation 81
4.5 Sphere Formation Assay 81
4.5.1 Sphere Formation for Characterization 81
4.5.2 Sphere Formation after UV Irradiation 82

4.6 Immunostaining and Imaging 83
4.6.1 Immunocytochemistry 83
4.6.2 Flow Cytometry 84
4.6.2.1 NGFRp75 and CD90 Staining of DSCs 84
4.6.2.2 Doubling Time 84
4.6.2.3 Evaluation of DNA Damage (CPDs) 84
4.6.2.4 Cell Cycle Analysis 86
4.6.2.5 Apoptosis Assay 87
4.6.2.6 Viability Assay 88
4.7 Transcriptional Analysis 88
4.7.1 RNA Isolation 88
4.7.2 Determination of RNA Concentration 89
4.7.3 Reverse Transcription 89
4.7.4 Quantitative PCR 90
4.8 MicroRNA Analysis 91
4.8.1 MicroRNA Isolation 91
4.8.2 FirePlex® MiRNA Assay 92
4.8.3 Cluster and Pathway Analysis 94
4.9 Statistical Evaluation 95

5 Results 96
5.1 Stem Cell Frequency of DSC Cultures 96
5.2 Enrichment of DSCs from DSC-Fibroblast Co-Cultures 97
5.2.1 Elimination of Fibroblasts with Geneticin 98
5.2.2 Separation of DSCs and Fibroblasts via Selective Detachment 99
5.2.3 Segregation of The Two Cell Types via Immunomagnetic Separation 101
5.2.3.1 Negative Selection 102
5.2.3.2 Positive Selection 106
5.2.3.3 Overall Assessment of The Different IMS Methods 107
5.3 Characterization of DSCs 108
5.3.1 Morphology and Gene Expression of The Skin Cell Types 108
5.3.2 Doubling Times of The Skin Cell Types 110
5.3.3 Differentiation of DSCs into Melanocytes 110
5.3.4 Sphere Formation of DSCs 115
5.4 UV-Induced DNA Damage Response 116
5.4.1 CPD Induction, DNA Repair, and Remaining DNA Damage 117
5.4.2 Cell Cycle Progression 119
5.4.3 Induction of Apoptosis 121
5.5 Effect of UV on The Differentiation Potential of DSCs 123
5.6 Effect of UV on The Sphere Formation Capability of DSCs 128
5.7 Effect of UV on The MicroRNA Expression 130
5.7.1 Baseline MicroRNA Expression Levels in DSCs, Melanocytes, and Melanoma Cells 132
5.7.2 MicroRNA Expression Following UV Irradiation 134

6 Discussion 136
6.1 Characterization of DSCs 136
6.2 Purification of DSCs 137
6.2.1 Treatment with Geneticin 138
6.2.2 Selective Detachment 139
6.2.3 Immunomagnetic Separation 141
6.2.3.1 Negative Selection 141
6.2.3.2 Positive Selection 145
6.2.3.3 Overall Assessment of IMS 146
6.2.4 Conclusion to Purification of DSCs 148
6.3 UV Damage Response 150
6.3.1 DNA Repair Capacity 150
6.3.2 Cell Cycle Progression 156
6.3.3 Induction of Apoptosis 160
6.3.4 Conclusion to UV Damage Response 166
6.4 Differentiation into Melanocytes 169
6.4.1 *In Vitro* Melanocytic Differentiation Potential of DSCs 169
6.4.2 Differentiation Following UV Irradiation 174
6.5 Sphere Formation 177
6.5.1 Sphere-Forming Potential of DSCs 178
6.5.2 Sphere Formation Following UV Irradiation 182
6.6 MicroRNA Expression 186
6.6.1 Baseline MicroRNA Expression 188
6.6.2 MicroRNA Expression Following UV Irradiation 192

7 Outlook 195

8 Appendix 200
8.1 Supplementary Figures 200
8.2 Supplementary Tables 204

References 213

Danksagung 257

Declaration on Oath / Eidesstattliche Versicherung 259

List of Figures

Figure 1.1 Structure of human skin. 1
Figure 1.2 Key signaling pathways in melanocyte development. 5
Figure 1.3 Regulation of melanocytes through paracrine factors. 8
Figure 1.4 Potency of stem cells. 13
Figure 1.5 UV wavelength range in the spectrum of electromagnetic radiation. 21
Figure 1.6 Erythema-weighted spectral effectiveness. 22
Figure 1.7 Penetration depth of UV radiation into human skin. 24
Figure 1.8 Chemical structures of pyrimidine dimers. 26
Figure 1.9 UV-induced damage response. 29
Figure 1.10 Melanoma theories. 50

Figure 4.1 Illustration of immunomagnetic separation in a column-based approach. 73
Figure 4.2 Schematic construction of the irradiation device. 78
Figure 4.3 Schematic setup of the 'sphere formation after UV irradiation' experiment. 82
Figure 4.4 Principle of the FirePlex® miRNA Assay. 92

Figure 5.1 Characterization of DSCs. 97
Figure 5.2 Geneticin treatment of DSC-fibroblast co-cultures. 99
Figure 5.3 Selective detachment of DSC-fibroblast co-cultures. 100
Figure 5.4 Negative selection (labeling of fibroblasts) of DSC-fibroblast co-cultures. 103
Figure 5.5 Negative selection (labeling of fibroblasts) of DSC-fibroblast co-cultures with higher initial DSC frequency. 105
Figure 5.6 Positive selection (labeling of DSCs) of DSC-fibroblast co-cultures. 106
Figure 5.7 Purity and recovery of DSCs for the individual selection methods. 107
Figure 5.8 Characterization of DSCs, fibroblasts, melanocytes and keratinocytes. 109
Figure 5.9 Morphology of DSC cultures during differentiation. 111
Figure 5.10 Transition from DSCs into melanocytes. 112
Figure 5.11 End of differentiation process. 113
Figure 5.12 Sphere formation ability in suspension culture. 116
Figure 5.13 CPD induction, repair time constant and remaining DNA damage after UVB irradiation. 118
Figure 5.14 Cell cycle distribution after UV irradiation. 120
Figure 5.15 Induction of apoptosis and cell counts after UV irradiation. 122
Figure 5.16 Differentiation in DSC-fibroblast co-cultures after UV irradiation. 124
Figure 5.17 Differentiation in MACS®-purified DSC cultures after UV irradiation. 125
Figure 5.18 Gene expression analysis of differentiation following UV irradiation. 127
Figure 5.19 Sphere formation after UV irradiation. 129
Figure 5.20 Baseline microRNA expression in DSCs compared to melanocytes and melanoma cells. 133
Figure 5.21 microRNA expression after UV irradiation. 135

Figure 8.1 Effect of prior usage of *Basic MicroBeads* on immunomagnetic separation. 200
Figure 8.2 Additional pictures of DSC cultures and staining at the end of differentiation. 201

Figure 8.3 Changes in stem cell frequency of DSC samples in apoptosis measurement. ... 202
Figure 8.4 Age of foreskin donors. ... 202
Figure 8.5 Proliferation of DSCs during repair kinetics. ... 203

List of Tables

Table 1.1 Paracrine factors with stimulating effect in human melanocyte regulation. 7

Table 3.1 Devices. 56
Table 3.2 Consumables. 57
Table 3.3 Reagents and chemicals. 58
Table 3.4 Composition of buffers and solutions. 60
Table 3.5 Composition of cell culture media. 62
Table 3.6 Kits. 63
Table 3.7 Primary antibodies. 64
Table 3.8 Secondary antibodies. 64
Table 3.9 mRNA primer sequences. 65
Table 3.10 Internet addresses for primer design. 65
Table 3.11 Custom human melanoma miRNA panel for FirePlex® miRNA Assay. 66
Table 3.12 Used software. 66

Table 4.1 BME-coating for adherent growing DSCs. 70
Table 4.2 Protocols for detachment of adherent growing cells. 71
Table 4.3 Radiation sources and filters. 78
Table 4.4 Irradiation protocols. 79
Table 4.5 Reaction mixture for reverse transcription. 89
Table 4.6 Reverse transcription thermocycler program. 90
Table 4.7 Reaction mixture for qPCR. 90
Table 4.8 qPCR thermocycler program. 90
Table 4.9 Reaction mixtures for FirePlex® miRNA Assay. 93
Table 4.10 miRNA PCR thermocycler program. 93

Table 5.1 Increase in melanocytic gene expression at day 16 of differentiation. 115
Table 5.2 Statistically significant cell cycle alterations following UV irradiation. 121
Table 5.3 Statistically significant induction of apoptosis. 123
Table 5.4 Most stable microRNAs for normalization. 131

Table 6.1 Comparison of EasySep™ column-free and MACS® automatic column-based selection technology. 148
Table 6.2 Summary of DNA damage response mechanisms in the different cell types. ... 167

Table 8.1 microRNA expression in malignant melanoma. 204
Table 8.2 Individual repair time constants τ of all donors with standard deviation. 206
Table 8.3 Apoptosis results from the individual donors. 207
Table 8.4 Most stable microRNAs - all eight cell strains analyzed separately. 208
Table 8.5 Most stable microRNAs - only DSC strains compared to each other. 208
Table 8.6 Most stable microRNAs - only melanocyte strains compared to each other. 208
Table 8.7 Most stable microRNAs - only melanoma cell strains compared to each other. 209
Table 8.8 Most stable microRNAs - comparison of cell type groups. 209

Table 8.9 Significantly altered GO terms of the 4-miRNA set overexpressed in DSCs from Figure 5.20C. 210
Table 8.10 Significantly altered GO terms of the 40 target genes of the 4-miRNA set downregulated in DSCs from Figure 5.20D. 211
Table 8.11 KEGG pathway analysis of the 40 target genes of the 4-miRNA set downregulated in DSCs from Figure 5.20D. 212

List of Abbreviations

Abbreviation	Meaning
5-hmC	5-Hydroxymethylcytosine
6-4PP	Pyrimidine (6-4) pyrimidone photoproduct
8-oxo-dG	8-Oxo-7,8-dihydro-2'-deoxyguanosine
A	Adenine
ACD	Adrenocortical dysplasia homologue
ACTB	β-Actin
ACTH	Adrenocorticotropic hormone
ADSC	Adipose-derived stem cell
AGO2	Argonaute RISC catalytic component 2
AKT	Protein kinase B
ANOVA	Analysis of variance
Apaf-1	Apoptotic protease activating factor-1
APC	Allophycocyanin
APEX1	Apurinic/apyrimidinic endodeoxyribonuclease 1
ARID2	AT-rich interaction domain 2
ASIP	Agouti signaling protein
ASR	Age-standardized rate (per 100,000/year)
ATM	Ataxia-telangiectasia mutated; protein kinase
ATR	Ataxia-telangiectasia and Rad3-related; protein kinase
a.u.	Arbitrary unit
BAP1	BRCA1-associated protein 1
BCC	Basal cell carcinoma
BDNF	Brain-derived neurotrophic factor
BER	Base excision repair
BME	Basement membrane extract
BMI1	B lymphoma Mo-MLV insertion region 1 homolog
BMP4	Bone morphogenetic protein 4
bp	Base pair(s)
BRAF	v-Raf murine sarcoma viral oncogene homolog B1
BRCA1	Breast cancer 1
BrdU	5-Bromo-2'-deoxyuridine
BSA	Bovine serum albumin
C	Cytosine
CAF	Cancer-associated fibroblast
cAMP	Cyclic adenosine monophosphate
CCN1	Cellular communication network factor 1
CD	Cluster of differentiation
CD90	Cluster of differentiation 90, also known as Thy-1
Cdc25A	Cell division cycle 25A

Abbreviation	Meaning
CDK	Cyclin-dependent kinase
CDKN2A	Cyclin-dependent kinase inhibitor 2A
cDNA	Complementary DNA
Chk1, Chk2	Checkpoint kinase 1, 2
CIE	International Commission on Illumination (*fra.: Commission Internationale de l'Éclairage*)
CPD	Cyclobutane pyrimidine dimer
CpG	Cytosine-guanine dinucleotide (in 5'→3' direction)
CRBC	CPD-retaining basal cell
CREB	cAMP response element-binding protein
CSA	Cockayne syndrome group A, also known as ERCC8
CSB	Cockayne syndrome group B, also known as ERCC6
CSC	Cancer stem cell
C_t	Cycle threshold
CTLA-4	Cytotoxic T-cell antigen 4
d	Diameter
DABCO	1,4-Diazabicyclo[2.2.2]octane
DAPI	4',6-Diamidino-2-phenylindole
ddH_2O	Double-distilled water, sterile-filtered
DDR	DNA damage response
dim	Fluorescence intensity of a uniformly positive population with lower intensity than a positive normal cell population
DKK1	Dickkopf-related protein 1
DMEM	Dulbecco's modified eagle medium
DMSO	Dimethyl sulfoxide
DNA	Deoxyribonucleic acid
DNA-PK	DNA protein kinase
DNase	Deoxyribonuclease
DNMT1	DNA methyltransferase 1
dNTP	Deoxyribonucleotide triphosphate
DSC	Dermal stem cell
E	Irradiance
ECM	Extracellular matrix
EDTA	Ethylenediaminetetraacetic acid
EdU	5-Ethynyl-2'-deoxyuridine
EMT	Epithelial-mesenchymal transition
ERCC1	Excision repair cross-complementation group 1
ERK1/2	Extracellular signal-regulated kinase 1/2 (MAP kinases)
ESC	Embryonic stem cell
ET-1, ET-2, ET-3	Endothelin-1, 2, 3
ETBR	Endothelin B receptor
EZH2	Enhancer of zeste homologue 2

Abbreviation	Meaning
F	Forward
FACS	Fluorescence-activated cell sorting
FADD	FAS-associated death domain protein
FAP-α	Fibroblast activation protein-α
FasL	Fas ligand
FBS	Fetal bovine serum
FC	Fold change
FFPE	Formalin-fixed paraffin-embedded
FGF-basic/bFGF	Basic fibroblast growth factor
FITC	Fluorescein isothiocyanate
FOXD3	Forkhead box D3
FOXO1, FOXO3	Forkhead box O1, O3
FRZB	Frizzled-related protein
g	Acceleration of gravity (9.81 m/s²)
g	Gram
G	Guanine
GGR	Global genome repair
GM-CSF	Granulocyte-macrophage colony-stimulating factor
GO	Gene Ontology
GSK3β	Glycogen synthase kinase-3β
h	Hour
H	Dose / radiant exposure
HaCaT	Human adult low Calcium high Temperature
HAT	Histone acetyltransferase
HBSS	Hanks' balanced salt solution
HDAC	Histone deacetylase
HEPES	4-(2-Hydroxyethyl)-1-piperazineethanesulfonic acid
hESC	Human embryonic stem cell
HFSC	Hair follicle stem cell
HGF	Hepatocyte growth factor
HIF1α	Hypoxia-inducible factor 1α
HKG	Housekeeping gene
HMB45	Human melanoma black-45, also known as Pmel17 or gp100
HPRT1	Hypoxanthine phosphoribosyltransferase 1
HSC	Hematopoietic stem cell
Hz	Hertz
ICC	Immunocytochemistry
IDH1	Isocitrate dehydrogenase 1
IdU	5-Iodo-2'-deoxyuridine
IgG	Immunoglobulin G
IL-1, IL-6, IL-8, IL-10	Interleukin 1, 6, 8, 10

Abbreviation	Meaning
IMS	Immunomagnetic separation
iPSC	Induced pluripotent stem cell
IQR	Interquartile range
IR	Infrared radiation (780 nm–1 mm)
IR-A	Infrared-A radiation (780 nm–1400 nm)
IR-B	Infrared-B radiation (1400 nm–3000 nm)
IR-C	Infrared-C radiation (3000 nm–1 mm)
ITS	Insulin-Transferrin-Selenium
J	Joule
K	Lysine
KEGG	Kyoto Encyclopedia of Genes and Genomes
KGF	Keratinocyte growth factor
KLF4	Kruppel-like factor 4
L	Liter
LDH	Lactate dehydrogenase
LIF	Leukemia inhibitory factor
LINE-1	Long interspersed nuclear element-1
m	Meter
M	Molar, mol/L
MACS	Magnetic-activated cell sorting
MAP2K1	Mitogen-activated protein kinase kinase 1
MAPK	Mitogen-activated protein kinase
Mc	Melanocyte
MC1R	Melanocortin-1 receptor
McSC	Melanocyte stem cells
MDM2	Mouse double minute 2 homolog
MED	Minimal erythema dose
MEK	Mitogen-activated protein kinase kinase, also known as MAP2K or MAPKK
mESC	Mouse embryonic stem cell
min	Minute
miR, miRNA	microRNA
MITF	Microphthalmia-associated transcription factor
MM	Malignant melanoma
MMP2, MMP9	Matrix metalloproteinase 2, 9
mRNA	Messenger RNA
MSC	Mesenchymal stem cell
α-MSH	Melanocyte-stimulating hormone
MSX1	Msh homeobox 1
MTA1	Metastasis-associated antigen 1
mTOR	Mechanistic target of rapamycin kinase
n/a	Not available

Abbreviation	Meaning
NCSC	Neural crest stem cell
NER	Nucleotide excision repair
NF1	Neurofibromin 1
NGF	Nerve growth factor
NGFRp75	Low-affinity nerve growth factor receptor p75, also known as CD271
NGS	Next-generation sequencing
NMSC	Non-melanoma skin cancer
NO	Nitric oxide
NRAS	Neuroblastoma RAS viral oncogene homolog
Nrf2	Nuclear factor erythroid 2-related factor 2
NRG-1	Neuregulin-1
NT-3, NT-4/5	Neurotrophin-3, -4/5
OCA2	Oculocutaneous albinism type 2
Oct-3/4	Octamer-binding transcription factor 3/4
OD_{230}, OD_{260}, OD_{280}	Optical density at 230, 260, or 280 nm
onco-miRNA	Oncogenic miRNA
ORA	Over-representation analysis / enrichment analysis
OTC	Organotypic culture
PAK1	p21 (RAC1) activated kinase 1
PARP1	Poly(ADP-ribose) polymerase 1
Pax3	Paired box 3
PBS	Phosphate-buffered saline
PCNA	Proliferating cell nuclear antigen
PCR	Polymerase chain reaction
PCR-H_2O	Nuclease-free, distilled water
PD-1	Programmed cell death 1
PDGFRα, PDGFRβ	Platelet-derived growth factor receptor α, β
PD-L1	Programmed cell death-ligand 1
PE	Phycoerythrin
PGE_2, $PGF_{2\alpha}$	Prostaglandin E_2, $F_{2\alpha}$
PI	Propidium iodide
PI3K	Phosphatidylinositol-3-kinase
PIB5PA	Phosphatidylinositol-4,5-biphosphate 5-phosphatase A
PKA	Protein kinase A
PKC	Protein kinase C
PMA	Phorbol 12-myristate 13-acetate, also known as 12-*O*-tetradecanoylphorbol-13-acetate (TPA)
Pmel	Premelanosome protein
POLE	DNA polymerase epsilon
POT1	Protection of telomeres 1
PPP6C	Protein phosphatase 6 catalytic subunit
PSC	Pluripotent stem cell

Abbreviation	Meaning
PTEN	Phosphatase and tensin homolog
PTM	Post-translational modification
pur	Purity
qPCR	Quantitative real-time PCR
R	Reverse
RAC1	Ras-related C3 botulinum toxin substrate 1
RAD51B	RAD51 paralog B
RASSF1A	Ras association domain family protein 1A
RB	Retinoblastoma protein
rec	Recovery
RNA	Ribonucleic acid
RNase	Ribonuclease
RNA-seq	RNA sequencing
ROS	Reactive oxygen species
RPA	Replication protein A
rpm	Revolutions per minute
RPMI	Roswell Park Memorial Institute
RT	Room temperature
s	Second
SCC	Squamous cell carcinoma
SCF	Stem cell factor
SE	Skin equivalent
Sema7a	Semaphorin 7a
Ser	Serine
SETDB1	SET domain bifurcated 1
sFRP2	Secreted frizzled-related protein 2
siRNA	Small interfering RNA
SIRT1	Sirtuin 1
SKP	Skin-derived precursor
SLC45A2	Solute carrier family 45 member 2
SNX31	Sorting Nexin 31
SOX2, SOX10	Sex-determining region Y-box 2, 10
ssDNA	Single-stranded DNA
STK19	Serine/threonine kinase 19
SWI/SNF	Switch/sucrose non-fermentable
τ	Repair time constant
T	Thymine
TAC	Transit-amplifying cell
TACC1	Transforming acidic coiled-coil containing protein 1
TAM	Tumor-associated macrophage
TBP	TATA-binding protein

Abbreviation	Meaning
TBS	Tris-buffered saline
TCF/LEF	T cell factor/lymphoid enhancer factor
TCR	Transcription-coupled repair
t_d	Doubling time
TE	Tris-EDTA
TERF2IP	Telomeric repeat binding factor 2, interacting protein
TERT	Telomerase reverse-transcriptase
TFIIH	Transcription factor IIH
TGF-β	Transforming growth factor-β
Tie2	Angiopoietin-1 receptor
TIMP3	Tissue inhibitor of metalloprotinease-3
TLS	Translesion DNA synthesis
TNF-α	Tumor necrosis factor
Tris	Tris-(hydroxymethyl)-aminomethan
TRP1	Tyrosinase-related protein 1
TRP2/DCT	Tyrosinase-related protein 2
TUNEL	Terminal desoxynucleotidyl transferase dUTP nick-end labeling
TYR	Tyrosinase
U	Unit (enzyme activity)
UTR	Untranslated region
UV	Ultraviolet radiation (100–400 nm)
UVA	Ultraviolet A radiation (315–400 nm)
UVB	Ultraviolet B radiation (280–315 nm)
UVC	Ultraviolet C radiation (100–280 nm)
VEGF	Vascular endothelial growth factor
VIS	Visible light (400–780 nm)
W	Watt
WHO	World Health Organization
XP	Xeroderma pigmentosum
XPA	Xeroderma pigmentosum group A
XPB	Xeroderma pigmentosum group B; DNA helicase
XPC	Xeroderma pigmentosum group C; DNA damage sensor
XPD	Xeroderma pigmentosum group D; DNA helicase
XPF	Xeroderma pigmentosum group F; endonuclease
XPG	Xeroderma pigmentosum group G; endonuclease
XRCC1	X-ray repair cross-complementing protein 1
ZEB1, ZEB2	Zinc-finger E-box binding homeobox 1, 2

Preliminary Remarks / Publications

For the creation of this thesis, texts, parts and figures were reused, adapted or changed from my following first-author publications (* shared first authorship).

Partial results of this work were published in:

- Mhamdi-Ghodbani M*, **Starzonek C***, Degenhardt S, Bender M, Said M, Greinert R, Volkmer B. UVB damage response of dermal stem cells as melanocyte precursors compared to keratinocytes, melanocytes, and fibroblasts from human foreskin. *J Photochem Photobiol B*. 2021 Jul;220:112216. doi: 10.1016/j.jphotobiol.2021.112216. Epub 2021 May 17. PMID: 34023595.

- **Starzonek C***, Mhamdi-Ghodbani M*, Henning S, Bender M, Degenhardt S, Chen IP, Said M, Greinert R, Volkmer B. Enrichment of Human Dermal Stem Cells from Primary Cell Cultures through the Elimination of Fibroblasts. *Cells*. 2023 Mar 21;12(6):949. doi: 10.3390/cells12060949. PMID: 36980290; PMCID: PMC10047019.

Abstract

Malignant melanoma is the most aggressive and lethal type of skin cancer with rising incidence worldwide. The unequivocal risk factor is exposure to solar and artificial UV radiation. Despite the central role of UV-induced cyclobutane pyrimidine dimers (CPDs), particularly in the formation of UV signature mutations, the precise cellular and molecular mechanisms driving melanomagenesis are far from being understood in detail. Moreover, the cell of origin remains a subject of debate, with discussions centering on whether transformation initiates in mature epidermal melanocytes or stem cell precursors. An alternative theory proposes a damaged extrafollicular dermal melanocyte stem cell as the earliest origin. Within human skin, multipotent neural crest-derived dermal stem cells (DSCs) may serve as a reservoir for epidermal melanocytes. Although DSCs are constantly exposed to solar UV radiation, potentially contributing to the onset of melanoma, there is still insufficient investigation into how DSCs react to UV-induced damage. Therefore, this study aimed to establish workflows for the *in vitro* investigation of DSCs as potential cell of origin and of their response to UV irradiation. The work focused on examining functional stem cell features and understanding protection mechanisms to determine if UV-induced cell damage poses a higher risk in DSCs.

It was demonstrated that DSCs isolated from human foreskin can serve as a model to study their potential relevance in the genesis of malignant melanoma. Cultivated in specific stem cell medium, primary DSC cultures exhibited neural crest stem cell characteristics, including the expression of relevant markers, the ability to form three-dimensional spheres, and the potential for melanocytic differentiation. However, fibroblast contamination was a serious limitation for certain applications, necessitating the enrichment of DSCs. Immunomagnetic separation with negative selection based on CD90 and alternative non-cell-specific approaches, such as Geneticin treatment or selective detachment, proved unsuitable for DSC purification. Highly enriched DSCs with a good recovery rate were obtained using column-based MACS® positive selection targeting NGFRp75. These purified DSCs maintained viability and differentiation potential, although further validation is needed. This *in vitro* purification marks a crucial advancement in DSC research.

A comparative study of the DNA damage response after UVA and UVB irradiation revealed that DSCs reacted similarly to fibroblasts and melanocytes, displaying functional DNA repair and apoptosis induction. Protective mechanisms in DSCs were not superior to those of differentiated skin cells. Interestingly, DSCs exhibited an exceptional cell cycle regulation with a lack of growth arrest following UV irradiation, potentially indicating deficiencies in cell

cycle checkpoints. This could lead to replication through unrepaired damage, mutations, and an elevated risk of transformation. Although initial evidence hints at a possibly heightened susceptibility of DSCs to UV-mediated carcinogenesis, further research is needed to establish a causal link between this specific radiation response and melanoma development.

UV irradiation predominantly had no impact on stem cell features and epigenetic regulation. Exposure to a single dose of UVA or UVB did not alter the expression of selected melanoma-specific microRNAs or the ability of DSCs to differentiate into melanocytes, neither impairing nor triggering differentiation. The radiation scheme might have been insufficient to induce UV-related effects, requiring multiple irradiations to adequately mimic physiological conditions. Irrespective of irradiation, a set of eight differentially expressed microRNAs allowed a clear distinction between DSCs, melanocytes, and melanoma cells, indicating significant differences in their overall baseline microRNA expression. By contrast, both single and multiple UVB exposures affected the sphere-forming potential of DSCs, resulting in reduced sphere counts. However, uncertainties arose regarding the influence of fibroblasts and cell aggregation in the utilized sphere formation assay, hindering a comprehensive evaluation of the results.

In summary, this study has successfully met its objectives by establishing workflows and methods that enabled an initial *in vitro* investigation of functional stem cell features and UV protection mechanisms in DSCs. While these findings yield a preliminary assessment of DSCs as potential cell of origin for malignant melanoma, they also raise questions for future investigations that could provide further insights into mechanisms underlying UV-induced melanomagenesis. Understanding how DSCs respond to UV exposure could enhance knowledge of early events in melanoma initiation, potentially improving prevention, early diagnosis, and the development of new treatment strategies.

Zusammenfassung

Das maligne Melanom ist die aggressivste und tödlichste Hautkrebsform mit steigender Inzidenz weltweit. Der Hauptrisikofaktor ist die Exposition gegenüber solarer und künstlicher UV-Strahlung. Trotz der zentralen Rolle von UV-induzierten Cyclobutan-Pyrimidin-Dimeren (CPDs), insbesondere bei der Entstehung von UV-Signaturmutationen, sind die genauen zellulären und molekularen Mechanismen der Melanomgenese noch nicht im Detail verstanden. Auch die Ursprungszelle ist weiterhin unklar, wobei sowohl die Transformation von reifen epidermalen Melanozyten als auch von Stammzellen diskutiert wird. Eine alternative Theorie vermutet eine geschädigte, extrafollikuläre, dermale melanozytäre Stammzelle als den frühesten Ursprung. In der menschlichen Haut könnten multipotente, aus der Neuralleiste stammende dermale Stammzellen (DSCs) als Reservoir für epidermale Melanozyten dienen. Obwohl DSCs ständig solarer UV-Strahlung ausgesetzt und möglicherweise in die Entstehung des malignen Melanoms involviert sind, ist das Wissen darüber, wie DSCs auf UV-induzierte Schäden reagieren, noch unzureichend. Ziel dieser Arbeit war es daher, Arbeitsabläufe für die *in vitro* Untersuchung von DSCs als potenzielle Ursprungszellen und ihrer Antwort auf UV-Bestrahlung zu etablieren. Der Fokus lag darauf, funktionelle Stammzelleigenschaften und Schutzmechanismen zu untersuchen, um festzustellen, ob UV-induzierte Zellschäden bei DSCs ein höheres Risiko darstellen.

Es wurde gezeigt, dass aus menschlicher Vorhaut isolierte DSCs als Modell dienen können, um ihre Relevanz bei der Entstehung des malignen Melanoms zu untersuchen. In speziellem Stammzellmedium kultivierte primäre DSC-Kulturen wiesen Merkmale von Stammzellen aus der Neuralleiste auf, wie die Expression relevanter Marker, die Fähigkeit zur Sphärenbildung und das Potenzial zur Melanozytendifferenzierung. Allerdings stellte die Kontamination mit Fibroblasten eine erhebliche Einschränkung für bestimmte Anwendungen dar, was eine Anreicherung der DSCs erforderlich machte. Magnetische Separation mit Negativselektion basierend auf CD90 sowie alternative, nicht-zellspezifische Ansätze, wie die Behandlung mit Geneticin oder selektive Ablöse, erwiesen sich als ungeeignet für die DSC-Aufreinigung. Hochangereicherte DSCs mit einer guten Ausbeute konnten mittels säulenbasierter MACS® Positivselektion gewonnen werden, die auf NGFRp75 abzielte. Die aufgereinigten DSCs behielten ihre Viabilität und Differenzierungsfähigkeit bei, es sind jedoch weitere Validierungen erforderlich. Diese *in vitro* Aufreinigung stellt einen entscheidenden Fortschritt in der DSC-Forschung dar.

Vergleichende Untersuchungen zur DNA-Schadensantwort nach UVA- und UVB-Bestrahlung zeigten, dass DSCs ähnlich wie Fibroblasten und Melanozyten mit einer funktionalen DNA-Reparatur und Apoptoseinduktion reagierten. Die Schutzmechanismen der DSCs schienen im Vergleich zu differenzierten Hautzellen nicht überlegen. Interessanterweise wiesen DSCs eine außergewöhnliche Regulation des Zellzyklus mit ausbleibendem Arrest nach UV-Bestrahlung auf, was möglicherweise auf Defizite in den Zellzykluskontrollpunkten hinweist. Dies könnte zu Zellteilung bei noch bestehenden Schäden, Mutationen und einem erhöhten Risiko der Transformation führen. Obwohl erste Hinweise auf eine eventuell erhöhte Anfälligkeit von DSCs für UV-vermittelte Karzinogenese hindeuten, sind weitere Untersuchungen erforderlich, um eine kausale Verbindung zwischen dieser spezifischen Strahlenantwort und der Melanomgenese herzustellen.

UV-Bestrahlung hatte überwiegend keinen Einfluss auf Stammzelleigenschaften und die epigenetische Regulation. Akute UVA- oder UVB-Exposition veränderte weder die Expression ausgewählter, Melanom-spezifischer miRNAs, noch beeinträchtigte oder stimulierte sie die Fähigkeit von DSCs, sich in Melanozyten zu differenzieren. Das Bestrahlungsschema könnte unzureichend gewesen sein, um UV-bedingte Effekte hervorzurufen, sodass mehrfache Bestrahlungen erforderlich sind, um physiologische Bedingungen angemessen zu imitieren. Unabhängig von der Bestrahlung ermöglichte ein Set aus acht differentiell exprimierten miRNAs eine eindeutige Unterscheidung zwischen DSCs, Melanozyten und Melanomzellen, was signifikante Unterschiede in der gesamten Baseline-miRNA-Expression vermuten lässt. Im Gegensatz dazu beeinflussten sowohl akute als auch mehrfache UVB-Bestrahlungen die Sphärenbildung und führten zu einer Verringerung der Sphärenanzahl. Es traten jedoch Unsicherheiten hinsichtlich des Einflusses von Fibroblasten und Zellaggregation im verwendeten Sphärenbildungs-Assay auf, was eine umfassende Bewertung der Ergebnisse verhinderte.

Insgesamt konnten erfolgreich Arbeitsabläufe und Methoden etabliert werden, die eine *in vitro* Untersuchung von funktionellen Stammzelleigenschaften und UV-Schutzmechanismen in DSCs ermöglichten. Diese Ergebnisse geben eine erste Einschätzung von DSCs als potenzielle Ursprungszellen für das maligne Melanom und werfen Fragen auf, die weitere Einblicke in die Mechanismen der UV-induzierten Melanomgenese liefern könnten. Das Verständnis dafür, wie DSCs auf UV-Exposition reagieren, könnte das Wissen über frühe Ereignisse bei der Initiierung von Melanomen verbessern und somit möglicherweise die Prävention, die Früherkennung und die Entwicklung neuer Behandlungsstrategien voranbringen.

1 Introduction

1.1 Structure of Human Skin

With an area of approximately 2 m², the skin is the largest human organ and accounts for about one sixth of the total body weight. It consists of different cell types and fulfills a variety of physiological tasks, such as maintenance of homeostasis, metabolic functions through vitamin D synthesis, and thermoregulation. In addition, the skin is a physical and immunological barrier against mechanical, chemical, physical, thermal and microbial environmental influences [1,2]. Having pain, heat, and tactile receptors, it is also an important peripheral sensory organ. In addition, the skin mediates immune-stimulatory effects through antigen presenting cells in the epidermis. The skin consists of three layers from the outside in: epidermis, dermis, and subcutaneous tissue (hypodermis) [1,3]. Figure 1.1A shows a schematic representation of the skin structure with the different skin layers.

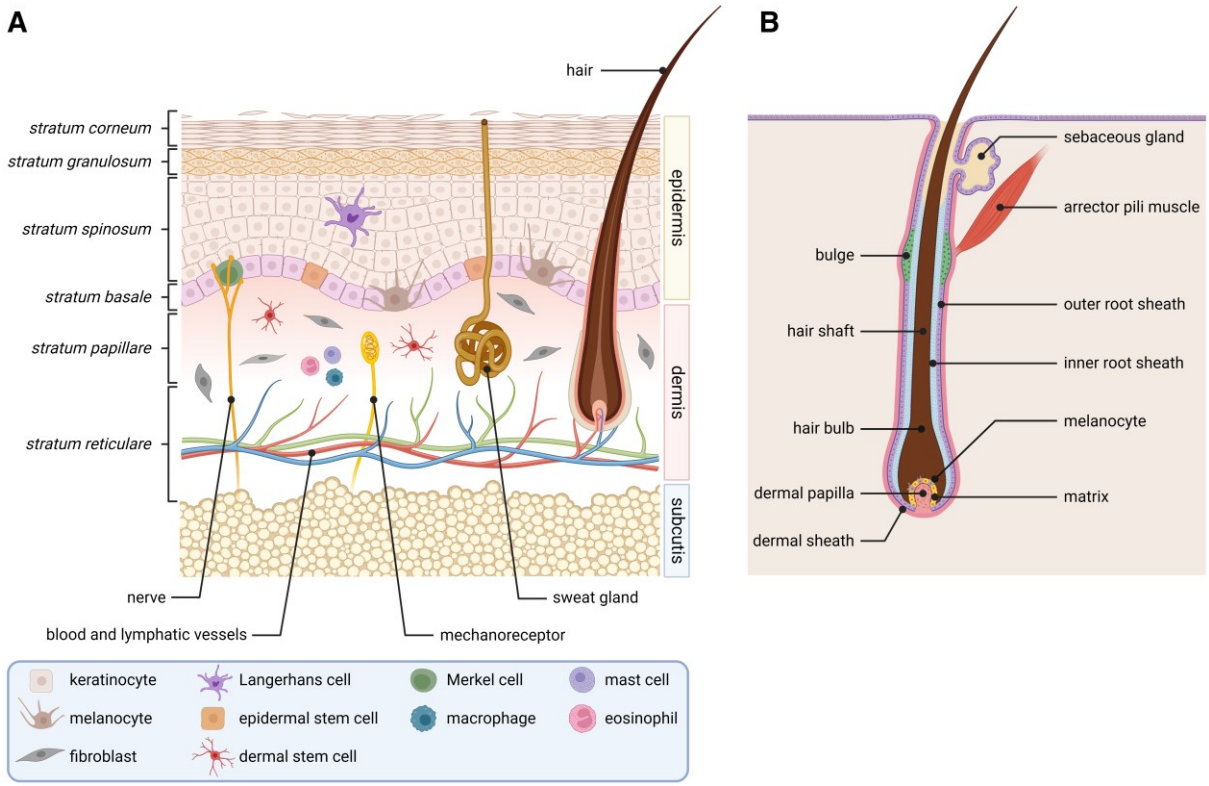

Figure 1.1 Structure of human skin. (**A**) The skin is made up of three layers: epidermis, dermis, and subcutaneous tissue. The epidermis is further divided into the superficial *stratum corneum* and three underlying layers of living cells. The dermis is the connective tissue underneath the epidermis. It contains collagen fibers, structural proteins, and many different cell types. The subcutaneous tissue consists mainly of fat and connective tissue (**B**) Anatomy of the hair follicle with attached sebaceous gland and arrector pili muscle (created with BioRender.com).

The thickness, texture, and color of the skin vary depending on the location in the body. In areas consistently subjected to pressure and friction, the skin is thicker and lacks hair follicles, for example on palms, soles, and the volar parts of fingers and toes [3,4].

1.1.1 Epidermis

The epidermis represents the covering of the body and therefore the primary interface to the environment. It is characterized as a stratified, cornificated squamous epithelium (30–300 µm thick) and is a classic proliferation tissue due to constant renewal. The epidermis consists mainly of keratinocytes (90–95%) in diverse stages of differentiation, forming four epidermal layers, which are characterized by different keratin proteins: *stratum corneum* (cornified layer), *stratum granulosum* (granular layer), *stratum spinosum* (spinous layer) and *stratum basale* (basal layer) [1,2] (Figure 1.1A). Keratinocytes derive from epidermal stem cells localized within the basal layer. There is a permanent cell migration from basal to superficial, while passing various differentiation stages up to the flattened, anuclear corneocytes, which ultimately form the *stratum corneum*. That way, the epidermis completely renews itself over the course of four weeks [2,5].

Further epidermal cell populations encompass melanocytes (see section 1.1.1.1), Langerhans cells, and Merkel cells. Langerhans cells, located in the spinous layer, act as antigen-presenting dendritic cells of the immune system. Merkel cells are associated with nerve cells and are a part of the tactile sense. They are localized in the basal layer, just like melanocytes [1,3].

1.1.1.1 Melanocytes

Melanocytes are a heterogeneous group of dendritic cells. They can be found in the skin (epidermis, hair) and the eye (iris), where they are part of the pigmentary system [6]. In human skin, melanocytes are located in the basal layer of the epidermis as the second most common cell type, determining the skin color [4]. The basal layer maintains a constant homeostatic ratio of 1:10 between melanocytes and keratinocytes throughout life that only changes during nevus or melanoma formation [7,8]. Melanocytic nevi (moles) are benign growths of melanocytes [9] that often have oncogenic mutations in BRAF (v-Raf murine sarcoma viral oncogene homolog B1) and NRAS (Neuroblastoma RAS viral oncogene homolog), proteins that are part of the MAPK signaling pathway [10]. A high number of nevi is associated with a significantly increased risk of developing melanoma [9].

Melanocytes are also present in the matrix of hair follicles (Figure 1.1B) with a denser proportion of 1:5, determining the hair color [11]. Hair follicle melanocytes and epidermal melanocytes are two biologically different populations in their own niches. Epidermal melanocytes are long-living cells, surviving in the epidermis for decades [12], although the exact duration is unknown. With age, their density decreases, morphological changes occur, and both tyrosinase activity [13] (a key protein in melanin synthesis) and proliferative activity [14] decline. Hair melanocytes, on the other hand, have a lifespan corresponding to the hair cycle, which is around 3–8 years [6]. Unlike hair follicle melanocytes, epidermal melanocytes rarely proliferate under natural conditions [11]. This requires the presence of growth factors, hormones, and cytokines, activating pathways like MAPK signaling, α-MSH/cAMP/PKA signaling, and endothelin/PKC signaling [6,15] (see section 1.1.1.3).

In this work, epidermal melanocytes were primarily of interest. Each melanocyte is connected to approximately 30–40 satellite keratinocytes through dendrites, forming the epidermal melanin unit [6,16]. Melanocytes play a crucial role in determining skin color and providing photoprotection. They synthesize melanin from tyrosine through melanogenesis, involving the enzymes tyrosinase (TYR), tyrosinase-related protein 1 (TRP1), and tyrosinase-related protein 2 (TRP2, or dopachrome tautomerase DCT). The melanin is produced and stored in cytoplasmic organelles called melanosomes, which are released to the surrounding keratinocytes via the melanocytes' dendrites. The exact melanosome transfer mechanism remains unclear but may include exo-/endocytosis, cytophagocytosis, tunneling nanotubes, or membrane vesicle-mediated transfer [17]. In keratinocytes, melanin is stored over the cell nuclei, providing UV protection by absorbing and scattering UV rays [5,6]. The process of melanogenesis in hair melanocytes is similar to that of epidermal melanocytes. However, hair graying results from the higher sensitivity of hair follicle melanocytes to aging influences, such as oxidative stress [6,13]. Melanin synthesis is regulated through intercellular communication among keratinocytes, fibroblasts, and melanocytes via paracrine signaling (see section 1.1.1.3) and can also be induced by environmental stimuli, e.g., UV radiation, chemical compounds, drugs, and stress (adaptive pigmentation) [18], whereby UVA is more potent than UVB in triggering pigmentation. Moreover, UV radiation darkens pre-existing melanin and leads to redistribution from the basal to suprabasal layers [19,20].

There are two major types of melanin: yellow-red pheomelanin and brown-black eumelanin. Skin color variation (constitutive pigmentation) is determined by the activity of melanocytes, meaning the quantity of produced melanin and the ratio of the different melanin types [8,19].

Especially the eumelanin content plays a crucial role in determining skin color and is greater in dark-skinned individuals. Variants in the melanocortin-1 receptor (MC1R), which induces eumelanin synthesis, result in reduced or absent receptor activity, favoring pheomelanin production. This is associated with phenotypes of fair skin, red hair, and freckling [21,22]. Eumelanin has better photoprotective properties against UV-induced damage and exhibits antioxidant activity [23]. Therefore, in lighter skin with less eumelanin, the risk of skin cancer is higher. Pheomelanin is associated with the pathogenesis of melanoma not only due to its weak UV protection capacity, but indeed also acts as a carcinogenic photosensitizer, amplifying UV-induced production of reactive oxygen species (ROS) and oxidative DNA damage. The pheomelanin pathway can induce a pro-oxidant state even without UV irradiation, promoting melanoma formation in a UV-independent fashion [24-26].

1.1.1.2 Differentiation into Melanocytes

Melanocytes derive from the neural crest during vertebrate development. The neural crest, a temporary embryonic structure formed between the neural tube and surface ectoderm during neurulation, gives rise to various cell populations, including (neuro-) ectodermal derivatives like neurons, glial cells and melanocytes, as well as mesenchymal progeny such as osteocytes [6,27]. A reliable marker for neural crest-derived stem and progenitor cells is the expression of low-affinity nerve growth factor receptor p75 (NGFRp75), also known as p75 neurotrophin receptor or CD271. NGFRp75 serves as the common receptor for neurotrophins, such as NGF, NT-3, NT-4/5, and BDNF, playing a role in survival, apoptosis, migration, and differentiation [28]. The interaction of neurotrophins with stem cell factor (SCF) guides neural crest cells towards the melanocytic lineage [28]. During embryonic development, neural crest cells evolve into melanoblasts, which are melanocyte precursors. These melanoblasts migrate through the dermis to their final destinations in the epidermis and hair follicle, where they undergo differentiation into melanocyte stem cells (McSC) and mature melanocytes [29,30]. Additionally, melanocytic precursors might also persist in the dermis [30-32]. The most common markers for melanoblasts are c-Kit, MITF (microphthalmia-associated transcription factor), SOX10 (sex-determining region Y-box 10), Pax3 (paired box 3), and DCT/TRP2 [6,33].

Numerous genes, epigenetic factors, and environmental factors, such as UV radiation and influences from surrounding keratinocytes and fibroblasts, regulate the differentiation of melanocytes. Key factors in this process include the transcription factors MITF, SOX10, and Pax3, the receptor tyrosine kinase c-Kit, the Wnt signaling pathway, and the G protein-coupled

endothelin B receptor (ETBR) [27,34] (Figure 1.2). The activity of these intrinsic factors is finely tuned and influenced by extracellular growth factors, including SCF (c-Kit ligand), Wnt proteins, endothelins, neuregulin-1, and α-MSH [27,33].

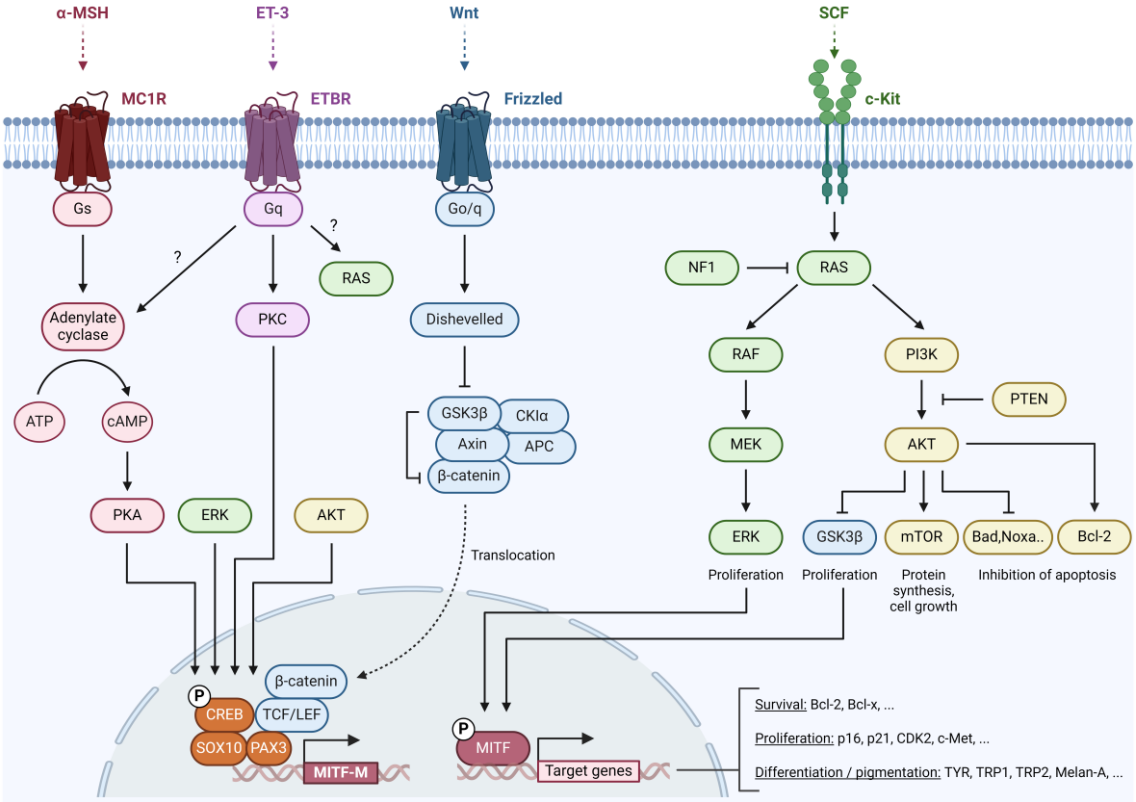

Figure 1.2 Key signaling pathways in melanocyte development. Schematic overview of the major network involved in melanocyte development, including the α-MSH/MC1R/PKA pathway, the endothelin/ETBR/PKC pathway, the Wnt/Frizzled/β-catenin pathway, and the SCF/c-Kit pathway with MAPK and PI3K/AKT signaling (created with BioRender.com, adapted from [35,36]).

In the course of melanoblast and melanocyte development, crucial pathways involve c-Kit, Wnt, and ETBR signaling, ultimately inducing MITF (Figure 1.2). Notch and α-MSH signaling also play a role. Signaling via the ETB receptor is required for melanoblast migration, survival, proliferation, and differentiation [37,38], with endothelins (ET) binding to ETBR triggering downstream pathways like PKC and MAPK. This cascade results in increased phosphorylation of MITF and the transcription factor CREB [34]. Additionally, CREB is able to activate MITF in response to MC1R-induced elevated cAMP signaling. The ligand α-MSH, for example released by keratinocytes, binds to the MC1 receptor, activating adenylate cyclase, which generates cAMP. The cAMP-dependent protein kinase A (PKA) subsequently phosphorylates and activates CREB, resulting in transcriptional activation of MITF [35]. c-Kit signaling is necessary for (embryonic) melanoblast migration, proliferation, and survival [34,37]. SCF-induced activation of c-Kit triggers receptor dimerization and activation of downstream events, including RAS, MAPK, and PI3K/AKT pathways [29,34].

The Notch pathway plays a crucial role during the embryonic period in inducing neural crest cells at the neural plate border [33]. Notch signaling through cell-cell interaction between membrane-bound ligands Delta and Jagged and the Notch receptor is also essential for maintenance of the immature status and survival of melanoblasts and neural crest stem cells (NCSCs) during both development and adulthood [37,39]. In mature melanocytes, Notch signaling is inactive; however, its activation can dedifferentiate and reprogram melanocytes into multipotent NCSCs [40]. Wnt/Frizzled/β-catenin signaling is essential for the induction and specification of melanocyte fate in NCSCs, inhibiting neuronal/glial differentiation. Conversely, the absence of Wnt signaling promotes neuronal cell fates [41,42]. In the canonical Wnt/β-catenin pathway, binding of Wnt ligands such as Wnt3a and Wnt7a to the Frizzled receptor leads to inhibition of glycogen synthase kinase-3β (GSK3β), thereby stabilizing β-catenin. This allows β-catenin to translocate into the nucleus, where it interacts with TCF/LEF family transcription factors to stimulate MITF transcription [29,34,43]. Furthermore, Wnt ligands suppress the Notch pathway through upregulation of the Notch inhibitor Numb. UV irradiation increases the secretion of Wnt7a by keratinocytes [42].

MITF is the master regulator in melanocyte development, proliferation, differentiation, migration, survival, dendrite formation, and melanin synthesis [44]. A pivotal step in committing neural crest cells to the melanocytic lineage involves the downregulation of the transcription factors FOXD3 and SOX2, which act as repressors of MITF [37]. Disruptions such as mutations or deletions in MITF cause melanocyte deficiency and pigmentation defects [27]. The MITF-M isoform is expressed almost exclusively in the melanocyte lineage, regulating propagation of melanoblasts during early development and melanogenesis in adult melanocytes. The transcription factors Pax3 and SOX10 collaborate with CREB and TCF/LEF to regulate and activate the MITF promotor [29,44]. The activity of CREB is controlled by phosphorylation through kinases AKT, ERK1/2, PKC, and PKA [23]. Besides transcriptional regulation, MITF also undergoes phosphorylation mediated by ERK1/2 and GSK3β [44].

MITF is responsible for controlling the expression of genes related to differentiation and pigmentation, including tyrosinase, TRP1, TRP2, and melanosomal proteins (Melan-A/MART-1, HMB45). Together with MITF, these melanocyte-specific proteins serve as the main markers for adult melanocytes [6]. Furthermore, MITF is involved in proliferation and survival through regulation of cell cycle- and apoptosis-related genes, such as CDK2, p16, and p21, as well as the anti-apoptotic Bcl-2, respectively [23,29,45]. MITF has also been reported to influence the expression of the microRNA-processing enzyme DICER [29,46].

The *in vitro* differentiation of pluripotent stem cells (PSCs) like embryonic stem cells (ESCs) or induced pluripotent stem cells (iPSCs) mirrors the *in vivo* process, involving sequential steps: differentiation into neural crest cells, followed by transformation into melanoblasts, and ultimately maturation into melanin-producing melanocytes [33]. Typically, protocols for melanocyte differentiation employ various factors such as SCF, endothelin-3, Wnt3a, bFGF, CHIR-99021, cAMP, BMP4, B27, ascorbic acid, along with feeder cells for the seeding of PSCs [33].

1.1.1.3 Regulation of Melanocytes

Melanocyte proliferation, differentiation, melanin synthesis, and dendrite formation are on the one hand controlled by genetic factors, but on the other hand also through the crosstalk between melanocytes, keratinocytes, and dermal fibroblasts. This communication involves cell-cell contacts (e.g., E-cadherin) and the secretion of paracrine factors (e.g., cytokines, proteins, growth factors) [7,12,15,47] (Table 1.1).

Table 1.1 Paracrine factors with stimulating effect in human melanocyte regulation.

Proliferation	Differentiation	Melanogenesis	Dendrite formation
SCF	SCF	SCF	SCF
GM-CSF	GM-CSF	GM-CSF	GM-CSF
ET-1	ET-1	ET-1	ET-1
HGF	HGF	HGF	HGF
α-MSH	-	α-MSH	α-MSH
β-endorphin	-	β-endorphin	β-endorphin
NRG-1	-	NRG-1	-
bFGF	-	-	bFGF
Sema7a	-	-	Sema7a*
NT-3	-	-	-
TGF-β	-	-	-
CCN1	-	-	-
FAP-α	-	-	-
-	Wnt7a	-	-
-	-	ACTH	ACTH
-	-	PGE_2, $PGF_{2\alpha}$	PGE_2, $PGF_{2\alpha}$
-	-	NO	NO
-	-	KGF	-
-	-	-	NGF
-	-	-	IL-6, IL-8

*SCF (stem cell factor), GM-CSF (granulocyte-macrophage colony-stimulating factor), ET-1 (endothelin-1), HGF (hepatocyte growth factor), α-MSH (melanocyte-stimulating hormone), NRG-1 (neuregulin-1), bFGF (basic fibroblast growth factor), Sema7a (semaphorin 7a), NT-3 (neurotrophin-3), TGF-β (transforming growth factor-β), FAP-α (fibroblast activation protein-α), ACTH (adrenocorticotropic hormone), PGE_2 (prostaglandin E_2), $PGF_{2\alpha}$ (prostaglandin $F_{2\alpha}$), NO (nitric oxide), KGF (keratinocyte growth factor), NGF (nerve growth factor), IL-6 (interleukin 6), IL-8 (interleukin 8). *depending on receptor and pathway. Not included in table but in text: CCN1 (cellular communication network factor 1), ET-2 (endothelin-2), ET-3 (endothelin-3), LIF (leukemia inhibitory factor), IL-1 (interleukin 1), DKK1 (Dickkopf-related protein 1), sFRP2 (secreted frizzled-related protein 2), TNF-α (tumor necrosis factor).*

In humans, keratinocyte-derived factors include SCF, α-MSH, ACTH, GM-CSF, ET-1, bFGF, NGF, HGF, PGE_2, $PGF_{2\alpha}$, IL-6, IL-8, β-endorphin, and Sema7a. Evidence for ET-2, ET-3, LIF, and IL-1α is currently limited to mice [12,15,47,48]. Dermal fibroblasts secrete SCF, bFGF, HGF, KGF, NT-3, NRG-1, TGF-β, ET-3, IL-1, sFRP2, Sema7a, CCN1, FAP-α, and DKK1 [7,10,12,49]. The binding of these factors to specific receptors on the melanoblast/melanocyte membrane leads to the activation of PKA, PKC, or MAPK signaling (Figure 1.3).

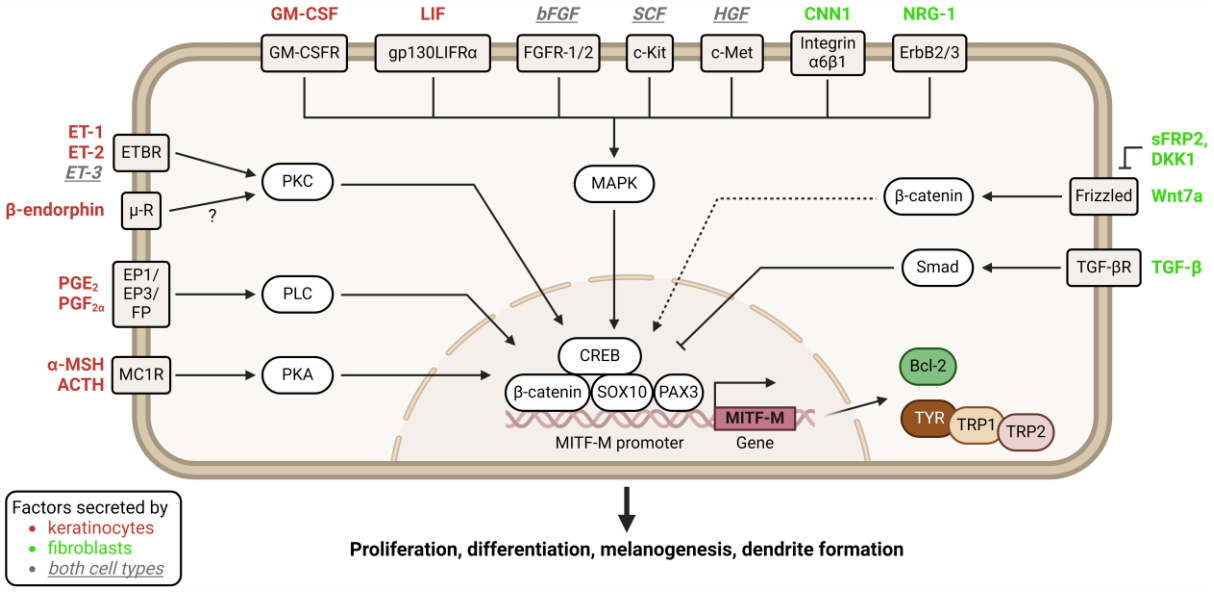

Figure 1.3 Regulation of melanocytes through paracrine factors. Mechanisms of keratinocyte- (red) and fibroblast-derived factors (green) on melanocytes. Factors secreted by both cell types are shown in gray. Binding of paracrine factors, including cytokines, proteins, and growth factors, to their specific receptors on the melanoblast/melanocyte membrane activates PKA, PKC, or MAPK signaling. UV exposure can induce the secretion (created with BioRender.com, adapted from [6,12,47]).

UV irradiation stimulates the secretion by keratinocytes, resulting in increased proliferation, differentiation, dendrite formation and melanogenesis in human melanocytes [47,50]. Moreover, DNA repair, antioxidant defense, and survival pathways are activated [23]. UV-inducible soluble factors include SCF, GM-CSF, ET-1, α-MSH, ACTH, Wnt7a, bFGF, NGF, PGE_2/$PGF_{2\alpha}$, NO, as well as pro-inflammatory cytokines IL-1α/1β, IL-6, and TNF-α [10,12,15,51]. For example, α-MSH and ACTH bind to the MC1 receptor on melanocytes, leading to cAMP production and activation of PKA and CREB, resulting in induction of MITF.

MITF-regulated genes control cell cycle and melanogenesis, blocking cell cycle progression and increasing eumelanin production [8,15,52]. Similar to ET-1 and NGF, α-MSH can induce the DNA damage response via p53, including nucleotide excision repair (NER), base excision repair (BER), and antioxidant genes. The three factors also inhibit UV-induced apoptosis by elevating levels of anti-apoptotic Bcl-2 [12,23].

The dysregulation of paracrine factors is linked to diverse pigmentary disorders, such as melasma, solar lentigines, post-inflammatory hyperpigmentation, and vitiligo. The malignant transformation of melanocytes into melanoma is characterized by the evasion of the control by keratinocytes (through downregulation of receptors crucial for cell-cell communication), autocrine production of growth factors, and insensitivity to growth-inhibitory factors [7]. The abnormal paracrine and autocrine production contributes to enhanced survival, proliferation, and resistance to therapies [12,49].

In addition to soluble secreted factors, skin cells also communicate through extracellular vesicles (EVs). Pigmentation in melanocytes can be regulated through keratinocyte-secreted exosomes in a miRNA-dependent manner, e.g., involving miR-3196 and miR-203, which control the expression and activity of melanosomal proteins like tyrosinase. UVB radiation alters the miRNA profile of exosomes, thereby stimulating pigmentation [50].

1.1.2 Dermis

The dermis is the connective tissue that lies underneath the epidermis. Both layers are separated by the dermal-epidermal junction including the basement membrane, which is composed of extracellular matrix (ECM) proteins, such as collagen, fibronectin, and elastin. The dermis supports the epidermis physically and with nutrients, and is responsible for mechanical strength as well as for the provision of immune cells. It contains blood vessels and lymphatic vessels, mechanoreceptors, nerve endings, and skin appendages such as hair follicles, sebaceous glands and sweat glands (Figure 1.1A). The dermis is composed of many cell types, including fibroblasts, blood vessel components (endothelial cells, smooth muscle cells, and blood vessel-associated fibroblasts/pericytes), lymphatic vessel components, neurons, tissue-resident immune cells (leukocytes), adipocytes, and dermal stem cells (DSCs, explained in detail in section 1.2.3). Connective tissue cells are classified as either resident (fixed) cells, meaning fibroblasts, fibrocytes, adipocytes, and stem cells, or wandering (transient) cells. The latter group comprises leukocytes such as eosinophils, lymphocytes, plasma cells, macrophages, monocytes, and mast cells. Fibroblasts are the primary cell type. They produce ECM proteins,

mainly collagen fibers, which contribute to the main substance of the dermis, forming a fibroelastic tissue that is responsible for the elasticity of the skin, tensile strength, and mechanical strength [1,2].

Human dermis is divided into the finely structured *stratum papillare* (papillary layer) in the upper area and the underlying coarsely structured *stratum reticulare* (reticular layer). The papillary dermis is a thin layer of loose connective tissue interlocked with the epidermis through dermal papillae. It consists of randomly distributed connective tissue cells, thin, poorly organized collagen fibers (primarily type I and III), and loose elastic fibers and is rich in capillaries, veins, and lymphatic vessels. In contrast, the reticular dermis is composed of meshed dense connective tissue featuring thick, well-organized collagen fibers (mainly type I) and coarse elastic fibers. Hair follicles, sebaceous glands, and sweat glands are located within this layer as well. Cell density is lower in the reticular layer than in the papillary layer [3,4,53,54].

1.1.3 Subcutaneous Tissue

The subcutaneous tissue (hypodermis) is located below the dermis, with the boundary between the two layers being rather indistinct. This layer is functionally connected to the skin, but not actually a part of it. It consists largely of subcutaneous adipose tissue and loose connective tissue, and contains nerves as well as larger blood vessels that supply the overlying layers of skin. The adipose tissue serves as pressure padding, energy storage and contributes to thermal insulation [1,3].

1.2 Stem Cells

Stem cells are unspecialized and immature cells that are responsible for the development of organ and tissue systems. They replenish lost cells throughout an organism's lifespan and thus play a crucial role in tissue homeostasis, regeneration, and wound repair [1,55,56]. The activity of stem cells varies depending on the organ they reside in. For example, bone marrow stem cells exhibit constant division, while stem cells in the pancreas have a low activity [56]. Stem cells are characterized by two features: the capacity for self-renewal and differentiation into mature cells building different tissues and organs. The term self-renewal refers to the ability of numerous mitotic cell divisions with resistance to senescence, permanent cell cycle arrest or differentiation. By contrast, precursor cells can only divide a few times before they differentiate and acquire lineage-specific characteristics. Differentiated cells are non-mitotic and have a limited lifespan.

Self-renewal of stem cells occurs either through symmetric or asymmetric division. In symmetric replication, the stem cell divides into two identical stem cells. Asymmetric replication means that one of the daughter cells remains an identical stem cell, while the other daughter cell—the so-called transit-amplifying cell (TAC)—divides a finite number of times until it enters terminal differentiation [1]. The balance between self-renewal and differentiation is essential for the physiological maintenance of tissues and organs [57].

Stem cells are located in a specialized microenvironment known as the stem cell niche, which governs their behavior and shields them from harmful influences. The niche is composed of stromal cells, ECM, and paracrine factors [57,58]. Progeny of stem cells, such as TACs, may also be an important component, providing feedback signals [59]. The stem cell niche is a key regulatory element for maintaining the functionality of the stem cell population and controlling cell fate [60]. The interplay between intrinsic mechanisms of the stem cell (gene expression, metabolism) and external signals from the surrounding cells (cell-cell contact, molecular crosstalking) regulates self-renewal, proliferation, survival, activation, and differentiation of stem cells [56]. When stem cells are separated from their specialized environment, they lose their stem cell identity and undergo differentiation [60].

Being a dynamic domain, the niches coevolve with the maturation of stem cells from embryonic development into adulthood. While fetal progenitors in emerging niches exhibit high proliferation, adult stem cells are mostly quiescent, meaning non-proliferating in the G0 phase [61]. The balance between stem cell quiescence and activity is a hallmark of a functional niche. Excessive stem cell production could lead to tumors [62]. Communication in the niche is bidirectional, with stem cells not only receiving signals from niche cells, but also actively emitting signals to influence the organization and function of their microenvironment in the adult organism. This has been demonstrated, for example, in hair follicle stem cells [63]. Dysregulation of stem cell behavior by the niche is implicated in disease onset [60]; e.g., genetic defects in the stem cell niche can contribute to the development of congenital myopathies [61].

Changes in both stem cells and their niche also play a role in the aging process, leading to reduced tissue homeostasis and repair upon injury in older individuals. Different mechanisms contribute to the aging-associated decline in stem cell function and number [64,65]. Lower self-renewal and differentiation capacity are caused by intrinsic transcriptional changes, epigenetic alterations, stress responses (mainly accumulation of DNA damage and oxidative stress), mitochondrial malfunction, telomere shortening, and deficiencies in DNA repair [66-69]. Aging is also marked by an increased number of stem cells entering senescence or deep quiescence

with limited reactivation potential [64]. Additionally, genotoxic stress can trigger differentiation of stem cells, leading to a depletion of stem cells [70]. Age-related alterations in the supporting niche result in a decline in niche function, contributing to stem cell defects [67]. These changes include transcriptomic shifts, accumulation of DNA damage, variations in cell and ECM composition of the niche, infiltration with immune cells, and changes in paracrine and soluble factors, such as decreased production of local self-renewal factors and an increase in inflammatory signals [60,64,65].

1.2.1 Potency of Stem Cells

The potency of a stem cell refers to its ability to differentiate into various cell types or tissues within the body. Stem cells can be classified according to their differentiation potential (Figure 1.4).

a. **Totipotent** stem cells have the highest potency and can give rise to all cell types of an organism, including extra-embryonic tissues. They are found in the zygote (fertilized egg) in the first three days after fertilization in the morula stage (16–32 cells). These totipotent stem cells develop into the embryo and the trophoblast as the extra-embryonic part and precursor of the placenta [55,56].
b. **Pluripotency** is the capacity to differentiate into cells of all three germ layers (endoderm, mesoderm, and ectoderm). During embryogenesis, the blastocyst develops from the morula on day five to six when there are approximately 70–100 cells. Pluripotent stem cells (PSCs) are then found in the inner cell mass (embryoblast) of the blastocyst. They have already lost the ability to differentiate into the trophoblast. Another source of pluripotent stem cells are induced pluripotent stem cells (iPSCs) which are artificially generated through genetic reprogramming of somatic cells in the laboratory [55,56].
c. **Multipotent** stem cells have a more limited differentiation spectrum and can differentiate into multiple cell types within a specific lineage or tissue, e.g., neural stem cells, mesenchymal stem cells (MSCs), or hematopoietic stem cells (HSCs) in the bone marrow, which can give rise to various blood cell types [56].
d. **Oligopotency** is the ability to differentiate into a few closely related cell types. An example is a myeloid stem cell derived from HSCs, which can give rise to different types of blood cells within the myeloid lineage, but not in the lymphoid lineage [56].
e. **Unipotent** stem cells can divide repeatedly, but only differentiate into one specialized cell type [56].

Cells with restricted differentiation capacity are sometimes labeled as **precursor or progenitor cells**. In addition to the limited potency, they also lack the ability of self-renewal, have a limited division capacity and a heightened differentiation level towards a specific cell type compared to conventional stem cells. Sometimes, the boundary between stem cell and precursor cell is not clearly defined [55]. Only multipotent and unipotent stem cells are found in the adult organism, allowing for the regeneration of cells and tissues.

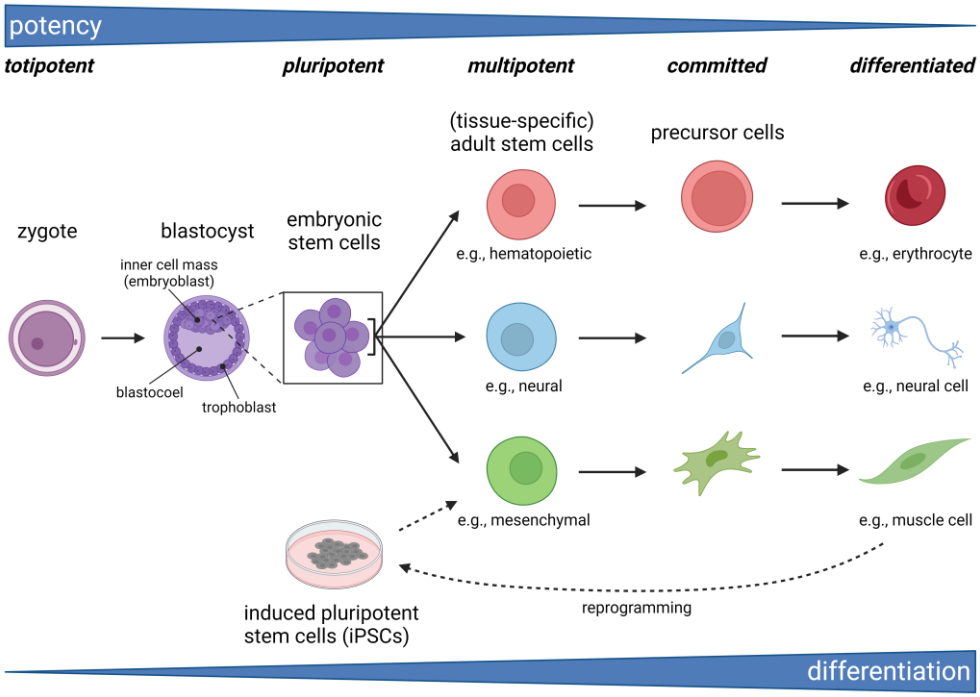

Figure 1.4 Potency of stem cells. Stem cells are categorized into different potency levels, including totipotent, pluripotent, multipotent, oligopotent, and unipotent, with the differentiation potential ranging from high to low. Totipotent stem cells found in the zygote exhibit the highest spectrum of differentiation, capable of giving rise to all cell types in the body. In contrast, oligopotent and unipotent precursor cells have the lowest potency and are restricted to differentiation into a few or only one defined cell type, respectively (created with BioRender.com).

When classified according to their occurrence, embryonic stem cells (ESCs) and adult (somatic) stem cells are distinguished. ESCs play a crucial role in the whole-body development and can be totipotent as well as pluripotent. During the initial divisions following fertilization, cells in the morula stage are still totipotent. In the blastocyst stage, pluripotent ESCs can be derived from the embryoblast/inner cell mass [55]. When the term ESCs is used, it usually refers to the pluripotent population. ESCs undergo symmetric cell division. Subsequently, they can further differentiate into multipotent and unipotent cells. The application and study of ESCs is controversial, raising ethical concerns and encountering legal obstacles [1,55].

Although pluripotency can occur naturally only in ESCs, induced pluripotent stem cells (iPSC) represent an alternative. iPSCs are genetically reprogrammed from adult somatic cells

through the introduction of reprogramming factors, such as Oct-3/4, SOX2, KLF4, and c-Myc [71] or SOX2, Oct-4, Lin28, and Nanog [72], using for example viral vectors or plasmids. This process induces changes in the epigenetic status and gene expression. iPSCs exhibit features similar to ESCs, including comparable morphology, gene expression patterns, self-renewal capacity, potential for differentiation into various cell types, and telomerase activity [1,56]. Consequently, iPSCs are highly attractive for both research and medical applications in disease modeling and stem cell therapy [73].

Adult stem cells are typically multipotent, exhibiting sufficient phenotypic plasticity to develop into different tissues, but some are also oligopotent or unipotent. They are present in regenerative tissues of adult organisms, distributed across nearly every organ and tissue, e.g., bone marrow, intestine, skin, muscle, brain, heart, adipose tissue, liver, reproductive organs, and blood [55]. Their primary role is to maintain and repair the tissue in which they reside, ensuring its functionality by replacing senescent or damaged cells [56]. This occurs via the process of asymmetric cell division [74]. However, there is evidence that certain tissue-based adult stem cells, for instance neural stem cells, may have a broader differentiation capacity than previously assumed [75,76]. Adult stem cells are located next to differentiated cells [57], mostly in a dormant, non-proliferating state (quiescence) within their stem cell niche to minimize metabolic and oxidative stress and prevent stem cell exhaustion, ensuring the prolonged maintenance of the stem cells in the tissue [69,77]. In response to tissue damage or cell loss, they are activated to proliferate and differentiate [78]. Mesenchymal stem cells (MSCs) exemplify adult stem cells, with populations found, among other places, in the bone marrow and subcutaneous adipose tissue [1]. The utilization of adult stem cells is usually free from ethical or legal concerns [55].

The potency of stem cells dictates their regenerative and therapeutic potential. Totipotent and pluripotent stem cells are highly valuable for research and potential medical applications due to their ability to generate a wide range of cell types. Hence, ESCs and iPSCs are promising for the use in regenerative medicine, transplantology and tissue engineering. However, they also come with ethical considerations, especially in the case of ESCs, and practical issues, bearing the risk of immunogenicity and tumorigenicity [1,73]. Therefore, multipotent and unipotent adult stem cells are highly advantageous for cell therapy and tissue engineering as well, since they lack these adverse effects and ethical issues, although they have more limited applications [55,78]. Especially MSCs are considered to have great potential and they are easy to isolate [1]. There are numerous preclinical and clinical studies on stem cell therapy worldwide, e.g., for

cardiovascular disorders, neurodegenerative diseases (like Parkinson's disease, Alzheimer's disease, Huntington's disease), macular degeneration, skin damage (e.g., chronic wounds, burn injuries), and type 1 diabetes. Moreover, stem cell therapy is already approved for certain applications, such as the use of limbal stem cells for eye burns or hematopoietic stem cell transplantation to treat leukemia [56,78,79]. Apart from the direct application of stem cells, there is an alternative method known as stem cell-based cell-free therapy. In this approach, only the bioactive molecules (e.g., growth factors and immunomodulatory molecules) generated by stem cells and enclosed in extracellular vesicles are extracted and utilized, since the regenerative effect primarily relies on these autocrine produced factors [55].

1.2.2 Types of Stem Cells in The Skin

The skin being a complex and highly regenerative organ, contains various precursor and stem cell populations. These skin stem cells play a dual role in maintaining skin homeostasis through continuous tissue regeneration and contributing to wound healing in response to injury [80], thereby preserving the integrity and functionality of the skin. The primary reservoirs for skin stem cells are the epidermis, hair follicles, and the dermis. Different types of stem cells include interfollicular epidermal stem cells, hair follicle stem cells, sebaceous gland stem cells, sweat gland stem cells, adipose-derived stem cells, melanocyte stem cells, and dermal stem cells.

Epidermal stem cells are located in the basal layer of the interfollicular epidermis, constituting 1–10% of the cells in this layer [81]. They are highly proliferative and possess a high degree of self-renewal potential. Asymmetric mitotic division generates a new epidermal stem cell and a TAC, which undergoes several divisions before leaving the basal layer to ultimately differentiate into keratinocytes [62,82]. Epidermal stem cells play a central role in the constant regeneration of the epidermis (epidermal homeostasis) and in wound repair [81].

The bulge region integrated into the outer root sheath of the hair follicle (Figure 1.1B) is the primary site for stem cells within the hair follicle [11] and contains multipotent epithelial stem cells, also termed **hair follicle stem cells** (HFSCs). These HFSCs give rise to various cell types within the follicle, including epithelial cells/follicular keratinocytes and sebaceous gland cells, but they can differentiate into interfollicular keratinocytes as well [62,83]. Their primary function is the regeneration of the hair follicle during the hair cycle. However, when skin integrity is severely compromised after injury, e.g., after burns, HFSCs are also involved in the repair of the epidermis [82,83], even though they are not typically responsible for building the interfollicular epidermis [84].

Sebaceous gland stem cells are located in the sebaceous glands associated with hair follicles [85] (Figure 1.1B). They have the capacity to generate both sebocytes and epidermal keratinocytes, potentially contributing to the regeneration of the epidermis and other skin structures following injury [62]. Sebocytes are responsible for producing lipids and sebum, an oily substance that lubricates the skin and hair, thereby protecting and moisturizing the skin [80,85].

Sweat gland stem cells are found in the sweat glands distributed throughout the skin. They encompass various subpopulations, with most of them having functions in sweat gland repair and maintenance. Another subpopulation includes epidermal stem cells [86]. The ability to form a stratified, interfollicular epidermis with keratinocytes [87] is indicative of a potential role of sweat gland stem cells in wound healing [88]. Sweat glands regulate body temperature by producing sweat and are a component of the innate immune system [86].

Adipose-derived stem cells (ADSCs) are MSCs located at the dermal papilla and dermal sheath of hair follicles (Figure 1.1B), in the interfollicular dermis, and subcutaneous tissue [89]. They produce ECM proteins and regulate skin homeostasis as well as wound healing [89]. During wound healing, ADSCs are activated to recruit fibroblasts [90]. ADSCs can also migrate into wounded sites, differentiating into dermal fibroblasts, endothelial cells, and keratinocytes [89]. Dermal fibroblasts may also originate from other MSCs in human skin or from fibrocytes, bone marrow-derived progenitor cells related to monocytes, which migrate from the bone marrow or blood to the site of dermal injury and participate in tissue restoration [91,92].

Melanocyte stem cells (McSCs) serve as a reservoir to replenish lost melanocytes during adulthood. The precise location of these cells in adult skin is a topic of ongoing debate. While there is a confirmed niche for McSCs in the hair follicle [11,93], studies have suggested additional localizations in dermis and epidermis [6]. Several reports even propose that peripheral nerves could potentially act as a McSC niche from which cutaneous melanocytes are recruited for skin regeneration and repair [94-96].

In the hair follicle, McSCs reside in the bulge region along with HFSCs (Figure 1.1B). These hair follicle McSCs replenish hair matrix melanocytes during each hair cycle [11]. They can also migrate to the basal layer of the surrounding epidermis and differentiate into epidermal melanocytes when needed [18], serving as a melanocyte reservoir for both hair and skin pigmentation [11]. Yu and colleagues were able to isolate adult stem cells with neural crest characteristics from human hair follicle bulge [93,97], which were different from previously identified lineage-specific McSCs from hair follicles. These cells expressed NCSC markers,

proliferated as spheres, and demonstrated self-renewal as well as differentiation into multiple lineages *in vitro*, namely neurons, smooth muscle cells, melanocytes [93], adipocytes, chondrocytes, and osteocytes [97].

In individuals with vitiligo—a pigmentary skin disorder characterized by the loss of melanocytes—the process of skin repigmentation typically occurs through 'follicular repigmentation', starting around hair follicles and expanding from there over the entire depigmented skin area [11]. However, occasional instances of repigmentation in areas without hair follicles, like the palms of the hands, suggest the existence of McSC niches in other (extrafollicular) skin structures [98,99]. Additionally, with aging, hair follicle McSCs lose their self-renewal ability; depletion and dysfunction of McSCs and hair matrix melanocytes result in hair graying [100,101]. In contrast, skin melanocytes maintain lifelong proliferative potential, and skin pigmentation persists even after hair graying, being also indicative of another, hair follicle-independent source of McSCs. While much research has been conducted in murine skin, studies on McSCs in human skin are limited. Nevertheless, findings from mice cannot simply be extrapolated to humans due to significant differences in skin structure and physiology between the two (e.g., skin thickness, distribution of melanocytes) [10,102,103]. Recent research suggests the presence of melanocyte precursor cells in human interfollicular epidermis. Michalak-Micka et al. identified a c-Kit^{-}/CD90^{+} cell population that has neural crest characteristics and can differentiate into multiple lineages *in vitro* [104]. It is further hypothesized that in humans, precursor cells for melanocytes could originate from dermal cell populations. However, a confined McSC niche in non-hairy skin has not yet been found. The growing evidence of a dermal melanocyte stem cell reservoir [30-32,105,106] is detailed in section 1.2.3.

The presence of stem cells in the dermis remains largely unexplored. So far, THE ONE **dermal stem cell** singularly responsible for the maintenance and repair of the dermis has not been identified. This issue is discussed in the following section.

1.2.3 Dermal Stem Cells

In the literature, the term 'dermal stem cell' is confoundingly used to describe various dermis-derived adult stem cell populations, employing different culture systems. The distinction is often challenging due to the terminological choices and the unclear origin in most cases. The studies described below demonstrate the presence of multipotent adult stem cell populations in the dermis; however, these populations are often not well-characterized. In *in vitro* examinations, the culture-initiating cell population is commonly undefined and heterogeneous,

being derived from the entire dermis. Consequently, the measured cell characteristics strongly rely on the culture system, including the isolation method and the utilized medium. Moreover, differences may arise depending on the specific anatomical location of the starting tissue [107].

While adult stem cells were traditionally thought to have stringent tissue-restricted differentiation potential, several findings indicate that they can also give rise to cells of different embryonic lineages [75,76,108,109]. Given the development of the dermis from mesenchymal precursors, one might hypothesize the existence of a multipotent embryonic mesenchymal precursor in the dermis responsible for homeostatic maintenance and regeneration. **Mesenchymal stem cells** (MSCs) are derived from the mesoderm and characterized by their ability of multi-lineage differentiation, with the extent of this capacity varying depending on the source in the body [110]. Usually, they can differentiate into cells of the osteogenic (bone), adipogenic (fat), chondrogenic (cartilage), and myogenic (muscle) lineages, while the potential to generate cells of the neurogenic lineage is still under debate. The existence of multipotent MSC-like cells in the dermis, demonstrating multi-lineage differentiation into mesodermal (osteocytes, adipocytes, myocytes) [110-112] and endodermal cells (hepatocytes) [112] was confirmed in several studies with human juvenile foreskin [110,111] and adult skin [112]. Other studies have demonstrated the additional potential of human dermis-derived stem cells for (ectodermal) neurogenic differentiation, generating cell types (neurons) that are not typically found in this tissue [105,113,114]. Besides MSCs, the dermis contains various other stem cell subpopulations, including neural crest stem cells (NCSCs) [115].

In a major breakthrough in the early 2000s, Toma and colleagues identified multipotent adult precursors with neural crest characteristics in the dermis. Initially discovered in juvenile and adult rodent and adult human skin [109], these cells termed **'skin-derived precursors' (SKPs)** were later also found in neonatal human foreskin [105]. SKPs express mesenchymal markers like fibronectin and vimentin, along with neural crest markers such as nestin, Pax3, Snail, and Slug, whereas NGFRp75 is expressed minimally or not at all [105]. Thus, Toma et al. suggested a novel, previously unidentified dermal stem cell population, as SKPs differ from bone marrow MSCs in expression profile, growth behavior, and morphology [109]. Their antigen profile mostly aligns with embryonic NCSCs [105] and shares similarities with the pattern of the neural crest-characteristic hair follicle-derived McSCs described by Yu et al. [97] (see section 1.2.2). *In vitro*, SKPs grow as self-renewing spheres and exhibit the capacity for multi-lineage differentiation into both neuroectodermal (neurons, glial cells, Schwann cells) and mesodermal cells (smooth muscle cells, adipocytes) [105], all of them representing neural crest progeny.

The fact that SKPs can differentiate into functional myelinating Schwann cells [116], a cell type only derived from the neural crest, supports a potential neural crest origin [105]. These findings suggest that SKPs are embryonic neural crest-related stem cells that persist in lower numbers in the skin after embryogenesis, with the potential to generate neural crest progeny found in the skin, including melanocytes [117]. Other studies have confirmed the neurogenic potential of rodent and human dermis-derived SKPs [118-120]. However, their overall function in skin remained uncertain.

The localization of these multipotent adult stem cells in the dermis and whether they have a confined niche are yet to be defined. Several studies concluded that the hair follicle dermal papilla and dermal sheath (Figure 1.1B) serve as niches for MSCs [115,121,122] and SKPs [117,123,124] in human and rodent skin. However, data from studies using foreskin tissue [105,110,111,113], which does not contain hair follicles, provide evidence that multipotent cells also exist in other extrafollicular zones of the dermis. A spatially restricted stem cell reservoir in non-hairy skin has not yet been identified.

After Toma et al. were the first to demonstrate the presence of multipotent adult stem cells in extrafollicular regions through the isolation of SKPs [105], neural crest-derived stem cells from the skin have been extensively studied. In search of melanocyte precursors beyond hair follicles, in 2010 the group led by Meenhard Herlyn at The Wistar Institute in Philadelphia, USA, reported on multipotent dermis-derived stem cells with neural crest-like characteristics that demonstrated melanocytic differentiation potential [31]. These **'dermal stem cells' or 'DSCs'** were isolated from human neonatal foreskin [125] and are the focus of this study. DSCs form three-dimensional spheres in human ESC medium, exhibiting self-renewal capabilities. They express NCSC markers NGFRp75 and nestin, along with the ESC marker Oct-4, while lacking expression of E-cadherin, N-cadherin, and melanocytic markers such as HMB45 or S100. *In vitro*, DSCs can differentiate into various neural crest-derived lineages, including melanocytes, neurons, Schwann cells, smooth muscle cells, chondrocytes, and adipocytes [31,126]. Consequently, DSCs are McSCs but retain flexibility to alter their fate depending on culture conditions. Foreskin-derived DSCs and SKPs [105] are similar but differ in some aspects, possibly attributable to the different culture media used: a melanocytic differentiation potential of SKPs is unknown and they lack solid expression of NGFRp75 and Oct-4.

Using a 3D human skin reconstruct model, Herlyn's group showed for the first time that DSCs differentiate into $HMB45^{+}/S100^{+}$ melanocytes, which migrate from the dermis to the epidermis and align at the basal layer [31,125]. Following contact with epidermal keratinocytes,

they gain E-cadherin, while losing NGFRp75 expression [31]. This process of differentiation is triggered by keratinocytes secreting Wnt ligands after UV irradiation [42]. The 3D model comprised dermal foreskin fibroblasts and DSCs embedded in collagen as the dermal compartment, and epidermal keratinocytes above as a stratified epidermis, separated by a functional basement membrane [102]. Staining of foreskin sections revealed no distinct niche but rather the distribution of individual DSCs throughout the entire dermis. Overall, the findings from Herlyn and colleagues provide strong evidence that DSCs serve as a reservoir for extrafollicular epidermal melanocytes in the more protected dermis [31,32]. Meanwhile, in the dermis of glabrous depigmented areas of vitiligo patients, NCSCs have indeed been identified [106] using Li et al.'s protocols [31]. Due to their features ($NGFRp75^+$/$nestin^+$, self-renewal capacity, melanocytic differentiation potential), these cells are very likely to be DSCs [106], thereby further confirming the existence of a dermal McSC niche.

All of these findings initiated a debate on whether DSCs are involved in pathological events such as malignant transformation into melanoma. Accordingly, early epigenetic or genetic changes might already occur in the dermis in melanocytic precursors [31], as discussed further in section 1.5.2.3.

When the term 'dermal stem cells' or 'DSCs' is used hereinafter, it refers to the melanocyte precursors from foreskin described by Herlyn's group.

1.3 UV Radiation

UV radiation is a form of electromagnetic radiation with wavelengths between ionizing radiation (<100 nm) and visible light (VIS; ~400–780 nm) on the electromagnetic spectrum (Figure 1.5). It is classified into three spectral bands: UVA (315–400 nm), UVB (280–315 nm) and UVC radiation (100–280 nm). UVA photons have the lowest energy at the longest wavelength, while UVC has the shortest wavelength but the highest energy. UVB covers the wavelength range between UVC and UVA radiation. Together with VIS and infrared radiation (IR), UV radiation is emitted by the sun. Each UV spectral band has a variety of effects on cells, tissues, and molecules [127,128]. UVA and UVB are classified as fully carcinogenic, meaning they have both tumor-causing and tumor-promoting effects [127,129]. Skin cancers primarily result from exposure to UV radiation, coming from the sun or from artificial sources such as tanning beds [127,130].

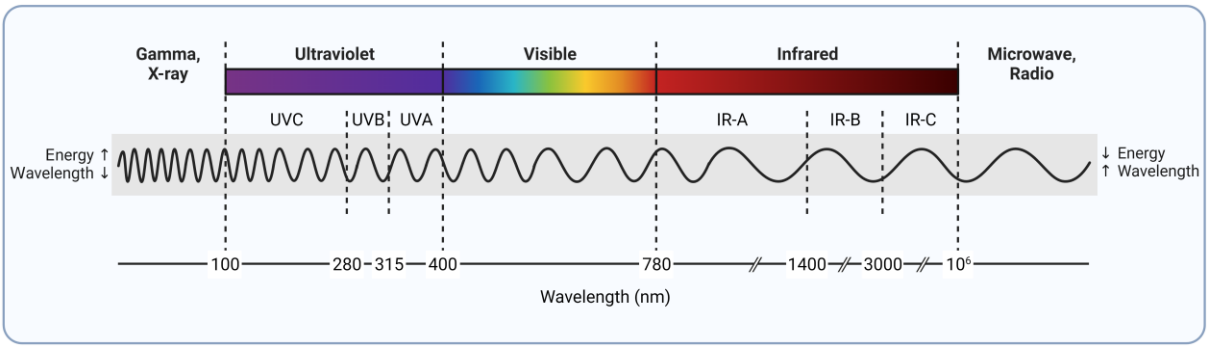

Figure 1.5 UV wavelength range in the spectrum of electromagnetic radiation. Ultraviolet radiation refers to electromagnetic radiation with wavelengths between 100–400 nm. It is divided into UVA (315–400 nm), UVB (280–315 nm), and UVC radiation (100–280 nm). Gamma and X-rays with shorter wavelengths <100 nm but higher energy belong to ionizing radiation. Visible light, infrared radiation (IR), microwaves and radio waves have lower energy but longer wavelengths than UV radiation (created with BioRender.com, adapted from [131]).

1.3.1 Physical Principles of UV Radiation

The energy of electromagnetic radiation is described by the following formulas according to the wave-particle duality:

$$c = \lambda \times v \quad \text{and} \qquad \text{Formula 1}$$

$$E = h \times v = h \times \frac{c}{\lambda} \qquad \text{Formula 2}$$

with E = energy of the radiation quantum (J)

h = Planck constant (6.626×10^{-34} Js)

v = frequency of the radiation quantum (Hz)

c = speed of light in vacuum (m/s)

λ = wavelength (nm)

The energy of electromagnetic radiation is therefore dependent on the wavelength λ. The longer the wavelength, the lower the energy and vice versa. The irradiance E (W/m²) is calculated from the radiant power per unit area.

$$E = \int_{\lambda_1}^{\lambda_2} E_\lambda(\lambda) d\lambda \qquad \text{Formula 3}$$

The dose or radiant exposure H (J/m²) describes the integral over time of the irradiance and thus the energy that acts on a surface over a defined period of time t [132].

$$H = \int_0^t E(t)dt \qquad \text{Formula 4}$$

The different UV spectral bands differ in their irradiance for inducing certain biological effects. Therefore, it is necessary to weigh UV radiation according to its biological effectiveness. The minimal erythema dose (MED) is often used as a measure of the biological effectiveness. It is defined as the lowest UV dose that causes a just noticeable reddening (erythema) on previously non-exposed skin 24 hours after exposure [133,134]. The MED is a subjective measure and varies greatly depending on the individual skin type, skin thickness, prior UV exposure, immune status, sex, season, and meteorological factors [135-137]. For a fair-skinned European with skin type II, the MED averages around 250–400 J/m² [127].

The calculation of erythema-weighted doses is based on standardization by the International Commission on Illumination (CIE). This weighting according to standardization is shown in Figure 1.6. The relative effectiveness decreases significantly with increasing wavelengths. Since nucleic acids and proteins exhibit absorbance maxima at 260 nm and 280 nm, respectively, UVB radiation (280–315 nm) has the highest biological effectiveness, while in the range of UVA rays (315–400 nm), it decreases by a factor of 1,000–10,000. Consequently, a much higher UVA dose is required to induce equivalent physiological effects compared to UVB radiation. UVC radiation (100–280 nm) is not shown due to its low proportion in solar radiation and low relevance in the development of skin cancer [138-140].

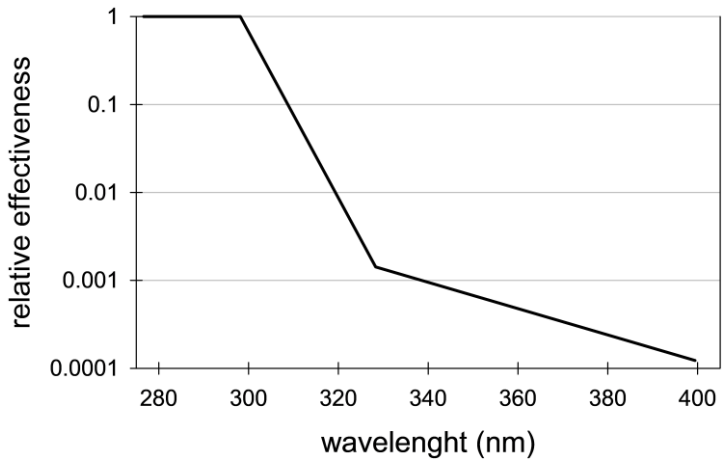

Figure 1.6 Erythema-weighted spectral effectiveness. The biological effectiveness varies depending on the spectral band. It is greatest with short-wave UV radiation (UVB). At increasing wavelengths shifting into the UVA range, it decreases sharply (adapted from [140]).

1.3.2 Solar UV Radiation

Solar radiation is largely optical radiation. Epidemiological studies together with molecular biological data confirm a causal association between exposure to solar radiation and the major types of skin cancer [141]. Therefore, solar radiation is classified as carcinogenic to humans [129]. The solar radiation spectrum on the Earth's surface (terrestrial radiation) is composed of 50% visible light (VIS), 45% infrared radiation (IR), and 5% UV radiation. Although UV radiation only accounts for such a small portion of the total terrestrial solar energy, it is responsible for a large portion of all known biological effects that are associated with harmful effects of solar radiation exposure [134,136].

Passing through the Earth's atmosphere, the sunlight is filtered and scattered by various atmospheric components, including ozone and other gaseous and pollutant particles. Especially the short-wave UV range is absorbed, resulting in almost complete absorption of UVC radiation by the ozone layer. UVB rays are also largely absorbed by the Earth's atmosphere, while nearly all of the emitted UVA radiation reaches the surface of the Earth [142]. Therefore, terrestrial UV radiation primarily consists of UVA (90–95%) and UVB radiation (5–10%) [129,134].

A variety of factors, such as the position of the sun, cloudiness, altitude, reflectance, and the atmospheric composition (ozone content, amount of scattering and absorbing particles, pollution) affect the intensity and the proportion of solar UV radiation at the Earth's surface that is biologically active for humans [134,143]. This results in diurnal, seasonal, and geographical variations [127,128,136]. Given the influencing factors mentioned above, climate change will also have an effect on terrestrial UV levels.

1.3.3 Penetration Depth of UV Radiation into Human Skin

Depending on the wavelength, solar radiation penetrates the human skin to varying degrees, with increasing wavelengths corresponding to greater penetration depth (Figure 1.7). The penetration depth is influenced by the absorption characteristics of chromophores and by tissue reflection [136,144] and can vary depending on the angle of entry and the thickness of the different skin layers. Absorption at specific wavelengths is primarily associated with distinct components of the skin. Around 280 nm, it is attributed to keratin in the epidermis and *stratum corneum*, while absorption at 425, 500, and 600 nm is linked to blood and fat in the dermis and subcutaneous tissue. At approximately 970 nm, water plays a central role in absorption. Melanin is a broadband UV absorber. Scattering and absorption of radiation in the different skin layers lead to a gradual, non-linear reduction of energy density with depth [145].

The *stratum corneum* is an effective barrier to UVC radiation, but since solar UVC is almost completely absorbed by the ozone layer, it is not considered further. The long-wavelength UVA rays are less scattered upon entering the epidermis compared to UVB. Approximately 20% of UVA and 9% of UVB radiation reach the basal layer of the epidermis, where epidermal stem cells and melanocytes are located [128]. UVA can penetrate deep into the dermis and one percent even transmits into the subcutaneous tissue, contributing to skin aging and wrinkling by damaging elastic fibers and collagen. UVB radiation, on the other hand, is almost entirely absorbed in the epidermis due to molecular interactions and only a small fraction reaches the dermis [5,127]. The wavelengths of VIS and infrared radiation (particularly IR-A) are able to penetrate deeper into the skin [136,146,147]. Around 20% of VIS arrives at the subcutaneous tissue, whereas for IR-A, larger percentages transmit into dermis (65%) and subcutaneous tissue (40%) [148]. Longer-wavelength IR-B and IR-C radiation are mostly absorbed in the epidermis by water and released as thermal energy to surrounding tissues [147].

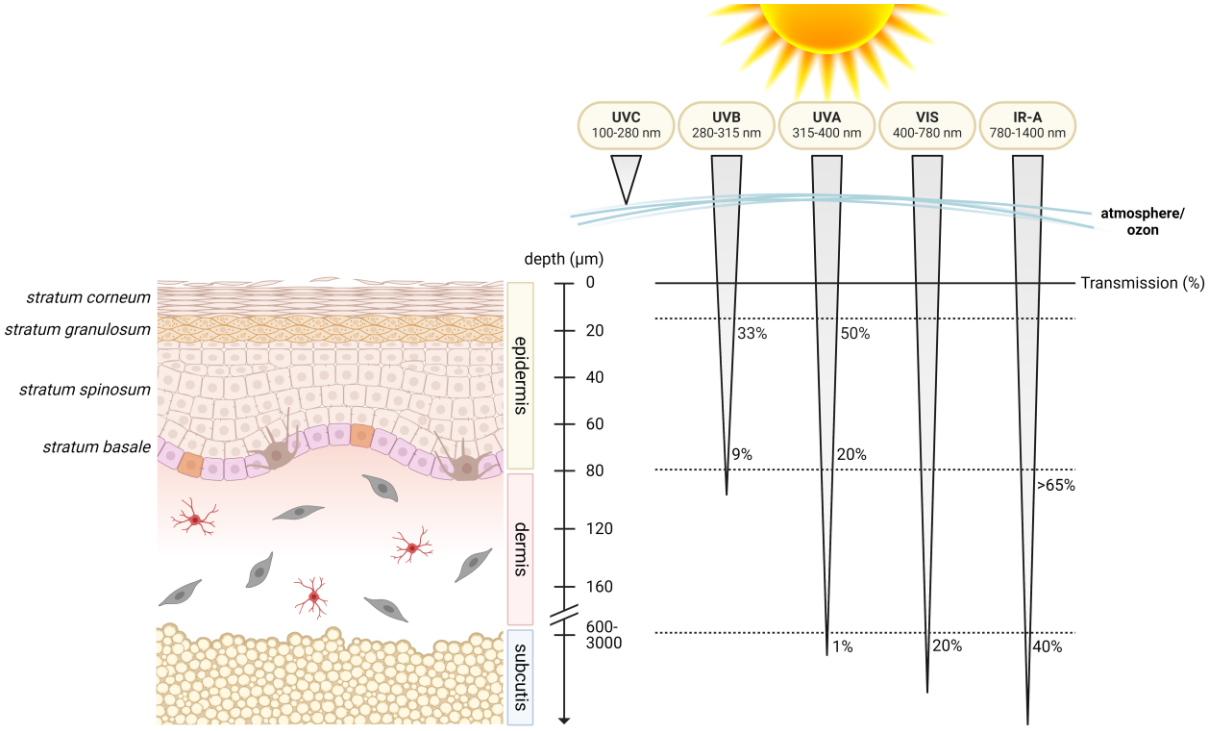

Figure 1.7 Penetration depth of UV radiation into human skin. The depth to which electromagnetic radiation penetrates the skin is dependent on its wavelength. Greater wavelength corresponds to increased penetration depth. UVC is almost completely absorbed by the ozone layer. UVB is largely absorbed in the epidermis, with a minor portion still penetrating into the upper dermis. UVA reaches deep into the dermis and even into the subcutaneous tissue. Both VIS and IR-A reach the subcutaneous tissue as well (created with BioRender.com, adapted from [5,149]).

1.3.4 Biological Effects of UV Radiation (on The Skin)

Exposure to UV radiation results in a variety of acute and long-term effects in the human body and can impair the integrity of the skin barrier. Solely UVA and UVB radiation are biologically relevant, since exposure to UVC is only possible through artificial sources such as electric-arc welding and germicidal lamps [127,128]. UV radiation triggers photochemical effects due to the absorption of photons by specific molecules. These effects are dependent on the dose and on the wavelength. The primary organs affected by UV radiation are skin and eyes [136]. However, effects to the eyes are not relevant for this work and not discussed in detail.

Acute adverse effects of UV exposure include erythema/sunburn, pigmentation (tanning), photodermatoses, photokeratitis, photoconjunctivitis, local and systemic immunosuppression [150,151]. At the molecular level, UV radiation causes DNA damage, such as cyclobutane pyrimidine dimers (CPDs) and pyrimidine (6-4) pyrimidone photoproducts (6-4PPs) [152], as well as the formation of free radicals and reactive oxygen species (ROS) [136].

UV radiation also has some beneficial biological effects, including vitamin D_3 synthesis in the skin. Recent research indicates that UV might even lower blood pressure [151,153]. Moreover, it is used therapeutically for the treatment of certain (inflammatory) skin diseases like vitiligo vulgaris, psoriasis, atopic dermatitis, cutaneous T-cell lymphoma, and cutaneous sclerosis due to its anti-inflammatory/immunosuppressive effect (e.g., phototherapy with narrowband UVB, psoralen + UVA (PUVA), UVA1) [154,155].

Chronic exposure to UV radiation leads to long-term adverse effects, such as photoaging of the skin (wrinkling, hyperpigmentation, loss of elasticity, dryness), eye damage like cataract, and ultimately photocarcinogenesis due to the accumulation of mutations [156]. Except for vitamin D_3 synthesis, both acute and chronic effects are causally linked to UV-induced DNA damage and are mainly attributed to CPDs [128,157]. UVB radiation is acknowledged as the primary cause of sunburn and skin cancer; however, both UVB and UVA contribute to the development of cutaneous tumors [5].

1.3.5 UV-Induced DNA Lesions

Exposure to UV radiation can lead to both direct and indirect DNA damage [57,141]. Absorption of UVB photons by DNA causes direct damage, most frequently resulting in dimerization of adjacent pyrimidine bases (cytosine, thymine). The two main photoproducts are CPD and 6-4PP [138,141] (Figure 1.8). 6-4PPs are generated by formation of a covalent bond between the C6 of the 5'-base and the C4 of the 3'-base. On the other hand, CPDs are formed

by the coupling of the 5,6-double bonded carbons of two adjacent pyrimidine nucleotides and are induced most frequently [141,152]. About 75% of UV-specific DNA lesions are CPDs, while 6-4PPs account for the remaining 25% [133,158]. The phenomenon of dark CPDs encompasses the formation of CPDs up to three hours after irradiation. This process involves chemiexcitation, where the energy is transferred to chemical intermediates such as melanin, which in turn transfer the energy to DNA molecules, resulting in the subsequent, time-delayed CPD formation [151,159].

DNA photolesions can lead to mutations and are involved in the development of cancer, with CPDs being considered to have a higher mutagenic potential [5,127,160]. 6-4PPs are typically repaired more efficiently and are less likely to cause mutations [138,161,162]. CPDs and 6-4PPs cause different biological effects in UV-damaged cells. For example, 6-4PPs tend to induce apoptosis as the initial cellular response, while CPDs are more often associated with cell cycle arrest followed by DNA repair [163,164].

Several studies have shown that CPDs are also the most common UVA-induced DNA damage in human skin cells and human skin *in vivo* [138,165,166]. The exact mechanism of induction by UVA, however, is still unknown [152,167]. Nevertheless, UVB radiation induces CPDs with an approximately 1,000- to 10,000-fold higher efficacy than UVA radiation [133,138,168].

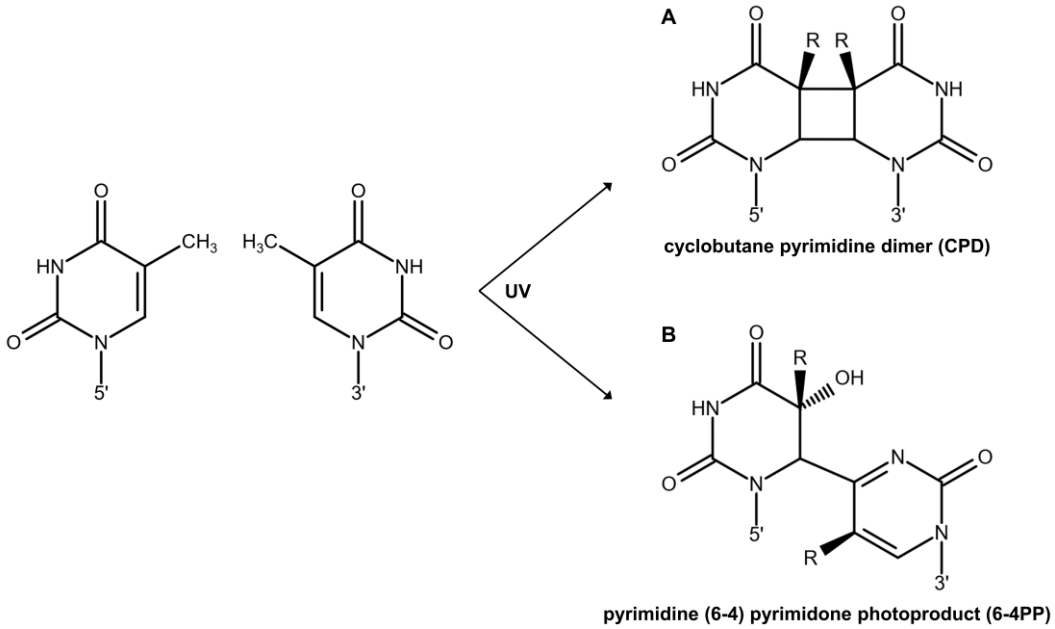

Figure 1.8 Chemical structures of pyrimidine dimers. The most common UV-induced DNA lesions are pyrimidine dimers, namely the cyclobutane pyrimidine dimer (CPD) and the pyrimidine (6-4) pyrimidone photoproduct (6-4PP) (created with Marvin JS).

The formation of CPDs is not uniform and depends on the base sequence and chromatin state, with lesions occurring more frequently in heterochromatin than in euchromatin. Thus, nucleosomes and other DNA-binding proteins affect CPD induction [169-171]. Most frequently, adjacent thymines undergo dimerization (TT). Thymine-cytosine or cytosine-thymine lesions (TC, CT) occur less often, and cytosine-cytosine dimers (CC) are extremely rare [138,152,156,166].

While TT dimers rarely lead to mutations, CC photolesions have a high mutagenicity, leading to the formation of specific UV signature mutations as a result of CC→TT tandem transitions [172]. Nevertheless, the predominant mutations are C→T transitions [138]. The prevailing emergence of mutations from cytosine-containing CPDs is likely attributed to two mechanisms. First, lesion bypass through error-prone DNA polymerases can result in incorrect base pairing of the damaged cytosine with adenine. Second, within the dimer, cytosine may deaminate to uracil, leading to the subsequent 'correct' insertion of adenine opposite uracil. During the next replication, thymine is inserted opposite the adenine, ultimately representing a C→T transition [141]. These signature mutations are found in UV-irradiated cells as well as in skin tumors, e.g., in the *p53* gene [129,133,173], a tumor suppressor with crucial roles in cell cycle regulation, DNA repair, and apoptosis (see section 1.4). Due to increased energy absorption, CPDs and thus C→T mutations are often induced at 5-methylcytosine within CpG dinucleotides [138,141]. This leads to UV-induced mutation hotspots within CpG islands in promoter regions, for example, of tumor suppressor genes like *p53*, impacting their activity [174]. Consequently, CPDs play a pivotal role in skin carcinogenesis and, along with UVB radiation, are considered one of the main causes of skin cancer [141].

However, also UVA is implicated in the promotion of skin cancer and causes characteristic signature mutation patterns [138,175]. With similar physiological doses, UVA-induced pyrimidine dimers might be even more mutagenic than those induced by UVB, attributed to a less effective UVA-triggered DNA damage response. UVA activates p53 to a significantly lesser extent, while cell cycle arrests and deceleration of DNA replication occur more frequently and prolonged after UVB exposure [152,176]. Consistent with these findings, the repair rate of UVA-induced CPDs in human skin is reported to be lower than that of UVB-induced CPDs. It is assumed that not only different cell cycle dynamics but also degradation of DNA repair proteins under oxidative stress contribute to this circumstance, although the precise underlying mechanisms remain unknown [165].

UV radiation causes additional cancer-promoting changes apart from CPDs, which also lead to mutations. Predominantly UVA radiation indirectly damages DNA by stimulating endogenous

cellular chromophores like porphyrins, flavins, melanin, and NADH. These chromophores interact with molecular oxygen, giving rise to free radicals and ROS, such as hydrogen peroxide (H_2O_2), hydroxyl radicals (OH^-), singlet oxygen ($^1O_2$), and superoxide anions (O_2^-). These ROS subsequently interact with membrane lipids, proteins, and also DNA bases and result in DNA-protein crosslinks, DNA single- and double-strand breaks, abasic sites, and oxidative base damage [24,177-179]. The DNA lesion 8-oxo-7,8-dihydro-2'-deoxyguanosine (8-oxo-dG) is the most common oxidative damage caused by UVA and leads to G→T transversions due to incorrect base pairing with adenine. These mutations were detected in skin tumors, suggesting a carcinogenic potential of oxidative damage [127,180].

This study primarily focuses on CPDs as UV-induced DNA damage, since they are responsible for the majority of UV-specific mutations.

1.4 DNA Damage Response

The DNA damage response (DDR) refers to an evolutionary conserved, complex network of interacting pathways designed to detect and regulate specific forms of DNA damage, aiming at preserving genomic stability [181]. Therefore, the DDR plays a crucial role in preventing carcinogenesis [57]. During differentiation, the DDR undergoes modifications, thereby establishing different levels of tolerance to DNA damage between stem cells and post-mitotic/somatic cells [182]. This section will focus primarily on the cellular response to UV exposure.

The formation of photoproducts through UV radiation triggers the DDR (Figure 1.9A). Activation of DNA damage checkpoints initiates multiple signaling cascades, including DNA repair, cell cycle arrest, transcriptional reprogramming [183], and chromatin remodeling [184,185]. As part of the DNA damage tolerance, the so-called translesion DNA synthesis (TLS) allows for DNA synthesis while UV-induced DNA lesions are still present, but may incorporate mutations [186]. This can lead to the inactivation of tumor suppressors, the activation of oncogenes, and in stem cells, the dysregulation of genes involved in differentiation and self-renewal [66]. All these factors can ultimately contribute to carcinogenesis. In case of extensive or irreparable DNA damage, apoptotic or senescent mechanisms are activated [183,186]. Another alternative outcome of the DDR in adult stem cells is the promotion of differentiation in response to excessive DNA damage [66,181]. The diverse pathways of the DDR are regulated by various transcriptional, post-translational, and epigenetic mechanisms [187-189].

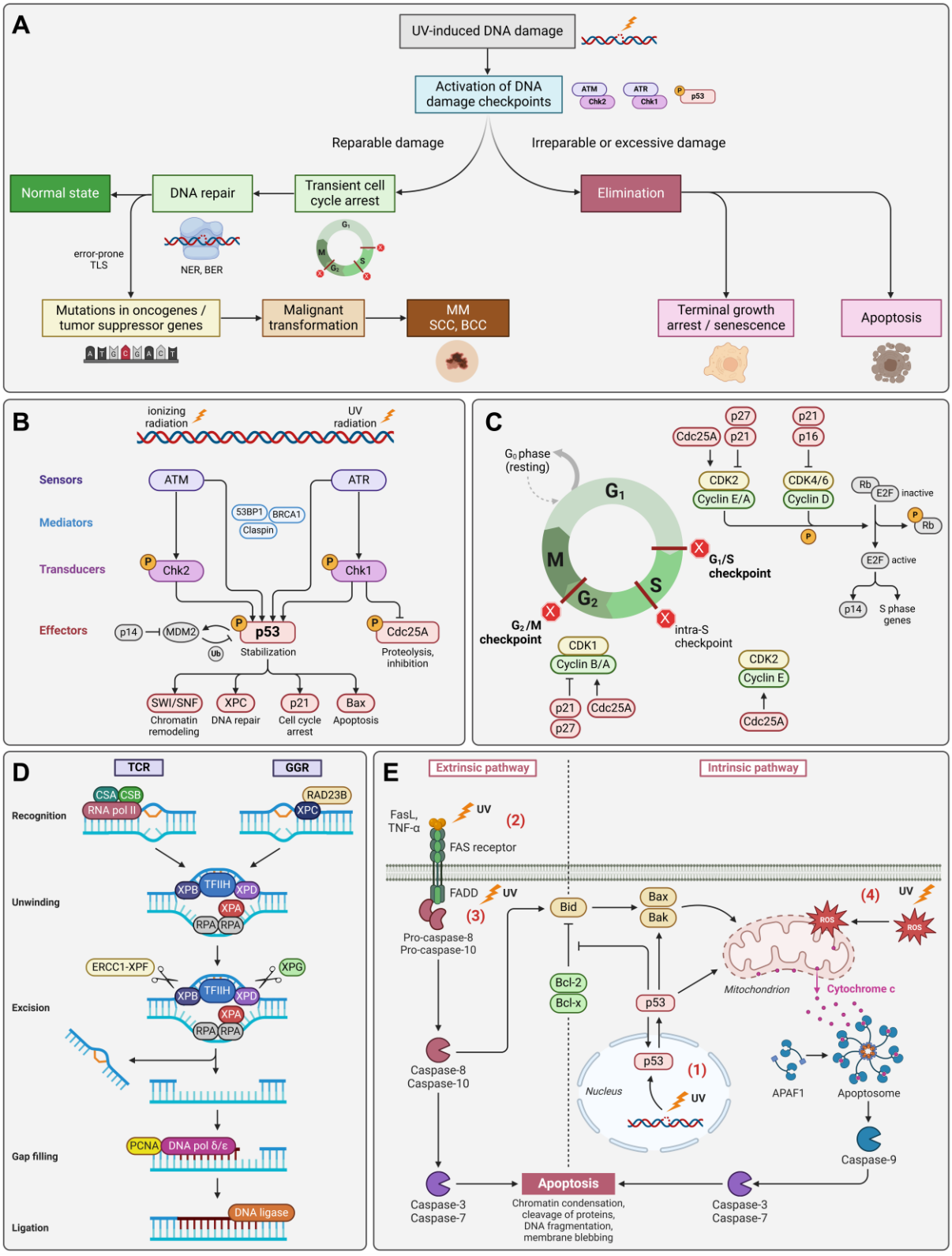

Figure 1.9 UV-induced damage response. (**A**) Schematic overview of the different outcomes in the DNA damage response to UV radiation. NER: nucleotide excision repair, BER: base excision repair, TLS: translesion DNA synthesis, MM: malignant melanoma, SCC: squamous cell carcinoma, BCC: basal cell carcinoma. (**B**) Induction of the DNA damage checkpoints with ATM and ATR as damage sensors. ATM: ataxia-telangiectasia mutated, ATR: ataxia-telangiectasia and Rad3-related (ATR). (**C**) Regulation of the cell cycle checkpoints following ATR checkpoint signaling and activation of p53. (**D**) Different steps of the nucleotide excision repair. TCR: transcription-coupled repair, GGR: global genome repair. (**E**) Extrinsic and intrinsic apoptosis pathways induced by UV radiation. The different

pathways (1–4) are further explained in section 1.4.4. ROS: reactive oxygen species (created with BioRender.com, D and E adapted from [184] and [5]).

1.4.1 DNA Damage Checkpoints

DNA damage checkpoints are constant cellular surveillance mechanisms that are activated in response to DNA damage, limiting the growth of damaged cells through various processes [66,183]. They consist of four components (Figure 1.9B):

- Sensors, e.g., ATM, ATR, DNA-PK
- Mediators, e.g., 53BP1, Claspin, BRCA1
- Signal transducers, e.g., Chk1, Chk2
- Effectors, e.g., p53, Cdc25A

The interaction of these proteins can result in either temporary cell cycle arrest and DNA repair, or the elimination of the damaged cell through apoptosis and/or cellular senescence [190]. In mammalian cells, the DDR is primarily regulated by two main kinases of the PI3K-like kinase family: ataxia-telangiectasia mutated (ATM) and ataxia-telangiectasia and Rad3-related (ATR). The damage sensor ATM acts primarily on DNA double-strand breaks from ionizing radiation, whereas ATR is activated by replication stress, such as unprocessed damage, stalled replicative DNA polymerase, or single-stranded DNA (ssDNA) [191,192]. UV-induced DNA damage is mainly detected by ATR [183], although in non-cycling cells, UV radiation can also activate the ATM pathway [186]. Mediators simultaneously interact with damage sensors, signal transducers, and effector molecules, contributing to signal transduction specificity [183]. ATR activates the checkpoint kinase 1 (Chk1), which phosphorylates effector proteins like tumor suppressor p53 and phosphatase Cdc25A [186] (Figure 1.9A).

One key element of the DDR is the transcription factor and tumor suppressor p53, the ‘guardian of the genome’ [191,193]. Under normal conditions, MDM2-mediated degradation keeps p53 at constant low levels [194]. Upon damage-induced phosphorylation by ATR and Chk1, p53 is stabilized [183,186], accumulates in the nucleus, and activates several downstream targets associated with cell cycle arrest (p21), DNA repair (e.g., PCNA, NER recognition protein XPC), apoptosis (pro-apoptotic proteins Bax, Noxa, Puma), senescence (p16, p19), antioxidant defense, and/or chromatin remodeling (interaction with remodeling complexes, e.g., SWI/SNF) [184,195-200]. Changes in chromatin structure are also mediated through the interaction of p53 with histone acetyltransferases (HATs) and histone deacetylases (HDACs) [191,201]. In addition, microRNAs that subsequently act in the DDR are also among the p53 targets [202].

Activation of p53 with low levels, involving the classical p53-MDM2 feedback loop, typically activates cell cycle arrest, while apoptosis is associated with high p53 levels lacking MDM2 accumulation [191].

The dynamics of p53 vary based on the stimulus and cell fate. UV radiation induces a single pulse of p53 activation with a dose-dependent increase in amplitude and duration. In response to DNA double-strand breaks (e.g., ionizing radiation), p53 displays pulsed dynamics with fixed amplitude and duration, but a dose-dependent number of pulses. These variations arise from ATR instead of ATM acting as a sensor for UV-induced damage, involving different negative feedback loops. Moreover, distinct dynamics determine diverse cell fates. Pulsatile kinetics are associated with cell cycle arrest and repair, whereas sustained levels lead to apoptosis and senescence [197]. Furthermore, p53 dynamics are also cell type-specific [203].

1.4.2 Cell Cycle Arrest

The ability to undergo cell cycle arrest after DNA damage is essential for maintaining genomic integrity and facilitating the repair of damage before DNA synthesis and subsequent cell divisions. The activation of checkpoints is controlled by the kinases ATM and ATR. ATR checkpoint signaling can induce different cell cycle checkpoints: G1/S, intra-S, and G2/M (Figure 1.9C). The ATR/Chk1-triggered proteolysis and inhibition of Cdc25A prevent the activation of cyclin-dependent kinases 2 and 1 (CDK2 and CDK1) that usually mediate the transition from G1 into S phase and the mitotic entry, respectively, temporarily arresting the cell cycle at G1/S and G2/M [186,192]. This initial, short-lasting arrest is accompanied by prolonged p53-mediated cell cycle checkpoint activation. Upon UV radiation, p53 also arrests the cell cycle in G1 and G2 phases [184], whereby p21 plays a crucial role as an inhibitor of several CDK complexes [191]. The stabilization of p53 after phosphorylation by ATR (at Ser15) and Chk1 (at Ser20) allows for the activation of p21 [183]. The p53-regulated G1/S arrest occurs through the inhibition of CDK2 by p21 [204]. Additionally, p21 binds to the cyclin D/CDK4 complex, preventing it from phosphorylating retinoblastoma protein (Rb), thereby inhibiting the transcription of E2F-dependent S phase genes [183]. On the other hand, the interaction of p21 with CDK2 can be enhanced by the release of p21 from cyclin D/CDK4 due to the disruption of the complex by p16 [205] and through p53-independent degradation of cyclin D [206]. In the G2/M arrest, p21 is involved in the inhibition of cyclin A- and cyclin B/CDK complexes, although p21 is not essential for this checkpoint [191]. The intra-S checkpoint is triggered by ATR-Chk1 signaling with the inhibition of Cdc25A and cyclin E/CDK2, inhibiting the firing of replication origins [183]. In addition to cell cycle arrest, p53

also activates a variety of DNA repair genes [207,208], chromatin remodeling [184,198], antioxidant defense, and apoptosis.

1.4.3 DNA Repair

Preserving the genomic integrity is essential for organismal development, cellular homeostasis, and cancer suppression. When DNA repair is absent or incomplete, DNA photolesions may lead to cell death and senescence, contributing to aging. Alternatively, the formation of mutations and genomic alterations can promote carcinogenesis [209]. Eukaryotic cells possess various highly conserved DNA repair mechanisms with differing fidelity levels. The activation of a specific mechanism depends on the type of DNA lesion and the cell cycle stage in which the cell resides [195,209]. Many organisms from bacteria to vertebrates are able to repair UV-induced pyrimidine dimers through photoreactivation with photolyase enzymes. These enzymes directly cleave CPDs and 6-4PPs into their corresponding monomers via a light-dependent reaction. However, humans are excluded from this, since placental mammals, due to evolutionary changes, lack the photolyase enzymes necessary for photoreactivation [175,183,210]. In humans, repair of UV-induced DNA damage is possible only through nucleotide and base excision mechanisms [186].

The primary pathway for repairing bulky, helix-distorting adducts like UV-induced pyrimidine dimers is the nucleotide excision repair (NER) (Figure 1.9D), where a lesion-containing oligonucleotide (~25–30 nucleotides long) is enzymatically removed and replaced by an intact sequence [211]. A distorted helix conformation inhibits physiological processes, such as replication and transcription [184]. 6-4PPs alter the helix structure more strongly than CPDs, leading to quicker detection and removal [186]. Additionally, the chromatin state (compactness) influences the recognition of UV-induced DNA lesions, affecting the rapidity and efficiency of NER [171,212].

NER comprises two distinct subpathways that differ in DNA damage recognition [211]. Global genome repair (GGR) operates throughout the entire genome, independent of transcription and replication, with initiation through the XPC-RAD23B complex detecting helix distortion. Transcription-coupled repair (TCR) targets only the transcribed strand of active, expressed genes during transcription through stalled RNA polymerase II at the damage site with the assistance of CSA and CSB [184,186]. Additionally, a mechanism called transcription domain-associated repair (DAR) involves proficient repair on both strands of transcribed genes in otherwise NER-deficient cells. This has been observed, for example, in neuron-like cells, appearing to be a subset of GGR, but the underlying molecular mechanism is unknown

[211,213]. Following damage recognition, both subpathways (GGR and TCR) share subsequent steps (Figure 1.9D): DNA unwinding by helicases XPB and XPD, subunits of the transcription factor IIH (TFIIH) complex; stabilization of the resulting single-strand structure by XPA and RPA; incision 5' and 3' to the damaged site via the endonucleases ERCC1-XPF and XPG, respectively; excision of the oligonucleotide; filling of the ssDNA gap through DNA synthesis by DNA polymerase δ or ε associated with PCNA, using the opposite DNA strand as a template; sealing of the new oligonucleotide by DNA ligase I or III [184,211,214].

p53 contributes to DNA repair by regulating transcription and directly interacting with components of the repair machinery (e.g., RPA), although the precise mechanisms remain unknown [191]. Additionally, p53 seems to recruit HAT complexes to enable access of NER factors to damaged sites through chromatin relaxation [191,201].

If a DNA lesion remains unrepaired or undergoes slow repair, TLS polymerases may read across the lesion during the S phase as part of a DNA damage tolerance mechanism. This process can potentially lead to the generation of mutations in an error-prone manner by incorporating incorrect nucleotides [186,215]. The significance of functional DNA repair in preventing photocarcinogenesis is exemplified by xeroderma pigmentosum (XP), a rare autosomal recessive congenital disorder affecting DNA repair due to mutations in NER genes, categorized into eight complementation groups/subtypes (XPA to XPG, XPV) [216]. Deficiencies in the repair capability of DNA photolesions result in hypersensitivity of the skin to sunlight and UV radiation, along with an almost 10,000-fold increase in non-melanoma skin cancers (NMSCs) and a 2,000-fold increase in malignant melanomas (MMs) among XP patients under 20 years old [217,218]. Approximately a quarter of XP patients also suffer from progressive neurological damage [216]. The majority of XP patients face premature death due to metastatic MMs and invasive squamous cell carcinomas (SCCs) [219]. Similarly, the autosomal recessive disorders trichothiodystrophy and Cockayne syndrome are characterized by mutations in the NER pathway as well. Patients exhibit features, such as developmental disorders, neurodegeneration, and premature aging, however, without solar hypersensitivity [158,218].

Oxidative UV-induced DNA damage like 8-oxo-dG is repaired via base excision repair (BER). In this repair process, typically individual damaged bases are replaced, but single-strand breaks are also addressed. Various DNA glycosylases detect modified DNA bases (such as oxidation, deamination, depurination, alkylation) and catalyze their excision, resulting in an abasic site.

The APEX1 endonuclease cleaves the DNA backbone, the gap is re-synthesized by DNA polymerase β and PCNA, and finally sealed through the XRCC1-ligase III complex [220,221].

1.4.4 Apoptosis

When DNA damage exceeds the cell's repair capacity or DNA repair fails, leaving unprocessed DNA lesions, cells usually enter a state of cellular senescence through permanent cell cycle arrest in G1 or undergo programmed cell death through apoptosis. By restricting replicative expansion, apoptosis serves as a protective, tumor-suppressing mechanism against unrepaired DNA lesions that could lead to mutations and carcinogenesis. This is particularly important in stem cells, where mutations otherwise could be passed on to self-renewing daughter cells and accumulate over time. UV radiation triggers apoptosis by causing DNA damage and ROS [5]. The emergence of epidermal sunburn cells following exposure to high-dose solar radiation is an example of UV-induced apoptosis in keratinocytes [222].

Apoptosis is an active process in which the cell undergoes successive breakdown without harming neighboring tissue. Characteristic features of apoptotic cells are: cell shrinkage; chromatin condensation; protein cleavage via caspases; DNA fragmentation via caspase-activated DNase, causing the characteristic 'nucleosome ladder' [5]; and formation of membrane-bound apoptotic bodies (membrane blebbing), which are phagocytosed by macrophages and dendritic cells [184]. Caspases, cysteine proteases, play a pivotal role in this process by cleaving the cell's own proteins, such as lamin (nuclear membrane) and actin (cytoskeleton), and activating secondary target proteins like DNase or other caspases through proteolysis. Necrosis, in contrast to apoptosis, is a passive process where massive damage leads to cellular swelling and disruption of the cell membrane, subsequently causing an inflammatory reaction [222].

Mammalian cells exhibit two pathways to induce apoptosis (Figure 1.9E). The intrinsic (mitochondrial) pathway is initiated from within the cell due to cellular stressors, regulated by pro-apoptotic (Bax, Bak, Bid, Bim, Puma, Noxa) and anti-apoptotic (Bcl-2, Bcl-x) members of the Bcl-2 protein family. Initially, excessive DNA damage activates p53, leading to the transcription of pro-apoptotic Bax and Bak. These proteins cause mitochondrial membrane permeabilization and subsequent release of cytochrome c from mitochondria into the cytosol. Cytochrome c forms a complex with apoptotic protease activating factor-1 (Apaf-1) called the apoptosome, which activates the caspase cascade, starting from initiator Caspase-9 and progressing to effector Caspase-3 and Caspase-7 [5,184].

Conversely, UV radiation can also initiate apoptosis independently of DNA photoproducts through the extrinsic (death receptor) pathway, involving the activation of membrane death receptors. This pathway is mitochondria-independent and starts with an external signal, such as Fas ligand (FasL) or autocrine and paracrine-released TNF-α, binding to death receptors in the plasma membrane (e.g., Fas receptor/CD95). Downstream signal transduction includes the recruitment of cytosolic FAS-associated death domain protein (FADD) and subsequent activation of the caspase cascade. This cascade starts with initiator Caspase-8 and Caspase-10, which cleave and activate effector Caspase-3 and Caspase-7 [5,184,222].

The capacity of p53 to trigger apoptosis could be considered its foremost role in suppressing tumors [191]. Phosphorylation of p53 at Ser46 is associated with the activation of various genes involved in both death receptor pathways (e.g., Fas) and mitochondrial pathways (e.g., Apaf-1, Bax, Noxa, Puma) [191,197]. Additionally, p53 can directly interact with the mitochondrion or members of the Bcl-2 protein family [191]. In melanocytes, both UVA- and UVB-induced apoptosis are p53-dependent, though the intracellular location of p53 differs [223]. UVA induces oxidative damage, disrupting the intracellular redox balance and causing the translocation of p53 to the mitochondria. In contrast, UVB induces DNA damage, leading to the expression of p53, which then translocates to the nucleus. Both mechanisms ultimately result in the translocation of Bax to the mitochondria, release of cytochrome c, and activation of caspases [200].

In summary, UV radiation can initiate apoptosis via several pathways (Figure 1.9E):

(1) DNA damage, leading to p53 activation and release of cytochrome c from mitochondria (intrinsic pathway) [222]
(2) Induction of death ligands and subsequent activation of death receptors, initiating the caspase cascade (extrinsic pathway) [222]
(3) Direct, ligand-independent activation of death receptors through the induction of receptor clustering [222], accompanied by the translocation of Bax to mitochondria and release of cytochrome c
(4) Overproduction of ROS, resulting in protein and DNA damage, and release of cytochrome c [5]

1.4.5 Transcriptional, Post-Translational, and Epigenetic Regulation

The DDR is regulated by a rapid cascade of post-translational modifications (PTMs), primarily phosphorylation through kinases (e.g., inhibition of Cdc25A), and a delayed transcriptional

response, involving changes in gene expression (e.g., transcription of p21). Additionally, post-transcriptional epigenetic regulation also contributes to this process [187-189,224].

Epigenetic generally refers to potentially heritable alterations in gene expression without modifying the primary DNA sequence. The three major epigenetic mechanisms include DNA methylation (addition of a methyl group at the C5-position of cytosine), histone modifications, and non-coding RNAs [225]. DNA hypermethylation in gene promoter regions is associated with transcriptional repression, whereas hypomethylation promotes gene activation.

In response to UV-induced DNA damage, histone modifications induce chromatin remodeling, resulting in either enhanced gene accessibility (euchromatin) or inactivation (heterochromatin) [185,226] to support chromosomal stability, depending on the type and location of the modification [227]. PTMs of the histone tails encompass acetylation, methylation, phosphorylation, and ubiquitination. Moreover, the specific type of modification dictates the cell's fate, determining whether it undergoes DNA repair [228] or apoptosis [229]. Certain histone modifications serve as binding site for repair and checkpoint proteins or act as signals, for instance, triggering chromatin condensation for apoptosis [184,230].

Non-coding RNAs that are implicated in post-transcriptional gene regulation and RNA silencing include small interfering RNAs (siRNAs) and microRNAs (miRNAs) [231]. miRNAs are small, endogenous, single-stranded RNA molecules with a length of about 18–25 nucleotides [232]. Their primary mode of action involves binding to the 3' untranslated region (3'UTR) of target mRNAs, thereby suppressing the protein translation or causing degradation of the mRNA, depending on the degree of complementarity [231]. Notably, a single miRNA can target hundreds of mRNAs, and conversely, each mRNA can be (cooperatively) regulated by multiple miRNAs [233,234]. miRNAs play integral roles in various physiological and pathological processes like embryonic development, cell differentiation, proliferation, carcinogenesis, tumor progression, and metastasis [232]. In the context of tumor development, miRNAs exhibit dual functionality as both tumor suppressors and oncogenes [235,236]. Recent research shows that miRNAs are involved in the initiation, maintenance, and termination of DDR signaling, introducing an additional layer of regulation and complexity to the intricately controlled cellular responses to UV radiation [187,189,237]. The regulation of UV-DDR by miRNAs is suggested to occur at an intermediate stage, positioned between rapid protein modifications within minutes and the much slower transcriptional reprogramming that requires several hours to days [188,189].

UV radiation causes dose-dependent transcriptional alterations in both skin and cultured skin cells. These changes vary significantly based on whether transient cell cycle arrest or apoptosis is triggered. Generally, UV irradiation results in global repression of transcriptional activity, characterized by a predominantly reduced gene expression [238,239], and leads to a short-term miRNA-mediated gene silencing by upregulation of UV-responsive miRNAs [188]. On the contrary, multiple genes associated with stress response, cell cycle regulation, DNA repair, apoptosis [238], immunity, inflammation, and pigmentation are upregulated [151,186]. The transcriptional targets [191] and miRNA expression changes [189] are quite similar in keratinocytes, melanocytes, and fibroblasts.

In the regulation of miRNAs during DDR, p53 plays a pivotal role as well. Certain miRNAs participating in survival and cell death processes are activated or repressed by p53 in response to DNA damage. The miR-34 family, including miR-34a, -34b, and -34c, is induced in a p53-dependent manner. These miRNAs promote cell cycle arrest at G1/S, apoptosis, and senescence by downregulating targets, such as cyclin E2, CDK4/6, E2F3, c-Myc, and Bcl-2 [187,202,240]. Notably, miR-34a stands out as the most significantly activated miRNA by p53 [202]. Other p53-induced miRNAs with anti-proliferative activity include mir-16 [188], miR-192, miR-215 [241], miR-15a, let-7 [202], miR-23a, miR-29, miR-194, and miR-605 [242], targeting for example Bcl-2 and RAS [202,242]. miR-16 suppresses Cdc25A, cyclin D1, and cyclin E, inducing cell cycle arrest [188], and influences the cell fate decision between apoptosis and senescence [243]. Conversely, p53 represses certain miRNAs like miR-221/222, which downregulate the CDK inhibitor p27 [202], and miR-17-92 cluster [242].

The regulation of miRNAs by p53 not only occurs on the transcriptional level, but also encompasses modulation of miRNA processing and maturation steps [237]. For example, the interaction of p53 with the Drosha processing complex leads to upregulation of growth-suppressive miR-16, miR-143, and miR-145 [236]. miR-145 represses c-Myc and CDK6, inhibiting cell proliferation and inducing apoptosis [244]. In addition, p53 may influence the processing of let-7, miR-200c, miR-107, miR-134, miR-449a, miR-503, and miR-21 [245].

On the one hand, miRNAs act downstream in the DDR, but conversely, they also actively participate in the regulation of core proteins, such as p53, p21, and Cdc25A [237]. For instance, p53 itself undergoes negative regulation by miR-125b and miR-504 [237]. The repression mediated by miR-125b contributes to maintaining a low baseline expression level of p53 [246]. Overexpression of these two miRNAs results in reduced p53 protein levels and enhances the tumorigenicity of cells *in vivo*. p21 is repressed by members of the miR-106b family, whose

overexpression potentially supports tumor cell proliferation by promoting cell cycle progression [247]. In the DDR of hESCs, miRNAs from the miR-302 family (miR-302a, -302b, -302c, and -302d) negatively regulate the p21 expression, contributing to a non-functional G1/S checkpoint after DNA damage [248]. Elevated expression of the miR-290 cluster may also contribute to the lack of G1/S checkpoint [249]. Furthermore, there is evidence indicating that Cdc25A can be inhibited by miR-21 [250], suggesting that miR-21 may be involved in cell cycle arrest in addition to the ATR-Chk1 signaling. However, the mechanism underlying the induction of miR-21 in response to DNA damage remains unknown [187]. Cdc25A is also targeted by miR-16 and miR-449a/b [188,237].

The majority of DNA repair proteins or genes undergo regulation through PTMs, such as ubiquitination, phosphorylation, methylation, and acetylation. Additionally, they are subject to post-transcriptional regulation by miRNAs [233]. For instance, miR-192 can suppress NER by inhibiting helicase XPB and endonuclease XPF [251]. Hypoxia-inducible miR-373 has the capacity to repress RAD23B, a key factor in the recognition of DNA lesions along with XPC [252]. Several members of the BER and TLS pathways are also regulated by miRNAs (miR-34c, miR-199a, miR-499 in BER; miR-145, miR-630, miR-96 in TLS) [233].

1.5 Skin Cancer

The term skin cancer refers to malignant neoplasms of the skin. Skin cancers are the most common group of cancers worldwide, showing an increasing incidence, particularly in older people [57,253]. Skin cancer is classified into malignant melanoma (MM), arising from cells of the melanocyte lineage, and non-melanoma skin cancer (NMSC). The latter category mainly includes basal cell carcinoma (BCC) and squamous cell carcinoma (SCC), both originating from epidermal keratinocytes [127,130,151]. Less common types of NMSCs are Merkel cell carcinoma, primary cutaneous B-cell lymphoma, Kaposi sarcoma, and dermatofibrosarcoma protuberans. In Germany, around 308,800 new skin cancer diagnoses are estimated for 2023, comprising 14% MMs, 52% BCCs, and 34% SCCs. After an increase in the total number of new skin cancer cases until 2015, the number has since stabilized at approximately 300,000 new cases per year [254].

The main etiological factor for the formation of cutaneous carcinomas is exposure to UV radiation from solar radiation or artificial sources such as tanning beds [138,144,255]. Further risk factors include carcinogenic substances, ionizing radiation, as well as age and immunosuppression but only in combination with UV radiation [130,151,256,257]. An

estimated 75% of MMs and 90% of NMSCs worldwide are causally related to UV exposure [127,130]. In certain countries, even more than 90% of MMs are attributable to UV radiation, including for example New Zealand, Australia, Norway, Denmark, and also Germany [258,259]. The risk of developing UV-induced skin cancer is also dependent on the skin color/pigmentation. Lighter pigmentation like in skin type I and II is associated with higher sensitivity to UV damage and thereby a higher skin cancer risk due to a decreased photoprotection from lower melanin levels [19,136,151,253,256]. Hence, darker-skinned populations have markedly lower melanoma incidence rates [253].

Photocarcinogenesis is a complex, multi-stage process [255]. The primary mechanisms include: (a) formation and accumulation of DNA photoproducts within cancer-related genes, resulting in DNA mutations that disrupt signal transduction pathways, influencing cell growth and cell cycle regulation, (b) promotion of cutaneous inflammation through UV-induced oxidative stress and DNA damage [57,151], and (c) suppression of anti-tumor immune responses through upregulation of immunosuppressive cytokines like interleukin 10 (IL-10), creating an environment conducive to cancer cell growth and progression [150,260,261].

The significant role that UV radiation plays in skin carcinogenesis is reflected in the occurrence of UV signature mutations in cutaneous tumors. The spectrum of hotspot (driver) mutations resulting from C→T transitions found in multiple genes in cutaneous melanoma (e.g., in *STK19*, the oncogene *RAC1*, and the tumor suppressor *PPP6C*) provides genomic evidence for a direct mutagenic role of UV radiation in MM pathogenesis [173,262]. Pleasance et al. demonstrated that up to 70% of the single nucleotide and dinucleotide substitutions in a melanoma metastasis were C→T and CC→TT signature mutations [263]. These UV-specific mutations are found in BCCs and SCCs as well, affecting genes like the tumor suppressor genes *patched*, *p16*, and *p53*, as well as the protooncogene *RAS*. UV-induced carcinogenesis often involves inactivation of one or more tumor suppressor genes or activation of growth-stimulating protooncogenes [156]. The tumor suppressor p53 is a crucial factor in cell cycle regulation, DNA repair, and apoptosis, and represents the most frequently mutated gene in skin tumors. UV signature mutations in *p53* are found in more than 50% of BCCs, often involving C→T transitions [264]. In SCCs, this applies to up to 90% of tumors, with mutations occurring predominantly in so-called hotspot regions of the *p53* gene, where repair rates of pre-mutagenic lesions like CPDs are reduced (‘repair coldspots’) [130,133]. Loss of p53 in the regulation of cell cycle and apoptosis promotes uncontrolled proliferation and transformation in the process of carcinogenesis. Besides dysregulation of signal transduction pathways and cell cycle, mutations can lead to a depletion of antioxidant defenses as well [255].

In addition to UV-induced genetic changes/mutations (in tumor suppressor genes and protooncogenes), epigenetic dysregulation also plays an important role in improper activation or silencing of genes in skin carcinogenesis [265]. Detailed information about epigenetic changes in the genesis of malignant melanoma can be found in section 1.5.2.2.

1.5.1 Non-Melanoma Skin Cancer

Frequently, diagnoses of NMSCs are not routinely recorded in cancer registries and occurrence of more than one lesion is not considered, leading to an under-estimated incidence [144]. Nevertheless, they are the most common malignant tumors in the European population and in fair-skinned people throughout the world. Their incidence increases with age [57,136] and is considerably higher among men than among women [266]. Worldwide, an estimated 1,198,073 people were diagnosed with NMSC in 2020 (data of first occurrence, excluding BCC) [267,268]. However, the World Health Organization (WHO) estimates 2–3 million cases per year [269], while the Global Burden of Disease Study even assumed 6.4 million NMSC cases worldwide in 2019 [270]. Australia (ASR=140.0 (per 100,000/year)) and New Zealand (ASR=127.5) had the highest incidence, followed by the United States (ASR=64.9) and Canada (ASR=60.6). Germany was ranked 8th with an ASR of 31.3. NMSCs caused 63,731 global deaths in 2020, with the highest mortality in Papua New Guinea (ASR=5.1), followed by Namibia (ASR=3.8) [267,268].

Basal cell carcinoma (BCC) is the most prevalent type of skin cancer and accounts for approximately 80% of NMSCs. These tumors mainly occur in the head and neck region, but also in less sun-exposed areas. Risk factors include high intermittent UV exposure in both childhood and adulthood, high cumulative lifetime dose, fair skin, and genetic predisposition. BCCs rarely metastasize, leading to a low mortality of <1% [128,130,151,256,264].

Squamous cell carcinoma (SCC) ranks as the second most common type of skin cancer, constituting 19% of NMSC. Usually, it originates from *in situ* carcinoma and is primarily found in high sun-exposed areas. High cumulative exposure to UV radiation is the primary risk factor, with other contributing factors including chronic exposure to ionizing radiation, heat, arsenic, as well as human papillomavirus. Compared to BCC, SCCs have a higher risk of metastasis and related mortality, but early diagnosis at small tumor sizes reduces the probability of metastasis and the mortality rate [130,151,256,264].

1.5.2 Malignant Melanoma

For the sake of completeness, it must be mentioned that the term ‘melanoma’ encompasses various melanocytic tumors, not only cutaneous melanoma of the skin but also extracutaneous melanomas, such as uveal melanoma of the eye and mucosal melanoma found, for example, on mucosal surfaces of the gastrointestinal and genital tracts [271]. However, these extracutaneous melanomas are much less common and not relevant to this work. When using the term malignant melanoma here, it always refers to cutaneous melanoma.

The incidence of malignant melanoma (MM) has been steadily increasing worldwide in the last 50 years, especially in the fair-skinned populations and among older age groups >50 years [136,253]. In some countries, however, incidence rates have stabilized or decreased in recent generations [151,253,272]. According to the Global Burden of Diseases Study 2015, the five world regions with the greatest MM incidence and mortality rates are Australasia (Australia, New Zealand), North America, Eastern Europe, Western Europe, and Central Europe [273]. An estimated 324,635 people worldwide were diagnosed with melanoma in 2020 (1.7% of all new cancer cases), including large geographic variations. The highest incidence rates were observed in Australia (ASR=36.6) and New Zealand (ASR=31.6), followed by Denmark (ASR=29.7) and the Netherlands (ASR=27.0). On the other hand, MM is rare in most African and Asian countries (ASR<1). Germany had the eighth-highest incidence (ASR=20.5) [151,253,267,268] and in 2023, an estimated 42,300 new melanoma cases with virtually equal distribution among men and women are predicted for Germany [254]. In most world regions, however, MM is more frequent among males [253,266]. Moreover, melanoma is nearly 30 times more common in White people than in Black people [274].

The MM is the most aggressive type of skin cancer, tends to metastasize early, and is associated with a high mortality rate [258,275]. Despite accounting for only about 10–20% of skin cancer cases, MM is responsible for the vast majority of skin cancer deaths [253,274] owing to the high potential of metastasis and therapy resistance [141]. Survival rates are usually lower in men [266,273] and for Black people [272]. The survival rate depends on various factors, including gender, tumor location, tumor thickness, and stage at diagnosis [258]. In the United States, the 5-year relative survival rate for individuals with localized melanoma (confined to the primary tumor without spreading) ranges from 80–99%, depending on the tumor thickness. For regional melanoma that has extended to nearby lymph nodes, the 5-year survival rate is 71%. If the MM has metastasized to distant parts of the body, the survival rate drops to approximately 32% [274]. In 2020, melanoma was responsible for 57,043 global deaths (0.6%

of all cancer deaths), with the highest mortality in New Zealand (ASR=4.7), followed by Norway (ASR=3.2). The lowest mortality rates are found in most African and Asian countries (ASR<1) [151,253,266-268]. Similar to the incidence, mortality has also plateaued or even decreased, partly due to the introduction of systemic therapies for advanced disease, including immune checkpoint inhibitors (anti-CTLA-4 and anti-PD-1 antibodies) and targeted therapies (BRAF and MEK inhibitors) for metastatic MM [151,253,272]. When extrapolating the melanoma burden based on the 2020 rates, global incidence is estimated to increase to 510,000 new cases (50% increase) and global mortality will increase to 96,000 deaths (68% increase) by 2040 [253].

The most relevant etiological factor for MM is high intermittent UV exposure with repeated childhood sunburns. Other key risk factors include a fair skin type, the presence of numerous or atypical melanocytic nevi (moles), and genetic predisposition [130,264,276,277]. While the average age at diagnosis is 65 [278], melanoma also frequently affects younger individuals, including those under 30 years old [276]. In younger ages, MM often occurs on less UV-exposed skin areas, such as trunk and limbs. Melanomas at these sites are strongly associated with nevi. In contrast, at older ages, MM arises on more UV-exposed sites like head and neck [128,253].

Cutaneous melanoma is classified into four histological subtypes that differ in growth patterns, anatomical site of origin, and molecular profile. The most common subtype is superficial spreading melanoma (50% of all MMs), frequent in fair-skinned individuals on trunk and legs. Other subtypes, with decreasing incidence, include nodular melanoma (16%), lentigo maligna melanoma (10%), and acral lentiginous melanoma (4%) [45,57]. Nodular melanoma is the most aggressive subtype, appearing as a firm lump on the skin surface, typically in fair-skinned people aged over 65. Lentigo maligna melanoma affects older patients with sun-damaged skin, primarily observed on face, ears, and neck. Acral lentiginous melanoma commonly affects individuals with darker skin and manifests as a dark spot on the soles or palms [279].

1.5.2.1 Melanomagenesis

The development of MM involves a complex interplay of genetic changes (mutations) and epigenetic alterations (miRNAs, non-coding RNAs, histone modifications, DNA methylation), which can be induced by UV radiation. The primary contributors to melanoma are UV exposure and genetic predisposition, whereby the association between sun exposure and MM appears to vary based on the location of the tumor. According to a dual pathway hypothesis [280], MM

can develop independent of nevi or from inside a benign nevus. Melanomas on less frequently exposed areas (trunk and limbs) are strongly linked to pre-existing benign nevi [151]. Approximately 25% of MMs are thought to originate from nevi [18], whereas in contrast, the majority of melanoma cases seem to arise without a connection to nevus. These melanomas, predominantly found in sun-exposed areas (head and neck), are associated with cumulative sun exposure [151] and have a higher mutational burden than those arising from nevi. Worldwide, an estimated 75% of MMs is attributed to UV radiation [130].

The precise cellular and molecular mechanisms underlying melanomagenesis are far from being understood in detail. However, it is generally accepted that, besides chromosomal aberrations (translocations, amplifications, deletions) [281] and UV-induced DNA lesions serving as mutagenesis precursors [282], dysregulation of signaling pathways plays a crucial role in MM development. This primarily involves the MAPK pathway, PI3K/PTEN/AKT pathway, cell cycle regulation pathways, MITF signaling pathways (related to pigmentation), and p53 pathways [279]. The activation of MAPK signaling, e.g., through activating *NRAS* and *BRAF* mutations, is a pivotal step in melanoma pathogenesis, leading to uncontrolled proliferation and survival. This is accompanied by the suppression of senescence through multiple mechanisms. These include the progression of cell cycle (via inactivation of *CDKN2A/p16*, *TERT*), activation of PI3K/AKT signaling (via loss of *PTEN* or *NF1*, activating *NRAS* mutation), and activation of Wnt/β-catenin signaling (via stabilization of β-catenin) [18,283,284]. Many of these pathways result in the amplification of MITF, which therefore plays a central role in melanoma biology and, for instance, causes the dysregulation of anti-apoptotic proteins [262]. The skin microenvironment, especially keratinocytes, contributes to the dysregulation of signaling pathways by suppressing senescence-related genes, while promoting the proliferation of transformed melanocytes [285].

When considering the mutational background driving melanomagenesis, it is essential to differentiate between familial (hereditary) and sporadic (non-familial) forms of melanoma. The majority of MM cases are sporadic, meaning that genetic changes (somatic mutations) are acquired throughout life and are not inherited, with UV radiation being the primary contributor. Owing to UV signature mutations, MM has the highest mutational burden among all cancers (>10 mutations/megabase) [258]. Hayward and colleagues' analysis of 140 cutaneous MM samples found a mean tumor mutational burden of around 50 mutations/megabase [286]. Numerous whole-genome sequencing studies have identified a variety of so-called 'early driver mutations' [262,263,286] occurring in key genes at critical points in the evolution of melanoma,

providing the mutated cell with a survival advantage. These genes control cell proliferation (*BRAF*, *NRAS*, *NF1*), cell cycle and replication (*CDKN2A*, *p53*, *TERT*), and metabolic pathways (*PTEN*, *KIT*) [45,286]. Additional driver mutations may include *RAC1*, *PPP6C*, *STK19*, *MAP2K1*, *SNX31*, *TACC1*, *IDH1*, *ARID2*, and *RB* [45,262].

The most common gene defects in cutaneous melanoma are activating mutations of the (proto)oncogenes *BRAF* (*BRAF*^{V600}, 50–60% of MMs), *NRAS* (*NRAS*^{Q61}, 20–25%), and *KIT* (<15%) [45,262]. The Kit receptor signaling pathway, inclusive of the MAPK signaling cascade with NRAS and BRAF, plays a key role in melanocytes, activating MITF and inducing cell growth and survival (see section 1.1.1.2) [35]. In melanoma, mutations in components of this pathway lead to its constitutive activation and contribute to oncogenesis. Additionally, 10–15% of MMs exhibit mutations in several tumor suppressor genes, including *p53*, *NF1*, *CDKN2A*, and *PTEN* [45]. Molecular classification of melanoma involves the subtypes *BRAF*-mutant, *RAS*-mutant, *NF1*-mutant, and the so-called 'triple wild-type' form (also called triple-negative or pan-negative; 10% of MMs), which lacks driver mutations in all three aforementioned genes [279]. The mutational profile can predict the response to and the efficacy of certain therapies. Therefore, molecular characterization is often conducted prior to therapy decision-making. *BRAF*^{V600} mutations predict responsiveness to BRAF inhibitors, *KIT* mutations to tyrosine kinase inhibitors, and *NRAS* mutations to MEK inhibitors [262].

In contrast to sporadic MM with somatic mutations, about 10% of cutaneous melanomas have a significant family history, with multiple close relatives also diagnosed with MM [253,258]. Genetic predisposition for familial (hereditary) melanoma is evident through an inheritance pattern of genetic changes (germline mutations) in a specific set of genes. These melanoma susceptibility genes are related to cell cycle control (*CDKN2A*, *CDK4*), DNA damage repair (*BAP1*, *PARP1*, *ATM*, *APEX1*, *RAD51B*, *POLE*), melanin synthesis (*MITF*, *MC1R*, *TYR*, *TRP1*, *ASIP*, *SLC45A2*, *OCA2*, *KIT*), and telomere length control (*TERT*, *POT1*, *ACD*, *TERF2IP*) [18,45,52,287]. Individuals with these germline mutations face an increased risk of developing primary melanomas and other malignancies, including pancreatic, lung, and breast cancer, as well as NMSC. Onset at an earlier age is a notable characteristic of familial melanoma [288].

The most significant and well-characterized genes involved in familial MM are *CDKN2A* and *MC1R*, with around 20–40% and 70–90% of familial MMs having mutations in these genes, respectively [288]. *CDKN2A* encodes the two tumor suppressors p16 and p14, which both function in cell cycle regulation. p16 inhibits CDK4 and CDK6 kinases, preventing Rb phosphorylation, thereby causing cell cycle arrest at the G1/S checkpoint and promotion of senescence. p14 inhibits MDM2-induced p53 ubiquitination and degradation, stabilizing p53

[289]. Inactivating mutations therefore result in uncontrolled cell cycle progression and bypass of senescence [18]. Melanoma primarily exhibits loss of p16, while p14 is often unaffected by the mutations [289]. The MC1 receptor is involved in eumelanin production and can also trigger nucleotide excision repair in melanocytes. Hence, loss-of-function mutations in *MC1R* increase susceptibility to UV radiation due to reduced photoprotection, less antioxidant defense, and impaired CPD repair. Accordingly, MM patients with *MC1R* variants have increased UV signature mutational burdens [290].

1.5.2.2 Epigenetic Dysregulation in Melanoma

Alterations to the epigenome are common in MM and are as crucial in development as distinct genetic events. These changes play a role not only in cancer initiation but also in progression and resistance to therapy [279,291]. Certain epigenetic marks can serve as important biomarkers for diagnosis and prediction of outcomes, and as targets for therapeutic interventions [279,292]. The epigenetic modifications encompass aberrant DNA methylation, histone modifications, and altered miRNA expression [293].

Changes in the DNA methylation pattern are a well-recognized hallmark of cancer, including both genome-wide (global) hypomethylation and site-specific hypermethylation of CpG islands in promoters. These patterns are also evident in melanoma [294]. Promoter hypermethylation is linked to transcriptional repression, while hypomethylation facilitates gene activation. Numerous studies provide evidence of dozens to hundreds of genes with epigenetic silencing due to promoter hypermethylation during MM development and progression, e.g., *Apaf-1*, *Caspase-8*, *E-cadherin*, *P-cadherin*, *endothelin-2*, *PCNA*, *PTEN*, *CDKN2A/p16/p14*, *RASSF1A* [295], *p27*, and *cyclin D2* [296]. For instance, inactivation of the cell death effector Apaf-1 results in defective apoptotic mechanisms and chemoresistance in melanomas [297]. Apaf-1 typically collaborates with cytochrome c and Caspase-9 to mediate apoptosis [296]. The tumor suppressors *PTEN*, *CDKN2A* (p16, p14), and *RASSF1A* are among the most frequently reported and best characterized hypermethylated genes in MM [293,298]. Silencing of *PTEN* increases AKT activity, since PTEN usually inhibits the PI3K/AKT pathway [299], and also serves as a predictor for poor survival [300]. Promoter hypermethylation of *CDKN2A*, encoding p16 and p14, is associated with increased tumor proliferation and reduced survival [301]. Hence, in melanoma, *CDKN2A* is silenced not only by chromosomal deletions and inactivating mutations but also by promoter hypermethylation [295,298]. RASSF1A, involved in cell cycle regulation and apoptosis through interactions with cyclins and RAS [302], exhibits increasing methylation levels with disease stage. Therefore, it might be a potential progression and prognosis

biomarker [303]. The dysregulated methylation of promoters in MM seems to be connected to an overexpression of the DNA methyltransferase DNMT1 [295].

Besides altered promoter methylation, melanoma also displays global hypomethylation within its genome [298], for example, in the repetitive *LINE-1* sequence [304]. Additionally, the loss of global 5-hydroxymethylcytosine (5-hmC) is an epigenetic hallmark of MM. High levels of 5-hmC are present in melanocytes and nevi, but decrease in primary and metastatic melanoma. The loss of 5-hmC is linked to poor prognosis, suggesting its potential as a diagnostic and prognostic biomarker [294].

Additional factors influencing gene expression encompass histone modifications and chromatin remodeling, which impact how DNA is packaged. Overexpression of the chromatin remodeling factor MTA1 may be implicated in melanoma development [295]. Histones can be modified by acetylation, methylation, phosphorylation, and ubiquitination. Generally, acetylation is linked to transcriptionally active chromatin, whereas deacetylation promotes chromatin condensation and repression of gene transcription. Upregulation of histone deacetylases HDAC1, 2, and 3 [305], as well as Sirtuin 1 (SIRT1) [306] plays a role in MM development, likely by promoting proliferation and DNA repair, while preventing apoptosis [295]. De-/hypoacetylation of histones leads to silencing of tumor suppressors such as p21 [307], PIB5PA (suppressor of PI3K/AKT signaling) [308], and pro-apoptotic factors Bim, Bax, and Bak in melanoma cells [293,309].

Histone methylation can result in either activation or repression, depending on the specific residue that is methylated. Trimethylation of lysine 27 (H3K27me3) and lysine 9 on histone H3 (H3K9me3) are associated with heterochromatin and gene silencing [295]. Overexpression of the histone methyltransferase EZH2, governing repressive H3K27me3, leads to transcriptional repression of tumor suppressors like p21. Protein levels of EZH2 increase from benign nevi to melanoma, with elevated levels being associated with MM progression and more aggressive tumor subtypes [310,311]. The histone methyltransferase SETDB1, mediating repressive H3K9me3, is also upregulated in MM but not in benign nevi or normal melanocytes. Its specific targets are unknown. Genomic amplification of SETDB1 has been shown to promote melanomagenesis in a zebrafish melanoma model [312].

miRNAs target various cellular processes and pathways involved in MM development and progression, acting as either oncogenic miRNAs (onco-miRNAs) or tumor-suppressive miRNAs [234,235,313] (see Appendix Table 8.1). Dysregulation of miRNA expression correlates with various hallmarks of MM pathogenesis, including promotion of proliferative

signaling, resistance to cell death, replicative immortality, migration/invasion or metastasis, and immune evasion [293,314]. Moreover, differential miRNA expression is linked to several clinicopathological variables, such as treatment resistance, cancer reoccurrence, and response to therapeutic agents [234]. Multiple miRNAs play a role in melanomagenesis by modulating the expression of genes involved in MAPK signaling, PI3K/AKT signaling, and cyclin/CDK-dependent cell cycle regulation [291,315]. The MAPK pathway is targeted, for example, by let-7 miRNAs, which are downregulated in MM, leading to MAPK activation and increased proliferation. Conversely, the activated MAPK pathway negatively regulates certain growth-inhibitory miRNAs, such as let-7i, miR-34a, miR-211, and miR-22, while upregulating growth-promoting miRNAs like miR-17, miR-92, and miR-221/222 [316].

Several notable **onco-miRNAs** upregulated in MM include miR-21 [317-319], miR-155 [234], miR-221/222 [320], and miR-182 [321,322]. **miR-21** increases proliferation, oxidative stress, angiogenesis, invasion, metastasis, genetic instability, and diminishes apoptosis by affecting crucial genes involved in these processes (e.g., suppression of PTEN, Apaf-1, TIMP3, FOXO1, p53; induction of PI3K, AKT, cyclin D1, Bcl-2, hTERT, VEGF, HIF1α) [317,318]. High miR-21 expression correlates with an advanced clinical stage and predicts poorer survival [323]. UV radiation has been shown to stimulate miR-21 expression in the skin [318]. Cellular responses to **miR-155** overexpression include immune evasion, tumor growth, and angiogenesis, for example through inhibition of TRP1 and MITF, whereas VEGF, MMP2, MMP9, and IL-1β are upregulated [234]. Levels of miR-155 are increased in MM cases with sentinel lymph node involvement [324]. The **miR-221/222** cluster suppresses the CDK inhibitor p27 (enhancing proliferation) and the c-Kit receptor (blocking differentiation) [320,325]. Serum miR-221 levels correlate with disease stage and tumor thickness, and rise again during recurrence. Therefore, miR-221 serves as potential MM biomarker for diagnosis, progression, and monitoring during follow-up [326]. Amplification of **miR-182** promotes tumor growth, invasion, and metastasis, while inhibiting apoptosis by directly repressing MITF and FOXO3, as well as its downstream target, the pro-apoptotic Bim [321,322].

The majority of dysregulated miRNAs in melanoma exhibit downregulation (see Appendix Table 8.1). Some of these **tumor suppressor miRNAs** include miR-205 [327-329], miR-125b [330,331], miR-211 [329,332,333], the let-7 family [334,335], miR-34a [315,336], miR-16 [337], miR-137 [338,339], miR-31 [340], miR-203 [329,341], and the miR-200 family [329,342]. Downstream targets of **miR-205** comprise E2F1 and E2F5, implicated in cell cycle progression and AKT pathway [327], as well as ZEB2, whose upregulation leads to E-cadherin

downregulation. Consequently, miR-205-mediated tumorigenesis may involve the promotion of epithelial-mesenchymal transition (EMT) and metastasis [328], in addition to increased proliferation. Expression of **miR-125b** is already diminished in atypical nevi [343]. Evidence indicates that miR-125b facilitates tumor progression by influencing proliferation, migration, cellular senescence, and apoptosis [317]. Cells with reduced levels show less spontaneous apoptosis [344]. **miR-211** stands out as one of the most differentially expressed miRNAs in MM. Downregulation decreases cellular adhesion and promotes invasive potential, partially through indirect inhibition of MITF [317,332]. Members of the **let-7 family** (let-7a, -7b, -7d, -7e, and -7g) contribute to MM development and progression as regulators of cell cycle and proliferation [314]. They target various cancer-promoting factors, such as NRAS, RAF, c-Myc, Rb, cyclin D, and CDK4 [335]. Let-7a also negatively regulates the adhesion molecule Integrin β3, implying increased invasive potential upon let-7a loss [334]. Downregulation of **miR-34a** and upregulation of its target, the transcription factor and E-cadherin inhibitor ZEB1, amplifies proliferation and migration [336]. In addition, miR-34a is a key mediator of p53, usually inducing cell cycle arrest, apoptosis, and senescence through inhibition of cyclin E2, CDK4/6, E2F3, c-Myc, and Bcl-2 [187,202,240]. **miR-16** exerts growth-suppressive functions, targeting Cdc25A, cyclin D1, and cyclin E [188], resulting in enhanced proliferation upon downregulation in MM. Expression of miR-16 positively correlates with longer survival, indicating diagnostic and prognostic potential [337]. Downregulation of the well-established tumor suppressor **miR-137** prevents apoptosis and promotes cell cycle progression. miR-137 usually targets MITF, which regulates anti-apoptotic Bcl-2, as well as EZH2, which induces the repression of p21 [339]. Low miR-137 levels indicate a poor prognosis for MM patients [338]. **miR-31** also serves as negative regulator of EZH2 and of oncogenic kinases [340]. Downregulation of **miR-203**, targeting E2F3 and BMI1, prevents cell cycle arrest and senescence [345], while enhancing the invasive potential [341]. Low miR-203 expression is associated with short overall survival, tumor thickness, and tumor stage [346]. Reduced expression of miR-200c from the **miR-200 family** (miR-200a, -200b, -200c) leads to BMI1-mediated E-cadherin downregulation, promotion of cell proliferation, and migration [342]. Loss of miR-200a is linked to decreased E-cadherin expression as well [347].

In the clinical context, miRNAs hold the potential for use in MM diagnosis, prognosis, or prediction of treatment responses, complementing established tissue markers (e.g., tumor stage, tumor thickness) and circulating molecular biomarkers (e.g., LDH, S100B, circulating tumor DNA) [234,292,348]. The remarkable stability of miRNAs in body fluids [349] and formalin-fixed paraffin-embedded (FFPE) tissues [350] presents a significant advantage in this regard.

For instance, miR-17-5p-mediated upregulation of PD-L1 in MM is associated with increased disease aggressiveness. Therefore, miR-17-5p may function as a marker for PD-L1 expression and predict the response to BRAF or MEK inhibitors [351]. The expression of a 4-miRNA set, in combination with disease stage, predicts the likelihood of developing brain metastases [352]. A 17-miRNAs panel (MELmiR-17) is capable of predicting stage, recurrence, and survival. Another seven-miRNA panel (MELmiR-7) signifies the presence of melanoma and more accurately characterizes the survival of MM patients than serum LDH and S100B [353].

1.5.2.3 Cell of Origin

The specific cell in which changes involved in carcinogenesis initially occur remained uncertain for a long time. Vital insights into the cellular origins of numerous solid tumors have been provided by genetic lineage-tracing experiments [354]. Furthermore, it was revealed that microenvironmental cues have a decisive impact on the tumor predisposition of cells. Cutaneous melanoma is a neuroectodermal tumor arising from cells of the neural crest-derived melanocyte lineage. However, there is still discussion on whether the gradual transformation to MM initiates from mature melanocytes or stem cell precursors [7,32,281,355-362]. Essentially, the stochastic model faces the cancer stem cell model of carcinogenesis.

The stochastic model implies that cancer development takes place through a series of genetic and epigenetic changes in somatic cells, followed by the clonal expansion of cells harboring advantageous mutations [57]. Consequently, according to this **'classical' hypothesis**, melanoma originates from a mature, fully differentiated epidermal melanocyte in a gradual transformation, during which it accumulates mutations in oncogenes and tumor suppressor genes over time, primarily due to UV exposure, providing survival and growth advantages [355,357] (Figure 1.10).

On the other hand, the cancer stem cell (CSC, also known as tumor-initiating cell) model proposes that cancer originates from the transformation of tissue-specific stem or progenitor cells that maintain stem cell-like properties in the tumor, such as the ability to self-renew [57,363,364]. For instance, there is compelling evidence indicating that stem cells might be the founder population in blood [365], brain [366], colon [367], prostate [368], pancreatic [369], and breast cancers [370]. Moreover, stem cells might also be involved in development of BCC [371] and SCC [372,373].

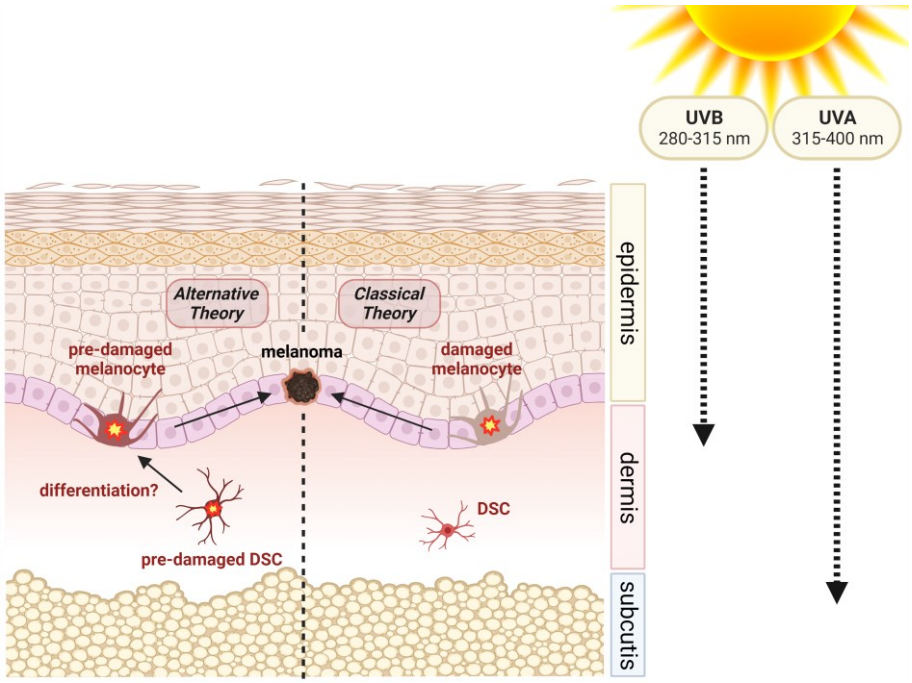

Figure 1.10 Melanoma theories. The classical theory states that malignant melanoma originates from a mature, fully differentiated melanocyte located in the basal layer of the epidermis, accumulating damage from UV exposure. According to the alternative theory proposed by Hoerter [357,358], the cell of origin is an extrafollicular melanocyte precursor in the dermis, a dermal stem cell (DSC), which is damaged in an early stage by UV radiation penetrating deeply into the skin. The pre-damaged DSC accumulates further damage during migration to the epidermis and differentiation into a melanocyte, subsequently leading to melanomagenesis (created with BioRender.com).

The detection of phenotypic heterogeneity, morphologic plasticity, embryonic-like differentiation potential, self-renewal capacity, high tumorigenicity, and cells with stem cell markers (CD20, CD133, CD34) in MM tumors and cell lines [355,356,374-376] also suggest the presence of CSCs and thus the involvement of mutated McSCs or progenitor cells in MM initiation, progression, and drug resistance [281,362]. In lentigo maligna melanoma, stem cells expressing the CSC markers CD113 and CD34 were identified in the outer root sheath of hair follicles, partly mixed with MM cells [355]. Certain characteristics of melanomas support the idea of a mutated stem cell as origin. Nevi and MMs may stem from the same source—a genetically defective stem cell—with the extent of the defective growth regulation determining whether the outcome is a benign or malignant neoplasia. Moreover, this model could offer a more straightforward explanation for delayed onset and tumor dormancy [356]. The CSC model contradicts the concept of dedifferentiation: stem-like features might also emerge during the transformation of melanocytes through a gradual dedifferentiation process involving genetic and/or epigenetic modifications that trigger a plastic, pluripotent phenotype [355,356]. This was demonstrated *in vivo* with lineage-tracing in a mouse model, where melanoma originated through the transcriptional reprogramming and dedifferentiation of mature epidermal melanocytes [359]. The generation and maintenance of CSCs are also significantly influenced

by the microenvironment, e.g., via growth factors secreted by endothelial cells and fibroblasts [281,364,377].

The **alternative theory** of MM initiation proposed by Hoerter et al. aligns with the CSC model and specifically suggests a damaged extrafollicular dermal McSC, such as a DSC, or a melanocyte precursor derived from it, as the earliest origin of melanoma [357,358] (Figure 1.10). Li and colleagues have proven the existence of multipotent neural crest-derived DSCs in the dermis of human non-hairy skin, serving as a dermal reservoir for epidermal melanocytes [31,32]. Given that adult stem cell populations are frequently more radiosensitive and more prone to tumor initiation than TACs and mature, differentiated cells [364,378], it is assumed that a melanocyte precursor is more susceptible to UV-induced damage than a fully differentiated melanocyte.

According to Hoerter's model, McSCs in their dermal niche are frequently exposed to solar (or artificial) UV radiation, especially to UVA in deeper layers, inducing photolesions (Figure 1.10). Damage to repair, apoptosis, and defense pathways will result in the progressive accumulation of DNA damage as well as genetic and epigenetic changes in dermal McSCs over the lifetime, with a higher likelihood in quiescent, non-proliferating McSCs [357], since DNA damage checkpoints and the majority of DNA repair mechanisms are cell cycle-dependent [182]. Similar to what is found in squamous cell carcinoma [379], UVA radiation, ROS-induced damage to (repair) proteins and DNA, and UVA fingerprint mutations could thus play a significant role as important carcinogens in the dermal stem cell compartment, especially in the early stages of MM initiation [32,357]. When a senescent, non-functional, or excessively damaged, apoptotic epidermal melanocyte needs replacement, a pre-damaged extrafollicular McSC will migrate to the epidermis to reestablish skin homeostasis [7]. The exact signaling mechanisms for this migration remain poorly understood and could originate from surrounding keratinocytes and fibroblasts [12] or from the dying cell itself [380]. The migration mechanism to the epidermis and differentiation into melanocytes has been demonstrated for DSCs in a 3D skin reconstruct model [31,102]. Secretion of Wnt ligands by keratinocytes, e.g., following UV irradiation, was identified as a stimulating factor [42]. The sequence of events remains uncertain regarding whether dermal McSCs initially undergo differentiation into melanocytes in the dermis before migrating to the epidermis and localizing at the basal membrane, or if they migrate first and subsequently complete the differentiation process in the epidermis [31]. During their differentiation/migration to the epidermis, dermal McSCs are subjected to increasing UVA and UVB doses, leading to further DNA damage and mutations, increasing the probability of transformation. Growth factors present in the epidermis are likely to stimulate

additional proliferation. If a damaged McSC reaches the epidermis without undergoing transformation, it may result in a pre-damaged melanocyte, which is more vulnerable to subsequent UV exposure [357,360].

DSCs share numerous phenotypic and biological similarities with certain melanoma cell populations, presumably CSCs. These features include self-renewal, differentiation into multiple neural crest-derived lineages, high migratory and invasive capabilities, association with mesenchymal cells, absence of melanocytic markers in late-stage tumors, expression of NCSC markers NGFRp75 and nestin, non-canonical Wnt signaling, and Notch activation [32,42]. MMs exhibiting these NCSC-like characteristics are associated with increased aggressiveness, invasiveness, higher metastatic ability, worse prognosis, as well as resistance to immune response and therapy [32,381-383]. This similarity between DSCs and CSCs could be an indication that transformed DSCs serve as CSCs and represent the cell of origin. Instead of progressing through pre-damaged melanocytes as intermediates and then undergoing dedifferentiation, the malignant transformation might occur directly from the stem cell [7,358,362].

Some studies have already described the vulnerability of McSCs or melanocyte precursors to UV radiation [358,361], along with their ability to develop melanomas [361,384,385]. Preliminary findings from zebrafish studies show that both UVA and UVB radiation can impair McSC function, resulting in abnormal pigmentation patterns and abnormal regrowth of the caudal fin [358]. Furthermore, neural crest cells and melanoblasts in zebrafish tend to undergo transformation due to *BRAF* and *p53* mutations more readily than mature melanocytes [384]. Discussions on the stem cell theory of MM initiation not only involve extrafollicular McSCs, but also consider the involvement of McSCs located in the bulge region of hair follicles [11,93,386,387]. Various research groups, utilizing *in vivo* lineage-tracing experiments in mouse models, have shown that hair follicle McSCs can act as melanoma cells of origin, and these MMs resemble human melanoma [361,385]. Moon et al. even demonstrated the induction of MM due to UV stimulation [361]. Irradiation with UVB was sufficient to initiate the activation, translocation, and malignant transformation of quiescent, adult hair follicle McSCs harboring a mutational load, in an inflammation-dependent process. These findings suggest that pre-damaged McSCs may persist in a quiescent state until UV radiation, acting as an extrinsic stimulus, triggers their activation and melanomagenesis [361]. While a melanoma-forming capacity of DSCs upon UV exposure is also supposed [32], this aspect is yet to be investigated.

Therefore, the examination of DSCs is of great importance for gaining a more detailed understanding of the mechanisms underlying MM development.

The McSC theory of melanomagenesis is further supported by several other aspects. Since skin stem cells are long-living cells, they are more likely to accumulate DNA damage and mutations with age compared to mature cells with a shorter lifespan [66,355]. Epidermal stem and progenitor cells in murine epidermis are prone to the accumulation of persistent CPDs upon chronic UV exposure, despite NER proficiency [388,389]. These CPD-retaining basal cells (CRBCs) evade apoptosis, thus serving as potential hotspots for subsequent mutagenesis and carcinogenesis [389]. Interestingly, CRBCs have been observed in unaffected skin tissue of BCC and MM patients as well [388]. Therefore, it is quite likely that McSCs and/or their progeny also accumulate DNA damage over time, contributing to melanomagenesis. Especially stem cells in a non-proliferating, dormant state (quiescence) would be susceptible to this process, since the global repression of transcription, a compacted chromatin structure, and the absence of DNA replication hamper DNA repair via NER [390]. Without active replication, repair through TCR might not function properly. Additionally, GGR seems to be arrested in quiescent cells, facilitating damage accumulation and formation of mutations at both transcribed and temporally silent genes [391]. Active and quiescent adult stem cell subpopulations coexist in the same tissue, whereby the majority is quiescent and non-proliferating [77]. In the mouse hair follicle, the coexistence of activated McSCs, quiescent McSCs, and differentiated melanocytes has been demonstrated [392].

The age-related decline in DNA repair pathways, owing to factors like UV-induced mutations, oxidative stress from mitochondria, or chemical exposures, renders aging adult stem cells more vulnerable to malignant transformation, since their processes of self-renewal, proliferation, survival, quiescence, differentiation, and migration from the stem cell niche may be altered [393]. Aging of hair follicle McSCs due to external influences is evident in the loss of their self-renewal ability and subsequent hair graying [100,101]. Therefore, it can be hypothesized that extrafollicular dermal McSCs may eventually exhibit age-related reductions in DNA repair capacity as well, leading to increased genomic instability [357,358].

2 Aim of This Work

Melanoma is the most aggressive and lethal type of skin cancer [258,275] and primarily linked to UV radiation as its main etiological factor. Numerous epidemiological and biological studies have provided substantial evidence for the causal relationship between UV exposure, which can induce genetic and epigenetic changes, and the development of melanoma [130]. UV-specific cyclobutane pyrimidine dimers (CPDs) and the resulting mutations play a crucial role in this process [138,141]. The identity of the original target cell responsible for acquiring the necessary alterations for transformation into melanoma remains elusive [32,356]. An alternative theory suggests the involvement of multipotent neural crest-derived melanocytic precursors in the dermis, known as dermal stem cells (DSCs), in the origin of melanoma [31,32,357,358]. Being constantly exposed to solar UV radiation in the human skin, DSCs are at risk of accumulating UV-induced mutations. Such pre-damaged cells may be more susceptible to malignant transformation. However, how DSCs react to UV-induced damage is still an insufficiently answered question. Consequently, developing an *in vitro* model to investigate the potential role of DSCs in melanoma development is of significant interest. It is imperative to examine the differentiation process and the DNA damage response (DDR) of DSCs, as UV radiation may induce alterations in these mechanisms that are conducive to malignant degeneration. Additionally, deficiencies in the DDR represent a crucial etiological factor in the multistep development of skin cancer [394]. Understanding the regulatory mechanisms in DSCs will help to define tumor-promoting changes.

Therefore, the aim of this thesis was to establish and initially investigate human multipotent DSCs as a novel model for melanomagenesis. This involved the isolation and propagation of primary DSCs from foreskin, as well as their characterization with respect to certain functional stem cell features. Thereafter, the main objective was to examine the response of DSCs to UV exposure.

I begin by discussing the issue of contaminating fibroblasts in primary DSC cultures and emphasize the importance of a high degree of DSC purification for accurate investigations. By comparing various methods, I show how effective enrichment of DSCs can be achieved in a reliable and reproducible manner without significantly affecting cell characteristics. Furthermore, I demonstrate an initial characterization of DSCs focusing on two essential functional properties of (neural crest) stem cells, the potential for melanocytic differentiation and sphere formation, while comparing native and purified DSC cultures.

Subsequently, I examine how DSCs respond to UV-induced DNA damage and whether UV irradiation affects stem cell characteristics or epigenetic regulation. These investigations involve both UVA and UVB radiation, with UVC wavelengths deemed insignificant for this study due to their absence in the terrestrial solar radiation spectrum. By comparing DSCs to differentiated skin cell types isolated from foreskin, I assess if the DDR in DSCs—including fundamental mechanisms, such as DNA repair, cell cycle regulation, and induction of apoptosis—exhibits any features or abnormalities that might render them more susceptible to tumorigenesis. Additionally, I investigate the effects of UV irradiation on DSC properties, specifically in terms of differentiation and sphere formation capability. Finally, using a selected melanoma-specific miRNA panel, I search for potential UV-induced miRNA patterns in DSCs that are associated with the development of melanoma.

Studying the effects of UV exposure on DSCs will be important for comprehending the role of radiation-damaged melanocyte stem cells in the etiology of cutaneous melanoma. The findings from these investigations might advance our understanding of the molecular and cellular risk factors that lead to UV-induced malignant transformation during melanoma development.

3 Materials

3.1 Devices

Table 3.1 Devices.

Device	Model	Manufacturer
Analytical balance	870-61	Kern & Sohn (Balingen-Frommern, Germany)
Aspirator	Accuvac Basic E 341 Battery	Weinmann (Hamburg, Germany) ATMOS MedizinTechnik (Lenzkirch, Germany)
autoMACS® Separator	Pro	Miltenyi Biotec (Bergisch Gladbach, Germany)
Beam combiner 45°, 315 nm	custom-made	S1 Optics (Nürtingen, Germany)
Beam combiner 45°, 400 nm	custom-made	S1 Optics (Nürtingen, Germany)
Camera	DX40C-285FW	Kappa opto-electronics GmbH (Gleichen, Germany)
Centrifuge	Micro Centrifuge AL Mikro 200 Mikro 22 R Rotina 46 Universal 320	Carl Roth GmbH (Karlsruhe, Germany) Hettich (Tuttlingen, Germany) Hettich (Tuttlingen, Germany) Hettich (Tuttlingen, Germany) Hettich (Tuttlingen, Germany)
EasySep™ Magnet	EasyEights™	StemCell Technologies (Vancouver, Canada)
Filter for UVA lamp (UVB filter)	Schott WG 320 long-pass	Schott AG (Mainz, Germany)
Filter for UVB lamp (UVA filter)	Asahi Spectra UV325 short-pass (ZUS0325)	Mountain Photonics GmbH (Landsberg am Lech, Germany)
Filter for UVB lamp (UVC filter)	Schott B270 long-pass	Reichmann-Feinoptik GmbH (Brokdorf, Germany)
Filter metal mesh		Modulor GmbH (Berlin, Germany)
Flow cytometer	Guava® easyCyte 8HT	Merck (Darmstadt, Germany)
Fluorescence microscope	DMRB	Leica (Wetzlar, Germany)
Fume hood	7590	Köttermann (Uetze/Hänigsen, Germany)
Hybridization Oven	Hybri 6/12	LTF Labortechnik GmbH (Wasserburg, Germany)
Incubator	CB 210	Binder GmbH (Tuttlingen, Germany)
Laminar flow hood class 2	Gelaire BSB-4A	Flow Laboratories GmbH (Meckenheim, Germany)
Magnetic stirrer	IKAMAG RH	IKA Labortechnik (Staufen, Germany)
Microscope	CKX53	Olympus (Hamburg, Germany)
pH meter	766 Calimatic	Knick Elektronische Messgeräte GmbH (Berlin, Germany)
Photometer	BioPhotometer 6131	Eppendorf (Hamburg, Germany)
Pipetting aid	Pipetus-Accu	Hirschmann (Eberstadt, Germany)
Plate Thermo-Shaker	PST-100HL	Biosan (Riga, Latvia)
Platform Shaker	KL2 Rotamax 120	Edmund Bühler GmbH (Bodelshausen, Germany) Heidolph Instruments GmbH (Schwabach, Germany)
Rocking platform shaker	WT14	Biometra GmbH (Göttingen, Germany)

Device	Model	Manufacturer
Shaking water bath	1083	GFL mbH (Burgwedel, Germany)
Thermal shaker	Thermomixer 5436 ThermoMixer C	Eppendorf (Hamburg, Germany) Eppendorf (Hamburg, Germany)
Thermocycler	qTOWER^3 G touch T-personal 48	Analytik Jena (Jena, Germany) Biometra (Göttingen, Germany)
UV irradiation lamp	KAUVIR	KAUVIR consortium, Technical University of Darmstadt (Darmstadt, Germany)
Vacuum manifold for 96-well filter plates		Firefly BioWorks (Cambridge, MA, USA)
Vortexer	All-in-one Vibrofix VF2	Biozym (Hessisch Oldendorf, Germany) IKA Labortechnik (Staufen, Germany)

3.2 Consumables

Table 3.2 Consumables.

Product	Manufacturer
autoMACS® Columns	Miltenyi Biotec (Bergisch Gladbach, Germany)
Cell culture dishes (35 mm, 60 mm, 94 mm)	Greiner Bio-One GmbH (Frickenhausen, Germany)
Cell culture flasks, adherent cells (25 cm², 75 cm²)	Greiner Bio-One GmbH (Frickenhausen, Germany)
Cell culture flasks, suspension cells (50 mL)	Greiner Bio-One GmbH (Frickenhausen, Germany)
Cell culture plates (6-well, 24-well)	Greiner Bio-One GmbH (Frickenhausen, Germany)
Cell scraper	Greiner Bio-One GmbH (Frickenhausen, Germany)
Cell strainer (40 µm, 100 µm)	Corning (Corning, NY, USA)
Centrifuge tubes (15 mL, 50 mL)	Greiner Bio-One GmbH (Frickenhausen, Germany)
Coverslips (13 mm)	VWR (Radnor, PA, USA)
Disposable syringe (5 mL, 10 mL)	Becton, Dickinson and Company (Franklin Lakes, NJ, USA)
Filter plates + Catch plates (96-well)	Abcam (Cambridge, UK)
Forceps	Carl Roth GmbH (Karlsruhe, Germany)
Freezing container, Mr. Frosty™	VWR (Radnor, PA, USA)
Freezing tubes (1 mL)	Greiner Bio-One GmbH (Frickenhausen, Germany)
Graduated pipettes	Karl Hecht GmbH (Sondheim v.d. Röhn, Germany)
Microplates ELISA, F-bottom (96-well)	Greiner Bio-One GmbH (Frickenhausen, Germany)
Microplates, V-bottom (96-well)	Greiner Bio-One GmbH (Frickenhausen, Germany)
Microscope slides	Karl Hecht GmbH (Sondheim v.d. Röhn, Germany)
Microtome blades, stainless steel, S35	FEATHER Safety Razor (Osaka, Japan)
Neubauer hemocytometer	Karl Hecht GmbH (Sondheim v.d. Röhn, Germany)
Pasteur pipettes	Henze (Elmshorn, Germany)
PCR strips	Greiner Bio-One GmbH (Frickenhausen, Germany) Bioplastics (Landgraaf, Niederlande)

Product	Manufacturer
Pipettes	Eppendorf (Hamburg, Germany)
Pipette tips	Greiner Bio-One GmbH (Frickenhausen, Germany) Ratiolab GmbH (Dreieich, Germany)
Pre-separation filters (30 µm)	Miltenyi Biotec (Bergisch Gladbach, Germany)
Reaction tubes (0.5 mL, 1.5 mL, 2 mL)	Greiner Bio-One GmbH (Frickenhausen, Germany)
Round-bottom polystyrene tubes (5 mL)	Corning (Corning, NY, USA)
Scissors	Carl Roth GmbH (Karlsruhe, Germany)
Sieve, stainless steel, coarse-meshed (75 mm)	Carl Roth GmbH (Karlsruhe, Germany)
Sterile filter, Millex®GP (0.22 µm)	Merck (Darmstadt, Germany)
Sterile filter, Steritop® 45 mm Neck Size (0.22 µm)	Merck (Darmstadt, Germany)
UV cuvette	Eppendorf (Hamburg, Germany)

3.3 Reagents

Table 3.3 Reagents and chemicals.

Product	Manufacturer
Accutase™ cell detachment solution	Capricorn Scientific (Ebsdorfergrund, Germany)
Acetone	Carl Roth GmbH (Karlsruhe, Germany)
Annexin-V-FITC, recombinant (50 µg/mL)	Biotium (Fremont, CA, USA)
L-Ascorbic acid	Sigma-Aldrich (Taufkirchen, Germany)
autoMACS® Rinsing solution	Miltenyi Biotec (Bergisch Gladbach, Germany)
autoMACS® Washing solution	Miltenyi Biotec (Bergisch Gladbach, Germany)
BSA	Carl Roth GmbH (Karlsruhe, Germany)
Calcium chloride $CaCl_2$	Carl Roth GmbH (Karlsruhe, Germany)
Calcium chloride dihydrate $CaCl_2 \times 2\ H_2O$	Carl Roth GmbH (Karlsruhe, Germany)
CHIR-99021	Biogems (Westlake Village, CA, USA)
Chloroform/Trichloromethane (99%)	Carl Roth GmbH (Karlsruhe, Germany)
Cholera toxin	Sigma-Aldrich (Taufkirchen, Germany)
Collagenase type IV (255 U/mg)	Gibco Life Technologies (Carlsbad, CA, USA)
Cultrex™ Stem Cell Qualified Reduced Growth Factor Basement Membrane Extract (8–12 mg/mL)	Bio-Techne (Minneapolis, MN, USA)
DABCO (99%)	Sigma-Aldrich (Taufkirchen, Germany)
DAPI	Sigma-Aldrich (Taufkirchen, Germany)
DermaLife K keratinocyte medium	Lifeline Cell Technology (Frederick, MD, USA)
DermaLife Ma melanocyte medium	Lifeline Cell Technology (Frederick, MD, USA)
Dexamethasone	Sigma-Aldrich (Taufkirchen, Germany)
Dibutyryl-cAMP	Biogems (Westlake Village, CA, USA)
Disodium hydrogen phosphate Na_2HPO_4	Merck (Darmstadt, Germany)

Product	Manufacturer
Disodium hydrogen phosphate dihydrate $Na_2HPO_4 \times 2\ H_2O$	Carl Roth GmbH (Karlsruhe, Germany)
Dispase II (0.5 U/mg)	Sigma-Aldrich (Taufkirchen, Germany)
DMEM, low glucose, pyruvate	Capricorn Scientific (Ebsdorfergrund, Germany)
DMEM powder	Gibco Life Technologies (Carlsbad, CA, USA)
DMSO	Carl Roth GmbH (Karlsruhe, Germany)
DNase I from bovine pancreas (min. 3,000 Kunitz U/mg)	SERVA Electrophoresis GmbH (Heidelberg, Germany)
EDTA Titriplex III (99%)	Merck (Darmstadt, Germany)
Endothelin-3	Sigma-Aldrich (Taufkirchen, Germany)
Ethanol (100%)	VWR (Radnor, PA, USA)
FBS (12A, CP18-2361)	Capricorn Scientific (Ebsdorfergrund, Germany)
FGF-basic, recombinant human	PeproTech (Hamburg, Germany)
FirePlex® Cytometer Run Buffer I (ab245836)	Abcam (Cambridge, UK)
Geltrex™ LDEV-Free Reduced Growth Factor Basement Membrane Matrix (12–18 mg/mL)	Gibco Life Technologies (Carlsbad, CA, USA)
Geneticin (50 mg/mL)	Gibco Life Technologies (Carlsbad, CA, USA)
Gentamycin (10 mg/mL)	Merck (Darmstadt, Germany)
D-glucose (dextrose)	Sigma-Aldrich (Taufkirchen, Germany)
Goat serum	Dako (Glostrup, Denmark)
Glycerol (99.5%)	Carl Roth GmbH (Karlsruhe, Germany)
HEPES	Carl Roth GmbH (Karlsruhe, Germany)
Hydrochloric acid HCl (32% = 10 M)	Carl Roth GmbH (Karlsruhe, Germany)
Isopropyl alcohol, for freezing container	Carl Roth GmbH (Karlsruhe, Germany)
ITS liquid medium supplement (100×)	Sigma-Aldrich (Taufkirchen, Germany)
Kanamycin	Carl Roth GmbH (Karlsruhe, Germany)
Linoleic acid-BSA (100 mg/mL)	Sigma-Aldrich (Taufkirchen, Germany)
MACS® BSA stock solution	Miltenyi Biotec (Bergisch Gladbach, Germany)
Magnesium chloride hexahydrate $MgCl_2 \times 6\ H_2O$	Carl Roth GmbH (Karlsruhe, Germany)
Magnesium sulfate $MgSO_4 \times H_2O$	Carl Roth GmbH (Karlsruhe, Germany)
MCDB 201 medium	Sigma-Aldrich (Taufkirchen, Germany) Biomol GmbH (Hamburg, Germany)
β-Mercaptoethanol	Gibco Life Technologies (Carlsbad, CA, USA)
Methanol	Carl Roth GmbH (Karlsruhe, Germany)
Mowiol 4-88	Carl Roth GmbH (Karlsruhe, Germany)
PBS tablets	Gibco Life Technologies (Carlsbad, CA, USA)
Penicillin + streptomycin 10,000 U/mL penicillin 10,000 µg/mL streptomycin	Gibco Life Technologies (Carlsbad, CA, USA)
Phenol red	Sigma-Aldrich (Taufkirchen, Germany)
PMA / TPA	Sigma-Aldrich (Taufkirchen, Germany)

Product	Manufacturer
Potassium chloride KCl	Carl Roth GmbH (Karlsruhe, Germany)
Potassium dihydrogen phosphate KH_2PO_4	Merck (Darmstadt, Germany)
Propidium iodide powder	Sigma-Aldrich (Taufkirchen, Germany)
Propidium iodide solution (100 µg/mL)	Miltenyi Biotec (Bergisch Gladbach, Germany)
Proteinase K (30 U/mg)	Sigma-Aldrich (Taufkirchen, Germany)
RNase A from bovine pancreas (85–110 Kunitz U/mg)	Sigma-Aldrich (Taufkirchen, Germany)
Roti®Block blocking and washing solution (10×)	Carl Roth GmbH (Karlsruhe, Germany)
RPMI 1640 powder	Gibco Life Technologies (Carlsbad, CA, USA)
SCF	PeproTech (Hamburg, Germany)
Sodium acetate $C_2H_3NaO_2$	Merck (Darmstadt, Germany)
Sodium chloride NaCl	Carl Roth GmbH (Karlsruhe, Germany)
Sodium hydrogen carbonate $NaHCO_3$	Carl Roth GmbH (Karlsruhe, Germany)
Soybean trypsin inhibitor	Sigma-Aldrich (Taufkirchen, Germany)
Staurosporine	Santa Cruz Biotechnology (Dallas, TX, USA)
StemPro™ hESC SFM medium includes DMEM/F-12+GlutaMAX™ medium, StemPro™ hESC supplement, and 25% BSA	Gibco Life Technologies (Carlsbad, CA, USA)
Sulfamethoxazole	Sigma-Aldrich (Taufkirchen, Germany)
TE-Buffer (100×)	Carl Roth GmbH (Karlsruhe, Germany)
Tris base $C_4H_{11}NO_3$	Carl Roth GmbH (Karlsruhe, Germany)
Tris hydrochloride $C_4H_{11}NO_3 \times HCl$	Carl Roth GmbH (Karlsruhe, Germany)
Trisodium citrate dihydrate $C_6H_5Na_3O_7 \times 2\ H_2O$	Merck (Darmstadt, Germany)
Triton X-100	Sigma-Aldrich (Taufkirchen, Germany)
Trypsin	Biochrom GmbH (Berlin, Germany)
Water, nuclease-free, sterile-filtered, double-distilled	Carl Roth GmbH (Karlsruhe, Germany) B. Braun Melsungen AG (Melsungen, Germany)
Wnt3a, recombinant human	R&D Systems (Minneapolis, MN, USA)

3.4 Buffers and Solutions

Table 3.4 Composition of buffers and solutions.

Name	Formula
Annexin incubation buffer	2.4 g/L HEPES (= 10 mM), 8.2 g/L NaCl (= 140 mM), 0.56 g/L $CaCl_2$ (= 5 mM) in ddH_2O. pH 7.4. Store at 4 °C.
Annexin staining solution	1.25 µg/mL Annexin-V-FITC, 1.25 µg/mL propidium iodide in Annexin incubation buffer.
L-Ascorbic acid (100 mM)	100 mg L-ascorbic acid in 5.678 mL ddH_2O. Store at -20 °C.
BSA (0.1%)	1 g/L BSA in $PBS^{-/-}$. Store at 4 °C.
BSA (3%)	30 g/L BSA in $PBS^{+/+}$. Store at 4 °C.
CHIR-99021 (3 mM)	1 mg CHIR-99021 in 716 µL DMSO. Store at -20 °C.

Name	Formula
Cholera toxin (10 µM)	0.5 mg cholera toxin in 589 µL ddH_2O. Store at 4 °C. For the preparation of medium, the stock solution (10 µM) was further diluted to 20 nM with ddH_2O, and from this dilution the required amount was taken.
Collagenase type IV (100,000 U/mL)	1 g collagenase type IV in 2.55 mL $HBSS^{+/+}$. Store at -20 °C.
Collagenase type IV (500 U/mL)	50 µL collagenase type IV (100,000 U/mL) in 10 mL $HBSS^{+/+}$. Sterile-filtered.
DAPI (10 µg/mL)	1 mg DAPI in 100 mL ddH_2O. Store at -20 °C. The solution was diluted 1:100 with ddH_2O to a concentration of 0.1 µg/mL before use.
Dexamethasone (25 µM)	25 mg dexamethasone in 2.548 mL ethanol (= 25 mM). From this stock, 10 µL in 10 mL ethanol. Store at -20 °C.
Dibutyryl-cAMP (100 mM)	25 mg dibutyryl-cAMP in 508.75 µL ddH_2O. Store at -20 °C.
Dispase II (0.48% = 2.4 U/mL)	480 mg dispase II in 100 mL $PBS^{-/-}$. pH 7.4, sterile-filtered. Store at -20 °C.
DNase I (20,000 U/mL)	25 mg DNase I in 3.75 mL sterile 0.15 M NaCl. Store at -20 °C.
Endothelin-3 (100 µM)	100 µg endothelin-3 in 378 µL $PBS^{-/-}$. Store at -20 °C.
FACS buffer (0.5% BSA/2 mM EDTA)	5 g/L BSA, 744 mg/L EDTA in $PBS^{-/-}$. pH 7.2. Store at 4 °C.
FGF-basic (100 µg/mL)	100 µg FGF-basic in 1 mL sterile 0.1% BSA/$PBS^{-/-}$. Store at -20 °C. For the preparation of medium, the stock solution (100 µg/mL) was further diluted to 10 µg/mL with 0.1% BSA/$PBS^{-/-}$, and from this dilution the required amount was taken.
Goat serum (5%)	500 µL goat serum, 9500 µL $PBS^{-/-}$. Store at 4 °C.
$HBSS^{+/+}$	140 mg/L $CaCl_2$, 100 mg/L $MgCl_2 \times 6\ H_2O$, 49 mg/L $MgSO_4 \times H_2O$, 400 mg/L KCl, 60 mg/L KH_2PO_4, 350 mg/L $NaHCO_3$, 8 g/L NaCl, 48 mg/L Na_2HPO_4, 1 g/L D-glucose, 10 mg/L phenol red, 100 U/mL penicillin, 100 µg/mL streptomycin in ddH_2O. pH 7.8, sterile-filtered. Store at 4 °C.
$HBSS^{-/-}$	400 mg/L KCl, 60 mg/L KH_2PO_4, 350 mg/L $NaHCO_3$, 8 g/L NaCl, 60 mg/L $Na_2HPO_4 \times 2\ H_2O$, 1 g/L D-glucose, 100 mg/L phenol red, 100 U/mL penicillin, 100 µg/mL streptomycin in ddH_2O. pH 7.8, sterile-filtered. Store at 4 °C.
HCl (2 M)	80 mL ddH_2O, 20 mL 10 M HCl.
Kanamycin (100 mg/mL)	5 g kanamycin in 50 mL ddH_2O. Sterile-filtered. Store at -20 °C.
MCDB 201 medium	1 g in 56 mL ddH_2O. pH 7.6, sterile-filtered. Store at 4 °C.
Mowiol mounting medium	Dissolve 2.4 g Mowiol 4-88 in 6 g glycerol for 1 h at RT, with stirring. Add 6 mL ddH_2O, stir for one more hour at RT. Add 12 mL 0.2 M tris-HCl, incubate for 2 h at 50 °C under periodical stirring (for 2 min every 20 minutes). Add 25 mg/mL DABCO. Store at -20 °C.
NaCl (0.15 M)	58.44 g/L NaCl in ddH_2O. Sterile-filtered.
$PBS^{+/+}$	Two tablets of PBS, 100 mg/L $MgCl_2 \times 6\ H_2O$, 132 mg/L $CaCl_2 \times 2\ H_2O$ in ddH_2O. pH 7.3.
$PBS^{-/-}$	Two tablets of PBS in 1 L ddH_2O. pH 7.3.
Phenol red (0.01 g/L)	0.1 mg phenol red in 10 mL $PBS^{-/-}$. Sterile-filtered. Store at 4 °C.
PMA (500 µM)	1 mg PMA in 3.242 mL DMSO. Store at -20 °C.
Propidium iodide (1 mg/mL)	10 mg propidium iodide in 10 mL $PBS^{-/-}$. Store at 4 °C.

Name	Formula
Proteinase K (50 µg/mL = 1.5 U/mL)	5 mg proteinase K in 100 mL $PBS^{+/+}$. Store at -20 °C. The solution was diluted 1:10 with $PBS^{+/+}$ to a concentration of 5 µg/mL = 0.15 U/mL before use.
RNase A (0.1%)	1 g/L RNase A in 10 mM sodium acetate. Heat to 100 °C for 15 min, allow to cool to RT. Adjust to pH 7.4 with 1 M tris-HCl. Store at -20 °C. The solution was diluted 1:10 with $PBS^{-/-}$ to a concentration of 0.01% before use.
Roti®Block-Triton (1×/0.125%)	10 mL 10× Roti®Block blocking and washing solution, 90 mL ddH_2O, 125 µL Triton X-100.
SCF (100 µg/mL)	50 µg SCF in 100 µL ddH_2O and 400 µL sterile 0.1% BSA/$PBS^{-/-}$. Store at -20 °C.
Selection buffer ES (2% FBS/1 mM EDTA)	2 mL FBS, 372 mg/L EDTA, 98 mL $PBS^{-/-}$. Store at 4 °C.
Selection buffer M (0.5% BSA/2 mM EDTA)	MACS® BSA stock solution diluted 1:20 with autoMACS® Rinsing solution. Store at 4 °C.
Sodium acetate (10 mM)	820 mg/L sodium acetate in ddH_2O. pH 5.2.
Soybean trypsin inhibitor (10 mg/mL)	25 mg soybean trypsin inhibitor in 2.5 mL ddH_2O. Sterile-filtered. Store at -20 °C.
Staurosporine (1 mM)	1 mg staurosporine in 2.143 mL DMSO. Store at -20 °C.
Sulfamethoxazole (20 mg/mL)	0.5 g sulfamethoxazole in 25 mL ethanol. Sterile-filtered. Store at -20 °C.
TBS (10×)	12.12 g/L tris base, 87.66 g/L NaCl in ddH_2O. pH 7.5. Store at 4 °C. The buffer was diluted 1:10 with ddH_2O to 1× concentration before use.
Tris-HCl (0.2 M)	31.52 g/L tris hydrochloride in ddH_2O. pH 8.5.
Tris-HCl (1 M)	157.6 g/L tris hydrochloride in ddH_2O. pH 8.1.
Trypsin (0.1%)	1 g/L trypsin powder, 2.6 g/L trisodium citrate dihydrate, 6 g/L NaCl, 0.2 g/L EDTA, 100 U/mL penicillin, 100 µg/mL streptomycin in ddH_2O. pH 7.8, sterile-filtered. Store at -20 °C.
Trypsin-EDTA (0.25%/0.02%)	2.5 g/L trypsin powder, 0.2 g/L EDTA in $PBS^{-/-}$. pH 7.5, sterile-filtered. Store at -20 °C.
Trypsin-EDTA (0.5%/0.2%)	5 g/L trypsin powder, 2 g/L EDTA in $PBS^{-/-}$. pH 7.5, sterile-filtered. Store at -20 °C.
Wnt3a (20 µg/mL)	10 µg Wnt3a in 500 µL sterile 0.1% BSA/$PBS^{-/-}$. Store at -20 °C.

3.5 Culture Media

Table 3.5 Composition of cell culture media.

Name	Formula
DMEM	13.38 g/L DMEM powder, 3.7 g/L $NaHCO_3$, 100 U/mL penicillin, 100 µg/mL streptomycin in ddH_2O. pH 7.3, sterile-filtered.
DMEM+10%FBS	13.38 g/L DMEM powder, 3.7 g/L $NaHCO_3$, 100 U/mL penicillin, 100 µg/mL streptomycin, 10% FBS. pH 7.3, sterile-filtered.
Freezing medium	70% FBS-free cell-specific medium, 20% FBS, 10% DMSO, sterile-filtered.
Keratinocyte medium	DermaLife K keratinocyte medium, 100 U/mL penicillin, 100 µg/mL streptomycin, 1 µg/L phenol red.

Name	Formula
Melanocyte differentiation medium	50% DMEM, 0.5% FBS, 30% DMEM low glucose, 20% MCDB 201 medium, 1× ITS liquid medium supplement, 1 mg/mL linoleic acid-BSA, 100 µM L-ascorbic acid, 100 ng/mL SCF, 50 nM dexamethasone, 20 pM cholera toxin, 100 nM PMA, 4 ng/mL FGF-basic, 100 nM endothelin-3, 20 ng/mL Wnt3a, 100 µM dibutyryl-cAMP, 3 µM CHIR-99021, 100 U/mL penicillin, 100 µg/mL streptomycin. Sterile-filtered.
Melanocyte medium	DermaLife Ma melanocyte medium, 100 U/mL penicillin, 100 µg/mL streptomycin, 100 µg/mL kanamycin, 1 µg/L phenol red.
RPMI+10%FBS	10.43 g/L RPMI 1640 medium, 2 g/L $NaHCO_3$, 100 U/mL penicillin, 100 µg/mL streptomycin, 10% FBS in ddH_2O. pH 7.3, sterile-filtered.
Stem cell medium	StemPro™ hESC SFM medium, 1.8% BSA, 1× StemPro™ hESC supplement (provided as a kit), 8 ng/mL FGF-basic, 0.1 mM β-mercaptoethanol, 100 U/mL penicillin, 100 µg/mL streptomycin, 100 µg/mL kanamycin, sterile-filtered.
Transport medium	13.38 g/L DMEM powder, 5.958 g/L HEPES, 100 U/mL penicillin, 100 µg/mL streptomycin, 100 µg/mL gentamycin, 100 µg/mL kanamycin in ddH_2O. pH 7.3, sterile-filtered.

3.6 Kits

Table 3.6 Kits.

Name	Cat. #	Manufacturer
Anti-PE MicroBeads	130-048-801	Miltenyi Biotec (Bergisch Gladbach, Germany)
Basic MicroBeads	130-048-001	Miltenyi Biotec (Bergisch Gladbach, Germany)
CD90 MicroBeads, human	130-096-253	Miltenyi Biotec (Bergisch Gladbach, Germany)
EasySep™ Human CD271 Positive Selection Kit II	17849	StemCell Technologies (Vancouver, Canada)
EasySep™ Human PE Positive Selection Kit II	17664	StemCell Technologies (Vancouver, Canada)
FirePlex® miRNA Assay Core Reagent Kit V2 - Biofluid	ab218342	Abcam (Cambridge, UK)
FirePlex® miRNA Assay Custom Particle Panel RGPC P1	ab254477	Abcam (Cambridge, UK)
Guava® ViaCount™ Reagent	4000-0040	Luminex Corporation (Austin, TX, USA)
miRNeasy Mini Kit	217004	Qiagen (Hilden, Germany)
Neural Crest Stem Cell (NCSC) MicroBeads, human	130-097-127	Miltenyi Biotec (Bergisch Gladbach, Germany)
peqGOLD DNase I Digest Kit	13-1091-01	VWR (Radnor, PA, USA)
peqGOLD Total RNA Kit	12-6834-02, replaced by 13-6834-02	PEQLAB Biotechnologie GmbH (Erlangen, Germany)
SensiFAST™ cDNA Synthesis Kit	BIO-65053	Bioline GmbH (Luckenwalde, Germany)
SensiMix™ SYBR No-ROX Kit	QT650-05	Bioline GmbH (Luckenwalde, Germany)

3.7 Antibodies

3.7.1 Primary Antibodies

Table 3.7 Primary antibodies.

Antigen, Label	Host	Clone	Application	Cat. #	Supplier
CD90, PE	Mouse	5E10	Flow, IMS	60045PE	StemCell Technologies (Vancouver, Canada)
CPD	Mouse	KTM53	Flow	MC-062	Kamiya Biomedical Company (Seattle, WA, USA)
NGFRp75 (intracellular)	Rabbit	EP1039Y	Flow, ICC	ab52987	Abcam (Cambridge, UK)
NGFRp75 (CD271), APC (surface)	Recom-binant	REA844	Flow	130-112-602	Miltenyi Biotec (Bergisch Gladbach, Germany)
CD90	Mouse	AS02	ICC	DIA100	Dianova (Hamburg, Germany)
HMB45	Mouse	-	ICC	sc-59305	Santa Cruz Biotechnology (Dallas, TX, USA)
Melan-A	Mouse	A103	ICC	M7196	Dako (Glostrup, Denmark)
Pan-keratin	Mouse	PAN-CK	ICC	MA5-13203	Thermo Fisher Scientific (Waltham, MA, USA)
TRP2	Mouse	C-9	ICC	sc-74439	Santa Cruz Biotechnology (Dallas, TX, USA)
CD90, PE	Mouse	DG3	IMS	130-117-388	Miltenyi Biotec (Bergisch Gladbach, Germany)

Flow: flow cytometry, ICC: immunocytochemistry, IMS: immunomagnetic separation.

3.7.2 Secondary Antibodies

Table 3.8 Secondary antibodies.

Antigen, Label	Host	Application	Cat. #	Supplier
Mouse IgG (H+L), FITC	Goat	Flow	115-095-062	Dianova (Hamburg, Germany)
Rabbit IgG (H+L) Cross-Adsorbed, APC	Goat	Flow	A10931	Thermo Fisher Scientific (Waltham, MA, USA)
Mouse IgG (H+L) Highly Cross-Adsorbed, Alexa Fluor 488	Goat	ICC	A11029	Thermo Fisher Scientific (Waltham, MA, USA)
Rabbit IgG (H+L) Cross-Adsorbed, Alexa Fluor 594	Goat	ICC	A11012	Thermo Fisher Scientific (Waltham, MA, USA)

Flow: flow cytometry, ICC: immunocytochemistry, IMS: immunomagnetic separation.

3.8 mRNA Primers for qPCR Expression Analysis

Primer sequences were taken from the literature or designed in-house. Primers were purchased from Biomers.net (Ulm, Germany), dissolved in 1× TE buffer, and forward and reverse primers were combined to an equimolar solution of 3 µM before use.

3.8.1 Primer Sequences

Table 3.9 mRNA primer sequences.

Gene		Sequence 5‘ → 3‘	Amplicon [bp]	Design
ACTB (*HKG*)	F	TTCCTGGGCATGGAGTC	84	[395]
	R	CAGGTCTTTGCGGATGTC		
FRZB	F	TGGAAGGATCGACTCGGTAAA	64	[40]
	R	TGAGTCCAAGATGACGAAGC		
HPRT1 (*HKG*)	F	TGACACTGGCAAAACAATGCA	94	[396]
	R	GGTCCTTTTCACCAGCAAGCT		
MITF	F	GAACACACACATTCACGAGCG	154	[397]
	R	CAATCAAGTTTCCCGAGACAG		
MSX1	F	AGCTGCCAGAAGATGCGCT	152	in-house [398]
	R	CGGCTTACGGTTCGTCTTGT		
Nestin	F	ACCTCAAGATGTCCCTCAGC	127	in-house [398]
	R	TCCAGCTTGGGGTCCTGA		
NGFRp75	F	GCTGCTGTTGCTGCTTCTG	180	in-house [398]
	R	TCGGAGAACGTCACGCTG		
TBP (*HKG*)	F	TTCGGAGAGTTCTGGGATTGTA	227	[399]
	R	TGGACTGTTCTTCACTCTTGGC		
TRP1	F	GCTCCAGACAACCTGGGATA	185	[400]
	R	TCAGTGAGGAGAGGCTGGTT		
TRP2	F	ACGCCTGGGTGCAGAGTC	86	[400]
	R	AGGGCCTTGTGTCGGCTC		
Tyrosinase	F	GTACAGGGATCTGCCAACGA	210	modified from [400]
	R	GCCCAGATCTTTGGATGAAATAA		

HKG: housekeeping gene. F: forward. R: reverse.

3.8.2 Internet Addresses for Primer Design

Table 3.10 Internet addresses for primer design.

URL	Accessed on
http://biotools.nubic.northwestern.edu/OligoCalc.html	February 11, 2019
http://bisearch.enzim.hu/?m=genompsearch	February 11, 2019
http://www.bioinformatics.org/sms/rev_comp.html	February 11, 2019
http://www.ensembl.org/Homo_sapiens/Info/Index	February 11, 2019
https://www.ncbi.nlm.nih.gov/tools/primer-blast/	February 11, 2019

3.9 MicroRNA Panel

Table 3.11 Custom human melanoma miRNA panel for FirePlex® miRNA Assay.

hsa-let-7a-5p	hsa-mir-145-5p	hsa-mir-193b-5p	hsa-mir-218-5p	hsa-mir-338-3p
hsa-let-7d-5p	hsa-mir-146b-5p	**hsa-mir-197-3p**	**hsa-mir-21-5p**	hsa-mir-33a-5p
hsa-let-7g-5p	hsa-mir-148a-3p	hsa-mir-199a-3p	hsa-mir-221-3p	hsa-mir-342-3p
hsa-let-7i-5p	hsa-mir-150-5p	hsa-mir-199a-5p	hsa-mir-222-3p	hsa-mir-34a-3p
hsa-mir-100-5p	hsa-mir-155-5p	hsa-mir-200c-3p	hsa-mir-23a-3p	hsa-mir-34a-5p
hsa-mir-101-3p	hsa-mir-15a-5p	hsa-mir-203a-3p	hsa-mir-23b-3p	hsa-mir-34b-3p
hsa-mir-124-3p	hsa-mir-15b-5p	hsa-mir-204-5p	hsa-mir-29a-3p	hsa-mir-425-5p
hsa-mir-1246	**hsa-mir-16-5p**	hsa-mir-205-5p	hsa-mir-29b-3p	hsa-mir-494-3p
hsa-mir-125b-5p	**hsa-mir-17-5p**	hsa-mir-20a-5p	hsa-mir-29c-3p	hsa-mir-509-3p
hsa-mir-132-3p	hsa-mir-182-5p	hsa-mir-20b-5p	hsa-mir-301a-3p	hsa-mir-92b-3p
hsa-mir-137	hsa-mir-185-5p	hsa-mir-210-3p	hsa-mir-30d-5p	**hsa-mir-93-5p**
hsa-mir-142-3p	hsa-mir-192-5p	hsa-mir-211-5p	hsa-mir-31-3p	
hsa-mir-142-5p	hsa-mir-193b-3p	hsa-mir-214-3p	hsa-mir-31-5p	

The nine most stable microRNAs for normalization are shown in bold. The five microRNAs highlighted in gray were excluded from the analysis due to low fluorescence values in measurements.

3.10 Software

Table 3.12 Used software.

Name	Version	Company
BioRender		BioRender (Toronto, Canada), https://www.biorender.com/
EHDView	x64, 3.7.9432	EHD imaging GmbH (Damme, Germany)
EndNote™	21.2	Clarivate Analytics (London, UK)
FirePlex® Analysis Workbench	2.0.274-ext	Abcam (Cambridge, UK)
Flowing Software	2.5.1	Perttu Terho, Turku Bioscience Centre (Turku, Finland)
Guava® InCyte™	3.1	Luminex Corporation (Austin, TX, USA)
ImageJ	1.50i	National Institutes of Health (Bethesda, MD, USA), https://www.imagej.nih.gov/ij/
Kappa Camera Control	1.4.2.9031	Kappa opto-electronics GmbH (Gleichen, Germany)
Marvin JS	23.13.0	Chemaxon (Budapest, Hungary)
Microsoft Office	2016	Microsoft Corporation (Redmond, WA, USA)
miRTargetLink	2.0	Saarland University (Saarbrücken, Germany), https://ccb-compute.cs.uni-saarland.de/mirtargetlink2/
ModFit LT	4.1	Verity Software House (Topsham, ME, USA)
qPCRsoft	4.1	Analytik Jena (Jena, Germany)
R	3.5.1 or higher	R Foundation for Statistical Computing (Vienna, Austria), https://www.r-project.org/
SigmaPlot	13.0	Systat Software Inc. (San José, CA, USA)

3.11 Cell Strains

3.11.1 Primary DSCs, Fibroblasts, Melanocytes, and Keratinocytes

All primary skin cells—including DSCs, fibroblasts, melanocytes, and keratinocytes—were isolated from human foreskins derived from routine circumcisions as discarded tissue, kindly provided by Dr. M. Said (Hamburg, Germany). The children's legal guardians gave their written informed consent before donation of foreskin samples, which were anonymized.

3.11.2 Melanoma Cells

Melanoma cells were available as frozen stocks from 2010 and 2013. Cells were previously isolated in the Department of Molecular Cell Biology from melanoma metastasis tissue that was not required for further diagnostics, obtained from surgery at the Department of Dermatology at the Elbe Clinics Stade-Buxtehude (Buxtehude, Germany). The patients gave their written informed consent before donation of metastasis tissue samples, which were anonymized.

4 Methods

4.1 Cell Culture

4.1.1 Isolation of Cells

All cells were isolated from human foreskins as previously described [31,125,126] with slight modifications [398]. After excision, the skin was stored at 4 °C in a sterile centrifuge tube containing 20 mL of transport medium (Table 3.5) and delivered to the laboratory within 48 h. Foreskins were washed in a 6-well cell culture plate in phosphate-buffered saline ($PBS^{-/-}$), 70% ethanol, and again in $PBS^{-/-}$, cut open with scissors and then into elongated stripes 2–3 mm wide. The foreskin stripes were washed three times for 10 min in a 6-well cell culture plate in $PBS^{-/-}$ containing 200 µg/mL gentamycin and 200 µg/mL sulfamethoxazole, at 200 rpm on a platform shaker. Afterwards, skin stripes were finally incubated in 5 mL of 0.48% dispase II overnight at 4 °C.

On the next day, epidermis and dermis were separated with forceps and collected in Ca^{2+}- and Mg^{2+}-free HBSS ($HBSS^{-/-}$) and $PBS^{-/-}$, respectively, until further processing to prevent from drying out. The dermis was finely chopped with a microtome blade and incubated in 5 mL of 500 U/mL collagenase type IV in Hanks' balanced salt solution with Ca^{2+} and Mg^{2+} ($HBSS^{+/+}$) at 37 °C for 1 h with shaking every 15 min. The resulting suspension was then diluted with 25 mL $HBSS^{-/-}$ and sequentially passed through a coarse-meshed sieve, a 100 µm cell strainer and a 40 µm cell strainer. Cells were counted and centrifuged at 200× g for 10–30 min, depending on the turbidity of the supernatant. Fibroblasts were cultured by seeding whole dermal cells at a density of 2×10^4 cells/cm² in RPMI+10%FBS (Table 3.5).

To obtain DSCs, whole dermal cells were seeded at a density of $0.8–1.0 \times 10^6$ cells/mL in stem cell medium (Table 3.5) in suspension culture flasks to be initially cultivated in spheres. For medium change, the whole content of the flasks including cells and medium was collected in a centrifuge tube. If cells were also attached to the bottom of the flasks, they were scraped off with a cell scraper beforehand. Cell aggregates/spheres were allowed to settle for 5–10 min. Then, half of the supernatant was aspirated and refilled with fresh stem cell medium. Only at the first medium change after isolation, the supernatant was not discarded but collected and mixed with fresh medium for further cultivation. After roughly two weeks of cultivation in suspension, the dermal spheres were dissociated (see section 4.1.2), and cells were seeded in cell culture vessels coated with basement membrane extract (BME) (see section 4.1.3) in order to let the cells proliferate and to obtain sufficient amounts of cells for subsequent experiments

with adherent growing cultures. Depending on the cell count, experiments with DSCs were performed with either single donor cell strains or a combination of multiple donor cell strains.

To prepare keratinocytes, one third of the epidermis was incubated in 2 mL 0.25%/0.02% trypsin-EDTA for 5 min at 37 °C. Afterwards, the suspension was vigorously pipetted up and down for 1–2 min with a Pasteur pipette, and diluted with 10 mL Dulbecco's modified Eagle medium (DMEM) containing 10% fetal bovine serum (DMEM+10%FBS). Cells were centrifuged at 200× g for 10 min, counted, and seeded at a density of 2.7–4.0 × 10^4 cells/cm² in keratinocyte medium (Table 3.5).

The isolation of melanocytes was adapted from a method by Herlyn and colleagues [401]. Two thirds of the epidermis were finely chopped with a microtome blade, incubated in 1–2 mL 0.5%/0.2% trypsin-EDTA for 5 min at 37 °C, and pipetted up and down 80 times with a Pasteur pipette. Trypsinization was stopped with 1 mg/mL soybean trypsin inhibitor and the suspension was further diluted with 10 mL DMEM+10%FBS. Cells were centrifuged for 10 min at 200× g, counted, and seeded in melanocyte medium (Table 3.5) at a density of 4.0–5.4 × 10^4 cells/cm². In the first 48–72 h, it was necessary to refrain from disturbing the melanocytes and avoid any repositioning.

Melanoma cells, derived from melanoma metastases in earlier isolations, were already available as frozen stocks. For experiments, melanoma cells were thawed and cultured in RPMI+10%FBS (Table 3.5) at a density of 1.6 × 10^4 cells/cm². All cells were cultured in an incubator with 5% CO_2 and 95% humidity at 37 °C. Half of the medium was changed twice each week or when required.

4.1.2 Dissociation of Dermal Spheres

Following a suspension cultivation period of 12–14 days after isolation, the dermal spheres were dissociated. The medium containing spheres and scraped-off cells was transferred to a centrifuge tube and allowed to settle for 10 min. Half of the medium was removed, and the resulting cell suspension was centrifuged at 200× g for 10 min. After aspiration of the supernatant, the pellet was resuspended in around 1 mL Accutase™ per cell culture flask and incubated at 37 °C for 1 h within a water bath, with occasional shaking. Spheres were additionally pipetted up and down with a graduated pipette and a Pasteur pipette for further dissociation. Subsequently, the cells were counted and centrifuged for 10 min at 200× g, before seeding into cell culture vessels coated with BME (see section 4.1.3) at a density of approximately 1.4–2.7 × 10^4 cells/cm² to enable adherent growth. Furthermore, following

dissociation of the spheres, the DSC frequency in the culture was determined via flow cytometry, using the stem cell marker NGFRp75 (see section 4.6.2.1).

4.1.3 Coating with Basement Membrane Extract for DSCs

For adherent cell growth of DSCs, coating of the cell culture vessels with basement membrane extract (BME) was necessary. This soluble mixture containing laminin, collagen IV, entactin, and heparin sulfate proteoglycan purified from Engelbreth-Holm-Swarm tumor cells resembles the basement membrane and gels at temperatures >15 °C. First, the thawed but cold extract (Geltrex™ or Cultrex™) was diluted 1:100 with pre-chilled DMEM low glucose to a final concentration of around 80–140 µg/mL. The dilution was applied to the cell culture vessels with the volumes shown in Table 4.1, and culture vessels were incubated at RT for at least 30 min. Flasks were placed on a rocking platform shaker for an even distribution. (Vessels with coating solution could also be stored in an incubator for several days.) The BME-coating solution was carefully aspirated immediately before seeding of DSCs.

Table 4.1 BME-coating for adherent growing DSCs.

Cell culture vessel	Volume of diluted BME
Cell culture dish (35 mm)	1.5 mL
Cell culture dish (60 mm)	2.5 mL
Cell culture dish (94 mm)	5 mL
Cell culture flask (25 cm²)	3 mL
Cell culture flask (75 cm²)	5 mL
Coverslip (13 mm) placed in 24-well cell culture plate	0.5 mL

4.1.4 Splitting of Cells

At 80–90% confluency of adherent cell cultures, the cells were detached and split according to the following cell-specific protocols (Table 4.2). In case of contamination of melanocyte cultures with keratinocytes, both cell types could be separated with this differential trypsinization protocol as melanocytes detached fast and keratinocytes remained behind. The number of obtained cells was determined using a Neubauer hemocytometer. After centrifugation at 200× g for 10 min, cells were either seeded in cell culture vessels for further cultivation and experiments, or cells were frozen.

Table 4.2 Protocols for detachment of adherent growing cells.

DSCs & DSC-fibroblast co-cultures	Fibroblasts	Melanocytes	Keratinocytes
Aspiration of medium	Aspiration of medium	Aspiration of medium	Aspiration of medium
Washing with $PBS^{-/-}$	$HBSS^{-/-}$, 10 min, 37 °C	Washing with $PBS^{-/-}$	Washing with $PBS^{-/-}$
Accutase™, 5 min, 37 °C	0.1% trypsin, 5 min, 37 °C	0.25%/0.02% trypsin-EDTA, 1 min, RT	0.25%/0.02% trypsin-EDTA, 5–10 min, 37 °C
Tapping of culture vessel and dissociation of cells	Tapping of culture vessel and dissociation of cells	Only slight tapping of culture vessel	Tapping of culture vessel and dissociation of cells
Addition of DMEM+10%FBS to dilute Accutase™ to stop detachment reaction	Addition of RPMI+10%FBS to stop detachment reaction	Addition of DMEM+10%FBS to stop detachment reaction	Addition of DMEM+10%FBS to stop detachment reaction

4.1.5 Freezing of Cells

Cells were detached according to the cell-specific protocol (Table 4.2) and centrifuged for 10 min at 200× g. The supernatant was aspirated and cells were resuspended in freshly prepared, cell-specific freezing medium with a concentration of 1–2 × 10^6 cells/1 mL per freezing tube. The tubes were placed in a freezing container and stored at -70 °C for at least one day. The freezing container, filled with isopropyl alcohol, allows for a controlled cooling rate of -1 °C/min. Afterwards tubes were transferred to liquid nitrogen (-196 °C) for long-term storage.

4.1.6 Thawing of Cells

Cells were taken out of the liquid nitrogen and thawed quickly at 37 °C in a water bath. The cell suspension was transferred to a centrifuge tube filled with 10 mL of DMEM+10%FBS and centrifuged at 200× g for 10 min. The supernatant was aspirated, cells were resuspended in the required amount of cell-specific culture medium (Table 3.5), and transferred to a culture flask. Approximately 0.7–1.5 × 10^6 cells/75 cm² flask were seeded in 13–15 mL medium or around 0.5–1 × 10^6 cells/25 cm² flask in 5 mL medium. Flasks for cultivation of DSCs were BME-coated (see section 4.1.3).

4.2 Enrichment of DSCs

Cultivating whole dermal cells obtained from foreskin dermis in stem cell medium leads to the natural growth of DSCs in heterogeneous co-cultures with fibroblasts (see section 5.1). Given

that the fibroblasts not only pose a minor contamination, but represent the majority of the DSC culture, these mixed cultures are subsequently referred to as ‘DSC-fibroblast co-cultures’.

4.2.1 Geneticin Treatment

Dissociated DSC-fibroblast co-cultures were seeded on BME-coated coverslips (13 mm) placed in 24-well cell culture plates (5.0–5.7 × 10^4 cells/coverslip) and in BME-coated cell culture dishes (3.1–3.9 × 10^4 cells/cm²) in stem cell medium. Starting the following day (day 0), the cultures were treated with 50 µg/mL or 100 µg/mL Geneticin for a total of two days. Subsequently, the cells were washed with $PBS^{-/-}$, fresh medium without Geneticin was added (day 2), and the cultures were maintained for a total of six days. Control cells were treated analogously, but without the addition of Geneticin. On days 0, 3, and 6 of the experiment, cell growth was monitored via light microscopy (Olympus CKX53 microscope with integrated camera and the EHDView software), the total number of cells grown in cell culture dishes was determined, and cells grown on coverslips were fixed for subsequent immunocytochemical staining (see section 4.6.1) to evaluate the proportion of DSCs in culture.

4.2.2 Selective Detachment

Dissociated DSC-fibroblast co-cultures were seeded in BME-coated cell culture dishes (2.6–3.1 × 10^4 cells/cm²) in stem cell medium. Upon reaching 80–90% confluency, cells were washed with $PBS^{-/-}$ and then incubated with the detachment reagents Accutase™ or trypsin-EDTA (0.25%/0.02%) for varying periods of time. For Accutase™ treatment, cells were collected at 1-, 2-, and 3-minute time points, while trypsin-EDTA treatment required incubation periods of 0.5, 1, and 2 min. Control cells were incubated for 5 min. At the respective points, the culture dish was tapped slightly, and the supernatant containing the detached cells was collected. The remaining adherent cells were monitored via light microscopy (Olympus CKX53 microscope with integrated camera and the EHDView software) and then further detached, reaching a total incubation time of 5 min. Subsequently, the cell count for each sample was measured, and the proportion of DSCs in culture was determined via flow cytometric staining of NGFRp75 and CD90 (see section 4.6.2.1). Cell viability was assessed through propidium iodide staining (1 µg/mL).

4.2.3 Immunomagnetic Separation

DSC-fibroblast co-cultures were subjected to both positive or negative immunomagnetic separation (IMS) (Figure 4.1), while also comparing EasySep™ column-free and MACS®

automatic column-based separation methods. Magnetic bead separation was performed on fresh DSC-fibroblast co-cultures grown on BME-coating prior to selection to allow the cells to proliferate and to obtain sufficient amounts of cells. The co-cultures were dissociated according to the cell-specific protocol (Table 4.2), and the resulting single-cell suspensions were subjected to separation protocols. The cell counts were determined before and in both fractions after the separation. The recovery was calculated as the ratio of the absolute number of DSCs in the purified fraction to the absolute number of DSCs in the initial sample.

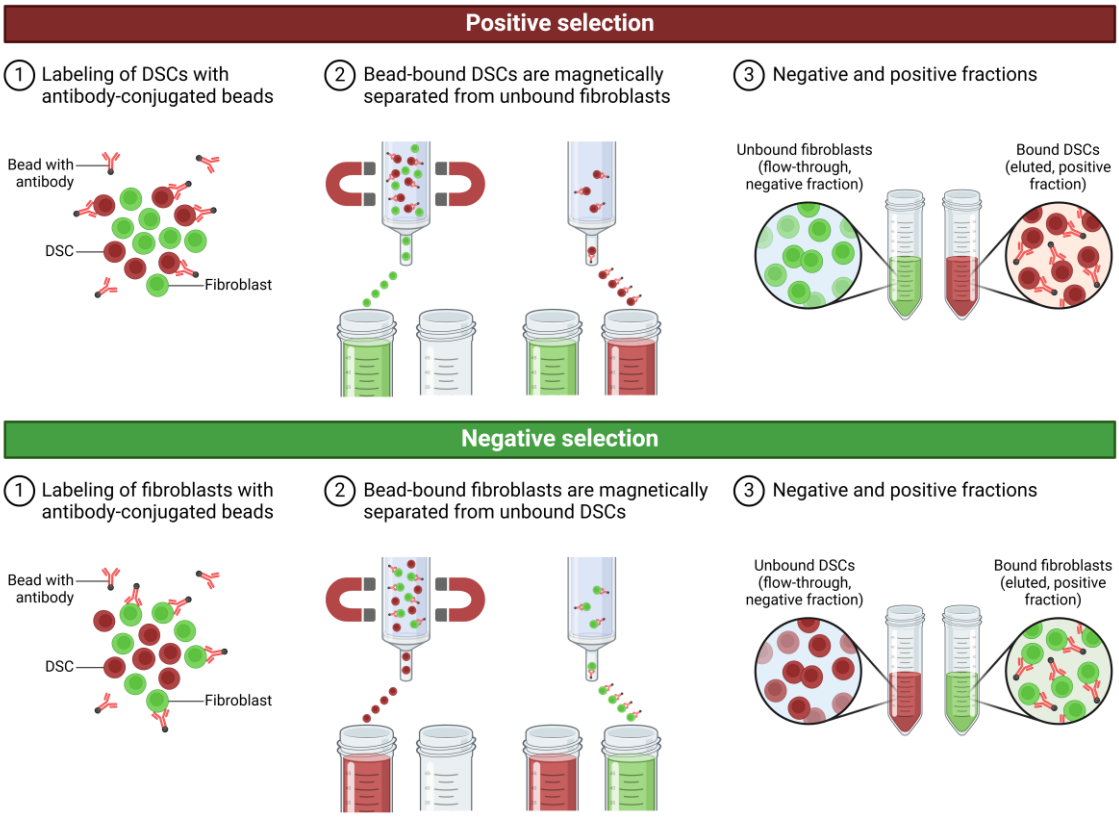

Figure 4.1 Illustration of immunomagnetic separation in a column-based approach. For positive selection, DSCs are labeled with beads via NGFRp75. Unbound fibroblasts pass through the magnetic field into the negative fraction, while labeled DSCs are retained in the column and eluted in the positive fraction. For negative selection, fibroblasts are labeled with beads via CD90. Unbound DSCs pass through the magnetic field into the negative fraction, while labeled fibroblasts are retained in the column and eluted in the positive fraction. For a column-free approach, a tube containing the labeled cell suspension is placed into a magnet. The supernatant with the unbound cells (negative fraction) is pipetted off, while the labeled cells are retained in the tube and subsequently resuspended (positive fraction) (created with BioRender.com).

4.2.3.1 EasySep™ Column-Free Separation

The EasySep™ column-free separation of fibroblasts and DSCs was performed using 5 mL polystyrene round-bottom tubes, the EasyEights™ EasySep™ Magnet, and EasySep™ Selection Kits from StemCell Technologies. $PBS^{-/-}$ containing 2% FBS and 1 mM EDTA was used as selection buffer (selection buffer ES).

For EasySep™ negative selection (labeling of fibroblasts), the *EasySep™ Human PE Positive Selection Kit II* along with a PE-conjugated anti-CD90 antibody (clone 5E10) was used according to the manufacturer's protocol, with slight modifications. Changes to the kit protocol included:

1. Up to 1×10^7 cells were resuspended in 1 mL of selection buffer ES (instead of 1×10^8 cells/mL).
2. Addition of 100 µL FcR blocker/mL of sample and 20 µL of PE-conjugated anti-CD90 antibody/mL of sample meaning 1 µg/mL antibody (within the recommended concentration range of 0.3–3 µg/mL) and incubation for 15 min at RT.
3. Wash step with centrifugation at 200× g for 10 min and resuspending of cell pellet in 1 mL selection buffer ES.
4. For an optimal ratio of the selection cocktail to antibody, 50 µL of selection cocktail/mL of sample (instead of 100 µL/mL) were added and incubated for 15 min at RT.
5. Due to the high number of fibroblasts to be captured, 100 µL of RapidSpheres™ (beads)/mL of sample (instead of 75 µL/mL) were added and incubated for 10 min at RT.
6. The sample was topped up with selection buffer ES to 2.5 mL and placed into the magnet for 10 min.
7. The supernatant was carefully pipetted off and transferred to a new tube.
8. Cells left in the tube were resuspended in 2.5 mL selection buffer ES, and the isolation step in the magnet was repeated with both the supernatant and the resuspended beads to a total of 2–3 separations.

For EasySep™ positive selection (labeling of DSCs), the *EasySep™ Human CD271 Positive Selection Kit II* was used. The procedure followed the manufacturer's protocol, with minor modifications:

1. Approximately $1–2 \times 10^7$ cells were resuspended in 1 mL of selection buffer ES (instead of 1×10^8 cells/mL).
2. Addition of 25 µL FcR blocker/mL of sample and 50 µL of selection cocktail/mL of sample and incubation for 15 min at RT.
3. Addition of 50 µL RapidSpheres™ (beads)/mL of sample and incubation for 5 min at RT.
4. The sample was topped up with selection buffer ES to 2.5 mL and placed into the magnet for 5 min.
5. The supernatant was carefully pipetted off and transferred to a new tube.

6. Cells left in the tube were resuspended in 2.5 mL selection buffer ES, and the isolation step in the magnet was repeated to a total of 3–4 separations.

The supernatant was designated as the negative fraction, while the leftover CD90-PE- or CD271(NGFRp75)-labeled cells bound to the magnetic beads were referred to as the positive fraction. Both of these cell suspensions obtained from magnetic separation were collected for immunostaining via flow cytometry (see section 4.6.2.1). The fraction containing the enriched DSCs was further cultivated for approximately 10–12 days.

4.2.3.2 MACS® Automatic Column-Based Separation

The MACS® automatic column-based separation was conducted with 5 mL polystyrene round-bottom tubes, the autoMACS® Pro Separator, autoMACS® Columns, and MACS® *MicroBeads* from Miltenyi Biotec. $PBS^{-/-}$ containing 0.5% bovine serum albumin (BSA) and 2 mM EDTA was used as selection buffer (selection buffer M). Prior to starting the separation protocol, the dissociated cell suspensions were filtered through 30 µm pre-separation filters to remove cell clumps that could potentially clog the columns. In addition, DNase I digestion was performed on the cell suspension to reduce non-specific binding and cell clumping caused by free DNA. Cells were treated with 200 U/mL DNase I diluted in 5 mL of DMEM+10%FBS for 5 min at RT. Subsequently, the samples were washed with 15 mL DMEM+10%FBS and subjected to separation. Cells and buffer were kept cold (4 °C) throughout the entire separation protocol.

Only one attempt of removing non-specific binding material prior to separation was conducted (see Appendix Figure 8.1), using *Basic MicroBeads* following the manufacturer's protocol:

1. Up to 1×10^7 cells were resuspended in 50 µL of selection buffer M.
2. Addition of 5 µL of pre-diluted (1:10) *Basic MicroBeads*/1×10^7 cells and incubation for 15 min at 4 °C.
3. Wash step by adding 2 mL of selection buffer M per 1×10^7 cells and centrifugation at 300× g for 5 min.
4. The cell pellet (up to 1×10^8 cells) was resuspended in selection buffer M to a total volume of 500 µL.
5. The sample was placed into the tube rack in the autoMACS® Pro Separator and subjected to the sensitive single-column depletion program *DepleteS* (loading rate of 1 mL/min) and the wash program *Rinse*.

6. The negative fraction, which contained the unbound cells, was then used for the separation protocols.

All other separations shown in the results section below were performed without the prior use of *Basic MicroBeads*.

For MACS® negative selection (labeling of fibroblasts), two different MACS® *MicroBeads* were tested.

(a) *Anti-PE MicroBeads* in combination with a PE-conjugated anti-CD90 antibody (clone DG3) were used according to the manufacturer's protocol, with minor adjustments:

1. Up to 1×10^7 cells were resuspended in selection buffer M, reaching a total volume of 200 µL (instead of 100 µL/1×10^7 cells).
2. Addition of 16 µL PE-conjugated anti-CD90 antibody/1×10^7 cells meaning 8 µg/mL antibody (instead of 2 µL/1×10^7 cells meaning 2 µg/mL) and incubation for 10 min at 4 °C protected from light.
3. Wash step with centrifugation at 300× g for 5 min and resuspending of cell pellet in selection buffer M to a total volume of 120 µL (instead of 80 µL/1×10^7 cells).
4. Due to the high number of anti-CD90 bound fibroblasts to be captured, the number of magnetic beads was increased four-fold. Specifically, 80 µL of *Anti-PE MicroBeads*/1×10^7 cells (instead of 20 µL/1×10^7 cells) were added and incubated for 15 min at 4 °C protected from light.
5. Wash step with centrifugation at 300× g for 5 min and resuspending of cell pellet in 1 mL of selection buffer M (instead of 500 µL).
6. The sample was placed into the tube rack in the autoMACS® Pro Separator and subjected to the single-column depletion program *Deplete* (loading rate of 4 mL/min) and the wash program *Rinse*.

(b) *CD90 MicroBeads* were used following the manufacturer's instructions, with slight modifications. Changes to the protocol included:

1. Up to 1×10^7 cells were resuspended in selection buffer M, reaching a total volume of 20 µL (instead of 80 µL/1×10^7 cells).
2. Due to the high number of fibroblasts to be captured, the number of magnetic beads was increased four-fold. Specifically, 80 µL of *CD90 MicroBeads*/1×10^7 cells (instead of 20 µL/1×10^7 cells) were added and incubated for 15 min at 4 °C.
3. Wash step with centrifugation at 300× g for 5 min and resuspending of cell pellet in 1 mL of selection buffer M (instead of 500 µL).

4. The sample was placed into the tube rack in the autoMACS® Pro Separator and subjected to the single-column depletion program *Deplete* (loading rate of 4 mL/min) or the more sensitive program *DepleteS* (loading rate of 1 mL/min), and the wash program *Rinse*.

For MACS® positive selection (labeling of DSCs), the *Neural Crest Stem Cell (NCSC) MicroBeads*, which are conjugated to anti-NGFRp75 antibodies, were used according to the manufacturer's protocol, with slight adjustments:

1. Up to 1×10^7 cells were resuspended in selection buffer M, reaching a total volume of 160 µL (instead of 80 µL/1×10^7 cells).
2. Addition of 40 µL *NCSC MicroBeads*/1×10^7 cells (instead of 20 µL/1×10^7 cells) and incubation for 15 min at 4 °C.
3. Wash step with centrifugation at 300× g for 5 min and resuspending of cell pellet in 1 mL of selection buffer M (instead of 500 µL).
4. The sample was placed into the tube rack in the autoMACS® Pro Separator and subjected to the double-column positive separation program *Posseld2* (loading rate of 4 mL/min) and the wash program *Rinse*.

Upon completion of the separation process, the autoMACS® Pro Separator collected two separate fractions: the negative cell fraction consisted of unlabeled cells that passed through the column without binding, whereas the positive cell fraction comprised the magnetically labeled cells (Figure 4.1). Subsequently, the fraction containing the enriched DSCs was further cultivated for approximately 10–12 days. The proportion of DSCs and fibroblasts in the culture was measured via flow cytometric staining of NGFRp75 and CD90 (see section 4.6.2.1) before, immediately after separation, and after several days of cultivation, to monitor whether fibroblasts were growing back in the purified DSC culture.

4.3 UV Irradiation

4.3.1 Irradiation Device

The UVA and the UVB sources used in these studies are part of a custom-made, patented solar simulating irradiation device (patent number 10 2022 102 915.8) that combines four different radiation sources (IR-A, visible light, UVA, UVB) with irradiances similar to the solar spectrum [402] (Figure 4.2). The lamps are arranged one above the other and can be regulated individually, thereby allowing different irradiation combinations to mimic different exposure

conditions. In this study, only UVA or UVB were used separately, therefore the IR-A and visible light sources are not considered further.

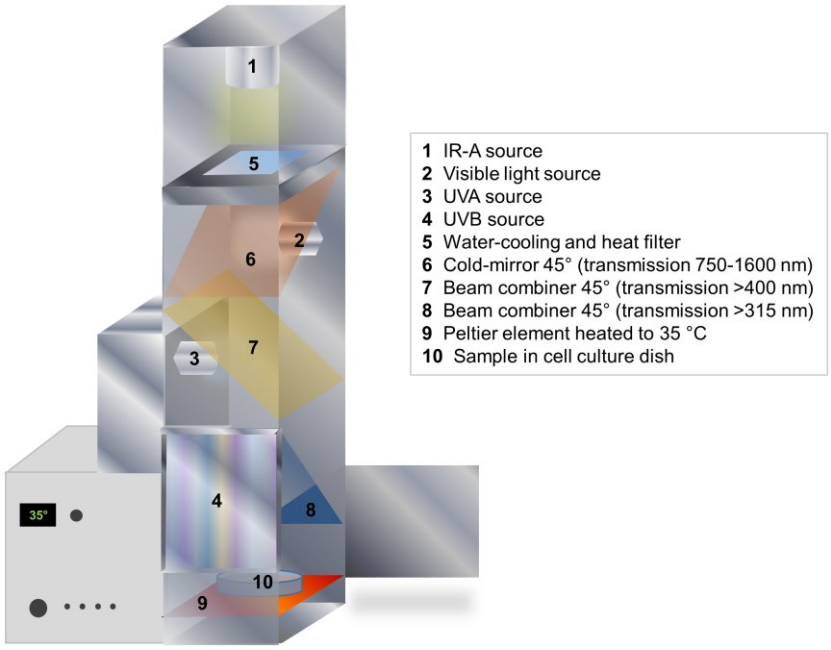

Figure 4.2 Schematic construction of the irradiation device. The solar simulating combination lamp includes radiation sources for IR-A, visible light, UVA, and UVB. The irradiance of each spectral band is similar to the solar spectrum. Different dichroic beam combiners and optional filters were used for the individual lamps [402]. The sample was placed centered at the bottom of the device on a heated Peltier element. By courtesy of Bente Siebels [403].

Different dichroic beam combiners/mirrors and optional filters (optical and metal mesh) were utilized to control the spectral ranges of the individual lamps (Table 4.3). For UVB irradiation, four units of PL-S 9W/12 2P UVB broadband tubes (Philips) were used. The UVB lamp was filtered with an Asahi Spectra UV325 short-pass filter to reduce the UVA radiation of the UVB source. Additionally, a Schott B270 UVB long-pass filter was used to filter out any UVC radiation (wavelengths <295 nm). A custom-made 315 nm (45°) beam combiner deflected the emission of the UVB lamp to the sample.

Table 4.3 Radiation sources and filters. [402]

Lamp	Source	Filters
UVA	Philips HPA CLEO flexpower 440 W	- Metal mesh filter - Schott WG 320 nm long-pass (UVB filter)
UVB	4× Philips PL-S 9W/12 2P	- Metal mesh filter - Schott B270 long-pass (UVC filter) - Asahi Spectra UV325 short-pass (UVA filter)

For UVA exposure, an HPA CLEO flexpower 440 W high-pressure lamp (Philips) was used. The UVA lamp was filtered with a Schott WG 320 nm long-pass filter to prevent cross-contamination with small amounts of UVB emitted from the UVA lamp [402]. A custom-made

400 nm (45°) beam combiner was used to deflect the emitted UVA radiation to the sample. In front of both UVA and UVB lamp, metal mesh filters with defined open apertures were incorporated.

For irradiation, the samples were placed centered at the bottom of the irradiation device on a heated Peltier element to maintain a constant temperature of 35 °C during irradiation (Figure 4.2). The homogeneous irradiation area of 17 cm × 17 cm allowed for the simultaneous irradiation of multiple cell culture dishes. Depending on the size, eight (35 mm diameter), four (60 mm), or two (94 mm) cell culture dishes could be irradiated at the same time.

4.3.2 Cell Preparation for Irradiation

Cells were seeded in cell culture dishes and cultured until they reached 80–90% confluency. The cell culture medium was aspirated and cells were washed once with $PBS^{-/-}$. To prevent cells from drying out during irradiation, 1, 3, or 5 mL of $PBS^{-/-}$ were added, depending on the size of the cell culture dish (35, 60, or 94 mm diameter, respectively). Control cells were treated analogously, but maintained at 35 °C in darkness for the duration of irradiation.

4.3.3 Irradiation of Cells

The irradiation protocols for the different experiments are listed in Table 4.4, including details on the spectral band, dose, irradiance, and time of analysis post-irradiation.

Table 4.4 Irradiation protocols.

Experiment	Spectral band	Dose *H*	Irradiance *E*	Time of analysis (post-irradiation)
CPD induction	UVB	285, (400) J/m²	0.713 W/m²	0 h
Repair kinetics	UVB	285, (400) J/m²	0.713 W/m²	0, 24, 48, 72, 96 h
Remaining DNA damage	UVB	285, (400) J/m²	0.713 W/m²	96 h
Cell cycle	UVB UVA	300, 900 J/m² 37, 74 kJ/m²	0.705 W/m² 39.16 W/m²	0, 16, 24, 48, 72 h
Apoptosis	UVB UVA	300, 900 J/m² 37, 74 kJ/m²	0.705 W/m² 39.16 W/m²	24, 48 h
Differentiation	UVB UVA	300 J/m² 37 kJ/m²	0.669 W/m² 36.71 W/m²	3, 10, 16 days of differentiation
Sphere formation	UVB UVA	300, 3×100, 900, 3×300 J/m² 37, 3×12.33, 74, 3×24.67 kJ/m²	0.669 W/m² 36.71 W/m²	48 h + additional 5 days in suspension
miRNAs	UVB UVA	300 J/m² 37 kJ/m²	0.669 W/m² 36.71 W/m²	6, 24 h

CPD induction, Repair kinetics, and Remaining DNA damage: DSC-fibroblast co-cultures, fibroblasts, and keratinocytes were irradiated with a single UVB dose of 285 J/m². Melanocytes, on the other hand, were exposed to two different doses of either 285 or 400 J/m² UVB, as the lower dose was insufficient to induce the same amount of CPDs as in the other cell types. Cells were harvested either directly after irradiation (0 h) or after further cultivation for 24, 48, 72, and 96 h. As negative controls, non-irradiated cells collected at 0 h and 96 h post sham-irradiation were included in the study.

Cell cycle: DSC-fibroblast co-cultures, fibroblasts, melanocytes and keratinocytes were irradiated with a single dose of 300 J/m² or 900 J/m² UVB, or with 37 kJ/m² or 74 kJ/m² UVA. Cells were harvested either directly after irradiation (0 h) or after further cultivation for 16, 24, 48, and 72 h. For every time point, non-irradiated cells served as negative controls.

Apoptosis: DSC-fibroblast co-cultures, fibroblasts, melanocytes and keratinocytes were irradiated with a single dose of 300 J/m² or 900 J/m² UVB, or with 37 kJ/m² or 74 kJ/m² UVA. Cells treated with 1 µM staurosporine for 3 h, a commonly used inducer of apoptosis, served as positive controls. Irradiated and staurosporine-treated cells were harvested after further cultivation for 24, and 48 h. For every time point, non-irradiated cells served as negative controls.

Differentiation: DSC-fibroblast co-cultures and purified DSCs were irradiated with a single dose of 300 J/m² UVB or 37 kJ/m² UVA one day before starting the differentiation. Cells were harvested on days 3, 10, and 16 of differentiation. As controls, non-irradiated cells in stem cell medium and non-irradiated cells in differentiation medium were included for every time point.

Sphere formation: Naturally enriched DSC-fibroblast co-cultures (cultures with naturally high number of DSCs) were irradiated as monolayer culture with 300 J/m², 3×100 J/m², 900 J/m², or 3×300 J/m² UVB, or with 37 kJ/m², 3×12.33 kJ/m², 74 kJ/m², or 3×24.67 kJ/m² UVA, harvested after 48 h, and further cultivated for 5 days in suspension culture. Non-irradiated cells served as controls.

microRNAs: Naturally enriched DSC-fibroblast co-cultures, purified DSCs, and melanocytes were irradiated with a single dose of 300 J/m² UVB or 37 kJ/m² UVA. Cells were lysed for miRNA analysis after further cultivation for 6 and 24 h. For every time point, non-irradiated cells served as controls. Non-irradiated melanoma cells were included for comparison.

4.4 Differentiation of DSCs into Melanocytes

4.4.1 Differentiation for Characterization

Differentiation assay was performed as previously described [31,125,126,398] with minor modifications. DSC-fibroblast co-cultures and purified DSCs were grown in BME-coated cell culture dishes (35 mm diameter) to 80–90% confluency. To start the differentiation, stem cell medium was replaced with freshly prepared melanocyte differentiation medium (Table 3.5), and cells were maintained for 2–3 weeks with medium changes twice a week (alternating between half and full medium change). Control cells were cultivated in stem cell medium for the same period and were treated analogously. The differentiation progress was monitored via light microscopy, immunocytochemistry (see section 4.6.1), and gene expression analysis (see section 4.7) at different times.

4.4.2 Differentiation after UV Irradiation

For irradiation experiments, upon 80–90% confluency, DSC-fibroblast co-cultures and purified DSCs grown in BME-coated cell culture dishes (35 mm diameter) were irradiated with a single dose of 300 J/m² UVB or 37 kJ/m² UVA (day -1), and subsequently cultured for another day in stem cell medium. Non-irradiated cells for differentiation and control cells were supplied with fresh stem cell medium. On the next day, cells were provided with freshly prepared melanocyte differentiation medium (Table 3.5) and maintained for 16 days with medium changes twice a week (alternating between half and full medium change). On days 3, 10, and 16, cells were monitored via light microscopy (Olympus CKX53 microscope with integrated camera and the EHDView software) and lysed for gene expression analysis (see section 4.7). Non-irradiated control cells for normalization were cultured in stem cell medium for the same period and were treated analogously.

4.5 Sphere Formation Assay

4.5.1 Sphere Formation for Characterization

The formation of spheres was examined using a DSC-fibroblast co-culture (17% DSCs), a MACS®-purified population from the same donor cell strain (87% DSCs), and two different fibroblast cultures. The adherently growing cells were enzymatically dissociated, filtered through a 40 µm cell strainer, and recultured in stem cell medium in suspension culture flasks. The two DSC samples were seeded with 2×10^6 cells, while the fibroblast strains were seeded

with 0.8×10^6 cells (#1) and 1.1×10^6 cells (#2). Sphere formation was monitored via light microscopy (Olympus CKX53 microscope with integrated camera and the EHDView software) for six days.

4.5.2 Sphere Formation after UV Irradiation

Naturally enriched DSC cultures with high stem cell proportions of 49%, 65%, and 89% were grown as monolayer in BME-coated cell culture dishes (94 mm diameter) to 80–90% confluency. Cells were irradiated once or multiple times with different doses of UVA or UVB (Figure 4.3). Multiple irradiations with 3×100 J/m² or 3×300 J/m² UVB, or with 3×12.33 kJ/m² or 3×24.67 kJ/m² UVA were carried out on three consecutive days. Single irradiation with 300 J/m² or 900 J/m² UVB, or with 37 kJ/m² or 74 kJ/m² UVA was conducted on the last day of the multiple irradiations schedule. Non-irradiated cells served as controls.

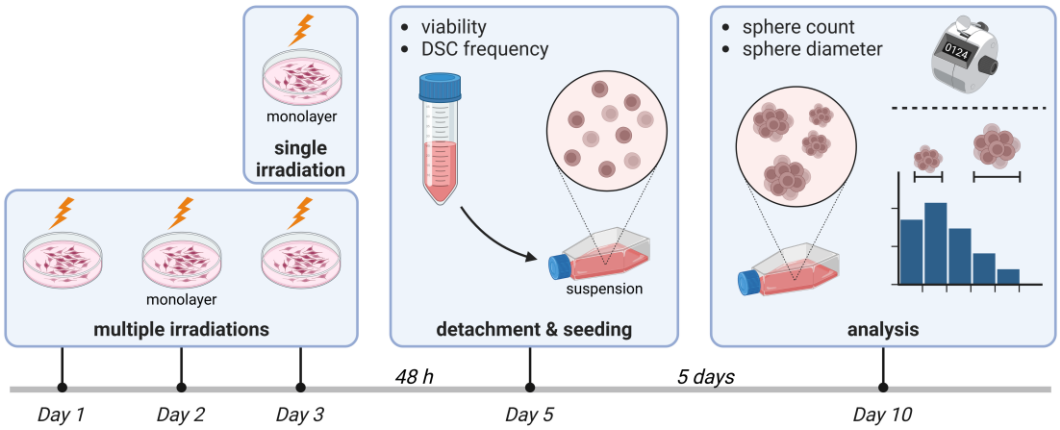

Figure 4.3 Schematic setup of the 'sphere formation after UV irradiation' experiment. DSC cultures were irradiated once or multiple times with different doses of UVA and UVB on three consecutive days. After 48 h, cells were detached and viability of DSCs as well as the DSC frequency were measured. Cells were seeded in suspension culture flasks and cultivated for five days. Formed spheres were analyzed for number of spheres and size (created with BioRender.com).

After 48 h following the last irradiation, cells were detached and viability of DSCs as well as the stem cell proportion were measured via flow cytometry (see section 4.6.2.6). Based on these data, in a multiple-cell plating approach [404], equal amounts of viable NGFRp75$^+$ cells were seeded in suspension culture flasks (2×10^6 cells for two donor cell strains and 0.6×10^6 cells for the third donor cell strain due to lower cell numbers). After five days of cultivation in suspension, for each sample, spheres were transferred to a 96-well flat-bottom ELISA microplate and allowed to settle for at least 5 min. From each well, pictures were taken at three predefined spots to count the number of spheres and to measure their size (diameter). The diameter of spheres was determined using digital image processing with an ImageJ macro that measured the area of each sphere. If necessary, the detection of the spheres was manually

corrected. Using the formula $d = 2 \cdot \sqrt{A/\pi}$, the area *A* was then calculated back to the diameter *d*. Only cell clusters with a diameter ≥25 µm were considered as spheres.

Statistical analysis was conducted in SigmaPlot 13.0 with multiple comparisons versus the control with One-way ANOVA followed by Dunnett's method. For viability results, the percentage of viable cells was used for statistics and depiction. The proportion of DSCs in the samples is displayed as binary logarithm of the fold change ($\log_2$(FC)) of DSC frequency, but for statistical analysis, fold changes (FC) were used instead of $\log_2$(FC). Statistics for sphere counts were performed using the raw counts, while the results are shown as relative values obtained through normalization relative to the respective control for each donor cell strain separately, followed by calculating the mean of all three donors. Regarding the size distribution of formed spheres, results are displayed as histogram showing the percentage of DSC spheres divided into defined ranges of 25 µm diameter, whereas statistics for sphere diameter were conducted with raw counts as well.

4.6 Immunostaining and Imaging

4.6.1 Immunocytochemistry

Cells grown on glass coverslips were washed with $PBS^{-/-}$ and fixed with ice-cold methanol and acetone for 5 min each at -20 °C. Slides were blocked with 3% BSA in PBS containing 0.9 mM Ca^{2+} and 0.5 mM Mg^{2+} ($PBS^{+/+}$) followed by 5% goat serum in $PBS^{-/-}$ both for 30 min at RT. Cells were incubated with primary antibodies specific for CD90 (clone AS02, 1 µg/mL), HMB45 (2 µg/mL), Melan-A (clone A103, 2 µg/mL), NGFRp75 (clone EP1039Y, 3 µg/mL), Pan-keratin (clone PAN-CK, 4 µg/mL), and TRP2 (clone C-9, 2 µg/mL) (Table 3.7) diluted in 3% BSA/$PBS^{+/+}$ for 2 h at 37 °C or overnight at 4 °C. After washing the slides with $PBS^{-/-}$, 4 µg/mL secondary anti-mouse and anti-rabbit antibodies conjugated to Alexa Fluor 488 or 594, respectively (Table 3.8), were incubated for 1 h at 37 °C. Finally, cells were washed with $PBS^{-/-}$, counterstained with 0.1 µg/mL DAPI for 5 min at RT, and again rinsed with $PBS^{-/-}$. Samples were embedded in Mowiol mounting medium, and examined using a Leica DMRB fluorescence microscope. Fluorescent images were taken with a DX40C-285FW camera and the Kappa Camera Control software.

4.6.2 Flow Cytometry

4.6.2.1 NGFRp75 and CD90 Staining of DSCs

Around 30,000–50,000 cells per sample were incubated with 0.3 µg/mL APC-conjugated recombinant anti-NGFRp75 antibody (clone REA844) and 0.5 µg/mL PE-conjugated mouse anti-CD90 antibody (clone 5E10) diluted in 50 µL FACS buffer for 10 min at 4 °C protected from light. Afterwards, 100 µL FACS buffer and 1 µg/mL propidium iodide were added to exclude dead cells. Samples were transferred to a 96-well microplate for measurement of 10,000 cells per sample via flow cytometry. The proportion of NGFRp75^{+} cells represented the frequency of DSCs.

4.6.2.2 Doubling Time

Dissociated cell cultures were seeded with a defined cell count in cell culture dishes (60 mm diameter) in cell-specific medium. DSC-fibroblast co-cultures, purified DSC cultures (both on BME-coating), melanocytes, and keratinocytes were seeded at a density of 8.9 × 10³ cells/cm², while fibroblasts were seeded with 9.3 × 10³ cells/cm². Starting the following day, biological replicates were harvested at four time points with an interval of 24 hours each. After detachment according to the cell-specific protocols (Table 4.2), cells were collected in a total volume of 5 mL. From each sample, three times 750 µL were transferred to 1.5 mL reaction tubes and centrifuged for 10 min at 200× g. Next, 700 µL of the supernatant was discarded and 100 µL PBS$^{-/-}$ was added to resuspend the cell pellet. Cell concentration was determined via flow cytometry measuring 20,000 cells. To distinguish between DSCs and fibroblasts in DSC cultures, they were additionally stained with 0.3 µg/mL APC-conjugated recombinant anti-NGFRp75 antibody (clone REA844) diluted in PBS$^{-/-}$ for 10 min at 4 °C protected from light prior to measurement.

For evaluation, each sample's technical triplicates were averaged to the cell count c. The natural logarithm of the cell count $\ln(c)$ of biological replicates was plotted against time, and a linear fit was applied for the exponential growth phase. Using the growth rate µ, which corresponds to the slope of the fit, the doubling time was calculated with the formula $t_d = \frac{\ln(2)}{\mu}$.

4.6.2.3 Evaluation of DNA Damage (CPDs)

Irradiated samples (285 J/m² or 400 J/m² UVB) and non-irradiated control samples from DSC-fibroblast co-cultures, fibroblasts, melanocytes, and keratinocytes were harvested at various

times (0, 24, 48, 72, and 96 h after (sham-)irradiation) according to the cell-specific protocol (Table 4.2), washed with $PBS^{-/-}$, and fixed overnight with ice-cold 70% ethanol at -20 °C. Staining for CPDs was carried out in a 96-well microplate with intermediate centrifugation at 500× g for 3 min, discarding the supernatant by overturning the microplate with a swift motion. First, 2.5×10^5 cells were rehydrated in tris-buffered saline (TBS) and then permeabilized for 10 min at RT in 1× Roti®Block blocking and washing solution containing 0.125% Triton X-100 (Roti®Block-Triton). For denaturation of DNA, cells were resuspended in 2 M HCl for 10 min at RT. Washing one time with Roti®Block-Triton and two times with $PBS^{+/+}$ was followed by a 10-minute incubation with 5 µg/mL (= 0.15 U/mL) proteinase K at 37 °C and 400 rpm in a plate thermo-shaker. Samples were again washed, one time with $PBS^{+/+}$ and two times with Roti®Block-Triton. The cells were incubated with 1 µg/mL mouse anti-CPD antibody (clone KTM53) in Roti®Block-Triton overnight at 4 °C and 150 rpm on a platform shaker. The next day, cells were washed two times with Roti®Block-Triton and then incubated with 15 µg/mL FITC-conjugated goat anti-mouse antibody in Roti®Block-Triton for 1 h at 37 °C and 400 rpm in a plate thermo-shaker. Samples were washed two times with Roti®Block-Triton and finally stained for 5 min at RT with 10 µg/mL propidium iodide in 0.01% RNase A. At least 5000 cells per sample were measured via flow cytometry. DSC-fibroblast co-cultures and fibroblast cultures were co-stained with 3 µg/mL rabbit anti-NGFRp75 antibody (clone EP1039Y) and 5 µg/mL APC-conjugated goat anti-rabbit antibody to exclude the undesired population in the respective cell culture when analyzing the measurement. For DSC-fibroblast co-cultures, the assessment exclusively focused on $NGFRp75^+$ cells. Conversely, in fibroblast cultures, the analysis was restricted to $NGFRp75^-$ cells.

Analysis of data and statistical computations were executed using Flowing Software 2.5.1, SigmaPlot 13.0, and R 3.5.1 or higher (https://www.r-project.org/). Only cells within the G1 phase were examined in order to exclude dividing cells with greater DNA content and doublets that may distort the results. The assessment of DNA damage induction was accomplished by quantifying the CPD content immediately post-exposure. CPD levels at the indicated points of time were used to analyze repair capacities, with the fitting of an exponential decay as a function of time ($N(t) = N_i \cdot e^{-\frac{t}{\tau}}$) providing an evaluation of the repair time constant τ. The repair time constant denotes the duration when the initially induced CPD amount diminished to 1/e, equivalent to 37%. Unrepaired DNA damage was measured by detecting CPDs 96 h after irradiation, relative to the initial CPD induction.

An ANOVA was performed on all data on CPD induction, repair time constant, and remaining damage. Data were checked for homogeneity of variance of residuals with Levene test and for normal distribution of residuals with Shapiro-Wilk test. Due to the normal distribution of the data sets, a pairwise *t*-test was employed to compare each cell type against the basemean (mean of all groups). In the examination of remaining DNA damage, no post-hoc tests were applied since ANOVA was not significant.

4.6.2.4 Cell Cycle Analysis

Measurement of the cell cycle phases was done through quantification of the DNA content via staining with the nucleic acid dye propidium iodide (PI). PI intercalates stoichiometrically into the cellular DNA, resulting in a fluorescence signal that is directly proportional to the DNA content [405].

DSC-fibroblast co-cultures, fibroblasts, melanocytes, and keratinocytes in 35 mm cell culture dishes were irradiated with a single dose of 300 J/m² or 900 J/m² UVB, or with 37 kJ/m² or 74 kJ/m² UVA. Non-irradiated cells served as controls. Cells were harvested after 0, 16, 24, 48, and 72 h according to the cell-specific protocol (Table 4.2), washed with $PBS^{-/-}$, and fixed overnight with ice-cold 70% ethanol at -20 °C. Staining of DNA was carried out in a 96-well microplate with intermediate centrifugation at 500× g for 3 min, discarding the supernatant by overturning the microplate with a swift motion. The staining protocol of DSC-fibroblast co-cultures differed from that of fibroblasts, melanocytes, and keratinocytes.

DSC-fibroblast co-cultures: At first, 2.8×10^5 cells were rehydrated in TBS and subsequently permeabilized in Roti®Block-Triton for 45 min at 4 °C. Cells were stained with 3 µg/mL rabbit anti-NGFRp75 antibody (clone EP1039Y) in Roti®Block-Triton for 1 h at 37 °C and 400 rpm in a plate thermo-shaker. Following two wash steps with Roti®Block-Triton, the samples were incubated with 5 µg/mL APC-conjugated goat anti-rabbit antibody in Roti®Block-Triton for 45 min at 37 °C and 400 rpm in a plate thermo-shaker. Cells were again washed two times with Roti®Block-Triton, and finally stained for 10 min at RT with 10 µg/mL propidium iodide in 0.01% RNase A, prior to measurement of 30,000 cells via flow cytometry.

Fibroblasts, melanocytes, keratinocytes: At first, 2.8×10^5 cells were rehydrated in TBS and subsequently permeabilized in Roti®Block-Triton for 5 min at RT. Finally, samples were incubated for 15 min at RT with 10 µg/mL propidium iodide in 0.01% RNase A, prior to measurement of 20,000 cells via flow cytometry.

Fitting of the cell cycle phases was done with ModFit LT 4.1 and a G1/G2 ratio of 1.9. DSC-fibroblast co-cultures were gated on NGFRp75^{+} cells in advance to exclude contaminating fibroblasts. Statistical analysis was performed in R 4.2.3 or higher. Differences were tested for significance with One-way ANOVA followed by Dunnett's test from R's DescTools package against non-irradiated controls for various factor combinations. Bonferroni adjustment was applied afterwards. Data was log-transformed before statistical testing as residual analysis revealed approximation of a normal distribution of model residuals after log-transformation.

4.6.2.5 Apoptosis Assay

Induction of apoptosis was measured via Annexin-V/PI staining combined with flow cytometric analysis. Annexin-V detects exposure of phosphatidylserine residues which are translocated to the outer layer of the plasma membrane via phospholipid scramblases during the early apoptotic process as an 'eat me' signal for macrophages [406,407]. Additional intake of the membrane-impermeant nucleic acid dye propidium iodide marks late apoptotic or necrotic cells that lost their membrane integrity [408].

DSC-fibroblast co-cultures, fibroblasts, melanocytes, and keratinocytes in 35 mm cell culture dishes were irradiated with a single dose of 300 J/m² or 900 J/m² UVB, or with 37 kJ/m² or 74 kJ/m² UVA. Non-irradiated cells served as controls. Cells treated with 1 µM staurosporine for 3 h served as positive controls. At 24 h and 48 h after irradiation or staurosporine treatment, cell culture supernatants were collected and cells were harvested according to the cell-specific protocol (Table 4.2). Harvested cells and supernatants were combined with a ratio of 0.5×10^5 cells plus half of the supernatant. A wash step in PBS$^{-/-}$ with centrifugation at 200× g for 10 min was followed by incubation in 50 µL Annexin staining solution for 15 min at RT protected from light. DSCs were simultaneously also stained with 0.3 µg/mL APC-conjugated recombinant anti-NGFRp75 antibody (clone REA844) to distinguish between DSCs and contaminating fibroblasts. Afterwards, 100 µL Annexin incubation buffer was added and samples were transferred to a 96-well microplate for measurement of 10,000 cells per sample via flow cytometry. The proportion of total apoptotic cells (early + late) and the proportion of NGFRp75^{+} cells, representing the DSC frequency, were evaluated with Guava® InCyte™ 3.1.

Statistical analysis of apoptotic cells was performed in R 4.2.3 or higher. Differences were tested for significance with One-way ANOVA followed by Dunnett's test from R's DescTools package against non-irradiated controls for various factor combinations. Bonferroni adjustment

was applied afterwards. Data was log-transformed before statistical testing as residual analysis revealed approximation of a normal distribution of model residuals after log-transformation.

Statistical analysis of DSC frequency was conducted in SigmaPlot 13.0 with multiple comparisons versus the control with One-way ANOVA followed by Dunnett's method. The proportion of DSCs was displayed as $\log_2$(FC) of DSC frequency, but for statistical analysis, fold changes were used instead of the binary logarithm of FC.

4.6.2.6 Viability Assay

Cell viability for the sphere formation assay was measured using *Guava® ViaCount™ Reagent*, which allows distinguishing viable and apoptotic/dead cells based on differential permeabilities of two DNA-binding dyes. The nuclear dye permeates all membranes and thereby stains all nucleated cells, while the viability dye only enters cells through defective membranes and therefore stains dying cells.

DSCs were harvested and 1×10^5 cells were resuspended in 15 µL $PBS^{-/-}$ plus 35 µL *Guava® ViaCount™ Reagent* containing 0.3 µg/mL APC-conjugated recombinant anti-NGFRp75 antibody (clone REA844). Samples were incubated for 10 min at RT protected from light. After addition of 100 µL *Guava® ViaCount™ Reagent* and further incubation for another 5 min, at least 20,000 cells per sample were measured via flow cytometry. Gated on $NGFRp75^+$ cells beforehand, the proportion of viable cells was evaluated with Guava® InCyte™ 3.1. Statistical analysis was performed in R 4.2.3 with multiple comparisons versus the control with One-way ANOVA followed by Dunnett's method, using the proportions of viable cells.

4.7 Transcriptional Analysis

Gene expression was measured using the qPCR method. Initially, the isolated mRNA was converted into cDNA through reverse transcription. Then, the relative number of transcripts was determined in a quantitative real-time approach.

4.7.1 RNA Isolation

Cells were lysed for gene expression analysis by washing with $PBS^{-/-}$ and then adding 400 µL of the lysis buffer from the RNA extraction kit directly to the cells in the cell culture dish. The cells were scraped off with a cell scraper, transferred to a 1.5 mL reaction tube and stored at -70 °C until further processing. Total RNA was extracted using *peqGOLD Total RNA Kit* including a DNase I digestion step using the *peqGOLD DNase I Digest Kit* according to the manufacturer's protocols. Briefly, the lysate was loaded onto a DNA Removing Column and

centrifuged at 12,000× g for 1 min. The filtrate was mixed with an equal volume of 400 µL 70% ethanol, loaded onto a PerfectBind RNA Column and centrifuged at 10,000× g for 1 min. The filtrate was discarded, as was the case with all subsequent centrifugation steps. The column was washed with 500 µL RNA Wash Buffer I, with centrifugation at 10,000× g for 15 s. Next, a DNase I digestion step was performed with 73.5 µL DNase I Digestion Buffer plus 1.5 µL RNase-free DNase I (20 Kunitz units/µL) for 15 min at RT, followed by addition of 400 µL RNA Wash Buffer I and another 5-minute incubation at RT. The column was centrifuged at 10,000× g for 15 s, and washed two times with 600 µL RNA Wash Buffer II. To completely dry the column matrix, the empty column was centrifuged at 10,000× g for 2 min. For elution of RNA, the column was placed into a fresh 1.5 mL reaction tube and 35–80 µL preheated (70 °C) PCR-H_2O, depending on the input of cells, were added to the column, incubated for 5 min, and centrifuged at 5,000× g for 1 min. The eluted RNA was stored at -70 °C.

4.7.2 Determination of RNA Concentration

The concentration of the RNA was determined photometrically by measuring the UV absorption at a wavelength of 260 nm (OD_{260}). First, a blank measurement was conducted with 5 µl PCR-H_2O + 60 µL TE buffer (1×). To measure the RNA samples, 5 µL of the sample were diluted with 60 µL of TE buffer (1×). One OD_{260} unit corresponded to 40 µg/mL RNA. The quality and degree of purity of the RNA were assessed with the OD_{260}/OD_{280} ratio and the OD_{260}/OD_{230} ratio.

4.7.3 Reverse Transcription

cDNA was synthesized with *SensiFAST™ cDNA Synthesis Kit*, which uses oligodT- and random-hexamer-primers for transcription. Between 0.3–1.0 µg of RNA was used as starting material and the synthesis was carried out according to the manufacturer's instructions. The protocol for the reaction mixture is displayed in Table 4.5 and the thermocycler program is shown in Table 4.6.

Table 4.5 Reaction mixture for reverse transcription.

Component	Volume [µL]
5× TransAmp Buffer	4
Reverse transcriptase	1
RNA (0.3–1.0 µg)	n
PCR-H_2O	15-n
Total	20

Table 4.6 Reverse transcription thermocycler program.

Step	Temperature	Duration
Primer annealing	25 °C	10 min
Reverse transcription	42 °C	15 min
Incubation	48 °C	15 min
Inactivation	85 °C	5 min

Finally, the reaction product was diluted 1:2.5 with 30 µL PCR-H_2O (at low input of 0.3 µg RNA) or 1:5 with 80 µL PCR-H_2O (at high input of up to 1 µg RNA) and stored at a temperature of -20 °C.

4.7.4 Quantitative PCR

Real-time quantitative polymerase chain reaction (RT-qPCR) was performed using *SensiMix™ SYBR No-ROX Kit* and gene-specific primers for FRZB, MITF, MSX1, nestin, NGFRp75, TRP1, TRP2, and tyrosinase (Table 3.9). Forward and reverse primers were utilized as an equimolar solution. The protocol for the qPCR reaction mixture is displayed in Table 4.7 and the qPCR thermocycler program is shown in Table 4.8.

Table 4.7 Reaction mixture for qPCR.

Component	Volume [µL]
SensiMix™ SYBR No-ROX (2×)	10
Primer [3 µM]	2
cDNA template	5
PCR-H_2O	3
Total	20

Table 4.8 qPCR thermocycler program.

PCR step		Temperature	Duration
Initial denaturation		95 °C	10 min
Denaturation	45 cycles	95 °C	15 s
Annealing		61.5 °C	20 s
Extension		72 °C	20 s
Melting curve		60–95 °C	10 min (ΔT 1 °C every 15 s)

For the qPCR program, 45 cycles and an annealing temperature of 61.5 °C were used as standard. Different combinations of the three reference housekeeping genes ACTB (β-actin), HPRT1 (hypoxanthine phosphoribosyltransferase 1), and TBP (TATA-binding protein) were used for normalization. Data analysis was conducted using qPCRsoft 4.1 by quantifying relative

to the controls using the $\Delta\Delta C_t$ method [409]. The relative changes in gene expression to the controls are depicted as binary logarithm, termed $\log_2$(fold change).

Characterization of DSCs: The gene expression analysis within dermal spheres (Figure 5.1B), in DSC-fibroblast co-cultures, and fibroblast cultures (Figure 5.8C) included NCSC genes NGFRp75, nestin, MSX1, FRZB. Data were normalized to HPRT1 and TBP. The calculation of fold changes was conducted relative to foreskin-derived melanocytes. An additive two-way ANOVA was performed. Data were checked for homogeneity of variance of residuals by Levene test, and for normal distribution of residuals by Shapiro-Wilk test. Given the normal distribution of the data sets, the comparison between the cell types for each gene was assessed using a t-test.

Differentiation of DSCs into melanocytes: Gene expression analysis of NGFRp75 and melanocytic markers MITF, tyrosinase, TRP1, and TRP2 as part of the differentiation assay (Figure 5.11D and Figure 5.18) included the reference housekeeping genes ACTB and TBP for normalization. Fold changes were calculated relative to (non-irradiated) DSCs grown in stem cell medium for the same time period (control cells).

4.8 MicroRNA Analysis

The miRNA expression was examined using one naturally enriched DSC-fibroblast co-culture (93% DSCs), two MACS®-purified DSC cultures (both 97%), two melanocyte cell strains, and three melanoma cell cultures. DSCs and melanocytes were irradiated with a single dose of 300 J/m² UVB or 37 kJ/m² UVA, and cells were lysed for miRNA expression analysis after 6 and 24 h. Non-irradiated cells served as controls. Melanoma cells were not irradiated.

4.8.1 MicroRNA Isolation

Cells were lysed by washing with $PBS^{-/-}$ and then adding 700 µL of QIAzol® Lysis Reagent from the miRNA extraction kit directly to the cells in the cell culture dish. The cells were scraped off with a pipette tip, transferred to a 1.5 mL reaction tube and stored at -70 °C until further processing. miRNA was extracted using *miRNeasy Mini Kit* (without a DNase digestion step) according to the manufacturer's protocol.

Briefly, the thawed cell lysate was incubated for 5 min at RT before addition of 140 µL chloroform. The sample was shaken for 15 s and incubated for 3 min at RT, followed by centrifugation at 4 °C at 12,000× g for 15 min. Next, 300 µL of the upper aqueous phase were mixed with 450 µL 100% ethanol and loaded onto a RNeasy® Mini Column. After

centrifugation at 8,000× g for 15 s, the filtrate was discarded, as was the case with all subsequent centrifugation steps. The column was washed once with 700 µL Buffer RWT, and twice with 500 µL Buffer RPE each, with centrifugation at 8,000× g for 15 s the first two times and for 2 min in the latter case. To completely dry the column matrix, the empty column was further centrifuged at 12,000× g for 1 min. For elution of miRNA, the column was placed into a fresh 1.5 mL reaction tube, 40 µL PCR-H_2O were added to the column and centrifuged at 8,000× g for 1 min. The eluted miRNA was stored at -70 °C. The concentration and degree of purity of the miRNA were determined photometrically as described in section 4.7.2. A dilution of 0.2 ng/µL was prepared from the miRNA samples using ddH_20.

4.8.2 FirePlex® MiRNA Assay

miRNA expression was analyzed using the *FirePlex® miRNA Assay Core Reagent Kit V2 - Biofluid* in combination with a custom multiplex melanoma panel (*FirePlex® miRNA Assay Custom Particle Panel RGPC P1*) comprising 63 miRNAs that were selected by colleagues via literature review (Table 3.11). This assay enables multiplex microRNA profiling with a high sensitivity using uniquely encoded hydrogel particles with miRNA-specific binding sites, and included the following steps: 1. Hybridization of miRNAs with particles. 2. End-labeling with universal adapter sequences. 3. Elution of miRNAs from particles. 4. PCR amplification of miRNAs using universal primers. 5. Re-hybridization of miRNAs to the particles. 6. Labeling with fluorescent reporter. 7. Detection of fluorescence via flow cytometry (Figure 4.4). miRNA expression was quantified based on fluorescence intensity [410].

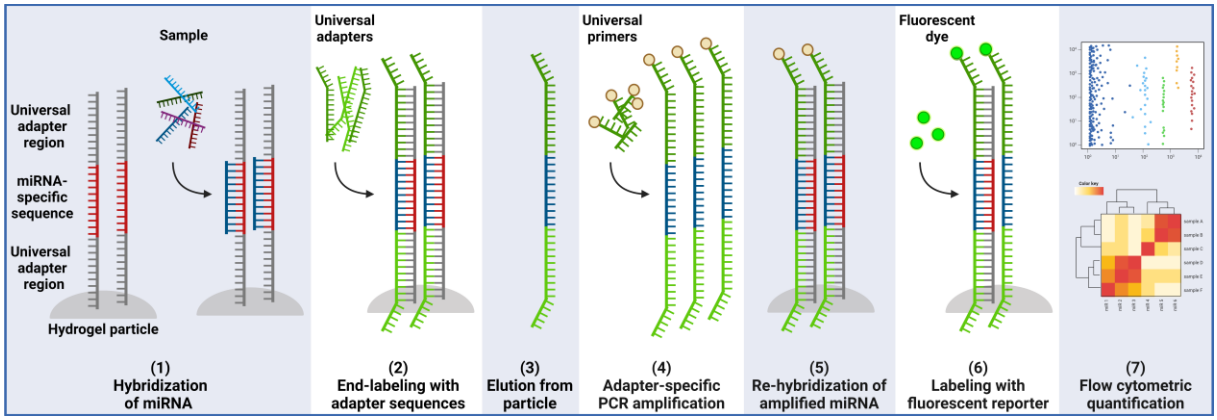

Figure 4.4 Principle of the FirePlex® miRNA Assay. (1) Binding of sample miRNAs to complementary sequences coupled to uniquely encoded hydrogel particles. (2) Ligation of universal adapter sequences to the universal adapter regions at the ends of the particle-bound sequences. (3) Elution of miRNA-adapter complexes. (4) Amplification of miRNA-adapter sequences in a PCR with universal primers that non-specifically hybridize with the adapter sequences. (5) Re-hybridization of the amplified miRNAs to the particles through the miRNA-specific sequence. (6) Labeling with fluorescent reporter. (7) Quantification of miRNA expression through flow cytometric detection of fluorescence. By courtesy of Marc Bender [411] (created with BioRender.com).

The procedure followed the manufacturer's protocol, with minor adjustments. For each sample, 35 µL of FirePlex® Particles per well were added to a 96-well Filter plate. Storage buffer was removed by applying vacuum using a vacuum manifold, and 25 µL of hybridization buffer were transferred to each well. A total of 5 ng miRNA were added by taking 25 µL of the 0.2 ng/µL dilution. A negative control was included with 25 µL ddH_2O instead of miRNA. Samples were incubated for 1 h at 38 °C and 1130 rpm in a plate thermo-shaker, and were afterwards rinsed twice with 165 µL 1× rinse buffer A, followed by application of vacuum. Next, 75 µL of 1× labeling mix (Table 4.9) were added and incubated for 1 h at RT and 1150 rpm in a plate thermo-shaker.

Table 4.9 Reaction mixtures for FirePlex® miRNA Assay.

1× labeling mix	PCR mix	1× reporter mix
78.4 µL labeling diluent	19.8 µL PCR buffer	64 µL RNase free H_2O
1.6 µL labeling buffer	2.4 µL primer mix	16 µL 5× reporter
0.4 µL labeling enzyme	1.2 µL dNTP mix	
	0.6 µL PCR enzyme	

After rinsing twice with 150 µL 1× rinse buffer B and once with 165 µL 1× rinse buffer A, followed by application of vacuum, 110 µL RNase-free H_2O were added and incubated for 30 min at 55 °C and 1130 rpm in a plate thermo-shaker. The Filter plate was placed on top of a 96-well Catch plate inside the vacuum manifold to transfer the eluant to the Catch plate upon application of vacuum. The Filter plate was filled with 1× rinse buffer A and stored at 4 °C until further use. In a separate PCR strip, 20 µL PCR master mix (Table 4.9) were mixed with 30 µL eluant and transferred to a thermocycler for amplification (Table 4.10).

Table 4.10 miRNA PCR thermocycler program.

Temperature		Duration
93 °C		15 s
93 °C	32 cycles	5 s
57 °C		30 s
68 °C		60 s
68 °C		5 min
94 °C		4 min

The stored Filter plate was emptied and 60 µL hybridization buffer as well as 20 µL PCR product were added to the respective well from which the corresponding eluant was taken. Samples were incubated for 30 min at 38 °C and 1130 rpm in a plate thermo-shaker. Next, wells were rinsed twice with 150 µL 1× rinse buffer B and once with 165 µL 1× rinse buffer A, followed by application of vacuum. Each well was supplied with 75 µL 1× reporter mix (Table

4.9) and incubated for 15 min at RT and 1150 rpm in a plate thermo-shaker. After rinsing twice with 165 µL 1× rinse buffer A, followed by application of vacuum, 175 µL FirePlex® Cytometer Run Buffer I were added and 12,000 particles per sample were measured via flow cytometry.

Data analysis was performed using the software FirePlex® Analysis Workbench 2.0.274-ext through normalization with the most stable miRNAs. miRNAs with a median fluorescence value <2.5 a.u. were excluded from the investigation. For further analysis in R 4.2.3 or higher, raw fluorescence values (corresponding to gene expression) were $\log_2$-transformed.

4.8.3 Cluster and Pathway Analysis

Hierarchical cluster analyses were conducted with the R package *ComplexHeatmap* [412] and are displayed as heatmaps with dendrogram. Baseline microRNA expression of DSCs, melanocytes, and melanoma cells was assessed from non-irradiated control samples. For DSCs and melanocytes, controls from 6 h and 24 h were combined. Significant differences of the differentially expressed microRNAs have been assessed with the R package *limma* as described by the authors [413]. Subsequent network analysis with miRTargetLink 2.0 [414] was executed using sets of differentially expressed miRNAs as input. This web application allows for the visualization of interactions between microRNAs and mRNA targets in the form of interactive networks. Networks include only target genes that are regulated by at least two of the input miRNAs.

Pathway analysis was conducted via enrichment analysis/over-representation analysis (ORA) to understand the functional roles of the miRNAs and target genes, and to identify enriched biological processes or pathways. ORA is a commonly used method to assess whether known functions or processes are over-represented/enriched in a list of genes, for example a set of differentially expressed genes [415]. GO (Gene Ontology) and KEGG (Kyoto Encyclopedia of Genes and Genomes) are the two most frequently used database resources for functional annotation and pathway analysis of genes. GO provides a defined vocabulary to describe the functions of genes and their products [416]. The category of ‘GO - Biological Process’ was used for analysis. KEGG includes pathway maps representing sets of molecular interactions and reactions in a biological process. It provides information about pathways, networks, diseases, drugs, and orthologs [417]. Enrichment analysis was performed with the miRNA sets using miEAA 2.0 [418], or alternatively with the target gene sets via GeneTrail 3.0 [419]. Both applications are integrated with the miRTargetLink 2.0 application.

4.9 Statistical Evaluation

Data analysis and statistical analysis are described directly under the respective method section. Statistical significance is indicated by asterisks. Significance levels were defined as follows: *$p \leq 0.05$, **$p \leq 0.01$, ***$p \leq 0.001$, ****$p \leq 0.0001$.

5 Results

This thesis aimed to establish and investigate multipotent DSCs as a novel model for melanomagenesis. This involved isolation and purification of primary DSCs from human foreskin. Initial characterization focused on melanocytic differentiation potential and sphere formation in both native and purified DSC cultures. The study further investigated the response of DSCs to UV exposure. Comparisons with differentiated skin cells assessed the DNA damage response in DSCs, examining DNA repair, cell cycle regulation, and apoptosis induction for abnormalities that potentially influence susceptibility to tumorigenesis. Moreover, the impact of UV irradiation on the melanocytic differentiation ability and the sphere-forming potential of DSCs were also studied. Finally, a melanoma-specific miRNA panel was used to identify potential UV-induced miRNA patterns in DSCs associated with melanoma development.

5.1 Stem Cell Frequency of DSC Cultures

DSCs were isolated from the dermis of human foreskins. Upon placement in stem cell medium, the dissociated dermal cells formed small cell clusters in suspension culture within the initial 3–5 days. These clusters transformed into free-floating or loosely adherent spheres over the subsequent days (Figure 5.1A). The expression levels of the neural crest stem cell (NCSC) marker NGFRp75 within these dermal spheres increased throughout the cultivation (Figure 5.1B). After approximately 14 days of cultivation in suspension, the dermal spheres were enzymatically dissociated, the stem cell frequency was measured via staining for NGFRp75 and CD90, and cells were subsequently cultivated on BME-coating to grow adherently.

Notably, the DSC frequency measurement revealed, that not only DSCs but also fibroblasts got incorporated into the dermal spheres. After the initial two-week cultivation period in stem cell medium, the proportion of DSCs in dissociated dermal spheres averaged only 10.5% (median 8.7%, IQR 5.7–13.3%) (Figure 5.1C). There was a great donor-dependent variation ranging between 0.7% (minimum outlier) and 35.7% (maximum outlier). The majority of the donor cell strains (66 out of 79, equivalent to around 83.5%) displayed a stem cell frequency below 15% (Figure 5.1D). Higher proportions of DSCs were rare and did not occur frequently. During cultivation, the stem cell content may decrease or increase but was usually relatively stable and varied only within a small percentage range. Cultures of DSCs seem to be particular cell cultures, which are more likely to be termed a heterogeneous co-culture of DSCs and fibroblasts (and maybe other dermal cells in a very small proportion) rather than a fibroblast-

contaminated DSC culture. As a result, the term ‘DSC-fibroblast co-cultures’ is used in the further course of the study to describe these mixed cultures.

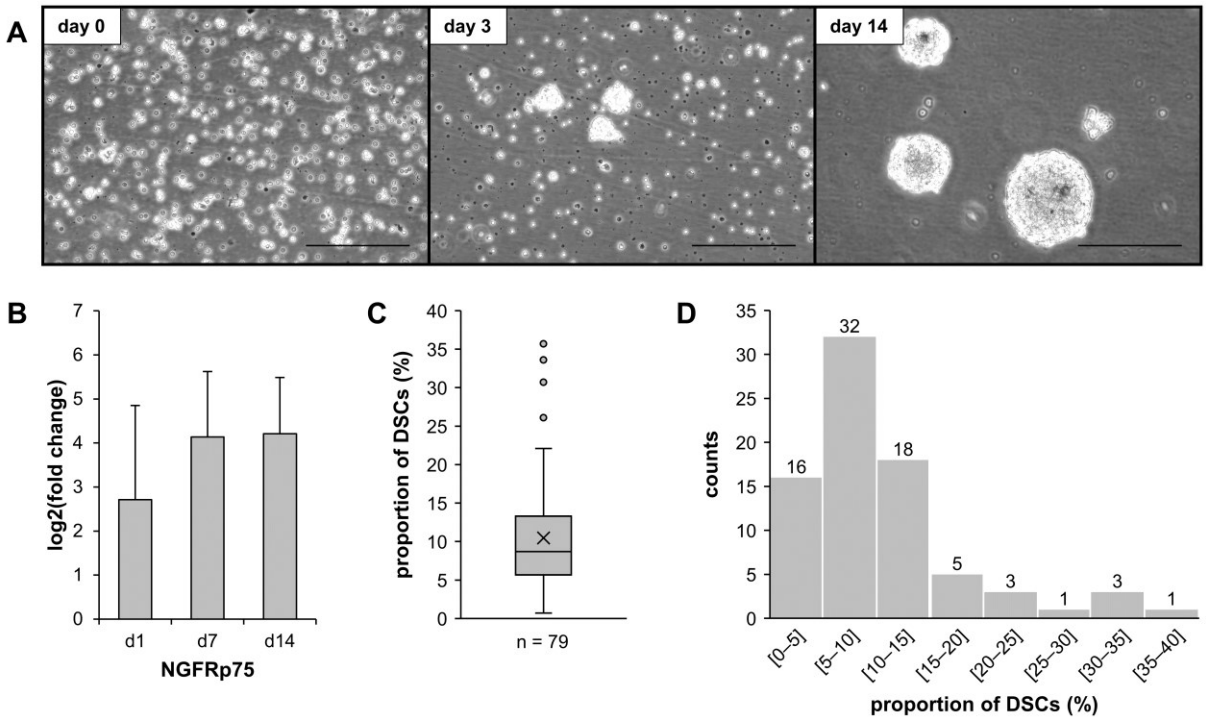

Figure 5.1 Characterization of DSCs. (**A**) Formation of dermal spheres in stem cell medium monitored at days 0, 3, and 6. Scale bars: 200 µm. (**B**) Gene expression analysis of NGFRp75 in dermal spheres during the 14-days cultivation period in stem cell medium. Values are presented as mean ± SDs. Sample size: n=3, with technical duplicates. Normalized on melanocytes. (**C**) Frequency of stem cells in DSC-fibroblast co-cultures. Dermal spheres were enzymatically dissociated after two weeks, and the percentage of DSCs (NGFRp75$^+$ cells) in the culture was determined via flow cytometry. Boxplot displaying the median with 25th/75th percentiles (inclusive method). The length of the box marks the interquartile range (IQR). The cross (×) inside the box indicates the mean DSC frequency. Dots represent outliers. Results from 79 donors. (**D**) The histogram shows the abundance distribution of DSC frequencies of individual donor cell strains divided into ranges of 5%. Results from 79 donors (adapted from [398] and [420]).

5.2 Enrichment of DSCs from DSC-Fibroblast Co-Cultures

The usage of DSC-fibroblast co-cultures does not pose a problem for experiments that involve flow cytometric analysis and immunocytochemistry as these methods allow for a cell-specific evaluation based on distinct cell surface markers and ensure exclusive examination of DSCs while excluding fibroblasts. However, certain experiments that cannot discriminate between cell populations (e.g., analysis of epigenetics, gene expression, miRNA expression, protein expression) are impracticable using co-cultures. Therefore, it was indispensable to establish a technique for enriching/purifying DSCs.

To diminish the substantial fibroblast population in DSC-fibroblast co-cultures and thus amplify the DSC frequency, three different methods were tested. Geneticin treatment and selective detachment were examined due to the benefits of simplicity and availability. Immunomagnetic separation was chosen for higher specificity. While these methods were well described and practical for various cell types, their application to DSCs had yet to be explored. The objective was to acquire highly pure or enriched populations of DSCs, targeting a minimum purity level of 85% or higher. These enriched DSCs would then be utilized for subsequent research delving into the genetic and epigenetic effects of UV irradiation on these cells.

5.2.1 Elimination of Fibroblasts with Geneticin

The antibiotic Geneticin exhibits varying cytotoxic effects on eukaryotic cells depending on their growth rates. Consequently, rapidly dividing cells are more susceptible to its impact compared to cells with lower proliferation rates. In this study, treatment with Geneticin was performed to selectively kill fibroblasts in DSC-fibroblast co-cultures. Additionally, the growth rates of both DSCs and the corresponding fibroblasts in (non-Geneticin-treated) co-cultures were assessed.

After three days of Geneticin treatment, cell densities were visibly reduced compared to the control cells. While untreated cells were nearly confluent by day six of the experiment, both concentrations of Geneticin caused distinct growth inhibition or cell death, and changes in cell morphology (Figure 5.2A). Quantitative analysis of the total cell numbers confirmed these observations. The control cells proliferated, exhibiting an average relative cell count of 2.3 ± 0.8 by day six (compared to the beginning of the experiment), whereas cell cultures treated with 50 µg/mL Geneticin showed stagnant cell counts (1.0 ± 0.3) at the same time point (Figure 5.2C). Samples subjected to 100 µg/mL Geneticin even displayed a continuous decline in cell numbers, resulting in a relative cell count of 0.6 ± 0.2 at the end of the experiment. Geneticin not only harmed fibroblasts, but also dramatically affected the frequency of DSCs, as revealed by immunocytochemical staining of the treated cultures (Figure 5.2B). Initially, DSCs accounted for $5.1 \pm 3.3\%$ of the total cell population at day 0. However, both concentrations of Geneticin caused a loss of stem cells, with the higher concentration of 100 µg/mL nearly eradicating DSCs ($0.1 \pm 0.1\%$) by day six (Figure 5.2D). The lower dose of 50 µg/mL Geneticin also diminished the proportion of DSCs to $1.4 \pm 1.6\%$ in the final culture. Instead of enriching the stem cell proportion in DSC-fibroblast co-cultures, treatment with Geneticin even reduced the DSC frequency.

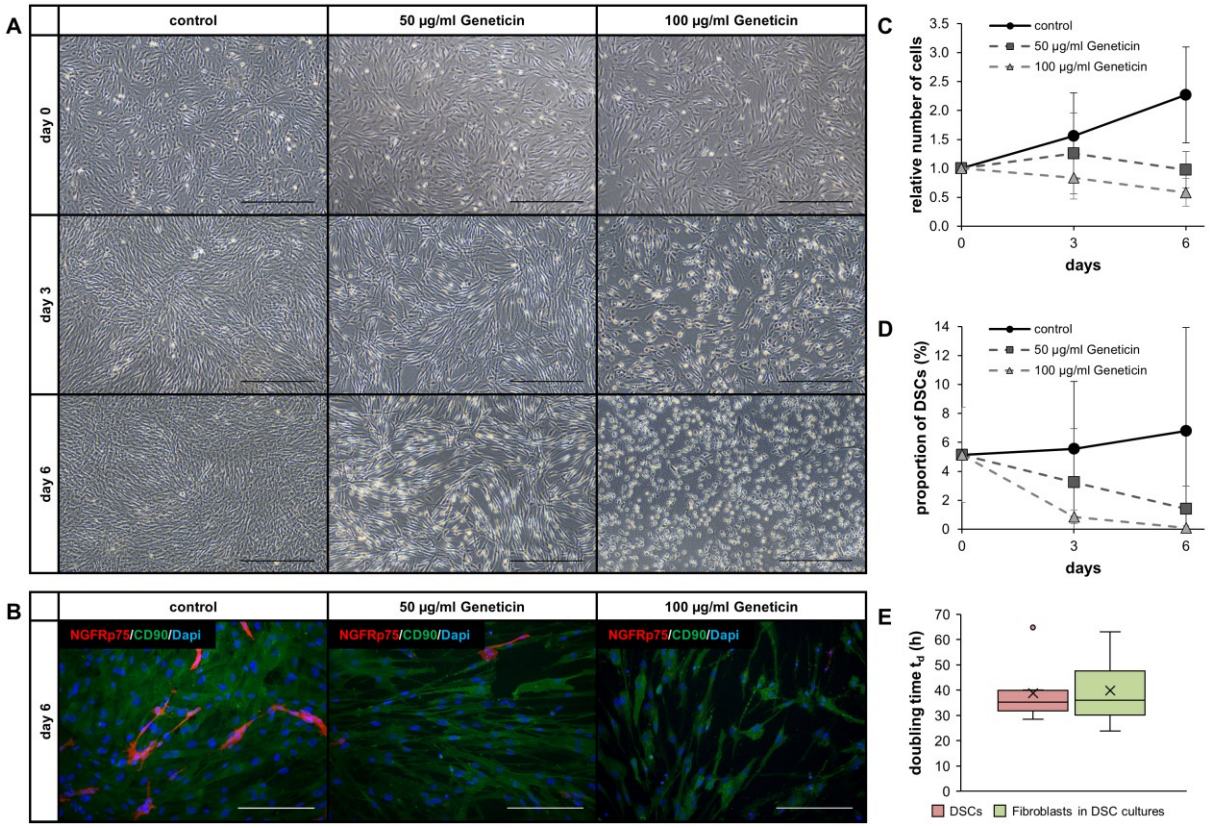

Figure 5.2 Geneticin treatment of DSC-fibroblast co-cultures. DSC-fibroblast co-cultures were cultured in stem cell medium without Geneticin or with 50 µg/mL or 100 µg/mL Geneticin for two days and monitored for a total of six days. (**A**) Cell growth recorded at days 0, 3, and 6. Scale bars: 500 µm. (**B**) Immunocytochemical staining for NCSC marker NGFRp75 (red) and fibroblast marker CD90 (green) at day 6. Nuclei were counterstained with DAPI (blue). Scale bars: 200 µm. (**C**) Number of total cells in relation to the cell count of control cells at day 0 and (**D**) frequency of DSCs in culture measured at days 0, 3, and 6. Values are presented as mean ± SDs. Sample size: n=3. (**E**) Doubling time of DSCs and the respective fibroblasts in the DSC-fibroblast co-cultures without Geneticin treatment. Boxplot displaying the median with 25th/75th percentiles (inclusive method). The length of the box marks the interquartile range (IQR). The cross (×) inside the box indicates the mean doubling time. Dots represent outliers. Sample size: n=7 (adapted from [420]).

The measurement of growth rates of the two cell types in co-cultures showed that, on average, both cell types proliferated at a similar rate, with DSCs doubling every 38.8 hours (median 35.2 h, IQR 31.8–39.8 h) and fibroblasts reduplicating every 39.7 hours (median 35.9 h, IQR 30.1–47.6 h) (Figure 5.2E).

5.2.2 Separation of DSCs and Fibroblasts via Selective Detachment

A second approach investigated whether DSCs and fibroblasts exhibit different adhesion properties, enabling the separation of both cell types from DSC-fibroblast co-cultures via selective detachment. For this, three donor cell strains with different stem cell proportions (<5%, 10–20%, >30%) were examined.

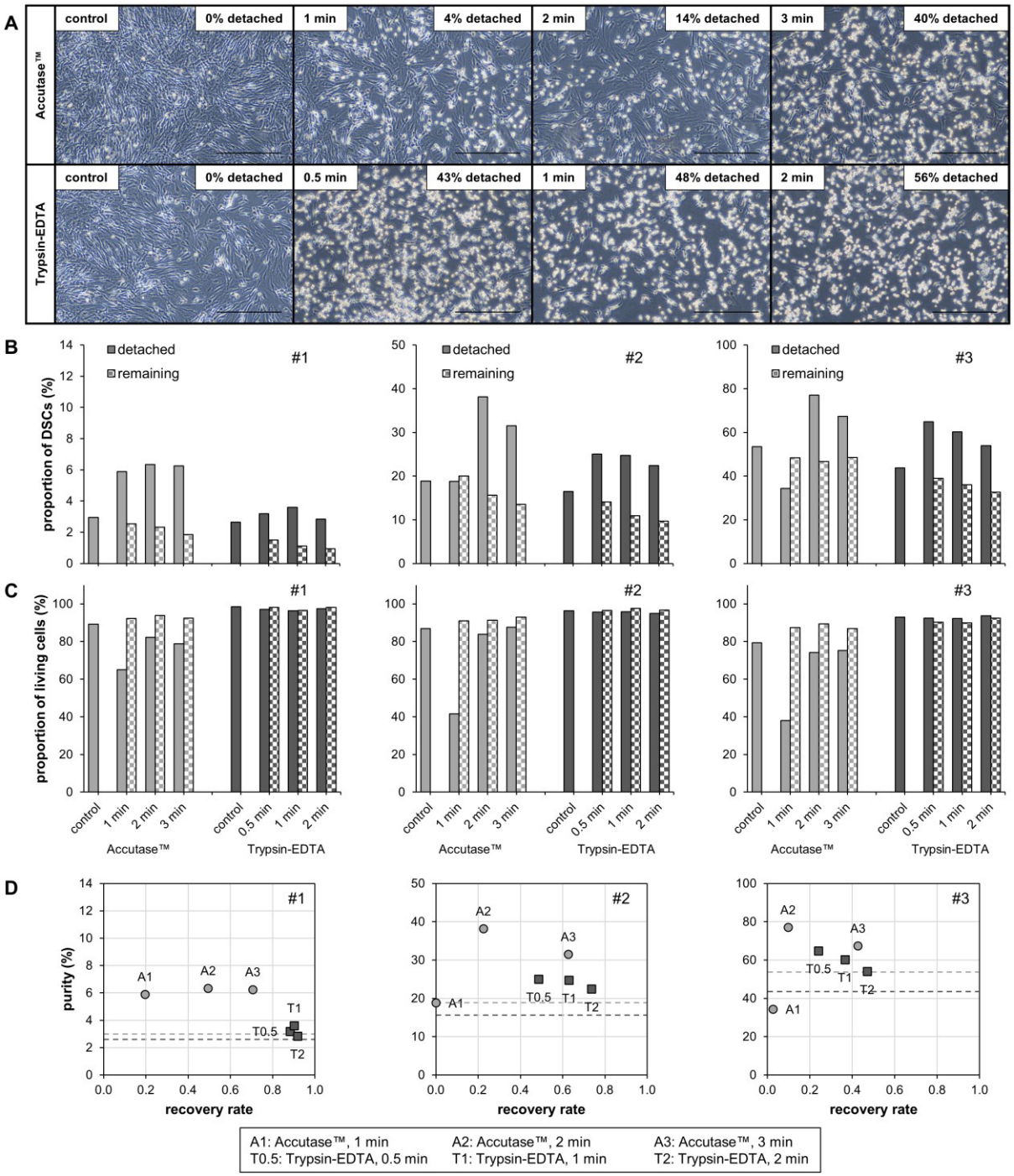

Figure 5.3 Selective detachment of DSC-fibroblast co-cultures. DSC-fibroblast co-cultures were incubated with Accutase™ for 1, 2, or 3 min or with trypsin-EDTA for 0.5, 1, or 2 min, and detached cells were collected. (**A**) Light microscopy of the remaining cells at the different time points of detachment with Accutase™ or trypsin-EDTA with the percentage of detached total cells. Scale bar: 500 µm. (**B**) Frequency of DSCs in samples measured using NGFRp75 staining. (**C**) Viability of total cells examined with propidium iodide. (**D**) Plot of recovery rate (*x*-axis) versus purity (*y*-axis) of detached cells at the individual incubation times. Purity: frequency of DSCs. Recovery rate: ratio of the absolute number of DSCs in the detached sample to the absolute number of DSCs before detachment. Dotted lines indicate the DSC frequency of control cells detached with Accutase™ (light gray) or trypsin-EDTA (dark gray). Results from three donor cell strains with different stem cell proportions (#1: <5%, #2: 10–20%, #3: >30%) (adapted from [420]).

In general, with Accutase™ cells detached more slowly compared with trypsin-EDTA, where a lot of cells were immediately released and floating in the supernatant (Figure 5.3A). Analysis revealed that fibroblasts seemed to adhere more strongly to the Geltrex™-coated cell culture vessel than DSCs. DSCs were therefore detached faster—with both Accutase™ and trypsin-EDTA—and were found at higher proportions in the detached samples, while showing decreasing frequencies in the remaining samples (Figure 5.3B). When using Accutase™, the highest increase in DSC frequency was observed at the 2-minute time point, ranging between 3.6–23.6 percentage points depending on the donor. For trypsin-EDTA, the strongest increase in DSC frequency occurred at the 0.5-minute or 1-minute time points, varying from 1.0–21.1 percentage points. Overall, Accutase™ resulted in a higher enrichment of DSCs compared to trypsin-EDTA. However, it's worth noting that those control cells which were detached with trypsin-EDTA (total detachment after 5 min) also showed lower DSC frequencies.

Regarding cell viability (Figure 5.3C), in all samples (detached, remaining, and controls) treated with trypsin-EDTA more than 90% of the cells were viable. In contrast, detachment with Accutase™ slightly impaired cell viability in general, as seen in the controls with 80–90% viable cells. Incubation with Accutase™ for 1 min significantly reduced the viability of the detached cells to 65%, 42%, and 38%, while cells collected at 2 min or 3 min showed higher values between 74-88%. The remaining cells, however, were not affected.

Apart from the purity of the detached DSCs, the recovery rate (or yield) is also crucial in assessing the success of this purification method. The recovery was calculated as the ratio of the absolute number of DSCs in the detached sample to the absolute number of DSCs before detachment. Naturally, the recovery rates increased with longer incubation times for both detachment solutions (Figure 5.3D), but higher recovery rates were always linked to decreasing purity. The highest purity was in turn associated with the second-lowest recovery, leaving almost no cells for further cultivation (Figure 5.3D, A2: Accutase™ for 2 min).

5.2.3 Segregation of The Two Cell Types via Immunomagnetic Separation

Immunomagnetic separation (IMS) was tested for better and more specific targeting, as this method relies on specific cell surface antigens and thus enables the enrichment of a particular cell population. This technique offers both negative selection (labeling of undesired cells) and positive selection (labeling of target cells) options, depending on the particular antigen that is used [421,422]. In this study, the fibroblast marker CD90 and the stem cell marker NGFRp75 (CD271) were chosen for negative and positive selections, respectively. These surface proteins

are well-described, cell-specific markers [32,423,424] that serve as the targets for many commercially available selection kits.

Co-cultures of DSCs and fibroblasts with a stem cell frequency averaging below 15%, which is characteristic for the majority of primary donor cell strains, underwent both negative and positive selection. Additionally, a comparison was made between the EasySep™ method (column-free) and the MACS® method (automatic column-based). At the beginning, numerous different strategies were tested, especially in the EasySep™ approach, yielding limited success, e.g., usage of self-coated beads, various magnets, different kits, varying cell numbers, adjustments in the volumes of labeling reagents and beads, repeatedly labeling with beads, and sequential separation (data not shown). The established and improved protocols were repeated multiple times, leading to the outcomes detailed below.

5.2.3.1 Negative Selection

The EasySep™ negative selection of DSC-fibroblast co-cultures involved depleting fibroblasts using anti-PE RapidSpheres™ in combination with a CD90-PE antibody. This resulted in an approximately four-fold increase in DSCs from 14.0 ± 3.3% in the pre sample to 59.4 ± 19.8% in the negative fraction (DSC fraction) (Figure 5.4A). However, a substantial amount of $CD90^+$ fibroblasts and occasionally also a smaller population of $CD90^-$/$NGFRp75^-$ double-negative cells remained in the negative fraction (Figure 5.4B). The separation led to significant loss of ($CD90^{dim}$) DSCs in the positive fraction (fibroblast fraction) (10.8 ± 4.7%), and showed a decrease in the stem cell frequency during the subsequent cultivation of the purified DSC fraction (48.8% on day 11–12) (Figure 5.4A+C). Fibroblast depletion with EasySep™ negative selection was not reliably reproducible, as evidenced by large variations across different experiments.

For negative selection (labeling of fibroblasts) with the MACS® approach, two different methods were used to label fibroblasts. The first method involved indirect labeling with *Anti-PE MicroBeads* in combination with a PE-conjugated anti-CD90 antibody. This led to a five-fold enrichment of DSCs from 9.6 ± 5.3% to 52.0 ± 24.8%, with minimal loss of stem cells in the positive fibroblast fraction (4.5 ± 2.6%) (Figure 5.4D). Nevertheless, a small population of double-negative cells ($CD90^-$/$NGFRp75^-$) and a considerable number of fibroblasts ($CD90^{dim}$) persisted in the negative DSC fraction (Figure 5.4E). On average, cultures were able to maintain the increased DSC frequency during subsequent cultivation for 11–12 days (52.8 ± 23.4%) (Figure 5.4D+F). This method showed huge standard deviations, too.

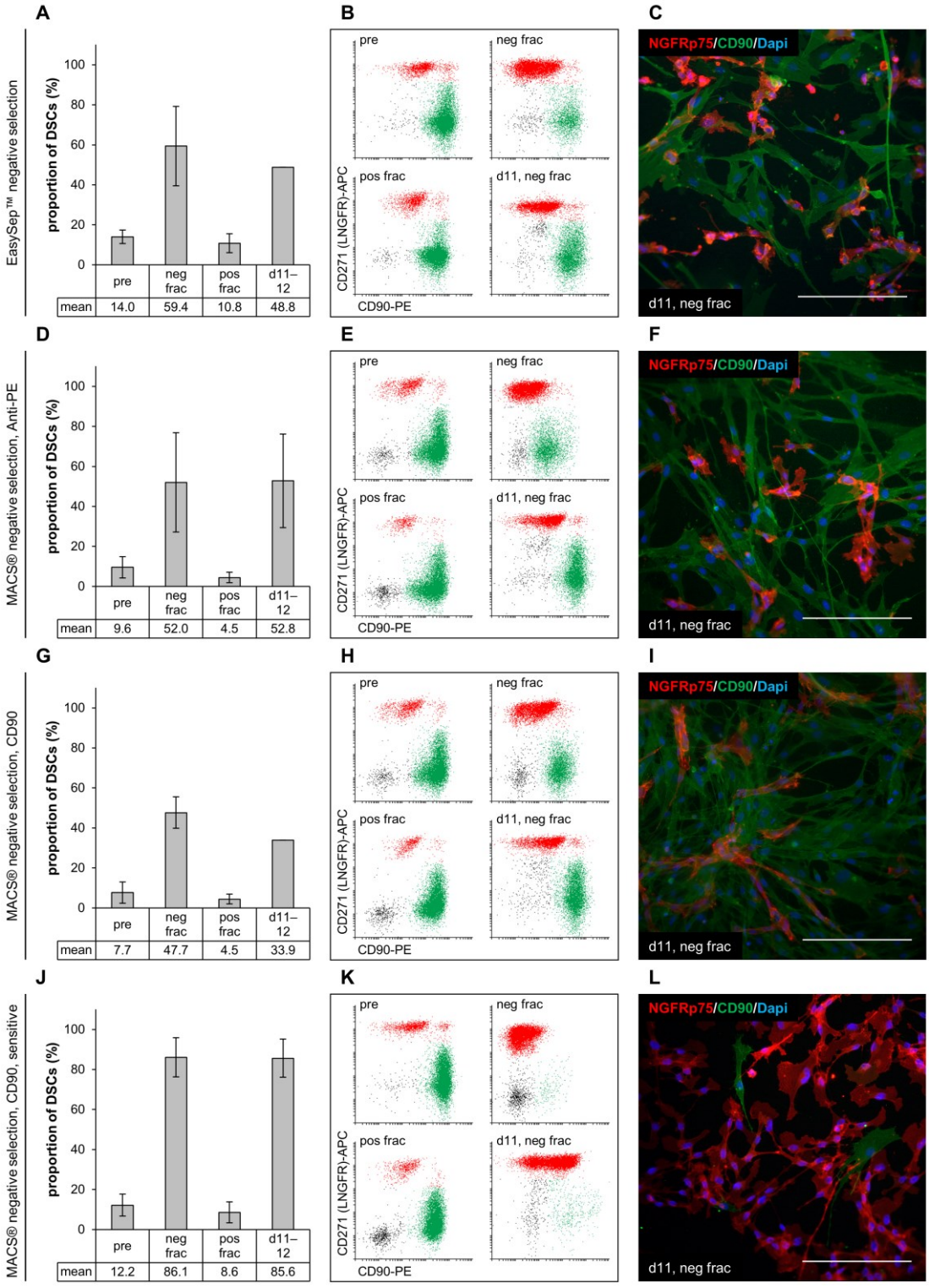

Figure 5.4 Negative selection (labeling of fibroblasts) of DSC-fibroblast co-cultures. (**A–C**) EasySep™ column-free negative selection with the *EasySep™ Human PE Positive Selection Kit II* in combination with a PE-conjugated anti-CD90 antibody. Sample size: n=5. (**D–F**) MACS® automatic column-based negative selection with *Anti-PE MicroBeads* in combination with a PE-conjugated anti-CD90 antibody and the autoMACS® Pro Separator. Program: *Deplete*. Sample size: n=3. (**G–I**) MACS® automatic column-based negative selection with *CD90 MicroBeads* and the autoMACS® Pro Separator. Program: *Deplete*. Sample size: n=2. (**J–L**) MACS® automatic column-based negative selection with *CD90 MicroBeads* and the autoMACS® Pro Separator. Sensitive Program: *DepleteS*. Sample size: n=3. Values are presented as mean ± SDs. Pre: initial sample, neg frac: DSC fraction, pos frac: fibroblast fraction, d11–12: 11–12 days of cultivation. Frequency of DSCs in the separate fractions

was determined via flow cytometry analysis of NGFRp75 (*y*-axis of dot plots) and CD90 (*x*-axis of dot plots) (**B+E+H+K**). Following separation, the enriched DSC fraction was cultivated in stem cell medium. After 11–12 days, the proportion of DSCs in culture was measured again via flow cytometry, and cells were additionally stained immunocytochemically for NGFRp75 (red) and CD90 (green) (**C+F+I+L**). Nuclei were counterstained with DAPI (blue). Scale bars: 200 µm (adapted from [420]).

A similar outcome was observed with the second MACS® negative selection method, which involved direct labeling of fibroblasts with *CD90 MicroBeads*. This method resulted in a comparable increase in DSC frequency from 7.7 ± 5.4% to 47.7 ± 7.8%, and only a minor proportion of stem cells was separated out with the fibroblast fraction (4.5 ± 2.5%) (Figure 5.4G). However, the DSC proportion declined to 33.9% on day 11–12 of subsequent cultivation (Figure 5.4H–I). Flow cytometry analysis revealed a similar distribution of cell populations as observed in the *Anti-PE MicroBeads* separation (Figure 5.4E). Surprisingly, both MACS® negative selection procedures yielded a significant number of $CD90^{-}$/$NGFRp75^{-}$ cells in the positive fibroblast fraction.

Effective purification of DSC-fibroblast co-cultures with a stem cell frequency below 15% was achieved using MACS® negative selection with *CD90 MicroBeads* (direct labeling) and a more sensitive separation program (*DepleteS*). The selection led to a remarkable seven-fold enrichment of DSCs from 12.2 ± 5.5% to 86.1 ± 9.8% (Figure 5.4J), along with a clear separation of the different cell populations in flow cytometry analysis (Figure 5.4K). The negative fraction (DSC fraction) still contained double-negative cells ($CD90^{-}$/$NGFRp75^{-}$), while all $CD90^{+}$ fibroblasts were successfully removed. However, a considerable amount of $NGFRp75^{+}$/$CD90^{dim}$ DSCs (8.6 ± 5.2%) got lost in the positive fibroblast fraction. The enriched cultures maintained a high DSC frequency during cultivation (85.6 ± 9.5% on day 11–12) (Figure 5.4J+L). Comparable results were obtained with MACS® *Anti-PE MicroBeads* and the sensitive separation program (data not shown).

A very small number of donor cell strains (see Figure 5.1C–D) initially displayed or spontaneously attained a relatively high frequency of DSCs (≥30%) during their growth. This led to the assumption that the purification process for these cultures would be more effective, given the reduced number of fibroblasts that required removal. Consequently, the negative selection (labeling of fibroblasts) was also implemented on DSC-fibroblast co-cultures that already had a higher proportion of stem cells. These cultures were enriched either naturally or through manual pre-enrichment using negative selection, as described earlier, with an intermediate cultivation step.

Employing the EasySep™ negative separation technique on these ‘pre high’ co-cultures (38.0 ± 2.6%) yielded a significantly enriched DSC fraction containing 88.4 ± 12.0% DSCs

(Figure 5.5A–B). The subsequent follow-up comprised only one experiment after 28 days, indicating that the cells required notably more time to proliferate, but cells were able to maintain the elevated stem cell content (89.8%) (Figure 5.5A+C). Furthermore, a large number of DSCs got lost in the positive fibroblast fraction (34.9 ± 10.1%).

Utilizing MACS® negative separation with *CD90 MicroBeads* on co-cultures of DSCs and fibroblasts with a higher initial proportion of stem cells led to an increase in the DSC frequency from 54.3 ± 5.0% to 77.0 ± 6.5%, accompanied by a notable loss of DSCs in the fibroblast fraction as well (49.4 ± 4.2%) (Figure 5.5D–E). Over an 11–12-days period, the proportion of stem cells decreased to 66.7 ± 10.8% (Figure 5.5D+F).

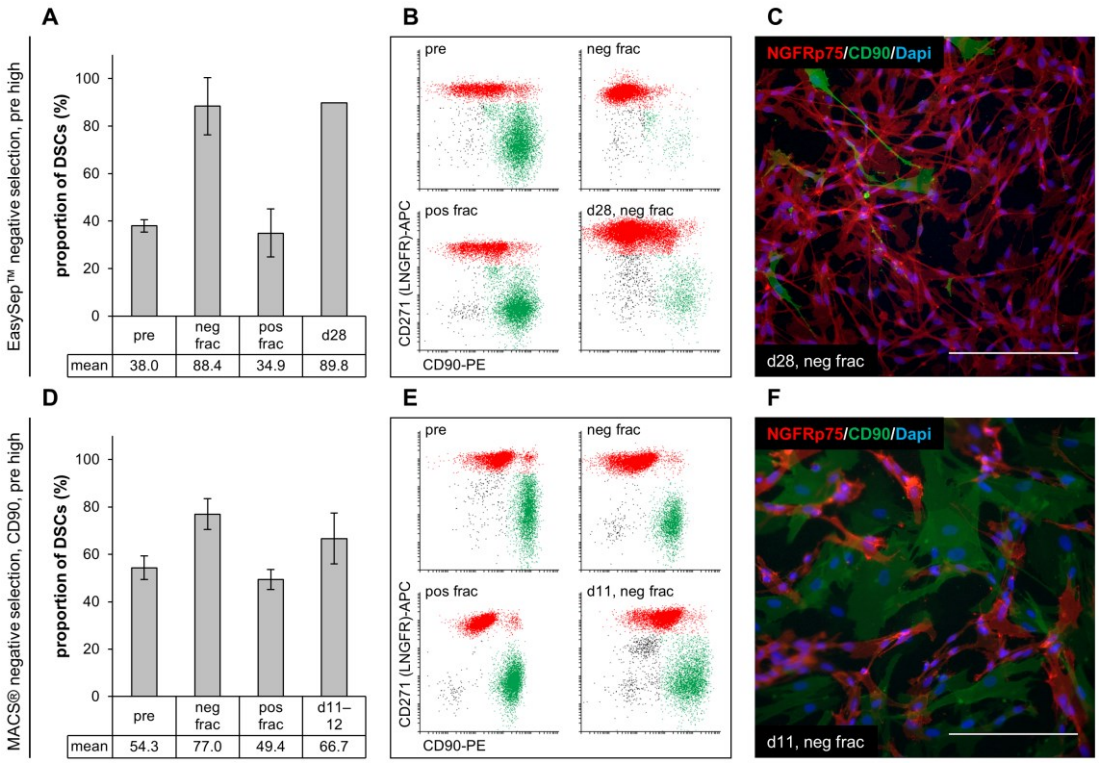

Figure 5.5 Negative selection (labeling of fibroblasts) of DSC-fibroblast co-cultures with higher initial DSC frequency. (**A–C**) EasySep™ column-free negative selection with the *EasySep™ Human PE Positive Selection Kit II* in combination with a PE-conjugated anti-CD90 antibody in cell cultures with higher initial DSC frequencies. Sample size: n=3. (**D–F**) MACS® automatic column-based negative selection with *CD90 MicroBeads* and the autoMACS® Pro Separator in cell cultures with higher initial DSC frequency. Program: *Deplete*. Sample size: n=2. Values are presented as mean ± SDs. Pre: initial sample, neg frac: DSC fraction, pos frac: fibroblast fraction, d28/d11–12: 28 or 11–12 days of cultivation. Frequency of DSCs in the separate fractions was determined via flow cytometry analysis of NGFRp75 (*y*-axis of dot plots) and CD90 (*x*-axis of dot plots). Following separation, the enriched DSC fraction was cultivated in stem cell medium. After 11–12 or 28 days, the proportion of DSCs in culture was measured again via flow cytometry, and cells were additionally stained immunocytochemically for NGFRp75 (red) and CD90 (green). Nuclei were counterstained with DAPI (blue). Scale bars: 200 µm (adapted from [420]).

5.2.3.2 Positive Selection

Since the outcomes of negative selection were unsatisfactory, a positive selection strategy was employed on DSC-fibroblast co-cultures with a stem cell frequency below 15%, which represented the majority of primary donor cell strains. This was done while comparing the separation methods of EasySep™ (column-free) and MACS® (automatic column-based).

The EasySep™ positive selection technique involving CD271(NGFRp75)-labeling of DSCs led to an enrichment of cultures. The positive fraction (DSC fraction) showed an average stem cell content of 61.8 ± 28.5%; a significant increase from the initial 11.1 ± 6.0% in the pre sample (Figure 5.6A). There was minimal loss of DSCs in the negative fraction (fibroblast fraction) with a proportion of 2.7 ± 2.4% stem cells (Figure 5.6B). During subsequent cultivation for 11–12 days, the DSC cultures maintained an average enrichment level of 56.1 ± 16.2% (Figure 5.6A+C). However, in some experiments, DSC separation was not well tolerated, resulting in morphological changes and poor attachment when cultivated after separation.

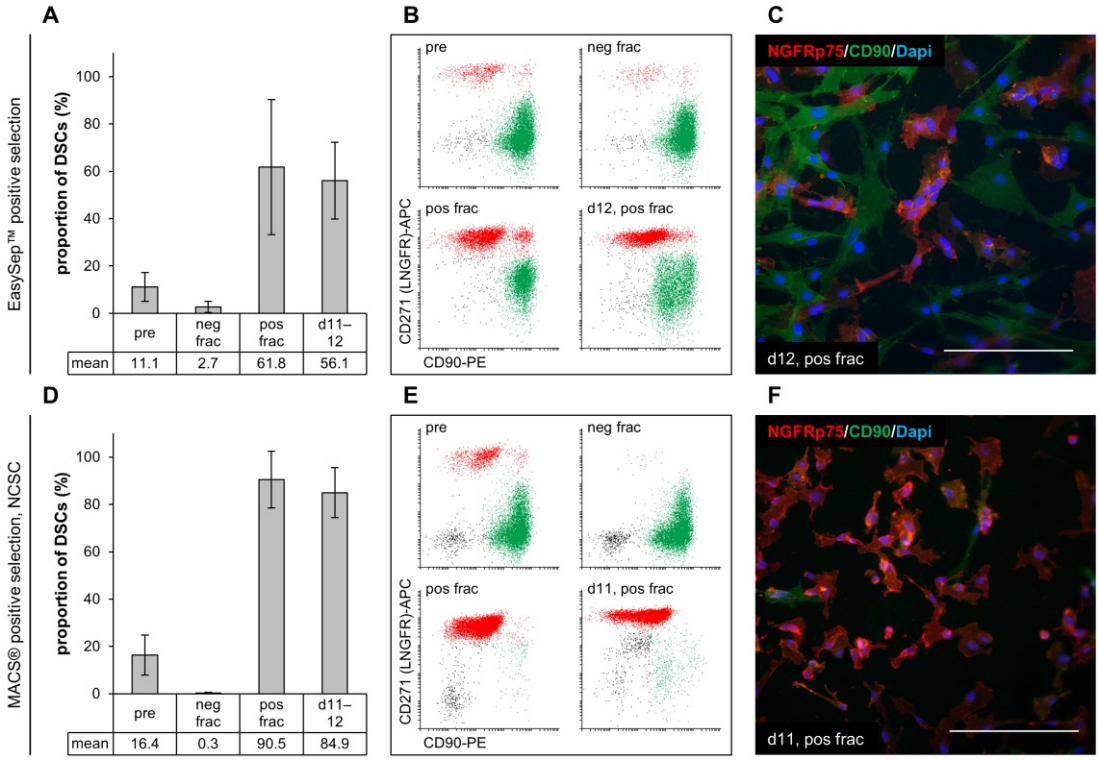

Figure 5.6 Positive selection (labeling of DSCs) of DSC-fibroblast co-cultures. (**A–C**) EasySep™ column-free positive selection with the *EasySep™ Human CD271 Positive Selection Kit II*. Sample size: n=6. (**D–F**) MACS® automatic column-based positive selection with *NCSC MicroBeads* and the autoMACS® Pro Separator. Program: *Posseld2*. Sample size: n=13. Values are presented as mean ± SDs. Pre: initial sample, neg frac: fibroblast fraction, pos frac: DSC fraction, d11–12: 11–12 days of cultivation. Frequency of DSCs in the separate fractions was determined via flow cytometry analysis of NGFRp75 (*y*-axis of dot plots) and CD90 (*x*-axis of dot plots). Following separation, the enriched DSC fraction was cultivated in stem cell medium. After 11–12 days, the proportion of DSCs

in culture was measured again via flow cytometry, and cells were additionally stained immunocytochemically for NGFRp75 (red) and CD90 (green). Nuclei were counterstained with DAPI (blue). Scale bars: 200 µm (adapted from [420]).

With MACS® positive selection using *NCSC MicroBeads* targeting NGFRp75, nearly pure DSC cultures were achieved. The positive fraction contained a high DSC content of 90.5 ± 12.0% compared to the initial 16.4 ± 8.4% in the pre sample. Importantly, there was negligible loss of stem cells in the negative fraction (0.3 ± 0.3%) (Figure 5.6D–E). A notable proportion of the other remaining cells in the positive DSC fraction were $CD90^{-}$/$NGFRp75^{-}$ cells, although the majority of them were effectively separated along with the fibroblast fraction (Figure 5.6E). DSC cultures that underwent purification via this method maintained a consistently high stem cell frequency, averaging 84.9 ± 10.5% throughout a 11–12-days cultivation period (Figure 5.6D+F).

5.2.3.3 Overall Assessment of The Different IMS Methods

To properly assess the efficacy of the individual separation methods for low initial DSC frequencies, the evaluation must consider not only the purity of the DSC cultures following selection (Figure 5.7A) but also the recovery rate or yield of the technique (Figure 5.7B). The recovery is the ratio of the absolute count of DSCs in the purified fraction to the absolute count of DSCs in the pre sample.

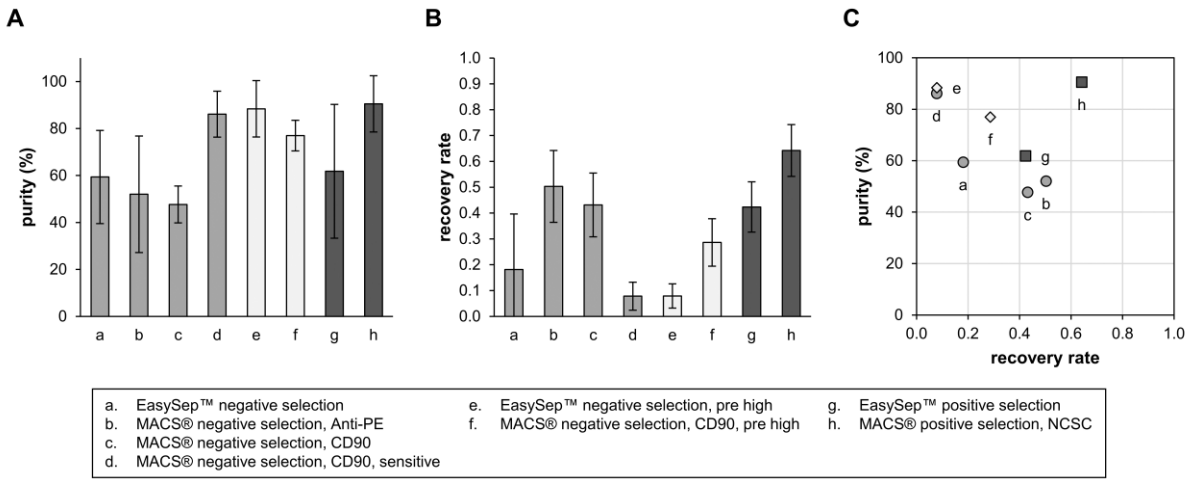

Figure 5.7 Purity and recovery of DSCs for the individual selection methods. (**A**) Purity: frequency of DSCs in the purified fraction after separation determined via flow cytometry analysis of NGFRp75. Values are presented as mean ± SDs. (**B**) Recovery rate: ratio of the absolute number of DSCs in the purified fraction after separation to the absolute number of DSCs in the pre sample. Values are presented as mean ± SDs. (**C**) Plot of recovery rate (*x*-axis) versus purity (*y*-axis) of the individual selection methods. Sample size: a. n=5; b. n=3; c. n=2; d. n=3; e. n=3; f. n=2; g. n=6; h. n=13 (adapted from [420]).

Regarding purity, the MACS® positive selection (Figure 5.7: h, purity 90.5 ± 12.0%, recovery 0.64 ± 0.10) and the MACS® negative selection (CD90) utilizing a more sensitive program (Figure 5.7: d, pur 86.1 ± 9.8%, rec 0.08 ± 0.05) worked best. However, the latter approach was deemed unfeasible due to an extremely low recovery rate, leaving very few cells available for subsequent cultivation or experiments.

For the other three negative selection methods (Figure 5.7: a, b, c) and the EasySep™ positive selection (Figure 5.7: g), comparable purity results within the range of 50–60% were observed. Nevertheless, upon evaluating the recovery rate, clear advantages were evident for the MACS® negative selection Anti-PE (Figure 5.7: b, pur 52.0 ± 24.8%, rec 0.50 ± 0.14), the MACS® negative selection CD90 (Figure 5.7: c, pur 47.7 ± 7.8%, rec 0.43 ± 0.12), and the EasySep™ positive selection (Figure 5.7: g, pur 61.8 ± 28.5%, rec 0.42 ± 0.10), over the EasySep™ negative selection (Figure 5.7: a, pur 59.4 ± 19.8%, rec 0.18 ± 0.22).

For samples with higher initial DSC frequencies (≥30%), both the EasySep™ negative selection (Figure 5.7: e, pur 88.4 ± 12.0%, rec 0.08 ± 0.05) and the MACS® negative selection (Figure 5.7: f, pur 77.0 ± 6.5%, rec 0.29 ± 0.09) achieved notable purity but simultaneously (very) low recovery rates. When plotting the recovery rate against the purity (Figure 5.7C), the MACS® positive selection (Figure 5.7: h) emerged as the optimal choice for enhancing DSC frequency in cell cultures, owing to its highest purity and highest recovery rate.

In the following experiments, both purified DSC cultures—obtained through MACS® positive selection with *NCSC MicroBeads* (see Figure 5.6D–F)—and DSC-fibroblast co-cultures were used in different experiments. Co-cultures were only used in those experiments where the analysis allowed for a distinction between DSCs and fibroblasts. To avoid ambiguity, it is stated explicitly where co-cultures and where enriched/purified DSCs were used.

5.3 Characterization of DSCs

5.3.1 Morphology and Gene Expression of The Skin Cell Types

This thesis frequently compared DSCs with other skin cell types, namely fibroblasts, melanocytes, and keratinocytes, to ensure a comprehensive analysis. All four skin cell types were successfully isolated from the same foreskin: DSCs and fibroblasts from the dermis, as well as melanocytes and keratinocytes from the epidermis. This procedure was reproducible using foreskin tissue from multiple different donors. The cells were identified based on their morphology and expression profile. Each cell type was cultured using cell-specific medium and showed characteristic cellular morphologies in monolayer culture (Figure 5.8A). To exclude

contaminations with other cell types (data not shown) and demonstrate the purity of the cultures, cell-specific markers were used for staining (Figure 5.8B). With the exception of DSC cultures, which—as mentioned above—also included fibroblasts (indicated by CD90 staining), all other cell cultures were pure. The presence of fibroblasts in DSC cultures was attributed to the fact that all dermal cells were initially seeded post-isolation, and fibroblasts displayed robust proliferation in the stem cell medium.

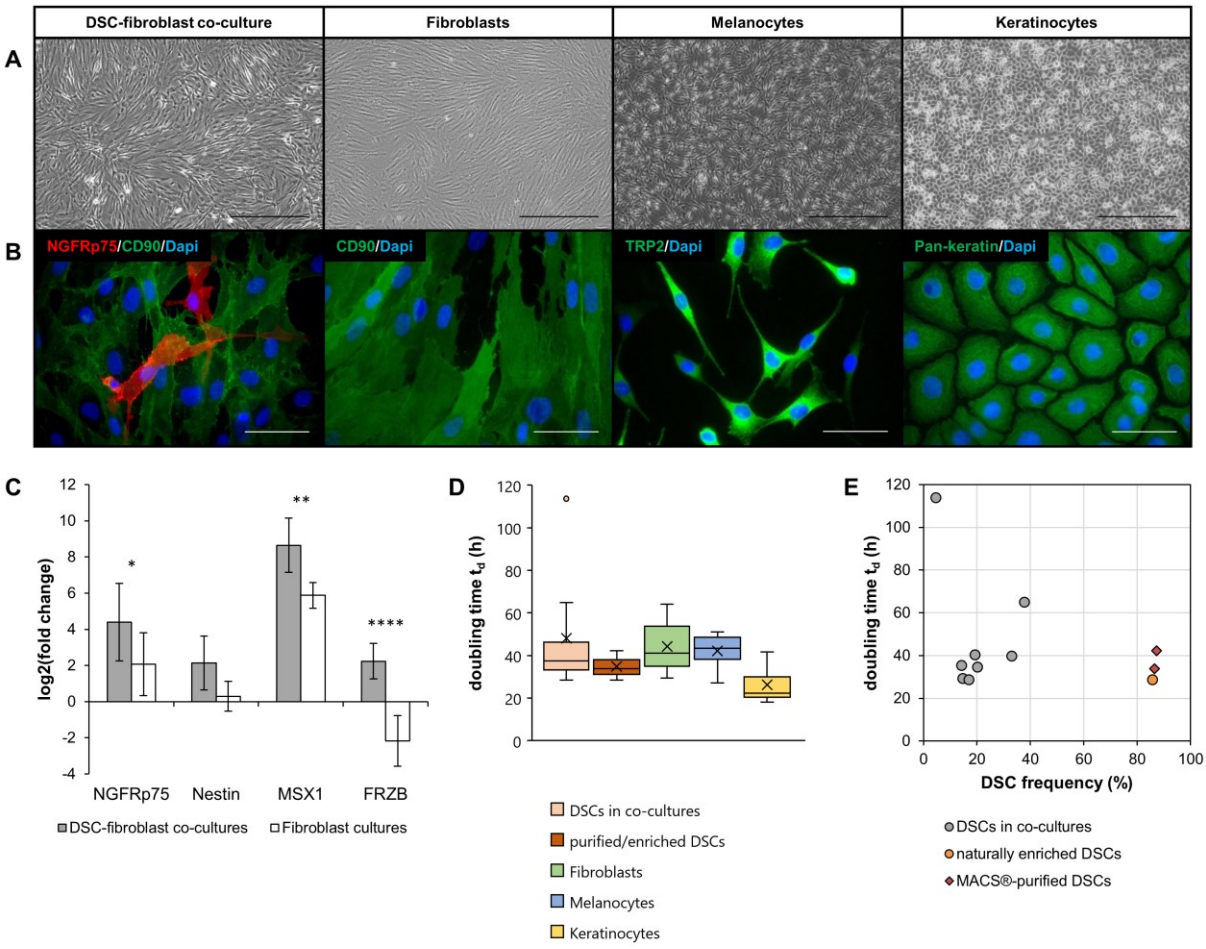

Figure 5.8 Characterization of DSCs, fibroblasts, melanocytes and keratinocytes. (**A**) Light microscopy of the four different skin cell types isolated from the same foreskin and cultured in the appropriate media. Scale bars: 500 µm. (**B**) Immunocytochemical staining for specific marker proteins NGFRp75, CD90, TRP2, and Pan-keratin. Scale bars: 50 µm (**C**) Gene expression analysis of NCSC genes NGFRp75, nestin, MSX1, and FRZB in DSC-fibroblast co-cultures and fibroblast cultures. Values are presented as mean ± SDs. Sample size: DSC-fibroblast co-cultures n=6, fibroblasts n=4, with technical duplicates. Normalized on melanocytes. t-test: *$p \leq 0.05$; **$p \leq 0.01$; ****$p \leq 0.0001$ (adapted from [398]). (**D**) Doubling times of DSCs, fibroblasts, melanocytes, and keratinocytes. DSCs are subdivided into DSCs in fibroblast-containing co-cultures and purified DSCs. Boxplots displaying the median with 25th/75th percentiles (inclusive method). The length of the box marks the interquartile range (IQR). The cross (×) inside the box indicates the mean doubling time. Dots represent outliers. Sample size: DSC-fibroblast co-cultures n=8, purified DSCs n=3, fibroblasts n=8, melanocytes n=7, keratinocytes n=10. (**E**) Plot of DSC frequency (*x*-axis) versus doubling time (*y*-axis) of different donor cell strains.

Examination of the expression profiles of NCSC-related genes revealed significantly elevated expression levels of NGFRp75 ($p = 0.021$), MSX1 ($p = 0.005$), and FRZB ($p < 0.0001$) in DSC-fibroblast co-cultures compared to fibroblast cultures derived from the same donor (Figure 5.8C). While nestin also displayed increased abundance in DSC-fibroblast co-cultures, the difference was not deemed statistically significant ($p = 0.056$). These findings underscore that the stem cell medium specifically promotes the proliferation and enrichment of stem cells, despite the concurrent presence of fibroblasts in the same culture. Low expression levels of stem cell-associated genes in fibroblast cultures suggested that a minor fraction of DSCs might have proliferated within the fibroblast cultures as well.

5.3.2 Doubling Times of The Skin Cell Types

DSCs not only displayed morphological differences to the other skin cells, but partially also differed in their proliferation rate (Figure 5.8D). Due to an extreme outlier among the DSCs in DSC-fibroblast co-cultures, the median was more suitable for comparison than the mean. The doubling time of DSCs in co-cultures with 37.4 h (IQR 33.1–46.2 h, mean 48.2 h) was slightly shorter than fibroblasts with 41.2 h (IQR 34.9–53.6 h, mean 44.3 h) and melanocytes with 43.3 h (IQR 38.2–48.5 h, mean 42.1 h), although this difference was quite small. Keratinocytes, on the other hand, proliferated considerably faster with a doubling time of 22.3 h (IQR 20.5–30.0 h, mean 26.3 h). Purified/enriched DSCs showed only minor changes in their proliferation rate and continued to double every 33.8 h (IQR 31.2–38.0 h, mean 34.9 h).

Additionally, it was investigated whether the stem cell frequency is a predictor of the proliferation rate. It was assumed that a higher proportion of stem cells may be the result of faster reduplication of DSCs in these cultures. Consequently, DSCs in cultures with a lower stem cell content would be expected to exhibit a longer doubling time compared to DSCs in cultures with a higher stem cell content. However, when plotting the DSC frequency of different donor cell strains against the DSC doubling time, no correlation between the two parameters was observed (Figure 5.8E).

5.3.3 Differentiation of DSCs into Melanocytes

As part of the functional characterization of DSCs, the aim was to investigate if *in vitro* cultured DSCs show multiple properties of NCSCs. A NCSC-characteristic gene expression in DSC-fibroblast co-cultures has already been demonstrated above (Figure 5.8C). The multipotency of DSCs was initially shown by Li and colleagues [31]. In this work, only melanocytes among the various progeny of the DSCs were relevant. Hence, the capability of DSCs to generate

differentiated melanocytes was evaluated in both DSC-fibroblast co-cultures and purified DSCs, to simultaneously verify if the differentiation potential of DSCs was affected by the enrichment via IMS. The progression of differentiation was tracked using light microscopy, immunocytochemistry, and gene expression analysis.

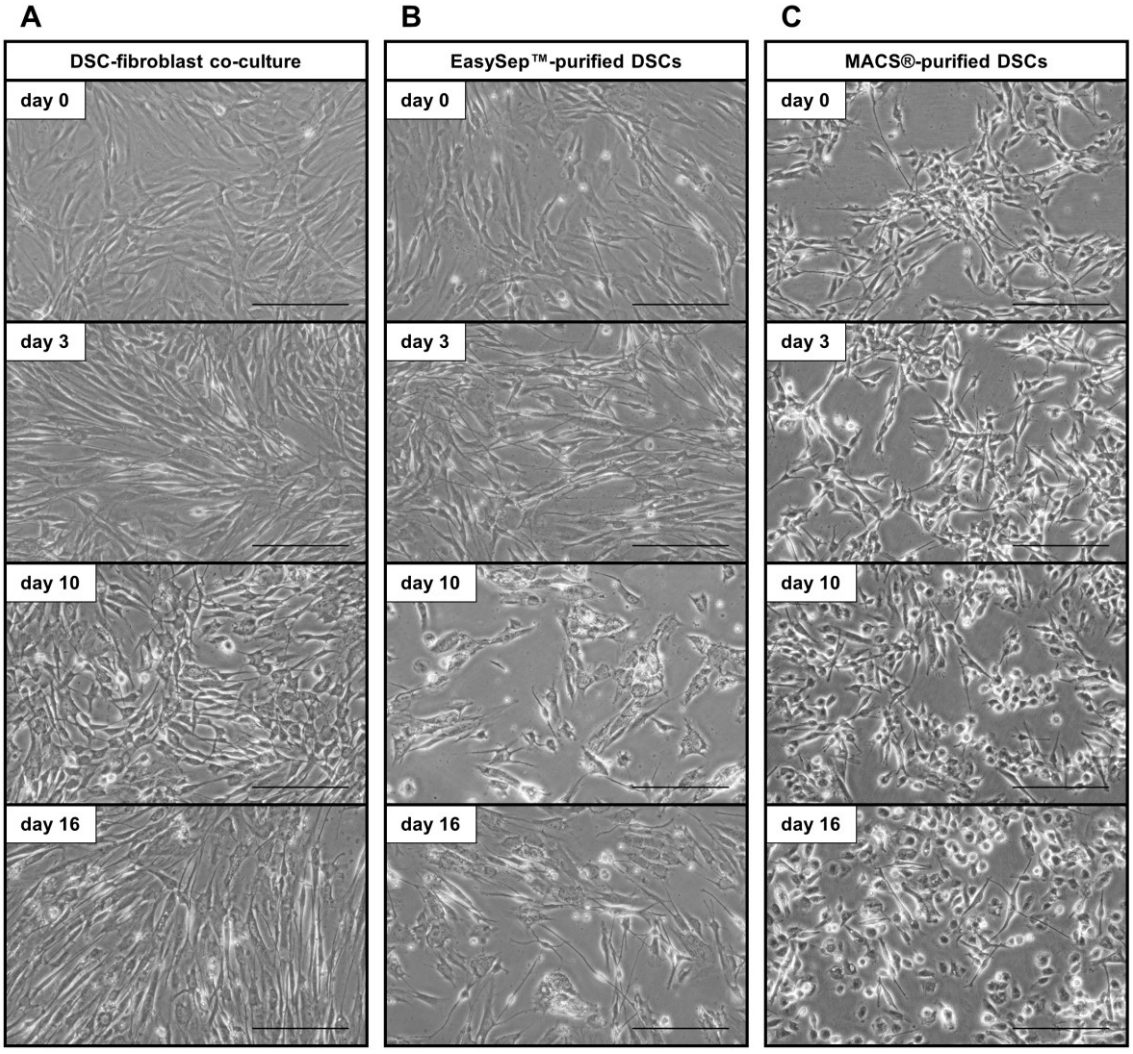

Figure 5.9 Morphology of DSC cultures during differentiation. Light microscopy of (**A**) a DSC-fibroblast co-culture (10% DSCs), (**B**) EasySep™ positive selection-purified DSCs (69% DSCs), and (**C**) MACS® positive selection-purified DSCs (97% DSCs) cultivated in melanocyte differentiation medium at days 0, 3, 10, and 16 of differentiation. Scale bars A–C: 200 µm.

During cultivation in melanocyte differentiation medium over a span of two to three weeks, the cells transitioned from a fibroblast-like morphology to a dendritic shape (Figure 5.9A–C). On day 0, the DSC fibroblast co-culture (containing 10% stem cells) had grown very densely (Figure 5.9A), while the EasySep™-purified DSCs (69% stem cells) displayed slightly less confluency (Figure 5.9B), and the MACS®-purified DSCs (97% stem cells) showed a network-like growth pattern (Figure 5.9C). As the differentiation progressed, cell density decreased in all three cultures, and the cell morphology became more distinct. Moreover, the cells reduced

in size, and an increasing number of long dendritic extensions became visible. By day 16, certain cells clearly exhibited the characteristic morphology of melanocytes (Figure 5.9A–C), especially in the MACS®-purified DSC cultures (see Appendix Figure 8.2A). However, in the DSC-fibroblast co-culture, identifying these cells was more challenging than in the purified cultures due to the presence of numerous large-sized fibroblasts and the resulting higher confluency.

Immunocytochemical staining was used to visualize the various stages of differentiation throughout the differentiation process, unveiling a heterogeneous cell culture. The representative pictures shown in Figure 5.10 derive from DSC-fibroblast co-cultures on day 13 of differentiation. Some cells displayed strong expression of NGFRp75, denoting DSCs (Figure 5.10A), while others exhibited concurrent expression of both NGFRp75 and the melanocyte marker HMB45, suggesting an ongoing differentiation process into melanocytes (Figure 5.10B). Notably, the expression of NGFRp75 was weaker in these double-positive cells compared to undifferentiated DSCs. Cells exclusively expressing HMB45 were also observed, indicative of terminally differentiated melanocytes (Figure 5.10A).

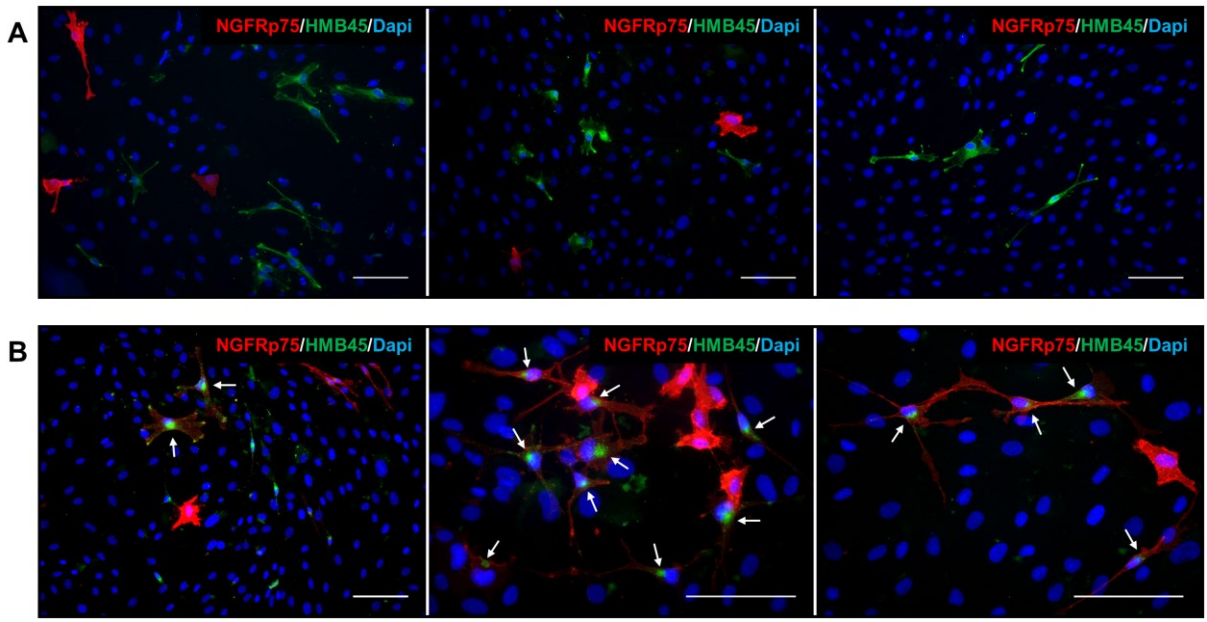

Figure 5.10 Transition from DSCs into melanocytes. Immunocytochemical staining for NCSC marker NGFRp75 (red), and melanocytic marker HMB45 (green) at day 13 in DSC-fibroblast co-cultures. (**A**) Co-existence of DSCs and differentiated melanocytes. (**B**) Arrows mark cells with expression of multiple markers. Nuclei were counterstained with DAPI (blue). Scale bars A–B: 100 µm.

Staining after 17–21 days at the end of the experiment revealed successful differentiation into melanocytes in DSC-fibroblast co-cultures (Figure 5.11A), EasySep™-purified DSC cultures (Figure 5.11B), and MACS®-purified DSC cultures (Figure 5.11C), reflected by cells with

strong expression of HMB45 and TRP2. However, the number of HMB45^{+} cells in EasySep™-purified DSCs appeared lower than in the other two cultures.

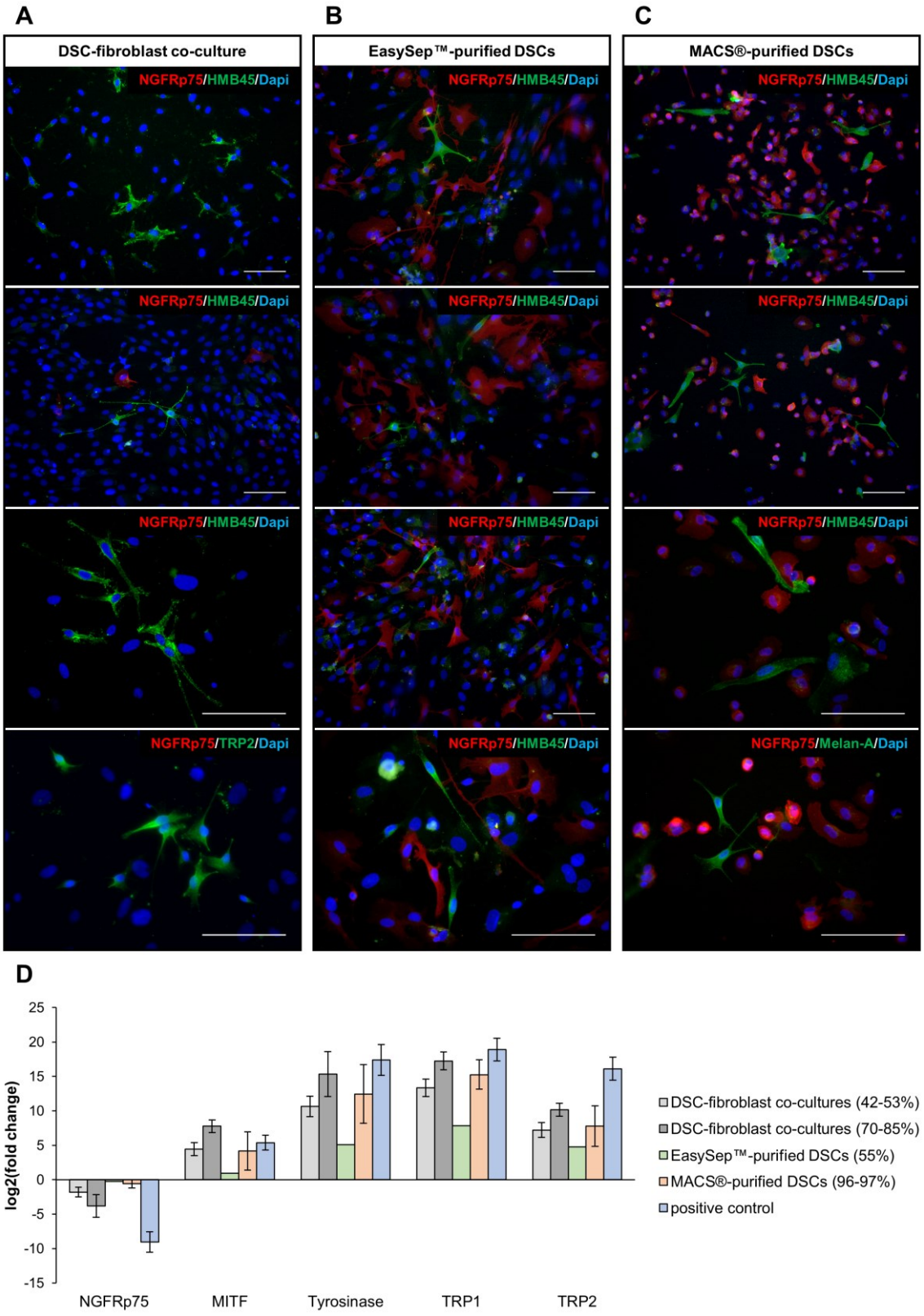

Figure 5.11 End of differentiation process. (**A–C**) Immunocytochemical staining for NCSC marker NGFRp75 (red), and melanocytic markers HMB45 (green), TRP2 (green), and Melan-A at the end of differentiation (day 17–21) in (**A**) DSC-fibroblast co-culture, (**B**) EasySep™ positive selection-purified

DSCs, and (**C**) MACS® positive selection-purified DSCs. Nuclei were counterstained with DAPI (blue). Scale bars: 100 µm. (**D**) Gene expression analysis of NGFRp75 and melanocytic markers (MITF, tyrosinase, TRP1, TRP2) at day 16 of differentiation in naturally enriched DSC-fibroblast co-cultures with 40–50% and 70–85% stem cell frequency, EasySep™-purified DSCs with 55% stem cells, and MACS®-purified DSCs with 96–97% stem cells. Foreskin-derived melanocytes served as positive control. Values are presented as mean ± SDs. Sample size with technical duplicates: DSC-fibroblast co-cultures (40–50%) n=2, DSC-fibroblast co-cultures (70–85%) n=2, EasySep™-purified DSCs n=1, MACS®-purified DSCs n=3. Normalized on the respective control cells cultivated in stem cell medium.

The melanocytes were mostly not evenly dispersed throughout the culture but instead clustered together in several small groups. Throughout the differentiation process, the percentage of NGFRp75$^+$ cells in DSC-fibroblast co-cultures declined (data not shown), resulting in little to no DSCs by the end of differentiation when the initial stem cell frequency was already relatively low (Figure 5.11A). In contrast, MACS®-purified DSC cultures continued to exhibit strong expression of NGFRp75 (Figure 5.11C), while EasySep™-purified DSC cultures also contained unstained cells, likely representing fibroblasts. Additional immunocytochemical staining of DSC-fibroblast co-cultures and MACS®-purified DSCs at the end of differentiation can be found in the Appendix Figure 8.2B–C.

For quantification of differentiation via qPCR, DSC-fibroblast co-cultures were divided into two groups (42–53% and 70–85%), depending on their DSC frequency at the start of differentiation. Despite their relatively high stem cell proportions, all of them were naturally enriched. The reduced NGFRp75 expression in DSC fibroblast co-cultures at day 16 of differentiation (3–14-fold reduction, depending on the initial DSC proportion) (Figure 5.11D) matched the observations of a decreasing DSC frequency in immunocytochemical staining (see Figure 5.11A). In purified DSC cultures (EasySep™ with 55%, MACS® with 96–97%), on the other hand, the NGFRp75 expression level remained stable. Gene expression analysis confirmed the successful differentiation into melanocytes in both DSC-fibroblast co-cultures and purified DSC cultures, as evidenced by the upregulated expression of all four melanocytic markers compared to control cells in stem cell medium. In general, TRP1 and tyrosinase exhibited the highest expression levels, and gene expression was more pronounced in cultures with a higher initial stem cell proportion (dark gray and light orange bars). With all four melanocytic genes, the most substantial upregulation was observed in DSC-fibroblast co-cultures with 70–85% stem cell content, followed by MACS®-purified DSCs (96–97%), and DSC-fibroblast co-cultures with 42–53% stem cell frequency (Table 5.1). EasySep™-purified DSCs (55%) consistently displayed the lowest gene expression, though it is important to note that these results were based on a single experiment.

Table 5.1 Increase in melanocytic gene expression at day 16 of differentiation. Values are the mean fold change.

	MITF	Tyrosinase	TRP1	TRP2
DSC-fibroblast co-cultures (70–85%)	219-fold	41,631-fold	155,831-fold	1,161-fold
MACS®-purified DSCs (96–97%)	18-fold	5,595-fold	39,219-fold	222-fold
DSC-fibroblast co-cultures (42–53%)	22-fold	1,610-fold	10,476-fold	147-fold
EasySep™-purified DSCs (55%)	2-fold	34-fold	228-fold	27-fold

Considering the stem cell content in this particular experiment, EasySep™-purified DSCs (55%) and the first group of DSC-fibroblast co-cultures (42–53%) had similar DSC frequencies, while MACS®-purified DSCs (96–97%) were more akin to the second group of DSC-fibroblast co-cultures (70–85%). When contrasting DSC-fibroblast co-cultures and purified DSCs with similar DSC frequencies, it became apparent that purified DSCs consistently displayed lower expression levels of melanocytic markers than co-cultures at day 16 of differentiation, whereby the difference for the MACS®-purified DSCs was only minimal.

5.3.4 Sphere Formation of DSCs

Another functional property of stem cells is their ability to form spherical structures when cultured in suspension [425], frequently employed to assess self-renewal capability, which is another common NCSC feature [426]. It is essential to mention that in this experiment, owing to the initial multiple-cell plating, only the capacity of sphere formation, not self-renewal, was examined. As demonstrated above, dermal cells produced spheres after their isolation from foreskin tissue. Now it was of interest, whether DSC cultures can persistently generate these stem cell-specific spheres throughout later passages, especially after being subjected to prolonged monolayer cultivation. In addition, it was essential to verify whether the purification procedure affected the potential for sphere formation. To address this, both the native cell population (17% DSCs) and an enriched population from the same donor cell strain (87% DSCs) were examined. Two fibroblast cultures were also incorporated into the analysis. Enzymatically dissociated and filtered cell cultures were seeded in suspension culture flask in stem cell medium and monitored over a span of six days.

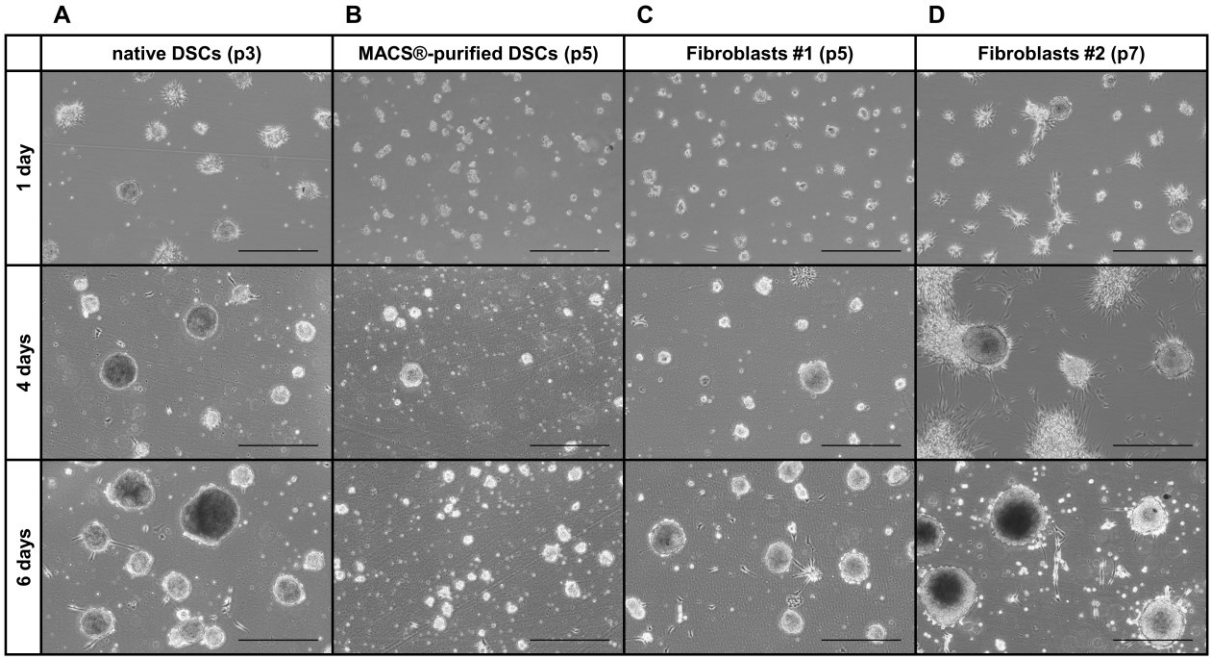

Figure 5.12 Sphere formation ability in suspension culture. Filtered cell suspensions of dissociated single cells from (**A**) a native DSC-fibroblast co-culture in passage 3 (17% DSCs), (**B**) the same DSC culture in passage 5 after purification via MACS® positive selection (87% DSCs), (**C**) a fibroblast culture in passage 5, and (**D**) another fibroblast culture in passage 7, were seeded in suspension culture flasks in stem cell medium. Formation of spheres was monitored at days 1, 4, and 6. Scale bars: 500 µm. The two fibroblast cultures were cultivated in RPMI+10%FBS prior to the experiment.

Within just one day, the native DSC-fibroblast co-culture formed spheres of remarkable size that continued to expand, culminating in large spheres by day six (Figure 5.12A). These spheres bore a close resemblance to the morphology of the dermal spheres, which were typically formed within the initial two weeks after isolation from foreskin (see Figure 5.1A). By contrast, the same DSC culture subjected to enrichment via MACS® positive selection displayed only small cell clusters on the first day, albeit in considerable numbers (Figure 5.12B). These clusters transformed into spheres in the following days but remained significantly smaller than the native spheres. Intriguingly, fibroblast cultures, previously cultivated in fibroblast-specific medium, were also able to generate spheres in stem cell medium (Figure 5.12C–D). The fibroblast spheres reached sizes comparable to the native DSC-fibroblast co-culture and arose similarly fast. One noticeable difference, however, was the tendency of fibroblast-derived spheres to frequently attach to the bottom of the cell culture flask. In addition, a notable number of cells exhibited adherent growth, either individually or forming larger colonies.

5.4 UV-Induced DNA Damage Response

In this section of the study, first investigations on the DNA damage response of DSCs following UV irradiation were performed. The main focus was on CPDs—displaying the main type of

DNA damage and a substantial result of UV exposure—and the mechanisms involved in overcoming DNA damage. All of the experiments shown in this section represent a comparative study of DSCs with three other skin cell types, in order to be able to classify the results of the DSCs adequately. Fibroblasts were chosen because they are direct neighbors of the DSCs in the same skin layer and therefore obtain the most similar exposure scenario. Melanocytes are of particular interest as direct progeny of DSCs. Keratinocytes are the skin cells that are most exposed to UV radiation and from which (other) skin tumors can derive.

The following experiments (subitems of section 5.4) were actually conducted with DSC-fibroblast co-cultures, since the enrichment of DSC cultures (see section 5.2) was not yet established. However, the methods of analysis allowed for the discrimination of DSCs and fibroblasts. Therefore, the findings shown for DSC cultures represent the results of the DSCs only, excluding the results from the fibroblasts grown in the same culture.

5.4.1 CPD Induction, DNA Repair, and Remaining DNA Damage

To evaluate DNA damage in terms of CPDs, cells were exclusively subjected to UVB irradiation and not UVA, given that UVB is the main cause of CPD induction. The UVB dose that was used in these experiments was comparable to the minimal erythema dose *in vivo*. For an adequate comparison, it was essential to ensure that same amounts of DNA lesions were induced in the different cell types.

The induction of CPDs after 285 J/m² UVB exposure showed almost identical levels and consistent variances among various donors in DSCs (604 ± 81 a.u.), fibroblasts (645 ± 79 a.u.), and keratinocytes (642 ± 95 a.u.) (Figure 5.13A). However, melanocytes exhibited a significantly lower CPD induction level, measuring 388 ± 131 a.u. ($p = 0.04$). By comparison, UVB irradiation with 285 J/m² induced nearly 40% fewer CPDs in melanocytes than in DSCs. In order to establish comparable initial levels of CPD induction, melanocytes were exposed to a UVB dose 40% higher, equivalent to 400 J/m². With this increased UVB dose, the prior lower level of initial DNA lesions turned into approximately 20% more CPDs in melanocytes (727 ± 185 a.u.) compared to DSCs, and exhibited a broader variance among different donor cell strains. This variance was most probably attributed to the utilization of other donor cell strains for the higher dose irradiation of melanocytes, deviating from the initial irradiation at the lower dose.

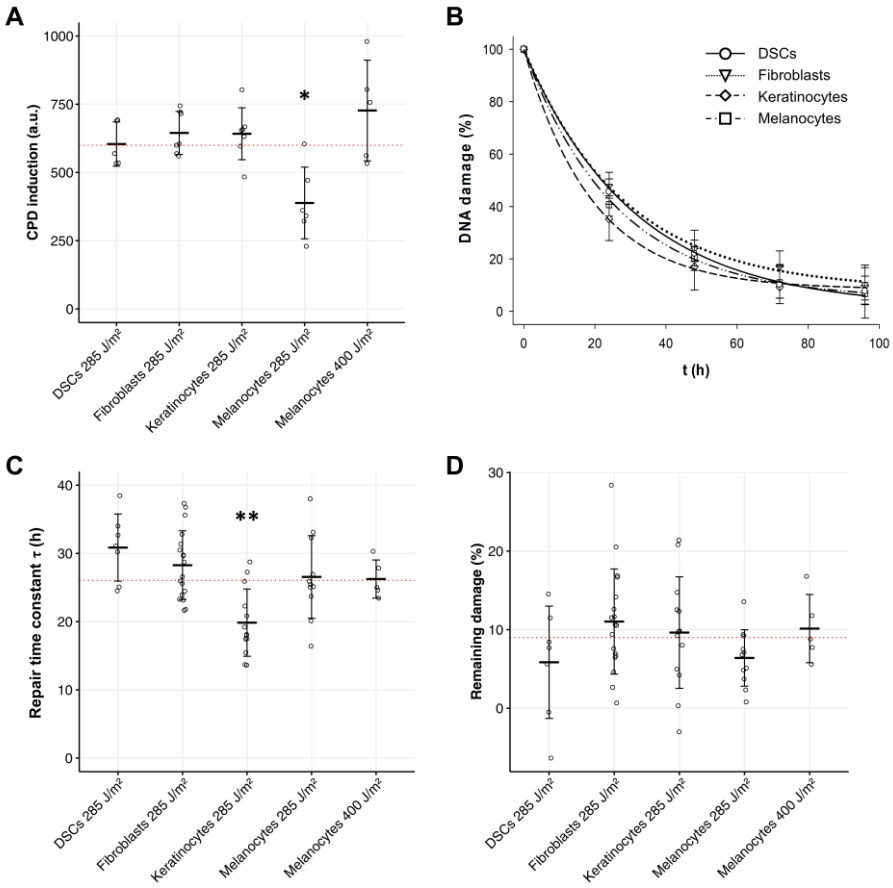

Figure 5.13 CPD induction, repair time constant and remaining DNA damage after UVB irradiation. Cells were irradiated with 285 J/m² UVB (melanocytes were irradiated with a single dose of 285 J/m² or 400 J/m² UVB), harvested at different times, and CPDs were measured via flow cytometry. (**A**) Induction of CPDs immediately post-irradiation. Sample size: DSCs n=5, fibroblasts n=7, keratinocytes n=7, melanocytes 285 J/m² n=6, melanocytes 400 J/m² n=5. (**B**) The fitting of an exponential decay to the CPD amount over five different points of time provided the repair time constant τ. Representative kinetics from combined results of multiple samples. Sample size: DSCs n=7, fibroblasts n=18, keratinocytes n=13, melanocytes n=11. Values are presented as mean ± SDs. (**C**) Repair time constant τ of the distinct cell types obtained by CPD kinetics. (**D**) Remaining CPD content at 96 h after irradiation. Sample size for C and D: DSCs n=7, fibroblasts n=18, keratinocytes n=13, melanocytes 285 J/m² n=11, melanocytes 400 J/m² n=5. Values in A, C, and D are presented as mean ± SDs. Red dotted lines indicate basemean. Pairwise t-test: *p ≤ 0.05; **p ≤ 0.01 (adapted from [398]).

The repair time constant τ (see Appendix Table 8.2) extracted from CPD kinetics (Figure 5.13B) served as a measure for the DNA repair rate. The analysis of the overall mean repair time constants revealed a gradual increase in repair times from melanocytes (τ = 26.6 ± 6.1 h) to fibroblasts (τ = 28.3 ± 5.0 h) and DSCs (τ = 30.9 ± 4.9 h) (Figure 5.13C). However, owing to τ values predominantly spanning between 22–34 h among different donors, these differences failed to reach statistical significance. In contrast, keratinocytes demonstrated significantly faster repair (τ = 19.9 ± 4.9 h; p = 0.004) in comparison to the other cell types. Remarkably, even with an enhanced initial CPD content after exposure to 400 J/m² UVB, melanocytes exhibited the same repair capacities (τ = 26.2 ± 2.8 h).

To further investigate DNA repair, the remaining DNA damage at the final point of the kinetics was determined. Assessing the quantity of unrepaired CPDs 96 h after UVB irradiation (285 J/m²), both fibroblasts (11.0 ± 6.7%) and keratinocytes (9.6 ± 7.1%) demonstrated nearly equivalent values (Figure 5.13D). These cell types exhibited a notably wide distribution, encompassing up to 28.4% and 21.4% of remaining CPDs, respectively. DSCs (5.9 ± 7.1%) and melanocytes (6.4 ± 3.6%) presented slightly lower mean percentages. Following exposure to 400 J/m² UVB, melanocytes left 10.1 ± 4.3% of initial CPDs unrepaired. The small disparities in remaining DNA damage among the four skin cell types did not yield statistical significance (ANOVA, $p = 0.216$).

5.4.2 Cell Cycle Progression

DNA repair is closely linked to cell cycle regulation to allow for proper removal of lesions before the cell proceeds to proliferate. Therefore, the investigation of the damage response of DSCs also included the analysis of the cell cycle distribution following UV irradiation. Measurement time points were selected based on first cell cycle findings of our group published by Mhamdi-Ghodbani et al. (2021) [398]. The final 96-hour point was replaced with an earlier point at 16 h post-irradiation. Additionally, this investigation was expanded beyond UVB exposure to also include UVA, each with two different doses.

It was noticeable that the baseline cell cycle distribution in non-irradiated controls at 0 h differed depending on the cell type. DSCs (G1: 68.0%, S: 18.3%, G2/M: 13.7%, Figure 5.14A) showed the highest resemblance to keratinocytes (G1: 68.3%, S: 20.9%, G2/M: 10.9%, Figure 5.14D), both having a G1-S-G2/M ratio of approximately 70:20:10. Fibroblasts (G1: 85.9%, S: 7.8%, G2/M: 6.4%, Figure 5.14B) and melanocytes (G1: 89.0%, S: 7.0%, G2/M: 4.0%, Figure 5.14C) also demonstrated similarity, characterized by a predominant G1 phase of >85%, and nearly equal shares of S and G2/M phases. Melanocytes displayed a very small G2/M phase. Conspicuously, after sham-irradiation, all cell types, except for DSCs, exhibited an increasing S phase proportion in control cells. Keratinocytes reached the largest S phase proportion after 16 h (Figure 5.14D), while fibroblasts and melanocytes took up to 24 h (Figure 5.14B+C), followed by a gradually declining S phase at the subsequent time points. By the 72-hour point, the cell cycle distribution appeared to have leveled off in all cell types, reaching nearly baseline distribution from the 0-hour point. DSC controls, on the other hand, showed an invariable cell cycle distribution throughout the whole experiment (Figure 5.14A).

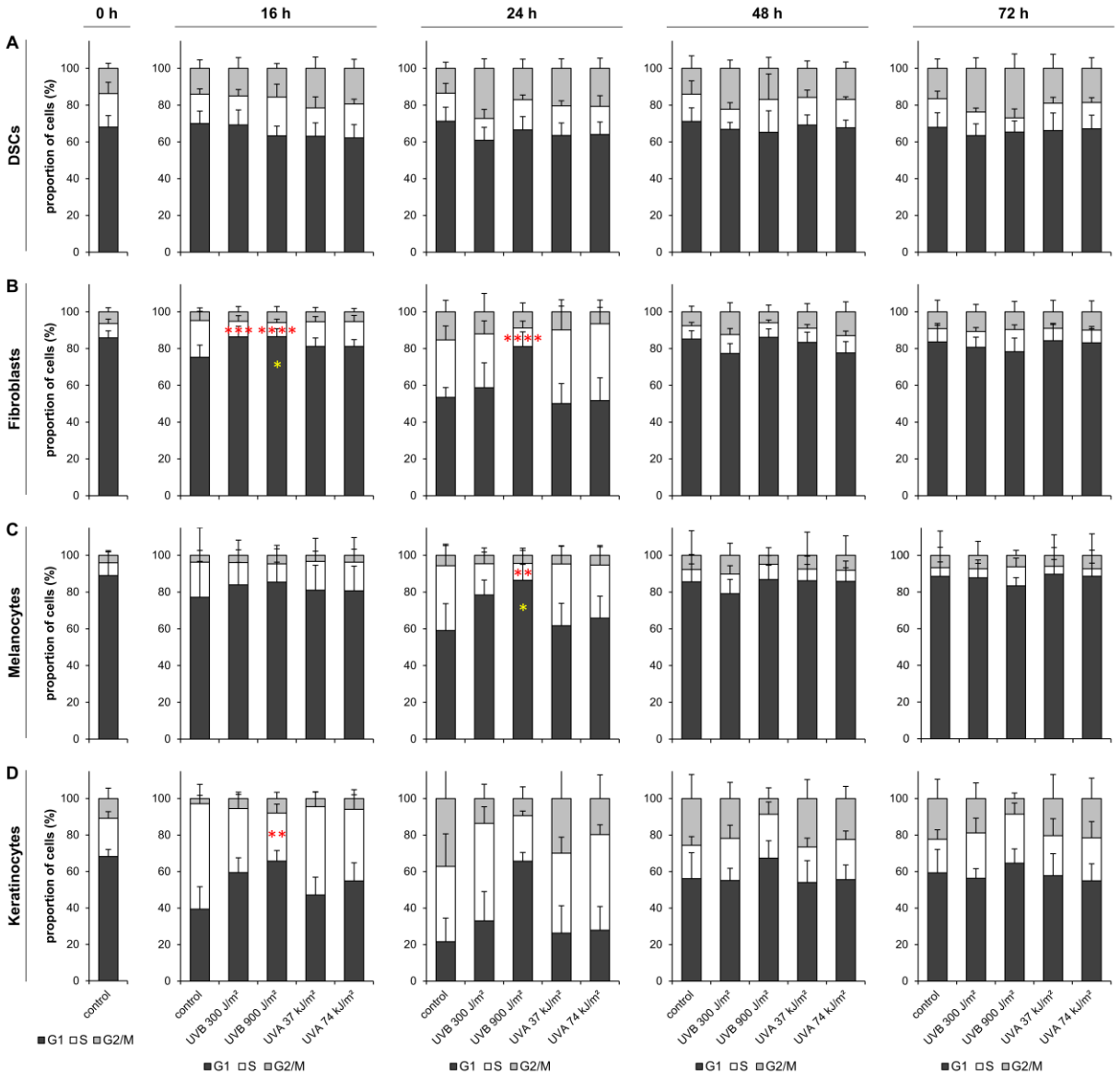

Figure 5.14 Cell cycle distribution after UV irradiation. Cells were irradiated with 300 or 900 J/m² UVB or with 37 or 74 kJ/m² UVA, and harvested after 0, 16, 24, 48, and 72 h. Distribution of the cell cycle phases was measured with propidium iodide staining via flow cytometry in (**A**) DSCs, (**B**) fibroblasts, (**C**) melanocytes, and (**D**) keratinocytes. Values are presented as mean ± SDs. Sample size: DSCs n=5, fibroblasts n=7, melanocytes n=7, keratinocytes n=5. Multiple comparisons versus the respective control (One-way ANOVA and Dunnett's method): *$p \leq 0.05$; **$p \leq 0.01$; ***$p \leq 0.001$; ****$p \leq 0.0001$.

UV irradiation resulted in notably different cell cycle progressions in DSCs compared to the other three skin cell types. DSCs did not exhibit any significant cell cycle alterations at all, neither with UVB nor with UVA exposure (Figure 5.14A). There were only slight indications of a G2 arrest after UVB irradiation; otherwise, the cell cycle distribution remained stable. On the contrary, especially 900 J/m² UVB induced a distinct arrest in the G1 phase, accompanied by a reduced S (and G2/M) phase in fibroblasts (Figure 5.14B), melanocytes (Figure 5.14C), and keratinocytes (Figure 5.14D) after 24 h. In fibroblasts and keratinocyte, this effect was already evident at 16 h post-irradiation. Similar tendencies were observed after exposure to

300 J/m² UVB, albeit statistically significant only in fibroblasts. After 48 h, the proportions of cell cycle phases in UVB-irradiated cells aligned with those of the control cells. Irradiation with UVA did not affect cell cycle regulation in any of the cell types, neither with 37 kJ/m² nor with 74 kJ/m². An overview of all significant alterations along with the corresponding p-values is displayed in Table 5.2.

Table 5.2 Statistically significant cell cycle alterations following UV irradiation.

Cell type	Time	Irradiation	Cell cycle phase with p-value	
Fibroblasts	16 h	300 J/m² UVB	S	p = 7.578e-4 (***)
	16 h	900 J/m² UVB	S	p = 2.072e-5 (****)
			G1	p = 0.042 (*)
	24 h	900 J/m² UVB	S	p = 1.336e-6 (****)
Melanocytes	24 h	900 J/m² UVB	S	p = 1.608e-3 (**)
			G1	p = 0.039 (*)
Keratinocytes	16 h	900 J/m² UVB	S	p = 2.769e-3 (**)

5.4.3 Induction of Apoptosis

Simultaneous to the cell cycle analysis, it was verified whether the applied UVB and UVA doses were tolerated by the examined skin cells, or if cell damage led to the induction of apoptosis. Additionally, the cell numbers were determined at harvesting and plotted against time. In none of the four cell types did irradiation with both UVA doses (37 kJ/m², 74 kJ/m²) or the lower UVB dose (300 J/m²) lead to the induction of apoptosis. Following exposure to the higher UVB dose of 900 J/m², DSCs showed a small increase in apoptotic cells 24 h after irradiation (21.4 ± 3.8%) as well as an obvious induction after 48 h (35.4 ± 18.1%) that were both, however, not deemed statistically significant (Figure 5.15A). This lack of statistical significance was most probably attributed to the high variability, since looking at the results from the different donors individually showed a clear effect of apoptosis induction after 900 J/m² UVB at both times (see Appendix Table 8.3). In line with this increase in apoptotic cells, the same samples showed a statistically significant simultaneous decrease in the DSC frequency following 900 J/m² UVB, with a fold change of 0.80 ($\log_2$(FC) = -0.33; p = 0.005) and 0.82 ($\log_2$(FC) = -0.30; p = 0.026) at 24 h and 48 h, respectively (see Appendix Figure 8.3). This higher UVB dose also induced apoptosis in fibroblasts after 48 h (17.0 ± 2.5%, p = 1.060e-9) (Figure 5.15B) as well as in melanocytes after both 24 h (23.4 ± 7.0%, p = 1.021e-3) and 48 h (26.6 ± 7.0%, p = 6.399e-4) (Figure 5.15C), whereas keratinocytes were not affected (Figure 5.15D).

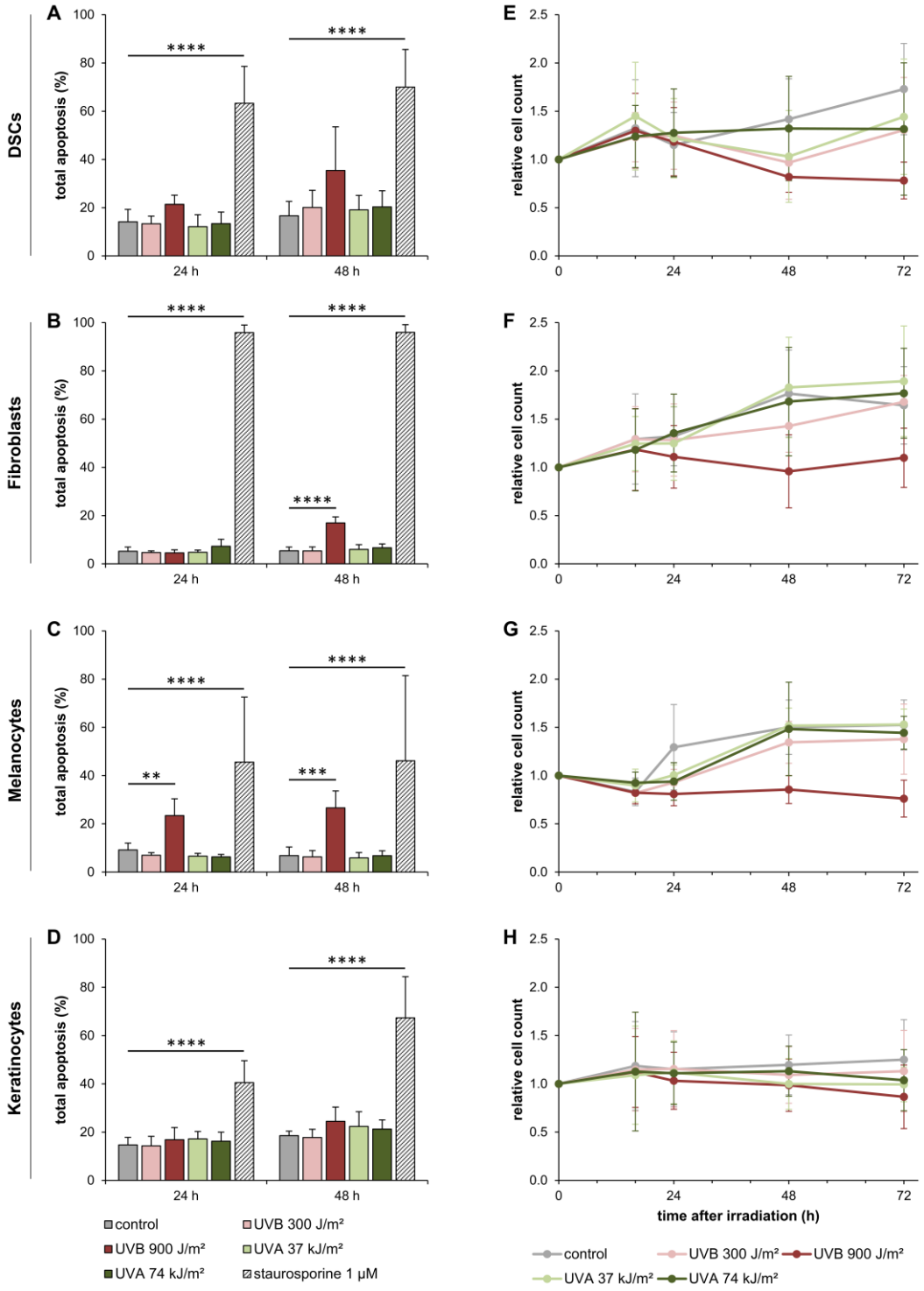

Figure 5.15 Induction of apoptosis and cell counts after UV irradiation. Cells were irradiated with 300 or 900 J/m² UVB or with 37 or 74 kJ/m² UVA, and harvested after 0, 16, 24, 48, and 72 h. (**A–D**) Proportion of total (early + late) apoptotic cells was measured after 24, and 48 h with Annexin-V assay via flow cytometry in (**A**) DSCs, (**B**) fibroblasts, (**C**) melanocytes, and (**D**) keratinocytes. Values are presented as mean ± SDs. Sample size: DSCs n=6, fibroblasts n=7, melanocytes n=6, keratinocytes n=6. Staurosporine-treated cells (1 µM for 3 h) served as positive controls. Multiple comparisons versus the respective control (One-way ANOVA and Dunnett's method): **p ≤ 0.01; ***p ≤ 0.001; ****p ≤ 0.0001. The individual results from each donor can be found in Appendix Table 8.3. (**E–H**) Cell counts at the time of harvest after 0, 16, 24, 48, and 72 h, relative to the counts of control cells at 0 h determined in (**E**) DSCs, (**F**) fibroblasts, (**G**) melanocytes, and (**H**) keratinocytes. Values are presented as mean ± SDs. Sample size: DSCs n=5, fibroblasts n=7, melanocytes n=6, keratinocytes n=5.

The positive controls confirmed the validity of the method with significantly increased amounts of apoptotic cells at both times in all four cell types, while revealing different susceptibility of the skin cells to the staurosporine treatment. Fibroblasts appeared to be most sensitive (24 h: 95.9 ± 3.1%; 48 h: 96.0 ± 3.2%), followed by DSCs (24 h: 63.3 ± 15.3%; 48 h: 70.0 ± 15.6%), keratinocytes (24 h: 40.5 ± 9.0%; 48 h: 67.3 ± 17.1%), and melanocytes (24 h: 45.6 ± 27.0%; 48 h: 46.1 ± 35.3%), including high donor-dependent variability in the last three cell types. An overview of all significant changes along with the corresponding p-values is displayed in Table 5.3.

Table 5.3 Statistically significant induction of apoptosis.

Cell type	Time	Treatment	p-value
DSCs	24 h	1 µM staurosporine	p = 4.863e-9 (****)
	48 h	1 µM staurosporine	p = 1.067e-6 (****)
Fibroblasts	24 h	1 µM staurosporine	p < 0.0001 (****)
	48 h	900 J/m² UVB 1 µM staurosporine	p = 1.060e-9 (****) p < 0.0001 (****)
Melanocytes	24 h	900 J/m² UVB 1 µM staurosporine	p = 1.021e-3 (**) p = 1.430e-7 (****)
	48 h	900 J/m² UVB 1 µM staurosporine	p = 6.399e-4 (***) p = 2.575e-5 (****)
Keratinocytes	24 h	1 µM staurosporine	p = 9.594e-7 (****)
	48 h	1 µM staurosporine	p = 5.232e-11 (****)

Corresponding to the induction of apoptosis, DSCs exhibited steadily decreasing cell counts when irradiated with 900 J/m² UVB (Figure 5.15E). They also showed a drop in cell numbers 48 h following 300 J/m² UVB and 37 kJ/m² UVA, although no apoptotic cells were detected. In fibroblasts, melanocytes, and keratinocytes, apoptosis results and cell count also correlated very well. Fibroblasts (Figure 5.15F) and melanocytes (Figure 5.15G) displayed lower cell numbers following exposure to 900 J/m² UVB, consistent with increased proportions of apoptotic cells, while in the other samples the cell count increased continuously. In keratinocytes, the similarly developing cell numbers of control and irradiated cells matched the absence of apoptosis (Figure 5.15H).

5.5 Effect of UV on The Differentiation Potential of DSCs

The capability of DSCs to differentiate into melanocytes was already proven in section 5.3.3. Since DSCs in the human skin are subjected to UV radiation, it was of utmost interest, if their differentiation potential is affected by UV radiation or if UV exposure promotes differentiation.

For this, DSC-fibroblast co-cultures and MACS® positive selection-purified DSCs were exposed to a single dose of 300 J/m² UVB or 37 kJ/m² UVA one day before starting the differentiation process. The progression of differentiation was tracked using light microscopy and gene expression analysis.

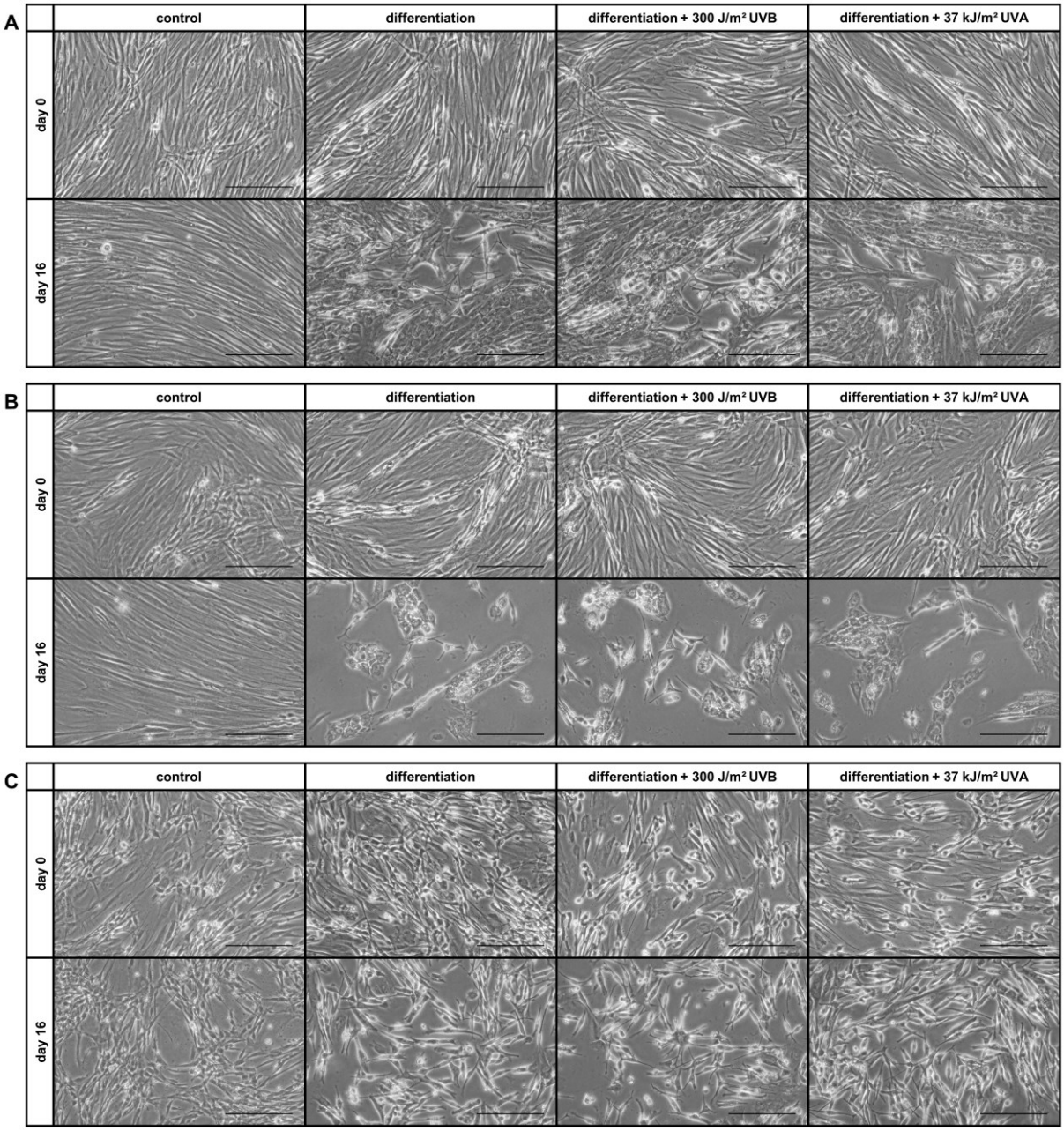

Figure 5.16 Differentiation in DSC-fibroblast co-cultures after UV irradiation. Light microscopy of three different DSC-fibroblast co-cultures with varying initial stem cell frequencies at days 0 and 16 of differentiation assay. Stem cell proportion: (**A**) 42% DSCs, (**B**) 55% DSCs, (**C**) 70% DSCs. Cells were cultivated in melanocyte differentiation medium and irradiation with a single dose of 300 J/m² UVB or 37 kJ/m² UVA was conducted one day prior to starting the differentiation. Control cells were cultivated in stem cell medium. Scale bars: 200 µm.

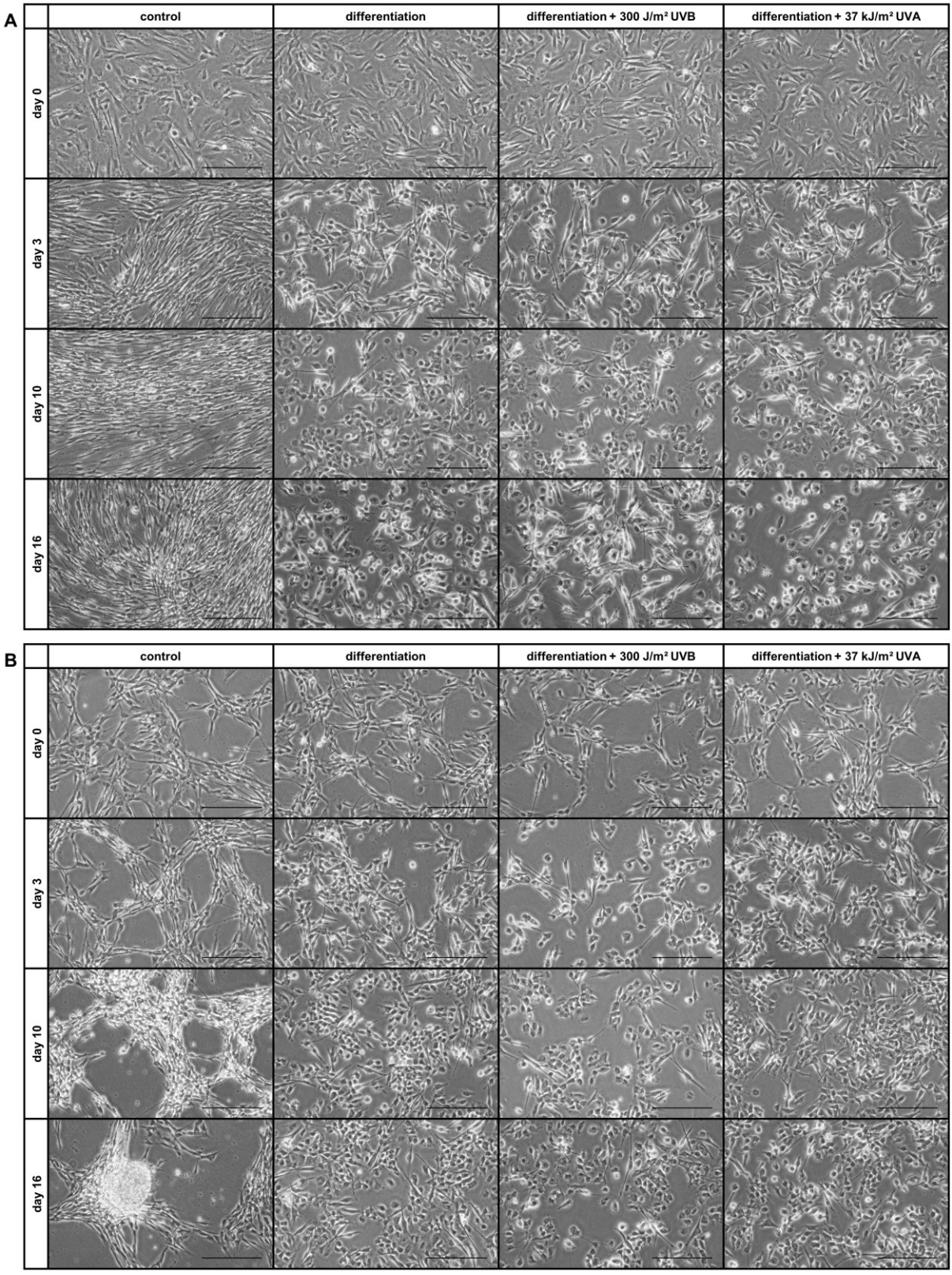

Figure 5.17 Differentiation in MACS®-purified DSC cultures after UV irradiation. Light microscopy of two different MACS® positive selection-purified DSC cultures at days 0, 3, 10 and 16 of differentiation assay. Purified DSCs in (**A**) and (**B**) both with 97% DSCs. Cells were cultivated in melanocyte differentiation medium and irradiation with a single dose of 300 J/m² UVB or 37 kJ/m² UVA was conducted one day prior to starting the differentiation. Control cells were cultivated in stem cell medium. Scale bars: 200 µm.

As previously demonstrated, the cultures exhibited lower cell density when supplied with differentiation medium in comparison to control cells cultured in stem cell medium (see section 5.3.3). It is noteworthy that different donor cell strains displayed different sensitivity to the differentiation medium (as well as to UV irradiation), strikingly illustrated in diverse DSC-fibroblast co-cultures. In one culture (initially 42% DSCs), dense cell growth continued (Figure 5.16A), whereas another culture (70% DSCs) exhibited a noticeably reduced confluency (Figure 5.16C), and in a third culture (55% DSCs), an exceptionally high number of cells died, leaving only individual cells and small colonies (Figure 5.16B).

A reduced confluency when cultured in differentiation medium was evident in the purified DSC cultures (97% DSCs) as well (Figure 5.17), which additionally also showed diverse growth patterns in stem cell medium. On the one hand, cultures with an initially uniform and widespread growth became denser over time and the DSCs appeared innervated to cluster together, consequently evolving network patterns at high confluency (Figure 5.17A). On the other hand, some donor cell strains already displayed a network-like growth pattern right after purification and in extreme cases, tended to form spheres upon a high cell count, despite the BME-coating (Figure 5.17B).

When DSC cultures were irradiated with UVB prior to differentiation, the previously described decline in cell density was even more pronounced. This effect was particularly noticeable in purified DSC cultures (Figure 5.17B), where the UVB-irradiated samples occasionally experienced complete cell death within the initial 7–10 days of the differentiation assay if the initial confluency was too low (data not shown). UVA irradiation, on the other hand, had minimal impact on the cell density of DSC-fibroblast co-cultures (Figure 5.16), and in purified DSCs, any reduction in confluency following UVA was only mildly pronounced (Figure 5.17). Hence, the morphology of UVA-exposed samples mostly resembled the non-irradiated differentiation samples. At day 16 of differentiation, in both DSC-fibroblast co-cultures (Figure 5.16) and purified DSC cultures (Figure 5.17), cells with distinct melanocyte-like morphology were detected, even after UV irradiation. Macroscopically, there was no observable difference in the number of these dendritic cells between irradiated and non-irradiated cultures.

At various times during the differentiation process, gene expression of multiple melanocytic markers and the NCSC marker NGFRp75 were examined. Overall, no differences were found between UVB-irradiated (‘diff + 300 J/m² UVB’) or UVA-irradiated cells (‘diff + 37 kJ/m² UVA’) and non-irradiated cells (‘diff’), neither in DSC-fibroblast co-cultures nor in MACS®-purified DSC cultures (Figure 5.18).

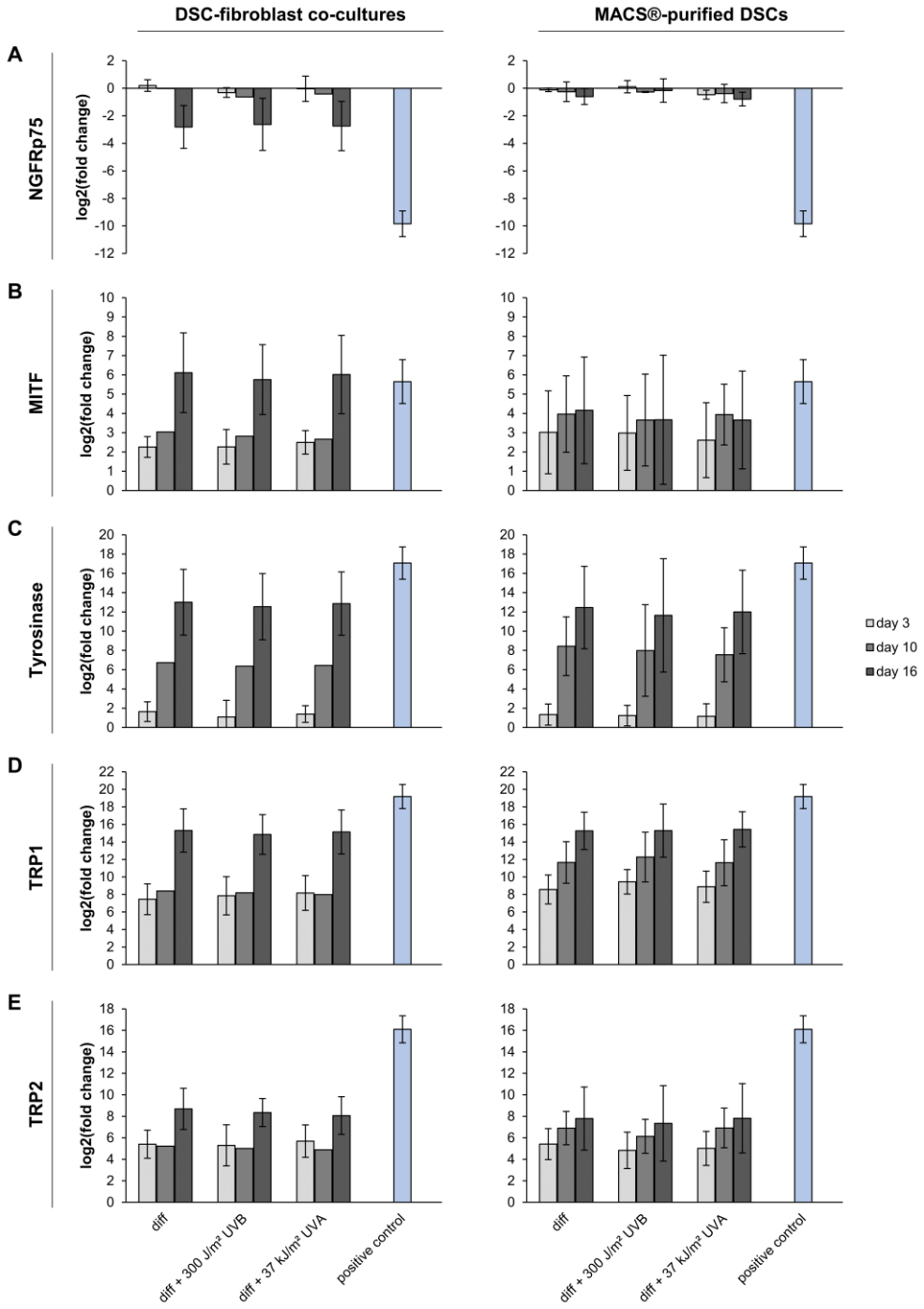

Figure 5.18 Gene expression analysis of differentiation following UV irradiation. Gene expression analysis of NGFRp75 (**A**) and melanocytic markers MITF (**B**), tyrosinase (**C**), TRP1 (**D**), and TRP2 (**E**) at days 3, 10, and 16 of differentiation in naturally enriched DSC-fibroblast co-cultures and MACS®-purified DSCs. Foreskin-derived melanocytes served as positive control. Values are presented as mean ± SDs. Sample size with technical duplicates: DSC-fibroblast co-cultures n=5 at day 3, n=1 at day 10, n=4 at day 16; MACS®-purified DSCs n=3 at all times. Normalized on the respective control cells cultivated in stem cell medium.

The expression levels of NGFRp75 in DSC-fibroblast co-cultures decreased throughout the differentiation, resulting in a 6–7-fold reduction ($\log_2(FC) \approx -2.7$) by day 16 in all samples, while in MACS®-purified DSCs, nearly no changes were observed (Figure 5.18A). Melanocytic genes were gradually upregulated over time in both DSC-fibroblast co-cultures

and purified DSCs, showing considerably high values at day 16. These final expression values were in the same range for DSC-fibroblast co-cultures and for purified DSCs. However, the upregulation occurred more rapidly in purified DSCs, as evidenced by higher expression levels at day 3 and 10. Among all the melanocytic genes examined, MITF was ultimately expressed with the lowest values (log_2(FC) = 4–6, corresponding to a 15–65-fold upregulation) at day 16 (Figure 5.18B), while tyrosinase was more abundant with log_2(FC) values ranging around 12–13 (corresponding to 4,000–8,000-fold upregulation) (Figure 5.18C). For both genes, the variance between different donors was noticeably larger in purified cells. TRP1 was upregulated the most, leading to an increase of up to 40,000-fold in both DSC-fibroblast co-cultures and purified DSCs (log_2(FC) ≈ 15) (Figure 5.18D). TRP2 expression was markedly lower with a 200–400-fold upregulation (log_2(FC) = 7.5–8.5) (Figure 5.18E). When interpreting these results, it is important to consider that there were datasets from only one donor cell strain available for DSC-fibroblast co-cultures on day 10.

5.6 Effect of UV on The Sphere Formation Capability of DSCs

In this section, the impact of UV irradiation on functional properties of DSCs was further investigated, assessing their ability to form spheres after UV exposure. Naturally enriched DSC cultures with stem cell frequencies of 49%, 65%, and 89% were irradiated with UVB or UVA in monolayer culture, either as a single dose or with multiple irradiations over three consecutive days, resulting in the same cumulative dose as the single irradiation. First, the viability of DSCs and the DSC frequency in culture were analyzed 48 h post-irradiation, before seeding them in suspension culture.

Compared to non-irradiated control cells (89.0 ± 2.3% viable cells), DSCs exposed to a total dose of 900 J/m² UVB showed significantly reduced viability, regardless of whether the dose was applied in a single irradiation (74.0 ± 4.2% viable cells, p = 1.270e-4) or fractionated over three days with 3×300 J/m² UVB (75.7 ± 2.5% viable cells, p = 4.999e-4) (Figure 5.19A). Exposure to 300 J/m² UVB and 3×100 J/m² UVB was well tolerated by the cells. Except for multiple irradiations with 3×24.67 kJ/m² UVA (79.6 ± 3.1% viable cells, p = 0.016), UVA had no significant effect on the viability.

Analogous to the cell viability results, the DSC frequency also decreased 48 h after single or fractionated irradiation with the higher UVB dose (Figure 5.19B). Exposure to 900 J/m² UVB resulted in an approximately 2-fold decrease of the DSC proportion (FC = 0.54 ± 0.16, log_2(FC) = -0.94 ± 0.48, p < 0.001), while 3×300 J/m² UVB led to a fold change of 0.64 ± 0.12

(log_2(FC) = -0.66 ± 0.28, $p < 0.001$). Following all other irradiation treatments, the stem cell content remained unchanged.

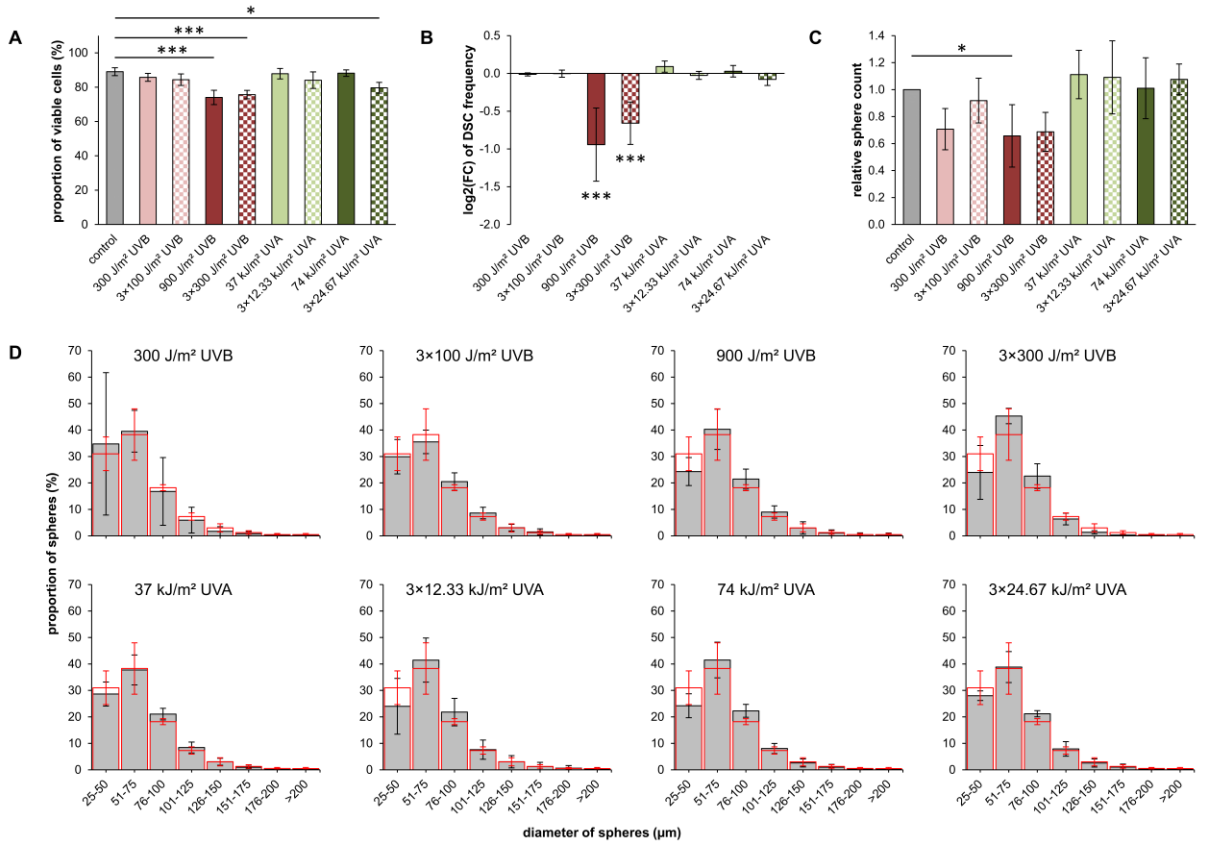

Figure 5.19 Sphere formation after UV irradiation. DSC cultures in monolayer were irradiated once or multiple times with 300, 3×100, 900, or 3×300 J/m² UVB, or with 37, 3×12.33, 74, or 3×24.67 kJ/m² UVA. After 48 h, cells were harvested and (**A**) viability of DSCs, gated on NGFRp75$^+$ cells as well as (**B**) fold changes in DSC frequency relative to non-irradiated control cells were measured via flow cytometry. Equal amounts of viable NGFRp75$^+$ cells were seeded in suspension culture flasks. After five days of cultivation, (**C**) numbers of spheres were determined relative to non-irradiated control cells and (**D**) diameters of spheres were measured. Size distribution of spheres in ranges of 25 µm diameter, determined using digital image processing. Red histogram overlay shows non-irradiated controls. Values are presented as mean ± SDs. Sample size: n=3. Multiple comparisons versus control (One-way ANOVA and Dunnett's method): *p ≤ 0.05; ***p ≤ 0.001.

Based on the DSC proportion and viability results, equal amounts of viable NGFRp75$^+$ cells were cultured in suspension, and examined for the number and diameter of formed spheres after five days. The count of spheres was calculated relative to the non-irradiated control (fold change) (Figure 5.19C). A notable reduction of 30–35% fewer spheres was observed following single irradiation with 300 J/m² UVB (FC = 0.71 ± 0.15) and 900 J/m² UVB (FC = 0.66 ± 0.23, p = 0.042), as well as after multiple irradiations with 3×300 J/m² UVB (FC = 0.69 ± 0.14). However, due to the large overall variance among all samples, these alterations were statistically significant only for 900 J/m² UVB. On average, UVA irradiation had no effect on the number of formed spheres.

The size distribution analysis of formed spheres illustrates the percentage of spheres falling within specific size ranges of 25 µm diameter steps (Figure 5.19D). There was heterogeneity in the size of the spheres, ranging from approximately 25 µm for the smallest to over 200 µm in diameter for the largest. The cutoff value as the minimum size of a structure to be considered a sphere rather than a cell cluster was set to 25 µm diameter. The histograms did not display a normal distribution with a symmetric bell shape but instead a unimodal distribution, mostly skewed to the right (toward greater sizes) without any outliers. The central peak consistently appeared in the 51–75 µm diameter range, with a higher proportion of spheres having a diameter >75 µm than <51 µm. Following any UV irradiation, both UVA and UVB, there was a tendency for fewer small spheres to be formed. In other words, the size distribution slightly shifted towards larger diameters upon irradiation, except for irradiation with 300 J/m² UVB, where notably high standard deviations were observed. In irradiated samples, the proportion of small spheres with a diameter of up to 50 µm was lower than in non-irradiated control cells (ANOVA, $p = 0.315$). Consequently, in the irradiated samples, larger percentages of spheres were observed in greater diameter ranges of 51–75 µm (ANOVA, $p = 0.162$) or 76–100 µm (ANOVA, $p = 0.076$) compared to the controls. However, these changes did not reach statistical significance.

5.7 Effect of UV on The MicroRNA Expression

In this section, at first, the baseline miRNA expression in DSCs was compared to that of melanocytes and melanoma cells. Further, it was investigated whether UV irradiation induces changes in the miRNA expression patterns of DSCs that are associated with the development of skin cancer. One naturally enriched DSC-fibroblast co-culture (93% DSCs) and two MACS® positive selection-purified DSC cultures (both 97%) were utilized. For comparison, two melanocyte cell strains derived from foreskin were also subjected to UV irradiation. Additionally, non-irradiated melanoma cells (MM) were included as an ‘endpoint’ of UV-induced melanomagenesis. These three melanoma cell cultures were obtained from different melanoma metastases.

During the evaluation of measured data, normalization is performed using the most stable miRNAs, typically around ten in number. Therefore, it was examined which miRNAs exhibited stability across the different cell types. Upon analyzing measurements from all eight donor cell strains separately (3 DSCs, 2 melanocytes, 3 MM), only one miRNA was found to be consistently stable in all eight cell strains: hsa-mir-23a-3p (see Appendix Table 8.4).

Comparing cell strains solely within their specific cell type led to more consistency. When comparing all three DSC strains to each other, at least three matching, stably expressed miRNAs were found (hsa-mir-23a-3p, hsa-mir-20a-5p, hsa-mir-17-5p) (see Appendix Table 8.5). Similarly, the comparison of the two melanocyte strains revealed eight matched, stably expressed miRNAs (hsa-mir-23a-3p, hsa-mir-20a-5p, hsa-mir-17-5p, hsa-mir-100-5p, hsa-mir-15a-5p, hsa-mir-23b-3p, hsa-mir-15b-5p, hsa-mir-221-3p) (see Appendix Table 8.6). Furthermore, when the three melanoma cell strains were compared among themselves, five matched, stably expressed miRNAs were identified (hsa-mir-23a-3p, hsa-mir-185-5p, hsa-mir-197-3p, hsa-mir-222-3p, hsa-mir-301a-3p) (see Appendix Table 8.7). This already indicated distinct differences in the miRNA expression patterns among the three different cell types.

Hence, it was considered to evaluate the measured data of the cell strains grouped by cell type, meaning all DSC strains together, all melanocyte strains together, and all melanoma cell strains together. Then, the three cell type groups were compared with regard to their most stable miRNAs. This analysis revealed an entirely different set of miRNAs compared to the previous assessments. Here, only two miRNAs were consistently expressed in a stable manner in all three groups (hsa-let-7g-5p, hsa-let-7i-5p) (see Appendix Table 8.8).

However, using the normalization methods described earlier, it would be possible to investigate only effects within individual cell types, such as the impact of UV irradiation on DSCs. A comparison between the cell types based on different normalizations would have been inadequate, due to fundamental differences. Especially if the transition from DSCs to melanocytes and then to malignant melanoma is to be investigated, a common normalizer is a prerequisite. Therefore, ultimately, the measurements of all different cell strains were analyzed together, ensuring that all presented results are based on the same normalization miRNAs. This led to the identification of the nine most stable miRNAs for normalization shown in Table 5.4.

Table 5.4 Most stable microRNAs for normalization.

hsa-mir-17-5p	hsa-let-7g-5p	hsa-let-7a-5p	hsa-let-7d-5p	hsa-let-7i-5p
hsa-mir-93-5p	hsa-mir-21-5p	hsa-mir-16-5p	hsa-mir-197-3p	

Following normalization, the five miRNAs hsa-mir-124-3p, hsa-mir-142-3p, hsa-mir-142-5p, hsa-mir-150-5p, and hsa-mir-182-5p were excluded from the analysis due to their low median expression values.

5.7.1 Baseline MicroRNA Expression Levels in DSCs, Melanocytes, and Melanoma Cells

Using the non-irradiated control cells, the baseline miRNA expression profile in DSCs was first investigated in comparison to their progeny, melanocytes, and to melanoma cells. Hierarchical cluster analysis of baseline miRNA expression revealed eight differentially expressed miRNAs in DSCs, which allowed a clear discrimination from melanocytes and melanoma cells (Figure 5.20A–B). This microRNA pattern included four overexpressed miRNAs in DSCs (hsa-mir-137, hsa-mir-15a-5p, hsa-mir-33a-5p, hsa-mir-494-3p) and, conversely, four miRNAs that were overexpressed in melanocytes and melanoma cells while downregulated in DSCs (hsa-mir-146b-5p, hsa-mir-204-5p, hsa-mir-222-3p, hsa-mir-34a-3p). Statistically significant differences in expression levels between DSCs and melanoma cells were observed for all eight miRNAs (hsa-mir-137, $p = 0.032$; hsa-mir-146b-5p, $p = 0.005$; hsa-mir-15a-5p, $p = 0.034$; hsa-mir-204-5p, $p = 0.037$; hsa-mir-222-3p, $p = 0.008$; hsa-mir-33a-5p, $p = 0.012$; hsa-mir-34a-3p, $p = 0.029$; hsa-mir-494-3p, $p = 0.007$). However, for the comparison of DSCs and melanocytes, only the differences in hsa-mir-146b-5p expression were deemed statistically significant ($p = 0.017$), although clearly visible disparities were also evident for hsa-mir-137, hsa-mir-204-5p, and hsa-mir-33a-5p (Figure 5.20A). The lack of statistical significance is most probably attributed to the smaller sample size of melanocytes. Notably, all three examined DSC cultures showed very similar expression levels, regardless of whether they were naturally enriched or MACS®-purified (Figure 5.20B).

To identify target genes of the eight differentially expressed miRNAs in DSCs, a network analysis was conducted. The search for targets regulated by at least two of the 4-miRNA set overexpressed in DSCs (hsa-mir-137, hsa-mir-15a-5p, hsa-mir-33a-5p, hsa-mir-494-3p) resulted in the identification of 39 targets (Figure 5.20C). These targets were not regulated by hsa-mir-137. Consequently, no targets were found that are regulated by all four miRNAs. Target genes (that should be inhibited) included, for instance, CDK6, MYC, BCL2, CCND1 (Cyclin D1), AGO2, RAD23B, and HIF1α. To identify biological processes and pathways in which the miRNAs are involved, an enrichment analysis/over-representation analysis (ORA) was conducted with regard to enriched KEGG pathways and Gene ontology (GO) terms. The top 20 biological processes repressed by the overexpressed miRNA set, obtained from the analysis of significantly changed GO terms, can be found in Appendix Table 8.9.

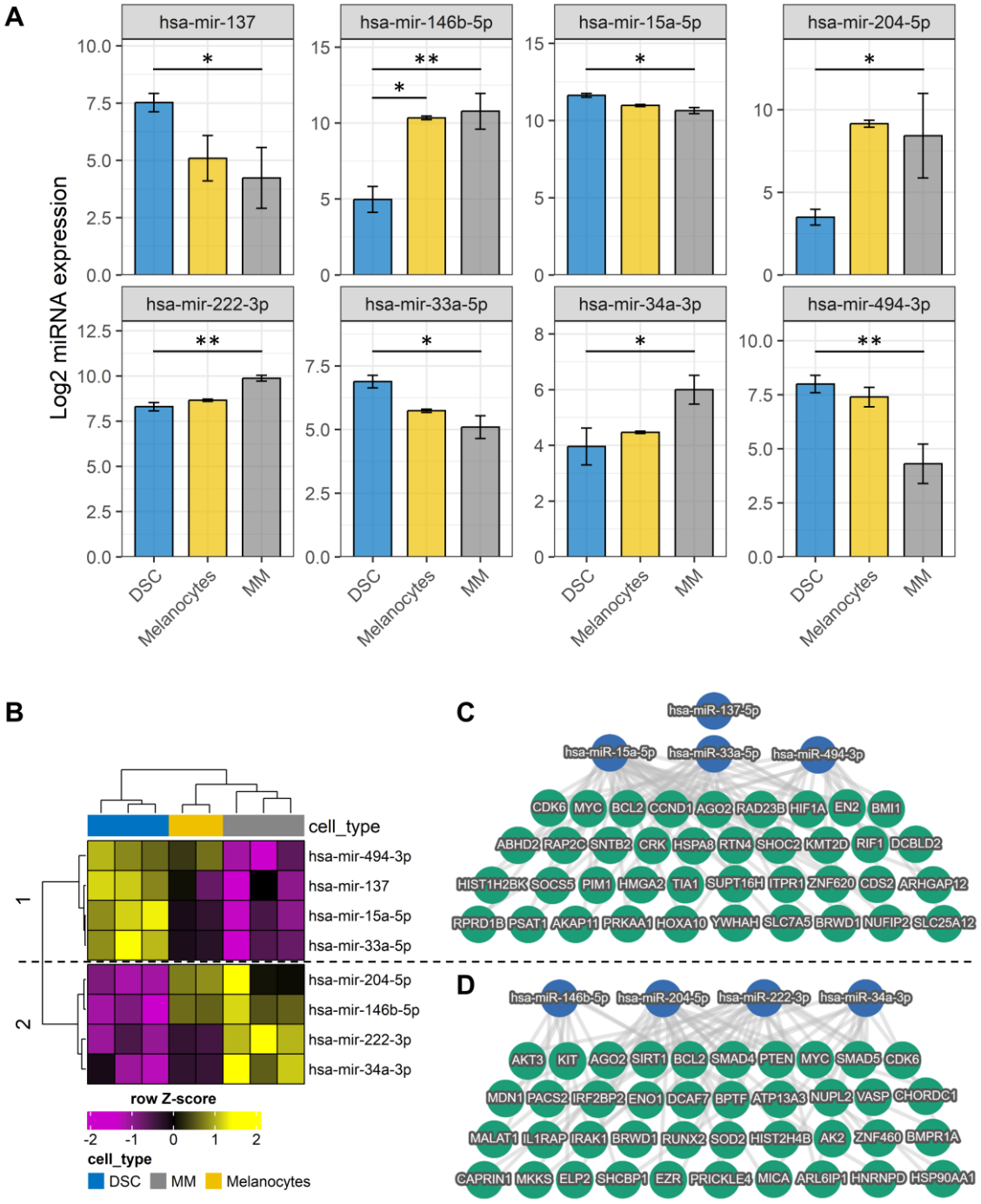

Figure 5.20 Baseline microRNA expression in DSCs compared to melanocytes and melanoma cells. Expression of a selected panel of miRNAs was measured via flow cytometry using the FirePlex® miRNA Assay. (**A**) Differential expression levels of eight miRNAs. Values are presented as mean ± SDs of log_2-transformed raw expression values. Sample size: DSCs n=3, melanocytes n=2, melanoma cells n=3, with technical duplicates. Significant differences have been assessed with the R package *limma*: *p ≤ 0.05; **p ≤ 0.01. (**B**) Hierarchical cluster analysis shows differentially expressed miRNAs between DSCs, melanocytes, and melanoma cells. Downregulated miRNAs are shown in purple, upregulated miRNAs in yellow as scaled and centered values (Z-score). The cell types are depicted with different colors above the heatmap. DSCs = blue, melanoma cells = gray, melanocytes = yellow. The individual clusters are visually highlighted by the division of the dendrograms. Sample size: DSCs n=3, melanocytes n=2, melanoma cells n=3, with technical duplicates. (**C**) Network analyses of the 4-miRNA set overexpressed in DSCs and (**D**) the 4-miRNA set downregulated in DSCs with target genes that are regulated by at least two of the four miRNAs (created with miRTargetLink 2.0, accessed on September 21, 2023).

For the 4-miRNA set that was downregulated in DSCs (hsa-mir-146b-5p, hsa-mir-204-5p, hsa-mir-222-3p, hsa-mir-34a-3p), searching for targets that are regulated by all four or by at least three of the miRNAs provided no results. A network analysis, considering a minimum of two shared targets, identified 40 target mRNAs (Figure 5.20D). Among the target genes (that should be upregulated) were, e.g., AKT3, KIT, SIRT1, PTEN, SMAD4, SMAD5, and there were overlaps with the targets of the overexpressed miRNAs, including CDK6, MYC, and BCL2. The subsequent ORA with the miRNA set as input did not yield any significantly altered GO terms. Therefore, ORA was alternatively performed with the target genes. The top 20 GO terms of activated biological processes are displayed in Appendix Table 8.10. The reduced expression of the four miRNAs and the subsequent induction of target genes were also associated with the significant activation of KEGG pathways shown in Appendix Table 8.11.

5.7.2 MicroRNA Expression Following UV Irradiation

To investigate the effect of UV irradiation on miRNA expression in DSCs, they were irradiated with a single dose of 300 J/m² UVB or 37 kJ/m² UVA, and harvested following 6 h and 24 h. Melanocytes were also irradiated in the same way, while melanoma cells remained non-irradiated. Hierarchical cluster analysis of the 58 miRNAs after irradiation revealed variations in the miRNA patterns (Figure 5.21). However, these differences were predominantly attributable to differences in cell lineages, as the samples clustered according to the three cell types. Within each cell type, samples from the same donor consistently grouped together, irrespective of irradiation, and allowed for a clear discrimination between the different cell strains. Consequently, there was no discernible impact from UV irradiation in DSCs and melanocytes, and no similarities were found between irradiated DSCs and melanoma cells or irradiated melanocytes and melanoma cells. Furthermore, there were no considerable differences between naturally enriched DSCs (labeled as DSC 02 in the figure) and MACS®-purified DSCs (labeled as DSC 17 and DSC 33). Rather, one of the MACS®-purified DSC cultures (DSC 17) differed from the other two DSC cultures in the expression of multiple miRNAs.

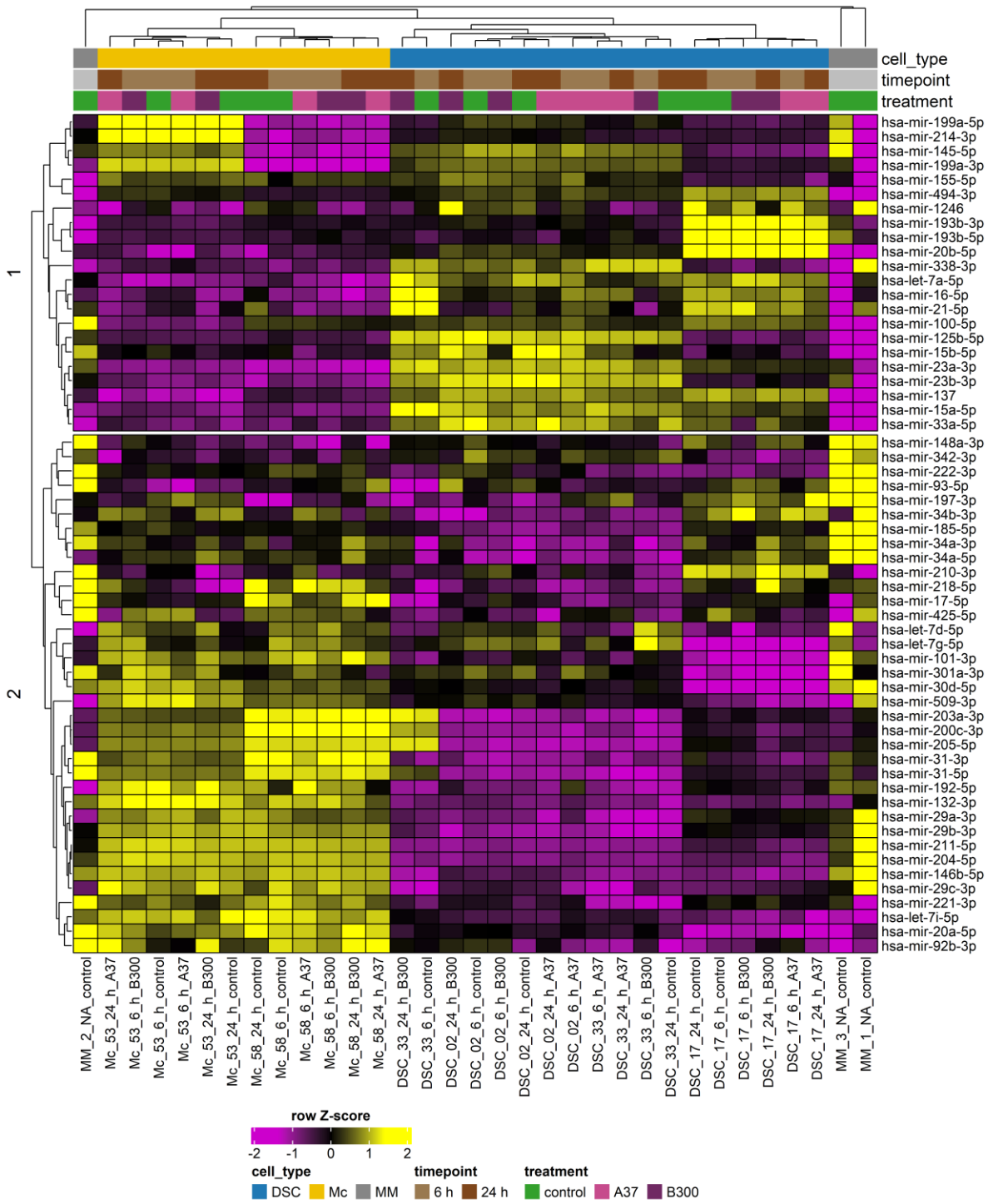

Figure 5.21 microRNA expression after UV irradiation. Cells were irradiated with a single dose of 300 J/m² UVB or 37 kJ/m² UVA, and harvested after 6 h and 24 h. Expression of a selected panel of miRNAs was measured via flow cytometry using the FirePlex® miRNA Assay. Hierarchical cluster analysis of 58 miRNAs following irradiation of DSCs and melanocytes (Mc), compared to non-irradiated melanoma cells (MM). Downregulated miRNAs are shown in purple, upregulated miRNAs in yellow as scaled and centered values (Z-score). The cell types, time points, and treatments are depicted with different colors above the heatmap. Cell types: DSCs = blue, melanocytes (Mc) = yellow, melanoma cells (MM) = gray. Time points: 6 h = light brown, 24 h = dark brown. Treatment: control = green, 37 kJ/m² UVA = pink, 300 J/m² UVB = purple. The individual clusters are visually highlighted by the division of the dendrograms. Sample size: DSCs n=3, melanocytes n=2, melanoma cells n=3, with technical duplicates.

6 Discussion

The first objectives of this study were the characterization and purification of DSCs derived from human foreskin. Subsequently, the investigation aimed to determine whether these cells exhibit any special features or abnormalities in their response to UV irradiation that may contribute to an increased risk of UV-induced malignant transformation.

6.1 Characterization of DSCs

DSCs were successfully isolated from human foreskin and expanded in cell culture using specific stem cell medium, following methodologies similar to those described by Li et al. [31,125]. DSCs grew in three-dimensional dermal spheres, which were found to be heterogeneous and also contained fibroblasts. This heterogeneity was attributed to the cultivation of all isolated dermal cells and the low percentage of DSCs present in the skin. The proportion of DSCs varied greatly among different donors, with fibroblasts predominantly representing the major cell population in these DSC-fibroblast co-cultures. The mean proportion of 10.5% NGFRp75^{+} DSCs in the dermal spheres is in agreement with the 12% reported by Herlyn's group [31]. To enable in-depth analysis of DSCs, a critical step involved the purification of DSC-fibroblast co-cultures, which was established by comparing different enrichment approaches. Detailed discussions of these results can be found in section 6.2.

Furthermore, multiple characteristics of neural crest stem cells (NCSCs) were confirmed, providing compelling evidence that the dermis-derived stem cells in this work were indeed the DSCs previously described by Herlyn's group [31,125,126]. The DSCs expressed NCSC-characteristic markers like NGFRp75, MSX1, and FRZB. They were able to form three-dimensional spheres in human ESC medium (discussed in section 6.5) and possessed the capability to differentiate into melanocytes upon appropriate stimulation with melanocyte differentiation medium (discussed in section 6.4). Inadvertent enrichment of melanocytic stem cells from the hair follicle instead of DSCs can be ruled out, as foreskin lacks hair follicles.

In monolayer culture, DSCs showed characteristic cellular morphology that differed from those of the other three foreskin-derived skin cell types (fibroblasts, melanocytes, keratinocytes), which were cultured using cell-specific medium. DSCs (median 37.4 h) proliferated at a rate similar to fibroblasts (41.2 h) and melanocytes (43.3 h), while keratinocytes (22.3 h) exhibited a significantly faster doubling time. A direct comparison with doubling times from the literature is challenging, as they may vary depending on factors such as age, passage, culture conditions, material (primary cultures, cell lines), and, in the case of primary cells, the body location from

which they were obtained [427,428]. For example, in studies by Moulin et al., doubling times of dermal fibroblasts ranged from 40–55 h [429], whereas Trokovic and colleagues found a range of 18–33 h [428]. Horvath et al. measured doubling times of 38–42 h for primary neonatal foreskin keratinocytes [430]. For melanocytes, the variations are even greater, with reports including values of 48 h or even multiple days [358,431]. There are no available comparative data for DSCs.

6.2 Purification of DSCs

After being isolated from foreskin, DSCs grew in co-cultures with fibroblasts. It is widely recognized that the presence of contaminating fibroblasts with high proliferative potential can result in the overgrowth of the desired cell population, even if the initial fibroblast contamination is minimal [423,424]. Moreover, their coexistence poses challenges in certain analyses where both cell types are indistinguishable. However, for various studies such as those involving epigenetics, gene expression, miRNA expression, and protein expression, it is crucial to work with enriched or pure DSC cultures. Hence, it was imperative to establish a method for eliminating this undesired cell population before conducting experiments. Numerous attempts to remove unwanted fibroblasts from cell cultures have been previously described for different cell lines and types. Traditional methods encompass:

(i) Adding antimitotic drugs like cytosine arabinoside (Ara-C) [432,433] or antibiotics such as Geneticin (G418) [434-436] into the cell culture medium.
(ii) Employing differential adhesion [437,438] and selective detachment techniques [439,440].
(iii) Cultivating in media without serum [440,441].
(iv) Utilizing immunomagnetic separation based on differential cell surface antigens [423,436,442].
(v) Employing fluorescence-activated cell sorting (FACS) that combines multiple parameters such as distinct surface markers, size, and granularity [443-446].

This study evaluated three approaches to reduce the significant fibroblast population in DSC-fibroblast co-cultures. Geneticin treatment and selective detachment were considered due to their simplicity and availability. Immunomagnetic separation was selected for its enhanced specificity. Although these methods have been well described for several cell types, their application to enrich DSCs in primary cell cultures containing fibroblasts had not been explored before.

6.2.1 Treatment with Geneticin

Geneticin is an aminoglycoside antibiotic and commonly used for selecting transfected cells. It functions by inhibiting protein synthesis, specifically targeting the elongation step in both prokaryotic and eukaryotic cells, thereby disrupting cell growth and proliferation. Its known variable cytotoxic effects on eukaryotic cells with different growth rates make it a valuable tool for eliminating contaminating fibroblasts from mixed cultures. Cytotoxicity becomes evident after 1–2 cell divisions, with the most pronounced impact on rapidly dividing cells. Additionally, Geneticin may induce Caspase-3-dependent apoptosis, ultimately leading to cell death [435,447].

In this study, treatment of DSC-fibroblast co-cultures with the antibiotic Geneticin failed in enriching the stem cell content. On the one hand, Geneticin caused a decrease in total cell numbers and the death of fibroblasts. On the other hand, it also resulted in distinct cell death among DSCs, leading to a decline in the stem cell frequency.

To compare the effectiveness of Geneticin treatment in different cell cultures, several aspects need to be considered, with the proliferation rate of the various cell populations being the most crucial factor since Geneticin acts on the most rapidly dividing cells. DSCs and fibroblasts exhibited similar growth rates in the co-cultures in stem cell medium. This similarity explains why both cell populations were affected similarly by the Geneticin treatment. While the minor population of DCSs in culture succumbed to the treatment, some of the outnumbering fibroblasts survived. In contrast, Geneticin has proven to be an effective eliminator of fibroblasts in melanocyte cultures from various tissues [447]. Melanocytes are slow-dividing cells with infrequent *in vivo* proliferation that show varying *in vitro* doubling time from 48 hours up to 10 days, depending on the growth conditions [358,431]. The fact that fibroblasts divide much faster with duplication ranging from roughly 40–55 hours [429] permits an effective purification of melanocyte cultures.

The response of cells to Geneticin is also influenced by their cell metabolism, leading to varying degrees of tolerance to this kind of cellular stress among different cell lines and types. Melanocytes, for instance, seem to have a natural resistance to Geneticin. By contrast, stem cells—and as confirmed in this study particularly DSCs—appear notably sensitive to this antibiotic. Maybe due to the sensitivity, Geneticin is not commonly used to enrich stem cell cultures. Additionally, variations in culture media compositions (e.g., serum, glutamine, insulin) could influence the impact of Geneticin, impeding the straightforward transfer of an established procedure from one cell culture condition to another. On top of that, the huge donor-

dependent variations observed in DSC cultures in general—which include differences in stem cell content, proliferation rate and possibly also cell metabolism/sensitivity—further complicate the establishment of a standardized protocol for Geneticin treatment of primary DSC cultures.

Moreover, one has to keep in mind that non-cell-specific agents such as Geneticin may also affect the proliferation, phenotype, and functional properties of the surviving cell population, potentially influencing downstream applications [436,445,446]. Despite being an efficacious and cost-effective method for eliminating fibroblasts from melanocyte cultures [435,436,447], Geneticin is not suitable for purifying DSC cultures.

6.2.2 Selective Detachment

The method of selective detachment becomes applicable when different cell populations in adherently growing cell cultures exhibit varying detachment properties, allowing for their release at different times during incubation. Depending on the particular cell culture, either fibroblasts detach first and can be removed with the supernatant [440], or fibroblasts initially remain attached due to stronger adhesion while the desired cells are released earlier [439]. In this study, two different detachment reagents, Accutase™ and trypsin-EDTA, were examined.

When selectively detaching DSC-fibroblast co-cultures, DSCs tended to detach more rapidly than fibroblasts, resulting in a slight enrichment of DSCs, albeit only by a small percentage. Detachment with Accutase™ yielded higher purity compared to trypsin-EDTA; however, it also resulted in lower viability and recovery rates, leaving an insufficient number of cells for subsequent experiments or cultivation. Notably, higher viability and recovery always came along with lower purity. Hence, extended cultivation periods would be necessary after the selective detachment protocol to propagate DSCs or to perform multiple cycles to enhance purity, resulting in undesirably high passages and significant time consumption. Similarly, Kisselbach et al. required multiple treatments of primary human CEC (corneal epithelial cell) cultures with trypsin-EDTA due to fibroblast regrowth, eventually leading to senescence of the desired cells. Consequently, they described this approach as simple and initially successful but inefficient [440]. On the contrary, this method has proven efficient for HDMEC (human dermal microvascular endothelial cell) cultures during the first week of primary cell culture, before fibroblasts proliferate excessively and the HDMECs adhere too strongly [439]. Considering the conditions of the DSC-fibroblast co-cultures in this study, it is likely that the number of fibroblasts was already too high, and the DSCs adhered too strongly to efficiently separate the

two cell types through selective detachment. In addition, the growth of the DSC-fibroblast co-cultures on BME-coating could make a selective detachment more difficult.

Comparing the detachment reagents, Accutase™ is generally considered a mild-acting enzyme that is gentle on cells. As a result, cells detached with Accutase™ are less likely to lose or alter their cell surface markers, maintaining their structural integrity and functionality. In contrast, trypsin is harsher and degrades many cell surface markers [448-450]. The degradation of surface proteins and ECM components during proteolytic enzyme digestion can impact the detectability of surface markers and reduce cell viability, especially in the case of stem cells [448]. Therefore, preserving the integrity of cell surface markers and receptors is essential for accurately characterizing and identifying the enriched DSC population. Consistent with the milder proteolytic activity, in this study, cells were detached more slowly with Accutase™; however, the decreased viability was unexpected. Multiple studies reported lower cell viability with trypsin compared to Accutase™, for example when dissociating epithelial cancer cells [451] or digesting neurospheres [452], whereas Accutase™ led to more apoptosis as a result of digestion. The authors ascribed the reduced apoptosis observed after trypsin dissociation to extensive disruption of the cell membrane by trypsin, hampering the detection of apoptotic cells via Annexin-V assay [451]. A compromised cell membrane structure could explain the consistently lower proportions of NGFRp75^{+} cells with trypsin-EDTA compared to Accutase™ shown here. By contrast, the results from this study agree with data from Skog et al. who found higher viability of trypsin-dissociated cells after digestion of epidermis, while in subsequent cultivation, Accutase™-dissociated cells seemed healthier in the long term [450]. These collective findings indicate that the impact of detachment reagents on the viability is strongly cell type-dependent.

So, while Accutase™ seemed to impair cell viability, trypsin appeared to slightly degrade NGFRp75 on the cell surface, leading to a decreased detection of stem cells. Recent studies have suggested that Accutase™ may also influence the expression of certain cell surface proteins and that cells require around one day of recovery time after detachment before conducting experiments [448]. In summary, due to low enrichment, reduced viability and low cell counts of DSCs, the method of selective detachment has also proven unsuitable for the purification of DSC cultures.

6.2.3 Immunomagnetic Separation

As a third approach to obtain pure DSC cultures, immunomagnetic separation (IMS) was performed using two different techniques: negative selection (labeling of undesired cells, fibroblasts) and positive selection (labeling of target cells, DSCs). Additionally, two widely used IMS approaches were compared: EasySep™ (column-free) technology from StemCell Technologies and the MACS® (automatic column-based) technology from Miltenyi Biotec. IMS is a well-established method for the separation of diverse cell populations based on specific cell surface antigens, enabling the enrichment of a particular cell type. In principle, specific antibodies bound to magnetic beads capture cells expressing the corresponding epitope. By using a magnetic field, the labeled cells are retained and therefore separated from unlabeled cells.

6.2.3.1 Negative Selection

Negative selection is usually preferred to positive selection, because the cells of interest remain 'untouched'—meaning they are not bound by antibodies and beads—and thus should remain functionally unaltered [453,454]. This approach also helps remove non-specifically labeled dead cells and debris [455]. However, compared to positive selection, negative selection is often less pure since it is challenging to target all unwanted cells, necessitating exact knowledge of the starting cell types and their unique surface markers [456].

In this study, with both EasySep™ and MACS® negative selection targeting the fibroblast marker CD90, a complete elimination of $CD90^{+/dim}$ fibroblasts was not achieved. Multiple purification steps may be required to fully remove the remaining fibroblasts [436]. Experiments with two consecutive purification steps were unsatisfactory: firstly, although the purity continued to increase, it did not reach the desired level, and secondly, the number of remaining cells was very low and not usable (data not shown). Besides the numerous $CD90^{+/dim}$ cells, there was also a subset of double-negative ($CD90^{-}$/$NGFRp75^{-}$) cells persisting within the purified (negative) DSC fraction post-selection, implying that separation based on the CD90 marker was insufficient for these cells [457]. It is unclear whether these cells were originally resided in the dermis of the skin and co-cultured over time, or if they represent fibroblasts with altered CD90 expression levels under stem cell medium cultivation conditions. Since fibroblasts are the most prevalent cell type in the dermis, it was assumed that the contaminating cells were fibroblasts. However, other dermal cell types could also be involved. This problem of inconclusive identification is not uncommon. Contaminating cells are often referred to as fibroblasts, even

though their origin and specific characteristics are uncertain [423]. When the double-negative cells are indeed cells other than fibroblasts, they could be eliminated using appropriate markers for immune/hematopoietic cells (CD45), endothelial and lymphatic cells (CD31, Tie2), and mesenchymal stem cells (CD106, CD105, CD73) [53,458].

CD90 is the most common and best characterized cell surface marker to separate fibroblasts [54]. However, it appears that using only this marker to target the unwanted cells was insufficient, also with regards to a possible $CD90^{dim}$ DSC subpopulation (see below). In the human body, various functionally distinct fibroblast subtypes exist. On the one hand, there is phenotypic diversity between different organs/tissues (anatomical diversity), but also within the same tissue or anatomical site (layer-specific diversity) [54,459]. Specifically, dermal fibroblasts represent a heterogeneous cell population of at least two lineages with different morphology, expression profiles, proliferation rates, and functions depending on their localization (papillary and reticular) (see section 1.1.2). Papillary fibroblasts have a lean, spindle-shaped morphology, they maintain an increased proliferative potential in culture, and exhibit a more undifferentiated phenotype, while reticular fibroblasts are characterized by a flatter, spread out, stellate shape, lower proliferative activity, and a more differentiated phenotype [459-461]. Several studies showed significant differences in the expression of several cell markers of these fibroblast subtypes in both cell culture and human skin [459,460,462-464]. Notably, there are varying reports regarding the expression of the cell marker CD90. While some sources state that all dermal fibroblasts express CD90 [54], others declare two subpopulations with differential CD90 expression. For instance, Korosec et al. identified the combination of the two cell surface markers FAP (fibroblast activation protein) and CD90 as a means to distinguish papillary ($FAP^+/CD90^-$) and reticular ($FAP^-/CD90^+$) dermal fibroblasts in human skin, while there was also a subpopulation that expressed both markers [53]. Papillary fibroblasts tend to acquire a reticular phenotype and morphology during long-term *in vitro* cultivation [53,460], possibly due to loss of signaling between papillary dermal fibroblasts and basal keratinocytes [463]. However, it is hypothesized that this transition might not apply to all cells and that those cells, which were not separated via CD90, were a remaining population of $CD90^-$ papillary fibroblasts. Consequently, this aspect could be one of the reasons for variances in purification quality and the varying proportion of double-negative cells observed in different donor cultures. The composition of the fibroblast population is probably already individually different right after the isolation from foreskin. Further disparities in the rapidness of the expression change of the subtypes and the duration of cultivation prior to purification might contribute to different prerequisites of individual DSC cultures.

Another important point to consider is the phenotypic stability of cells, influenced by the microenvironment. Extrinsic signals play a significant role in preserving cellular identity during *ex vivo* cultivation. There is evidence indicating that fibroblasts undergo a notable shift in their expression of cell surface markers when transitioning to *in vitro* cell culture [53,458,465]. Therefore, depending on the culture conditions and environment, markers allegedly attributed to a specific cell type may not be reliably used. It cannot be excluded that the stem cell medium might contribute to a change in the cell identity of the fibroblasts, potentially resulting in a reduction or loss of specific antigens like CD90, rendering them less susceptible to CD90 antibodies. Moreover, the presence of BSA in the stem cell medium might not be conducive to optimal CD90 expression and fibroblast proliferation, as they typically require FBS [440,441]. Deprivation of FBS from medium is a method to partially eliminate contaminating fibroblasts, especially from non-serum dependent cell cultures [440,441]. However, fibroblasts proliferated well in the stem cell medium, otherwise they would have been naturally diluted during cultivation.

Altogether, dermal fibroblasts represent a complex group of cells, and it is advisable to consider additional markers for their separation from DSCs to target all subtypes effectively. While there are multiple specific markers available for both fibroblast subtypes, there is generally a lack of unique surface markers. A comprehensive review of the literature has identified a range of surface markers that could be combined with CD90 to cover both subtypes (e.g., FAP, CD39, CD36, CD26, PDGFRα, PDGFRβ, CD13) [54,461,462]. To perform immunomagnetic separation with the highest possible effectiveness and to eliminate the $CD90^{-}$/$NGFRp75^{-}$ cell population, a phenotypic analysis of the co-culture would be necessary, in order to identify and characterize all the included cell types and their specific properties, for example through single-cell RNA-seq analysis.

Another issue encountered with negative selection was the loss of many DSCs in the (positive) fibroblast fraction during the selection process, possibly due to non-specific binding, endocytosis of beads [466], or the presence of a $CD90^{dim}$ DSC subpopulation. In humans, CD90 has been identified on a variety of stem cells such as mesenchymal stem cells (MSCs), hematopoietic stem cells, and keratinocytic stem cells as well as on fibroblasts, neurons and endothelial cells [440], but has not yet been described as a marker on DSCs. The selection efficiency can be hampered by non-specific binding between cells and antibodies or magnetic beads [454,467], but also by sticky dead cells and cell debris that bind to antibodies, beads, and living cells, preventing the correct binding of antibodies and causing cell aggregation [421,454].

Introducing a dead cell removal kit and/or DNase digestion before separation can mitigate these issues. While pre-incubating with *Basic MicroBeads* in the MACS® method was ineffective (see Appendix Figure 8.1), a prior DNase digestion and cell suspension filtering led to better results and thus were included in the protocol. This could account for the minimal loss of DSCs in the positive fraction as compared to the EasySep™ method, advising the incorporation of DNase digestion, filtering, and possibly a dead cell removal kit in the EasySep™ protocol as well. In addition, working with the EasySep™ RapidSpheres™ at room temperature might have favored endocytosis/internalization of the beads [468] and non-specific binding, so that working at 4 °C like the MACS® approach should also be considered. Further research is required to uncover reasons for the loss of ($CD90^{dim}$) DSCs during negative selection and improve separation efficiency. Varying parameters such as the incubation times, the concentrations of beads and antibodies are promising approaches.

Applying the more sensitive *DepleteS* program in the MACS® negative separation led to high purity of DSCs, but with an extremely low recovery rate, making this approach practically non-applicable to conduct downstream experiments. To obtain sufficient cells, extended culture of these purified DSCs is necessary, causing additional costs for the expensive stem cell medium, and risking a decreasing DSC frequency due to rapid growth of surviving fibroblasts.

Successful negative selection was also achieved with cultures having a higher initial proportion of DSCs (≥30%) using both EasySep™ and MACS®, yielding high purity but (very) low recovery rates. However, DSC-fibroblast co-cultures with a high DSC frequency were rare. Among the seventy-nine donor cell strains examined in this study, only four, representing five percent, exhibited natural enrichment, indicating that this is an exception rather than the rule. These findings suggest that a two-step sequential negative selection approach with intermediate cultivation might yield high purity, but low output would result in several weeks of propagation between the separations.

These negative selection results contrast with studies that have effectively removed fibroblasts from endothelial cell cultures [424] or human umbilical vein endothelial cells (HUVECs) [440] using CD90-dependent IMS, possibly due to different culture conditions affecting CD90 expression in fibroblasts, as mentioned above. This study utilized naturally occurring DSC-fibroblast co-cultures cultivated in stem cell medium. In contrast, the other research groups experimentally mixed fibroblasts, cultured in their appropriate medium, just before selection, potentially leading to different CD90 expression patterns. Another essential aspect to consider is the fibroblast percentage in co-culture. While this study exhibited an average fibroblast

content of 90%, the highest fibroblast contamination in the other reports reached around 50% [424,440]. As a result, adequately comparing these studies to the presented results is difficult.

6.2.3.2 Positive Selection

Given the unsatisfactory outcomes of the negative selection, a positive selection strategy targeting the stem cell marker NGFRp75 (CD271) was implemented for DSCs. Positive selection typically yields highly purified cells by specifically targeting the desired cell type. In comparison to negative selection, it offers a higher cell yield and quicker performance when dealing with multiple unwanted cell populations, as it requires only one antibody [456]. Nevertheless, it is possible that cell debris and dead cells are also selected due to non-specific binding [455]. However, a notable disadvantage of this approach is that the target cells become bound to antibodies or other labeling agents (e.g., beads), potentially impacting downstream assays and influencing cell viability and proliferation. Labeling of the desired cells is associated with the risk of inducing artificial cell activation [422,456,466] and potentially altering cellular function [454,468].

Both positive selection methods resulted in DSC enrichment; however, the EasySep™ positive selection exhibited unreliability across various experiments and occasionally was not well tolerated by the DSCs, leading to atypical cell morphology and poor attachment post-separation. Impaired stem cell proliferation (observation) led to a rapid decline in DSC frequency and a resurgence of fibroblasts. It is recognized that magnetic particles can introduce adverse effects on cell phenotype, function [469,470], and viability [471-473], suggesting a potential impact on the DSCs via the antibodies and RapidSpheres™ they remained attached to. The amount of labeling reagent is an important aspect in positive selection [455]. A low bead number may lead to target cell loss, but an overly high number of beads might impede proper cell growth afterwards [442]. Thus, a reduction of labeling reagent and the incorporation of a post-separation bead removal step might enhance cell viability and support the maintenance of the enriched DSC frequency.

In contrast, MACS® positive selection yielded highly enriched DSC cultures in a reproducible manner. Notably, DSCs showed better tolerance to this method although they remained attached to the beads as well. This discrepancy could be attributed to the small size (explained in detail below under section 6.2.3.3) and the biodegradability of MACS® *MicroBeads*. They are internalized via endocytosis and subsequently degraded in lysosomes within a few hours to days [474,475]. Additionally, magnetic beads are diluted through cell division in proliferating

cells, while they can persist on and within non-dividing cells for up to two weeks after separation [476]. Indeed, MACS®-purified DSCs demonstrated superior post-separation proliferation compared to EasySep™-purified DSCs (observed as faster reached confluence and higher cell numbers after the same cultivation period), implying faster dilution of MACS® *MicroBeads* than EasySep™ RapidSpheres™. This aligns with previous studies comparing MACS® and EasySep™ technologies for isolating monocytes and osteoprogenitor cells through positive selection, where MACS® outperformed EasySep™ in terms of yield and purity [468,477].

Further research is recommended to comprehensively understand the impact of both technologies (MACS® and EasySep™) on DSC functionality, especially regarding their potential to differentiate into melanocytes. In particular, examination of bead persistence on and inside the cells [476] is crucial. Several studies have demonstrated that MACS®-purified cells maintain viability and functionality after positive selection [423,436]. Meyers et al. showed that human perivascular stem/stromal cells maintained their multilineage differentiation capacity and were even effective in repairing bone defects *in vivo* after positive MACS® selection [478]. Initial experiments with MACS®-purified DSCs indicated that their differentiation potential persists and is not significantly impaired post-positive selection (see section 6.4), though further verification is required.

Despite the substantial enrichment achieved through positive selection, residual $CD90^+$ fibroblasts and double-negative ($CD90^-$/$NGFRp75^-$) cells were still present in the purified DSC fraction. This cell contamination after separation is likely attributed to direct non-specific binding between undesired cells and magnetic beads [454,467], or the adhesive nature of dead cells and cell debris, causing non-specific aggregation involving antibodies, beads, and living cells [421,454]. The DNase digestion, pre-selection cell suspension filtration, and handling at 4 °C in the MACS® approach presumably contributed to its superior purification compared to EasySep™, and these steps should be incorporated into the latter method as well. The use of *Basic MicroBeads* in the MACS® separation to remove material non-specifically binding to magnetic beads, however, did not influence the separation efficiency (see Appendix Figure 8.1).

6.2.3.3 Overall Assessment of IMS

Balancing purity and recovery is crucial, but optimizing one parameter often compromises the other [455]. In negative selection, increasing antibody volume, bead amount, and incubation duration could enhance fibroblast targeting and purity, but might elevate non-specific binding

of DSCs, thus reducing recovery. During the negative selection approaches, already significant DSC loss occurred within the fibroblast fraction, especially in the EasySep™ method, contributing to its poor recovery rate. This makes increased labeling reagents more feasible for MACS® negative selection. Conversely, high purity negative selection approaches (see Figure 5.7: d, e, f) could potentially enhance recovery by reducing labeling reagents or incubation times, albeit at the cost of purity. In terms of positive selection, purity could be improved by shortening incubation times, yet recovery might decrease [455].

IMS efficiency depends on factors like binding of antibodies and beads to cells, magnetic susceptibility, and magnetic field strength [455,456]. Divergences in viability and proliferation of enriched DSCs following positive separation may arise from different bead technologies. Column-free approaches typically utilize micro-sized paramagnetic beads with diameters ranging from 0.5 to 5 µm [466]. EasySep™ uses bispecific tetrameric antibody complexes (TACs, included in the selection cocktail) to link labeled target cells to dextran-coated RapidSpheres™, but specific particle size information is lacking from the manufacturer. However, literature cites sizes ranging from 150 nm [466,476] to 200 nm [422]. Conversely, the MACS® technique by Miltenyi Biotec utilizes nano-sized superparamagnetic MACS® *MicroBeads*—around 50 nm in size—the smallest commercially available beads for cell isolation [475]. These MACS® *MicroBeads* are said to be biodegradable, non-toxic, compatible with various downstream applications, and should maintain cell viability and proliferation [453].

The weaker magnetic field used in column-free methods (EasySep™) necessitates extensive labeling and/or large beads, potentially promoting non-specific labeling and epitope saturation, which could affect downstream applications like flow cytometry. More importantly, this impacts cell viability, cell characteristics, and triggers cell activation [466,479] as well as biological alterations [468]. In contrast, the stronger magnetic field in column-based methods (MACS®) allows minimal labeling and smaller (nano-sized) beads, reducing non-specific labeling and epitope blocking. Minimal cell stress and preservation of cell functionality make column-based approaches better tolerated by target cells [478].

In summary, each method has distinct advantages and disadvantages, as listed in Table 6.1. For time-sensitive molecular analyses like gene expression profiling or signal transduction assays, the MACS® method is preferable.

Table 6.1 Comparison of EasySep™ column-free and MACS® automatic column-based selection technology. [480,481]

EasySep™ Column-Free	MACS® Automatic Column-Based
- considerably cheaper	- more expensive
- minimum space requirements	- device takes up a lot of space in the laminar flow hood
- lower risk of sample loss	- samples can get lost through clogging of columns or intake of air bubbles
	- new columns are needed periodically
	- excessive washing necessary to avoid contaminations
- time-consuming	- fast protocol
- labor-intensive	- easy handling [478]
- lower recovery, more loss of cells	- better separation
- success is strongly dependent on the handling of the executing person	- standardized separation, well reproducible
- weak magnetic field	- strong magnetic field [453,466]
- thereby extensive labeling and/or larger beads required [456]	- thereby minimal labeling and smaller beads (nano-sized) are sufficient [456]
• leads to epitope saturation	• no epitope blocking [478]
• promotes non-specific labeling	• less non-specific labeling
• impacts the viability and cell characteristics	• little cell stress
• can lead to activation of cells [466,479] and biological alteration [468]	• preservation of cell functionality • well tolerated by target cells

6.2.4 Conclusion to Purification of DSCs

Increasing evidence suggests that neural crest-derived DSCs in human skin might play a role in (UV-induced) melanomagenesis. DSCs obtained from human foreskin provide a suitable platform to investigate the underlying mechanisms. However, due to the considerable number of contaminating fibroblasts in primary DSC cultures, it becomes imperative to purify these DSC-fibroblast co-cultures for certain investigations. Various methods such as Geneticin treatment and selective detachment to remove fibroblasts prove inadequate for effective DSC enrichment. Negative selection techniques were suboptimal and would require further optimization to achieve the desired level of purity. Overall, positive selection through MACS® technology emerged as the optimal choice for purifying DSCs from primary cell cultures. Assessing multiple parameters like purity, recovery rate, and proliferation capability post-separation, this approach was perceived to be superior to all other methods examined in this

study. The simple and convenient MACS® positive selection protocol detailed in this study presents an appealing tool for enriching DSCs in upcoming experiments.

Overall, non-cell-specific methods appear to be generally less effective, offering lower chances of successful purification. However, further cell-specific methods relying on established surface markers like NGFRp75 may also work very well. Based on the successful results with MACS® positive selection, it is assumed that fluorescence-activated cell sorting (FACS) via NGFRp75 would also be a suitable method to separate DSCs and fibroblasts. This approach usually provides high purity and can be more specific, because cells can be sorted based on multiple parameters at once (different surface markers, size, granularity) [438,482]. Moreover, FACS allows separating more than one population simultaneously [443]. However, the sorting process with FACS is sophisticated and slow [438], and requires expensive technology as well as specialized operators [443,482]. Additionally, just like immunomagnetic separation, the binding of antibodies may lead to activation of intracellular signal transduction and changes in cell functionality [443]. Unfortunately, it was not possible to conduct FACS in this study since it is mostly provided only at core facilities.

The *in vitro* purification and expansion of enriched DSCs mark a crucial development in investigating the effects of UV radiation on their ability to differentiate into melanocytes, and exploring genetic and epigenetic changes. Consequently, enriched DSCs represent a novel and unique model for investigating their potential involvement in the development of malignant melanoma, possibly improving the understanding of melanomagenesis.

Purified DSCs are also a prerequisite for the establishment of a stable DSC cell line, which would greatly facilitate the study of these cells. Adult neural crest-derived skin stem cells pose a challenge in long-term cultivation due to their limited proliferation potential and gradual loss of multipotency over time [40]. A cell line would mitigate this issue. One potential drawback with purified DSCs could be that with the removal of fibroblasts the last remaining component of the skin microenvironment is eliminated. This could result in purified DSCs losing their stem cell properties over time in culture. The resolution of this concern through the establishment of a stable cell line remains to be investigated. Organotypic cultures (OTCs) with a fibroblast-derived matrix mimic the structure of human skin and resembles the *in vivo* dermal microenvironment [483-485]. The inclusion of purified DSCs in these 3D skin tissue experiments would reduce uncertainties associated with the absence of a microenvironment.

6.3 UV Damage Response

The response of human adult stem cells to DNA damage is still an insufficiently answered question. Existing studies on the DNA damage response (DDR) predominantly involve ESCs, iPSCs, or murine stem cells in combination with ionizing radiation, H_2O_2, or UVC exposure [486-489]. However, none of these investigations have incorporated an examination of human DSCs as McSCs in response to UVB and UVA radiation. Due to significant variations in DDR mechanisms among stem cells from different tissues, at different developmental stages, and different activity levels, mechanisms observed in one stem cell population cannot be readily extrapolated to another [195]. For instance, during development, fetal stem cells might be more susceptible to elimination upon damage to establish an immaculate stem cell pool with lifelong functionality, whereas in adult stem cells, the emphasis may shift towards survival and DNA repair as crucial factors for preserving tissue homeostasis [195]. Moreover, only a limited number of studies have conducted a comparative analysis between stem cells and their downstream progenitors or across various types of skin cells. Emerging evidence suggests that DNA repair and DDR exhibit variations depending on cell type and differentiation stage, with stem cells addressing DNA damage differently than their somatic counterparts [182,190]. Therefore, this study stands as one of the first presentations of comparative data on the UV damage response in DSCs in contrast to diverse differentiated skin cells derived from human foreskin, including fibroblasts, melanocytes, and keratinocytes.

To minimize interindividual variabilities caused by age, ethnicity, and skin type that can influence damage induction and repair [490-493], all four cell types were obtained from juvenile foreskin. This provided the benefit of exclusively comparing primary cell cultures without the need of cell lines. Previous reports showed an age-related reduction in the repair capacity of fibroblasts [494,495], while in human keratinocytes, DNA repair was unaffected by age [496,497]. The donors in this study displayed consistent ethnicity and age, with 129 of 148 donors (87%) being younger than a year, and 108 of 148 donors (73%) being even younger than six months (see Appendix Figure 8.4). The donor's skin types were not classified according to the Fitzpatrick scale, but—based on observations—most of them ranged from fair to medium brown, with dark brown being rare.

6.3.1 DNA Repair Capacity

The individual radiation risk of stem cells differs from that of differentiated cells, due to disparities in DDR, cell cycle regulation, gene expression, chromatin structure, and epigenetic

patterns [498-502]. Stem cells, with their high proliferation potential, are more prone to replication-associated mutations. Additionally, the lifelong residence of stem cells in tissue increases their risk to accumulate genetic and epigenetic changes, thereby acquiring genomic instability [503]. Radiation-induced damage or mutations can disseminate in the stem cell pool through self-renewal or be transferred to daughter cells [190]. Therefore, both embryonic and adult stem cells possess highly efficient DNA repair mechanisms and an exceptional DDR to prevent these processes and maintain normal function [181,182]. However, protective mechanisms in DSCs following UV exposure have hardly been explored. The first part of the damage response analysis examined whether DSCs exhibit different repair capacities compared to more differentiated skin cells, contrasting the rate (using the repair time constant τ) and the efficacy (using remaining DNA damage) of DNA repair.

This necessitated the induction of equivalent levels of CPDs beforehand. Melanocytes showed significantly lower CPD induction compared to the other skin cells when exposed to the same dose of 285 J/m² UVB. This difference was most probably attributed to the presence of melanin, as the melanocytes displayed diverse pigmentation intensities during cell culture, mirroring the donor's skin phenotype [504]. Absorption and scattering of UV radiation by melanin acts as a protective mechanism, resulting in an inverse correlation between UVB-induced CPDs and melanin content/skin type [19,23,492,493,505]. Additional factors that may also influence the extent of damage induction include nucleus size and chromatin compactness [171,506-508]. Comparable initial CPD levels were induced by irradiating melanocytes with a higher UVB dose of 400 J/m².

When left unrepaired, UV-induced DNA damage has the potential to induce genetic mutations and genomic instability, contributing to cancer initiation and progression [211]. Deficiencies in the repair of photolesions are a significant etiological factor in the multistep development of skin cancer [394]. Following UVB exposure, there were indications that DSCs removed CPDs at the slowest pace, however without statistical significance. Hence, while DSCs, fibroblasts, and melanocytes exhibited comparable repair time constants τ (~27–31 h), keratinocytes demonstrated the fastest DNA repair. Their repair time constants shown here after 285 J/m² UVB exposure (~20 h) align with the repair kinetics of HaCaT keratinocytes following irradiation with 300 J/m² UVB (21 h) [394]. The repair rate of melanocytes was independent of the initial quantity of CPDs, consistent with findings from numerous *in vitro* and *in vivo* studies including cultured melanocytes, as well as animal models and humans with diverse skin pigmentation [19,492].

Rate and efficiency of nucleotide excision repair (NER) of UV-induced photoproducts are described to vary greatly across cell types [211,509,510]. The process of differentiation is often associated with a decline in DNA repair capacity [511]. Removal of DNA lesions is crucial in actively replicating cells, particularly from active genes. In contrast, terminally differentiated, post-mitotic cells—which no longer replicate their DNA—could potentially refrain from repair, at least for non-expressed genes, displaying restricted DNA repair/DDR [182,211,510]. Nouspikel and Hanawalt's review summarized several types of (terminally) differentiated cells, including neurons [512], macrophages [213], and muscle cells [513], where the removal of CPDs via NER is progressively downregulated throughout cellular differentiation [510]. This repair attenuation in terminally differentiated cells, as opposed to proliferating cells, solely involves global genome repair (GGR), while in active genes both the transcribed and non-transcribed strand undergo proficient repair through transcription-coupled repair (TCR) and transcription domain-associated repair (DAR) [509]. Base excision repair (BER) can also be downregulated in terminally differentiated cells [182]. Why is there such a significant difference in repair rates among the differentiated skin cells in this study, meaning fibroblasts and melanocytes in comparison to keratinocytes? Fibroblasts and especially melanocytes represent highly differentiated cells that might have attenuated DNA repair capabilities, at least *in vivo* in their normal physiological setting in the skin, where melanocytes also exhibit poor proliferation ability [23]. On the other hand, keratinocytes are highly proliferative in the skin compared to other cell types and can be found in all stages of differentiation in the epidermis, from undifferentiated to terminally differentiated. These conditions would match the repair results. However, cell culture represents an artificial environment that drives all cells to proliferate, even against their natural behavior. Although the foreskin-derived fibroblasts and melanocytes regained their proliferative potential in cell culture following isolation, their DNA repair was in fact slower compared to keratinocytes, similar to what might be expected *in vivo* based on differentiation and proliferative states. Accordingly, in earlier UVB studies, keratinocytes outperformed fibroblasts in pace and efficiency of CPD removal [514,515]. As the primary target for UV radiation and UV-induced cutaneous malignancies, keratinocytes might possess specialized strategies for maintaining genomic integrity, including efficient and rapid DNA repair mechanisms.

Given the context of restricted DNA repair in terminally differentiated cells [182,211,510] and the decrease in DNA repair capacity during the differentiation process [511], it was unexpected that DSCs, holding high differentiation potential, did not repair faster than the differentiated skin cells in this study, or at least faster than fibroblasts and melanocytes. Usually, both

embryonic and adult stem cells are equipped with a superior DDR [181]. Human mesenchymal stem cells (MSCs) repair UVB-induced CPDs more rapidly than dermal fibroblasts [516]. Higher NER capacity has been reported in adult stem cells from the monocytic [213] and neural lineage [512] compared to their differentiated progeny, macrophages and neurons, respectively. The repair of CPDs induced by UVA and UVC is significantly greater in keratinocyte stem cells and generally basal epidermal cells than in upper epidermal layer keratinocytes [496,517]. Adult neural stem cells [518] and keratinocyte stem cells [519] have also demonstrated superior repair capacities to ionizing radiation compared to their more differentiated counterparts. Moreover, enhanced expression and activity of BER components have been found in murine neural stem cells [520]. Human pluripotent stem cells (PSCs), such as hESCs and iPSCs, possess highly active DDR mechanisms as well. Their DNA repair capacities, both for NER and BER, surpass those of non-pluripotent, differentiated cells [511]. For example, hESCs exhibit enhanced BER activity compared to foreskin fibroblasts in response to various types of DNA lesions induced by H_2O_2 (oxidized bases), UVC (pyrimidine dimers), and ionizing radiation (single- and double-strand breaks) [487]. The NER of UVC-induced CPDs is even 2–3 times faster in hESCs and iPSCs than in fibroblasts, supposedly caused by enhanced GGR [486] and increased expression of multiple components involved in DNA damage signaling, checkpoint function, and DNA repair [487,488].

The question arises as to why DSCs do not demonstrate a higher NER capacity than differentiated cells. The robust and faster repair observed in PSCs is likely attributable to their accelerated proliferation and cell cycle progression (see section 6.3.2). PSCs, like ESCs and iPSCs, progress through G1 phase relatively fast compared to committed somatic cells to support self-renewal and maintain pluripotency [521,522]. They are characterized by short G1 and G2 phases and a large S phase [523,524]. This necessitates rapid and efficient repair in G1 prior to the next DNA replication in the S phase, especially considering that ESCs fail to activate the G1/S and intra-S checkpoints in response to DNA lesions [181,488]. In contrast to ESCs, adult stem cells, depending on the specific tissue, tend to be predominantly in a quiescent state, residing in the G0 phase of cell cycle with restricted or halted proliferation to reduce intrinsic cell stress and prevent stem cell exhaustion [69]. Recent studies indicate the coexistence of active and quiescent stem cell subpopulations in the same tissue, serving for tissue replenishment and as backup population, respectively [77]. Similar to terminally differentiated cells (see above), (temporarily) quiescent but not terminally differentiated cells, such as growth-arrested mouse embryo fibroblasts [391] or B lymphocytes [525], also show attenuated DNA repair. This applies to quiescent adult stem cells as well [190]. Regarding the

DDR, quiescence poses a challenge since DNA damage checkpoints and numerous repair pathways are cell cycle dependent [190]. The dormant state involves global repression of transcription, condensed chromatin, and absence of DNA replication [390]. These factors impede DNA repair through TCR, while GGR also seems to be arrested in quiescent cells. Consequently, in quiescent, non-proliferating (stem) cells, the accumulation of mutations at both transcribed and temporally silent genes and/or imperfect repair could potentially contribute to cancer-causing mutations [391]. So, could quiescence be the reason why DSCs do not have a better repair capacity than the other skin cells? The DSCs in these experiments were actively proliferating during repair kinetics (see Appendix Figure 8.5), indicating that at least a certain portion of the DSCs in cell culture is not (anymore) in a quiescent state and should exhibit a normal DDR. If quiescent DSCs were also isolated from foreskin, it is likely that they were mostly excluded during the initial two-week cultivation in free-floating dermal spheres. Formation of spheres primarily involves actively proliferating cells, conflicting with a quiescent state [425]. This may result in the elimination of quiescent DSCs prior to subsequent experiments. Under physiological conditions in human skin, however, DSCs are likely to also exist in a quiescent state, which accordingly could be associated with low/halted proliferation and attenuated DNA repair.

Throughout the entire study, the DSCs proliferated at approximately the same rate as fibroblasts and melanocytes, evident in only slightly shorter doubling times for DSCs. Additionally, the baseline cell cycle proportions in DSCs differed from the extremely short G1 and large S phase described in ESCs [523,524]. Even after UV irradiation, the cell cycle distribution did not indicate enhanced proliferation of DSCs. Consequently, unlike ESCs, DSCs appear to be less proliferative and progress through the G1 phase at a slower rate, suggesting that a faster repair, as observed in PSCs, may not be necessary. In contrast, keratinocytes demonstrated the shortest doubling times and, after UV irradiation, the highest proliferative activity, as indicated by a markedly increase in the S phase proportion and a decrease in the G1 phase. In this case, the rapid DNA repair, associated with the shortest repair time constant, aligns with the quick progression through the cell cycle. Consequently, there is some evidence that in these investigations, the proliferative ability of the various isolated skin cells in cell culture may have significantly influenced the rapidity of CPD repair.

Another possible reason why DSCs do not display the superior DNA repair attributed to stem cells [181] could be their lower potency (multipotency) compared to pluripotent ESCs or iPSCs. The one-step further differentiation might have already led to a reduction in DNA repair

capacity [511]. This could explain why in the case of DSCs, even after a potential exit from quiescence following isolation, there is not a significant difference in repair times compared to differentiated skin cells (fibroblasts and melanocytes) *in vitro*.

The findings of this study therefore indicate that for the applied UVB dose of 285 J/m²:

(i) CPD repair rates in DSCs are either comparable or even marginally slower than those in differentiated skin cells.

(ii) Repair of photolesions in DSCs might still be equally 'efficient' as in other human skin cells, as indicated by similar unrepaired CPD levels at the investigated time following irradiation.

The remaining DNA damage did not correlate with the repair time constants, as keratinocytes removed DNA lesions more rapidly but to the same extent as the other cell types. However, it is important to note that determining the final residual damage precisely may require more time for the repair curve to plateau, potentially beyond 96 h after irradiation. Additionally, both the repair time and the remaining DNA damage do not allow for an adequate assessment of the actual efficiency of CPD repair. In essence, a short repair time is preferable as it reduces the likelihood of cell division in the presence of persisting DNA damage, thereby decreasing the risk of mutation incorporation through error-prone translesion DNA synthesis (TLS) polymerases [526]. However, faster repair is not necessarily synonymous with better or more efficient outcomes; it could also be more prone to errors, suggesting that a slow but thorough repair may be advantageous. The actual efficiency of DNA repair can only be determined through mutation frequency analysis [527]. For instance, this method was used to demonstrate that mouse embryonic stem cells (mESCs) efficiently remove photolesions at low UVC doses [489]. The necessity of mutation frequency analysis to determine final repair efficiency is emphasized by the discovery that NER-proficient epidermal stem and progenitor cells in murine epidermis still accumulate persistent CPDs upon chronic UV exposure [388,389] and then evade apoptosis, rendering these CPD-retaining basal cells (CRBCs) predisposed to mutagenesis and carcinogenesis [389]. Thus, a functioning DNA repair with minimal remaining damage does not automatically imply efficient DNA repair if mutations result from it.

The pronounced donor-dependent interindividual variabilities observed in these results are not uncommon and have been noted in previous reports. Studies on *in situ* irradiation of human skin [490] and *in vitro* irradiation of primary keratinocytes and fibroblasts [394] have demonstrated variability in CPD induction, repair time constants, and remaining damage as well. This high variability might reflect individual variations in the degree of tolerable damage

and/or the saturation of the enzymatic repair system [394,490]. The involvement of the circadian clock in the NER activity [528] and the state of chromatin [171,212] may represent further reasons for the measured variabilities. Both the quantity of UV damage and the percentage of removed photoproducts have been shown to be influenced by the circadian time at which cultured cells and mouse skin are exposed to UV radiation, owing to differing chromatin condensation [506] and oscillating expression of certain NER proteins [529]. Bee et al. reported that the formation and removal of photolesions are highest at maximum chromatin relaxation [506]. Since the cells in this study were not synchronized, it is quite likely that varying chromatin compactness in different donor cell strains may have affected the CPD induction levels and the accessibility of DNA for repair proteins, which has direct implications for repair time and remaining DNA damage, leading to high variabilities.

6.3.2 Cell Cycle Progression

The cell cycle plays a crucial role in the DDR by enabling a temporary arrest to facilitate the repair of DNA damage. Before examining the cell cycle response to UV radiation, the baseline cell cycle distribution of the four skin cell types was compared. The baseline distribution of the cell cycle phases in the non-irradiated samples (0 h) was quite similar to our former studies [398]. Minor deviations, such as a slightly larger S phase observed in all cells in this study, can be attributed to donor-dependent interindividual variabilities and the utilization of two different evaluation software products (Flowing Software in Mhamdi-Ghodbani et al. [398] vs. ModFit LT in this study). Additionally, different cell densities due to varying rates of cell growth, different levels of medium consumption, and working with non-synchronized cells can have an impact as well.

The predominantly high G1 and small S phase of melanocytes observed at baseline (0 h) in this study suggested low proliferation in cell culture, reflecting the actual *in vivo* situation under normal physiological conditions, since in human skin, melanocyte mitosis is rare [530]. Terminally differentiated melanocytes demonstrate high levels of CDK inhibitors (e.g., p27, p16), dephosphorylated Rb (retinoblastoma protein), and decreased levels of cyclin D1, leading to the inhibition of cell cycle progression [6,14]. In contrast, DSCs exhibited a smaller baseline proportion of G1 compared to fibroblasts and melanocytes, suggesting a higher proliferative potential, despite the fact that *in vivo*, adult stem cells are predominantly in a non-proliferative state, depending on the organ or tissue [503]. The baseline cell cycle distribution of keratinocytes resembled that of DSCs. Measurement of the general doubling times revealed that DSCs proliferated only slightly faster than fibroblasts and melanocytes, whereas keratinocytes

reduplicated with the fastest pace. Differences in baseline cell cycle parameters between stem cells and committed somatic cells were described before. In hESC [521] and mESCs [522], a short G1 phase supports self-renewal and maintains pluripotency, since susceptibility to differentiation is higher in G1 [499]. The rapid progression through G1 in hESCs is associated with high transcription of G1-related CDK4/cyclin D2, whereas CDK inhibitors p21, p27, and p57 are expressed at very low levels [521]. In general, pluripotent stem cells like ESCs and iPSCs exhibit rapid proliferation, characterized by short G1 and G2 phases and a large proportion of cells in S phase. During early stages of differentiation, cell division times increase, accompanied by an elongation of the G1 phase [499,523,524]. In differentiated cells, the G1 proportion predominates. For cultured cells, inhibition of cell proliferation in G1 is typically a necessary step for the process of differentiation [531]. This is in agreement with the high baseline G1 proportions seen in fibroblasts and melanocytes in this survey. Compared to an extremely small G1 proportion (19%) and large fraction of actively proliferating S phase cells (66%) in hESCs [521], the results of the DSCs (68.0% G1, 18.3% S) indicate that DSCs are less proliferative than ESCs, but seem at least more proliferative than the fibroblasts and melanocytes in this study.

Cell proliferation in fibroblasts, melanocytes, and keratinocytes appeared to be stimulated by the addition of fresh medium at the beginning of the experiment, as evidenced by a strong increase in S phase in the initial 24 h (also evidenced by cell counts of controls at harvest for apoptosis measurement), with the most pronounced effect observed in keratinocytes. Notably, among these cells, keratinocytes are also the most proliferating cells in skin tissue. In contrast, melanocytes only divide continuously when removed from their physiological niche and cultured in a laboratory setting [532,533]. Unlike the other three cell types, DSCs appeared to proliferate at a constant rate throughout the whole experiment without further stimulation, reflected by the steady cell cycle distribution. DSCs indeed proliferated during cultivation as seen by increasing percentage of NGFRp75^{+} cells during repair kinetics (see Appendix Figure 8.5). The varying baseline cell cycle distributions across different cell types may influence their response to DNA damage. For instance, in human skin fibroblasts, declined DNA repair capacities have been demonstrated to correlate with alterations in cell cycle parameters [494].

For efficient repair of damage and maintenance of genomic integrity, cells undergo temporary growth arrest at various cell cycle checkpoints. Low UV doses trigger a transient cell cycle arrest (with transient p53 induction), while high doses induce cell death via apoptosis or permanent cell cycle arrest and senescence (with a slower, but more sustained and pronounced

p53 induction) [238,534], leading to a loss of pluripotency in ESCs [66,181]. The findings of this thesis indicate that the cell cycle response to DNA damage varies depending on the skin cell type. UV irradiation had no impact on the cell cycle profile of DSCs, whereas fibroblasts, melanocytes, and keratinocytes experienced a transient cell cycle arrest in the G1 phase following exposure to a high dose of 900 J/m² UVB.

These results are partly consistent with previous cell cycle data from our group, using a UVB dose comparable to the lower UVB dose of 300 J/m² in this study. Back then, we also observed no alterations in DSCs and a temporary cell cycle arrest in fibroblasts (with tendencies of an arrest in melanocytes and keratinocytes). However, the observed arrest occurred in the S and not in the G1 phase, accompanied by a reduced G1 proportion [398]. These disparities are most likely a result of differences in experimental setups. In the former experiments, we used control cells only at the beginning of the experiment, whereas in this study, control cells were implemented for every single measurement time point. Interestingly, the control cells in this study showed a pronounced S phase at the initial two points following sham-irradiation, possibly due to the supply of fresh medium and initiated proliferation. Hence, comparison of irradiated cells to their respective controls at the same time revealed an arrest in the G1 phase, resulting in a diminished portion of S phase cells. In our previous study, however, controls were harvested directly at the beginning, lacking introduction of fresh medium unlike in the irradiated cells, thus exhibiting an insufficient basis for comparison [398]. This underlines the importance of employing adequate controls to exclude all other possible confounding effects. Rünger et al. have also demonstrated a cell cycle arrest in G1 in foreskin fibroblasts following UVB exposure when cells were synchronized before irradiation, and in the S phase in non-synchronized cells [176]. Other studies reported an S phase arrest in fibroblasts, while keratinocytes remained unaffected, however, they lacked sufficient controls, hindering a thorough evaluation and comparability of the results [515].

The findings presented here suggest that the utilized UVA doses of 37 kJ/m² and 74 kJ/m² did not cause sufficient damage to induce cell cycle arrest in any of the skin cell types. Other studies have observed UVA-related cell cycle effects in HaCaT keratinocytes only at higher doses of 100 kJ/m² or more [402]. In primary foreskin fibroblasts, UVA mostly fails in activating cell cycle checkpoints or induces only short-lasting alterations [176]. Using equimutagenic doses, UVA (up to 300 kJ/m²) leads to less effective cell cycle arrest and lower activation of p53 compared to UVB (up to 300 J/m²) [176]. In this study, the applied doses were not equimutagenic, making a direct comparison of UVA and UVB effects challenging. The UVB

doses had a comparatively higher biological effectiveness, explaining the more robust cell cycle arrest observed in melanocytes, fibroblasts, and keratinocytes following UVB irradiation.

Unlike DSCs, which showed no alterations in the cell cycle in this work, studies of MSCs reported that MSCs exhibit a cell cycle arrest after both low-dose (250 J/m²) and high-dose (1000 J/m²) UVB irradiation that is, however, significantly less pronounced than in dermal fibroblasts. Simultaneously, this arrest is accompanied by a dose-dependent increase in p53 and p21 protein levels in MSCs [516]. The constant cell cycle distribution of DSCs after UV exposure resembles previous reports of human ESCs that lack proper G1/S checkpoint due to the absence of the p21 protein following UVC irradiation [535]. This also aligns with the low expression levels of CDK inhibitors such as p21 in hESCs as described by Becker et al. (see above) [521]. Moreover, the absence of hypophosphorylated Rb seems to play a role as well [536]. Other studies, on the other hand, demonstrate that hESCs are indeed capable of activating the G1/S checkpoint after UVC exposure through downregulation of CDK2. However, this activation also occurs in a p21- and p53-independent manner, mediated by checkpoint kinases Chk1 and Chk2, and the loss of phosphatase Cdc25A [537]. Likewise, following exposure to ionizing radiation, hESCs experience an ATM-dependent transient cell cycle arrest in the G2 phase [538]. Similar to hESCs, iPSCs can temporarily arrest the cell cycle at the G2 phase after ionizing radiation, but not at the G1/S checkpoint [488]. Multiple reports suggest that hESCs can modulate the CDK activity to promote and/or inhibit cell cycle progression [537]. The activity profile of cell cycle regulators in ESCs differs significantly from that in specialized somatic cells, with CDKs and cyclins not exhibiting the typical oscillating peaks of restricted activity [499,539]. The organized regulation of processes typically responsible for prompting somatic cells to undergo apoptosis or temporarily pause the cell cycle for DNA damage repair thus seems to be absent in ESC. Moreover, the p53-induced cell cycle arrest appears to interfere with the maintenance of pluripotency and self-renewal in ESCs, which is why p53 can guide ESCs with DNA damage towards differentiation instead of promoting DNA repair to maintain intact DNA [524]. Overall, it seems that the p53-p21-pathway in hESCs does not follow the typical regulation of cell cycle observed in somatic cells [540]. Whether this phenomenon of an atypical cell cycle structure also applies to DSCs and contributes to cell cycle progression instead of an arrest following UV exposure requires further investigation in subsequent studies. A lack of growth arrest in response to UVB irradiation would increase the probability of insufficient DNA repair, eventually leading to mutations and genomic instability.

In summary, the DSCs not only failed to exhibit any cell cycle arrest post-irradiation, but also did not manifest the changes in baseline cell cycle distribution observed in the non-irradiated controls of the other three cell types (increased S phase within the initial 24 h, implying proliferation due to the addition of fresh medium). These findings point to an exceptionally cell type-specific regulation of the cell cycle in DSCs, both in general and in response to UV irradiation, that does not resemble any of the observed patterns in the other examined skin cell types.

6.3.3 Induction of Apoptosis

Together with proliferation and differentiation, apoptosis is an essential process to ensure tissue homeostasis in the human epidermis [380,541]. In its function as a protective mechanism, apoptosis represents a double-edged sword, especially concerning stem cells. A high susceptibility to cell death ensures rapid removal of damaged cells from the stem cell pool, preventing stem cell dysfunction or malignant transformation, but at the same time would lead to faster stem cell exhaustion in the tissue and aging [190]. Conversely, resistance to apoptosis would ensure the survival of the stem cell population and the preservation of tissue regeneration. However, this comes at the expense of the long-term maintenance of genomic integrity, allowing for the accumulation and propagation of cancerous mutations in the stem cell pool through self-renewal [195]. Therefore, achieving a delicate balance in the mechanism of apoptosis is particularly important for stem cells to prevent the accumulation of irreparable DNA damage and mutations that would be permanently transferred to daughter cells [542].

In this study, keratinocytes were completely resistant to apoptosis when exposed to single UVB (300 J/m² or 900 J/m²) or UVA irradiation (37 kJ/m² or 74 kJ/m²), whereas the higher dose of UVB induced apoptosis in DSCs, fibroblasts, and melanocytes. Although the induction of apoptosis in DSCs after 900 J/m² UVB was not statistically significant due to high variability, the effect of apoptosis induction was clearly evident when examining the individual donor cell strains separately. Additionally, not only were fewer total cell counts measured simultaneously, but the frequency of DSCs also decreased, strongly indicating cell death. This implies that many DSCs were already damaged to a degree that rendered them undetectable with the anti-NGFRp75 antibody. Indeed, the apoptotic fraction in the DSC samples exhibited a weaker NGFRp75 signal intensity than the viable DSCs, particularly pronounced in the staurosporine-treated cells (data not shown), suggesting damage to the cell membrane. A diminished cell count and reduced proportion of stem cells may also arise from a more substantial impairment of DSC proliferation compared to fibroblasts in the same culture. However, as the cell cycle distribution

following UV irradiation did not indicate an impact on the proliferation rate of DSCs, cell death appears to be a more plausible cause. Consistently, the sphere formation assay also demonstrated a significantly decreased viability and reduced DSC frequency after UVB irradiation with 900 J/m² (see section 6.5.2), providing further support for the observed induction of apoptosis in DSCs. The generally higher baseline proportion of apoptotic cells in DSC controls compared to the other skin cells might be explained by the use of a different detachment reagent. Other studies have indicated that detachment with Accutase™ results in more apoptotic cells compared to, for example, trypsin [451]. Overall, DSCs behaved similarly to fibroblasts and melanocytes regarding the induction of apoptosis, and in all four skin cell types (DSCs, fibroblasts, melanocytes, keratinocytes), cell numbers and apoptosis results provided a consistent picture. The decrease in cell counts observed in fibroblasts and melanocytes following exposure to 900 J/m² UVB, in comparison to the non-irradiated controls, could be attributed to a combination of cell cycle arrest, leading to halted proliferation, and induced cell death.

When stem cells experience irreparable DNA damage, they tend to undergo early senescence or apoptosis to prevent the accumulation of genetic damage. For instance, both hESCs and iPSCs are very sensitive to DNA damage and thereby more prone to apoptosis [181], despite their enhanced CPD repair capabilities (see section 6.3.1). Even at low UVC doses (5–10 J/m²), which induce minimal or no apoptosis in non-pluripotent cells like fibroblasts and lymphoblasts, they display high rates of apoptosis [486,535]. The increased propensity for apoptosis in ESCs and iPSCs is attributed to several factors, including a lack of G1/S checkpoint activation [535,543,544], the presence of constitutively active pro-apoptotic Bax [542], and constitutive mitochondrial priming, which shifts the balance of pro-apoptotic and anti-apoptotic proteins closer to the apoptotic threshold [181,545]. Moreover, this hypersensitivity of ESCs to UV irradiation is linked to highly expressed p53 as compared to differentiated cells [546,547] and its accumulation in response to UV exposure [548,549]. Favoring cell death over DNA repair is assumed to be a strategy of pluripotent stem cells to maintain genomic integrity and avoid the propagation of mutated cells [489,535]. In line with this, the rate of spontaneous mutations in ESCs is notably lower than in somatic cells [544]. Similarly, in DSCs, the DDR also appears to lean towards apoptosis rather than cell cycle arrest for DNA repair, at least after exposure to 900 J/m² UVB. However, further verification of this hypothesis requires an examination of DNA repair at this higher dose, where apoptosis induction was observed in DSCs. The repair data presented in this study are based on a lower dose of 285 J/m² UVB. Following a similar dose of 300 J/m² UVB, no apoptosis was detected, suggesting that DNA

repair remains the preferred response over cell death at lower doses. In addition, the DSCs in this study were not as hypersensitive to UV as described for ESCs and iPSCs, leading to the speculation that DSCs may not express p53 as highly as PSCs.

In adult stem cells, the response to DNA damage in terms of cell death is less straightforward compared to PSCs, with instances of both sensitivity and resistance. In the interfollicular epidermis, the proliferating and less differentiated cells in the basal layer are more susceptible to UV-mediated apoptosis than the more committed progeny in the suprabasal layers [195]. Following UV irradiation, a sustained activation of p53 is observed in the longer-lived basal epidermal cells compared to suprabasal cells [550]. Additionally, there is an Nrf2 gradient with higher expression in suprabasal layers, leading to increased activation of antioxidant defense and less apoptosis in suprabasal keratinocytes [551,552]. In agreement with this, studies have shown that keratinocyte stem cells exhibit significant photosensitivity to UVA irradiation (100 kJ/m²), resulting in decreased viability and colony-forming ability [517]. By contrast, a UVB dose of 400 J/m², similar to the lower dose used in this study, does not induce apoptosis in keratinocyte stem cells [553]. Another example of insensitivity are multipotent hair follicle bulge stem cells that are resistant to ionizing radiation-induced apoptosis, displaying enhanced survival owing to high expression of anti-apoptotic Bcl-2 and rapid DNA repair compared to other epidermal cells [554]. Hair follicle melanocyte stem cells located in the same niche also avoid apoptosis; instead, they are eliminated through premature differentiation [70]. Human mesenchymal stem cells (MSCs) are more resistant to UVB exposure than dermal fibroblasts, showing higher viability and, if any, very low apoptosis rates after irradiation with 250 J/m² or 1000 J/m² UVB. In contrast, fibroblasts experience significant apoptosis induction. On the contrary, MSCs demonstrate increased senescence rates, while in fibroblasts senescence is not induced [516], suggesting that MSCs may evade apoptosis by undergoing senescence [516,555]. In future studies, senescence should be investigated as an additional endpoint to elucidate whether it plays a role in DSCs as well.

Altogether, there are great differences in the sensitivity of tissue-specific stem cells to DNA damage and apoptosis throughout the entire body [195]. The extent of p53 activation and the expression levels of the anti-apoptotic protein Bcl-2 apparently play a pivotal role in these differences [190]. The discrepancies among various stem cell populations arise from the fact that the sensitivity of adult stem cells to genotoxic stress is dependent on the proliferation rate [190]. Tissues characterized by high proliferation, like embryonic tissue and the intestinal epithelium [556], display heightened susceptibility to DNA damage caused by both endogenous

factors (e.g., replication stress) and exogenous sources (e.g., irradiation) [181]. In contrast, adult stem cells that proliferate slowly or are in a quiescent state, such as colon stem cells, demonstrate increased resistance to DNA-damaging agents, making them more susceptible to the accumulation of mutations and the potential for carcinogenesis [190,556].

As mentioned above, there were indications of membrane damage and compromised cell surface antigen expression in DSCs after UV irradiation, as evidenced by the decreased intensity of the NGFRp75 staining signal in flow cytometry within the apoptotic fraction. This raises the concern that apoptotic DSCs with an impaired NGFRp75 signal may be mistakenly omitted from the analysis when gating with fibroblasts, resulting in the underestimation of apoptotic cell numbers. To eliminate the possibility of an affected cell membrane causing false-negative NGFRp75 signals and excluding DSCs, experiments with purified DSC cultures should be conducted, as no gating based on surface markers is necessary to distinguish DSCs from fibroblasts in such cultures. Preliminary experiments with purified DSC cultures also showed no apoptosis after 300 J/m² UVB, whereas notably higher apoptosis rates were measured after 900 J/m² UVB compared to the DSC-fibroblast co-cultures in this study (Mhamdi-Ghodbani, unpublished data). Extensive disruption of the cell membrane can also hinder the detection of apoptotic cells via the Annexin-V assay, as shown in other studies where, despite reduced viability, only few apoptotic cells could be detected with the Annexin-V assay, likely due to this reason [451,452]. Annexin-V binds to cell membrane structures, specifically phosphatidylserine, resulting from morphological and biochemical changes during apoptosis [408]. This implies that the cell membrane must remain sufficiently intact for accurate detection of phosphatidylserine. Although the Annexin-V assay is widely employed for apoptosis detection, it might be worthwhile to consider an additional membrane-independent apoptosis assay. For example, measuring mitochondrial cytochrome c release could be an alternative, but this might exclude the induction of apoptosis via the extrinsic pathway. Caspase-3 is a well-established, early, and specific apoptosis marker commonly used [557]. Activation of Caspase-3 and -7 even precedes the translocation of phosphatidylserine residues to the membrane surface, since Caspase-3/7 cleave and activate scramblase Xkr8, which is responsible for the phosphatidylserine switch during apoptosis [558,559].

A review of the existing literature on the other three skin cell types revealed a mixture of consistent and contradictory findings. Consistently, other studies also report no significant induction of apoptosis in foreskin fibroblasts after 300 J/m² UVB, and even a considerably higher UVA dose of 300 kJ/m² shows no effect [176]. The results obtained in this work are

further supported by studies of primary human skin cells, revealing that epidermal keratinocytes are less affected by solar-simulated radiation than dermal fibroblasts regarding various cellular damage biomarkers such as ROS generation, mitochondrial DNA damage, and nuclear DNA damage [560]. In colony formation assays, keratinocytes display higher survival rates than fibroblasts when exposed to UVA, UVB [561], and oxidizing agents [514]. Contradictorily, TUNEL assays demonstrate that keratinocytes are more susceptible to UVB-induced and oxidizing agent-induced apoptosis than fibroblasts [514]. Irradiation with 500 J/m² UVB was shown to induce apoptosis in foreskin keratinocytes via suppression of Bcl-2 expression and activation of Caspase-3, -8, and -9 [562]. Another report showed that exposure to a slightly higher dose of 90 kJ/m² UVA could indeed induce cell death, as evidenced by significantly reduced viability in mouse embryonic fibroblasts (MEFs), human foreskin fibroblasts, and adult human epidermal keratinocytes (HEKs) [563]. Larsson et al.'s studies show that irradiation with similar UVA (30–60 kJ/m²) and UVB doses (150–300 J/m²) to those used here lead to an increased number of apoptotic cells in both foreskin melanocytes and keratinocytes [564]. Discrepancies in the results across different studies may arise from variations in experimental settings and the use of different UV sources with varying irradiances and emission spectra, potentially containing contaminating wavelengths to different extents. Additionally, factors such as different cell types, cell densities, and media, as well as varied analysis and evaluation methods contribute to the diversity of outcomes.

Cells in the skin respond differently to UV irradiation. Following high-dose UV exposure, keratinocytes undergo apoptosis, typically perceived as sunburned cells [222], whereas melanocytes display higher resistance, surviving acute sunburn with elevated amounts of DNA lesions [57]. However, at low UVB or UVA doses, keratinocytes in the skin are protected from UV-induced apoptosis, partly due to sustained activation of Nrf2, a transcription factor that induces antioxidant defense (glutathione and cysteine). The baseline expression level of Nrf2 is roughly two-fold higher in keratinocytes compared to fibroblasts and melanocytes [551,552]. Apoptosis pathways in keratinocytes might be less pronounced or absent at lower UV doses in order to maintain tissue structure and skin barrier integrity in the face of permanent damage from chronic UV exposure [209]. This potential insensitivity of keratinocytes to apoptosis at lower doses is counterbalanced by the skin's natural process of terminal differentiation of epidermal keratinocytes in the cornified layer, including the loss of nuclei, that basically represents physiological apoptosis [5]. This aligns with the findings of the keratinocytes in this study, which omitted apoptosis while repairing CPDs, using more moderate UV doses that would not trigger excessive sunburn. However, in the skin, the basal epidermal cells are indeed

sensitive to UV-induced apoptosis compared to the suprabasal keratinocytes [195]. The composition of the keratinocyte cultures in this study following isolation from foreskin epidermis remains uncertain—whether they consist of undifferentiated keratinocytes from the lower layers, prevailing due to their higher division potential, or more differentiated keratinocytes from suprabasal layers, which are numerically superior. Considering previous literature findings and the results of this work, it is reasonable to assume the latter—a composition of more differentiated keratinocytes from suprabasal layers, which are less sensitive to UV radiation.

In this investigation, melanocytes displayed the highest susceptibility to apoptosis. This was surprising in view of the facts that they typically constitutively express the anti-apoptotic protein Bcl-2 in both skin and cell culture settings [565], are slowly proliferating, and considered more resistant to apoptosis than keratinocytes [193]. Additionally, it is assumed that the presence of melanin likely resulted in less extensive damage in melanocytes compared to other skin cells [492,493] and hence, one would rather expect less apoptosis induction. One unique factor distinguishing melanocytes from other cells is precisely this melanin, prompting speculation about its potential active role in apoptosis induction. Melanocytes inherently possess higher baseline levels of oxidative stress compared to keratinocytes and fibroblasts due to melanin synthesis, with this pro-oxidant state rendering them particularly vulnerable to oxidative stress [166,566]. Melanin amplifies UV-induced production of ROS and oxidative DNA damage. Studies have shown that upon UVB and UVA irradiation, survival is significantly lower and accumulation of oxidative DNA damage higher in melanocytes than in keratinocytes, respectively, attributed to (pheo)melanin acting as an endogenous photosensitizer [24,166]. Overall, melanin and its intermediates exert cytotoxicity and damage melanocytes through oxidative stress [18], promoting the induction of apoptosis following UV exposure. This concept of melanin-mediated apoptosis, described by Yamaguchi et al., is supported by multiple *in vivo* (human and animals) and *in vitro* studies [20]. Thus, apoptosis can be initiated not only by DNA damage but also by melanin-triggered damage. Accordingly, UV-induced apoptosis is significantly greater in darker skin [20]. The pathways involved in this mechanism seem to include Ser46-phosphorylated p53 while being Caspase-3-independent [567]. Photothermolysis through the generation of heat from absorbed UV energy may also contribute [20]. Therefore, the active involvement of melanin, contributing to a prevailing pro-oxidative state that promotes ROS damage, and triggering melanin-mediated apoptosis could be causative for the slightly higher sensitivity of melanocytes to UVB compared to the other three cell types. Moreover, evidence suggests that keratinocytes have better antioxidant activity

than fibroblasts, based on higher heme oxygenase activity and higher ferritin levels [568]. This collectively could explain why apoptosis occurred in melanocytes and fibroblasts, but not in keratinocytes. The extent of antioxidant defense in DSCs remains to be investigated.

6.3.4 Conclusion to UV Damage Response

The DNA damage response (DDR) plays a crucial role in UV carcinogenesis. The competition between the repair rate and the time available for DNA repair within the cell cycle ultimately determines the extent of unrepaired lesions that could lead to mutations. Stem cells are particularly susceptible to DNA damage accumulation and genomic instability due to their longevity and often non-proliferating, quiescent state [503]. While DDR mechanisms are highly active in pluripotent stem cells [511], active in somatic cells, and not fully active in terminally differentiated cells, the activity of DDR mechanisms in adult stem cells is tissue-specific and varies with developmental stages [182]. One could hypothesize that DSCs, in comparison to more differentiated skin cells, possess uniquely robust protection mechanisms in order to maintain genomic integrity.

The findings presented in this study revealed that, despite DSCs not displaying superior DDR, the various skin cell types exhibited different responses to UV radiation. Generally, effects were only observed after UVB exposure, with UVA having no discernible influence. This can be attributed to the use of relatively low UVA doses, and furthermore, UVB is the primary determinant of cell cycle arrest and cell death [402]. When comparing with previous literature, it is crucial to note that the radiation source in this study mimics solar UVB by blocking wavelengths below 295 nm. This is an essential difference to other lamps used in earlier studies, which frequently include some contaminating UVC wavelengths. This difference may potentially account for variations in the reported outcomes. The damage caused by the same UVB dose, or in other words, the same extent of damage (at least in DSCs, fibroblasts, and keratinocytes; melanocytes probably even with lower CPD induction), seems to be perceived differently by the diverse skin cells (Table 6.2). Keratinocytes exhibited cell cycle arrest for DNA repair without the induction of apoptosis. In contrast, melanocytes and fibroblasts demonstrated both cell cycle arrest and apoptosis. DSCs, on the other hand, did not induce cell cycle arrest but exhibited some degree of apoptosis, though not excessively strong.

Table 6.2 Summary of DNA damage response mechanisms in the different cell types.

Cell type	DNA repair 285 J/m² UVB	Cell cycle arrest 900 J/m² UVB	Induction of apoptosis 900 J/m² UVB
DSCs	+	-	+
Fibroblasts	+	++	++
Melanocytes	+	++	++
Keratinocytes	++	++	-

In general, this study unveiled a very coherent picture regarding the CPD repair rate and proliferation ability. A higher proliferative potential, indicated by short doubling times and increased S phase proportions in cell cycle analysis, was associated with faster DNA repair times, likely to ensure completed DNA repair before the next cell division. Consequently, the rapidly proliferating keratinocytes repaired DNA more quickly than DSCs, fibroblasts, and melanocytes, all of which shared similar doubling times and repair time constants. Only the cell cycle distribution of DSCs after UV irradiation, marked by a lack of cell cycle arrest, got out of line. Furthermore, a consistent correlation emerged between the rapidity of DNA repair and susceptibility to apoptosis (albeit assessed at different doses). Keratinocytes, being the most rapidly repairing cells, did not undergo apoptosis, whereas DSCs, melanocytes, and fibroblasts, characterized by slower repair time constants, were able to induce apoptosis. This connection of rapid DNA repair contributing to resistance to cell death was demonstrated, for instance, in hair follicle bulge stem cells [554].

The results from the CPD repair analysis suggest that DSCs possess a functional DNA repair system for UV-induced CPDs, comparable to that of fibroblasts and melanocytes in terms of both rapidity and remaining damage. However, the extent to which the efficiency of DNA repair matches or differs from that of other cells remains uncertain. Moreover, it can be hypothesized that DSCs seem to prefer apoptosis over cell cycle arrest. The notable absence of cell cycle arrest following exposure to both low and high doses of UVB and UVA, along with ongoing proliferation, constrains the available time for DNA repair before replication. This predisposes DSCs to the accumulation of mutations and/or the possibility of undergoing extensive apoptosis [535]. Indeed, certain donor cell strains exhibited pronounced apoptosis induction following exposure to the higher UVB dose. However, overall, the proportion of apoptotic cells seemed not large enough to assume the elimination of all stem cells with unrepaired damage. For the surviving cell population, these circumstances definitely increase the potential for resumed DNA synthesis and replication while a substantial amount of DNA lesions remains in their genome. Damage bypass by TLS polymerases lacking proof-reading activity is recognized to

be error-prone and result in high mutagenesis [526,535]. Therefore, it is crucial to further clarify whether DSCs repair the CPDs correctly or if, due to a repair process that is equally fast but less accurate, more mutations are incorporated compared to differentiated skin cells that exhibited cell cycle arrest. This necessitates mutation frequency analysis.

In addition, it is important to elucidate the mechanisms underlying the UV-induced DDR in DSCs and the consequences of absent cell cycle arrest in more detail. In future investigations, the examination of gene and protein expression of cell cycle regulators, including Cdc25A, Rb, cyclins, CDKs, and particularly p53 and p21, is crucial to decipher the behavior at different checkpoints and determine whether DSCs exhibit deficiencies in the cell cycle checkpoints, similar to ESCs [535]. p53 plays a pivotal role in activating cell cycle checkpoints (via activation of p21) and inducing apoptosis [191,197,204]. It is very likely that the activation of the G1/S checkpoint in fibroblasts, melanocytes, and keratinocytes with UVB was mediated by p53 and p21. Therefore, it would be intriguing to investigate whether the lack of growth arrest in DSCs is influenced by changes in these two proteins. Another challenge is to understand the dynamics of p53 in DSCs, as p53 kinetics vary depending on the stimulus, degree of stress, and cell fate [197]. The proteins p21 and p53 are not only essential for regulating cell cycle regulation and inducing apoptosis, but are also deemed to function as negative regulators of translesion DNA synthesis (TLS) [535]. Cells with reduced expression levels of these proteins are more prone to engage in error-prone TLS to bypass DNA damage. Additionally, cells lacking p21 or p53 demonstrate an increased incidence of TLS-associated mutations [569]. In this context, a loss of p53 and p21 would be even more detrimental. In subsequent investigations, it is advisable to include the cell type-specific expression analysis of genes associated with DNA damage checkpoints (e.g., ATR, Chk1), DNA repair pathways (e.g., XP proteins), and apoptosis (members of the Bcl-2 protein family). The role of miRNAs in the regulation of the DDR could also be of interest [237]. However, all of these studies cannot be performed with DSC-fibroblast co-cultures. Since the purification of DSC cultures was not yet established during the examination of DNA repair, cell cycle, and apoptosis as part of this thesis, the corresponding studies can only now be conducted in the course of the joint project ‘UV-DHDS: Effekte von UV-Exposition auf die Differenzierung von humanen dermalen Stammzellen in der Melanom-Genese’ (02NUK083).

In summary, the findings reported here might indicate that DSCs lack proper cell cycle checkpoints. In this context, their repair capacity may be insufficient to preserve genomic integrity. Unrepaired DNA damage in DSCs could be passed on to their self-renewing progeny

and accumulate over time. If tumor-suppressing mechanisms, such as limiting replication through apoptosis, are not functioning effectively, pre-damaged stem cells may acquire malignant potential. This is particularly noteworthy in the context of skin carcinogenesis, given that DSCs are targets of UVB and UVA radiation in the human skin. Considering the ability of DSCs to differentiate into melanocytes, initial damage prior to differentiation may elevate the subsequent potential for transformation. Therefore, it is of significant importance to investigate DSCs as potential sources of melanoma and examine their biological response to UV radiation.

6.4 Differentiation into Melanocytes

6.4.1 *In Vitro* Melanocytic Differentiation Potential of DSCs

DSCs were previously shown to be multipotent, possessing the ability to differentiate into various neural crest-derived cell types, including melanocytes, neurons, Schwann cells, smooth muscle cells, chondrocytes, and adipocytes [31,126]. With regard to the alternative theory of melanoma initiation proposed by Hoerter et al. [357,358], the focus in this study was on melanocytes as progeny. Therefore, only the potential of DSCs for melanocytic differentiation was examined. Additionally, it was verified whether the differentiation ability was affected by enrichment via immunomagnetic separation (IMS). A comparison of DSC fibroblast co-cultures, EasySep™-purified DSCs, and MACS®-purified DSCs confirmed that differentiation into melanocytes following stimulation with melanocyte differentiation medium was successful in all three cases. This was evidenced by the observation of melanocyte-like cell morphology with long dendritic extensions, the presence of melanocytic markers in immunocytochemistry, and the expression of melanocyte-specific genes. The transition from DSCs to melanocytes was validated by the co-expression of both the DSC marker NGFRp75 and the melanocyte marker HMB45.

The detected reduction in NGFRp75 expression levels in DSC-fibroblast co-cultures during differentiation is logical, considering both the decrease in cell density and the visually noticeable decline in DSC frequency, while the fibroblasts remained present. Stem cells likely disappeared from the culture due to differentiation and presumably also due to cell death. In the purified cultures, the NGFRp75 expression values remained unchanged, given the negligible proportion of fibroblasts and the relatively low proportion of differentiated melanocytes at the end. Purified DSCs seemingly exhibited a slightly faster increase in the expression of melanocytic markers (as observed in the UV experiment), but this might be attributed to the presence of fibroblasts during analysis of DSC-fibroblast co-cultures as well. Ultimately,

considerably high final expression of melanocytic genes was detected in all cultures, co-cultures and purified cultures, confirming successful differentiation into melanocytes, albeit with some differences.

Regardless of the degree of purification, melanocytic gene expression levels were higher in cultures with a larger initial stem cell proportion (see Table 5.1), either due to the fewer fibroblasts in the analysis or because a greater number of DSCs might actually enhance the differentiation process. Comparison between purified DSCs and DSC-fibroblast co-cultures indicated that purified DSCs remained viable and retained their differentiation capability after IMS. However, the enrichment with EasySep™ positive selection appeared to impact the differentiation ability of DSCs more than the MACS® positive selection, as displayed by the lowest expression values of melanocytic genes in EasySep™-purified DSCs. On the other hand, the differentiation potential of MACS®-purified DSCs persisted and was, if at all, only minimally impaired, agreeing with studies by Meyers et al., where human perivascular stem/stromal cells maintained their differentiation capacity following positive MACS® selection [478]. Consistent with these results were the visual observations of lower numbers of melanocytes in EasySep™-purified DSCs. The reason for the seemingly more compromised differentiation ability after EasySep™ positive selection could be the potentially better tolerability of MACS® *MicroBeads* due to their biodegradability [453,475], smaller size [422,466,475], and lower bead persistence [476] compared to the EasySep™ RapidSpheres™, as described in section 6.2.3.2. However, it is important to note that these were only initial experiments that require further validation with larger sample size.

The similar (as observed in the UV experiment) or even higher final melanocytic marker expression in DSC-fibroblast co-cultures compared to purified DSC cultures supports the notion of slightly better differentiation in co-cultures, as they contained a relatively lower amount of stem cells. The diminished differentiation ability of purified DSCs could stem from functional alterations caused by the separation process and/or the beads. Magnetic particles have the potential to induce adverse effects on cell phenotype, function [454,468-470], and viability [471-473]. Alternatively, the presence of fibroblasts in the culture may influence the differentiation of DSCs, and the purified DSCs might lack the influence and signals of fibroblasts as their microenvironment. The stem cell niche or microenvironment is known to have a significant impact on stem cell features, such as differentiation potential, and to play a crucial role in controlling stem cell behavior [56,60]. For instance, the differentiation potential of epidermal stem cells is heavily defined by the local microenvironment, with fibroblasts being

indispensable for a functional stem cell niche. Therefore, epidermal stem cells cannot be maintained in culture indefinitely without losing their stemness [58]. Fibroblasts play a major role in tissue development and the differentiation of keratinocytes, among other functions, by triggering epigenetic changes. The underlying molecular mechanisms, however, are not well understood [54]. It is expected that fibroblasts in the dermis play a major role in the differentiation of melanocyte stem cells (McSCs) as well [7], as part of their microenvironment. Additionally, paracrine factors from fibroblasts contribute to the regulation of melanocytes, influencing processes such as proliferation and melanogenesis [12,49]. Thus, it is plausible that fibroblasts in DSC-fibroblast co-cultures may release paracrine signals, creating a differentiation-promoting microenvironment. The clustering of differentiating cells in small groups could be indicative of such microenvironmental influences; specific locations may create differentiation-favoring conditions, leading to nearby cells undergoing differentiation. Whether purified DSCs, similar to epidermal stem cells, lose their stemness in long-term cultivation lacking fibroblasts is unclear and warrants further investigation. Finally, it must be noted that a direct comparison of the differentiation potential between DSC-fibroblast co-cultures and purified DSCs from different donors is challenging due to significant interindividual variability [570]. For a more accurate assessment, co-cultures and purified cultures from the same donor cell strain should be utilized.

Besides potential influences from fibroblasts, the *in vitro* differentiation process is primarily regulated by the factors present in the differentiation medium, mimicking the signals that McSCs usually receive when they undergo differentiation in the skin (see section 1.1.1.2). The composition of the differentiation medium utilized in this study (see Table 3.5) was based on research conducted by the Herlyn laboratory with hESCs [571], hair follicle McSCs [93], and DSCs [31]. For *in vitro* differentiation, the interplay of the three growth factors endothelin-3, SCF, and Wnt3a is indispensable to obtain melanocytes that ultimately express characteristic melanocyte markers (MITF, tyrosinase, TRP1, TRP2) and produce melanin [31,32,571]. They activate key pathways for melanocyte development—ETBR, c-Kit, and Wnt signaling (see section 1.1.1.2).

Early studies by Yamane and colleagues demonstrated melanocytic differentiation of mouse ESCs, requiring co-cultivation on a stromal cell line as feeder cells. The differentiation was strictly dependent on SCF, enhanced by endothelin-3 and dexamethasone, while being independent of Wnt3a, possibly due to stromal cell production of this factor. They also used bFGF, PMA, and cholera toxin based on their promoting effects [572-574]. The Herlyn laboratory later adapted this protocol for human cells, highlighting the indispensable role of

Wnt3a in human melanocyte differentiation. Fang et al. derived melanocytes from human ESCs without feeder cells using Wnt3a-conditioned medium and fibronectin-coating, initially involving the formation of embryoid bodies. These melanocytes correctly integrated into the basal epidermal layer of reconstructed skin [571]. This protocol was also effective for melanocytic differentiation of human iPSC [575]. The critical role of Wnt signaling was supported by further studies showing its necessity for neural crest induction in human PSCs [576,577]. Endothelin-3 and SCF signaling are crucial for the maintenance and survival of both melanocyte precursors [578] and differentiated melanocytes [579].

Li et al. and Yu et al. from the Herlyn laboratory used the same conditions for differentiating DSCs [31] and hair follicle McSCs [93] into melanocytes. In addition to Wnt3a, SCF, and endothelin-3, the differentiation media contained dexamethasone, cholera toxin, PMA, bFGF, insulin-transferrin-selenium (ITS), linoleic acid-BSA, L-ascorbic acid, FBS, low-glucose DMEM, MCDB 201, and DMEM [31,93,571]. PMA and cholera toxin activate PKC and increase intracellular cAMP, respectively [571,575]. They are commonly used in melanocyte medium as growth enhancers [532,580]. Dexamethasone and bFGF also support melanocyte growth in culture [571,581]. Furthermore, PMA has been shown to induce neural crest cell differentiation into melanocytes and melanin synthesis through MITF upregulation [582]. In the present work, cAMP and CHIR-99021 were added to the medium, similar to other reports [104,581]. CHIR-99021 is a GSK3β inhibitor, further activating the canonical Wnt pathway [577]. cAMP promotes differentiation and pigment production in melanocytes, typically activated by α-MSH/MC1R signaling, leading to the expression of genes like MITF [583].

Zabierowski et al. suggested a crucial role for Wnt signaling in DSCs. The canonical Wnt pathway seems to be repressed in DSCs due to the high expression of Wnt inhibitors (DKKs and sFRPs). Conversely, non-canonical Wnt signaling appears to maintain the multipotent state of DSCs. The induction of differentiation involves a Wnt3a-mediated switch from the non-canonical to canonical Wnt pathway [32]. The functionality of DSC differentiation is preserved when Wnt3a is substituted with recombinant Wnt7a [42]. In 3D skin reconstructs, exogenous Wnt3a is not required for the differentiation of DSCs [32], as it is likely expressed by the epidermal keratinocytes [584].

In addition to a suitable composition of the cell culture media, the coating of the cell culture vessels plays a crucial role in differentiation. Depending on the concentration, various mechanisms such as stem cell maintenance, differentiation into melanocytes, or differentiation

into other cells can be triggered or supported. Mechanical stimulation, as a third important factor promoting the differentiation of stem cells *in vitro* [55], was not considered in this work.

The DSCs appeared to be quite sensitive to artificially induced differentiation. The reduced cell density in differentiation medium compared to control cells in stem cell medium indicates that the cells were stressed and exhibited lower cell proliferation or even underwent cell death. In DSC-fibroblast co-cultures, cellular stress was observed through a decrease in cell density and DSC frequency. In purified cultures, due to the high DSC frequency, the stress manifested only in the cell density. The reduced confluency and the observation of cells floating in the medium strongly suggested that cell death occurred as a consequence of the switch to the differentiation medium. This aligns with the findings of Li et al., who also reported a great amount of dying cells in differentiation medium and a significant decrease in NGFRp75 expression [31]. The change in culture conditions to a differentiation medium also induces apoptosis in other cell types, such as in skeletal myoblasts [585]. In future experiments, the extent of cell death during differentiation of DSCs should be analyzed. If the cultures indeed also exhibited reduced proliferative activity, this could be due to the differentiation of cells instead of proliferation or because the differentiation medium possibly does not promote proliferation as much as the stem cell medium. Generally, differentiation medium is designed to promote differentiation rather than sustained proliferation. However, *in vitro* differentiation does not necessarily result in a permanent stop of cell division for all cells. Some cells may still undergo limited proliferation in differentiation medium, while others may enter a state of growth arrest. Whether and how (symmetric or asymmetric) the DSCs continue to replicate in the differentiation medium could be tracked using proliferation markers like Ki67 or by using dye dilution with DNA-traceable dyes like BrdU, IdU, or EdU, which are titrated out as cells divide [586,587]. However, it is important to note that these tracking dyes may affect biological processes in the DSCs, potentially impacting both proliferation and differentiation [588,589]. By monitoring NGFRp75, a DNA-traceable dye, and a differentiation marker, it is further possible to investigate whether replicating DSCs are able to differentiate or not. In order to differentiate, cells need to enter cell cycle arrest, and usually, the rate of proliferation decreases when cells differentiate [590,591]. Studies with ESCs have shown that proteins involved in promoting cell cycle progression prevent differentiation and vice versa [536], leading to the downregulation of proliferation at the onset of differentiation.

At the end of the differentiation assay, both melanocytes and DSCs were present in the cultures. This shows that not all DSCs underwent differentiation into melanocytes, and a lot of them

instead maintained their stem cell character. It is unclear why this occurs and which factors determine whether a DSC undergoes differentiation or not. Defining the percentage of DSCs that differentiate into melanocytes is challenging, especially if the stem cells continue to proliferate, albeit possibly at a slower rate. To ascertain the proportion of differentiated DSCs, a proliferation assay would be necessary in this case as well.

In the differentiation experiments, interindividual variabilities were also evident, as the sensitivity of DSC cultures (to the differentiation medium and to UV irradiation) was highly dependent on the donor. Often, sensitivity appeared to be associated with the stem cell frequency, with cultures having a higher stem cell content being more sensitive and especially purified DSC cultures tending to exhibit a higher likelihood of cell death during the differentiation assay. However, this cannot be the sole reason, and other interindividual variances must also play a role, as this rule did not always hold true. In DSC-fibroblast co-cultures with a lower stem cell content, the presence of more robust fibroblasts likely contributed to the cultures appearing visually less sensitive.

In conclusion, DSCs isolated from foreskin possess a melanocytic differentiation potential, which persists even after purification with IMS, albeit with a slightly reduced ability. Possible factors contributing to this include potential impairment of cell function due to the purification process and the presence of attached beads, as well as the absence of influences from fibroblasts as a supporting microenvironment. Positive selection via the EasySep™ method had a stronger impact on DSCs compared to the MACS® approach. It is noteworthy that the only minimal reduction in differentiation capability following MACS® positive selection does not hinder differentiation experiments with these purified DSCs.

6.4.2 Differentiation Following UV Irradiation

By subjecting DSCs to a single UVB (300 J/m²) or UVA dose (37 kJ/m²) one day before initiating differentiation, the aim was to investigate whether UV irradiation affects the differentiation capability. Both DSC-fibroblast co-cultures and purified DSCs were able to differentiate into melanocytes after UV irradiation. The significant increase in the gene expression of melanocytic markers and the observed number of cells with melanocyte-like morphology were consistent with those in non-irradiated cultures. Likewise, MSCs preserve their multi-lineage differentiation potential after single irradiation with a similar UVB dose of 250 J/m² [516]. In the scenario of UV irradiation influencing differentiation, there were two potential outcomes. On the one hand, there could be less differentiation due to senescence or

cell death resulting from DNA damage. On the other hand, UV-induced differentiation might act as an escape and anti-tumor mechanism, removing DSCs from the stem cell pool to prevent the accumulation of persistent damage and the dissemination of mutations [592,593]. Especially considering that in ESCs with DNA damage, p53 activation can promote differentiation instead of DNA repair [524], this hypothesis seems plausible. Cell stressors, encompassing oxidative and genetic damage, are recognized as significant mediators of cell fate decisions [69,593]. Genotoxic stress (ionizing radiation) [70] and UV radiation [594] have the potential to induce stem cell differentiation through damage induction. For instance, it has been shown that epidermal stem cells with DNA double-strand breaks are selectively eliminated from the niche through differentiation [595]. In hematopoietic stem cells (HSCs), the accumulation of ROS and DNA damage can lead to a loss of quiescence and self-renewal ability, followed by subsequent differentiation [593]. Ionizing radiation triggers differentiation of hair follicle McSCs into mature melanocytes, leading to hair graying [70]. Undifferentiated human melanocytes in the interfollicular epidermis differentiate in response to genotoxic damage from radiotherapy (ionizing radiation) [596]. Furthermore, foreskin keratinocytes undergo further differentiation upon irradiation with 100–250 J/m² UVB as a response to DNA damage [594]. The osteogenic differentiation potential of MSCs also increases after 250 J/m² UVB exposure, while their adipogenic and chondrogenic differentiation is relatively unaffected [516]. However, in the current study, none of the two hypotheses could be confirmed for UV irradiation of DSCs. Neither a decrease in differentiation potential nor an increase in triggered differentiation was observed. Single UV irradiation with the applied doses of 300 J/m² UVB or 37 kJ/m² UVA had no discernible effect on the differentiation ability of DSCs.

It is assumed that a single irradiation prior to differentiation might be insufficient to induce UV-related effects in DSCs. The investigations should be extended with multiple irradiations, since DSCs are constantly exposed to UV radiation during their migration from the dermis to the epidermis [357]. Whether DSCs migrate to the epidermis first and subsequently complete the differentiation process, or if they undergo differentiation into melanocytes in the dermis before migrating or even during migration remains to be investigated [31]. To mimic the physiological conditions, depending on the scenario, it may therefore be relevant to expose DSCs to UV radiation not only before but also during the differentiation process. There were indeed attempts of multiple irradiations in combination with the differentiation assay (data not shown). However, this approach proved to be highly challenging, since DSCs exhibited extreme sensitivity to UV irradiation during differentiation, resulting in significant cell death. As demonstrated in the results of this study, DSCs with preceding UV irradiation already suffered

more compared to non-irradiated cells in the following differentiation, with an increased amount of dying cells. Especially prior UVB irradiation led to reduced cell density or sometimes even cell death across the entire sample (data not shown). In contrast, the UVA-exposed DSC cultures did not visually differ from the non-irradiated differentiation samples.

Generally, DSCs appear to be highly sensitive during differentiation. When exposed to damage from UVB radiation during this process, there is evidently an increased initiation of cell death, indicating a protective mechanism against UV-induced damage during differentiation. A protein that plays a crucial role in cell death is p53. It not only induces cell cycle arrest, DNA repair, apoptosis, and senescence upon DNA damage, but is intriguingly also implicated in the regulation of embryonic development and differentiation in adult tissues, exhibiting a dual function—acting as either an inhibitor or an inducer, depending on the cell type and fate [597,598]. In osteogenic [599] and adipocyte precursors [600], p53 functions as negative regulator of differentiation. Instead, in neural precursors [601], myoblasts [602], and HSCs [603], it plays a crucial role in promoting differentiation through multiple possible mechanisms. One possibility is that p53 can induce differentiation with its ability to suppress stem cell self-renewal [604], for instance, by inhibiting the transcription of *Nanog* and *Oct-4*, as shown in mESCs [544,605] and hESCs [199]. Other reports suggest the p53-dependent block of cell cycle progression in G0/G1 phase as a mechanism behind differentiation by p53 [540]. Both p53-driven apoptosis and p53-driven differentiation appear to be strategies employed by ESCs to maintain the genomic stability of the entire population. Whether p53 also plays a promoting role in the differentiation of McSCs like DSCs into melanocytes, remains to be investigated. If this were the case, the differentiating cells, with their elevated p53 level, might be more prone to rapid induction of cell death in response to damage during differentiation, facilitated by a quick switch between the two pathways.

Additionally, the key apoptotic regulator Caspase-3 can also mediate differentiation or exhibit pro-differentiation effects in ESCs [606], HSCs [607], myoblasts [608], osteoblasts [609], and neural progenitors [610], for instance, by limiting self-renewal, thus providing another link between differentiation and apoptosis. Moreover, cAMP present in the differentiation medium can trigger both differentiation and apoptosis in certain cell types, depending on the expression of pro- and anti-apoptotic regulators [611-613]. All these findings suggest that there could be multifaceted reasons for the increased susceptibility of DSCs to apoptosis during differentiation. Whether this indeed beneficial process of cell death following irradiation during differentiation also occurs *in vivo* in human skin, thereby preventing the differentiation of possibly pre-damaged DSCs into melanocytes as part of an anti-tumor

mechanism [69], remains uncertain. This could be explored, for example, using organotypic cultures (OTCs), whose fibroblast-derived matrix closely resembles the dermal microenvironment *in vivo* [483-485], similar to how Li et al. demonstrated the migration process of DSCs from the dermis to the epidermis in a 3D model [31,125].

It is notable that cell death in DSCs appears to be triggered in response to various extrinsic cellular stresses, including UV irradiation, loss of cell-cell contact, or changes in cultivation conditions with different growth factors. Stem cells, given their characteristics and functions, are particularly vulnerable to stresses, with apoptosis and senescence serving as anti-cancer mechanisms [69]. hESCs, mESCs, and iPSCs react highly sensitive to environmental influences, displaying an increased tendency toward apoptosis in response to low UVC exposure (5–10 J/m²), ionizing radiation, other DNA-damaging agents, replication inhibitors, and oxidative stress inducers. This sensitivity may represent a strategy to ensure the genomic integrity of the whole stem cell population by sacrificing damaged cells [486,535,538,614]. Consequently, it would be interesting to investigate the extent to which UV irradiation during differentiation induces cell death in DSCs.

Taken together, single irradiation with a low UVB or UVA dose prior to differentiation has no effect on the differentiation ability of DSCs. However, it seems that both UV exposure and cultivation in differentiation medium create a dual stress scenario for DSCs. This complicates the execution of differentiation experiments in combination with multiple UV irradiation before or during differentiation. Additionally, the varying sensitivity of different donor cell strains adds complexity to the establishment of a uniform irradiation regimen. Nevertheless, to further investigate the differentiation ability of DSCs in the context of UV damage and melanomagenesis, conducting chronic irradiation experiments is imperative. Future studies should also explore the impact of UV irradiation before and during differentiation on the expression of tumor suppressor genes (e.g., p16, p14, p53) and key melanoma driver genes (e.g., BRAF, NRAS, MITF, c-Kit) in the differentiated melanocytes.

6.5 Sphere Formation

Originally introduced by Reynolds and Weiss in 1992, sphere-forming culture with growth of cells in non-adherent conditions, was initially used for isolating neural stem cells from the adult brain, known as the neurosphere assay [615]. Since then, this technique has found widespread application in the identification, enrichment, and proliferation of various adult stem cells, populations with stem-cell properties [616,617], and cancer stem cells (CSCs), due to their

capability to grow in suspension culture [404,425]. The assay's outcome is significantly influenced by crucial parameters such as medium composition, seeding cell density, and cultivation duration. Notably, there is considerable variability in cell density reported across different studies [425].

On one hand, the gold standard for assessing the self-renewal capacity or clonal properties of stem cells is the sphere formation assay with single-cell plating using serial dilution [404,425]. This method ensures clonality as each sphere originates from a single cell through proliferation. However, it has the drawback of extended assay duration, attributed to the reduced sphere-forming efficiency with single-cell plating, linked to the absence of autocrine and/or paracrine signals released by co-cultured cells [425].

On the other hand, another commonly used approach is the sphere formation assay with multiple-cell plating, where seeding density varies greatly between studies [404]. Although this approach generally results in faster sphere formation, a limitation is the potential aggregation of cells within spheres due to their tendency to merge, especially at higher cell densities. Consequently, this method is unsuitable for measuring self-renewal ability or clonality [425].

6.5.1 Sphere-Forming Potential of DSCs

Following the confirmation of NCSC marker gene expression and the melanocytic differentiation potential of DSCs, another functional characteristic of stem cells—the ability to form three-dimensional spherical structures in suspension culture [425]—was also explored. The study aimed to determine if the sphere-forming potential observed in the initial generation of dermal spheres after the isolation of DSCs from foreskin persists in later passages following extended cultivation. To maintain similar seeding conditions as in the initial cultivation, a multi-cell plating approach was used.

It was confirmed that native DSC cultures were still able to form stem cell-specific spheres in human ESC medium, even in later passages. The morphology closely resembled the dermal spheres formed in the initial weeks after isolation. Consequently, this stem cell feature was preserved even after prolonged monolayer cultivation of DSC-fibroblast co-cultures. Moreover, the investigation revealed that DSCs maintained the ability to form spheres after purification via MACS® positive selection, as demonstrated by a purified population from the same donor cell strain. Notably, after purification, the generated spheres exhibited a significantly smaller size. This size difference could be attributed to two possible reasons. Firstly, the selection procedure may have influenced cell properties and function [466,468,479], affecting sphere formation potential. However, given the retained differentiation potential after positive

selection (see section 6.4.1), it would be surprising why only the capability for sphere generation is impaired. The sphere-forming capacity of purified DSCs may, however, be diminished through prolonged cultivation in later passages, independent of the enrichment process. In comparison, it is commonly assumed that stem cells produce larger spheres, while progenitor cells, having lost their ability for self-renewal, generate smaller spheres [425]. Secondly, it should be considered that fibroblasts were present in the spheres of the native DSC-fibroblast co-culture used for comparison—just as observed in dermal spheres which typically predominantly consisted of fibroblasts, resulting in a relatively low stem cell frequency (see Figure 5.1C–D). Since DSCs have a considerably smaller size than fibroblasts (own observations in ICC and flow cytometry), the absence of large-sized fibroblasts in spheres of purified DSCs is most likely primarily accountable for the smaller size compared to the native DSC-fibroblast co-culture. It is also conceivable that fibroblasts might release paracrine factors that enhance the cellular merging process, and consequently, these factors are absent in purified DSC cultures.

Intriguingly, fibroblast cultures (previously cultured in RPMI+10%FBS) also generated three-dimensional spherical structures when cultured in stem cell medium. These fibroblast spheres exhibited comparable sizes to those observed in the DSC-fibroblast co-culture and were generated similarly fast. The initial question arose about why fibroblasts can survive in a non-adherent culture. *In vivo*, anchorage-dependent cells that lose cell-cell and cell-matrix contacts undergo apoptosis through anoikis, while cells with anchorage independence or a motile phenotype resist anoikis [618]. Some cells, notably cancer cells, are excluded from anoikis or gain resistance. Similarly, in cell culture, cells that typically grow attached to the culture flask or an extracellular matrix usually die when cultured in suspension. Stem cells and cells with stem cell-like properties are able proliferate without adhesion solely through cell-cell interaction in a free-floating sphere culture [617]. When stem cells differentiate and thereby lose typical stem cell properties, their survival in suspension is significantly reduced, as demonstrated for skin-derived precursor [616]. Fibroblasts are typically not known for their ability to form spheres or aggregates under standard *in vitro* culture conditions. However, research indicates that normal fibroblasts can demonstrate anchorage independence and anoikis resistance [618], leading to the formation of spheres [619]. Furthermore, the resistance to anoikis in fibroblasts is implicated in pulmonary fibrosis, contributing to excessive proliferation [620]. In the current study, when cultivated in stem cell medium, dermal fibroblasts seem to exhibit induced or intrinsic properties that promote their survival in suspension. The specific culture conditions, featuring various growth factors, including basic fibroblast growth factor

(bFGF), appear to stimulate fibroblasts to organize into three-dimensional structures. Within stem cell medium, dermal fibroblasts thus seem mostly anchorage-independent, but not entirely. Strikingly, fibroblast-derived spheres tended to attach to the bottom of the cell culture flask, and a substantial number of cells continued to grow adherently. This heterogeneity in growth behavior could suggest acquired/induced anchorage independence.

The findings of fibroblast-derived spheres resemble previous studies conducted by our group, which also demonstrated sphere formation of fibroblast cultures in the same stem cell medium (StemPro™ hESC SFM medium), with induced gene expression of NCSC markers NGFRp75 and nestin compared to fibroblasts cultivated in RPMI+10%FBS [621]. In contrast, as part of their studies on DSCs, Li et al. cultivated melanocytes and fibroblasts from foreskin in stem cell medium as well, but used a different human embryonic stem cell medium, specifically HESCM4 conditioned by mouse embryonic fibroblasts (MEFs). Despite strong proliferation, fibroblasts in their study did not form spheres and instead grew in adherent monolayer cultures. Melanocytes even died within two weeks [31]. This raises questions about the discrepancy in the fibroblasts' sphere-forming ability and simultaneously suggests a significant influence of the stem cell medium used in this study. It seems that the StemPro™ hESC SFM medium not only promotes the growth of stem cells, but also facilitates the universal formation of spheres/aggregation of cells in a non-stem cell-specific manner. The possibility that Li and colleagues may have used adherent cell culture flasks compared to suspension cell culture flasks in this work, accounting for the difference, can be dismissed, as fibroblast cultures also formed spheres in adherent cell culture flasks in the StemPro™ hESC SFM medium (data not shown).

While it was previously known that fibroblasts were present in the spheres of DSC-fibroblast co-cultures, it was unexpected that pure fibroblast cultures were also able to form spheres. Various explanations could account for this phenomenon. It cannot be ruled out that a minor population of DSCs may have still been present in the fibroblast cultures in these experiments, potentially initiating the process of sphere generation. Additionally, various studies not only report the existence of a ($CD45^{-}/CD73^{+}/CD90^{+}/CD105^{+}$) fibroblast population with mesenchymal stem cell-like characteristics in the dermis of juvenile foreskin [111], but also suggest that dermal fibroblasts are a heterogeneous population containing diverse progenitors with varying differentiation potential [113]. The fibroblast spheres could also represent skin-derived precursors (SKPs) [105,109]. Hill and colleagues demonstrated the ability of human dermal fibroblast cultures to form SKPs after monolayer culture, regardless of their origin (hair-dense and hair-sparse body regions; adult skin and neonatal foreskin) [622]. These SKPs

expressed neural crest, embryonic, and mesenchymal stem cell markers and exhibited morphological and functional similarities to traditional SKPs. They observed first SKP spheres within 7–11 days and spheres took an average 21 days to form [622]. One could assume that these stem cell-like fibroblasts [111] and progenitor cells [113,622] might have been (still) present in the fibroblast cultures used here and, when stimulated by the stem cell medium, led to the formation of spheres. However, the rapid formation of the fibroblast spheres (within one day and at the latest after four days) makes this hypothesis, as well as the notion of a few remaining DSCs as sphere initiators, rather unlikely. To ascertain if sphere initiation is indeed restricted to stem cells, it becomes imperative to utilize fibroblast cultures or other cell cultures that have been verified not to contain any stem cells. Additionally, a more in-depth examination of the involved cells, including their antigen and expression profiles, is necessary to provide a thorough explanation for the phenomenon of fibroblast spheres.

Another aspect to be considered in this discussion is that the spheres, due to multi-cell seeding, lack clonality, making cell merging a possibility. Factors such as excessively high seeding cell density, experimenter-induced cell movement [623], and intrinsic mobility of spheres contribute to cell aggregation and fusion of spheres [425]. The latter has been observed in neurospheres even at low cell densities [623]. The integration of fibroblasts into spheres owing to the natural tendency of cells to reaggregate, just like in tissue, is also a plausible occurrence. The observed formation of spheres at the utilized cell densities is evidently not solely attributed to the proliferation or self-renewal of a single stem cell but also involves the merging of cells. The inclusion of fibroblasts in dermal spheres and co-culture spheres serves as clear evidence of this phenomenon, as otherwise, the occurrence of mixed spheres including DSCs and fibroblasts would not be possible. In such mixed spheres, both classical sphere formation through proliferation/self-renewal of DSCs and cell aggregation of fibroblasts, due to high density or to establish cell-cell contacts, likely play a role. This assumption gains support from the rapidity of sphere formation in DSC-fibroblast co-culture, which did not align with the measured doubling times of DSCs and the results of Herlyn’s group, who obtained small colonies only after 15 days and typical spheres after 90 days from single cells [31]. Therefore, aggregation of cells could have contributed to the formation of fibroblast spheres as well. To verify if the fibroblast spheres indeed arise through proliferation, demonstrating sphere-forming ability, or simply from cell merging, it is recommended to conduct a sphere formation assay with single-cell seeding or live cell imaging. Another method to distinguish cell proliferation from aggregation involves labeling with the tracing dye carboxyfluorescein diacetate succinimidyl ester (CFDA-SE). In this approach, a dissociated single-cell suspension is labeled

and cultured together with an unlabeled counterpart, and resulting spheres are examined for fluorescence. If spheres consist exclusively of either labeled or unlabeled cells, they form through cell proliferation/self-renewal. However, if spheres are a mixture of labeled and unlabeled cells, then cell aggregation also plays a role [97].

In summary, it is not conclusively understood why under seemingly identical conditions (except for the medium) there was no sphere formation in fibroblast cultures in the study by Li et al. [31] compared to impressive generation of fibroblast spheres observed in this work. However, the evidence, especially the rapidity of sphere formation in fibroblast cultures, primarily suggests the influence of the different stem cell medium and significant involvement of cell aggregation. Consequently, a sphere formation assay with multiple-cell plating is unquestionably not a unique functional assay for stem cells. Pastrana and colleagues phrased it quite explicit in their review: “Instead, sphere-forming assays evaluate the potential of a cell to behave as a stem cell when removed from its *in vivo* niche” [425].

In conclusion, it is important to highlight that this thesis focused solely on investigating the sphere formation (or aggregation) potential of DSCs, not their self-renewal. If the self-renewal ability of DSCs is to be explored, as a characteristic feature of NCSCs [426], a different sphere formation assay would be required. An optimal self-renewal assay includes the serial dilution of dissociated spheres for single-cell plating in 96-well microplates. This excludes merging of cells, ensuring that the formation of spheres is solely attributable to the proliferation of a single cell [31,425].

6.5.2 Sphere Formation Following UV Irradiation

The ability of DSCs to generate stem cell-specific three-dimensional spherical structures was further investigated in response to UV irradiation. Three naturally enriched DSC-fibroblast co-cultures (with 49%, 65%, and 89% stem cell content) were initially irradiated in monolayer culture, using varying doses of UVA and UVB either as a single or multiple exposures. Irradiation with 900 J/m² UVB significantly decreased viability and DSC frequency when applied both as a single or fractionated exposure over three days (3×300 J/m² UVB). This aligns with the apoptosis results in DSCs mentioned earlier, which involved an increased proportion of apoptotic cells and a reduction in stem cell content 48 h after irradiation with the same UVB dose (see section 6.3.3). The reason for the decreased viability following 3×24.67 kJ/m² UVA, although the DSC frequency remained unchanged and application of the same cumulative dose

in a single irradiation had no effect, remains unclear. This reduction was less pronounced compared to the impact of UVB.

The previously irradiated cells were seeded with equal amounts of viable DSCs in suspension culture flasks and were cultivated for five days. While there is no standardized parameter for assessing spheres, different approaches encompass the mean diameter of spheres, morphological description, relative area occupied by spheres, and the number of spheres being the most frequently used measure [404]. In this study, the evaluation of spheres was based on sphere count and size in terms of diameter. Similar to the other UV experiments in this study, UVA showed no detectable influence on the number of formed spheres. In contrast, exposure to 300 J/m², 900 J/m², and 3×300 J/m² UVB resulted in a notable reduction in the number of spheres, suggesting a potential impact of UVB on sphere formation ability. In light of this diminished sphere count after UVB irradiation, three hypothetical scenarios could be considered: (i) Further cell death of UVB-irradiated DSCs may have decreased the number of available cells for sphere formation. (ii) If no additional cell death occurred, there might actually be an impairment of cellular function, making DSCs less prone to forming spherical structures. (iii) UVB radiation may have influenced DSCs in a way that they form fewer but larger spheres.

In the analysis of size distribution, the observed heterogeneity in sphere size, characterized by a right-skewed distribution where smaller spheres constituted the majority of the population, resembled findings of other sphere formation studies. For example, Zhou and colleagues examined human cancer cell lines and mESCs using multiple-cell plating, reporting a size range of 50–350 µm, with smaller spheres being predominant [404]. In this study, a comparable size range was identified, with the largest measured sphere having a diameter of 374 µm. Spheres exceeding 200 µm were uncommon and were thus combined into a single category. According to the literature, spheres are typically assessed in the size range of 40–150 µm in diameter [425]. Here, the minimum threshold was set at 25 µm based on optical assessment of the formed structures.

It was observed that after all irradiations (except for 300 J/m² UVB), there was a tendency for fewer small and more large spheres to be generated compared to non-irradiated controls, meaning the size distribution slightly shifted towards greater diameter upon irradiation. Surprisingly, this effect was evident even after UVA exposure, despite the absence of any previously demonstrated impact by UVA. It is important to note that these changes lacked statistical significance, likely due to the small sample size of n=3 and relatively large variances. However, the described effect partly became very clear when considering individual donor cell

strains. As the different donor cell strains had varying stem cell contents, the question arose whether differences in DSC frequency or the presence of fibroblasts could contribute to the variability in sphere formation. However, this aspect was not pursued further, given the complexity and diversity of interindividual variability [570], which cannot be adequately represented and discussed, especially in combination with other influencing factors like UV irradiation. For a more precise investigation into the role of fibroblasts in sphere formation, one would need to use the same purified DSCs and mix them with varying ratios of fibroblasts, as such effects cannot be reliably measured across different donors. Consequently, despite the differing starting conditions of the donor cell strains, it was decided not to consider them separately.

Since the used DSC cultures were not completely pure, the formed spheres contained fibroblasts in addition to DSCs. As demonstrated previously, spheres appear to arise not only from the proliferation of a single cell but also from the aggregation of multiple cells, including fibroblasts, which can also generate spheres in the utilized stem cell medium (see Figure 5.12 and section 6.5.1). Unfortunately, due to their size, the spheres formed in this experiment could not be fully dissociated, preventing the accurate measurement of the final stem cell and fibroblast content. Nevertheless, it was confirmed that fibroblasts were indeed present within the spheres (data not shown).

The question arose as to the reasons behind the overall increase in sphere size following UV irradiation. One consideration is that fibroblasts might have an impact on sphere size, akin to the characterization experiment. In that experiment, when comparing the same donor cell strain in its native state (17% DSCs) to a purified state (87% DSCs) with an equal total number of seeded cells, the spheres were notably larger in the native culture (see Figure 5.12). In this UV experiment, for samples with a reduced DSC frequency after irradiation, a higher total number of cells was seeded in suspension to maintain the same absolute number of DSCs as the starting point. This was equivalent to a relatively greater number of fibroblasts in the culture. Consequently, these additional large-sized fibroblasts could have contributed to a larger sphere diameter through aggregation within the spheres. In that case, the effect should have been restricted to specific treatments where a diminished stem cell content was observed, namely the samples irradiated with the higher UVB dose. However, the trend of a shifted size distribution towards larger spheres was observed universally in all irradiated samples (with one exception), even in those where the DSC content remained constant compared to the control. In this experiment, it seemed that fibroblasts had minimal or no influence on the varying sizes of the

spheres after UV irradiation. The previously noted impact of UVB on viability, DSC frequency, and sphere count did not manifest in the size distribution of the spheres.

Consequently, it appeared that the altered size distribution was neither dependent on fibroblasts nor on specific wavelengths but rather represented a general radiation effect. When assuming that sphere size might be indicative of the proliferation/differentiation status and the responsiveness to growth factors of the parental clone-forming cell [425], larger sphere size could have resulted either from an amplified sphere-forming ability or, conversely, from an increased sensitivity to growth factors. Another plausible hypothesis that has emerged is that cells become generally stickier after irradiation due to changes in the surface condition/membrane damage. This phenomenon has been observed, for example, in the irradiation of hESCs (I. Schröder, personal communication, September 18, 2023). An increased stickiness could facilitate sphere formation, resulting in larger spheres by involving more cells and potentially even the fusion of small spheres. This theory would at least provide an explanation for the universal occurrence of the size shift effect. In the apoptosis investigations, there were indeed indications that UV irradiation led to membrane damage, impacting the detection with specific antibodies. This finding could serve as an indication of the suspected increase in stickiness in this sphere formation experiment, albeit the understanding of the mechanisms remains rudimentary.

The utilized sphere formation assay and analysis methods had certain limitations and pitfalls, which will be briefly discussed below.

(1) As previously mentioned, the seeding cell density is the most critical parameter in the sphere formation assay, influencing clonality and sphere number. This is attributed to the impact of autocrine/paracrine signals on sphere-forming efficiency and the tendency for cell aggregation at high cell density [425]. A density of 0.2–20 cells/µl culture medium is considered suitable for clonal growth [425]. Since the purpose of the sphere formation assays in this study was not to investigate self-renewal/clonality, the seeding densities were not chosen based on these guidelines and, in fact, significantly exceeded them (up to 20 times more cells). However, interpreting results from high-density seeded cultures becomes challenging due to cell aggregation and the fusion of spheres [425]. Additionally, moving the cell culture flasks during the growth phase further increases the occurrence of cell aggregation [623]. For an adequate assessment of UV influence, it should be considered to switch to low-density conditions to mitigate possible other

confounding effects. To circumvent some of the described issues, such as experimenter- and intrinsic mobility-induced aggregation, modifications of the traditional sphere assays have been developed, such as cultivation in semi-adherent conditions [425].

(2) The chosen methods of analysis have a certain susceptibility to errors, but they were selected as accurately as possible. The assessment of sphere count and diameter relied on representative images, with no assurance that the actual state was precisely reflected. Additionally, for a truly precise measurement of the diameter, the spheres would need to be perfectly round, which is not the case in a natural system. The most accurate representation of sphere size would be through the volume of a sphere. However, determining volume through images is not a suitable method for the reasons mentioned above and, as a result, was not carried out. Other parameters described in the literature also have their limitations, making it clear that there is no single perfect parameter [404].

In conclusion, it is affirmed that UVB irradiation is less well-tolerated and affects the viability, stem cell frequency, and sphere count of DSCs. However, whether the altered size distribution of the spheres is a result of an impact on cellular function or rather caused by structural changes remains uncertain and requires further investigation. The precise influence of UV irradiation on the stem cell's sphere formation ability could not be conclusively clarified. To mitigate uncertainties related to the influence of fibroblasts on sphere size, which may potentially obscure actual irradiation effects, it is recommended to conduct this experiment using highly MACS®-purified DSC cultures. Moreover, investigating the impact of UV irradiation on sphere formation in an assay with single cells through serial dilution should be considered, as this approach would also eliminate cell stickiness as a potential influencing factor.

6.6 MicroRNA Expression

In terms of preliminary experiments, the expression of microRNAs (miRNAs) in DSCs was conclusively examined, since these molecules play a pivotal role in various cellular processes and mechanisms in stem cells, including the regulation of cell cycle [624], stemness and differentiation [625-628], the DNA damage response (DDR) [237], and carcinogenesis [629]. It is well-established that miRNAs significantly contribute to the development, progression, and metastasis of malignant melanoma (MM) [235] and to this day, several differentially expressed miRNAs have been identified in MM [291,314]. During the initiation of cancer,

miRNAs exert their influence not only within cells (see section 1.5.2.2) but also externally. The crosstalk between transforming cells and the surrounding microenvironment is a crucial factor. miRNAs play a decisive role in the evolution of the tumor microenvironment [630], for instance, in regulating cancer-associated fibroblasts (CAFs), T cells, tumor-associated macrophages (TAMs), tumor-associated MSCs, and endothelial cells [235]. Hence, the specific biological characteristics of cells undergoing transformation might be evident in their miRNA expression pattern [631].

The miRNA analysis in this investigation utilized a custom multiplex melanoma panel comprising 63 miRNAs that were selected by colleagues based on a literature review. While these miRNAs are known to be dysregulated in MM, they are not exclusively specific to melanoma and are also identified in other types of cancers. For instance, miR-21 exhibits upregulation in melanoma, as well as in various other cancer types such as lymphoma, glioblastoma, breast, lung, prostate, and pancreas cancer [319]. The prominent upregulated onco-miRNAs in melanoma include miR-21, miR-155, miR-221/222, and miR-182. Conversely, frequently downregulated tumor suppressor miRNAs encompass miR-205, miR-125b, miR-211, the let-7 family, miR-34a, miR-16, miR-137, miR-31, miR-203, and the miR-200 family [314,317], all of which are part of the utilized panel.

Several miRNAs from the panel are also linked to or involved in the DDR (see section 1.4.5), a pivotal player in tumor prevention. The dysregulation of DDR mechanisms, such as cell cycle arrest and apoptosis, is a crucial process in carcinogenesis. For instance, miR-34a and miR-34b from the miR-34 family are induced in a p53-dependent manner and promote cell cycle arrest, apoptosis, and senescence [187,202,240]. Moreover, p53 induces various other miRNAs, including miR-192 [241], miR-16 [188], miR-15a, let-7 miRNAs [202], miR-145 [236], miR-200c, and miR-21 [245], while suppressing miR-221 [202]. miR-125b negatively regulates p53, contributing to the low baseline expression of p53 under normal conditions [246]. Additionally, miR-21 [250] and miR-16 [188,237] can inhibit Cdc25A. The involvement of these miRNAs in the regulation and execution of the DDR underscores their significance in tumorigenesis.

To investigate miRNA expression in DSCs, both without and with UV irradiation, it was imperative to utilize highly purified DSC cultures to avoid analyzing miRNAs expressed by co-cultured fibroblasts, for example, in the context of radiation-induced bystander effects [632]. Therefore, one naturally enriched and two MACS® positive selection-purified DSC cultures were used. The comparison involved two foreskin-derived melanocyte cell strains and three melanoma cell strains from metastases. Already during the evaluation of the measured data for

the selection of suitable stable miRNAs for normalization, it became apparent that the three cell types seemingly exhibit distinct miRNA expression patterns. Despite this, all measurements from the various cell strains were analyzed collectively to enable an adequate comparison based on the same normalization, although the nine most stable miRNAs obtained from this analysis not necessarily corresponded to the most stable miRNAs in the individual cell types. For future investigations, it is recommended to include miRNAs proven not to be cell-type specific, ensuring identification of these miRNAs as the most stable ones across all cell types. This approach would enhance the reliability of normalization for comprehensive comparisons.

6.6.1 Baseline MicroRNA Expression

In an initial investigation using the non-irradiated control cells, the focus was on determining potential differences in the baseline miRNA expression between DSCs and their differentiated progeny, melanocytes, as well as melanoma (MM) cells. A panel of eight differentially expressed miRNAs was successfully identified, clearly distinguishing between DSCs on one side and melanocytes and MM cells on the other. Among these, four miRNAs were overexpressed in DSCs, whereas the other four were downregulated in comparison to the other two cell types. The observed differences between DSCs and MM cells were consistently statistically significant. However, in the comparison between DSCs and melanocytes, only one of the eight miRNAs demonstrated statistical significance, likely attributable to the smaller sample size of melanocytes. Notably, melanocytes emerged as a bridge between DSCs and melanoma cells concerning the baseline expression of these eight miRNAs, occasionally exhibiting greater similarity to DSCs, other times to MM cells, or positioning between the expression values of DSCs and melanoma cells. As an additional observation, the uniformity observed across all three analyzed DSC cell strains provided an initial indication that purification with MACS® positive selection apparently does not affect the baseline miRNA expression of DSCs, at least not for the investigated miRNAs, as evidenced by minimal standard deviations.

The set of four miRNAs overexpressed in DSCs, while being downregulated in both melanoma cells and melanocytes, consisted of hsa-mir-137, hsa-mir-15a-5p, hsa-mir-33a-5p, and hsa-mir-494-3p. This observation is in agreement with existing literature, where all four miRNAs are reported to undergo downregulation in melanoma and melanoma cells. The tumor suppressor **miR-137**, in addition to melanoma [338,339], is also found to be reduced in other cancers, e.g., colorectal cancer, head and neck squamous cell carcinoma, and glioblastoma [633]. Functionally, miR-137 targets MITF, which regulates anti-apoptotic Bcl-2, and EZH2, which

usually represses the CDK inhibitor p21. Elevated levels of miR-137, as observed in DSCs, may result in the downregulation of MITF and EZH2, facilitating apoptosis and cell cycle arrest [339]. Other studies indicate miR-137-mediated cell cycle arrest through the targeting of Cdc42 and CDK6 [634]. Furthermore, miR-137 is associated with cell cycle regulation and control of cell fate determination in neural stem cells, where its high expression reduces proliferation and accelerates neuronal differentiation [635,636]. **miR-15a**, reported to be downregulated in melanoma [315] and other cancer types like leukemia, multiple myeloma, non-small cell lung cancer, and breast cancer [637], can be induced by p53 [202]. It targets cyclin D2, cyclin E1, and Bcl-2 [335,638], implicating its involvement in cell cycle regulation and apoptosis induction. The tumor suppressor **miR-33a**, significantly downregulated in melanoma and melanoma cells [639-641], typically inhibits the activation of the PI3K/AKT/mTOR pathway by targeting SNAI2 (Slug). Overexpression of miR-33a-5p in melanoma cells *in vitro* suppresses proliferation, invasion, migration, EMT, and promotes apoptosis [640]. miR-33a targets HIF1α directly [641] and p27 indirectly [639]. **mir-494**, downregulated in melanoma and melanoma cell lines [642,643] and also in breast cancer [644], is described as a tumor suppressor, inhibiting proliferation via the MAPK signaling pathway by targeting PAK1 [644]. However, there are conflicting reports about an oncogenic function of miR-494 in colorectal cancer, as it represses PTEN, leading to the activation of the PI3K/AKT signaling pathway, promoting cell migration and invasion [645].

The four miRNAs, which exhibited downregulation in DSCs but were overexpressed in melanocytes and MM cells, included hsa-mir-146b-5p, hsa-mir-204-5p, hsa-mir-222-3p, and hsa-mir-34a-3p. Reports on the involvement of **miR-146b** in melanoma are contradictory. Levati et al. describe reduced expression in melanoma cell lines [646]. During the photoaging process in dermal fibroblasts, miR-146b-5p is also downregulated [647]. Conversely, other studies indicate increased expression in melanoma [325,648] and melanoma cell lines [631]. This aligns with the expression results presented here, where miR-146b was overexpressed in MM cells and downregulated in DSCs. It is noteworthy that in melanocytes, this miRNA also demonstrated surprisingly high expression with a significant difference compared to DSCs. In ESCs and iPSCs, the expression of miR-146b-5p promotes differentiation towards the neural lineage by targeting SMAD4, thereby reducing Oct-4 expression [649]. Stevanato et al. also described miR-146b-5p upregulation in differentiated human neural stem cells [650]. In this context, reduced baseline expression in DSCs is plausible to maintain stemness, and the increased expression in melanocytes could be attributed to the differentiation process. Similarly, the literature regarding **miR-204** is characterized by ambiguity. Some studies

indicate upregulation in melanoma cell lines [631], while the majority reports miR-204 as downregulated [651] or even lost as a key event in melanoma [652], exerting tumor-suppressive functions through the targeting of Bcl-2 [653]. This contradicts the expression levels observed here, especially the elevated expression in melanocytes. However, findings of very low miR-204 levels in neural stem cells compared to high levels in differentiated brain tissues, attributed to miR-204 suppressing self-renewal and stemness [654], could explain the downregulation in DSCs. Oncogenic **miR-222** levels are reported to be stepwise upregulated during melanoma transformation, while being nearly undetectable in normal melanocytes [320]. Overexpression is also demonstrated in glioblastoma, multiple myeloma, breast, liver, pancreatic, prostate, gastric, and colorectal cancer [655]. miR-222-mediated suppression of p27 (resulting in cell cycle transition), the c-Kit receptor (blocking differentiation), and PTEN (activating PI3K/AKT signaling) enhances cell proliferation and invasion [320,325,335]. These findings align with the results showing high miR-222 expression in melanoma cells in this study. Additionally, there is evidence suggesting that miR-222 might promote differentiation by regulating the expression of differentiation-related genes [656], and that inhibiting miR-222 secures the expression of stem cell markers [657]. Possibly, this might also apply to the low miR-222 expression observed in DSCs. **miR-34a** is a tumor suppressor and key effector of p53-mediated DDR. It promotes cell cycle arrest, apoptosis, and senescence through the downregulation of cyclin E2, CDK4/6, E2F3, c-Myc, and Bcl-2 [187,202,240]. Consequently, the downregulation of miR-34a in DSCs may have implications for their DDR. Another target of miR-34a is the E-cadherin inhibitor ZEB1, decreasing proliferation and migration [336]. Being lost in various cancer cell lines and commonly deleted in neuroblastoma, non-small cell lung cancer [187,202,240], breast, liver, pancreatic, prostate cancer [624], and melanoma [315,336], the overexpression observed in MM cells in this study contradicts the reported findings. In addition to the anti-proliferative potential, miR-34a is capable of repressing stemness factors like Oct-4, KLF4, LIN28A, SOX2, Nanog, Notch, and Myc, thereby preventing backsliding to pluripotency and promoting differentiation [658,659]. Similarly, miR-34a-3p exhibits significantly lower expression in epidermal stem cells compared to differentiated keratinocytes [660]. Therefore, downregulation of miR-34a in DSCs might contribute to maintaining stemness.

The divergence observed in the miRNA expression pattern of melanoma cells in this study, when compared to existing literature, is comprehensible. Other previous studies also show partially contradictory results. Studies on miRNA dysregulation in melanoma face certain limitations [314]. Prior reports often compared human melanoma cell lines with primary epidermal melanocytes, or melanoma tissue (primary or metastatic) was contrasted with benign

nevi or normal skin. However, there are inherent differences between *in vivo* tumor tissue and *in vitro* cell lines, and likely also between primary and metastatic melanoma tissue. In addition, the choice of the presumed initiating cell for comparison is crucial for the outcomes of these analyses. It is still unknown whether a melanocyte or a melanocyte stem cell, such as a DSC, serves as the cell of origin for malignant melanoma. However, its baseline miRNA expression may vary depending on the state of differentiation [314] as indicated with the findings here, comparable with the differential miRNA expression profile between epidermal stem cells and differentiated keratinocytes [660]. This aspect is important to consider when comparing miRNA levels in melanoma cells to those of DSCs in this study, as deregulated miRNAs described in the literature might not be directly applicable to this specific comparison. It is also crucial to note that miRNA expression may not necessarily correspond to miRNA activity, similar to the relationship between mRNA and protein levels and activity. Consequently, investigating the activity of differentially expressed miRNAs is essential to validate their functionality [314]. Additionally, variations in tissues from different individuals contribute to partially contradictory results.

Conducting network analyses for both the 4-miRNA set overexpressed and downregulated in DSCs yielded two clusters with various targets, encompassing tumor suppressors (e.g., PTEN) and oncogenes (e.g., Myc, Bcl-2). Some of these targets are known to be implicated in the regulation of proliferation, cell cycle, DNA repair, and apoptosis. Notably, there was partial overlap among the targets for the two 4-miRNA sets. For the sake of completeness, enrichment analyses/over-representation analyses (ORA) were also conducted regarding enriched KEGG pathways and GO terms to identify biological processes and pathways in which the differentially expressed miRNAs are involved. However, these results were not further investigated. Given that the relatively limited number of examined miRNAs in the panel were preselected based on their involvement in melanoma (and other cancers), the outcome of the pathway analyses is predetermined and biased. Therefore, it is not surprising that the ORA of the downregulated 4-miRNA set revealed involvement in proliferation and various cancer pathways.

Furthermore, limitations arose from the constrained number of miRNAs utilized in the pathway analysis. The inclusion of only four miRNAs as input limits the statistical power to detect significantly enriched pathways. The fact that already eight out of the 58 examined miRNAs (initially 63 minus five barely-expressed miRNAs) were differentially expressed in this relatively small panel implies that the DSCs generally differ significantly in their baseline

miRNA pattern compared to the other two cell types. A broader investigation would likely unveil a multitude of differentially expressed miRNAs. Typically, miRNAs influence multiple targets and operate in collaboration with other miRNAs, forming a complex network of miRNA-target interactions [314]. Therefore, conducting an ORA with solely four identified miRNAs from a highly selected, tumor/melanoma-specific panel only allows for a very limited and guided analysis, leading to an oversimplification of potential effects. Consequently, the interpretative power of the pathway analyses presented here is restricted regarding general baseline differences between the cell types. While these pitfalls were acknowledged in advance, the baseline expression of these selected miRNAs was nevertheless explored for an initial assessment.

In summary, this study has provided preliminary indications of notably distinct baseline miRNA expression patterns in DSCs compared to melanocytes and melanoma cells, even with a thematically highly selected miRNA panel. For a more comprehensive understanding, larger-scale analyses are urgently needed.

6.6.2 MicroRNA Expression Following UV Irradiation

UV radiation is known to induce changes in miRNAs expression in the skin, being implicated in various processes like photoaging [661,662], pigmentation [50], DDR [188,663], and also oncogenic pathways [189,664-666]. In addition to a general miRNA response to UV, there are also wavelength-specific miRNA responses. The differential expression of miRNAs varies depending on whether cells are exposed to UVA or UVB [667,668].

Growing evidence suggests that UV radiation causes dysregulation of miRNAs associated with photocarcinogenesis and melanomagenesis [666,669,670]. This includes UV-mediated deregulation of miRNAs due to oxidative stress, contributing to known signal transduction pathways underlying melanoma development. These UV-induced, redox-sensitive miRNAs include, e.g., upregulation of miR-22, miR-21, miR-30b, miR-146a, miR-155, and miR-182, as well as downregulation of miR-29c, miR-34b, miR-34c, miR-125b, miR-148, miR-199a, miR-206, miR-200c, and miR-193b. This dysregulation results in increased proliferation, migration, and invasion, while apoptosis is inhibited [669]. Additionally, UV-stimulated exosomal trafficking of melanoma-promoting miRNAs is suggested, for example, miR-21-enriched exosomes secreted by keratinocytes upon UV irradiation and taken up by melanocytes [671].

To examine whether UV irradiation also induces alterations in the miRNA expression profile of DSCs that are associated with melanoma development, DSCs were exposed to a single dose

of 300 J/m² UVB or 37 kJ/m² UVA. miRNA expression was then analyzed at two different times following exposure. Melanocytes were also irradiated for comparison, and melanoma cells (without irradiation) were included in the analysis as a reference for melanoma-specific miRNA patterns. The investigation addressed the following questions:

a) Is there a radiation effect with differentially expressed miRNAs evident in DSCs and/or melanocytes?
b) Does UV irradiation induce changes in the miRNA expression patterns of DSCs and/or melanocytes resembling melanoma cells and thus associated with melanoma development?

In this experimental setup, no significant irradiation effect was observed at any time, neither with UVA nor with UVB, as the hierarchical cluster analysis primarily reflected differences based on cell types and donors rather than the irradiation treatment. The primary driver for miRNA expression heterogeneity was cell type differences, demonstrated by distinct clustering according to cell type. Additionally, donor-dependent differences within the cell types were noticeable, enabling a clear distinction between individual donors. Irradiated DSCs and melanocytes lacked a clear distinction from their respective non-irradiated controls, suggesting that there was no UV-induced up- or downregulation within both cell types, despite some of the analyzed miRNAs being involved in the DDR. Furthermore, there was no clustering of irradiated DSCs or melanocytes with the melanoma cells, indicating that after UV irradiation, no miRNA patterns associated with the development of melanoma were found in DSCs and melanocytes. Overall, interindividual variability was more pronounced than any putative irradiation effect in this setting. With this single application of the chosen UVB and UVA doses, only minimal changes in miRNA expression were observed. Therefore, no miRNA signature for different cell types responding to UV was identified.

Similar to the investigation of differentiation following UV irradiation, a single exposure appears insufficient to elicit UV-related effects in miRNA expression. It is conceivable that the chosen doses may have been too low, although, for comparison, research on keratinocytes demonstrated that after irradiation with the same dose of 300 J/m² UVB, a considerable number of miRNAs were differentially expressed, many of which were also included in the panel used here [672]. In future research, it is advisable to consider multiple irradiations. Clear epigenetic dysregulation is likely to manifest gradually through chronic irradiation, akin to genetic changes that develop over an extended period, ultimately contributing to transformation and the occurrence of skin cancer in old age. This assumption gains support from the examination of

miRNA expression in mouse skin, where almost no changes were observed after acute exposure, but a significantly higher number of differentially expressed miRNAs emerged in response to chronic UV exposure. These miRNAs were associated with pathways related to PI3K/AKT signaling, MAPK signaling, and melanoma [664].

Notably, the expression pattern of all examined miRNAs in DSCs did not exhibit significant similarity to either melanocytes, which might have been anticipated given their progeny relationship, or melanoma cells, as might have been expected within the context of the cancer stem cell hypothesis (see section 1.5.2.3). The previously reported similarities between DSCs and certain melanoma cell populations, presumably CSCs, in other studies [32,42] could not be confirmed on the miRNA level. However, it is worth noting that only a small, selected miRNA panel was investigated. To provide an accurate assessment of similarities or differences in the overall miRNA patterns of the different analyzed cell types, a comprehensive analysis of the entire miRNAome is necessary.

The most advanced method for miRNA analysis currently is RNA-seq using next-generation sequencing (NGS) [673]. Future studies utilizing NGS will be essential to evaluate how changes in the miRNA pattern contribute to the DDR of DSCs and the potential malignant transformation into melanoma. Investigating not only changes in intracellular miRNA expression following UV irradiation but also alterations in the secretion of miRNAs, such as in exosomes, holds promise. For example, it has been demonstrated that after multiple UV irradiations, human foreskin melanocytes release exosomes containing specific miRNAs, which induce premature senescence and suppress critical DNA repair genes involved in the GGR and TCR pathways [674].

7 Outlook

This study investigated how DSCs, considered as a potential cell of origin for malignant melanoma, respond to UV irradiation regarding various processes. Additionally, DSCs were examined for specific cell characteristics and the purification of DSC cultures was established. The outcomes of this work not only pose several questions, but also present new opportunities for future research on these cells.

Concerning the immunomagnetic separation to purify DSCs, it was hypothesized that there could be distinct subpopulations of dermal fibroblasts [53,459,462-464] and, additionally, small proportions of other dermal cells present within the co-cultures, aside from DSCs and fibroblasts. This presence could potentially hinder effective purification through negative selection based on CD90. Phenotypic analysis of DSC-fibroblast co-cultures with respective markers is necessary to characterize all potential cell types, e.g., CD31, Tie2 for endothelial and lymphatic cells; CD45, CD34, CD14, CD11b for hematopoietic/immune cells [53,458]; CD106, CD105, CD73 for mesenchymal stem cells (MSCs) [115,675]. Positive selection with the MACS® approach proved successful, with DSCs maintaining viability and proliferative capacity, providing a promising tool to enrich DSCs in upcoming experiments. To use these purified DSCs as a model for studying melanomagenesis, it is crucial to ensure that normal DSC characteristics are preserved after purification. Initial investigations of sphere formation ability, differentiation potential, and miRNA expression suggest that this is true. However, further validation is necessary to confirm that the functionality is indeed retained.

The melanocytic differentiation potential of both DSC-fibroblast co-cultures and purified DSCs was confirmed, albeit with a slightly reduced ability in purified DSCs. This raised the question whether fibroblasts *in vitro* could positively influence the differentiation of melanocyte stem cells, as expected in the dermis [7]. To address this, a purified DSC culture should be manually recombined with varying proportions of fibroblasts to subsequently compare the differentiation potential. Additional experiments are necessary to investigate proliferation (using DNA-traceable dye labeling [586,587]), apoptosis, and senescence during differentiation. It is also essential to examine whether DSCs maintain their differentiation potential over extended periods of cultivation. The role of p53 may be of interest as well, not only as an apoptosis regulator but also as a potential regulator of differentiation in adult stem cells [597,598]. To gain comprehensive insights, transcriptomic/proteomic profiles in DSCs/differentiating cells at various times and in response to UV radiation are necessary. This investigation should

encompass not only cell-specific markers but also tumor suppressor genes and key melanoma driver genes.

Further studies are required to explore differentiation at the epigenetic level, given the relationship between epigenetic modifications, stem cell behavior, and fate. Stem cell identity, including self-renewal and differentiation potential, is known to be also regulated epigenetically through DNA methylation, histone modifications, and miRNAs [676,677]. Especially miRNAs play a pivotal role, with various stem cell types exhibiting unique miRNA expression profiles [678]. During differentiation, significant changes in the epigenetic profile occur, involving the silencing of pluripotency genes and activation of specific signaling pathways for a given cell type [56,676]. There is a growing number of miRNAs targeting genes or pathways involved in melanocyte differentiation and biology, including an extensive network centered around MITF [679].

The sphere-forming potential of DSCs remained unaltered following both UV irradiation and purification with MACS® positive selection. However, the findings raised questions about the role of fibroblasts and cell aggregation in the sphere formation process [425]. It is recommended to use a considerably lower cell density for the multiple-cell plating method, working with highly MACS®-purified DSC cultures. To prevent cell merging and evaluate the self-renewal capacity or clonal properties of DSCs, a sphere formation assay with single-cell plating using serial dilution may be utilized [404,425].

The results from the miRNA expression analysis indicate significant differences in the overall baseline miRNA pattern of DSCs compared to melanocytes and melanoma cells. For a more comprehensive understanding, a larger-scale analysis of the entire miRNAome is mandatory, e.g., through RNA-seq utilizing next-generation sequencing [673].

No discernible impact on both miRNA expression and differentiation potential was observed with single UV irradiation. To mimic physiological conditions where DSCs are continuously exposed to UV radiation [357], further experiments involving multiple irradiations are essential. Depending on the migration scenario of the DSCs, even irradiation during the differentiation process could be relevant. Additionally, exploring the involvement of exosomes during differentiation could be of interest. Exosomes, small extracellular vesicles with a diameter of 30–150 nm, contain mRNAs, lipids, proteins, microRNAs, and long non-coding RNAs [680]. They play an important role in intercellular communication in response to UV radiation [681,682], in melanocyte regulation [50], and melanoma progression/EMT [683]. Exosomes secreted by irradiated fibroblasts, keratinocytes, or melanocytes might be added to DSC

cultures during differentiation to investigate a potential stimulatory effect of epigenetic cell-cell communication.

In the comparative analysis of the UV damage response, partially cell-specific responses to UV radiation were identified. DSCs demonstrated functional DNA repair of UV-induced CPDs and the ability to induce apoptosis, similar to the responses observed in fibroblasts and melanocytes. However, it is important to emphasize that the actual efficiency of DNA repair should be assessed through mutation frequency analysis [527]. The results also provided strong indications of a unique cell cycle regulation in DSCs, as they lacked cell cycle arrest following UV irradiation. Subsequent studies should focus on elucidating the mechanisms governing the DNA damage response (DDR) by conducting gene and protein expression analyses of checkpoint, repair, apoptosis, and cell cycle regulators, particularly of p53, as a key mediator of the DDR, and its effector p21. This might clarify whether DSCs also have non-functioning cell cycle checkpoints [535] and an atypical p53-p21 axis [540] as observed in ESCs. Additionally, exploring senescence and the role of miRNAs as part of the DDR [237] may be of interest as well.

In certain investigations, the use of purified DSCs is crucial to avoid potential interference with results stemming from contaminating fibroblasts. Additionally, the establishment of a stable DSC cell line from purified DSCs through transduction with TERT should be considered to minimize the impact of interindividual variances. Ideally, generating cell lines from approximately three DSC cell strains from different donors is recommended to avoid being confined to the individual characteristics of a single donor. However, a potential drawback associated with purified DSCs, and possibly DSC cell lines, could be the absence of the microenvironment to which the stem cells are accustomed in the skin and *in vitro* co-culture with fibroblasts. The stem cell niche or microenvironment significantly influences stem cell features and plays a crucial role in various processes [56,60]. Moreover, cancer-associated fibroblasts (CAFs) in the tumor microenvironment are known to support and regulate tumor growth and immune escape during carcinogenesis [684,685]. Consequently, it can be assumed that in the development of malignant melanoma from DSCs as the initiating cell, the surrounding fibroblasts in the dermis might play an important role [7]. The impact of long-term cultivation without fibroblasts on stem cell properties of DSCs remains to be investigated.

Although cell culture has been and still remains a valuable model for studying basal cell mechanisms, caution should be taken when extrapolating the knowledge derived from this cell system to human tissue. Cells exhibit different behavior in 3D culture and in contact with other

cells [686,687]. Hence, skin as a whole organ might differ in its response to environmental influences. In this context, the crosstalk between stem cells and their niche plays a significant role [56,63]. However, 2D monocultures fail to replicate the *in situ* phenotype [688] and neglect the roles of intercellular communication and homeostasis in shaping how a cell responds and adapts to radiation [686,687]. To accurately mimic the actual behavior of DSCs in tissue, the microenvironment must closely resemble the native counterpart. Acknowledging the structure-function relationship [2] and the potential role of bystander effects after UV irradiation [689-691], makes organotypic culture (OTC) or skin equivalent (SE) models desirable for *in vitro* 3D skin tissue experiments. OTCs partially recreate the complexity of the physiological situation and the anatomical features of human skin more accurately [102], closing the gap between 2D culture and animal models. The fibroblast-derived matrix of OTCs closely resembles the dermal microenvironment *in vivo* [483-485] and provides a suitable platform for embedding DSCs. The incorporation of immune cells in OTCs would be a further step towards creating a physiologically relevant environment [692,693], considering the critical role played by the immune system and its modification by UV radiation in melanomagenesis [261]. Altogether, experiments with OTCs are desirable for an improved understanding of biological processes and signaling pathways in DSCs and to assess the influence of surrounding cells on the cell fate following UV irradiation (e.g., signals for self-renewal or differentiation).

The influence of the whole solar spectrum, combining UVB, UVA, visible light (VIS), and infrared-A (IR-A), on DSCs is an area of potential interest. While the (harmful) effects of the IR and VIS components of solar radiation on the skin are less thoroughly characterized compared to UV effects [560], it is recognized that both IR and VIS exert influences on the skin, for instance, contributing to photoaging. VIS has been demonstrated to induce ROS and matrix metalloproteinases [694,695] and can also stimulate skin pigmentation [696]. IR-A, through the activation of MAPK signaling, promotes the production of ROS and matrix metalloproteinases as well [697-699]. Evidence suggests that VIS and IR can have both beneficial and detrimental effects on the skin [700,701]. However, relatively little is known about whether the different spectral bands, UVB, UVA, VIS, and IR-A influence each other. Recent studies have described both additive/synergistic and modulatory/antagonistic interactions [402]. In primary fibroblasts, the combination of UV, VIS, and IR increases the generation of ROS, mitochondrial DNA damage, and nuclear DNA damage, although these effects are not observed in keratinocytes, indicating cell type-dependent responses [560]. Jantschitsch et al. demonstrated that IR-A exposure mediates resistance to UV-induced apoptosis through the reduction of DNA damage and modulated expression of apoptosis-related

genes, potentially elevating the risk for carcinogenesis [702]. Consequently, the effects of the whole solar spectrum on DSCs might be even more complex.

Addressing these open questions will have profound implications for understanding the response of DSCs to UV-induced DNA damage, the preservation of genome integrity, and how disruption of these mechanisms may contribute to the onset of melanomagenesis.

8 Appendix

8.1 Supplementary Figures

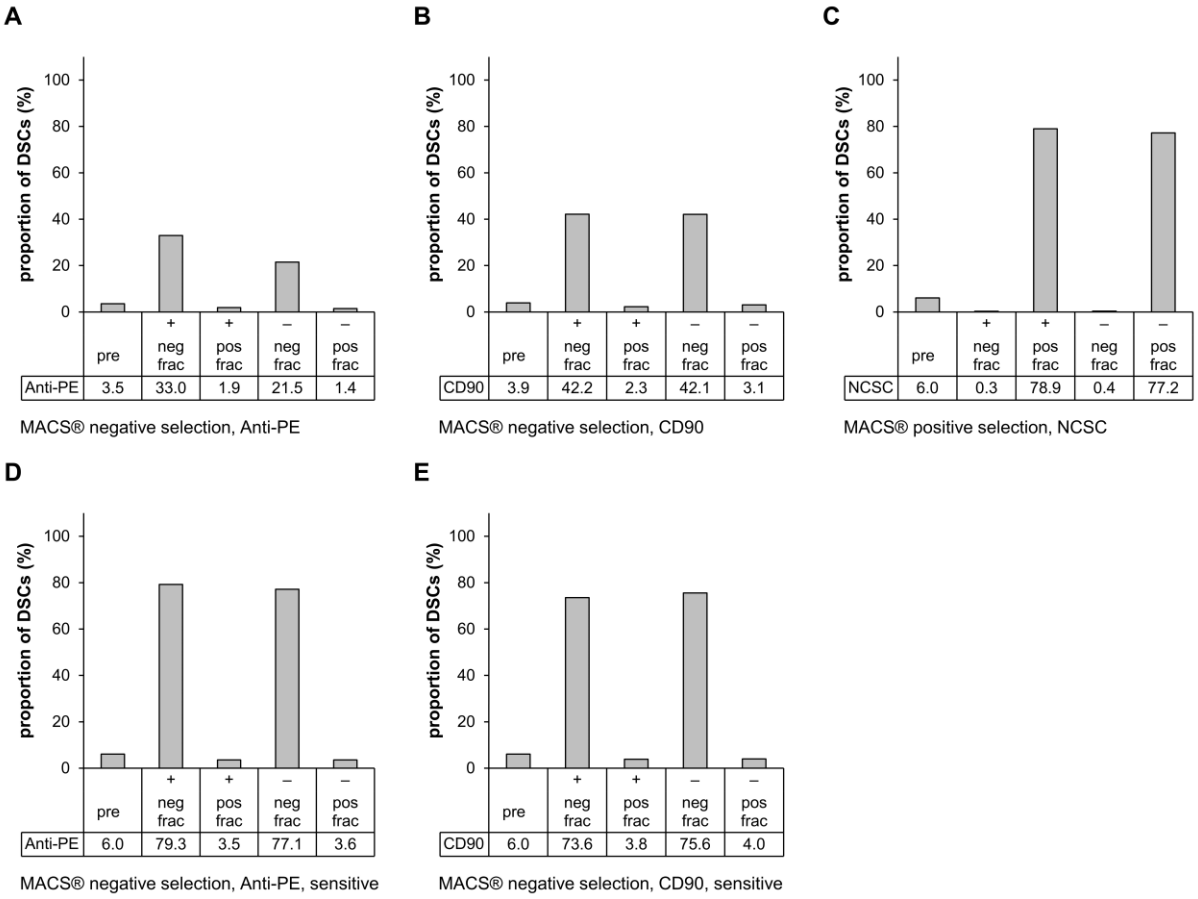

Figure 8.1 Effect of prior usage of *Basic MicroBeads* on immunomagnetic separation. Comparison of separation results with prior usage (+) and without prior usage (-) of *Basic MicroBeads* to remove non-specific binding material. (**A**) MACS® automatic column-based negative selection with *Anti-PE MicroBeads* in combination with a PE-conjugated anti-CD90 antibody and the autoMACS® Pro Separator. Program: *Deplete*. Sample size: n=1. (**B**) MACS® automatic column-based negative selection with *CD90 MicroBeads* and the autoMACS® Pro Separator. Program: *Deplete*. Sample size: n=1. (**C**) MACS® automatic column-based positive selection with *Neural Crest Stem Cell (NCSC) MicroBeads* and the autoMACS® Pro Separator. Program: *Posseld2*. Sample size: n=1. (**D**) MACS® automatic column-based negative selection with *Anti-PE MicroBeads* in combination with a PE-conjugated anti-CD90 antibody and the autoMACS® Pro Separator. Sensitive Program: *DepleteS*. Sample size: n=1. (**E**) MACS® automatic column-based negative selection with *CD90 MicroBeads* and the autoMACS® Pro Separator. Sensitive Program: *DepleteS*. Sample size: n=1. Pre: initial sample, neg frac: unlabeled fraction, pos frac: labeled fraction. Frequency of DSCs in the separate fractions was determined via flow cytometry analysis of NGFRp75 and CD90 (adapted from [420]).

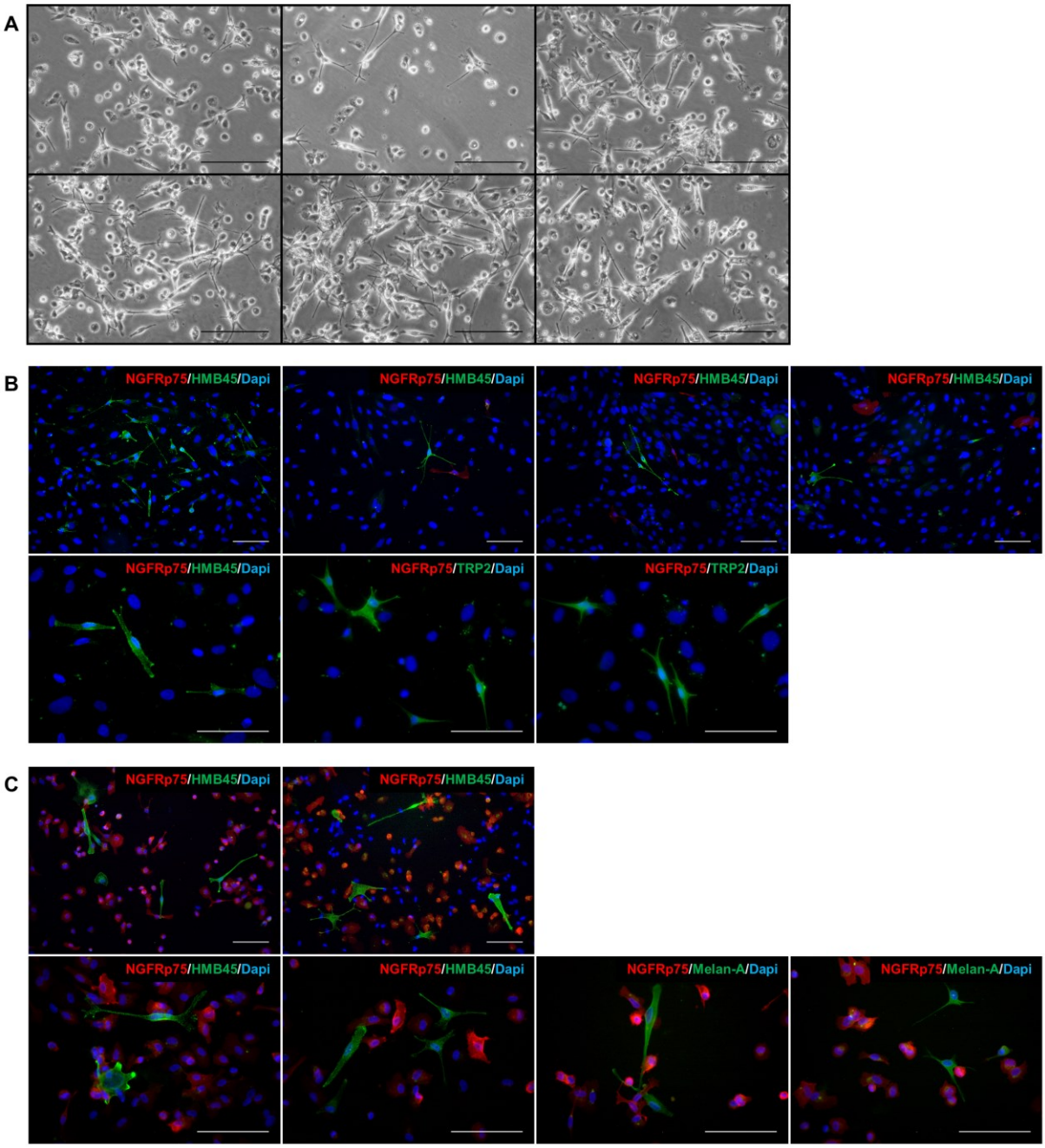

Figure 8.2 Additional pictures of DSC cultures and staining at the end of differentiation. (**A**) Collection of light microscopy pictures of MACS®-purified DSC cultures at the end of differentiation (day 16), showing multiple cells with morphological characteristics of melanocytes. Scale bars: 200 µm. (**B–C**) Collection of immunocytochemical staining for NCSC marker NGFRp75 (red), and melanocytic markers HMB45 (green), TRP2 (green), and Melan-A at the end of differentiation (day 17-20) in (**B**) DSC-fibroblast co-culture, and (**C**) MACS® positive selection-purified DSCs. Nuclei were counterstained with DAPI (blue). Scale bars: 100 µm.

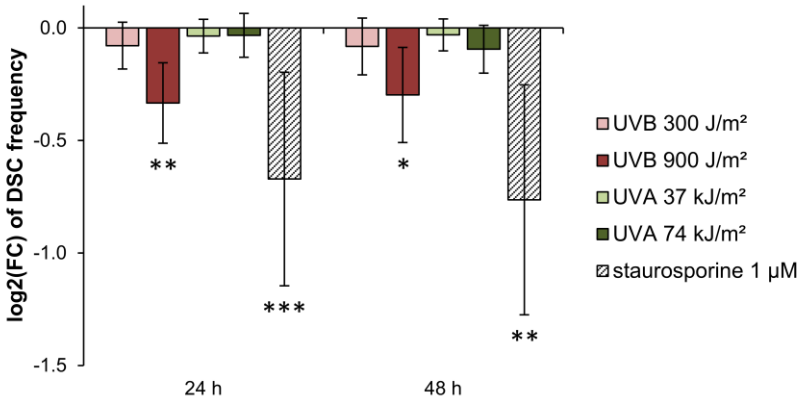

Figure 8.3 Changes in stem cell frequency of DSC samples in apoptosis measurement. Fold changes in DSC frequency relative to non-irradiated control cells measured via flow cytometry. Values are presented as mean ± SDs. Sample size: n=6. Multiple comparisons versus control (One-way ANOVA and Dunnett's method): *$p \leq 0.05$; **$p \leq 0.01$; ***$p \leq 0.001$. Significant changes: 24 h, 900 J/m² UVB $p = 0.005$; 24 h, staurosporine $p < 0.001$; 48 h, 900 J/m² UVB $p = 0.026$; 48 h, staurosporine $p = 0.002$.

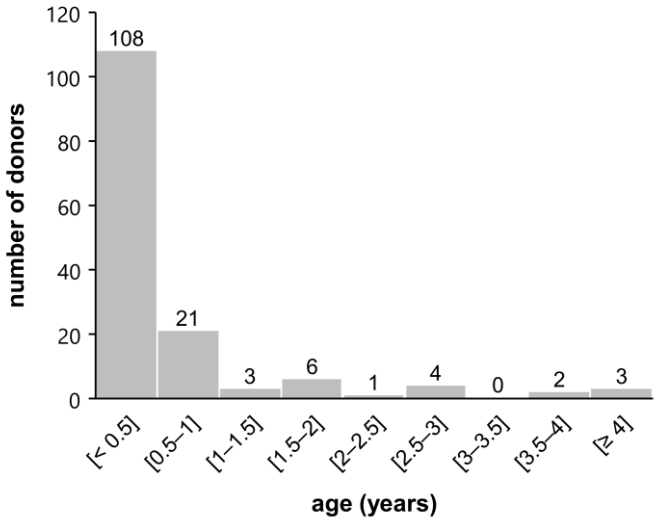

Figure 8.4 Age of foreskin donors. The histogram shows the abundance distribution of the age of foreskin donors at the time of circumcision, divided into ranges of 0.5 years. Results from 148 donors.

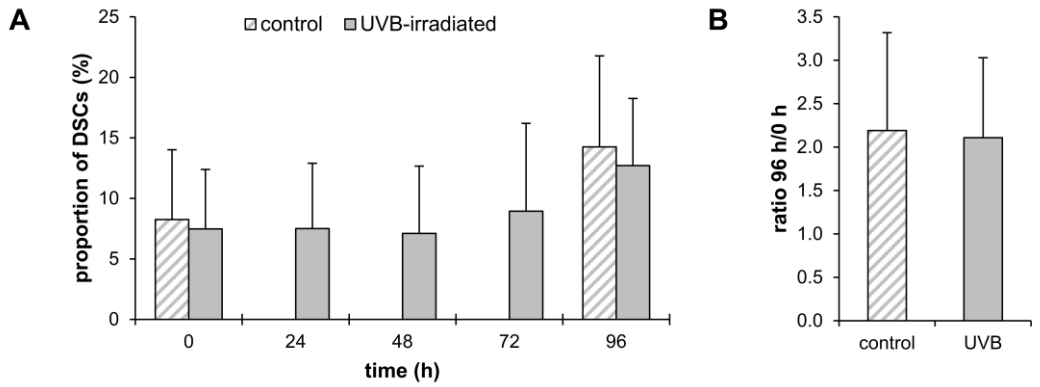

Figure 8.5 Proliferation of DSCs during repair kinetics. (**A**) Percentage of NGFRp75^{+} cells in sham-irradiated and UVB-irradiated DSC-fibroblast co-cultures during repair kinetics. (B) Ratio of DSC frequency at 96 h to DSC frequency at 0 h. Values are presented as mean ± SDs from n=5 independent experiments, with technical duplicates or triplicates. After exposure to 285 J/m² UVB, DSCs continued to proliferate similar to non-irradiated control cells over the period of 96 h (adapted from [398]).

8.2 Supplementary Tables

Table 8.1 microRNA expression in malignant melanoma.

Upregulated (oncogenic) miRNAs ↑		Downregulated (tumor-suppressive) miRNAs ↓	
miR-106b	reviewed by [315]	let-7 family (let-7a, -7b, -7d, -7e, and -7g)	[334,335]
miR-135a	reviewed by [291]	miR-101	reviewed by [703]
miR-146a	reviewed by [315]	miR-124	reviewed by [315]
miR-149	reviewed by [313]	miR-125b	[330,331]
miR-15b	[704]	miR-126	reviewed by [234]
miR-150	reviewed by [291]	miR-137	[338,339]
miR-155	[324]; reviewed by [234]	miR-138	reviewed by [315]
miR-17	reviewed by [316]	miR-139	reviewed by [291]
miR-18a	reviewed by [291]	miR-140	reviewed by [291]
miR-182	[321,322]	miR-143	reviewed by [315]
miR-21	[318,319,323]	miR-145	reviewed by [234,315]
miR-210	reviewed by [313]	miR-148	reviewed by [293]
miR-214	reviewed by [314]	miR-15a	reviewed by [315]
miR-221/222	[320,325,326]	miR-16	[337]
miR-25	reviewed by [315]	miR-18b	reviewed by [313]
miR-30b/d	reviewed by [314]	miR-183	[631]
miR-301a	reviewed by [315]	miR-185	reviewed by [315]
miR-376	[631]	miR-192	[631]
miR-449a	reviewed by [293]	miR-193b	reviewed by [234]
miR-603	reviewed by [291]	miR-194	reviewed by [315]
miR-633	reviewed by [291]	miR-195	reviewed by [313]
miR-92	reviewed by [316]	miR-196a	reviewed by [234]
		miR-199	reviewed by [313]
		miR-200 family (miR-200a, -200b, -200c)	[329,342,347]
		miR-201	reviewed by [235]
		miR-203	[329,341]
		miR-204	[651-653]
		miR-205	[327-329]
		miR-206	reviewed by [234]
		miR-211	[329,332,333]
		miR-216a/b	reviewed by [315]
		miR-218	reviewed by [315]
		miR-22	reviewed by [291]
		miR-224	[631]
		miR-23a/b	reviewed by [315]

Upregulated (oncogenic) miRNAs ↑	Downregulated (tumor-suppressive) miRNAs ↓	
	miR-26a	reviewed by [703]
	miR-27b	reviewed by [291]
	miR-29c	[705]
	miR-31	[340]
	miR-33a	[639-641]
	miR-335	[631]
	miR-34a/b/c	[336], reviewed by [315]
	miR-342	reviewed by [291]
	mir-365	reviewed by [315]
	miR-375	reviewed by [313]
	miR-429	reviewed by [315]
	miR-488	reviewed by [315]
	miR-548b	reviewed by [291]
	miR-9	reviewed by [314]
	miR-96	[631]
	miR-99a	reviewed by [293]

Table 8.2 Individual repair time constants τ of all donors with standard deviation. (adapted from [398])

ID	DSCs 285 J/m² (n=7)	Fibroblasts 285 J/m² (n=18)	Keratinocytes 285 J/m² (n=13)	Melanocytes 285 J/m² (n=11)	Melanocytes 400 J/m² (n=5*)
5/19	n/a	23.1±3.1 h	n/a	n/a	n/a
6/19	n/a	29.8±2.1 h	n/a	n/a	n/a
7/19	n/a	30.5±3.4 h	n/a	23.7±9.1 h	n/a
8/19	n/a	21.6±3.0 h	n/a	n/a	n/a
9/19	n/a	23.3±4.5 h	n/a	n/a	n/a
14/19	n/a	24.4±3.9 h	28.7±7.3 h	16.4±1.8 h	n/a
15/19	n/a	29.7±3.0 h	18.1±1.4 h	20.1±3.4 h	n/a
16/19	n/a	36.8±4.7 h	13.6±1.8 h	25.1±2.0 h	n/a
19/19	30.2±3.0 h	31.3±2.8 h	15.5±1.6 h	n/a	n/a
20/19	34.0±5.3 h	35.6±2.5 h	18.0±2.8 h	n/a	n/a
21/19	n/a	26.6±2.2 h	17.5±1.5 h	25.1±3.0 h	n/a
27/19	38.5±9.0 h	32.8±4.3 h	13.7±1.5 h	25.4±3.2 h	25.0±2.6 h
28/19	31.1±11.3 h	37.3±4.7 h	27.2±5.4 h	n/a	n/a
36/19	25.1±6.5 h	25.6±3.5 h	25.9±3.5 h	33.1±2.9 h	24.6±3.9 h
37/19	32.7±5.3 h	28.7±3.9 h	22.3±3.1 h	27.0±5.9 h	27.9±4.3 h
48/19	n/a	26.0±1.6 h	17.4±2.2 h	25.9±2.6 h	30.3±5.1 h
49/19	24.5±6.4 h	21.8±2.0 h	20.8±2.9 h	38.0±10.1 h	23.4±3.8 h
51/19	n/a	23.9±1.7 h	19.2±2.1 h	32.3±1.7 h	n/a

*n/a: not available (due to poor growth or contaminations); *: Additional irradiation with 400 J/m² UVB was performed with freeze-thawed melanocytes of the five indicated donors, based on previously gathered results.*

Table 8.3 Apoptosis results from the individual donors. Proportion of total apoptotic cells (%).

Cell type	Time	ID	control	UVB 300 J/m²	UVB 900 J/m²	UVA 37 kJ/m²	UVA 74 kJ/m²	staurosporine 1 µM
DSCs	24 h	48/20	13.1	11.8	25.0	10.8	14.7	59.3
		50/20	8.8	9.6	23.2	5.9	8.8	48.3
		51/20	10.9	11.5	15.2	10.1	9.6	47.5
		03/21	15.0	14.6	22.2	13.5	13.1	82.9
		04/21	23.6	18.7	24.2	20.9	22.1	80.4
		07/21	13.5	13.8	18.6	11.6	12.0	61.4
	48 h	48/20	11.6	14.6	30.5	15.7	14.2	73.2
		50/20	25.0	31.5	66.7	26.8	29.4	54.2
		51/20	12.6	16.6	20.9	19.7	15.4	49.7
		03/21	10.7	12.9	19.6	9.8	14.3	83.4
		04/21	18.5	19.9	28.5	19.2	21.9	89.0
		07/21	21.5	25.2	46.4	23.5	26.7	70.5
Fibroblasts	24 h	47/20	6.9	5.3	6.8	6.6	12.2	98.0
		48/20	5.5	5.2	5.2	4.9	6.9	97.9
		50/20	8.0	5.2	4.5	4.0	5.2	97.0
		51/20	3.6	4.1	3.7	4.7	9.8	98.6
		02/21	4.5	5.2	3.8	4.6	4.4	96.7
		05/21	3.5	3.7	3.0	4.1	4.5	92.8
		06/21	4.6	4.3	5.0	4.8	7.9	90.3
	48 h	47/20	5.2	4.7	20.1	5.5	9.1	89.4
		48/20	4.0	3.9	14.8	5.1	4.9	98.1
		50/20	7.6	6.1	16.5	5.7	5.3	95.5
		51/20	4.3	4.2	13.9	5.3	6.7	98.5
		02/21	4.8	6.8	15.2	6.4	7.3	98.1
		05/21	4.5	3.8	18.7	3.9	5.3	95.9
		06/21	7.6	8.0	19.6	10.1	8.0	96.5
Melanocytes	24 h	47/20	13.4	7.1	27.3	6.2	6.0	17.5
		48/20	8.3	6.1	13.8	6.8	6.2	25.3
		50/20	8.4	7.4	33.3	8.1	6.7	29.0
		51/20	11.5	8.2	26.5	7.6	8.1	45.5
		06/21	7.9	7.7	18.7	6.0	5.5	83.2
		18/20	5.6	5.4	20.8	5.0	5.4	72.9
	48 h	47/20	3.6	4.8	27.7	4.1	4.2	15.5
		48/20	3.4	2.8	17.7	3.7	6.4	13.4
		50/20	7.5	7.9	27.8	6.2	7.3	33.7
		51/20	4.7	4.8	32.0	5.1	5.1	33.7
		06/21	9.4	8.8	35.5	6.6	8.3	90.5
		18/20	12.3	9.0	19.0	9.7	9.5	90.2
Keratinocytes	24 h	27/19	11.5	10.9	14.2	16.1	14.0	50.7
		30/19	12.6	10.8	13.5	11.6	10.3	49.2
		08/21	20.0	20.1	23.1	19.5	18.5	28.8
		17/21	16.5	16.1	14.9	17.9	20.1	31.4
		18/21	14.5	16.7	23.4	19.7	15.7	43.6
		04/19	13.1	11.3	11.9	18.5	19.1	39.6
	48 h	27/19	17.9	16.0	30.5	32.0	26.0	80.3
		30/19	16.1	17.3	15.7	18.9	16.2	88.1
		08/21	19.8	17.7	25.4	18.1	19.8	42.1
		17/21	20.5	24.2	30.6	19.4	24.2	73.1
		18/21	20.2	14.1	24.9	28.2	23.2	66.9
		04/19	16.6	17.3	19.9	17.7	18.0	53.7

Table 8.4 Most stable microRNAs - all eight cell strains analyzed separately.

DSC 02	DSC 33	DSC 17	Mc 53	Mc 58	MM 1	MM 2	MM 3
mir-20a-5p	mir-15b-5p	mir-222-3p	mir-17-5p	mir-23a-3p	mir-185-5p	mir-210-3p	mir-193b-5p
mir-100-5p	mir-23a-3p	mir-193b-5p	mir-15a-5p	mir-15a-5p	mir-197-3p	mir-222-3p	mir-145-5p
mir-16-5p	mir-17-5p	mir-185-5p	mir-199a-3p	mir-17-5p	mir-338-3p	mir-197-3p	mir-301a-3p
mir-23a-3p	mir-100-5p	mir-23a-3p	mir-15b-5p	mir-20a-5p	mir-222-3p	mir-301a-3p	mir-185-5p
let-7i-5p	let-7i-5p	mir-20a-5p	mir-23b-3p	mir-23b-3p	mir-301a-3p	mir-185-5p	mir-197-3p
mir-15a-5p	mir-15a-5p	mir-137	mir-20a-5p	mir-15b-5p	mir-17-5p	mir-30d-5p	mir-222-3p
mir-17-5p	mir-93-5p	mir-221-3p	mir-23a-3p	mir-221-3p	mir-23a-3p	mir-425-5p	mir-199a-5p
mir-21-5p	let-7a-5p	mir-23b-3p	mir-100-5p	mir-100-5p	mir-20a-5p	mir-23a-3p	mir-23a-3p
mir-20b-5p	mir-20a-5p	mir-29a-3p	mir-221-3p	let-7d-5p	let-7a-5p	mir-93-5p	mir-15b-5p
mir-93-5p	mir-23b-3p	mir-17-5p	mir-30d-5p	mir-93-5p	mir-15a-5p	mir-15a-5p	mir-29b-3p

Table 8.5 Most stable microRNAs - only DSC strains compared to each other. Cell strains analyzed separately.

DSC 02	DSC 33	DSC 17
mir-20a-5p	mir-15b-5p	mir-222-3p
mir-100-5p	mir-23a-3p	mir-193b-5p
mir-16-5p	mir-17-5p	mir-185-5p
mir-23a-3p	mir-100-5p	mir-23a-3p
let-7i-5p	let-7i-5p	mir-20a-5p
mir-15a-5p	mir-15a-5p	mir-137
mir-17-5p	mir-93-5p	mir-221-3p
mir-21-5p	let-7a-5p	mir-23b-3p
mir-20b-5p	mir-20a-5p	mir-29a-3p
mir-93-5p	mir-23b-3p	mir-17-5p

Table 8.6 Most stable microRNAs - only melanocyte strains compared to each other. Cell strains analyzed separately.

Mc 53	Mc 58
mir-17-5p	mir-23a-3p
mir-15a-5p	mir-15a-5p
mir-199a-3p	mir-17-5p
mir-15b-5p	mir-20a-5p
mir-23b-3p	mir-23b-3p
mir-20a-5p	mir-15b-5p
mir-23a-3p	mir-221-3p
mir-100-5p	mir-100-5p
mir-221-3p	let-7d-5p
mir-30d-5p	mir-93-5p

Table 8.7 Most stable microRNAs - only melanoma cell strains compared to each other. Cell strains analyzed separately.

MM 1	MM 2	MM 3
mir-185-5p	mir-210-3p	mir-193b-5p
mir-197-3p	mir-222-3p	mir-145-5p
mir-338-3p	mir-197-3p	mir-301a-3p
mir-222-3p	mir-301a-3p	mir-185-5p
mir-301a-3p	mir-185-5p	mir-197-3p
mir-17-5p	mir-30d-5p	mir-222-3p
mir-23a-3p	mir-425-5p	mir-199a-5p
mir-20a-5p	mir-23a-3p	mir-23a-3p
let-7a-5p	mir-93-5p	mir-15b-5p
mir-15a-5p	mir-15a-5p	mir-29b-3p

Table 8.8 Most stable microRNAs - comparison of cell type groups. Cell strains from same cell type combined for analysis.

DSC combined	Mc combined	MM combined
mir-17-5p	mir-15a-5p	mir-222-3p
mir-100-5p	mir-222-3p	mir-15a-5p
mir-93-5p	mir-15b-5p	mir-23a-3p
let-7a-5p	let-7i-5p	let-7g-5p
let-7i-5p	let-7d-5p	mir-301a-3p
mir-23a-3p	mir-185-5p	let-7a-5p
mir-148a-3p	mir-17-5p	mir-20b-5p
let-7d-5p	let-7g-5p	let-7i-5p
mir-16-5p	mir-29a-3p	mir-16-5p
let-7g-5p	mir-23b-3p	mir-15b-5p

Table 8.9 Significantly altered GO terms of the 4-miRNA set overexpressed in DSCs from Figure 5.20C. Determined using miEAA 2.0, accessed on September 21, 2023.

Rank	GO term		p_{adj}
1	GO:0006914	autophagy	0.026
2	GO:0051649	establishment of localization in cell	0.026
3	GO:0016236	macroautophagy	0.026
4	GO:0060341	regulation of cellular localization	0.026
5	GO:0050796	regulation of insulin secretion	0.026
6	GO:0090276	regulation of peptide hormone secretion	0.026
7	GO:0014823	response to activity	0.026
8	GO:0030073	insulin secretion	0.027
9	GO:0071398	cellular response to fatty acid	0.037
10	GO:0030072	peptide hormone secretion	0.037
11	GO:0046883	regulation of hormone secretion	0.039
12	GO:0071900	regulation of protein serine/threonine kinase activity	0.042
13	GO:0034097	response to cytokine	0.042
14	GO:0007154	cell communication	0.044
15	GO:0034620	cellular response to unfolded protein	0.044
16	GO:0016311	dephosphorylation	0.044
17	GO:0008543	fibroblast growth factor receptor signaling pathway	0.044
18	GO:0060548	negative regulation of cell death	0.044
19	GO:0006796	phosphate-containing compound metabolic process	0.044
20	GO:0043388	positive regulation of DNA binding	0.044

Table 8.10 Significantly altered GO terms of the 40 target genes of the 4-miRNA set downregulated in DSCs from Figure 5.20D. Determined using GeneTrail 3.0, accessed on September 21, 2023.

Rank	GO term		p_{adj}
1	GO:0080135	regulation of cellular response to stress	4.156e-7
2	GO:0007166	cell surface receptor signaling pathway	5.432e-6
3	GO:0019221	cytokine-mediated signaling pathway	5.432e-6
4	GO:0010468	regulation of gene expression	5.432e-6
5	GO:0090344	negative regulation of cell aging	1.782e-5
6	GO:2001141	regulation of RNA biosynthetic process	1.782e-5
7	GO:0051171	regulation of nitrogen compound metabolic process	1.782e-5
8	GO:1903506	regulation of nucleic acid-templated transcription	1.782e-5
9	GO:0006355	regulation of transcription, DNA-templated	1.782e-5
10	GO:0010628	positive regulation of gene expression	2.402e-5
11	GO:0007167	enzyme linked receptor protein signaling pathway	2.783e-5
12	GO:0008284	positive regulation of cell population proliferation	3.723e-5
13	GO:0051252	regulation of RNA metabolic process	3.723e-5
14	GO:0007178	transmembrane receptor protein serine/threonine kinase signaling pathway	3.723e-5
15	GO:0019222	regulation of metabolic process	4.101e-5
16	GO:2000772	regulation of cellular senescence	5.320e-5
17	GO:0051152	positive regulation of smooth muscle cell differentiation	6.861e-5
18	GO:0071456	cellular response to hypoxia	7.236e-5
19	GO:0006357	regulation of transcription by RNA polymerase II	7.236e-5
20	GO:0048513	animal organ development	9.414e-5

Table 8.11 KEGG pathway analysis of the 40 target genes of the 4-miRNA set downregulated in DSCs from Figure 5.20D. Determined using GeneTrail 3.0, accessed on September 21, 2023.

Rank	KEGG pathway	Gene	p_{adj}
1	MicroRNAs in cancer	BCL2, CDK6, EZR, MYC, PTEN, SIRT1	3.814e-5
2	Small cell lung cancer	AKT3, BCL2, CDK6, MYC, PTEN	3.814e-5
3	FoxO signaling pathway	AKT3, PTEN, SIRT1, SMAD4, SOD2	9.157e-5
4	PI3K-AKT signaling pathway	AKT3, BCL2, CDK6, HSP90AA1, KIT, MYC, PTEN	9.157e-5
5	Pathways in cancer	AKT3, BCL2, CDK6, HSP90AA1, KIT, MYC, PTEN, SMAD4	9.157e-5
6	Signaling pathways regulating pluripotency of stem cells	AKT3, BMPR1A, MYC, SMAD4, SMAD5	9.157e-5
7	Breast cancer	AKT3, CDK6, KIT, MYC, PTEN	9.199e-5
8	Central carbon metabolism in cancer	AKT3, KIT, MYC, PTEN	9.199e-5
9	Cellular senescence	AKT3, CDK6, MYC, PTEN, SIRT1	9.891e-5
10	Chronic myeloid leukemia	AKT3, CDK6, MYC, SMAD4	9,891e-5
11	Hepatitis B	AKT3, BCL2, IRAK1, MYC, SMAD4	9,891e-5
12	Hepatocellular carcinoma	AKT3, CDK6, MYC, PTEN, SMAD4	1.045e-4
13	Colorectal cancer	AKT3, BCL2, MYC, SMAD4	1.297e-4
14	TGF-beta signaling pathway	BMPR1A, MYC, SMAD4, SMAD5	1.683e-4
15	Prostate cancer	AKT3, BCL2, HSP90AA1, PTEN	1.767e-4
16	Epstein-Barr virus infection	AKT3, BCL2, CDK6, IRAK1, MYC	1.813e-4
17	Fluid shear stress and atherosclerosis	AKT3, BCL2, BMPR1A, HSP90AA1	5.518e-4
18	Measles	AKT3, BCL2, CDK6, IRAK1	5.518e-4
19	Gastric cancer	AKT3, BCL2, MYC, SMAD4	6.615e-4
20	Endometrial cancer	AKT3, MYC, PTEN	6.656e-4

References

1. Nourian Dehkordi, A.; Mirahmadi Babaheydari, F.; Chehelgerdi, M.; Raeisi Dehkordi, S. Skin tissue engineering: wound healing based on stem-cell-based therapeutic strategies. *Stem Cell Res Ther* **2019**, *10*(1), 111, doi:10.1186/s13287-019-1212-2.

2. Roger, M.; Fullard, N.; Costello, L.; Bradbury, S.; Markiewicz, E.; O'Reilly, S.; Darling, N.; Ritchie, P.; Maatta, A.; Karakesisoglou, I.; Nelson, G.; von Zglinicki, T.; Dicolandrea, T.; Isfort, R.; Bascom, C.; Przyborski, S. Bioengineering the microanatomy of human skin. *J Anat* **2019**, *234*(4), 438-455, doi:10.1111/joa.12942.

3. Yousef, H.; Alhajj, M.; Sharma, S. Anatomy, Skin (Integument), Epidermis. In *StatPearls*; Treasure Island (FL), 2022.

4. Arda, O.; Goksugur, N.; Tuzun, Y. Basic histological structure and functions of facial skin. *Clin Dermatol* **2014**, *32*(1), 3-13, doi:10.1016/j.clindermatol.2013.05.021.

5. Lee, C.H.; Wu, S.B.; Hong, C.H.; Yu, H.S.; Wei, Y.H. Molecular Mechanisms of UV-Induced Apoptosis and Its Effects on Skin Residential Cells: The Implication in UV-Based Phototherapy. *Int J Mol Sci* **2013**, *14*(3), 6414-6435, doi:10.3390/ijms14036414.

6. Cichorek, M.; Wachulska, M.; Stasiewicz, A.; Tyminska, A. Skin melanocytes: biology and development. *Postepy Dermatol Alergol* **2013**, *30*(1), 30-41, doi:10.5114/pdia.2013.33376.

7. Haass, N.K.; Herlyn, M. Normal human melanocyte homeostasis as a paradigm for understanding melanoma. *J Investig Dermatol Symp Proc* **2005**, *10*(2), 153-163, doi:10.1111/j.1087-0024.2005.200407.x.

8. Yardman-Frank, J.M.; Fisher, D.E. Skin pigmentation and its control: From ultraviolet radiation to stem cells. *Exp Dermatol* **2021**, *30*(4), 560-571, doi:10.1111/exd.14260.

9. Hauschild, A.; Egberts, F.; Garbe, C.; Bauer, J.; Grabbe, S.; Hamm, H.; Kerl, H.; Reusch, M.; Rompel, R.; Schlaeger, M.; expert group "Melanocytic nevi". Melanocytic nevi. *J Dtsch Dermatol Ges* **2011**, *9*(9), 723-734, doi:10.1111/j.1610-0387.2011.07741.x.

10. Wang, J.X.; Fukunaga-Kalabis, M.; Herlyn, M. Crosstalk in skin: melanocytes, keratinocytes, stem cells, and melanoma. *J Cell Commun Signal* **2016**, *10*(3), 191-196, doi:10.1007/s12079-016-0349-3.

11. Nishimura, E.K. Melanocyte stem cells: a melanocyte reservoir in hair follicles for hair and skin pigmentation. *Pigment Cell Melanoma Res* **2011**, *24*(3), 401-410, doi:10.1111/j.1755-148X.2011.00855.x.

12. Upadhyay, P.R.; Ho, T.; Abdel-Malek, Z.A. Participation of keratinocyte- and fibroblast-derived factors in melanocyte homeostasis, the response to UV, and pigmentary disorders. *Pigment Cell Melanoma Res* **2021**, *34*(4), 762-776, doi:10.1111/pcmr.12985.

13. Kauser, S.; Westgate, G.E.; Green, M.R.; Tobin, D.J. Human hair follicle and epidermal melanocytes exhibit striking differences in their aging profile which involves catalase. *J Invest Dermatol* **2011**, *131*(4), 979-982, doi:10.1038/jid.2010.397.

14. Bennett, D.C.; Medrano, E.E. Molecular regulation of melanocyte senescence. *Pigment Cell Res* **2002**, *15*(4), 242-250, doi:10.1034/j.1600-0749.2002.02036.x.

15. Hirobe, T. Role of keratinocyte-derived factors involved in regulating the proliferation and differentiation of mammalian epidermal melanocytes. *Pigment Cell Res* **2005**, *18*(1), 2-12, doi:10.1111/j.1600-0749.2004.00198.x.

16. Nordlund, J.J. The melanocyte and the epidermal melanin unit: an expanded concept. *Dermatol Clin* **2007**, *25*(3), 271-281, vii, doi:10.1016/j.det.2007.04.001.

17. Tadokoro, R.; Takahashi, Y. Intercellular transfer of organelles during body pigmentation. *Curr Opin Genet Dev* **2017**, *45*132-138, doi:10.1016/j.gde.2017.05.001.

18. Bertrand, J.U.; Steingrimsson, E.; Jouenne, F.; Bressac-de Paillerets, B.; Larue, L. Melanoma Risk and Melanocyte Biology. *Acta Derm Venereol* **2020**, *100*(11), adv00139, doi:10.2340/00015555-3494.

19. Fajuyigbe, D.; Young, A.R. The impact of skin colour on human photobiological responses. *Pigment Cell Melanoma Res* **2016**, *29*(6), 607-618, doi:10.1111/pcmr.12511.

20. Yamaguchi, Y.; Beer, J.Z.; Hearing, V.J. Melanin mediated apoptosis of epidermal cells damaged by ultraviolet radiation: factors influencing the incidence of skin cancer. *Arch Dermatol Res* **2008**, *300 Suppl 1*S43-50, doi:10.1007/s00403-007-0807-0.

21. Garcia-Borron, J.C.; Sanchez-Laorden, B.L.; Jimenez-Cervantes, C. Melanocortin-1 receptor structure and functional regulation. *Pigment Cell Res* **2005**, *18*(6), 393-410, doi:10.1111/j.1600-0749.2005.00278.x.

22. Nasti, T.H.; Timares, L. MC1R, eumelanin and pheomelanin: their role in determining the susceptibility to skin cancer. *Photochem Photobiol* **2015**, *91*(1), 188-200, doi:10.1111/php.12335.

23. Abdel-Malek, Z.A.; Kadekaro, A.L.; Swope, V.B. Stepping up melanocytes to the challenge of UV exposure. *Pigment Cell Melanoma Res* **2010**, *23*(2), 171-186, doi:10.1111/j.1755-148X.2010.00679.x.

24. Jin, S.G.; Padron, F.; Pfeifer, G.P. UVA Radiation, DNA Damage, and Melanoma. *ACS Omega* **2022**, *7*(37), 32936-32948, doi:10.1021/acsomega.2c04424.

25. Mitra, D.; Luo, X.; Morgan, A.; Wang, J.; Hoang, M.P.; Lo, J.; Guerrero, C.R.; Lennerz, J.K.; Mihm, M.C.; Wargo, J.A.; Robinson, K.C.; Devi, S.P.; Vanover, J.C.; D'Orazio, J.A.; McMahon, M.; Bosenberg, M.W.; Haigis, K.M.; Haber, D.A.; Wang, Y.; Fisher, D.E. An ultraviolet-radiation-independent pathway to melanoma carcinogenesis in the red hair/fair skin background. *Nature* **2012**, *491*(7424), 449-453, doi:10.1038/nature11624.

26. Napolitano, A.; Panzella, L.; Monfrecola, G.; d'Ischia, M. Pheomelanin-induced oxidative stress: bright and dark chemistry bridging red hair phenotype and melanoma. *Pigment Cell Melanoma Res* **2014**, *27*(5), 721-733, doi:10.1111/pcmr.12262.

27. Sommer, L. Generation of melanocytes from neural crest cells. *Pigment Cell Melanoma Res* **2011**, *24*(3), 411-421, doi:10.1111/j.1755-148X.2011.00834.x.

28. Tomellini, E.; Lagadec, C.; Polakowska, R.; Le Bourhis, X. Role of p75 neurotrophin receptor in stem cell biology: more than just a marker. *Cell Mol Life Sci* **2014**, *71*(13), 2467-2481, doi:10.1007/s00018-014-1564-9.

29. Gelmi, M.C.; Houtzagers, L.E.; Strub, T.; Krossa, I.; Jager, M.J. MITF in Normal Melanocytes, Cutaneous and Uveal Melanoma: A Delicate Balance. *Int J Mol Sci* **2022**, *23*(11), doi:10.3390/ijms23116001.

30. Gleason, B.C.; Crum, C.P.; Murphy, G.F. Expression patterns of MITF during human cutaneous embryogenesis: evidence for bulge epithelial expression and persistence of dermal melanoblasts. *J Cutan Pathol* **2008**, *35*(7), 615-622, doi:10.1111/j.1600-0560.2007.00881.x.

31. Li, L.; Fukunaga-Kalabis, M.; Yu, H.; Xu, X.; Kong, J.; Lee, J.T.; Herlyn, M. Human dermal stem cells differentiate into functional epidermal melanocytes. *J Cell Sci* **2010**, *123*(Pt 6), 853-860, doi:10.1242/jcs.061598.

32. Zabierowski, S.E.; Fukunaga-Kalabis, M.; Li, L.; Herlyn, M. Dermis-derived stem cells: a source of epidermal melanocytes and melanoma? *Pigment Cell Melanoma Res* **2011**, *24*(3), 422-429, doi:10.1111/j.1755-148X.2011.00847.x.

33. Mirea, M.A.; Eckensperger, S.; Hengstschlager, M.; Mikula, M. Insights into Differentiation of Melanocytes from Human Stem Cells and Their Relevance for Melanoma Treatment. *Cancers (Basel)* **2020**, *12*(9), doi:10.3390/cancers12092508.

34. Hou, L.; Pavan, W.J. Transcriptional and signaling regulation in neural crest stem cell-derived melanocyte development: do all roads lead to Mitf? *Cell Res* **2008**, *18*(12), 1163-1176, doi:10.1038/cr.2008.303.

35. Hocker, T.L.; Singh, M.K.; Tsao, H. Melanoma genetics and therapeutic approaches in the 21st century: moving from the benchside to the bedside. *J Invest Dermatol* **2008**, *128*(11), 2575-2595, doi:10.1038/jid.2008.226.

36. Ostrowski, S.M.; Fisher, D.E. Biology of Melanoma. *Hematol Oncol Clin North Am* **2021**, *35*(1), 29-56, doi:10.1016/j.hoc.2020.08.010.

37. Mort, R.L.; Jackson, I.J.; Patton, E.E. The melanocyte lineage in development and disease. *Development* **2015**, *142*(4), 620-632, doi:10.1242/dev.106567.

38. Reid, K.; Turnley, A.M.; Maxwell, G.D.; Kurihara, Y.; Kurihara, H.; Bartlett, P.F.; Murphy, M. Multiple roles for endothelin in melanocyte development: regulation of progenitor number and stimulation of differentiation. *Development* **1996**, *122*(12), 3911-3919, doi:10.1242/dev.122.12.3911.

39. Moriyama, M.; Osawa, M.; Mak, S.S.; Ohtsuka, T.; Yamamoto, N.; Han, H.; Delmas, V.; Kageyama, R.; Beermann, F.; Larue, L.; Nishikawa, S. Notch signaling via Hes1 transcription factor maintains survival of melanoblasts and melanocyte stem cells. *J Cell Biol* **2006**, *173*(3), 333-339, doi:10.1083/jcb.200509084.

40. Zabierowski, S.E.; Baubet, V.; Himes, B.; Li, L.; Fukunaga-Kalabis, M.; Patel, S.; McDaid, R.; Guerra, M.; Gimotty, P.; Dahmane, N.; Herlyn, M. Direct reprogramming of melanocytes to neural crest stem-like cells by one defined factor. *Stem Cells* **2011**, *29*(11), 1752-1762, doi:10.1002/stem.740.

41. Dorsky, R.I.; Moon, R.T.; Raible, D.W. Control of neural crest cell fate by the Wnt signalling pathway. *Nature* **1998**, *396*(6709), 370-373, doi:10.1038/24620.

42. Fukunaga-Kalabis, M.; Hristova, D.M.; Wang, J.X.; Li, L.; Heppt, M.V.; Wei, Z.; Gyurdieva, A.; Webster, M.R.; Oka, M.; Weeraratna, A.T.; Herlyn, M. UV-Induced Wnt7a in the Human Skin Microenvironment Specifies the Fate of Neural Crest-Like Cells via Suppression of Notch. *J Invest Dermatol* **2015**, *135*(6), 1521-1532, doi:10.1038/jid.2015.59.

43. Takeda, K.; Yasumoto, K.; Takada, R.; Takada, S.; Watanabe, K.; Udono, T.; Saito, H.; Takahashi, K.; Shibahara, S. Induction of melanocyte-specific microphthalmia-associated transcription factor by Wnt-3a. *J Biol Chem* **2000**, *275*(19), 14013-14016, doi:10.1074/jbc.c000113200.

44. Levy, C.; Khaled, M.; Fisher, D.E. MITF: master regulator of melanocyte development and melanoma oncogene. *Trends Mol Med* **2006**, *12*(9), 406-414, doi:10.1016/j.molmed.2006.07.008.

45. Timar, J.; Ladanyi, A. Molecular Pathology of Skin Melanoma: Epidemiology, Differential Diagnostics, Prognosis and Therapy Prediction. *Int J Mol Sci* **2022**, *23*(10), doi:10.3390/ijms23105384.

46. Levy, C.; Khaled, M.; Robinson, K.C.; Veguilla, R.A.; Chen, P.H.; Yokoyama, S.; Makino, E.; Lu, J.; Larue, L.; Beermann, F.; Chin, L.; Bosenberg, M.; Song, J.S.; Fisher, D.E. Lineage-specific transcriptional regulation of DICER by MITF in melanocytes. *Cell* **2010**, *141*(6), 994-1005, doi:10.1016/j.cell.2010.05.004.

47. Hirobe, T. How are proliferation and differentiation of melanocytes regulated? *Pigment Cell Melanoma Res* **2011**, *24*(3), 462-478, doi:10.1111/j.1755-148X.2011.00845.x.

48. Hirobe, T. Keratinocytes regulate the function of melanocytes. *Dermatologica Sinica* **2014**, *32*(4), 200-204, doi:10.1016/j.dsi.2014.05.002.

49. Wang, Y.; Viennet, C.; Robin, S.; Berthon, J.Y.; He, L.; Humbert, P. Precise role of dermal fibroblasts on melanocyte pigmentation. *J Dermatol Sci* **2017**, *88*(2), 159-166, doi:10.1016/j.jdermsci.2017.06.018.

50. Lo Cicero, A.; Delevoye, C.; Gilles-Marsens, F.; Loew, D.; Dingli, F.; Guere, C.; Andre, N.; Vie, K.; van Niel, G.; Raposo, G. Exosomes released by keratinocytes modulate melanocyte pigmentation. *Nat Commun* **2015**, *6*7506, doi:10.1038/ncomms8506.

51. Yamada, T.; Hasegawa, S.; Inoue, Y.; Date, Y.; Yamamoto, N.; Mizutani, H.; Nakata, S.; Matsunaga, K.; Akamatsu, H. Wnt/beta-catenin and kit signaling sequentially regulate melanocyte stem cell differentiation in UVB-induced epidermal pigmentation. *J Invest Dermatol* **2013**, *133*(12), 2753-2762, doi:10.1038/jid.2013.235.

52. Aoude, L.G.; Wadt, K.A.; Pritchard, A.L.; Hayward, N.K. Genetics of familial melanoma: 20 years after CDKN2A. *Pigment Cell Melanoma Res* **2015**, *28*(2), 148-160, doi:10.1111/pcmr.12333.

53. Korosec, A.; Frech, S.; Gesslbauer, B.; Vierhapper, M.; Radtke, C.; Petzelbauer, P.; Lichtenberger, B.M. Lineage Identity and Location within the Dermis Determine the Function of Papillary and Reticular Fibroblasts in Human Skin. *J Invest Dermatol* **2019**, *139*(2), 342-351, doi:10.1016/j.jid.2018.07.033.

54. Sorrell, J.M.; Caplan, A.I. Fibroblasts-a diverse population at the center of it all. *Int Rev Cell Mol Biol* **2009**, *276*161-214, doi:10.1016/S1937-6448(09)76004-6.

55. Bacakova, L.; Zarubova, J.; Travnickova, M.; Musilkova, J.; Pajorova, J.; Slepicka, P.; Kasalkova, N.S.; Svorcik, V.; Kolska, Z.; Motarjemi, H.; Molitor, M. Stem cells: their source, potency and use in regenerative therapies with focus on adipose-derived stem cells - a review. *Biotechnol Adv* **2018**, *36*(4), 1111-1126, doi:10.1016/j.biotechadv.2018.03.011.

56. Zakrzewski, W.; Dobrzynski, M.; Szymonowicz, M.; Rybak, Z. Stem cells: past, present, and future. *Stem Cell Res Ther* **2019**, *10*(1), 68, doi:10.1186/s13287-019-1165-5.

57. International Agency for Research on Cancer (IARC). *World Cancer Report: Cancer Research for Cancer Prevention.* Wild, C., Weiderpass, E., Stewart, B., Eds.; Lyon, France: International Agency for Research on Cancer, 2020. https://publications.iarc.fr/586

58. Boehnke, K.; Falkowska-Hansen, B.; Stark, H.J.; Boukamp, P. Stem cells of the human epidermis and their niche: composition and function in epidermal regeneration and carcinogenesis. *Carcinogenesis* **2012**, *33*(7), 1247-1258, doi:10.1093/carcin/bgs136.

59. Hsu, Y.C.; Fuchs, E. A family business: stem cell progeny join the niche to regulate homeostasis. *Nat Rev Mol Cell Biol* **2012**, *13*(2), 103-114, doi:10.1038/nrm3272.

60. Voog, J.; Jones, D.L. Stem cells and the niche: a dynamic duo. *Cell Stem Cell* **2010**, *6*(2), 103-115, doi:10.1016/j.stem.2010.01.011.

61. Hicks, M.R.; Pyle, A.D. The emergence of the stem cell niche. *Trends Cell Biol* **2023**, *33*(2), 112-123, doi:10.1016/j.tcb.2022.07.003.

62. Zouboulis, C.C.; Adjaye, J.; Akamatsu, H.; Moe-Behrens, G.; Niemann, C. Human skin stem cells and the ageing process. *Exp Gerontol* **2008**, *43*(11), 986-997, doi:10.1016/j.exger.2008.09.001.

63. Li, K.N.; Tumbar, T. Hair follicle stem cells as a skin-organizing signaling center during adult homeostasis. *EMBO J* **2021**, *40*(11), e107135, doi:10.15252/embj.2020107135.

64. Brunet, A.; Goodell, M.A.; Rando, T.A. Ageing and rejuvenation of tissue stem cells and their niches. *Nat Rev Mol Cell Biol* **2023**, *24*(1), 45-62, doi:10.1038/s41580-022-00510-w.

65. Rudolph, K.L. Stem cell aging. *Mech Ageing Dev* **2021**, *193*111394, doi:10.1016/j.mad.2020.111394.

66. Behrens, A.; van Deursen, J.M.; Rudolph, K.L.; Schumacher, B. Impact of genomic damage and ageing on stem cell function. *Nat Cell Biol* **2014**, *16*(3), 201-207, doi:10.1038/ncb2928.

67. Ge, Y.; Miao, Y.; Gur-Cohen, S.; Gomez, N.; Yang, H.; Nikolova, M.; Polak, L.; Hu, Y.; Verma, A.; Elemento, O.; Krueger, J.G.; Fuchs, E. The aging skin microenvironment dictates stem cell behavior. *Proc Natl Acad Sci U S A* **2020**, *117*(10), 5339-5350, doi:10.1073/pnas.1901720117.

68. Lopez-Otin, C.; Blasco, M.A.; Partridge, L.; Serrano, M.; Kroemer, G. The hallmarks of aging. *Cell* **2013**, *153*(6), 1194-1217, doi:10.1016/j.cell.2013.05.039.

69. Tower, J. Stress and stem cells. *Wiley Interdiscip Rev Dev Biol* **2012**, *1*(6), 789-802, doi:10.1002/wdev.56.

70. Inomata, K.; Aoto, T.; Binh, N.T.; Okamoto, N.; Tanimura, S.; Wakayama, T.; Iseki, S.; Hara, E.; Masunaga, T.; Shimizu, H.; Nishimura, E.K. Genotoxic stress abrogates renewal of melanocyte stem cells by triggering their differentiation. *Cell* **2009**, *137*(6), 1088-1099, doi:10.1016/j.cell.2009.03.037.

71. Takahashi, K.; Tanabe, K.; Ohnuki, M.; Narita, M.; Ichisaka, T.; Tomoda, K.; Yamanaka, S. Induction of pluripotent stem cells from adult human fibroblasts by defined factors. *Cell* **2007**, *131*(5), 861-872, doi:10.1016/j.cell.2007.11.019.

72. Yu, J.; Vodyanik, M.A.; Smuga-Otto, K.; Antosiewicz-Bourget, J.; Frane, J.L.; Tian, S.; Nie, J.; Jonsdottir, G.A.; Ruotti, V.; Stewart, R.; Slukvin, II; Thomson, J.A. Induced pluripotent stem cell lines derived from human somatic cells. *Science* **2007**, *318*(5858), 1917-1920, doi:10.1126/science.1151526.

73. Takahashi, K.; Yamanaka, S. Induced pluripotent stem cells in medicine and biology. *Development* **2013**, *140*(12), 2457-2461, doi:10.1242/dev.092551.

74. Yamashita, Y.M.; Yuan, H.; Cheng, J.; Hunt, A.J. Polarity in stem cell division: asymmetric stem cell division in tissue homeostasis. *Cold Spring Harb Perspect Biol* **2010**, *2*(1), a001313, doi:10.1101/cshperspect.a001313.

75. Bjornson, C.R.; Rietze, R.L.; Reynolds, B.A.; Magli, M.C.; Vescovi, A.L. Turning brain into blood: a hematopoietic fate adopted by adult neural stem cells in vivo. *Science* **1999**, *283*(5401), 534-537, doi:10.1126/science.283.5401.534.

76. Clarke, D.L.; Johansson, C.B.; Wilbertz, J.; Veress, B.; Nilsson, E.; Karlstrom, H.; Lendahl, U.; Frisen, J. Generalized potential of adult neural stem cells. *Science* **2000**, *288*(5471), 1660-1663, doi:10.1126/science.288.5471.1660.

77. Li, L.; Clevers, H. Coexistence of quiescent and active adult stem cells in mammals. *Science* **2010**, *327*(5965), 542-545, doi:10.1126/science.1180794.

78. Gurusamy, N.; Alsayari, A.; Rajasingh, S.; Rajasingh, J. Adult Stem Cells for Regenerative Therapy. *Prog Mol Biol Transl Sci* **2018**, *160*1-22, doi:10.1016/bs.pmbts.2018.07.009.

79. Trounson, A.; McDonald, C. Stem Cell Therapies in Clinical Trials: Progress and Challenges. *Cell Stem Cell* **2015**, *17*(1), 11-22, doi:10.1016/j.stem.2015.06.007.

80. Gonzales, K.A.U.; Fuchs, E. Skin and Its Regenerative Powers: An Alliance between Stem Cells and Their Niche. *Dev Cell* **2017**, *43*(4), 387-401, doi:10.1016/j.devcel.2017.10.001.

81. Schneider, T.E.; Barland, C.; Alex, A.M.; Mancianti, M.L.; Lu, Y.; Cleaver, J.E.; Lawrence, H.J.; Ghadially, R. Measuring stem cell frequency in epidermis: a quantitative in vivo functional assay for long-term repopulating cells. *Proc Natl Acad Sci U S A* **2003**, *100*(20), 11412-11417, doi:10.1073/pnas.2034935100.

82. Blanpain, C.; Fuchs, E. Epidermal stem cells of the skin. *Annu Rev Cell Dev Biol* **2006**, *22*339-373, doi:10.1146/annurev.cellbio.22.010305.104357.

83. Blanpain, C.; Lowry, W.E.; Geoghegan, A.; Polak, L.; Fuchs, E. Self-renewal, multipotency, and the existence of two cell populations within an epithelial stem cell niche. *Cell* **2004**, *118*(5), 635-648, doi:10.1016/j.cell.2004.08.012.

84. Ito, M.; Liu, Y.; Yang, Z.; Nguyen, J.; Liang, F.; Morris, R.J.; Cotsarelis, G. Stem cells in the hair follicle bulge contribute to wound repair but not to homeostasis of the epidermis. *Nat Med* **2005**, *11*(12), 1351-1354, doi:10.1038/nm1328.

85. Geueke, A.; Niemann, C. Stem and progenitor cells in sebaceous gland development, homeostasis and pathologies. *Exp Dermatol* **2021**, *30*(4), 588-597, doi:10.1111/exd.14303.

86. Brandenburger, M.; Kruse, C. Heterogeneity of Sweat Gland Stem Cells. *Adv Exp Med Biol* **2019**, *1169*55-62, doi:10.1007/978-3-030-24108-7_3.

87. Biedermann, T.; Pontiggia, L.; Bottcher-Haberzeth, S.; Tharakan, S.; Braziulis, E.; Schiestl, C.; Meuli, M.; Reichmann, E. Human eccrine sweat gland cells can reconstitute a stratified epidermis. *J Invest Dermatol* **2010**, *130*(8), 1996-2009, doi:10.1038/jid.2010.83.

88. Lu, C.P.; Polak, L.; Rocha, A.S.; Pasolli, H.A.; Chen, S.C.; Sharma, N.; Blanpain, C.; Fuchs, E. Identification of stem cell populations in sweat glands and ducts reveals roles in homeostasis and wound repair. *Cell* **2012**, *150*(1), 136-150, doi:10.1016/j.cell.2012.04.045.

89. Mazini, L.; Rochette, L.; Admou, B.; Amal, S.; Malka, G. Hopes and Limits of Adipose-Derived Stem Cells (ADSCs) and Mesenchymal Stem Cells (MSCs) in Wound Healing. *Int J Mol Sci* **2020**, *21*(4), doi:10.3390/ijms21041306.

90. Schmidt, B.A.; Horsley, V. Intradermal adipocytes mediate fibroblast recruitment during skin wound healing. *Development* **2013**, *140*(7), 1517-1527, doi:10.1242/dev.087593.

91. Chong, S.G.; Sato, S.; Kolb, M.; Gauldie, J. Fibrocytes and fibroblasts-Where are we now. *Int J Biochem Cell Biol* **2019**, *116*105595, doi:10.1016/j.biocel.2019.105595.

92. Ishida, Y.; Kimura, A.; Takayasu, T.; Eisenmenger, W.; Kondo, T. Detection of fibrocytes in human skin wounds and its application for wound age determination. *Int J Legal Med* **2009**, *123*(4), 299-304, doi:10.1007/s00414-009-0320-4.

93. Yu, H.; Fang, D.; Kumar, S.M.; Li, L.; Nguyen, T.K.; Acs, G.; Herlyn, M.; Xu, X. Isolation of a novel population of multipotent adult stem cells from human hair follicles. *Am J Pathol* **2006**, *168*(6), 1879-1888, doi:10.2353/ajpath.2006.051170.

94. Budi, E.H.; Patterson, L.B.; Parichy, D.M. Post-embryonic nerve-associated precursors to adult pigment cells: genetic requirements and dynamics of morphogenesis and differentiation. *PLoS Genet* **2011**, *7*(5), e1002044, doi:10.1371/journal.pgen.1002044.

95. Dupin, E.; Real, C.; Glavieux-Pardanaud, C.; Vaigot, P.; Le Douarin, N.M. Reversal of developmental restrictions in neural crest lineages: transition from Schwann cells to glial-melanocytic precursors in vitro. *Proc Natl Acad Sci U S A* **2003**, *100*(9), 5229-5233, doi:10.1073/pnas.0831229100.

96. Nichols, D.H.; Weston, J.A. Melanogenesis in cultures of peripheral nervous tissue. I. The origin and prospective fate of cells giving rise to melanocytes. *Dev Biol* **1977**, *60*(1), 217-225, doi:10.1016/0012-1606(77)90120-8.

97. Yu, H.; Kumar, S.M.; Kossenkov, A.V.; Showe, L.; Xu, X. Stem cells with neural crest characteristics derived from the bulge region of cultured human hair follicles. *J Invest Dermatol* **2010**, *130*(5), 1227-1236, doi:10.1038/jid.2009.322.

98. Davids, L.M.; du Toit, E.; Kidson, S.H.; Todd, G. A rare repigmentation pattern in a vitiligo patient: a clue to an epidermal stem-cell reservoir of melanocytes? *Clin Exp Dermatol* **2009**, *34*(2), 246-248, doi:10.1111/j.1365-2230.2008.02793.x.

99. Falabella, R. Vitiligo and the melanocyte reservoir. *Indian J Dermatol* **2009**, *54*(4), 313-318, doi:10.4103/0019-5154.57604.

100. Jo, S.K.; Lee, J.Y.; Lee, Y.; Kim, C.D.; Lee, J.H.; Lee, Y.H. Three Streams for the Mechanism of Hair Graying. *Ann Dermatol* **2018**, *30*(4), 397-401, doi:10.5021/ad.2018.30.4.397.

101. Nishimura, E.K.; Granter, S.R.; Fisher, D.E. Mechanisms of hair graying: incomplete melanocyte stem cell maintenance in the niche. *Science* **2005**, *307*(5710), 720-724, doi:10.1126/science.1099593.

102. Li, L.; Fukunaga-Kalabis, M.; Herlyn, M. The three-dimensional human skin reconstruct model: a tool to study normal skin and melanoma progression. *J Vis Exp* **2011**, (54), doi:10.3791/2937.

103. Zomer, H.D.; Trentin, A.G. Skin wound healing in humans and mice: Challenges in translational research. *J Dermatol Sci* **2018**, *90*(1), 3-12, doi:10.1016/j.jdermsci.2017.12.009.

104. Michalak-Micka, K.; Buchler, V.L.; Zapiorkowska-Blumer, N.; Biedermann, T.; Klar, A.S. Characterization of a melanocyte progenitor population in human interfollicular epidermis. *Cell Rep* **2022**, *38*(9), 110419, doi:10.1016/j.celrep.2022.110419.

105. Toma, J.G.; McKenzie, I.A.; Bagli, D.; Miller, F.D. Isolation and characterization of multipotent skin-derived precursors from human skin. *Stem Cells* **2005**, *23*(6), 727-737, doi:10.1634/stemcells.2004-0134.

106. Kumar, R.; Parsad, D.; Rani, S.; Bhardwaj, S.; Srivastav, N. Glabrous lesional stem cells differentiated into functional melanocytes: new hope for repigmentation. *J Eur Acad Dermatol Venereol* **2016**, *30*(9), 1555-1560, doi:10.1111/jdv.13686.

107. Wong, C.E.; Paratore, C.; Dours-Zimmermann, M.T.; Rochat, A.; Pietri, T.; Suter, U.; Zimmermann, D.R.; Dufour, S.; Thiery, J.P.; Meijer, D.; Beermann, F.; Barrandon, Y.; Sommer, L. Neural crest-derived cells with stem cell features can be traced back to multiple lineages in the adult skin. *J Cell Biol* **2006**, *175*(6), 1005-1015, doi:10.1083/jcb.200606062.

108. Joshi, C.V.; Enver, T. Plasticity revisited. *Curr Opin Cell Biol* **2002**, *14*(6), 749-755, doi:10.1016/s0955-0674(02)00392-7.

109. Toma, J.G.; Akhavan, M.; Fernandes, K.J.; Barnabe-Heider, F.; Sadikot, A.; Kaplan, D.R.; Miller, F.D. Isolation of multipotent adult stem cells from the dermis of mammalian skin. *Nat Cell Biol* **2001**, *3*(9), 778-784, doi:10.1038/ncb0901-778.

110. Bartsch, G.; Yoo, J.J.; De Coppi, P.; Siddiqui, M.M.; Schuch, G.; Pohl, H.G.; Fuhr, J.; Perin, L.; Soker, S.; Atala, A. Propagation, expansion, and multilineage differentiation of human somatic stem cells from dermal progenitors. *Stem Cells Dev* **2005**, *14*(3), 337-348, doi:10.1089/scd.2005.14.337.

111. Lorenz, K.; Sicker, M.; Schmelzer, E.; Rupf, T.; Salvetter, J.; Schulz-Siegmund, M.; Bader, A. Multilineage differentiation potential of human dermal skin-derived fibroblasts. *Exp Dermatol* **2008**, *17*(11), 925-932, doi:10.1111/j.1600-0625.2008.00724.x.

112. Lysy, P.A.; Smets, F.; Sibille, C.; Najimi, M.; Sokal, E.M. Human skin fibroblasts: From mesodermal to hepatocyte-like differentiation. *Hepatology* **2007**, *46*(5), 1574-1585, doi:10.1002/hep.21839.

113. Chen, F.G.; Zhang, W.J.; Bi, D.; Liu, W.; Wei, X.; Chen, F.F.; Zhu, L.; Cui, L.; Cao, Y. Clonal analysis of nestin(-) vimentin(+) multipotent fibroblasts isolated from human dermis. *J Cell Sci* **2007**, *120*(Pt 16), 2875-2883, doi:10.1242/jcs.03478.

114. Shih, D.T.; Lee, D.C.; Chen, S.C.; Tsai, R.Y.; Huang, C.T.; Tsai, C.C.; Shen, E.Y.; Chiu, W.T. Isolation and characterization of neurogenic mesenchymal stem cells in human scalp tissue. *Stem Cells* **2005**, *23*(7), 1012-1020, doi:10.1634/stemcells.2004-0125.

115. Sellheyer, K.; Krahl, D. Skin mesenchymal stem cells: prospects for clinical dermatology. *J Am Acad Dermatol* **2010**, *63*(5), 859-865, doi:10.1016/j.jaad.2009.09.022.

116. McKenzie, I.A.; Biernaskie, J.; Toma, J.G.; Midha, R.; Miller, F.D. Skin-derived precursors generate myelinating Schwann cells for the injured and dysmyelinated nervous system. *J Neurosci* **2006**, *26*(24), 6651-6660, doi:10.1523/JNEUROSCI.1007-06.2006.

117. Fernandes, K.J.; McKenzie, I.A.; Mill, P.; Smith, K.M.; Akhavan, M.; Barnabe-Heider, F.; Biernaskie, J.; Junek, A.; Kobayashi, N.R.; Toma, J.G.; Kaplan, D.R.; Labosky, P.A.; Rafuse, V.; Hui, C.C.; Miller, F.D. A dermal niche for multipotent adult skin-derived precursor cells. *Nat Cell Biol* **2004**, *6*(11), 1082-1093, doi:10.1038/ncb1181.

118. Biernaskie, J.A.; McKenzie, I.A.; Toma, J.G.; Miller, F.D. Isolation of skin-derived precursors (SKPs) and differentiation and enrichment of their Schwann cell progeny. *Nat Protoc* **2006**, *1*(6), 2803-2812, doi:10.1038/nprot.2006.422.

119. Fernandes, K.J.; Kobayashi, N.R.; Gallagher, C.J.; Barnabe-Heider, F.; Aumont, A.; Kaplan, D.R.; Miller, F.D. Analysis of the neurogenic potential of multipotent skin-derived precursors. *Exp Neurol* **2006**, *201*(1), 32-48, doi:10.1016/j.expneurol.2006.03.018.

120. Gingras, M.; Champigny, M.F.; Berthod, F. Differentiation of human adult skin-derived neuronal precursors into mature neurons. *J Cell Physiol* **2007**, *210*(2), 498-506, doi:10.1002/jcp.20889.

121. Jahoda, C.A.; Whitehouse, J.; Reynolds, A.J.; Hole, N. Hair follicle dermal cells differentiate into adipogenic and osteogenic lineages. *Exp Dermatol* **2003**, *12*(6), 849-859, doi:10.1111/j.0906-6705.2003.00161.x.

122. Richardson, G.D.; Arnott, E.C.; Whitehouse, C.J.; Lawrence, C.M.; Reynolds, A.J.; Hole, N.; Jahoda, C.A. Plasticity of rodent and human hair follicle dermal cells: implications for cell therapy and tissue engineering. *J Investig Dermatol Symp Proc* **2005**, *10*(3), 180-183, doi:10.1111/j.1087-0024.2005.10101.x.

123. Biernaskie, J.; Paris, M.; Morozova, O.; Fagan, B.M.; Marra, M.; Pevny, L.; Miller, F.D. SKPs derive from hair follicle precursors and exhibit properties of adult dermal stem cells. *Cell Stem Cell* **2009**, *5*(6), 610-623, doi:10.1016/j.stem.2009.10.019.

124. Hunt, D.P.; Morris, P.N.; Sterling, J.; Anderson, J.A.; Joannides, A.; Jahoda, C.; Compston, A.; Chandran, S. A highly enriched niche of precursor cells with neuronal and glial potential within the hair follicle dermal papilla of adult skin. *Stem Cells* **2008**, *26*(1), 163-172, doi:10.1634/stemcells.2007-0281.

125. Li, L.; Fukunaga-Kalabis, M.; Herlyn, M. Isolation and cultivation of dermal stem cells that differentiate into functional epidermal melanocytes. *Methods Mol Biol* **2012**, *806*15-29, doi:10.1007/978-1-61779-367-7_2.

126. Li, L.; Fukunaga-Kalabis, M.; Herlyn, M. Isolation, characterization, and differentiation of human multipotent dermal stem cells. *Methods Mol Biol* **2013**, *989*235-246, doi:10.1007/978-1-62703-330-5_18.

127. D'Orazio, J.; Jarrett, S.; Amaro-Ortiz, A.; Scott, T. UV radiation and the skin. *Int J Mol Sci* **2013**, *14*(6), 12222-12248, doi:10.3390/ijms140612222.

128. Strahlenschutzkommission (SSK). Schutz des Menschen vor den Gefahren solarer UV-Strahlung und UV-Strahlung in Solarien. Empfehlung Der Strahlenschutzkommission; Bonn: Strahlenschutzkommission, 2016, Available online: https://www.ssk.de/SharedDocs/Beratungsergebnisse/DE/2016/2016-02-11_Empf_UV-Schutz_KT.html (accessed on November 14, 2023).

129. El Ghissassi, F.; Baan, R.; Straif, K.; Grosse, Y.; Secretan, B.; Bouvard, V.; Benbrahim-Tallaa, L.; Guha, N.; Freeman, C.; Galichet, L.; Cogliano, V.; Group, W.H.O.I.A.f.R.o.C.M.W. A review of human carcinogens--part D: radiation. *Lancet Oncol* **2009**, *10*(8), 751-752, doi:10.1016/s1470-2045(09)70213-x.

130. Leiter, U.; Keim, U.; Garbe, C. Epidemiology of Skin Cancer: Update 2019. *Adv Exp Med Biol* **2020**, *1268*123-139, doi:10.1007/978-3-030-46227-7_6.

131. Bundesanstalt für Arbeitsschutz und Arbeitsmedizin. Ratgeber zur Gefährdungsbeurteilung. Handbuch für Arbeitsschutzfachleute; Dortmund: Bundesanstalt für Arbeitsschutz und Arbeitsmedizin, 2016, doi:10.21934/baua:fachbuch20160901, (accessed on September 5, 2023).

132. CIE / International Organization for Standardization. Erythema reference action spectrum and standard erythema dose. ISO/CIE 17166:1999, Vienna, Austria **1999**.

133. Greinert, R.; de Vries, E.; Erdmann, F.; Espina, C.; Auvinen, A.; Kesminiene, A.; Schuz, J. European Code against Cancer 4th Edition: Ultraviolet radiation and cancer. *Cancer Epidemiol* **2015**, *39 Suppl 1*S75-83, doi:10.1016/j.canep.2014.12.014.

134. International Agency for Research on Cancer (IARC). *IARC Monographs on the Evaluation of Carcinogenic Risks to Humans. Volume 100. A Review of Human Carcinogens. Part D: Radiation* WHO Press: Lyon, France, 2012. http://monographs.iarc.fr/ENG/Monographs/vol100D/mono100D.pdf

135. de Gruijl, F.R. UV adaptation: Pigmentation and protection against overexposure. *Exp Dermatol* **2017**, *26*(7), 557-562, doi:10.1111/exd.13332.

136. Modenese, A.; Korpinen, L.; Gobba, F. Solar Radiation Exposure and Outdoor Work: An Underestimated Occupational Risk. *Int J Environ Res Public Health* **2018**, *15*(10), doi:10.3390/ijerph15102063.

137. Tan, Y.; Wang, F.; Fan, G.; Zheng, Y.; Li, B.; Li, N.; Liu, Y.; Wang, X.; Liu, W.; Krutmann, J.; Zou, Y.; Wang, S. Identification of factors associated with minimal erythema dose variations in a large-scale population study of 22 146 subjects. *J Eur Acad Dermatol Venereol* **2020**, *34*(7), 1595-1600, doi:10.1111/jdv.16206.

138. Cadet, J.; Douki, T. Formation of UV-induced DNA damage contributing to skin cancer development. *Photochem Photobiol Sci* **2018**, *17*(12), 1816-1841, doi:10.1039/c7pp00395a.

139. Honigsmann, H. Erythema and pigmentation. *Photodermatol Photoimmunol Photomed* **2002**, *18*(2), 75-81, doi:10.1034/j.1600-0781.2002.180204.x.

140. Scientific Committee on Consumer Products (SCCP). Opinion on Biological effects of ultraviolet radiation relevant to health with particular reference to sunbeds for cosmetic purposes; European Commission, 2006, Available online: https://www.euroskin.eu/downloads/sccpsunbeds2006.pdf (accessed on September 5, 2023).

141. Pfeifer, G.P.; Besaratinia, A. UV wavelength-dependent DNA damage and human non-melanoma and melanoma skin cancer. *Photochem Photobiol Sci* **2012**, *11*(1), 90-97, doi:10.1039/c1pp05144j.

142. Lucas, R.M.; Ponsonby, A.L. Ultraviolet radiation and health: friend and foe. *Med J Aust* **2002**, *177*(11-12), 594-598, doi:10.5694/j.1326-5377.2002.tb04979.x.

143. Ortonne, J.P.; Schwarz, T. [Clinical aspects and pathogenesis of UV-induced pigmentary disorders]. *J Dtsch Dermatol Ges* **2003**, *1*(4), 274-284, doi:10.1046/j.1610-0387.2003.03002.x.

144. Strahlenschutzkommission (SSK). Dosis-Wirkungsbeziehung für den Zusammenhang von UV-Strahlung und Hautkrebs. Stellungnahme der Strahlenschutzkommission; Bonn: Strahlenschutzkommission, 2023, Available online: https://test39.gsb.itzbund.de/SharedDocs/Beratungsergebnisse/DE/2023/2023-02-03_Stg_Dosiswirkungsbeziehungen_UV.html (accessed on November 14, 2023).

145. Finlayson, L.; Barnard, I.R.M.; McMillan, L.; Ibbotson, S.H.; Brown, C.T.A.; Eadie, E.; Wood, K. Depth Penetration of Light into Skin as a Function of Wavelength from 200 to 1000 nm. *Photochem Photobiol* **2022**, *98*(4), 974-981, doi:10.1111/php.13550.

146. Austin, E.; Geisler, A.N.; Nguyen, J.; Kohli, I.; Hamzavi, I.; Lim, H.W.; Jagdeo, J. Visible light. Part I: Properties and cutaneous effects of visible light. *J Am Acad Dermatol* **2021**, *84*(5), 1219-1231, doi:10.1016/j.jaad.2021.02.048.

147. Horton, L.; Brady, J.; Kincaid, C.M.; Torres, A.E.; Lim, H.W. The effects of infrared radiation on the human skin. *Photodermatol Photoimmunol Photomed* **2023**, *39*(6), 549-555, doi:10.1111/phpp.12899.

148. Schroeder, P.; Haendeler, J.; Krutmann, J. The role of near infrared radiation in photoaging of the skin. *Exp Gerontol* **2008**, *43*(7), 629-632, doi:10.1016/j.exger.2008.04.010.

149. Bruls, W.A.; Slaper, H.; van der Leun, J.C.; Berrens, L. Transmission of human epidermis and stratum corneum as a function of thickness in the ultraviolet and visible wavelengths. *Photochem Photobiol* **1984**, *40*(4), 485-494, doi:10.1111/j.1751-1097.1984.tb04622.x.

150. Gonzalez Maglio, D.H.; Paz, M.L.; Leoni, J. Sunlight Effects on Immune System: Is There Something Else in addition to UV-Induced Immunosuppression? *Biomed Res Int* **2016**, *2016*1934518, doi:10.1155/2016/1934518.

151. Neale, R.E.; Lucas, R.M.; Byrne, S.N.; Hollestein, L.; Rhodes, L.E.; Yazar, S.; Young, A.R.; Berwick, M.; Ireland, R.A.; Olsen, C.M. The effects of exposure to solar radiation on human health. *Photochem Photobiol Sci* **2023**, *22*(5), 1011-1047, doi:10.1007/s43630-023-00375-8.

152. Courdavault, S.; Baudouin, C.; Charveron, M.; Canguilhem, B.; Favier, A.; Cadet, J.; Douki, T. Repair of the three main types of bipyrimidine DNA photoproducts in human keratinocytes exposed to UVB and UVA radiations. *DNA Repair (Amst)* **2005**, *4*(7), 836-844, doi:10.1016/j.dnarep.2005.05.001.

153. Weller, R.B.; Macintyre, I.M.; Melville, V.; Farrugia, M.; Feelisch, M.; Webb, D.J. The effect of daily UVA phototherapy for 2 weeks on clinic and 24-h blood pressure in individuals with mild hypertension. *J Hum Hypertens* **2023**, *37*(7), 548-553, doi:10.1038/s41371-022-00729-2.

154. Barros, N.M.; Sbroglio, L.L.; Buffara, M.O.; Baka, J.; Pessoa, A.S.; Azulay-Abulafia, L. Phototherapy. *An Bras Dermatol* **2021**, *96*(4), 397-407, doi:10.1016/j.abd.2021.03.001.

155. Vangipuram, R.; Feldman, S.R. Ultraviolet phototherapy for cutaneous diseases: a concise review. *Oral Dis* **2016**, *22*(4), 253-259, doi:10.1111/odi.12366.

156. Matsumura, Y.; Ananthaswamy, H.N. Toxic effects of ultraviolet radiation on the skin. *Toxicol Appl Pharmacol* **2004**, *195*(3), 298-308, doi:10.1016/j.taap.2003.08.019.

157. Jans, J.; Garinis, G.A.; Schul, W.; van Oudenaren, A.; Moorhouse, M.; Smid, M.; Sert, Y.G.; van der Velde, A.; Rijksen, Y.; de Gruijl, F.R.; van der Spek, P.J.; Yasui, A.; Hoeijmakers, J.H.; Leenen, P.J.; van der Horst, G.T. Differential role of basal keratinocytes in UV-induced immunosuppression and skin cancer. *Mol Cell Biol* **2006**, *26*(22), 8515-8526, doi:10.1128/MCB.00807-06.

158. Moriwaki, S. Human DNA repair disorders in dermatology: A historical perspective, current concepts and new insight. *J Dermatol Sci* **2016**, *81*(2), 77-84, doi:10.1016/j.jdermsci.2015.09.008.

159. Premi, S.; Wallisch, S.; Mano, C.M.; Weiner, A.B.; Bacchiocchi, A.; Wakamatsu, K.; Bechara, E.J.; Halaban, R.; Douki, T.; Brash, D.E. Photochemistry. Chemiexcitation of melanin derivatives induces DNA photoproducts long after UV exposure. *Science* **2015**, *347*(6224), 842-847, doi:10.1126/science.1256022.

160. Ichihashi, M.; Ueda, M.; Budiyanto, A.; Bito, T.; Oka, M.; Fukunaga, M.; Tsuru, K.; Horikawa, T. UV-induced skin damage. *Toxicology* **2003**, *189*(1-2), 21-39, doi:10.1016/s0300-483x(03)00150-1.

161. Mitchell, D.L.; Haipek, C.A.; Clarkson, J.M. (6-4)Photoproducts are removed from the DNA of UV-irradiated mammalian cells more efficiently than cyclobutane pyrimidine dimers. *Mutat Res* **1985**, *143*(3), 109-112, doi:10.1016/s0165-7992(85)80018-x.

162. You, Y.H.; Lee, D.H.; Yoon, J.H.; Nakajima, S.; Yasui, A.; Pfeifer, G.P. Cyclobutane pyrimidine dimers are responsible for the vast majority of mutations induced by UVB irradiation in mammalian cells. *J Biol Chem* **2001**, *276*(48), 44688-44694, doi:10.1074/jbc.M107696200.

163. Boros, G.; Miko, E.; Muramatsu, H.; Weissman, D.; Emri, E.; van der Horst, G.T.; Szegedi, A.; Horkay, I.; Emri, G.; Kariko, K.; Remenyik, E. Identification of Cyclobutane Pyrimidine Dimer-Responsive Genes Using UVB-Irradiated Human Keratinocytes Transfected with In Vitro-Synthesized Photolyase mRNA. *PLoS One* **2015**, *10*(6), e0131141, doi:10.1371/journal.pone.0131141.

164. Lo, H.L.; Nakajima, S.; Ma, L.; Walter, B.; Yasui, A.; Ethell, D.W.; Owen, L.B. Differential biologic effects of CPD and 6-4PP UV-induced DNA damage on the induction of apoptosis and cell-cycle arrest. *BMC Cancer* **2005**, *5*135, doi:10.1186/1471-2407-5-135.

165. Mouret, S.; Baudouin, C.; Charveron, M.; Favier, A.; Cadet, J.; Douki, T. Cyclobutane pyrimidine dimers are predominant DNA lesions in whole human skin exposed to UVA radiation. *Proc Natl Acad Sci U S A* **2006**, *103*(37), 13765-13770, doi:10.1073/pnas.0604213103.

166. Mouret, S.; Forestier, A.; Douki, T. The specificity of UVA-induced DNA damage in human melanocytes. *Photochem Photobiol Sci* **2012**, *11*(1), 155-162, doi:10.1039/c1pp05185g.

167. Courdavault, S.; Baudouin, C.; Charveron, M.; Favier, A.; Cadet, J.; Douki, T. Larger yield of cyclobutane dimers than 8-oxo-7,8-dihydroguanine in the DNA of UVA-irradiated human skin cells. *Mutat Res* **2004**, *556*(1-2), 135-142, doi:10.1016/j.mrfmmm.2004.07.011.

168. Cadet, J.; Mouret, S.; Ravanat, J.L.; Douki, T. Photoinduced damage to cellular DNA: direct and photosensitized reactions. *Photochem Photobiol* **2012**, *88*(5), 1048-1065, doi:10.1111/j.1751-1097.2012.01200.x.

169. Garcia-Nieto, P.E.; Schwartz, E.K.; King, D.A.; Paulsen, J.; Collas, P.; Herrera, R.E.; Morrison, A.J. Carcinogen susceptibility is regulated by genome architecture and predicts cancer mutagenesis. *EMBO J* **2017**, *36*(19), 2829-2843, doi:10.15252/embj.201796717.

170. Hauer, M.H.; Seeber, A.; Singh, V.; Thierry, R.; Sack, R.; Amitai, A.; Kryzhanovska, M.; Eglinger, J.; Holcman, D.; Owen-Hughes, T.; Gasser, S.M. Histone degradation in response to DNA damage enhances chromatin dynamics and recombination rates. *Nat Struct Mol Biol* **2017**, *24*(2), 99-107, doi:10.1038/nsmb.3347.

171. Pfeifer, G.P. Formation and processing of UV photoproducts: effects of DNA sequence and chromatin environment. *Photochem Photobiol* **1997**, *65*(2), 270-283, doi:10.1111/j.1751-1097.1997.tb08560.x.

172. Douki, T.; Cadet, J. Individual determination of the yield of the main UV-induced dimeric pyrimidine photoproducts in DNA suggests a high mutagenicity of CC photolesions. *Biochemistry* **2001**, *40*(8), 2495-2501, doi:10.1021/bi0022543.

173. Brash, D.E. UV signature mutations. *Photochem Photobiol* **2015**, *91*(1), 15-26, doi:10.1111/php.12377.

174. Mitchell, D.; Fernandez, A. The photobiology of melanocytes modulates the impact of UVA on sunlight-induced melanoma. *Photochem Photobiol Sci* **2012**, *11*(1), 69-73, doi:10.1039/c1pp05146f.

175. Jans, J.; Schul, W.; Sert, Y.G.; Rijksen, Y.; Rebel, H.; Eker, A.P.; Nakajima, S.; van Steeg, H.; de Gruijl, F.R.; Yasui, A.; Hoeijmakers, J.H.; van der Horst, G.T. Powerful skin cancer protection by a CPD-photolyase transgene. *Curr Biol* **2005**, *15*(2), 105-115, doi:10.1016/j.cub.2005.01.001.

176. Runger, T.M.; Farahvash, B.; Hatvani, Z.; Rees, A. Comparison of DNA damage responses following equimutagenic doses of UVA and UVB: a less effective cell cycle arrest with UVA may render UVA-induced pyrimidine dimers more mutagenic than UVB-induced ones. *Photochem Photobiol Sci* **2012**, *11*(1), 207-215, doi:10.1039/c1pp05232b.

177. Cadet, J.; Douki, T.; Ravanat, J.L.; Di Mascio, P. Sensitized formation of oxidatively generated damage to cellular DNA by UVA radiation. *Photochem Photobiol Sci* **2009**, *8*(7), 903-911, doi:10.1039/b905343n.

178. Greinert, R.; Volkmer, B.; Henning, S.; Breitbart, E.W.; Greulich, K.O.; Cardoso, M.C.; Rapp, A. UVA-induced DNA double-strand breaks result from the repair of clustered oxidative DNA damages. *Nucleic Acids Res* **2012**, *40*(20), 10263-10273, doi:10.1093/nar/gks824.

179. Wischermann, K.; Popp, S.; Moshir, S.; Scharfetter-Kochanek, K.; Wlaschek, M.; de Gruijl, F.; Hartschuh, W.; Greinert, R.; Volkmer, B.; Faust, A.; Rapp, A.; Schmezer, P.; Boukamp, P. UVA radiation causes DNA strand breaks, chromosomal aberrations and tumorigenic transformation in HaCaT skin keratinocytes. *Oncogene* **2008**, *27*(31), 4269-4280, doi:10.1038/onc.2008.70.

180. Wondrak, G.T.; Jacobson, M.K.; Jacobson, E.L. Endogenous UVA-photosensitizers: mediators of skin photodamage and novel targets for skin photoprotection. *Photochem Photobiol Sci* **2006**, *5*(2), 215-237, doi:10.1039/b504573h.

181. Vitale, I.; Manic, G.; De Maria, R.; Kroemer, G.; Galluzzi, L. DNA Damage in Stem Cells. *Mol Cell* **2017**, *66*(3), 306-319, doi:10.1016/j.molcel.2017.04.006.

182. Fortini, P.; Ferretti, C.; Dogliotti, E. The response to DNA damage during differentiation: pathways and consequences. *Mutat Res* **2013**, *743-744*160-168, doi:10.1016/j.mrfmmm.2013.03.004.

183. Sancar, A.; Lindsey-Boltz, L.A.; Unsal-Kacmaz, K.; Linn, S. Molecular mechanisms of mammalian DNA repair and the DNA damage checkpoints. *Annu Rev Biochem* **2004**, *73*39-85, doi:10.1146/annurev.biochem.73.011303.073723.

184. Farrell, A.W.; Halliday, G.M.; Lyons, J.G. Chromatin structure following UV-induced DNA damage-repair or death? *Int J Mol Sci* **2011**, *12*(11), 8063-8085, doi:10.3390/ijms12118063.

185. Polo, S.E.; Almouzni, G. Chromatin dynamics after DNA damage: The legacy of the access-repair-restore model. *DNA Repair (Amst)* **2015**, *36*114-121, doi:10.1016/j.dnarep.2015.09.014.

186. Lee, J.W.; Ratnakumar, K.; Hung, K.F.; Rokunohe, D.; Kawasumi, M. Deciphering UV-induced DNA Damage Responses to Prevent and Treat Skin Cancer. *Photochem Photobiol* **2020**, *96*(3), 478-499, doi:10.1111/php.13245.

187. Boucas, J.; Riabinska, A.; Jokic, M.; Herter-Sprie, G.S.; Chen, S.; Hopker, K.; Reinhardt, H.C. Posttranscriptional regulation of gene expression-adding another layer of complexity to the DNA damage response. *Front Genet* **2012**, *3*159, doi:10.3389/fgene.2012.00159.

188. Pothof, J.; Verkaik, N.S.; van, I.W.; Wiemer, E.A.; Ta, V.T.; van der Horst, G.T.; Jaspers, N.G.; van Gent, D.C.; Hoeijmakers, J.H.; Persengiev, S.P. MicroRNA-mediated gene silencing modulates the UV-induced DNA-damage response. *EMBO J* **2009**, *28*(14), 2090-2099, doi:10.1038/emboj.2009.156.

189. Syed, D.N.; Khan, M.I.; Shabbir, M.; Mukhtar, H. MicroRNAs in skin response to UV radiation. *Curr Drug Targets* **2013**, *14*(10), 1128-1134, doi:10.2174/13894501113149990184.

190. Mandal, P.K.; Blanpain, C.; Rossi, D.J. DNA damage response in adult stem cells: pathways and consequences. *Nat Rev Mol Cell Biol* **2011**, *12*(3), 198-202, doi:10.1038/nrm3060.

191. Latonen, L.; Laiho, M. Cellular UV damage responses--functions of tumor suppressor p53. *Biochim Biophys Acta* **2005**, *1755*(2), 71-89, doi:10.1016/j.bbcan.2005.04.003.

192. Saldivar, J.C.; Cortez, D.; Cimprich, K.A. The essential kinase ATR: ensuring faithful duplication of a challenging genome. *Nat Rev Mol Cell Biol* **2017**, *18*(10), 622-636, doi:10.1038/nrm.2017.67.

193. Pustisek, N.; Situm, M. UV-radiation, apoptosis and skin. *Coll Antropol* **2011**, *35 Suppl 2*339-341.

194. Moll, U.M.; Petrenko, O. The MDM2-p53 interaction. *Mol Cancer Res* **2003**, *1*(14), 1001-1008.

195. Blanpain, C.; Mohrin, M.; Sotiropoulou, P.A.; Passegue, E. DNA-damage response in tissue-specific and cancer stem cells. *Cell Stem Cell* **2011**, *8*(1), 16-29, doi:10.1016/j.stem.2010.12.012.

196. el-Deiry, W.S. Regulation of p53 downstream genes. *Semin Cancer Biol* **1998**, *8*(5), 345-357, doi:10.1006/scbi.1998.0097.

197. Friedel, L.; Loewer, A. The guardian's choice: how p53 enables context-specific decision-making in individual cells. *FEBS J* **2022**, *289*(1), 40-52, doi:10.1111/febs.15767.

198. Lee, D.; Kim, J.W.; Seo, T.; Hwang, S.G.; Choi, E.J.; Choe, J. SWI/SNF complex interacts with tumor suppressor p53 and is necessary for the activation of p53-mediated transcription. *J Biol Chem* **2002**, *277*(25), 22330-22337, doi:10.1074/jbc.M111987200.

199. Qin, H.; Yu, T.; Qing, T.; Liu, Y.; Zhao, Y.; Cai, J.; Li, J.; Song, Z.; Qu, X.; Zhou, P.; Wu, J.; Ding, M.; Deng, H. Regulation of apoptosis and differentiation by p53 in human embryonic stem cells. *J Biol Chem* **2007**, *282*(8), 5842-5852, doi:10.1074/jbc.M610464200.

200. Waster, P.K.; Ollinger, K.M. Redox-dependent translocation of p53 to mitochondria or nucleus in human melanocytes after UVA- and UVB-induced apoptosis. *J Invest Dermatol* **2009**, *129*(7), 1769-1781, doi:10.1038/jid.2008.421.

201. Rubbi, C.P.; Milner, J. p53 is a chromatin accessibility factor for nucleotide excision repair of DNA damage. *EMBO J* **2003**, *22*(4), 975-986, doi:10.1093/emboj/cdg082.

202. Hermeking, H. p53 enters the microRNA world. *Cancer Cell* **2007**, *12*(5), 414-418, doi:10.1016/j.ccr.2007.10.028.

203. Stewart-Ornstein, J.; Lahav, G. p53 dynamics in response to DNA damage vary across cell lines and are shaped by efficiency of DNA repair and activity of the kinase ATM. *Sci Signal* **2017**, *10*(476), doi:10.1126/scisignal.aah6671.

204. Hafner, A.; Bulyk, M.L.; Jambhekar, A.; Lahav, G. The multiple mechanisms that regulate p53 activity and cell fate. *Nat Rev Mol Cell Biol* **2019**, *20*(4), 199-210, doi:10.1038/s41580-019-0110-x.

205. Bartek, J.; Lukas, J. Mammalian G1- and S-phase checkpoints in response to DNA damage. *Curr Opin Cell Biol* **2001**, *13*(6), 738-747, doi:10.1016/s0955-0674(00)00280-5.

206. Agami, R.; Bernards, R. Distinct initiation and maintenance mechanisms cooperate to induce G1 cell cycle arrest in response to DNA damage. *Cell* **2000**, *102*(1), 55-66, doi:10.1016/s0092-8674(00)00010-6.

207. Adimoolam, S.; Ford, J.M. p53 and DNA damage-inducible expression of the xeroderma pigmentosum group C gene. *Proc Natl Acad Sci U S A* **2002**, *99*(20), 12985-12990, doi:10.1073/pnas.202485699.

208. Ford, J.M. Regulation of DNA damage recognition and nucleotide excision repair: another role for p53. *Mutat Res* **2005**, *577*(1-2), 195-202, doi:10.1016/j.mrfmmm.2005.04.005.

209. Weeden, C.E.; Asselin-Labat, M.L. Mechanisms of DNA damage repair in adult stem cells and implications for cancer formation. *Biochim Biophys Acta Mol Basis Dis* **2018**, *1864*(1), 89-101, doi:10.1016/j.bbadis.2017.10.015.

210. Berardesca, E.; Bertona, M.; Altabas, K.; Altabas, V.; Emanuele, E. Reduced ultraviolet-induced DNA damage and apoptosis in human skin with topical application of a photolyase-containing DNA repair enzyme cream: clues to skin cancer prevention. *Mol Med Rep* **2012**, *5*(2), 570-574, doi:10.3892/mmr.2011.673.

211. Nouspikel, T. DNA repair in mammalian cells : Nucleotide excision repair: variations on versatility. *Cell Mol Life Sci* **2009**, *66*(6), 994-1009, doi:10.1007/s00018-009-8737-y.

212. Adar, S.; Hu, J.; Lieb, J.D.; Sancar, A. Genome-wide kinetics of DNA excision repair in relation to chromatin state and mutagenesis. *Proc Natl Acad Sci U S A* **2016**, *113*(15), E2124-2133, doi:10.1073/pnas.1603388113.

213. Nouspikel, T.P.; Hyka-Nouspikel, N.; Hanawalt, P.C. Transcription domain-associated repair in human cells. *Mol Cell Biol* **2006**, *26*(23), 8722-8730, doi:10.1128/MCB.01263-06.

214. Scharer, O.D. Nucleotide excision repair in eukaryotes. *Cold Spring Harb Perspect Biol* **2013**, *5*(10), a012609, doi:10.1101/cshperspect.a012609.

215. Chang, D.J.; Cimprich, K.A. DNA damage tolerance: when it's OK to make mistakes. *Nat Chem Biol* **2009**, *5*(2), 82-90, doi:10.1038/nchembio.139.

216. Lehmann, A.R.; McGibbon, D.; Stefanini, M. Xeroderma pigmentosum. *Orphanet J Rare Dis* **2011**, *6*70, doi:10.1186/1750-1172-6-70.

217. Bradford, P.T.; Goldstein, A.M.; Tamura, D.; Khan, S.G.; Ueda, T.; Boyle, J.; Oh, K.S.; Imoto, K.; Inui, H.; Moriwaki, S.; Emmert, S.; Pike, K.M.; Raziuddin, A.; Plona, T.M.; DiGiovanna, J.J.; Tucker, M.A.; Kraemer, K.H. Cancer and neurologic degeneration in xeroderma pigmentosum: long term follow-up characterises the role of DNA repair. *J Med Genet* **2011**, *48*(3), 168-176, doi:10.1136/jmg.2010.083022.

218. DiGiovanna, J.J.; Kraemer, K.H. Shining a light on xeroderma pigmentosum. *J Invest Dermatol* **2012**, *132*(3 Pt 2), 785-796, doi:10.1038/jid.2011.426.

219. Black, J.O. Xeroderma Pigmentosum. *Head Neck Pathol* **2016**, *10*(2), 139-144, doi:10.1007/s12105-016-0707-8.

220. Maynard, S.; Schurman, S.H.; Harboe, C.; de Souza-Pinto, N.C.; Bohr, V.A. Base excision repair of oxidative DNA damage and association with cancer and aging. *Carcinogenesis* **2009**, *30*(1), 2-10, doi:10.1093/carcin/bgn250.

221. Robertson, A.B.; Klungland, A.; Rognes, T.; Leiros, I. DNA repair in mammalian cells: Base excision repair: the long and short of it. *Cell Mol Life Sci* **2009**, *66*(6), 981-993, doi:10.1007/s00018-009-8736-z.

222. Kulms, D.; Schwarz, T. Molecular mechanisms of UV-induced apoptosis. *Photodermatol Photoimmunol Photomed* **2000**, *16*(5), 195-201, doi:10.1034/j.1600-0781.2000.160501.x.

223. Noonan, F.P.; De Fabo, E.C. UVB and UVA initiate different pathways to p53-dependent apoptosis in melanocytes. *J Invest Dermatol* **2009**, *129*(7), 1608-1610, doi:10.1038/jid.2009.116.

224. Wan, G.; Mathur, R.; Hu, X.; Zhang, X.; Lu, X. miRNA response to DNA damage. *Trends Biochem Sci* **2011**, *36*(9), 478-484, doi:10.1016/j.tibs.2011.06.002.

225. Zhang, L.; Lu, Q.; Chang, C. Epigenetics in Health and Disease. *Adv Exp Med Biol* **2020**, *1253*3-55, doi:10.1007/978-981-15-3449-2_1.

226. Portela, A.; Esteller, M. Epigenetic modifications and human disease. *Nat Biotechnol* **2010**, *28*(10), 1057-1068, doi:10.1038/nbt.1685.

227. Schick, S.; Fournier, D.; Thakurela, S.; Sahu, S.K.; Garding, A.; Tiwari, V.K. Dynamics of chromatin accessibility and epigenetic state in response to UV damage. *J Cell Sci* **2015**, *128*(23), 4380-4394, doi:10.1242/jcs.173633.

228. Palomera-Sanchez, Z.; Zurita, M. Open, repair and close again: chromatin dynamics and the response to UV-induced DNA damage. *DNA Repair (Amst)* **2011**, *10*(2), 119-125, doi:10.1016/j.dnarep.2010.10.010.

229. Fullgrabe, J.; Hajji, N.; Joseph, B. Cracking the death code: apoptosis-related histone modifications. *Cell Death Differ* **2010**, *17*(8), 1238-1243, doi:10.1038/cdd.2010.58.

230. Altaf, M.; Saksouk, N.; Cote, J. Histone modifications in response to DNA damage. *Mutat Res* **2007**, *618*(1-2), 81-90, doi:10.1016/j.mrfmmm.2006.09.009.

231. Sand, M.; Gambichler, T.; Sand, D.; Skrygan, M.; Altmeyer, P.; Bechara, F.G. MicroRNAs and the skin: tiny players in the body's largest organ. *J Dermatol Sci* **2009**, *53*(3), 169-175, doi:10.1016/j.jdermsci.2008.10.004.

232. Morales, S.; Monzo, M.; Navarro, A. Epigenetic regulation mechanisms of microRNA expression. *Biomol Concepts* **2017**, *8*(5-6), 203-212, doi:10.1515/bmc-2017-0024.

233. Natarajan, V. Regulation of DNA repair by non-coding miRNAs. *Noncoding RNA Res* **2016**, *1*(1), 64-68, doi:10.1016/j.ncrna.2016.10.002.

234. Thyagarajan, A.; Tsai, K.Y.; Sahu, R.P. MicroRNA heterogeneity in melanoma progression. *Semin Cancer Biol* **2019**, *59*208-220, doi:10.1016/j.semcancer.2019.05.021.

235. Poniewierska-Baran, A.; Sluczanowska-Glabowska, S.; Malkowska, P.; Sierawska, O.; Zadroga, L.; Pawlik, A.; Niedzwiedzka-Rystwej, P. Role of miRNA in Melanoma Development and Progression. *Int J Mol Sci* **2022**, *24*(1), doi:10.3390/ijms24010201.

236. Suzuki, H.I.; Yamagata, K.; Sugimoto, K.; Iwamoto, T.; Kato, S.; Miyazono, K. Modulation of microRNA processing by p53. *Nature* **2009**, *460*(7254), 529-533, doi:10.1038/nature08199.

237. Hu, H.; Gatti, R.A. MicroRNAs: new players in the DNA damage response. *J Mol Cell Biol* **2011**, *3*(3), 151-158, doi:10.1093/jmcb/mjq042.

238. Gentile, M.; Latonen, L.; Laiho, M. Cell cycle arrest and apoptosis provoked by UV radiation-induced DNA damage are transcriptionally highly divergent responses. *Nucleic Acids Res* **2003**, *31*(16), 4779-4790, doi:10.1093/nar/gkg675.

239. Nieto Moreno, N.; Olthof, A.M.; Svejstrup, J.Q. Transcription-Coupled Nucleotide Excision Repair and the Transcriptional Response to UV-Induced DNA Damage. *Annu Rev Biochem* **2023**, *92*81-113, doi:10.1146/annurev-biochem-052621-091205.

240. Chang, T.C.; Wentzel, E.A.; Kent, O.A.; Ramachandran, K.; Mullendore, M.; Lee, K.H.; Feldmann, G.; Yamakuchi, M.; Ferlito, M.; Lowenstein, C.J.; Arking, D.E.; Beer, M.A.; Maitra, A.; Mendell, J.T. Transactivation of miR-34a by p53 broadly influences gene expression and promotes apoptosis. *Mol Cell* **2007**, *26*(5), 745-752, doi:10.1016/j.molcel.2007.05.010.

241. Georges, S.A.; Biery, M.C.; Kim, S.Y.; Schelter, J.M.; Guo, J.; Chang, A.N.; Jackson, A.L.; Carleton, M.O.; Linsley, P.S.; Cleary, M.A.; Chau, B.N. Coordinated regulation of cell cycle transcripts by p53-Inducible microRNAs, miR-192 and miR-215. *Cancer Res* **2008**, *68*(24), 10105-10112, doi:10.1158/0008-5472.CAN-08-1846.

242. Olejniczak, M.; Kotowska-Zimmer, A.; Krzyzosiak, W. Stress-induced changes in miRNA biogenesis and functioning. *Cell Mol Life Sci* **2018**, *75*(2), 177-191, doi:10.1007/s00018-017-2591-0.

243. Issler, M.V.C.; Mombach, J.C.M. MicroRNA-16 feedback loop with p53 and Wip1 can regulate cell fate determination between apoptosis and senescence in DNA damage response. *PLoS One* **2017**, *12*(10), e0185794, doi:10.1371/journal.pone.0185794.

244. Sachdeva, M.; Zhu, S.; Wu, F.; Wu, H.; Walia, V.; Kumar, S.; Elble, R.; Watabe, K.; Mo, Y.Y. p53 represses c-Myc through induction of the tumor suppressor miR-145. *Proc Natl Acad Sci U S A* **2009**, *106*(9), 3207-3212, doi:10.1073/pnas.0808042106.

245. Boominathan, L. The tumor suppressors p53, p63, and p73 are regulators of microRNA processing complex. *PLoS One* **2010**, *5*(5), e10615, doi:10.1371/journal.pone.0010615.

246. Le, M.T.; Teh, C.; Shyh-Chang, N.; Xie, H.; Zhou, B.; Korzh, V.; Lodish, H.F.; Lim, B. MicroRNA-125b is a novel negative regulator of p53. *Genes Dev* **2009**, *23*(7), 862-876, doi:10.1101/gad.1767609.

247. Ivanovska, I.; Ball, A.S.; Diaz, R.L.; Magnus, J.F.; Kibukawa, M.; Schelter, J.M.; Kobayashi, S.V.; Lim, L.; Burchard, J.; Jackson, A.L.; Linsley, P.S.; Cleary, M.A. MicroRNAs in the miR-106b family regulate p21/CDKN1A and promote cell cycle progression. *Mol Cell Biol* **2008**, *28*(7), 2167-2174, doi:10.1128/MCB.01977-07.

248. Dolezalova, D.; Mraz, M.; Barta, T.; Plevova, K.; Vinarsky, V.; Holubcova, Z.; Jaros, J.; Dvorak, P.; Pospisilova, S.; Hampl, A. MicroRNAs regulate p21(Waf1/Cip1) protein expression and the DNA damage response in human embryonic stem cells. *Stem Cells* **2012**, *30*(7), 1362-1372, doi:10.1002/stem.1108.

249. Wang, Y.; Baskerville, S.; Shenoy, A.; Babiarz, J.E.; Baehner, L.; Blelloch, R. Embryonic stem cell-specific microRNAs regulate the G1-S transition and promote rapid proliferation. *Nat Genet* **2008**, *40*(12), 1478-1483, doi:10.1038/ng.250.

250. Wang, P.; Zou, F.; Zhang, X.; Li, H.; Dulak, A.; Tomko, R.J., Jr.; Lazo, J.S.; Wang, Z.; Zhang, L.; Yu, J. microRNA-21 negatively regulates Cdc25A and cell cycle progression in colon cancer cells. *Cancer Res* **2009**, *69*(20), 8157-8165, doi:10.1158/0008-5472.CAN-09-1996.

251. Xie, Q.H.; He, X.X.; Chang, Y.; Sun, S.Z.; Jiang, X.; Li, P.Y.; Lin, J.S. MiR-192 inhibits nucleotide excision repair by targeting ERCC3 and ERCC4 in HepG2.2.15 cells. *Biochem Biophys Res Commun* **2011**, *410*(3), 440-445, doi:10.1016/j.bbrc.2011.05.153.

252. Crosby, M.E.; Kulshreshtha, R.; Ivan, M.; Glazer, P.M. MicroRNA regulation of DNA repair gene expression in hypoxic stress. *Cancer Res* **2009**, *69*(3), 1221-1229, doi:10.1158/0008-5472.CAN-08-2516.

253. Arnold, M.; Singh, D.; Laversanne, M.; Vignat, J.; Vaccarella, S.; Meheus, F.; Cust, A.E.; de Vries, E.; Whiteman, D.C.; Bray, F. Global Burden of Cutaneous Melanoma in 2020 and Projections to 2040. *JAMA Dermatol* **2022**, *158*(5), 495-503, doi:10.1001/jamadermatol.2022.0160.

254. Katalinic, A. Update - Prognose und Zahlen zu Hautkrebs in Deutschland; Krebsregisters Schleswig-Holstein, 2023, Available online: https://www.krebsregister-sh.de/wp-content/uploads/2023/04/Zahlen_Hautkrebs_2023.pdf (accessed on October 16, 2023).

255. Nishisgori, C. Current concept of photocarcinogenesis. *Photochem Photobiol Sci* **2015**, *14*(9), 1713-1721, doi:10.1039/c5pp00185d.

256. Armstrong, B.K.; Kricker, A. The epidemiology of UV induced skin cancer. *J Photochem Photobiol B* **2001**, *63*(1-3), 8-18, doi:10.1016/s1011-1344(01)00198-1.

257. Karagas, M.R.; McDonald, J.A.; Greenberg, E.R.; Stukel, T.A.; Weiss, J.E.; Baron, J.A.; Stevens, M.M. Risk of basal cell and squamous cell skin cancers after ionizing radiation therapy. For The Skin Cancer Prevention Study Group. *J Natl Cancer Inst* **1996**, *88*(24), 1848-1853, doi:10.1093/jnci/88.24.1848.

258. Arnold, M.; de Vries, E.; Whiteman, D.C.; Jemal, A.; Bray, F.; Parkin, D.M.; Soerjomataram, I. Global burden of cutaneous melanoma attributable to ultraviolet radiation in 2012. *Int J Cancer* **2018**, *143*(6), 1305-1314, doi:10.1002/ijc.31527.

259. Keim, U.; Gandini, S.; Amaral, T.; Katalinic, A.; Holleczek, B.; Flatz, L.; Leiter, U.; Whiteman, D.; Garbe, C. Cutaneous melanoma attributable to UVR exposure in Denmark and Germany. *Eur J Cancer* **2021**, *159*98-104, doi:10.1016/j.ejca.2021.09.044.

260. Piskin, G.; Bos, J.D.; Teunissen, M.B. Neutrophils infiltrating ultraviolet B-irradiated normal human skin display high IL-10 expression. *Arch Dermatol Res* **2005**, *296*(7), 339-342, doi:10.1007/s00403-004-0522-z.

261. Schrom, K.P.; Kim, I.; Baron, E.D. The Immune System and Pathogenesis of Melanoma and Non-melanoma Skin Cancer. *Adv Exp Med Biol* **2020**, *1268*211-226, doi:10.1007/978-3-030-46227-7_11.

262. Hodis, E.; Watson, I.R.; Kryukov, G.V.; Arold, S.T.; Imielinski, M.; Theurillat, J.P.; Nickerson, E.; Auclair, D.; Li, L.; Place, C.; Dicara, D.; Ramos, A.H.; Lawrence, M.S.; Cibulskis, K.; Sivachenko, A.; Voet, D.; Saksena, G.; Stransky, N.; Onofrio, R.C.; Winckler, W.; et al. A landscape of driver mutations in melanoma. *Cell* **2012**, *150*(2), 251-263, doi:10.1016/j.cell.2012.06.024.

263. Pleasance, E.D.; Cheetham, R.K.; Stephens, P.J.; McBride, D.J.; Humphray, S.J.; Greenman, C.D.; Varela, I.; Lin, M.L.; Ordonez, G.R.; Bignell, G.R.; Ye, K.; Alipaz, J.; Bauer, M.J.; Beare, D.; Butler, A.; Carter, R.J.; Chen, L.; Cox, A.J.; Edkins, S.; Kokko-Gonzales, P.I.; et al. A comprehensive catalogue of somatic mutations from a human cancer genome. *Nature* **2010**, *463*(7278), 191-196, doi:10.1038/nature08658.

264. Boukamp, P. UV-induced skin cancer: similarities--variations. *J Dtsch Dermatol Ges* **2005**, *3*(7), 493-503, doi:10.1111/j.1610-0387.2005.05037.x.

265. Cheng, J.B.; Cho, R.J. Genetics and epigenetics of the skin meet deep sequence. *J Invest Dermatol* **2012**, *132*(3 Pt 2), 923-932, doi:10.1038/jid.2011.436.

266. Sung, H.; Ferlay, J.; Siegel, R.L.; Laversanne, M.; Soerjomataram, I.; Jemal, A.; Bray, F. Global Cancer Statistics 2020: GLOBOCAN Estimates of Incidence and Mortality Worldwide for 36 Cancers in 185 Countries. *CA Cancer J Clin* **2021**, *71*(3), 209-249, doi:10.3322/caac.21660.

267. Global Cancer Observatory, owned by the World Health Organization/International Agency for Research on Cancer. Cancer Today. 2020. Available online: https://gco.iarc.fr/today/online-analysis-table (accessed on October 10, 2023).

268. World Cancer Research Fund International. Skin cancer statistics. 2022. Available online: https://www.wcrf.org/cancer-trends/skin-cancer-statistics/ (accessed on October 10, 2023).

269. World Health Organization. Radiation: Ultraviolet (UV) radiation and skin cancer. How common is skin cancer? 2017. Available online: https://www.who.int/news-room/questions-and-answers/item/radiation-ultraviolet-(uv)-radiation-and-skin-cancer (accessed on October 13, 2023).

270. Global Burden of Disease 2019 Cancer Collaboration; Kocarnik, J.M.; Compton, K.; Dean, F.E.; Fu, W.; Gaw, B.L.; Harvey, J.D.; Henrikson, H.J.; Lu, D.; Pennini, A.; Xu, R.; Ababneh, E.; Abbasi-Kangevari, M.; Abbastabar, H.; Abd-Elsalam, S.M.; Abdoli, A.; Abedi, A.; Abidi, H.; Abolhassani, H.; Adedeji, I.A.; et al. Cancer Incidence, Mortality, Years of Life Lost, Years Lived With Disability, and Disability-Adjusted Life Years for 29 Cancer Groups From 2010 to 2019: A Systematic Analysis for the Global Burden of Disease Study 2019. *JAMA Oncol* **2022**, *8*(3), 420-444, doi:10.1001/jamaoncol.2021.6987.

271. Carvajal, R.; Maniar, R. Extracutaneous Melanoma. *Hematol Oncol Clin North Am* **2021**, *35*(1), 85-98, doi:10.1016/j.hoc.2020.09.004.

272. Siegel, R.L.; Miller, K.D.; Wagle, N.S.; Jemal, A. Cancer statistics, 2023. *CA Cancer J Clin* **2023**, *73*(1), 17-48, doi:10.3322/caac.21763.

273. Karimkhani, C.; Green, A.C.; Nijsten, T.; Weinstock, M.A.; Dellavalle, R.P.; Naghavi, M.; Fitzmaurice, C. The global burden of melanoma: results from the Global Burden of Disease Study 2015. *Br J Dermatol* **2017**, *177*(1), 134-140, doi:10.1111/bjd.15510.

274. American Cancer Society. Cancer Facts & Figures 2023; Atlanta: American Cancer Society, 2023, Available online: https://www.cancer.org/content/dam/cancer-org/research/cancer-facts-and-statistics/annual-cancer-facts-and-figures/2023/2023-cancer-facts-and-figures.pdf (accessed on October 16, 2023).

275. Weinstock, M.A. Death from skin cancer among the elderly: epidemiological patterns. *Arch Dermatol* **1997**, *133*(10), 1207-1209.

276. American Cancer Society. Cancer Facts & Figures 2020; Atlanta: American Cancer Society, 2020, Available online: https://www.cancer.org/content/dam/cancer-org/research/cancer-facts-and-statistics/annual-cancer-facts-and-figures/2020/cancer-facts-and-figures-2020.pdf (accessed on October 16, 2023).

277. Gandini, S.; Sera, F.; Cattaruzza, M.S.; Pasquini, P.; Abeni, D.; Boyle, P.; Melchi, C.F. Meta-analysis of risk factors for cutaneous melanoma: I. Common and atypical naevi. *Eur J Cancer* **2005**, *41*(1), 28-44, doi:10.1016/j.ejca.2004.10.015.

278. Saginala, K.; Barsouk, A.; Aluru, J.S.; Rawla, P.; Barsouk, A. Epidemiology of Melanoma. *Med Sci (Basel)* **2021**, *9*(4), doi:10.3390/medsci9040063.

279. Zob, D.L.; Augustin, I.; Caba, L.; Panzaru, M.C.; Popa, S.; Popa, A.D.; Florea, L.; Gorduza, E.V. Genomics and Epigenomics in the Molecular Biology of Melanoma-A Prerequisite for Biomarkers Studies. *Int J Mol Sci* **2022**, *24*(1), doi:10.3390/ijms24010716.

280. Laskar, R.; Ferreiro-Iglesias, A.; Bishop, D.T.; Iles, M.M.; Kanetsky, P.A.; Armstrong, B.K.; Law, M.H.; Goldstein, A.M.; Aitken, J.F.; Giles, G.G.; Australian Melanoma Family Study Investigators; Leeds Case-Control Study Investigators; Robbins, H.A.; Cust, A.E. Risk factors for melanoma by anatomical site: an evaluation of aetiological heterogeneity. *Br J Dermatol* **2021**, *184*(6), 1085-1093, doi:10.1111/bjd.19705.

281. Schatton, T.; Frank, M.H. Cancer stem cells and human malignant melanoma. *Pigment Cell Melanoma Res* **2008**, *21*(1), 39-55, doi:10.1111/j.1755-148X.2007.00427.x.

282. Greinert, R.; Boguhn, O.; Harder, D.; Breitbart, E.W.; Mitchell, D.L.; Volkmer, B. The dose dependence of cyclobutane dimer induction and repair in UVB-irradiated human keratinocytes. *Photochem Photobiol* **2000**, *72*(5), 701-708, doi:10.1562/0031-8655(2000)072<0701:tddocd>2.0.co;2.

283. Conde-Perez, A.; Gros, G.; Longvert, C.; Pedersen, M.; Petit, V.; Aktary, Z.; Viros, A.; Gesbert, F.; Delmas, V.; Rambow, F.; Bastian, B.C.; Campbell, A.D.; Colombo, S.; Puig, I.; Bellacosa, A.; Sansom, O.; Marais, R.; Van Kempen, L.C.; Larue, L. A caveolin-dependent and PI3K/AKT-independent role of PTEN in beta-catenin transcriptional activity. *Nat Commun* **2015**, *6*8093, doi:10.1038/ncomms9093.

284. Delmas, V.; Beermann, F.; Martinozzi, S.; Carreira, S.; Ackermann, J.; Kumasaka, M.; Denat, L.; Goodall, J.; Luciani, F.; Viros, A.; Demirkan, N.; Bastian, B.C.; Goding, C.R.; Larue, L. Beta-catenin induces immortalization of melanocytes by suppressing p16INK4a expression and cooperates with N-Ras in melanoma development. *Genes Dev* **2007**, *21*(22), 2923-2935, doi:10.1101/gad.450107.

285. Sadangi, S.; Milosavljevic, K.; Castro-Perez, E.; Lares, M.; Singh, M.; Altameemi, S.; Beebe, D.J.; Ayuso, J.M.; Setaluri, V. Role of the Skin Microenvironment in Melanomagenesis: Epidermal Keratinocytes and Dermal Fibroblasts Promote BRAF Oncogene-Induced Senescence Escape in Melanocytes. *Cancers (Basel)* **2022**, *14*(5), doi:10.3390/cancers14051233.

286. Hayward, N.K.; Wilmott, J.S.; Waddell, N.; Johansson, P.A.; Field, M.A.; Nones, K.; Patch, A.M.; Kakavand, H.; Alexandrov, L.B.; Burke, H.; Jakrot, V.; Kazakoff, S.; Holmes, O.; Leonard, C.; Sabarinathan, R.; Mularoni, L.; Wood, S.; Xu, Q.; Waddell, N.; Tembe, V.; et al. Whole-genome landscapes of major melanoma subtypes. *Nature* **2017**, *545*(7653), 175-180, doi:10.1038/nature22071.

287. Law, M.H.; Bishop, D.T.; Lee, J.E.; Brossard, M.; Martin, N.G.; Moses, E.K.; Song, F.; Barrett, J.H.; Kumar, R.; Easton, D.F.; Pharoah, P.D.P.; Swerdlow, A.J.; Kypreou, K.P.; Taylor, J.C.; Harland, M.; Randerson-Moor, J.; Akslen, L.A.; Andresen, P.A.; Avril, M.F.; Azizi, E.; et al. Genome-wide meta-analysis identifies five new susceptibility loci for cutaneous malignant melanoma. *Nat Genet* **2015**, *47*(9), 987-995, doi:10.1038/ng.3373.

288. Zocchi, L.; Lontano, A.; Merli, M.; Dika, E.; Nagore, E.; Quaglino, P.; Puig, S.; Ribero, S. Familial Melanoma and Susceptibility Genes: A Review of the Most Common Clinical and Dermoscopic Phenotypic Aspect, Associated Malignancies and Practical Tips for Management. *J Clin Med* **2021**, *10*(16), doi:10.3390/jcm10163760.

289. Kreuger, I.Z.M.; Slieker, R.C.; van Groningen, T.; van Doorn, R. Therapeutic Strategies for Targeting CDKN2A Loss in Melanoma. *J Invest Dermatol* **2023**, *143*(1), 18-25 e11, doi:10.1016/j.jid.2022.07.016.

290. Robles-Espinoza, C.D.; Roberts, N.D.; Chen, S.; Leacy, F.P.; Alexandrov, L.B.; Pornputtapong, N.; Halaban, R.; Krauthammer, M.; Cui, R.; Timothy Bishop, D.; Adams, D.J. Germline MC1R status influences somatic mutation burden in melanoma. *Nat Commun* **2016**, *7*12064, doi:10.1038/ncomms12064.

291. Abd-Allah, G.M.; Ismail, A.; El-Mahdy, H.A.; Elsakka, E.G.E.; El-Husseiny, A.A.; Abdelmaksoud, N.M.; Salman, A.; Elkhawaga, S.Y.; Doghish, A.S. miRNAs as potential game-changers in melanoma: A comprehensive review. *Pathol Res Pract* **2023**, *244*154424, doi:10.1016/j.prp.2023.154424.

292. Greenberg, E.S.; Chong, K.K.; Huynh, K.T.; Tanaka, R.; Hoon, D.S. Epigenetic biomarkers in skin cancer. *Cancer Lett* **2014**, *342*(2), 170-177, doi:10.1016/j.canlet.2012.01.020.

293. Sarkar, D.; Leung, E.Y.; Baguley, B.C.; Finlay, G.J.; Askarian-Amiri, M.E. Epigenetic regulation in human melanoma: past and future. *Epigenetics* **2015**, *10*(2), 103-121, doi:10.1080/15592294.2014.1003746.

294. Lian, C.G.; Xu, Y.; Ceol, C.; Wu, F.; Larson, A.; Dresser, K.; Xu, W.; Tan, L.; Hu, Y.; Zhan, Q.; Lee, C.W.; Hu, D.; Lian, B.Q.; Kleffel, S.; Yang, Y.; Neiswender, J.; Khorasani, A.J.; Fang, R.; Lezcano, C.; Duncan, L.M.; et al. Loss of 5-hydroxymethylcytosine is an epigenetic hallmark of melanoma. *Cell* **2012**, *150*(6), 1135-1146, doi:10.1016/j.cell.2012.07.033.

295. Rothhammer, T.; Bosserhoff, A.K. Epigenetic events in malignant melanoma. *Pigment Cell Res* **2007**, *20*(2), 92-111, doi:10.1111/j.1600-0749.2007.00367.x.

296. Schinke, C.; Mo, Y.; Yu, Y.; Amiri, K.; Sosman, J.; Greally, J.; Verma, A. Aberrant DNA methylation in malignant melanoma. *Melanoma Res* **2010**, *20*(4), 253-265, doi:10.1097/CMR.0b013e328338a35a.

297. Soengas, M.S.; Capodieci, P.; Polsky, D.; Mora, J.; Esteller, M.; Opitz-Araya, X.; McCombie, R.; Herman, J.G.; Gerald, W.L.; Lazebnik, Y.A.; Cordon-Cardo, C.; Lowe, S.W. Inactivation of the apoptosis effector Apaf-1 in malignant melanoma. *Nature* **2001**, *409*(6817), 207-211, doi:10.1038/35051606.

298. Giunta, E.F.; Arrichiello, G.; Curvietto, M.; Pappalardo, A.; Bosso, D.; Rosanova, M.; Diana, A.; Giordano, P.; Petrillo, A.; Federico, P.; Fabozzi, T.; Parola, S.; Riccio, V.; Mucci, B.; Vanella, V.; Festino, L.; Daniele, B.; Ascierto, P.A.; Ottaviano, M.; On Behalf Of Scito Youth. Epigenetic Regulation in Melanoma: Facts and Hopes. *Cells* **2021**, *10*(8), doi:10.3390/cells10082048.

299. Mirmohammadsadegh, A.; Marini, A.; Nambiar, S.; Hassan, M.; Tannapfel, A.; Ruzicka, T.; Hengge, U.R. Epigenetic silencing of the PTEN gene in melanoma. *Cancer Res* **2006**, *66*(13), 6546-6552, doi:10.1158/0008-5472.CAN-06-0384.

300. Lahtz, C.; Stranzenbach, R.; Fiedler, E.; Helmbold, P.; Dammann, R.H. Methylation of PTEN as a prognostic factor in malignant melanoma of the skin. *J Invest Dermatol* **2010**, *130*(2), 620-622, doi:10.1038/jid.2009.226.

301. Straume, O.; Smeds, J.; Kumar, R.; Hemminki, K.; Akslen, L.A. Significant impact of promoter hypermethylation and the 540 C>T polymorphism of CDKN2A in cutaneous melanoma of the vertical growth phase. *Am J Pathol* **2002**, *161*(1), 229-237, doi:10.1016/S0002-9440(10)64174-0.

302. Spugnardi, M.; Tommasi, S.; Dammann, R.; Pfeifer, G.P.; Hoon, D.S. Epigenetic inactivation of RAS association domain family protein 1 (RASSF1A) in malignant cutaneous melanoma. *Cancer Res* **2003**, *63*(7), 1639-1643.

303. Tanemura, A.; Terando, A.M.; Sim, M.S.; van Hoesel, A.Q.; de Maat, M.F.; Morton, D.L.; Hoon, D.S. CpG island methylator phenotype predicts progression of malignant melanoma. *Clin Cancer Res* **2009**, *15*(5), 1801-1807, doi:10.1158/1078-0432.CCR-08-1361.

304. Pramio, D.T.; Pennacchi, P.C.; Maria-Engler, S.S.; Campos, A.H.; Duprat, J.P.; Carraro, D.M.; Krepischi, A.C. LINE-1 hypomethylation and mutational status in cutaneous melanomas. *J Investig Med* **2016**, *64*(4), 899-904, doi:10.1136/jim-2016-000066.

305. Bandyopadhyay, D.; Mishra, A.; Medrano, E.E. Overexpression of histone deacetylase 1 confers resistance to sodium butyrate-mediated apoptosis in melanoma cells through a p53-mediated pathway. *Cancer Res* **2004**, *64*(21), 7706-7710, doi:10.1158/0008-5472.CAN-03-3897.

306. Wang, C.; Wang, M.W.; Tashiro, S.; Onodera, S.; Ikejima, T. Roles of SIRT1 and phosphoinositide 3-OH kinase/protein kinase C pathways in evodiamine-induced human melanoma A375-S2 cell death. *J Pharmacol Sci* **2005**, *97*(4), 494-500, doi:10.1254/jphs.fpj04055x.

307. Florenes, V.A.; Skrede, M.; Jorgensen, K.; Nesland, J.M. Deacetylase inhibition in malignant melanomas: impact on cell cycle regulation and survival. *Melanoma Res* **2004**, *14*(3), 173-181, doi:10.1097/01.cmr.0000129576.49313.26.

308. Ye, Y.; Jin, L.; Wilmott, J.S.; Hu, W.L.; Yosufi, B.; Thorne, R.F.; Liu, T.; Rizos, H.; Yan, X.G.; Dong, L.; Tay, K.H.; Tseng, H.Y.; Guo, S.T.; de Bock, C.E.; Jiang, C.C.; Wang, C.Y.; Wu, M.; Zhang, L.J.; Hersey, P.; Scolyer, R.A.; Zhang, X.D. PI(4,5)P2 5-phosphatase A regulates PI3K/Akt signalling and has a tumour suppressive role in human melanoma. *Nat Commun* **2013**, *4*1508, doi:10.1038/ncomms2489.

309. Zhang, X.D.; Gillespie, S.K.; Borrow, J.M.; Hersey, P. The histone deacetylase inhibitor suberic bishydroxamate regulates the expression of multiple apoptotic mediators and induces mitochondria-dependent apoptosis of melanoma cells. *Mol Cancer Ther* **2004**, *3*(4), 425-435.

310. Fan, T.; Jiang, S.; Chung, N.; Alikhan, A.; Ni, C.; Lee, C.C.; Hornyak, T.J. EZH2-dependent suppression of a cellular senescence phenotype in melanoma cells by inhibition of p21/CDKN1A expression. *Mol Cancer Res* **2011**, *9*(4), 418-429, doi:10.1158/1541-7786.MCR-10-0511.

311. Tiffen, J.; Gallagher, S.J.; Hersey, P. EZH2: an emerging role in melanoma biology and strategies for targeted therapy. *Pigment Cell Melanoma Res* **2015**, *28*(1), 21-30, doi:10.1111/pcmr.12280.

312. Ceol, C.J.; Houvras, Y.; Jane-Valbuena, J.; Bilodeau, S.; Orlando, D.A.; Battisti, V.; Fritsch, L.; Lin, W.M.; Hollmann, T.J.; Ferre, F.; Bourque, C.; Burke, C.J.; Turner, L.; Uong, A.; Johnson, L.A.; Beroukhim, R.; Mermel, C.H.; Loda, M.; Ait-Si-Ali, S.; Garraway, L.A.; et al. The histone

methyltransferase SETDB1 is recurrently amplified in melanoma and accelerates its onset. *Nature* **2011**, *471*(7339), 513-517, doi:10.1038/nature09806.

313. Aftab, M.N.; Dinger, M.E.; Perera, R.J. The role of microRNAs and long non-coding RNAs in the pathology, diagnosis, and management of melanoma. *Arch Biochem Biophys* **2014**, *563*60-70, doi:10.1016/j.abb.2014.07.022.

314. Segura, M.F.; Greenwald, H.S.; Hanniford, D.; Osman, I.; Hernando, E. MicroRNA and cutaneous melanoma: from discovery to prognosis and therapy. *Carcinogenesis* **2012**, *33*(10), 1823-1832, doi:10.1093/carcin/bgs205.

315. Ghafouri-Fard, S.; Gholipour, M.; Taheri, M. MicroRNA Signature in Melanoma: Biomarkers and Therapeutic Targets. *Front Oncol* **2021**, *11*608987, doi:10.3389/fonc.2021.608987.

316. Fattore, L.; Costantini, S.; Malpicci, D.; Ruggiero, C.F.; Ascierto, P.A.; Croce, C.M.; Mancini, R.; Ciliberto, G. MicroRNAs in melanoma development and resistance to target therapy. *Oncotarget* **2017**, *8*(13), 22262-22278, doi:10.18632/oncotarget.14763.

317. Latchana, N.; Ganju, A.; Howard, J.H.; Carson III, W.E. MicroRNA dysregulation in melanoma. *Surg Oncol* **2016**, *25*(3), 184-189, doi:10.1016/j.suronc.2016.05.017.

318. Melnik, B.C. MiR-21: an environmental driver of malignant melanoma? *J Transl Med* **2015**, *13*202, doi:10.1186/s12967-015-0570-5.

319. Satzger, I.; Mattern, A.; Kuettler, U.; Weinspach, D.; Niebuhr, M.; Kapp, A.; Gutzmer, R. microRNA-21 is upregulated in malignant melanoma and influences apoptosis of melanocytic cells. *Exp Dermatol* **2012**, *21*(7), 509-514, doi:10.1111/j.1600-0625.2012.01510.x.

320. Felicetti, F.; Errico, M.C.; Bottero, L.; Segnalini, P.; Stoppacciaro, A.; Biffoni, M.; Felli, N.; Mattia, G.; Petrini, M.; Colombo, M.P.; Peschle, C.; Care, A. The promyelocytic leukemia zinc finger-microRNA-221/-222 pathway controls melanoma progression through multiple oncogenic mechanisms. *Cancer Res* **2008**, *68*(8), 2745-2754, doi:10.1158/0008-5472.CAN-07-2538.

321. Liu, X.; Li, H.; Wu, G.; Cui, S. miR-182 promotes cell proliferation and invasion by inhibiting APC in melanoma. *Int J Clin Exp Pathol* **2018**, *11*(4), 1900-1908.

322. Segura, M.F.; Hanniford, D.; Menendez, S.; Reavie, L.; Zou, X.; Alvarez-Diaz, S.; Zakrzewski, J.; Blochin, E.; Rose, A.; Bogunovic, D.; Polsky, D.; Wei, J.; Lee, P.; Belitskaya-Levy, I.; Bhardwaj, N.; Osman, I.; Hernando, E. Aberrant miR-182 expression promotes melanoma metastasis by repressing FOXO3 and microphthalmia-associated transcription factor. *Proc Natl Acad Sci U S A* **2009**, *106*(6), 1814-1819, doi:10.1073/pnas.0808263106.

323. Jiang, L.; Lv, X.; Li, J.; Li, J.; Li, X.; Li, W.; Li, Y. The status of microRNA-21 expression and its clinical significance in human cutaneous malignant melanoma. *Acta Histochem* **2012**, *114*(6), 582-588, doi:10.1016/j.acthis.2011.11.001.

324. Grignol, V.; Fairchild, E.T.; Zimmerer, J.M.; Lesinski, G.B.; Walker, M.J.; Magro, C.M.; Kacher, J.E.; Karpa, V.I.; Clark, J.; Nuovo, G.; Lehman, A.; Volinia, S.; Agnese, D.M.; Croce, C.M.; Carson III, W.E. miR-21 and miR-155 are associated with mitotic activity and lesion depth of borderline melanocytic lesions. *Br J Cancer* **2011**, *105*(7), 1023-1029, doi:10.1038/bjc.2011.288.

325. Igoucheva, O.; Alexeev, V. MicroRNA-dependent regulation of cKit in cutaneous melanoma. *Biochem Biophys Res Commun* **2009**, *379*(3), 790-794, doi:10.1016/j.bbrc.2008.12.152.

326. Kanemaru, H.; Fukushima, S.; Yamashita, J.; Honda, N.; Oyama, R.; Kakimoto, A.; Masuguchi, S.; Ishihara, T.; Inoue, Y.; Jinnin, M.; Ihn, H. The circulating microRNA-221 level in patients with malignant melanoma as a new tumor marker. *J Dermatol Sci* **2011**, *61*(3), 187-193, doi:10.1016/j.jdermsci.2010.12.010.

327. Dar, A.A.; Majid, S.; de Semir, D.; Nosrati, M.; Bezrookove, V.; Kashani-Sabet, M. miRNA-205 suppresses melanoma cell proliferation and induces senescence via regulation of E2F1 protein. *J Biol Chem* **2011**, *286*(19), 16606-16614, doi:10.1074/jbc.M111.227611.

328. Liu, S.; Tetzlaff, M.T.; Liu, A.; Liegl-Atzwanger, B.; Guo, J.; Xu, X. Loss of microRNA-205 expression is associated with melanoma progression. *Lab Invest* **2012**, *92*(7), 1084-1096, doi:10.1038/labinvest.2012.62.

329. Xu, Y.; Brenn, T.; Brown, E.R.; Doherty, V.; Melton, D.W. Differential expression of microRNAs during melanoma progression: miR-200c, miR-205 and miR-211 are downregulated in melanoma and act as tumour suppressors. *Br J Cancer* **2012**, *106*(3), 553-561, doi:10.1038/bjc.2011.568.

330. Alegre, E.; Sanmamed, M.F.; Rodriguez, C.; Carranza, O.; Martin-Algarra, S.; Gonzalez, A. Study of circulating microRNA-125b levels in serum exosomes in advanced melanoma. *Arch Pathol Lab Med* **2014**, *138*(6), 828-832, doi:10.5858/arpa.2013-0134-OA.

331. Kappelmann, M.; Kuphal, S.; Meister, G.; Vardimon, L.; Bosserhoff, A.K. MicroRNA miR-125b controls melanoma progression by direct regulation of c-Jun protein expression. *Oncogene* **2013**, *32*(24), 2984-2991, doi:10.1038/onc.2012.307.

332. Boyle, G.M.; Woods, S.L.; Bonazzi, V.F.; Stark, M.S.; Hacker, E.; Aoude, L.G.; Dutton-Regester, K.; Cook, A.L.; Sturm, R.A.; Hayward, N.K. Melanoma cell invasiveness is regulated by miR-211 suppression of the BRN2 transcription factor. *Pigment Cell Melanoma Res* **2011**, *24*(3), 525-537, doi:10.1111/j.1755-148X.2011.00849.x.

333. Mazar, J.; DeYoung, K.; Khaitan, D.; Meister, E.; Almodovar, A.; Goydos, J.; Ray, A.; Perera, R.J. The regulation of miRNA-211 expression and its role in melanoma cell invasiveness. *PLoS One* **2010**, *5*(11), e13779, doi:10.1371/journal.pone.0013779.

334. Muller, D.W.; Bosserhoff, A.K. Integrin beta 3 expression is regulated by let-7a miRNA in malignant melanoma. *Oncogene* **2008**, *27*(52), 6698-6706, doi:10.1038/onc.2008.282.

335. Schultz, J.; Lorenz, P.; Gross, G.; Ibrahim, S.; Kunz, M. MicroRNA let-7b targets important cell cycle molecules in malignant melanoma cells and interferes with anchorage-independent growth. *Cell Res* **2008**, *18*(5), 549-557, doi:10.1038/cr.2008.45.

336. Xu, Y.; Guo, B.; Liu, X.; Tao, K. miR-34a inhibits melanoma growth by targeting ZEB1. *Aging (Albany NY)* **2021**, *13*(11), 15538-15547, doi:10.18632/aging.203114.

337. Guo, S.; Guo, W.; Li, S.; Dai, W.; Zhang, N.; Zhao, T.; Wang, H.; Ma, J.; Yi, X.; Ge, R.; Wang, G.; Gao, T.; Li, C. Serum miR-16: A Potential Biomarker for Predicting Melanoma Prognosis. *J Invest Dermatol* **2016**, *136*(5), 985-993, doi:10.1016/j.jid.2015.12.041.

338. Li, N. Low Expression of Mir-137 Predicts Poor Prognosis in Cutaneous Melanoma Patients. *Med Sci Monit* **2016**, *22*140-144, doi:10.12659/msm.895207.

339. Luo, C.; Tetteh, P.W.; Merz, P.R.; Dickes, E.; Abukiwan, A.; Hotz-Wagenblatt, A.; Holland-Cunz, S.; Sinnberg, T.; Schittek, B.; Schadendorf, D.; Diederichs, S.; Eichmuller, S.B. miR-137 inhibits the invasion of melanoma cells through downregulation of multiple oncogenic target genes. *J Invest Dermatol* **2013**, *133*(3), 768-775, doi:10.1038/jid.2012.357.

340. Asangani, I.A.; Harms, P.W.; Dodson, L.; Pandhi, M.; Kunju, L.P.; Maher, C.A.; Fullen, D.R.; Johnson, T.M.; Giordano, T.J.; Palanisamy, N.; Chinnaiyan, A.M. Genetic and epigenetic loss of microRNA-31 leads to feed-forward expression of EZH2 in melanoma. *Oncotarget* **2012**, *3*(9), 1011-1025, doi:10.18632/oncotarget.622.

341. Chang, X.; Sun, Y.; Han, S.; Zhu, W.; Zhang, H.; Lian, S. MiR-203 inhibits melanoma invasive and proliferative abilities by targeting the polycomb group gene BMI1. *Biochem Biophys Res Commun* **2015**, *456*(1), 361-366, doi:10.1016/j.bbrc.2014.11.087.

342. Liu, S.; Tetzlaff, M.T.; Cui, R.; Xu, X. miR-200c inhibits melanoma progression and drug resistance through down-regulation of BMI-1. *Am J Pathol* **2012**, *181*(5), 1823-1835, doi:10.1016/j.ajpath.2012.07.009.

343. Holst, L.M.; Kaczkowski, B.; Glud, M.; Futoma-Kazmierczak, E.; Hansen, L.F.; Gniadecki, R. The microRNA molecular signature of atypic and common acquired melanocytic nevi: differential expression of miR-125b and let-7c. *Exp Dermatol* **2011**, *20*(3), 278-280, doi:10.1111/j.1600-0625.2010.01163.x.

344. Glud, M.; Manfe, V.; Biskup, E.; Holst, L.; Dirksen, A.M.; Hastrup, N.; Nielsen, F.C.; Drzewiecki, K.T.; Gniadecki, R. MicroRNA miR-125b induces senescence in human melanoma cells. *Melanoma Res* **2011**, *21*(3), 253-256, doi:10.1097/CMR.0b013e328345333b.

345. Noguchi, S.; Mori, T.; Otsuka, Y.; Yamada, N.; Yasui, Y.; Iwasaki, J.; Kumazaki, M.; Maruo, K.; Akao, Y. Anti-oncogenic microRNA-203 induces senescence by targeting E2F3 protein in human melanoma cells. *J Biol Chem* **2012**, *287*(15), 11769-11777, doi:10.1074/jbc.M111.325027.

346. Wang, K.; Zhang, Z.W. Expression of miR-203 is decreased and associated with the prognosis of melanoma patients. *Int J Clin Exp Pathol* **2015**, *8*(10), 13249-13254.

347. van Kempen, L.C.; van den Hurk, K.; Lazar, V.; Michiels, S.; Winnepenninckx, V.; Stas, M.; Spatz, A.; van den Oord, J.J. Loss of microRNA-200a and c, and microRNA-203 expression at the invasive front of primary cutaneous melanoma is associated with increased thickness and disease progression. *Virchows Arch* **2012**, *461*(4), 441-448, doi:10.1007/s00428-012-1309-9.

348. Mumford, S.L.; Towler, B.P.; Pashler, A.L.; Gilleard, O.; Martin, Y.; Newbury, S.F. Circulating MicroRNA Biomarkers in Melanoma: Tools and Challenges in Personalised Medicine. *Biomolecules* **2018**, *8*(2), doi:10.3390/biom8020021.

349. Ho, P.T.B.; Clark, I.M.; Le, L.T.T. MicroRNA-Based Diagnosis and Therapy. *Int J Mol Sci* **2022**, *23*(13), doi:10.3390/ijms23137167.

350. Liu, A.; Tetzlaff, M.T.; Vanbelle, P.; Elder, D.; Feldman, M.; Tobias, J.W.; Sepulveda, A.R.; Xu, X. MicroRNA expression profiling outperforms mRNA expression profiling in formalin-fixed paraffin-embedded tissues. *Int J Clin Exp Pathol* **2009**, *2*(6), 519-527.

351. Audrito, V.; Serra, S.; Stingi, A.; Orso, F.; Gaudino, F.; Bologna, C.; Neri, F.; Garaffo, G.; Nassini, R.; Baroni, G.; Rulli, E.; Massi, D.; Oliviero, S.; Piva, R.; Taverna, D.; Mandala, M.; Deaglio, S. PD-L1 up-regulation in melanoma increases disease aggressiveness and is mediated through miR-17-5p. *Oncotarget* **2017**, *8*(9), 15894-15911, doi:10.18632/oncotarget.15213.

352. Hanniford, D.; Zhong, J.; Koetz, L.; Gaziel-Sovran, A.; Lackaye, D.J.; Shang, S.; Pavlick, A.; Shapiro, R.; Berman, R.; Darvishian, F.; Shao, Y.; Osman, I.; Hernando, E. A miRNA-Based Signature Detected in Primary Melanoma Tissue Predicts Development of Brain Metastasis. *Clin Cancer Res* **2015**, *21*(21), 4903-4912, doi:10.1158/1078-0432.CCR-14-2566.

353. Stark, M.S.; Klein, K.; Weide, B.; Haydu, L.E.; Pflugfelder, A.; Tang, Y.H.; Palmer, J.M.; Whiteman, D.C.; Scolyer, R.A.; Mann, G.J.; Thompson, J.F.; Long, G.V.; Barbour, A.P.; Soyer, H.P.; Garbe, C.; Herington, A.; Pollock, P.M.; Hayward, N.K. The Prognostic and Predictive Value of Melanoma-related MicroRNAs Using Tissue and Serum: A MicroRNA Expression Analysis. *EBioMedicine* **2015**, *2*(7), 671-680, doi:10.1016/j.ebiom.2015.05.011.

354. Blanpain, C. Tracing the cellular origin of cancer. *Nat Cell Biol* **2013**, *15*(2), 126-134, doi:10.1038/ncb2657.

355. Bongiorno, M.R.; Doukaki, S.; Malleo, F.; Arico, M. Identification of progenitor cancer stem cell in lentigo maligna melanoma. *Dermatol Ther* **2008**, *21 Suppl 1*S1-5, doi:10.1111/j.1529-8019.2008.00193.x.

356. Grichnik, J.M.; Burch, J.A.; Schulteis, R.D.; Shan, S.; Liu, J.; Darrow, T.L.; Vervaert, C.E.; Seigler, H.F. Melanoma, a tumor based on a mutant stem cell? *J Invest Dermatol* **2006**, *126*(1), 142-153, doi:10.1038/sj.jid.5700017.

357. Hoerter, J.D.; Bradley, P.; Casillas, A.; Chambers, D.; Denholm, C.; Johnson, K.; Weiswasser, B. Extrafollicular dermal melanocyte stem cells and melanoma. *Stem Cells Int* **2012**, *2012*407079, doi:10.1155/2012/407079.

358. Hoerter, J.D.; Bradley, P.; Casillas, A.; Chambers, D.; Weiswasser, B.; Clements, L.; Gilbert, S.; Jiao, A. Does melanoma begin in a melanocyte stem cell? *J Skin Cancer* **2012**, *2012*571087, doi:10.1155/2012/571087.

359. Kohler, C.; Nittner, D.; Rambow, F.; Radaelli, E.; Stanchi, F.; Vandamme, N.; Baggiolini, A.; Sommer, L.; Berx, G.; van den Oord, J.J.; Gerhardt, H.; Blanpain, C.; Marine, J.C. Mouse Cutaneous Melanoma Induced by Mutant BRaf Arises from Expansion and Dedifferentiation of Mature Pigmented Melanocytes. *Cell Stem Cell* **2017**, *21*(5), 679-693 e676, doi:10.1016/j.stem.2017.08.003.

360. Kyrgidis, A.; Tzellos, T.G.; Triaridis, S. Melanoma: Stem cells, sun exposure and hallmarks for carcinogenesis, molecular concepts and future clinical implications. *J Carcinog* **2010**, *9*3, doi:10.4103/1477-3163.62141.

361. Moon, H.; Donahue, L.R.; Choi, E.; Scumpia, P.O.; Lowry, W.E.; Grenier, J.K.; Zhu, J.; White, A.C. Melanocyte Stem Cell Activation and Translocation Initiate Cutaneous Melanoma in Response to UV Exposure. *Cell Stem Cell* **2017**, *21*(5), 665-678 e666, doi:10.1016/j.stem.2017.09.001.

362. Zabierowski, S.E.; Herlyn, M. Melanoma stem cells: the dark seed of melanoma. *J Clin Oncol* **2008**, *26*(17), 2890-2894, doi:10.1200/JCO.2007.15.5465.

363. Reya, T.; Morrison, S.J.; Clarke, M.F.; Weissman, I.L. Stem cells, cancer, and cancer stem cells. *Nature* **2001**, *414*(6859), 105-111, doi:10.1038/35102167.

364. White, A.C.; Lowry, W.E. Refining the role for adult stem cells as cancer cells of origin. *Trends Cell Biol* **2015**, *25*(1), 11-20, doi:10.1016/j.tcb.2014.08.008.

365. Bonnet, D.; Dick, J.E. Human acute myeloid leukemia is organized as a hierarchy that originates from a primitive hematopoietic cell. *Nat Med* **1997**, *3*(7), 730-737, doi:10.1038/nm0797-730.

366. Singh, S.K.; Hawkins, C.; Clarke, I.D.; Squire, J.A.; Bayani, J.; Hide, T.; Henkelman, R.M.; Cusimano, M.D.; Dirks, P.B. Identification of human brain tumour initiating cells. *Nature* **2004**, *432*(7015), 396-401, doi:10.1038/nature03128.

367. Ricci-Vitiani, L.; Lombardi, D.G.; Pilozzi, E.; Biffoni, M.; Todaro, M.; Peschle, C.; De Maria, R. Identification and expansion of human colon-cancer-initiating cells. *Nature* **2007**, *445*(7123), 111-115, doi:10.1038/nature05384.

368. Collins, A.T.; Berry, P.A.; Hyde, C.; Stower, M.J.; Maitland, N.J. Prospective identification of tumorigenic prostate cancer stem cells. *Cancer Res* **2005**, *65*(23), 10946-10951, doi:10.1158/0008-5472.CAN-05-2018.

369. Li, C.; Heidt, D.G.; Dalerba, P.; Burant, C.F.; Zhang, L.; Adsay, V.; Wicha, M.; Clarke, M.F.; Simeone, D.M. Identification of pancreatic cancer stem cells. *Cancer Res* **2007**, *67*(3), 1030-1037, doi:10.1158/0008-5472.CAN-06-2030.

370. Al-Hajj, M.; Wicha, M.S.; Benito-Hernandez, A.; Morrison, S.J.; Clarke, M.F. Prospective identification of tumorigenic breast cancer cells. *Proc Natl Acad Sci U S A* **2003**, *100*(7), 3983-3988, doi:10.1073/pnas.0530291100.

371. Peterson, S.C.; Eberl, M.; Vagnozzi, A.N.; Belkadi, A.; Veniaminova, N.A.; Verhaegen, M.E.; Bichakjian, C.K.; Ward, N.L.; Dlugosz, A.A.; Wong, S.Y. Basal cell carcinoma preferentially arises from stem cells within hair follicle and mechanosensory niches. *Cell Stem Cell* **2015**, *16*(4), 400-412, doi:10.1016/j.stem.2015.02.006.

372. Lapouge, G.; Youssef, K.K.; Vokaer, B.; Achouri, Y.; Michaux, C.; Sotiropoulou, P.A.; Blanpain, C. Identifying the cellular origin of squamous skin tumors. *Proc Natl Acad Sci U S A* **2011**, *108*(18), 7431-7436, doi:10.1073/pnas.1012720108.

373. White, A.C.; Tran, K.; Khuu, J.; Dang, C.; Cui, Y.; Binder, S.W.; Lowry, W.E. Defining the origins of Ras/p53-mediated squamous cell carcinoma. *Proc Natl Acad Sci U S A* **2011**, *108*(18), 7425-7430, doi:10.1073/pnas.1012670108.

374. Fang, D.; Nguyen, T.K.; Leishear, K.; Finko, R.; Kulp, A.N.; Hotz, S.; Van Belle, P.A.; Xu, X.; Elder, D.E.; Herlyn, M. A tumorigenic subpopulation with stem cell properties in melanomas. *Cancer Res* **2005**, *65*(20), 9328-9337, doi:10.1158/0008-5472.CAN-05-1343.

375. Hendrix, M.J.; Seftor, E.A.; Hess, A.R.; Seftor, R.E. Molecular plasticity of human melanoma cells. *Oncogene* **2003**, *22*(20), 3070-3075, doi:10.1038/sj.onc.1206447.

376. Monzani, E.; Facchetti, F.; Galmozzi, E.; Corsini, E.; Benetti, A.; Cavazzin, C.; Gritti, A.; Piccinini, A.; Porro, D.; Santinami, M.; Invernici, G.; Parati, E.; Alessandri, G.; La Porta, C.A. Melanoma contains CD133 and ABCG2 positive cells with enhanced tumourigenic potential. *Eur J Cancer* **2007**, *43*(5), 935-946, doi:10.1016/j.ejca.2007.01.017.

377. Lee, J.T.; Herlyn, M. Microenvironmental influences in melanoma progression. *J Cell Biochem* **2007**, *101*(4), 862-872, doi:10.1002/jcb.21204.

378. Ueno, M.; Aoto, T.; Mohri, Y.; Yokozeki, H.; Nishimura, E.K. Coupling of the radiosensitivity of melanocyte stem cells to their dormancy during the hair cycle. *Pigment Cell Melanoma Res* **2014**, *27*(4), 540-551, doi:10.1111/pcmr.12251.

379. Agar, N.S.; Halliday, G.M.; Barnetson, R.S.; Ananthaswamy, H.N.; Wheeler, M.; Jones, A.M. The basal layer in human squamous tumors harbors more UVA than UVB fingerprint mutations: a role for UVA in human skin carcinogenesis. *Proc Natl Acad Sci U S A* **2004**, *101*(14), 4954-4959, doi:10.1073/pnas.0401141101.

380. Brock, C.K.; Wallin, S.T.; Ruiz, O.E.; Samms, K.M.; Mandal, A.; Sumner, E.A.; Eisenhoffer, G.T. Stem cell proliferation is induced by apoptotic bodies from dying cells during epithelial tissue maintenance. *Nat Commun* **2019**, *10*(1), 1044, doi:10.1038/s41467-019-09010-6.

381. Diener, J.; Sommer, L. Reemergence of neural crest stem cell-like states in melanoma during disease progression and treatment. *Stem Cells Transl Med* **2021**, *10*(4), 522-533, doi:10.1002/sctm.20-0351.

382. Radke, J.; Rossner, F.; Redmer, T. CD271 determines migratory properties of melanoma cells. *Sci Rep* **2017**, *7*(1), 9834, doi:10.1038/s41598-017-10129-z.

383. Redmer, T.; Walz, I.; Klinger, B.; Khouja, S.; Welte, Y.; Schafer, R.; Regenbrecht, C. The role of the cancer stem cell marker CD271 in DNA damage response and drug resistance of melanoma cells. *Oncogenesis* **2017**, *6*(1), e291, doi:10.1038/oncsis.2016.88.

384. Baggiolini, A.; Callahan, S.J.; Montal, E.; Weiss, J.M.; Trieu, T.; Tagore, M.M.; Tischfield, S.E.; Walsh, R.M.; Suresh, S.; Fan, Y.; Campbell, N.R.; Perlee, S.C.; Saurat, N.; Hunter, M.V.; Simon-Vermot, T.; Huang, T.H.; Ma, Y.; Hollmann, T.; Tickoo, S.K.; Taylor, B.S.; et al. Developmental chromatin programs determine oncogenic competence in melanoma. *Science* **2021**, *373*(6559), eabc1048, doi:10.1126/science.abc1048.

385. Sun, Q.; Lee, W.; Mohri, Y.; Takeo, M.; Lim, C.H.; Xu, X.; Myung, P.; Atit, R.P.; Taketo, M.M.; Moubarak, R.S.; Schober, M.; Osman, I.; Gay, D.L.; Saur, D.; Nishimura, E.K.; Ito, M. A novel mouse model demonstrates that oncogenic melanocyte stem cells engender melanoma resembling human disease. *Nat Commun* **2019**, *10*(1), 5023, doi:10.1038/s41467-019-12733-1.

386. Garcia, A.M.; McLaren, C.E.; Meyskens, F.L., Jr. Melanoma: is hair the root of the problem? *Pigment Cell Melanoma Res* **2011**, *24*(1), 110-118, doi:10.1111/j.1755-148X.2010.00782.x.

387. Huang, X.; Protheroe, M.D.; Al-Jumaily, A.M.; Chalmers, A.N.; Paul, S.P.; Fu, X. Simulation of UV power absorbed by follicular stem cells during sun exposure and possible implications for melanoma development. *J Opt Soc Am A Opt Image Sci Vis* **2019**, *36*(4), 628-635, doi:10.1364/JOSAA.36.000628.

388. Mitchell, D.L.; Volkmer, B.; Breitbart, E.W.; Byrom, M.; Lowery, M.G.; Greinert, R. Identification of a non-dividing subpopulation of mouse and human epidermal cells exhibiting high levels of persistent ultraviolet photodamage. *J Invest Dermatol* **2001**, *117*(3), 590-595, doi:10.1046/j.0022-202x.2001.01442.x.

389. Nijhof, J.G.; van Pelt, C.; Mulder, A.A.; Mitchell, D.L.; Mullenders, L.H.; de Gruijl, F.R. Epidermal stem and progenitor cells in murine epidermis accumulate UV damage despite NER proficiency. *Carcinogenesis* **2007**, *28*(4), 792-800, doi:10.1093/carcin/bgl213.

390. Long, L.J.; Lee, P.H.; Small, E.M.; Hillyer, C.; Guo, Y.; Osley, M.A. Regulation of UV damage repair in quiescent yeast cells. *DNA Repair (Amst)* **2020**, *90*102861, doi:10.1016/j.dnarep.2020.102861.

391. Bielas, J.H. Non-transcribed strand repair revealed in quiescent cells. *Mutagenesis* **2006**, *21*(1), 49-53, doi:10.1093/mutage/gei073.

392. Lee, S.; An, L.; Soloway, P.D.; White, A.C. Dynamic regulation of chromatin accessibility during melanocyte stem cell activation. *Pigment Cell Melanoma Res* **2023**, *36*(6), 531-541, doi:10.1111/pcmr.13112.

393. Kenyon, J.; Gerson, S.L. The role of DNA damage repair in aging of adult stem cells. *Nucleic Acids Res* **2007**, *35*(22), 7557-7565, doi:10.1093/nar/gkm1064.

394. Greinert, R.; Breibart, E.W.; Mitchell, D.; Smida, J.; Volkmer, B. Characterisation of human keratinocytes by measuring cellular repair capacity of UVB-induced DNA damage and monitoring of cytogenetic changes in melanoma cell lines. *Radiation Protection Dosimetry* **2000**, *91*(1-3), 41-45, doi:10.1093/oxfordjournals.rpd.a033232.

395. Szabo, A.; Perou, C.M.; Karaca, M.; Perreard, L.; Palais, R.; Quackenbush, J.F.; Bernard, P.S. Statistical modeling for selecting housekeeper genes. *Genome Biol* **2004**, *5*(8), R59, doi:10.1186/gb-2004-5-8-r59.

396. Vandesompele, J.; De Preter, K.; Pattyn, F.; Poppe, B.; Van Roy, N.; De Paepe, A.; Speleman, F. Accurate normalization of real-time quantitative RT-PCR data by geometric averaging of multiple internal control genes. *Genome Biol* **2002**, *3*(7), doi:10.1186/gb-2002-3-7-research0034.

397. Adijanto, J.; Castorino, J.J.; Wang, Z.X.; Maminishkis, A.; Grunwald, G.B.; Philp, N.J. Microphthalmia-associated transcription factor (MITF) promotes differentiation of human retinal pigment epithelium (RPE) by regulating microRNAs-204/211 expression. *J Biol Chem* **2012**, *287*(24), 20491-20503, doi:10.1074/jbc.M112.354761.

398. Mhamdi-Ghodbani, M.; Starzonek, C.; Degenhardt, S.; Bender, M.; Said, M.; Greinert, R.; Volkmer, B. UVB damage response of dermal stem cells as melanocyte precursors compared to keratinocytes, melanocytes, and fibroblasts from human foreskin. *J Photochem Photobiol B* **2021**, *220*112216, doi:10.1016/j.jphotobiol.2021.112216.

399. Radonic, A.; Thulke, S.; Mackay, I.M.; Landt, O.; Siegert, W.; Nitsche, A. Guideline to reference gene selection for quantitative real-time PCR. *Biochem Biophys Res Commun* **2004**, *313*(4), 856-862, doi:10.1016/j.bbrc.2003.11.177.

400. Seo, E.Y.; Jin, S.P.; Sohn, K.C.; Park, C.H.; Lee, D.H.; Chung, J.H. UCHL1 Regulates Melanogenesis through Controlling MITF Stability in Human Melanocytes. *J Invest Dermatol* **2017**, *137*(8), 1757-1765, doi:10.1016/j.jid.2017.03.024.

401. The Wistar Institute. Herlyn Lab Cell Culture Techniques; Philadelphia: The Wistar Institute, 2017, Available online: https://www.wistar.org/wp-content/uploads/2023/10/Herlyn-Lab-Cell-Culture-Techniques-2017.pdf (accessed on January 22, 2019).

402. Plitta-Michalak, B.; Stricker, N.; Pavez Lorie, E.; Chen, I.; Pollet, M.; Krutmann, J.; Volkmer, B.; Greinert, R.; Boukamp, P.; Rapp, A. Development and characterisation of an irradiation device for biomedical studies covering the solar spectrum with individual regulated spectral bands. *Photochem Photobiol Sci* **2022**, *21*(9), 1701-1717, doi:10.1007/s43630-022-00252-w.

403. Siebels, B. Epigenetische Veränderungen und Reparaturkinetik in humanen Keratinozyten (HaCaT) nach der chronischen Kombinationsbestrahlung (UVA+UVB+VIS+IRA) aus dem solaren Spektrum. Bachelor thesis, University of Hamburg, 2019.

404. Zhou, X.; Wang, G.; Sun, Y. A reliable parameter to standardize the scoring of stem cell spheres. *PLoS One* **2015**, *10*(5), e0127348, doi:10.1371/journal.pone.0127348.

405. Darzynkiewicz, Z.; Juan, G.; Bedner, E. Determining cell cycle stages by flow cytometry. *Curr Protoc Cell Biol* **2001**, *Chapter 8*Unit 8 4, doi:10.1002/0471143030.cb0804s01.

406. Marino, G.; Kroemer, G. Mechanisms of apoptotic phosphatidylserine exposure. *Cell Res* **2013**, *23*(11), 1247-1248, doi:10.1038/cr.2013.115.

407. Segawa, K.; Nagata, S. An Apoptotic 'Eat Me' Signal: Phosphatidylserine Exposure. *Trends Cell Biol* **2015**, *25*(11), 639-650, doi:10.1016/j.tcb.2015.08.003.

408. Crowley, L.C.; Marfell, B.J.; Scott, A.P.; Waterhouse, N.J. Quantitation of Apoptosis and Necrosis by Annexin V Binding, Propidium Iodide Uptake, and Flow Cytometry. *Cold Spring Harb Protoc* **2016**, *2016*(11), doi:10.1101/pdb.prot087288.

409. Livak, K.J.; Schmittgen, T.D. Analysis of relative gene expression data using real-time quantitative PCR and the 2(-Delta Delta C(T)) Method. *Methods* **2001**, *25*(4), 402-408, doi:10.1006/meth.2001.1262.

410. Abcam. FirePlex® miRNA Assay. 2017. Available online: https://docs.abcam.com/pdf/kits/FirePlex-miRNA-Assay.pdf (accessed on July 4, 2022).

411. Bender, M. Solar simulated radiation and progression of cutaneous squamous cell carcinoma: the role of miRNAs and TGF-β1. Dissertation, University of Hamburg, 2023.

412. Gu, Z.; Eils, R.; Schlesner, M. Complex heatmaps reveal patterns and correlations in multidimensional genomic data. *Bioinformatics* **2016**, *32*(18), 2847-2849, doi:10.1093/bioinformatics/btw313.

413. Ritchie, M.E.; Phipson, B.; Wu, D.; Hu, Y.; Law, C.W.; Shi, W.; Smyth, G.K. limma powers differential expression analyses for RNA-sequencing and microarray studies. *Nucleic Acids Res* **2015**, *43*(7), e47, doi:10.1093/nar/gkv007.

414. Kern, F.; Aparicio-Puerta, E.; Li, Y.; Fehlmann, T.; Kehl, T.; Wagner, V.; Ray, K.; Ludwig, N.; Lenhof, H.P.; Meese, E.; Keller, A. miRTargetLink 2.0-interactive miRNA target gene and target pathway networks. *Nucleic Acids Res* **2021**, *49*(W1), W409-W416, doi:10.1093/nar/gkab297.

415. Maleki, F.; Ovens, K.; Hogan, D.J.; Kusalik, A.J. Gene Set Analysis: Challenges, Opportunities, and Future Research. *Front Genet* **2020**, *11*654, doi:10.3389/fgene.2020.00654.

416. Gene Ontology Consortium. Gene Ontology Consortium: going forward. *Nucleic Acids Res* **2015**, *43*(Database issue), D1049-1056, doi:10.1093/nar/gku1179.

417. Kanehisa, M.; Sato, Y.; Kawashima, M. KEGG mapping tools for uncovering hidden features in biological data. *Protein Sci* **2022**, *31*(1), 47-53, doi:10.1002/pro.4172.

418. Kern, F.; Fehlmann, T.; Solomon, J.; Schwed, L.; Grammes, N.; Backes, C.; Van Keuren-Jensen, K.; Craig, D.W.; Meese, E.; Keller, A. miEAA 2.0: integrating multi-species microRNA enrichment analysis and workflow management systems. *Nucleic Acids Res* **2020**, *48*(W1), W521-W528, doi:10.1093/nar/gkaa309.

419. Gerstner, N.; Kehl, T.; Lenhof, K.; Muller, A.; Mayer, C.; Eckhart, L.; Grammes, N.L.; Diener, C.; Hart, M.; Hahn, O.; Walter, J.; Wyss-Coray, T.; Meese, E.; Keller, A.; Lenhof, H.P. GeneTrail 3: advanced high-throughput enrichment analysis. *Nucleic Acids Res* **2020**, *48*(W1), W515-W520, doi:10.1093/nar/gkaa306.

420. Starzonek, C.; Mhamdi-Ghodbani, M.; Henning, S.; Bender, M.; Degenhardt, S.; Chen, I.P.; Said, M.; Greinert, R.; Volkmer, B. Enrichment of Human Dermal Stem Cells from Primary Cell Cultures through the Elimination of Fibroblasts. *Cells* **2023**, *12*(6), doi:10.3390/cells12060949.

421. Ravelo, K.M.; Andersen, N.D.; Monje, P.V. Magnetic-Activated Cell Sorting for the Fast and Efficient Separation of Human and Rodent Schwann Cells from Mixed Cell Populations. *Methods Mol Biol* **2018**, *1739*87-109, doi:10.1007/978-1-4939-7649-2_6.

422. Zborowski, M.; Chalmers, J.J. Magnetic cell sorting. *Methods Mol Biol* **2005**, *295*291-300, doi:10.1385/1-59259-873-0:291.

423. Peng, K.; Sant, D.; Andersen, N.; Silvera, R.; Camarena, V.; Pinero, G.; Graham, R.; Khan, A.; Xu, X.M.; Wang, G.; Monje, P.V. Magnetic separation of peripheral nerve-resident cells underscores key molecular features of human Schwann cells and fibroblasts: an immunochemical and transcriptomics approach. *Sci Rep* **2020**, *10*(1), 18433, doi:10.1038/s41598-020-74128-3.

424. Saalbach, A.; Aust, G.; Haustein, U.F.; Herrmann, K.; Anderegg, U. The fibroblast-specific MAb AS02: a novel tool for detection and elimination of human fibroblasts. *Cell Tissue Res* **1997**, *290*(3), 593-599, doi:10.1007/s004410050964.

425. Pastrana, E.; Silva-Vargas, V.; Doetsch, F. Eyes wide open: a critical review of sphere-formation as an assay for stem cells. *Cell Stem Cell* **2011**, *8*(5), 486-498, doi:10.1016/j.stem.2011.04.007.

426. Trentin, A.; Glavieux-Pardanaud, C.; Le Douarin, N.M.; Dupin, E. Self-renewal capacity is a widespread property of various types of neural crest precursor cells. *Proc Natl Acad Sci U S A* **2004**, *101*(13), 4495-4500, doi:10.1073/pnas.0400629101.

427. Gruber, H.E.; Somayaji, S.; Riley, F.; Hoelscher, G.L.; Norton, H.J.; Ingram, J.; Hanley, E.N., Jr. Human adipose-derived mesenchymal stem cells: serial passaging, doubling time and cell senescence. *Biotech Histochem* **2012**, *87*(4), 303-311, doi:10.3109/10520295.2011.649785.

428. Trokovic, R.; Weltner, J.; Noisa, P.; Raivio, T.; Otonkoski, T. Combined negative effect of donor age and time in culture on the reprogramming efficiency into induced pluripotent stem cells. *Stem Cell Res* **2015**, *15*(1), 254-262, doi:10.1016/j.scr.2015.06.001.

429. Moulin, V.J.; Mayrand, D.; Laforce-Lavoie, A.; Larochelle, S.; Genest, H. In Vitro Culture Methods of Skin Cells for Optimal Skin Reconstruction by Tissue Engineering. In *Regenerative Medicine and Tissue Engineering*, Daniel, E., Ed.; IntechOpen: Rijeka, 2011; pp. 195-208.

430. Horvath, S.; Lu, A.T.; Cohen, H.; Raj, K. Rapamycin retards epigenetic ageing of keratinocytes independently of its effects on replicative senescence, proliferation and differentiation. *Aging (Albany NY)* **2019**, *11*(10), 3238-3249, doi:10.18632/aging.101976.

431. De Luca, M.; D'Anna, F.; Bondanza, S.; Franzi, A.T.; Cancedda, R. Human epithelial cells induce human melanocyte growth in vitro but only skin keratinocytes regulate its proper differentiation in the absence of dermis. *J Cell Biol* **1988**, *107*(5), 1919-1926, doi:10.1083/jcb.107.5.1919.

432. Calderon-Martinez, D.; Garavito, Z.; Spinel, C.; Hurtado, H. Schwann cell-enriched cultures from adult human peripheral nerve: a technique combining short enzymatic dissociation and treatment with cytosine arabinoside (Ara-C). *J Neurosci Methods* **2002**, *114*(1), 1-8, doi:10.1016/s0165-0270(01)00493-9.

433. Lehmann, H.C.; Chen, W.; Mi, R.; Wang, S.; Liu, Y.; Rao, M.; Hoke, A. Human Schwann cells retain essential phenotype characteristics after immortalization. *Stem Cells Dev* **2012**, *21*(3), 423-431, doi:10.1089/scd.2010.0513.

434. Gledhill, K.; Guo, Z.; Umegaki-Arao, N.; Higgins, C.A.; Itoh, M.; Christiano, A.M. Melanin Transfer in Human 3D Skin Equivalents Generated Exclusively from Induced Pluripotent Stem Cells. *PLoS One* **2015**, *10*(8), e0136713, doi:10.1371/journal.pone.0136713.

435. Halaban, R.; Alfano, F.D. Selective elimination of fibroblasts from cultures of normal human melanocytes. *In Vitro* **1984**, *20*(5), 447-450, doi:10.1007/BF02619590.

436. Li, S.; Zenkel, M.; Kruse, F.E.; Giessl, A.; Schlotzer-Schrehardt, U. Identification, Isolation, and Characterization of Melanocyte Precursor Cells in the Human Limbal Stroma. *Int J Mol Sci* **2022**, *23*(7), doi:10.3390/ijms23073756.

437. Hsiao, F.S.; Cheng, C.C.; Peng, S.Y.; Huang, H.Y.; Lian, W.S.; Jan, M.L.; Fang, Y.T.; Cheng, E.C.; Lee, K.H.; Cheng, W.T.; Lin, S.P.; Wu, S.C. Isolation of therapeutically functional mouse bone marrow mesenchymal stem cells within 3 h by an effective single-step plastic-adherent method. *Cell Prolif* **2010**, *43*(3), 235-248, doi:10.1111/j.1365-2184.2010.00674.x.

438. Tomlinson, M.J.; Tomlinson, S.; Yang, X.B.; Kirkham, J. Cell separation: Terminology and practical considerations. *J Tissue Eng* **2013**, *4*2041731412472690, doi:10.1177/2041731412472690.

439. Henrot, P.; Laurent, P.; Levionnois, E.; Leleu, D.; Pain, C.; Truchetet, M.E.; Cario, M. A Method for Isolating and Culturing Skin Cells: Application to Endothelial Cells, Fibroblasts, Keratinocytes, and Melanocytes From Punch Biopsies in Systemic Sclerosis Skin. *Front Immunol* **2020**, *11*566607, doi:10.3389/fimmu.2020.566607.

440. Kisselbach, L.; Merges, M.; Bossie, A.; Boyd, A. CD90 Expression on human primary cells and elimination of contaminating fibroblasts from cell cultures. *Cytotechnology* **2009**, *59*(1), 31-44, doi:10.1007/s10616-009-9190-3.

441. Komiyama, T.; Nakao, Y.; Toyama, Y.; Asou, H.; Vacanti, C.A.; Vacanti, M.P. A novel technique to isolate adult Schwann cells for an artificial nerve conduit. *J Neurosci Methods* **2003**, *122*(2), 195-200, doi:10.1016/s0165-0270(02)00320-5.

442. Bourland, J.; Mayrand, D.; Tremblay, N.; Moulin, V.J.; Fradette, J.; Auger, F.A. Isolation and Culture of Human Dermal Microvascular Endothelial Cells. *Methods Mol Biol* **2019**, *1993*79-90, doi:10.1007/978-1-4939-9473-1_7.

443. Liao, X.; Makris, M.; Luo, X.M. Fluorescence-activated Cell Sorting for Purification of Plasmacytoid Dendritic Cells from the Mouse Bone Marrow. *J Vis Exp* **2016**, (117), doi:10.3791/54641.

444. Manohar, S.M.; Shah, P.; Nair, A. Flow cytometry: principles, applications and recent advances. *Bioanalysis* **2021**, *13*(3), 181-198, doi:10.4155/bio-2020-0267.

445. Polisetti, N.; Schlotzer-Schrehardt, U.; Reinhard, T.; Schlunck, G. Isolation and enrichment of melanocytes from human corneal limbus using CD117 (c-Kit) as selection marker. *Sci Rep* **2020**, *10*(1), 17588, doi:10.1038/s41598-020-74869-1.

446. Willemsen, M.; Luiten, R.M.; Teunissen, M.B.M. Instant isolation of highly purified human melanocytes from freshly prepared epidermal cell suspensions. *Pigment Cell Melanoma Res* **2020**, *33*(5), 763-766, doi:10.1111/pcmr.12882.

447. Sobiepanek, A.; Kowalska, P.D.; Soszyńska, M.; Ścieżyńska, A. Implementation of Geneticin in the in vitro cell culture and in vivo studies. *Review and Research on Cancer Treatment* **2020**, *6*(1), 79-87.

448. Lai, T.Y.; Cao, J.; Ou-Yang, P.; Tsai, C.Y.; Lin, C.W.; Chen, C.C.; Tsai, M.K.; Lee, C.Y. Different methods of detaching adherent cells and their effects on the cell surface expression of Fas receptor and Fas ligand. *Sci Rep* **2022**, *12*(1), 5713, doi:10.1038/s41598-022-09605-y.

449. Quan, Y.; Yan, Y.; Wang, X.; Fu, Q.; Wang, W.; Wu, J.; Yang, G.; Ren, J.; Wang, Y. Impact of cell dissociation on identification of breast cancer stem cells. *Cancer Biomark* **2012**, *12*(3), 125-133, doi:10.3233/CBM-130300.

450. Skog, M.; Sivler, P.; Steinvall, I.; Aili, D.; Sjoberg, F.; Elmasry, M. The Effect of Enzymatic Digestion on Cultured Epithelial Autografts. *Cell Transplant* **2019**, *28*(5), 638-644, doi:10.1177/0963689719833305.

451. Gobin, C.M.; Menefee, J.N.; Lattimore, C.C.; Doty, A.; Fredenburg, K.M. Cell Dissociation Enzymes Affect Annexin V/Flow-Cytometric Apoptotic Assay Outcomes After miRNA-based Transient Transfection. *Anticancer Res* **2022**, *42*(6), 2819-2825, doi:10.21873/anticanres.15763.

452. Li, T.; Li, C.; Zhang, C.Y.; Zhao, J. Effect of accutase or trypsin dissociation on the apoptosis of human striatum-derived neural stem cells. *Zhongguo Yi Xue Ke Xue Yuan Xue Bao* **2015**, *37*(2), 185-194, doi:10.3881/j.issn.1000-503X.2015.02.009.

453. Miltenyi, S.; Muller, W.; Weichel, W.; Radbruch, A. High gradient magnetic cell separation with MACS. *Cytometry* **1990**, *11*(2), 231-238, doi:10.1002/cyto.990110203.

454. Moore, D.K.; Motaung, B.; du Plessis, N.; Shabangu, A.N.; Loxton, A.G.; SU-IRG Consortium. Isolation of B-cells using Miltenyi MACS bead isolation kits. *PLoS One* **2019**, *14*(3), e0213832, doi:10.1371/journal.pone.0213832.

455. Peters, C.E.; Woodside, S.M.; Eaves, A.C. Isolation of subsets of immune cells. *Methods Mol Biol* **2005**, *302*95-116, doi:10.1385/1-59259-903-6:095.

456. Frenea-Robin, M.; Marchalot, J. Basic Principles and Recent Advances in Magnetic Cell Separation. *Magnetochemistry* **2022**, *8*(1), 11, doi:10.3390/magnetochemistry8010011.

457. Jiang, D.; Rinkevich, Y. Defining Skin Fibroblastic Cell Types Beyond CD90. *Front Cell Dev Biol* **2018**, *6*133, doi:10.3389/fcell.2018.00133.

458. Walmsley, G.G.; Rinkevich, Y.; Hu, M.S.; Montoro, D.T.; Lo, D.D.; McArdle, A.; Maan, Z.N.; Morrison, S.D.; Duscher, D.; Whittam, A.J.; Wong, V.W.; Weissman, I.L.; Gurtner, G.C.; Longaker, M.T. Live fibroblast harvest reveals surface marker shift in vitro. *Tissue Eng Part C Methods* **2015**, *21*(3), 314-321, doi:10.1089/ten.TEC.2014.0118.

459. Janson, D.G.; Saintigny, G.; van Adrichem, A.; Mahe, C.; El Ghalbzouri, A. Different gene expression patterns in human papillary and reticular fibroblasts. *J Invest Dermatol* **2012**, *132*(11), 2565-2572, doi:10.1038/jid.2012.192.

460. Janson, D.; Saintigny, G.; Mahe, C.; El Ghalbzouri, A. Papillary fibroblasts differentiate into reticular fibroblasts after prolonged in vitro culture. *Exp Dermatol* **2013**, *22*(1), 48-53, doi:10.1111/exd.12069.

461. Rippa, A.L.; Kalabusheva, E.P.; Vorotelyak, E.A. Regeneration of Dermis: Scarring and Cells Involved. *Cells* **2019**, *8*(6), doi:10.3390/cells8060607.

462. Driskell, R.R.; Lichtenberger, B.M.; Hoste, E.; Kretzschmar, K.; Simons, B.D.; Charalambous, M.; Ferron, S.R.; Herault, Y.; Pavlovic, G.; Ferguson-Smith, A.C.; Watt, F.M. Distinct fibroblast lineages determine dermal architecture in skin development and repair. *Nature* **2013**, *504*(7479), 277-281, doi:10.1038/nature12783.

463. Philippeos, C.; Telerman, S.B.; Oules, B.; Pisco, A.O.; Shaw, T.J.; Elgueta, R.; Lombardi, G.; Driskell, R.R.; Soldin, M.; Lynch, M.D.; Watt, F.M. Spatial and Single-Cell Transcriptional Profiling Identifies Functionally Distinct Human Dermal Fibroblast Subpopulations. *J Invest Dermatol* **2018**, *138*(4), 811-825, doi:10.1016/j.jid.2018.01.016.

464. Tabib, T.; Morse, C.; Wang, T.; Chen, W.; Lafyatis, R. SFRP2/DPP4 and FMO1/LSP1 Define Major Fibroblast Populations in Human Skin. *J Invest Dermatol* **2018**, *138*(4), 802-810, doi:10.1016/j.jid.2017.09.045.

465. Lynch, M.D.; Watt, F.M. Fibroblast heterogeneity: implications for human disease. *J Clin Invest* **2018**, *128*(1), 26-35, doi:10.1172/JCI93555.

466. Grutzkau, A.; Radbruch, A. Small but mighty: how the MACS-technology based on nanosized superparamagnetic particles has helped to analyze the immune system within the last 20 years. *Cytometry A* **2010**, *77*(7), 643-647, doi:10.1002/cyto.a.20918.

467. Chalmers, J.J.; Xiong, Y.; Jin, X.; Shao, M.; Tong, X.; Farag, S.; Zborowski, M. Quantification of non-specific binding of magnetic micro- and nanoparticles using cell tracking velocimetry: Implication for magnetic cell separation and detection. *Biotechnol Bioeng* **2010**, *105*(6), 1078-1093, doi:10.1002/bit.22635.

468. Marques, G.S.; Silva, Z.; Videira, P.A. Antitumor Efficacy of Human Monocyte-Derived Dendritic Cells: Comparing Effects of two Monocyte Isolation Methods. *Biol Proced Online* **2018**, *20*4, doi:10.1186/s12575-018-0069-6.

469. Farrell, E.; Wielopolski, P.; Pavljasevic, P.; van Tiel, S.; Jahr, H.; Verhaar, J.; Weinans, H.; Krestin, G.; O'Brien, F.J.; van Osch, G.; Bernsen, M. Effects of iron oxide incorporation for long term cell tracking on MSC differentiation in vitro and in vivo. *Biochem Biophys Res Commun* **2008**, *369*(4), 1076-1081, doi:10.1016/j.bbrc.2008.02.159.

470. Meinhardt, K.; Kroeger, I.; Abendroth, A.; Muller, S.; Mackensen, A.; Ullrich, E. Influence of NK cell magnetic bead isolation methods on phenotype and function of murine NK cells. *J Immunol Methods* **2012**, *378*(1-2), 1-10, doi:10.1016/j.jim.2012.01.008.

471. Mahmoudi, M.; Azadmanesh, K.; Shokrgozar, M.A.; Journeay, W.S.; Laurent, S. Effect of nanoparticles on the cell life cycle. *Chem Rev* **2011**, *111*(5), 3407-3432, doi:10.1021/cr1003166.

472. Shen, M.J.; Olsthoorn, R.C.L.; Zeng, Y.; Bakkum, T.; Kros, A.; Boyle, A.L. Magnetic-Activated Cell Sorting Using Coiled-Coil Peptides: An Alternative Strategy for Isolating Cells with High Efficiency and Specificity. *ACS Appl Mater Interfaces* **2021**, *13*(10), 11621-11630, doi:10.1021/acsami.0c22185.

473. Van de Walle, A.; Perez, J.E.; Abou-Hassan, A.; Hémadi, M.; Luciani, N.; Wilhelm, C. Magnetic nanoparticles in regenerative medicine: what of their fate and impact in stem cells? *Materials Today Nano* **2020**, *11*( ), 100084, doi:10.1016/j.mtnano.2020.100084.

474. Muller, P.; Gaebel, R.; Lemcke, H.; Steinhoff, G.; David, R. Data on the fate of MACS(R) MicroBeads intramyocardially co-injected with stem cell products. *Data Brief* **2017**, *13*569-574, doi:10.1016/j.dib.2017.06.035.

475. Muller, P.; Gaebel, R.; Lemcke, H.; Wiekhorst, F.; Hausburg, F.; Lang, C.; Zarniko, N.; Westphal, B.; Steinhoff, G.; David, R. Intramyocardial fate and effect of iron nanoparticles co-injected with MACS(R) purified stem cell products. *Biomaterials* **2017**, *135*74-84, doi:10.1016/j.biomaterials.2017.05.002.

476. Laghmouchi, A.; Hoogstraten, C.; Falkenburg, J.H.F.; Jedema, I. Long-term in vitro persistence of magnetic properties after magnetic bead-based cell separation of T cells. *Scand J Immunol* **2020**, *92*(3), e12924, doi:10.1111/sji.12924.

477. Olbrich, M.; Rieger, M.; Reinert, S.; Alexander, D. Isolation of osteoprogenitors from human jaw periosteal cells: a comparison of two magnetic separation methods. *PLoS One* **2012**, *7*(10), e47176, doi:10.1371/journal.pone.0047176.

478. Meyers, C.A.; Xu, J.; Zhang, L.; Chang, L.; Wang, Y.; Asatrian, G.; Ding, C.; Yan, N.; Zou, E.; Broderick, K.; Lee, M.; Peault, B.; James, A.W. Skeletogenic Capacity of Human Perivascular Stem Cells Obtained Via Magnetic-Activated Cell Sorting. *Tissue Eng Part A* **2019**, *25*(23-24), 1658-1666, doi:10.1089/ten.TEA.2019.0031.

479. Oren, A.; Husebo, C.; Iversen, A.C.; Austgulen, R. A comparative study of immunomagnetic methods used for separation of human natural killer cells from peripheral blood. *J Immunol Methods* **2005**, *303*(1-2), 1-10, doi:10.1016/j.jim.2005.04.022.

480. Miltenyi Biotec. Magnetic Cell Separation. 2022. Available online: https://www.miltenyibiotec.com/DE-en/resources/macs-handbook/macs-technologies/cell-separation/magnetic-cell-separation.html (accessed on May 9, 2022).

481. Miltenyi Biotec. MACS® Cell Separation, Select the best. 2022. Available online: https://www.miltenyibiotec.com/_Resources/Persistent/b5349effdd595b72195e588aff033be3e24706bd/IM0020021.pdf (accessed on May 9, 2022).

482. Poirier, J. Chapter 5 - Genetic profiling of tumors in PDX models. In *Patient Derived Tumor Xenograft Models*, Uthamanthyl, R., Tinkey, P., Eds.; Academic Press: London, 2015; pp. 149–159.

483. El Ghalbzouri, A.; Commandeur, S.; Rietveld, M.H.; Mulder, A.A.; Willemze, R. Replacement of animal-derived collagen matrix by human fibroblast-derived dermal matrix for human skin equivalent products. *Biomaterials* **2009**, *30*(1), 71-78, doi:10.1016/j.biomaterials.2008.09.002.

484. Pavez Lorie, E.; Boukamp, P. Methods in cell biology: Cell-derived matrices. *Methods Cell Biol* **2020**, *156*309-332, doi:10.1016/bs.mcb.2019.11.012.

485. Berning, M.; Pratzel-Wunder, S.; Bickenbach, J.R.; Boukamp, P. Three-Dimensional In Vitro Skin and Skin Cancer Models Based on Human Fibroblast-Derived Matrix. *Tissue Eng Part C Methods* **2015**, *21*(9), 958-970, doi:10.1089/ten.TEC.2014.0698.

486. Luo, L.Z.; Gopalakrishna-Pillai, S.; Nay, S.L.; Park, S.W.; Bates, S.E.; Zeng, X.; Iverson, L.E.; O'Connor, T.R. DNA repair in human pluripotent stem cells is distinct from that in non-pluripotent human cells. *PLoS One* **2012**, *7*(3), e30541, doi:10.1371/journal.pone.0030541.

487. Maynard, S.; Swistowska, A.M.; Lee, J.W.; Liu, Y.; Liu, S.T.; Da Cruz, A.B.; Rao, M.; de Souza-Pinto, N.C.; Zeng, X.; Bohr, V.A. Human embryonic stem cells have enhanced repair of multiple forms of DNA damage. *Stem Cells* **2008**, *26*(9), 2266-2274, doi:10.1634/stemcells.2007-1041.

488. Momcilovic, O.; Knobloch, L.; Fornsaglio, J.; Varum, S.; Easley, C.; Schatten, G. DNA damage responses in human induced pluripotent stem cells and embryonic stem cells. *PLoS One* **2010**, *5*(10), e13410, doi:10.1371/journal.pone.0013410.

489. Van Sloun, P.P.; Jansen, J.G.; Weeda, G.; Mullenders, L.H.; van Zeeland, A.A.; Lohman, P.H.; Vrieling, H. The role of nucleotide excision repair in protecting embryonic stem cells from genotoxic effects of UV-induced DNA damage. *Nucleic Acids Res* **1999**, *27*(16), 3276-3282, doi:10.1093/nar/27.16.3276.

490. Hemminki, K.; Xu, G.; Le Curieux, F. Ultraviolet radiation-induced photoproducts in human skin DNA as biomarkers of damage and its repair. *IARC Sci Publ* **2001**, *154*69-79.

491. Kemp, M.G.; Spandau, D.F.; Travers, J.B. Impact of Age and Insulin-Like Growth Factor-1 on DNA Damage Responses in UV-Irradiated Human Skin. *Molecules* **2017**, *22*(3), doi:10.3390/molecules22030356.

492. Smit, N.P.; Vink, A.A.; Kolb, R.M.; Steenwinkel, M.J.; van den Berg, P.T.; van Nieuwpoort, F.; Roza, L.; Pavel, S. Melanin offers protection against induction of cyclobutane pyrimidine dimers and 6-4 photoproducts by UVB in cultured human melanocytes. *Photochem Photobiol* **2001**, *74*(3), 424-430, doi:10.1562/0031-8655(2001)074<0424:mopaio>2.0.co;2.

493. Tadokoro, T.; Kobayashi, N.; Zmudzka, B.Z.; Ito, S.; Wakamatsu, K.; Yamaguchi, Y.; Korossy, K.S.; Miller, S.A.; Beer, J.Z.; Hearing, V.J. UV-induced DNA damage and melanin content in human skin differing in racial/ethnic origin. *FASEB J* **2003**, *17*(9), 1177-1179, doi:10.1096/fj.02-0865fje.

494. Hazane, F.; Sauvaigo, S.; Douki, T.; Favier, A.; Beani, J.C. Age-dependent DNA repair and cell cycle distribution of human skin fibroblasts in response to UVA irradiation. *J Photochem Photobiol B* **2006**, *82*(3), 214-223, doi:10.1016/j.jphotobiol.2005.10.004.

495. Takahashi, Y.; Moriwaki, S.; Sugiyama, Y.; Endo, Y.; Yamazaki, K.; Mori, T.; Takigawa, M.; Inoue, S. Decreased gene expression responsible for post-ultraviolet DNA repair synthesis in aging: a possible mechanism of age-related reduction in DNA repair capacity. *J Invest Dermatol* **2005**, *124*(2), 435-442, doi:10.1111/j.0022-202X.2004.23591.x.

496. Liu, S.C.; Parsons, S.; Hanawalt, P.C. DNA repair in cultured keratinocytes. *J Invest Dermatol* **1983**, *81*(1 Suppl), 179s-183s, doi:10.1111/1523-1747.ep12541076.

497. Moriwaki, S.; Takahashi, Y. Photoaging and DNA repair. *J Dermatol Sci* **2008**, *50*(3), 169-176, doi:10.1016/j.jdermsci.2007.08.011.

498. Godini, R.; Lafta, H.Y.; Fallahi, H. Epigenetic modifications in the embryonic and induced pluripotent stem cells. *Gene Expr Patterns* **2018**, *29*1-9, doi:10.1016/j.gep.2018.04.001.

499. Liu, L.; Michowski, W.; Kolodziejczyk, A.; Sicinski, P. The cell cycle in stem cell proliferation, pluripotency and differentiation. *Nat Cell Biol* **2019**, *21*(9), 1060-1067, doi:10.1038/s41556-019-0384-4.

500. Martello, G.; Smith, A. The nature of embryonic stem cells. *Annu Rev Cell Dev Biol* **2014**, *30*647-675, doi:10.1146/annurev-cellbio-100913-013116.

501. Mujoo, K.; Butler, E.B.; Pandita, R.K.; Hunt, C.R.; Pandita, T.K. Pluripotent Stem Cells and DNA Damage Response to Ionizing Radiations. *Radiat Res* **2016**, *186*(1), 17-26, doi:10.1667/RR14417.1.

502. Zheng, H.; Xie, W. The role of 3D genome organization in development and cell differentiation. *Nat Rev Mol Cell Biol* **2019**, *20*(9), 535-550, doi:10.1038/s41580-019-0132-4.

503. Rossi, D.J.; Jamieson, C.H.; Weissman, I.L. Stems cells and the pathways to aging and cancer. *Cell* **2008**, *132*(4), 681-696, doi:10.1016/j.cell.2008.01.036.

504. Wakamatsu, K.; Kavanagh, R.; Kadekaro, A.L.; Terzieva, S.; Sturm, R.A.; Leachman, S.; Abdel-Malek, Z.; Ito, S. Diversity of pigmentation in cultured human melanocytes is due to differences in the type as well as quantity of melanin. *Pigment Cell Res* **2006**, *19*(2), 154-162, doi:10.1111/j.1600-0749.2006.00293.x.

505. Hauser, J.E.; Kadekaro, A.L.; Kavanagh, R.J.; Wakamatsu, K.; Terzieva, S.; Schwemberger, S.; Babcock, G.; Rao, M.B.; Ito, S.; Abdel-Malek, Z.A. Melanin content and MC1R function independently affect UVR-induced DNA damage in cultured human melanocytes. *Pigment Cell Res* **2006**, *19*(4), 303-314, doi:10.1111/j.1600-0749.2006.00315.x.

506. Bee, L.; Marini, S.; Pontarin, G.; Ferraro, P.; Costa, R.; Albrecht, U.; Celotti, L. Nucleotide excision repair efficiency in quiescent human fibroblasts is modulated by circadian clock. *Nucleic Acids Res* **2015**, *43*(4), 2126-2137, doi:10.1093/nar/gkv081.

507. Takata, H.; Hanafusa, T.; Mori, T.; Shimura, M.; Iida, Y.; Ishikawa, K.; Yoshikawa, K.; Yoshikawa, Y.; Maeshima, K. Chromatin compaction protects genomic DNA from radiation damage. *PLoS One* **2013**, *8*(10), e75622, doi:10.1371/journal.pone.0075622.

508. Tang, N.; Bueno, M.; Meylan, S.; Incerti, S.; Tran, H.N.; Vaurijoux, A.; Gruel, G.; Villagrasa, C. Influence of chromatin compaction on simulated early radiation-induced DNA damage using Geant4-DNA. *Med Phys* **2019**, *46*(3), 1501-1511, doi:10.1002/mp.13405.

509. Nouspikel, T. DNA repair in differentiated cells: some new answers to old questions. *Neuroscience* **2007**, *145*(4), 1213-1221, doi:10.1016/j.neuroscience.2006.07.006.

510. Nouspikel, T.; Hanawalt, P.C. DNA repair in terminally differentiated cells. *DNA Repair (Amst)* **2002**, *1*(1), 59-75, doi:10.1016/s1568-7864(01)00005-2.

511. Sjakste, N.; Riekstina, U. DNA damage and repair in differentiation of stem cells and cells of connective cell lineages: A trigger or a complication? *Eur J Histochem* **2021**, *65*(2), doi:10.4081/ejh.2021.3236.

512. Nouspikel, T.; Hanawalt, P.C. Terminally differentiated human neurons repair transcribed genes but display attenuated global DNA repair and modulation of repair gene expression. *Mol Cell Biol* **2000**, *20*(5), 1562-1570, doi:10.1128/MCB.20.5.1562-1570.2000.

513. Ho, L.; Hanawalt, P.C. Gene-specific DNA repair in terminally differentiating rat myoblasts. *Mutat Res* **1991**, *255*(2), 123-141, doi:10.1016/0921-8777(91)90047-s.

514. D'Errico, M.; Lemma, T.; Calcagnile, A.; Proietti De Santis, L.; Dogliotti, E. Cell type and DNA damage specific response of human skin cells to environmental agents. *Mutat Res* **2007**, *614*(1-2), 37-47, doi:10.1016/j.mrfmmm.2006.06.009.

515. D'Errico, M.; Teson, M.; Calcagnile, A.; Proietti De Santis, L.; Nikaido, O.; Botta, E.; Zambruno, G.; Stefanini, M.; Dogliotti, E. Apoptosis and efficient repair of DNA damage protect human keratinocytes against UVB. *Cell Death Differ* **2003**, *10*(6), 754-756, doi:10.1038/sj.cdd.4401224.

516. Lopez Perez, R.; Brauer, J.; Ruhle, A.; Trinh, T.; Sisombath, S.; Wuchter, P.; Grosu, A.L.; Debus, J.; Saffrich, R.; Huber, P.E.; Nicolay, N.H. Human mesenchymal stem cells are resistant to UV-B irradiation. *Sci Rep* **2019**, *9*(1), 20000, doi:10.1038/s41598-019-56591-9.

517. Metral, E.; Bechetoille, N.; Demarne, F.; Damour, O.; Rachidi, W. Keratinocyte stem cells are more resistant to UVA radiation than their direct progeny. *PLoS One* **2018**, *13*(9), e0203863, doi:10.1371/journal.pone.0203863.

518. Shimura, T.; Sasatani, M.; Kawai, H.; Kamiya, K.; Kobayashi, J.; Komatsu, K.; Kunugita, N. A comparison of radiation-induced mitochondrial damage between neural progenitor stem cells and differentiated cells. *Cell Cycle* **2017**, *16*(6), 565-573, doi:10.1080/15384101.2017.1284716.

519. Harfouche, G.; Vaigot, P.; Rachidi, W.; Rigaud, O.; Moratille, S.; Marie, M.; Lemaitre, G.; Fortunel, N.O.; Martin, M.T. Fibroblast growth factor type 2 signaling is critical for DNA repair in human keratinocyte stem cells. *Stem Cells* **2010**, *28*(9), 1639-1648, doi:10.1002/stem.485.

520. Hildrestrand, G.A.; Diep, D.B.; Kunke, D.; Bolstad, N.; Bjoras, M.; Krauss, S.; Luna, L. The capacity to remove 8-oxoG is enhanced in newborn neural stem/progenitor cells and decreases in juvenile mice and upon cell differentiation. *DNA Repair (Amst)* **2007**, *6*(6), 723-732, doi:10.1016/j.dnarep.2006.12.008.

521. Becker, K.A.; Ghule, P.N.; Therrien, J.A.; Lian, J.B.; Stein, J.L.; van Wijnen, A.J.; Stein, G.S. Self-renewal of human embryonic stem cells is supported by a shortened G1 cell cycle phase. *J Cell Physiol* **2006**, *209*(3), 883-893, doi:10.1002/jcp.20776.

522. Coronado, D.; Godet, M.; Bourillot, P.Y.; Tapponnier, Y.; Bernat, A.; Petit, M.; Afanassieff, M.; Markossian, S.; Malashicheva, A.; Iacone, R.; Anastassiadis, K.; Savatier, P. A short G1 phase is an intrinsic determinant of naive embryonic stem cell pluripotency. *Stem Cell Res* **2013**, *10*(1), 118-131, doi:10.1016/j.scr.2012.10.004.

523. Boward, B.; Wu, T.; Dalton, S. Concise Review: Control of Cell Fate Through Cell Cycle and Pluripotency Networks. *Stem Cells* **2016**, *34*(6), 1427-1436, doi:10.1002/stem.2345.

524. Tsubouchi, T.; Fisher, A.G. Reprogramming and the pluripotent stem cell cycle. *Curr Top Dev Biol* **2013**, *104*223-241, doi:10.1016/B978-0-12-416027-9.00007-3.

525. Hyka-Nouspikel, N.; Lemonidis, K.; Lu, W.T.; Nouspikel, T. Circulating human B lymphocytes are deficient in nucleotide excision repair and accumulate mutations upon proliferation. *Blood* **2011**, *117*(23), 6277-6286, doi:10.1182/blood-2010-12-326637.

526. Goodman, M.F.; Woodgate, R. Translesion DNA polymerases. *Cold Spring Harb Perspect Biol* **2013**, *5*(10), a010363, doi:10.1101/cshperspect.a010363.

527. Klein, H.L.; Bacinskaja, G.; Che, J.; Cheblal, A.; Elango, R.; Epshtein, A.; Fitzgerald, D.M.; Gomez-Gonzalez, B.; Khan, S.R.; Kumar, S.; Leland, B.A.; Marie, L.; Mei, Q.; Mine-Hattab, J.; Piotrowska, A.; Polleys, E.J.; Putnam, C.D.; Radchenko, E.A.; Saada, A.A.; Sakofsky, C.J.; et al. Guidelines for DNA recombination and repair studies: Cellular assays of DNA repair pathways. *Microb Cell* **2019**, *6*(1), 1-64, doi:10.15698/mic2019.01.664.

528. Sancar, A.; Lindsey-Boltz, L.A.; Kang, T.H.; Reardon, J.T.; Lee, J.H.; Ozturk, N. Circadian clock control of the cellular response to DNA damage. *FEBS Lett* **2010**, *584*(12), 2618-2625, doi:10.1016/j.febslet.2010.03.017.

529. Gaddameedhi, S.; Selby, C.P.; Kaufmann, W.K.; Smart, R.C.; Sancar, A. Control of skin cancer by the circadian rhythm. *Proc Natl Acad Sci U S A* **2011**, *108*(46), 18790-18795, doi:10.1073/pnas.1115249108.

530. Jimbow, K.; Roth, S.I.; Fitzpatrick, T.B.; Szabo, G. Mitotic activity in non-neoplastic melanocytes in vivo as determined by histochemical, autoradiographic, and electron microscope studies. *J Cell Biol* **1975**, *66*(3), 663-670, doi:10.1083/jcb.66.3.663.

531. Li, V.C.; Kirschner, M.W. Molecular ties between the cell cycle and differentiation in embryonic stem cells. *Proc Natl Acad Sci U S A* **2014**, *111*(26), 9503-9508, doi:10.1073/pnas.1408638111.

532. Eisinger, M.; Marko, O. Selective proliferation of normal human melanocytes in vitro in the presence of phorbol ester and cholera toxin. *Proc Natl Acad Sci U S A* **1982**, *79*(6), 2018-2022, doi:10.1073/pnas.79.6.2018.

533. Herlyn, M.; Rodeck, U.; Mancianti, M.; Cardillo, F.M.; Lang, A.; Ross, A.H.; Jambrosic, J.; Koprowski, H. Expression of melanoma-associated antigens in rapidly dividing human melanocytes in culture. *Cancer Res* **1987**, *47*(12), 3057-3061.

534. Latonen, L.; Taya, Y.; Laiho, M. UV-radiation induces dose-dependent regulation of p53 response and modulates p53-HDM2 interaction in human fibroblasts. *Oncogene* **2001**, *20*(46), 6784-6793, doi:10.1038/sj.onc.1204883.

535. Hyka-Nouspikel, N.; Desmarais, J.; Gokhale, P.J.; Jones, M.; Meuth, M.; Andrews, P.W.; Nouspikel, T. Deficient DNA damage response and cell cycle checkpoints lead to accumulation of point mutations in human embryonic stem cells. *Stem Cells* **2012**, *30*(9), 1901-1910, doi:10.1002/stem.1177.

536. Ter Huurne, M.; Stunnenberg, H.G. G1-phase progression in pluripotent stem cells. *Cell Mol Life Sci* **2021**, *78*(10), 4507-4519, doi:10.1007/s00018-021-03797-8.

537. Barta, T.; Vinarsky, V.; Holubcova, Z.; Dolezalova, D.; Verner, J.; Pospisilova, S.; Dvorak, P.; Hampl, A. Human embryonic stem cells are capable of executing G1/S checkpoint activation. *Stem Cells* **2010**, *28*(7), 1143-1152, doi:10.1002/stem.451.

538. Momcilovic, O.; Choi, S.; Varum, S.; Bakkenist, C.; Schatten, G.; Navara, C. Ionizing radiation induces ataxia telangiectasia mutated-dependent checkpoint signaling and G(2) but not G(1) cell cycle arrest in pluripotent human embryonic stem cells. *Stem Cells* **2009**, *27*(8), 1822-1835, doi:10.1002/stem.123.

539. Ballabeni, A.; Park, I.H.; Zhao, R.; Wang, W.; Lerou, P.H.; Daley, G.Q.; Kirschner, M.W. Cell cycle adaptations of embryonic stem cells. *Proc Natl Acad Sci U S A* **2011**, *108*(48), 19252-19257, doi:10.1073/pnas.1116794108.

540. Maimets, T.; Neganova, I.; Armstrong, L.; Lako, M. Activation of p53 by nutlin leads to rapid differentiation of human embryonic stem cells. *Oncogene* **2008**, *27*(40), 5277-5287, doi:10.1038/onc.2008.166.

541. Raj, D.; Brash, D.E.; Grossman, D. Keratinocyte apoptosis in epidermal development and disease. *J Invest Dermatol* **2006**, *126*(2), 243-257, doi:10.1038/sj.jid.5700008.

542. Dumitru, R.; Gama, V.; Fagan, B.M.; Bower, J.J.; Swahari, V.; Pevny, L.H.; Deshmukh, M. Human embryonic stem cells have constitutively active Bax at the Golgi and are primed to undergo rapid apoptosis. *Mol Cell* **2012**, *46*(5), 573-583, doi:10.1016/j.molcel.2012.04.002.

543. Hong, Y.; Stambrook, P.J. Restoration of an absent G1 arrest and protection from apoptosis in embryonic stem cells after ionizing radiation. *Proc Natl Acad Sci U S A* **2004**, *101*(40), 14443-14448, doi:10.1073/pnas.0401346101.

544. Xu, Y. A new role for p53 in maintaining genetic stability in embryonic stem cells. *Cell Cycle* **2005**, *4*(3), 363-364, doi:10.4161/cc.4.3.1529.

545. Liu, J.C.; Guan, X.; Ryan, J.A.; Rivera, A.G.; Mock, C.; Agrawal, V.; Letai, A.; Lerou, P.H.; Lahav, G. High mitochondrial priming sensitizes hESCs to DNA-damage-induced apoptosis. *Cell Stem Cell* **2013**, *13*(4), 483-491, doi:10.1016/j.stem.2013.07.018.

546. Sabapathy, K.; Klemm, M.; Jaenisch, R.; Wagner, E.F. Regulation of ES cell differentiation by functional and conformational modulation of p53. *EMBO J* **1997**, *16*(20), 6217-6229, doi:10.1093/emboj/16.20.6217.

547. Solozobova, V.; Blattner, C. Regulation of p53 in embryonic stem cells. *Exp Cell Res* **2010**, *316*(15), 2434-2446, doi:10.1016/j.yexcr.2010.06.006.

548. Corbet, S.W.; Clarke, A.R.; Gledhill, S.; Wyllie, A.H. P53-dependent and -independent links between DNA-damage, apoptosis and mutation frequency in ES cells. *Oncogene* **1999**, *18*(8), 1537-1544, doi:10.1038/sj.onc.1202436.

549. Solozobova, V.; Rolletschek, A.; Blattner, C. Nuclear accumulation and activation of p53 in embryonic stem cells after DNA damage. *BMC Cell Biol* **2009**, *10*46, doi:10.1186/1471-2121-10-46.

550. Finlan, L.E.; Nenutil, R.; Ibbotson, S.H.; Vojtesek, B.; Hupp, T.R. CK2-site phosphorylation of p53 is induced in DeltaNp63 expressing basal stem cells in UVB irradiated human skin. *Cell Cycle* **2006**, *5*(21), 2489-2494, doi:10.4161/cc.5.21.3393.

551. Ikehata, H.; Yamamoto, M. Roles of the KEAP1-NRF2 system in mammalian skin exposed to UV radiation. *Toxicol Appl Pharmacol* **2018**, *360*69-77, doi:10.1016/j.taap.2018.09.038.

552. Schafer, M.; Dutsch, S.; auf dem Keller, U.; Navid, F.; Schwarz, A.; Johnson, D.A.; Johnson, J.A.; Werner, S. Nrf2 establishes a glutathione-mediated gradient of UVB cytoprotection in the epidermis. *Genes Dev* **2010**, *24*(10), 1045-1058, doi:10.1101/gad.568810.

553. Wray, H.; Mackenzie, I.C.; Storey, A.; Navsaria, H. alpha6 Integrin and CD44 enrich for a primary keratinocyte population that displays resistance to UV-induced apoptosis. *PLoS One* **2012**, *7*(10), e46968, doi:10.1371/journal.pone.0046968.

554. Sotiropoulou, P.A.; Candi, A.; Mascre, G.; De Clercq, S.; Youssef, K.K.; Lapouge, G.; Dahl, E.; Semeraro, C.; Denecker, G.; Marine, J.C.; Blanpain, C. Bcl-2 and accelerated DNA repair mediates resistance of hair follicle bulge stem cells to DNA-damage-induced cell death. *Nat Cell Biol* **2010**, *12*(6), 572-582, doi:10.1038/ncb2059.

555. Ko, E.; Lee, K.Y.; Hwang, D.S. Human umbilical cord blood-derived mesenchymal stem cells undergo cellular senescence in response to oxidative stress. *Stem Cells Dev* **2012**, *21*(11), 1877-1886, doi:10.1089/scd.2011.0284.

556. Merritt, A.J.; Potten, C.S.; Watson, A.J.; Loh, D.Y.; Nakayama, K.; Nakayama, K.; Hickman, J.A. Differential expression of bcl-2 in intestinal epithelia. Correlation with attenuation of apoptosis in colonic crypts and the incidence of colonic neoplasia. *J Cell Sci* **1995**, *108 (Pt 6)*2261-2271, doi:10.1242/jcs.108.6.2261.

557. Crowley, L.C.; Waterhouse, N.J. Detecting Cleaved Caspase-3 in Apoptotic Cells by Flow Cytometry. *Cold Spring Harb Protoc* **2016**, *2016*(11), doi:10.1101/pdb.prot087312.

558. Suzuki, J.; Denning, D.P.; Imanishi, E.; Horvitz, H.R.; Nagata, S. Xk-related protein 8 and CED-8 promote phosphatidylserine exposure in apoptotic cells. *Science* **2013**, *341*(6144), 403-406, doi:10.1126/science.1236758.

559. Suzuki, J.; Imanishi, E.; Nagata, S. Xkr8 phospholipid scrambling complex in apoptotic phosphatidylserine exposure. *Proc Natl Acad Sci U S A* **2016**, *113*(34), 9509-9514, doi:10.1073/pnas.1610403113.

560. Hudson, L.; Rashdan, E.; Bonn, C.A.; Chavan, B.; Rawlings, D.; Birch-Machin, M.A. Individual and combined effects of the infrared, visible, and ultraviolet light components of solar radiation on damage biomarkers in human skin cells. *FASEB J* **2020**, *34*(3), 3874-3883, doi:10.1096/fj.201902351RR.

561. Otto, A.I.; Riou, L.; Marionnet, C.; Mori, T.; Sarasin, A.; Magnaldo, T. Differential behaviors toward ultraviolet A and B radiation of fibroblasts and keratinocytes from normal and DNA-repair-deficient patients. *Cancer Res* **1999**, *59*(6), 1212-1218.

562. Lee, C.H.; Yu, C.L.; Liao, W.T.; Kao, Y.H.; Chai, C.Y.; Chen, G.S.; Yu, H.S. Effects and interactions of low doses of arsenic and UVB on keratinocyte apoptosis. *Chem Res Toxicol* **2004**, *17*(9), 1199-1205, doi:10.1021/tx049938m.

563. Zhivagui, M.; Hoda, A.; Valenzuela, N.; Yeh, Y.Y.; Dai, J.; He, Y.; Nandi, S.P.; Otlu, B.; Van Houten, B.; Alexandrov, L.B. DNA damage and somatic mutations in mammalian cells after irradiation with a nail polish dryer. *Nat Commun* **2023**, *14*(1), 276, doi:10.1038/s41467-023-35876-8.

564. Larsson, P.; Andersson, E.; Johansson, U.; Ollinger, K.; Rosdahl, I. Ultraviolet A and B affect human melanocytes and keratinocytes differently. A study of oxidative alterations and apoptosis. *Exp Dermatol* **2005**, *14*(2), 117-123, doi:10.1111/j.0906-6705.2005.00238.x.

565. Plettenberg, A.; Ballaun, C.; Pammer, J.; Mildner, M.; Strunk, D.; Weninger, W.; Tschachler, E. Human melanocytes and melanoma cells constitutively express the Bcl-2 proto-oncogene in situ and in cell culture. *Am J Pathol* **1995**, *146*(3), 651-659.

566. Denat, L.; Kadekaro, A.L.; Marrot, L.; Leachman, S.A.; Abdel-Malek, Z.A. Melanocytes as instigators and victims of oxidative stress. *J Invest Dermatol* **2014**, *134*(6), 1512-1518, doi:10.1038/jid.2014.65.

567. Yamaguchi, Y.; Takahashi, K.; Zmudzka, B.Z.; Kornhauser, A.; Miller, S.A.; Tadokoro, T.; Berens, W.; Beer, J.Z.; Hearing, V.J. Human skin responses to UV radiation: pigment in the upper epidermis protects against DNA damage in the lower epidermis and facilitates apoptosis. *FASEB J* **2006**, *20*(9), 1486-1488, doi:10.1096/fj.06-5725fje.

568. Applegate, L.A.; Noel, A.; Vile, G.; Frenk, E.; Tyrrell, R.M. Two genes contribute to different extents to the heme oxygenase enzyme activity measured in cultured human skin fibroblasts and keratinocytes: implications for protection against oxidant stress. *Photochem Photobiol* **1995**, *61*(3), 285-291, doi:10.1111/j.1751-1097.1995.tb03973.x.

569. Avkin, S.; Sevilya, Z.; Toube, L.; Geacintov, N.; Chaney, S.G.; Oren, M.; Livneh, Z. p53 and p21 regulate error-prone DNA repair to yield a lower mutation load. *Mol Cell* **2006**, *22*(3), 407-413, doi:10.1016/j.molcel.2006.03.022.

570. Board on Life Sciences; Division on Earth and Life Studies; National Academies of Sciences, Engineering, and Medicine. Interindividual Variability: New Ways to Study and Implications for Decision Making: Workshop in Brief. **2016**, *Mar 22*, doi:10.17226/23413.

571. Fang, D.; Leishear, K.; Nguyen, T.K.; Finko, R.; Cai, K.; Fukunaga, M.; Li, L.; Brafford, P.A.; Kulp, A.N.; Xu, X.; Smalley, K.S.; Herlyn, M. Defining the conditions for the generation of melanocytes from human embryonic stem cells. *Stem Cells* **2006**, *24*(7), 1668-1677, doi:10.1634/stemcells.2005-0414.

572. Kunisada, T.; Yamane, T.; Aoki, H.; Yoshimura, N.; Ishizaki, K.; Motohashi, T. Development of melanocytes from ES cells. *Methods Enzymol* **2003**, *365*341-349, doi:10.1016/s0076-6879(03)65024-x.

573. Motohashi, T.; Aoki, H.; Yoshimura, N.; Kunisada, T. Induction of melanocytes from embryonic stem cells and their therapeutic potential. *Pigment Cell Res* **2006**, *19*(4), 284-289, doi:10.1111/j.1600-0749.2006.00317.x.

574. Yamane, T.; Hayashi, S.; Mizoguchi, M.; Yamazaki, H.; Kunisada, T. Derivation of melanocytes from embryonic stem cells in culture. *Dev Dyn* **1999**, *216*(4-5), 450-458, doi:10.1002/(SICI)1097-0177(199912)216:4/5<450::AID-DVDY13>3.0.CO;2-0.

575. Ohta, S.; Imaizumi, Y.; Okada, Y.; Akamatsu, W.; Kuwahara, R.; Ohyama, M.; Amagai, M.; Matsuzaki, Y.; Yamanaka, S.; Okano, H.; Kawakami, Y. Generation of human melanocytes from induced pluripotent stem cells. *PLoS One* **2011**, *6*(1), e16182, doi:10.1371/journal.pone.0016182.

576. Menendez, L.; Yatskievych, T.A.; Antin, P.B.; Dalton, S. Wnt signaling and a Smad pathway blockade direct the differentiation of human pluripotent stem cells to multipotent neural crest cells. *Proc Natl Acad Sci U S A* **2011**, *108*(48), 19240-19245, doi:10.1073/pnas.1113746108.

577. Mica, Y.; Lee, G.; Chambers, S.M.; Tomishima, M.J.; Studer, L. Modeling neural crest induction, melanocyte specification, and disease-related pigmentation defects in hESCs and patient-specific iPSCs. *Cell Rep* **2013**, *3*(4), 1140-1152, doi:10.1016/j.celrep.2013.03.025.

578. Aoki, H.; Motohashi, T.; Yoshimura, N.; Yamazaki, H.; Yamane, T.; Panthier, J.J.; Kunisada, T. Cooperative and indispensable roles of endothelin 3 and KIT signalings in melanocyte development. *Dev Dyn* **2005**, *233*(2), 407-417, doi:10.1002/dvdy.20340.

579. Wehrle-Haller, B. The role of Kit-ligand in melanocyte development and epidermal homeostasis. *Pigment Cell Res* **2003**, *16*(3), 287-296, doi:10.1034/j.1600-0749.2003.00055.x.

580. Hu, D.N.; McCormick, S.A.; Ritch, R.; Pelton-Henrion, K. Studies of human uveal melanocytes in vitro: isolation, purification and cultivation of human uveal melanocytes. *Invest Ophthalmol Vis Sci* **1993**, *34*(7), 2210-2219.

581. Hosaka, C.; Kunisada, M.; Koyanagi-Aoi, M.; Masaki, T.; Takemori, C.; Taniguchi-Ikeda, M.; Aoi, T.; Nishigori, C. Induced pluripotent stem cell-derived melanocyte precursor cells undergoing differentiation into melanocytes. *Pigment Cell Melanoma Res* **2019**, *32*(5), 623-633, doi:10.1111/pcmr.12779.

582. Prince, S.; Wiggins, T.; Hulley, P.A.; Kidson, S.H. Stimulation of melanogenesis by tetradecanoylphorbol 13-acetate (TPA) in mouse melanocytes and neural crest cells. *Pigment Cell Res* **2003**, *16*(1), 26-34, doi:10.1034/j.1600-0749.2003.00008.x.

583. Rodriguez, C.I.; Setaluri, V. Cyclic AMP (cAMP) signaling in melanocytes and melanoma. *Arch Biochem Biophys* **2014**, *563*22-27, doi:10.1016/j.abb.2014.07.003.

584. Jia, L.; Zhou, J.; Peng, S.; Li, J.; Cao, Y.; Duan, E. Effects of Wnt3a on proliferation and differentiation of human epidermal stem cells. *Biochem Biophys Res Commun* **2008**, *368*(3), 483-488, doi:10.1016/j.bbrc.2008.01.097.

585. Dee, K.; Freer, M.; Mei, Y.; Weyman, C.M. Apoptosis coincident with the differentiation of skeletal myoblasts is delayed by caspase 3 inhibition and abrogated by MEK-independent constitutive Ras signaling. *Cell Death Differ* **2002**, *9*(2), 209-218, doi:10.1038/sj.cdd.4400930.

586. Flomerfelt, F.A.; Gress, R.E. Analysis of Cell Proliferation and Homeostasis Using EdU Labeling. *Methods Mol Biol* **2016**, *1323*211-220, doi:10.1007/978-1-4939-2809-5_18.

587. Tario, J.D., Jr.; Conway, A.N.; Muirhead, K.A.; Wallace, P.K. Monitoring Cell Proliferation by Dye Dilution: Considerations for Probe Selection. *Methods Mol Biol* **2018**, *1678*249-299, doi:10.1007/978-1-4939-7346-0_12.

588. Kohlmeier, F.; Maya-Mendoza, A.; Jackson, D.A. EdU induces DNA damage response and cell death in mESC in culture. *Chromosome Res* **2013**, *21*(1), 87-100, doi:10.1007/s10577-013-9340-5.

589. Zhao, H.; Halicka, H.D.; Li, J.; Biela, E.; Berniak, K.; Dobrucki, J.; Darzynkiewicz, Z. DNA damage signaling, impairment of cell cycle progression, and apoptosis triggered by 5-ethynyl-2'-deoxyuridine incorporated into DNA. *Cytometry A* **2013**, *83*(11), 979-988, doi:10.1002/cyto.a.22396.

590. Myster, D.L.; Duronio, R.J. To differentiate or not to differentiate? *Curr Biol* **2000**, *10*(8), R302-304, doi:10.1016/s0960-9822(00)00435-8.

591. Ruijtenberg, S.; van den Heuvel, S. Coordinating cell proliferation and differentiation: Antagonism between cell cycle regulators and cell type-specific gene expression. *Cell Cycle* **2016**, *15*(2), 196-212, doi:10.1080/15384101.2015.1120925.

592. Santos, M.A.; Faryabi, R.B.; Ergen, A.V.; Day, A.M.; Malhowski, A.; Canela, A.; Onozawa, M.; Lee, J.E.; Callen, E.; Gutierrez-Martinez, P.; Chen, H.T.; Wong, N.; Finkel, N.; Deshpande, A.; Sharrow, S.; Rossi, D.J.; Ito, K.; Ge, K.; Aplan, P.D.; Armstrong, S.A.; Nussenzweig, A. DNA-damage-induced differentiation of leukaemic cells as an anti-cancer barrier. *Nature* **2014**, *514*(7520), 107-111, doi:10.1038/nature13483.

593. Weiss, C.N.; Ito, K. DNA damage: a sensible mediator of the differentiation decision in hematopoietic stem cells and in leukemia. *Int J Mol Sci* **2015**, *16*(3), 6183-6201, doi:10.3390/ijms16036183.

594. de Pedro, I.; Alonso-Lecue, P.; Sanz-Gomez, N.; Freije, A.; Gandarillas, A. Sublethal UV irradiation induces squamous differentiation via a p53-independent, DNA damage-mitosis checkpoint. *Cell Death Dis* **2018**, *9*(11), 1094, doi:10.1038/s41419-018-1130-8.

595. Kato, T.; Liu, N.; Morinaga, H.; Asakawa, K.; Muraguchi, T.; Muroyama, Y.; Shimokawa, M.; Matsumura, H.; Nishimori, Y.; Tan, L.J.; Hayano, M.; Sinclair, D.A.; Mohri, Y.; Nishimura, E.K. Dynamic stem cell selection safeguards the genomic integrity of the epidermis. *Dev Cell* **2021**, *56*(24), 3309-3320 e3305, doi:10.1016/j.devcel.2021.11.018.

596. Fesse, P.; Nyman, J.; Hermansson, I.; Book, M.L.; Ahlgren, J.; Turesson, I. Human cutaneous interfollicular melanocytes differentiate temporarily under genotoxic stress. *iScience* **2022**, *25*(10), 105238, doi:10.1016/j.isci.2022.105238.

597. Almog, N.; Rotter, V. Involvement of p53 in cell differentiation and development. *Biochim Biophys Acta* **1997**, *1333*(1), F1-27, doi:10.1016/s0304-419x(97)00012-7.

598. Molchadsky, A.; Rivlin, N.; Brosh, R.; Rotter, V.; Sarig, R. p53 is balancing development, differentiation and de-differentiation to assure cancer prevention. *Carcinogenesis* **2010**, *31*(9), 1501-1508, doi:10.1093/carcin/bgq101.

599. Wang, X.; Kua, H.Y.; Hu, Y.; Guo, K.; Zeng, Q.; Wu, Q.; Ng, H.H.; Karsenty, G.; de Crombrugghe, B.; Yeh, J.; Li, B. p53 functions as a negative regulator of osteoblastogenesis, osteoblast-dependent osteoclastogenesis, and bone remodeling. *J Cell Biol* **2006**, *172*(1), 115-125, doi:10.1083/jcb.200507106.

600. Hallenborg, P.; Feddersen, S.; Madsen, L.; Kristiansen, K. The tumor suppressors pRB and p53 as regulators of adipocyte differentiation and function. *Expert Opin Ther Targets* **2009**, *13*(2), 235-246, doi:10.1517/14712590802680141.

601. Armesilla-Diaz, A.; Bragado, P.; Del Valle, I.; Cuevas, E.; Lazaro, I.; Martin, C.; Cigudosa, J.C.; Silva, A. p53 regulates the self-renewal and differentiation of neural precursors. *Neuroscience* **2009**, *158*(4), 1378-1389, doi:10.1016/j.neuroscience.2008.10.052.

602. Porrello, A.; Cerone, M.A.; Coen, S.; Gurtner, A.; Fontemaggi, G.; Cimino, L.; Piaggio, G.; Sacchi, A.; Soddu, S. p53 regulates myogenesis by triggering the differentiation activity of pRb. *J Cell Biol* **2000**, *151*(6), 1295-1304, doi:10.1083/jcb.151.6.1295.

603. Soddu, S.; Blandino, G.; Citro, G.; Scardigli, R.; Piaggio, G.; Ferber, A.; Calabretta, B.; Sacchi, A. Wild-type p53 gene expression induces granulocytic differentiation of HL-60 cells. *Blood* **1994**, *83*(8), 2230-2237.

604. Meletis, K.; Wirta, V.; Hede, S.M.; Nister, M.; Lundeberg, J.; Frisen, J. p53 suppresses the self-renewal of adult neural stem cells. *Development* **2006**, *133*(2), 363-369, doi:10.1242/dev.02208.

605. Lin, T.; Chao, C.; Saito, S.; Mazur, S.J.; Murphy, M.E.; Appella, E.; Xu, Y. p53 induces differentiation of mouse embryonic stem cells by suppressing Nanog expression. *Nat Cell Biol* **2005**, *7*(2), 165-171, doi:10.1038/ncb1211.

606. Fujita, J.; Crane, A.M.; Souza, M.K.; Dejosez, M.; Kyba, M.; Flavell, R.A.; Thomson, J.A.; Zwaka, T.P. Caspase activity mediates the differentiation of embryonic stem cells. *Cell Stem Cell* **2008**, *2*(6), 595-601, doi:10.1016/j.stem.2008.04.001.

607. Janzen, V.; Fleming, H.E.; Riedt, T.; Karlsson, G.; Riese, M.J.; Lo Celso, C.; Reynolds, G.; Milne, C.D.; Paige, C.J.; Karlsson, S.; Woo, M.; Scadden, D.T. Hematopoietic stem cell responsiveness to exogenous signals is limited by caspase-3. *Cell Stem Cell* **2008**, *2*(6), 584-594, doi:10.1016/j.stem.2008.03.012.

608. Fernando, P.; Kelly, J.F.; Balazsi, K.; Slack, R.S.; Megeney, L.A. Caspase 3 activity is required for skeletal muscle differentiation. *Proc Natl Acad Sci U S A* **2002**, *99*(17), 11025-11030, doi:10.1073/pnas.162172899.

609. Miura, M.; Chen, X.D.; Allen, M.R.; Bi, Y.; Gronthos, S.; Seo, B.M.; Lakhani, S.; Flavell, R.A.; Feng, X.H.; Robey, P.G.; Young, M.; Shi, S. A crucial role of caspase-3 in osteogenic differentiation of bone marrow stromal stem cells. *J Clin Invest* **2004**, *114*(12), 1704-1713, doi:10.1172/JCI20427.

610. Fernando, P.; Brunette, S.; Megeney, L.A. Neural stem cell differentiation is dependent upon endogenous caspase 3 activity. *FASEB J* **2005**, *19*(12), 1671-1673, doi:10.1096/fj.04-2981fje.

611. Chen, T.C.; Hinton, D.R.; Zidovetzki, R.; Hofman, F.M. Up-regulation of the cAMP/PKA pathway inhibits proliferation, induces differentiation, and leads to apoptosis in malignant gliomas. *Lab Invest* **1998**, *78*(2), 165-174.

612. Insel, P.A.; Wilderman, A.; Zhang, L.; Keshwani, M.M.; Zambon, A.C. Cyclic AMP/PKA-promoted apoptosis: insights from studies of S49 lymphoma cells. *Horm Metab Res* **2014**, *46*(12), 854-862, doi:10.1055/s-0034-1384519.

613. Seite, P.; Ruchaud, S.; Hillion, J.; Gendron, M.C.; Bruland, O.; Segal-Bendirdjian, E.; Doskeland, S.O.; Lillehaug, J.R.; Lanotte, M. Ectopic expression of Bcl-2 switches over nuclear signalling for cAMP-induced apoptosis to granulocytic differentiation. *Cell Death Differ* **2000**, *7*(11), 1081-1089, doi:10.1038/sj.cdd.4400730.

614. Guo, Y.L.; Chakraborty, S.; Rajan, S.S.; Wang, R.; Huang, F. Effects of oxidative stress on mouse embryonic stem cell proliferation, apoptosis, senescence, and self-renewal. *Stem Cells Dev* **2010**, *19*(9), 1321-1331, doi:10.1089/scd.2009.0313.

615. Reynolds, B.A.; Weiss, S. Generation of neurons and astrocytes from isolated cells of the adult mammalian central nervous system. *Science* **1992**, *255*(5052), 1707-1710, doi:10.1126/science.1553558.

616. Borena, B.M.; Meyer, E.; Chiers, K.; Martens, A.; Demeyere, K.; Broeckx, S.Y.; Duchateau, L.; Spaas, J.H. Sphere-forming capacity as an enrichment strategy for epithelial-like stem cells from equine skin. *Cell Physiol Biochem* **2014**, *34*(4), 1291-1303, doi:10.1159/000366338.

617. Min, S.O.; Lee, S.W.; Bak, S.Y.; Kim, K.S. Ideal sphere-forming culture conditions to maintain pluripotency in a hepatocellular carcinoma cell lines. *Cancer Cell Int* **2015**, *15*95, doi:10.1186/s12935-015-0240-y.

618. Frisch, S.M.; Francis, H. Disruption of epithelial cell-matrix interactions induces apoptosis. *J Cell Biol* **1994**, *124*(4), 619-626, doi:10.1083/jcb.124.4.619.

619. Busch, S.; Andersson, D.; Bom, E.; Walsh, C.; Stahlberg, A.; Landberg, G. Cellular organization and molecular differentiation model of breast cancer-associated fibroblasts. *Mol Cancer* **2017**, *16*(1), 73, doi:10.1186/s12943-017-0642-7.

620. Yin, J.; Wang, J.; Zhang, X.; Liao, Y.; Luo, W.; Wang, S.; Ding, J.; Huang, J.; Chen, M.; Wang, W.; Fang, S.; Chao, J. A missing piece of the puzzle in pulmonary fibrosis: anoikis resistance promotes fibroblast activation. *Cell Biosci* **2022**, *12*(1), 21, doi:10.1186/s13578-022-00761-2.

621. Zabihi, N. Methodenetablierung zur Isolierung und Charakterisierung humaner, dermaler Stammzellen aus adulter Haut. Bachelor thesis, Hamburg University of Applied Sciences, 2015.

622. Hill, R.P.; Gledhill, K.; Gardner, A.; Higgins, C.A.; Crawford, H.; Lawrence, C.; Hutchison, C.J.; Owens, W.A.; Kara, B.; James, S.E.; Jahoda, C.A. Generation and characterization of multipotent stem cells from established dermal cultures. *PLoS One* **2012**, *7*(11), e50742, doi:10.1371/journal.pone.0050742.

623. Coles-Takabe, B.L.; Brain, I.; Purpura, K.A.; Karpowicz, P.; Zandstra, P.W.; Morshead, C.M.; van der Kooy, D. Don't look: growing clonal versus nonclonal neural stem cell colonies. *Stem Cells* **2008**, *26*(11), 2938-2944, doi:10.1634/stemcells.2008-0558.

624. Mens, M.M.J.; Ghanbari, M. Cell Cycle Regulation of Stem Cells by MicroRNAs. *Stem Cell Rev Rep* **2018**, *14*(3), 309-322, doi:10.1007/s12015-018-9808-y.

625. Aberdam, D.; Candi, E.; Knight, R.A.; Melino, G. miRNAs, 'stemness' and skin. *Trends Biochem Sci* **2008**, *33*(12), 583-591, doi:10.1016/j.tibs.2008.09.002.

626. Huang, X.A.; Lin, H. The microRNA regulation of stem cells. *Wiley Interdiscip Rev Dev Biol* **2012**, *1*(1), 83-95, doi:10.1002/wdev.5.

627. Shenoy, A.; Blelloch, R.H. Regulation of microRNA function in somatic stem cell proliferation and differentiation. *Nat Rev Mol Cell Biol* **2014**, *15*(9), 565-576, doi:10.1038/nrm3854.

628. Shim, J.; Nam, J.W. The expression and functional roles of microRNAs in stem cell differentiation. *BMB Rep* **2016**, *49*(1), 3-10, doi:10.5483/BMBRep.2016.49.1.217.

629. Garg, M. MicroRNAs, stem cells and cancer stem cells. *World J Stem Cells* **2012**, *4*(7), 62-70, doi:10.4252/wjsc.v4.i7.62.

630. Suzuki, H.I.; Katsura, A.; Matsuyama, H.; Miyazono, K. MicroRNA regulons in tumor microenvironment. *Oncogene* **2015**, *34*(24), 3085-3094, doi:10.1038/onc.2014.254.

631. Gaur, A.; Jewell, D.A.; Liang, Y.; Ridzon, D.; Moore, J.H.; Chen, C.; Ambros, V.R.; Israel, M.A. Characterization of microRNA expression levels and their biological correlates in human cancer cell lines. *Cancer Res* **2007**, *67*(6), 2456-2468, doi:10.1158/0008-5472.CAN-06-2698.

632. Wang, J.; Ma, W.; Si, C.; Zhang, M.; Qian, W.; Park, G.; Zhou, B.; Luo, D. Exosome-mediated miR-4655-3p contributes to UV radiation-induced bystander effects. *Exp Cell Res* **2022**, *418*(1), 113247, doi:10.1016/j.yexcr.2022.113247.

633. Tamim, S.; Vo, D.T.; Uren, P.J.; Qiao, M.; Bindewald, E.; Kasprzak, W.K.; Shapiro, B.A.; Nakaya, H.I.; Burns, S.C.; Araujo, P.R.; Nakano, I.; Radek, A.J.; Kuersten, S.; Smith, A.D.; Penalva, L.O. Genomic analyses reveal broad impact of miR-137 on genes associated with malignant transformation and neuronal differentiation in glioblastoma cells. *PLoS One* **2014**, *9*(1), e85591, doi:10.1371/journal.pone.0085591.

634. Zhu, X.; Li, Y.; Shen, H.; Li, H.; Long, L.; Hui, L.; Xu, W. miR-137 inhibits the proliferation of lung cancer cells by targeting Cdc42 and Cdk6. *FEBS Lett* **2013**, *587*(1), 73-81, doi:10.1016/j.febslet.2012.11.004.

635. Channakkar, A.S.; Singh, T.; Pattnaik, B.; Gupta, K.; Seth, P.; Adlakha, Y.K. MiRNA-137-mediated modulation of mitochondrial dynamics regulates human neural stem cell fate. *Stem Cells* **2020**, *38*(5), 683-697, doi:10.1002/stem.3155.

636. Sun, G.; Ye, P.; Murai, K.; Lang, M.F.; Li, S.; Zhang, H.; Li, W.; Fu, C.; Yin, J.; Wang, A.; Ma, X.; Shi, Y. miR-137 forms a regulatory loop with nuclear receptor TLX and LSD1 in neural stem cells. *Nat Commun* **2011**, *2*529, doi:10.1038/ncomms1532.

637. Liu, T.; Xu, Z.; Ou, D.; Liu, J.; Zhang, J. The miR-15a/16 gene cluster in human cancer: A systematic review. *J Cell Physiol* **2019**, *234*(5), 5496-5506, doi:10.1002/jcp.27342.

638. Cimmino, A.; Calin, G.A.; Fabbri, M.; Iorio, M.V.; Ferracin, M.; Shimizu, M.; Wojcik, S.E.; Aqeilan, R.I.; Zupo, S.; Dono, M.; Rassenti, L.; Alder, H.; Volinia, S.; Liu, C.G.; Kipps, T.J.; Negrini, M.; Croce, C.M. miR-15 and miR-16 induce apoptosis by targeting BCL2. *Proc Natl Acad Sci U S A* **2005**, *102*(39), 13944-13949, doi:10.1073/pnas.0506654102.

639. Tian, F.; Wei, H.; Tian, H.; Qiu, Y.; Xu, J. miR-33a is downregulated in melanoma cells and modulates cell proliferation by targeting PCTAIRE1. *Oncol Lett* **2016**, *11*(4), 2741-2746, doi:10.3892/ol.2016.4321.

640. Zhang, Z.R.; Yang, N. MiR-33a-5p inhibits the growth and metastasis of melanoma cells by targeting SNAI2. *Neoplasma* **2020**, *67*(4), 813-824, doi:10.4149/neo_2020_190823N811.

641. Zhou, J.; Xu, D.; Xie, H.; Tang, J.; Liu, R.; Li, J.; Wang, S.; Chen, X.; Su, J.; Zhou, X.; Xia, K.; He, Q.; Chen, J.; Xiong, W.; Cao, P.; Cao, K. miR-33a functions as a tumor suppressor in melanoma by targeting HIF-1alpha. *Cancer Biol Ther* **2015**, *16*(6), 846-855, doi:10.1080/15384047.2015.1030545.

642. Bellenghi, M.; Pontecorvi, G.; Care, A. On exosome functional role in cancer: miR-494 complex regulation in melanoma cells and corresponding exosomes. *Transl Cancer Res* **2019**, *8*(3), 725-728, doi:10.21037/tcr.2019.04.08.

643. Li, J.; Chen, J.; Wang, S.; Li, P.; Zheng, C.; Zhou, X.; Tao, Y.; Chen, X.; Sun, L.; Wang, A.; Cao, K.; Tang, S.; Zhou, J. Blockage of transferred exosome-shuttled miR-494 inhibits melanoma growth and metastasis. *J Cell Physiol* **2019**, *234*(9), 15763-15774, doi:10.1002/jcp.28234.

644. Zhan, M.N.; Yu, X.T.; Tang, J.; Zhou, C.X.; Wang, C.L.; Yin, Q.Q.; Gong, X.F.; He, M.; He, J.R.; Chen, G.Q.; Zhao, Q. MicroRNA-494 inhibits breast cancer progression by directly targeting PAK1. *Cell Death Dis* **2017**, *8*(1), e2529, doi:10.1038/cddis.2016.440.

645. Sun, H.B.; Chen, X.; Ji, H.; Wu, T.; Lu, H.W.; Zhang, Y.; Li, H.; Li, Y.M. miR-494 is an independent prognostic factor and promotes cell migration and invasion in colorectal cancer by directly targeting PTEN. *Int J Oncol* **2014**, *45*(6), 2486-2494, doi:10.3892/ijo.2014.2665.

646. Levati, L.; Alvino, E.; Pagani, E.; Arcelli, D.; Caporaso, P.; Bondanza, S.; Di Leva, G.; Ferracin, M.; Volinia, S.; Bonmassar, E.; Croce, C.M.; D'Atri, S. Altered expression of selected microRNAs in melanoma: antiproliferative and proapoptotic activity of miRNA-155. *Int J Oncol* **2009**, *35*(2), 393-400.

647. Li, W.; Zhou, B.R.; Hua, L.J.; Guo, Z.; Luo, D. Differential miRNA profile on photoaged primary human fibroblasts irradiated with ultraviolet A. *Tumour Biol* **2013**, *34*(6), 3491-3500, doi:10.1007/s13277-013-0927-4.

648. Sand, M.; Skrygan, M.; Sand, D.; Georgas, D.; Gambichler, T.; Hahn, S.A.; Altmeyer, P.; Bechara, F.G. Comparative microarray analysis of microRNA expression profiles in primary cutaneous malignant melanoma, cutaneous malignant melanoma metastases, and benign melanocytic nevi. *Cell Tissue Res* **2013**, *351*(1), 85-98, doi:10.1007/s00441-012-1514-5.

649. Zhang, N.; Lyu, Y.; Pan, X.; Xu, L.; Xuan, A.; He, X.; Huang, W.; Long, D. miR-146b-5p promotes the neural conversion of pluripotent stem cells by targeting Smad4. *Int J Mol Med* **2017**, *40*(3), 814-824, doi:10.3892/ijmm.2017.3064.

650. Stevanato, L.; Sinden, J.D. The effects of microRNAs on human neural stem cell differentiation in two- and three-dimensional cultures. *Stem Cell Res Ther* **2014**, *5*(2), 49, doi:10.1186/scrt437.

651. Palkina, N.; Komina, A.; Aksenenko, M.; Moshev, A.; Savchenko, A.; Ruksha, T. miR-204-5p and miR-3065-5p exert antitumor effects on melanoma cells. *Oncol Lett* **2018**, *15*(6), 8269-8280, doi:10.3892/ol.2018.8443.

652. Galasso, M.; Morrison, C.; Minotti, L.; Corra, F.; Zerbinati, C.; Agnoletto, C.; Baldassari, F.; Fassan, M.; Bartolazzi, A.; Vecchione, A.; Nuovo, G.J.; Di Leva, G.; D'Atri, S.; Alvino, E.; Previati, M.; Nickoloff, B.J.; Croce, C.M.; Volinia, S. Loss of miR-204 expression is a key event in melanoma. *Mol Cancer* **2018**, *17*(1), 71, doi:10.1186/s12943-018-0819-8.

653. Luan, W.; Qian, Y.; Ni, X.; Bu, X.; Xia, Y.; Wang, J.; Ruan, H.; Ma, S.; Xu, B. miR-204-5p acts as a tumor suppressor by targeting matrix metalloproteinases-9 and B-cell lymphoma-2 in malignant melanoma. *Onco Targets Ther* **2017**, *10*1237-1246, doi:10.2147/OTT.S128819.

654. Ying, Z.; Li, Y.; Wu, J.; Zhu, X.; Yang, Y.; Tian, H.; Li, W.; Hu, B.; Cheng, S.Y.; Li, M. Loss of miR-204 expression enhances glioma migration and stem cell-like phenotype. *Cancer Res* **2013**, *73*(2), 990-999, doi:10.1158/0008-5472.CAN-12-2895.

655. Song, J.; Ouyang, Y.; Che, J.; Li, X.; Zhao, Y.; Yang, K.; Zhao, X.; Chen, Y.; Fan, C.; Yuan, W. Potential Value of miR-221/222 as Diagnostic, Prognostic, and Therapeutic Biomarkers for Diseases. *Front Immunol* **2017**, *8*56, doi:10.3389/fimmu.2017.00056.

656. Ahn, H.J.; Jung, J.E.; Park, K.S. miRNA-222 modulates differentiation of mouse embryonic stem cells. *Dev Reprod* **2011**, *15*(4), 331-338.

657. Aldaz, B.; Sagardoy, A.; Nogueira, L.; Guruceaga, E.; Grande, L.; Huse, J.T.; Aznar, M.A.; Diez-Valle, R.; Tejada-Solis, S.; Alonso, M.M.; Fernandez-Luna, J.L.; Martinez-Climent, J.A.; Malumbres, R. Involvement of miRNAs in the differentiation of human glioblastoma multiforme stem-like cells. *PLoS One* **2013**, *8*(10), e77098, doi:10.1371/journal.pone.0077098.

658. Jain, A.K.; Allton, K.; Iacovino, M.; Mahen, E.; Milczarek, R.J.; Zwaka, T.P.; Kyba, M.; Barton, M.C. p53 regulates cell cycle and microRNAs to promote differentiation of human embryonic stem cells. *PLoS Biol* **2012**, *10*(2), e1001268, doi:10.1371/journal.pbio.1001268.

659. Li, W.J.; Wang, Y.; Liu, R.; Kasinski, A.L.; Shen, H.; Slack, F.J.; Tang, D.G. MicroRNA-34a: Potent Tumor Suppressor, Cancer Stem Cell Inhibitor, and Potential Anticancer Therapeutic. *Front Cell Dev Biol* **2021**, *9*640587, doi:10.3389/fcell.2021.640587.

660. Song, Z.; Liu, D.; Peng, Y.; Li, J.; Zhang, Z.; Ning, P. Differential microRNA expression profile comparison between epidermal stem cells and differentiated keratinocytes. *Mol Med Rep* **2015**, *11*(3), 2285-2291, doi:10.3892/mmr.2014.2886.

661. Greussing, R.; Hackl, M.; Charoentong, P.; Pauck, A.; Monteforte, R.; Cavinato, M.; Hofer, E.; Scheideler, M.; Neuhaus, M.; Micutkova, L.; Mueck, C.; Trajanoski, Z.; Grillari, J.; Jansen-Durr, P. Identification of microRNA-mRNA functional interactions in UVB-induced senescence of human diploid fibroblasts. *BMC Genomics* **2013**, *14*224, doi:10.1186/1471-2164-14-224.

662. Srivastava, A.; Karlsson, M.; Marionnet, C.; Bernerd, F.; Gueniche, A.; Rawadi, C.E.L.; Stahle, M.; Sonkoly, E.; Breton, L.; Pivarcsi, A. Identification of chronological and photoageing-associated microRNAs in human skin. *Sci Rep* **2018**, *8*(1), 12990, doi:10.1038/s41598-018-31217-8.

663. Cha, H.J.; Kim, O.Y.; Lee, G.T.; Lee, K.S.; Lee, J.H.; Park, I.C.; Lee, S.J.; Kim, Y.R.; Ahn, K.J.; An, I.S.; An, S.; Bae, S. Identification of ultraviolet B radiation-induced microRNAs in normal human dermal papilla cells. *Mol Med Rep* **2014**, *10*(4), 1663-1670, doi:10.3892/mmr.2014.2418.

664. Singh, A.; Willems, E.; Singh, A.; Ong, I.M.; Verma, A.K. Ultraviolet radiation-induced differential microRNA expression in the skin of hairless SKH1 mice, a widely used mouse model for dermatology research. *Oncotarget* **2016**, *7*(51), 84924-84937, doi:10.18632/oncotarget.12913.

665. Valacchi, G.; Pambianchi, E.; Coco, S.; Pulliero, A.; Izzotti, A. MicroRNA Alterations Induced in Human Skin by Diesel Fumes, Ozone, and UV Radiation. *J Pers Med* **2022**, *12*(2), doi:10.3390/jpm12020176.

666. Zhou, B.R.; Xu, Y.; Luo, D. Effect of UVB irradiation on microRNA expression in mouse epidermis. *Oncol Lett* **2012**, *3*(3), 560-564, doi:10.3892/ol.2012.551.

667. Dziunycz, P.; Iotzova-Weiss, G.; Eloranta, J.J.; Lauchli, S.; Hafner, J.; French, L.E.; Hofbauer, G.F. Squamous cell carcinoma of the skin shows a distinct microRNA profile modulated by UV radiation. *J Invest Dermatol* **2010**, *130*(11), 2686-2689, doi:10.1038/jid.2010.169.

668. Kraemer, A.; Chen, I.P.; Henning, S.; Faust, A.; Volkmer, B.; Atkinson, M.J.; Moertl, S.; Greinert, R. UVA and UVB irradiation differentially regulate microRNA expression in human primary keratinocytes. *PLoS One* **2013**, *8*(12), e83392, doi:10.1371/journal.pone.0083392.

669. Pecorelli, A.; Valacchi, G. Oxidative-Stress-Sensitive microRNAs in UV-Promoted Development of Melanoma. *Cancers (Basel)* **2022**, *14*(13), doi:10.3390/cancers14133224.

670. Sha, J.; Gastman, B.R.; Morris, N.; Mesinkovska, N.A.; Baron, E.D.; Cooper, K.D.; McCormick, T.; Arbesman, J.; Harter, M.L. The Response of microRNAs to Solar UVR in Skin-Resident Melanocytes Differs between Melanoma Patients and Healthy Persons. *PLoS One* **2016**, *11*(5), e0154915, doi:10.1371/journal.pone.0154915.

671. Melnik, B.C.; John, S.M.; Carrera-Bastos, P.; Schmitz, G. MicroRNA-21-Enriched Exosomes as Epigenetic Regulators in Melanomagenesis and Melanoma Progression: The Impact of Western Lifestyle Factors. *Cancers (Basel)* **2020**, *12*(8), doi:10.3390/cancers12082111.

672. Zhou, B.R.; Xu, Y.; Permatasari, F.; Liu, W.L.; Li, W.; Guo, X.F.; Huang, Q.H.; Guo, Z.; Luo, D. Characterization of the miRNA profile in UVB-irradiated normal human keratinocytes. *Exp Dermatol* **2012**, *21*(4), 317-319, doi:10.1111/j.1600-0625.2012.01465.x.

673. Guanzon, D.; Iljas, J.D.; Rice, G.E.; Salomon, C. Using a Next-Generation Sequencing Approach to Profile MicroRNAs from Human Origin. *Methods Mol Biol* **2018**, *1710*203-217, doi:10.1007/978-1-4939-7498-6_16.

674. Sha, J.; Arbesman, J.; Harter, M.L. Premature senescence in human melanocytes after exposure to solar UVR: An exosome and UV-miRNA connection. *Pigment Cell Melanoma Res* **2020**, *33*(5), 671-684, doi:10.1111/pcmr.12888.

675. Dominici, M.; Le Blanc, K.; Mueller, I.; Slaper-Cortenbach, I.; Marini, F.; Krause, D.; Deans, R.; Keating, A.; Prockop, D.; Horwitz, E. Minimal criteria for defining multipotent mesenchymal stromal cells. The

International Society for Cellular Therapy position statement. *Cytotherapy* **2006**, *8*(4), 315-317, doi:10.1080/14653240600855905.

676. Bloushtain-Qimron, N.; Yao, J.; Shipitsin, M.; Maruyama, R.; Polyak, K. Epigenetic patterns of embryonic and adult stem cells. *Cell Cycle* **2009**, *8*(6), 809-817, doi:10.4161/cc.8.6.7938.

677. Gangaraju, V.K.; Lin, H. MicroRNAs: key regulators of stem cells. *Nat Rev Mol Cell Biol* **2009**, *10*(2), 116-125, doi:10.1038/nrm2621.

678. Rajabi, H.; Aslani, S.; Abhari, A.; Sanajou, D. Expression Profiles of MicroRNAs in Stem Cells Differentiation. *Curr Pharm Biotechnol* **2020**, *21*(10), 906-918, doi:10.2174/1389201021666200219092520.

679. Mione, M.; Bosserhoff, A. MicroRNAs in melanocyte and melanoma biology. *Pigment Cell Melanoma Res* **2015**, *28*(3), 340-354, doi:10.1111/pcmr.12346.

680. Doyle, L.M.; Wang, M.Z. Overview of Extracellular Vesicles, Their Origin, Composition, Purpose, and Methods for Exosome Isolation and Analysis. *Cells* **2019**, *8*(7), doi:10.3390/cells8070727.

681. Shen, Z.; Sun, J.; Shao, J.; Xu, J. Ultraviolet B irradiation enhances the secretion of exosomes by human primary melanocytes and changes their exosomal miRNA profile. *PLoS One* **2020**, *15*(8), e0237023, doi:10.1371/journal.pone.0237023.

682. Waster, P.; Eriksson, I.; Vainikka, L.; Ollinger, K. Extracellular vesicles released by melanocytes after UVA irradiation promote intercellular signaling via miR21. *Pigment Cell Melanoma Res* **2020**, *33*(4), 542-555, doi:10.1111/pcmr.12860.

683. Xiao, D.; Barry, S.; Kmetz, D.; Egger, M.; Pan, J.; Rai, S.N.; Qu, J.; McMasters, K.M.; Hao, H. Melanoma cell-derived exosomes promote epithelial-mesenchymal transition in primary melanocytes through paracrine/autocrine signaling in the tumor microenvironment. *Cancer Lett* **2016**, *376*(2), 318-327, doi:10.1016/j.canlet.2016.03.050.

684. Biffi, G.; Tuveson, D.A. Diversity and Biology of Cancer-Associated Fibroblasts. *Physiol Rev* **2021**, *101*(1), 147-176, doi:10.1152/physrev.00048.2019.

685. Yamamoto, Y.; Kasashima, H.; Fukui, Y.; Tsujio, G.; Yashiro, M.; Maeda, K. The heterogeneity of cancer-associated fibroblast subpopulations: Their origins, biomarkers, and roles in the tumor microenvironment. *Cancer Sci* **2023**, *114*(1), 16-24, doi:10.1111/cas.15609.

686. Smalley, K.S.; Lioni, M.; Herlyn, M. Life isn't flat: taking cancer biology to the next dimension. *In Vitro Cell Dev Biol Anim* **2006**, *42*(8-9), 242-247, doi:10.1290/0604027.1.

687. Sun, T.; Jackson, S.; Haycock, J.W.; MacNeil, S. Culture of skin cells in 3D rather than 2D improves their ability to survive exposure to cytotoxic agents. *J Biotechnol* **2006**, *122*(3), 372-381, doi:10.1016/j.jbiotec.2005.12.021.

688. Berking, C.; Herlyn, M. Human skin reconstruct models: a new application for studies of melanocyte and melanoma biology. *Histol Histopathol* **2001**, *16*(2), 669-674, doi:10.14670/HH-16.669.

689. Hansda, S.; Ghosh, R. Bystander effect of ultraviolet A radiation protects A375 melanoma cells by induction of antioxidant defense. *J Environ Sci Health C Toxicol Carcinog* **2022**, *40*(1), 46-67, doi:10.1080/26896583.2021.1994820.

690. Whiteside, J.R.; McMillan, T.J. A bystander effect is induced in human cells treated with UVA radiation but not UVB radiation. *Radiat Res* **2009**, *171*(2), 204-211, doi:10.1667/RR1508.1.

691. Widel, M. Bystander effect induced by UV radiation; why should we be interested? *Postepy Hig Med Dosw (Online)* **2012**, *66*828-837, doi:10.5604/17322693.1019532.

692. Arjmand, B.; Hamidpour, S.K.; Tayanloo-Beik, A.; Arjmand, R.; Rezaei-Tavirani, M.; Namazi, N.; Ojagh, H.; Larijani, B. Incorporating NK Cells in a Three-Dimensional Organotypic Culture System for Human Skin Stem Cells: Modeling Skin Diseases and Immune Cell Interplay. *Methods Mol Biol* **2023**, doi:10.1007/7651_2023_504.

693. Bergers, L.; Reijnders, C.M.A.; van den Broek, L.J.; Spiekstra, S.W.; de Gruijl, T.D.; Weijers, E.M.; Gibbs, S. Immune-competent human skin disease models. *Drug Discov Today* **2016**, *21*(9), 1479-1488, doi:10.1016/j.drudis.2016.05.008.

694. Liebel, F.; Kaur, S.; Ruvolo, E.; Kollias, N.; Southall, M.D. Irradiation of skin with visible light induces reactive oxygen species and matrix-degrading enzymes. *J Invest Dermatol* **2012**, *132*(7), 1901-1907, doi:10.1038/jid.2011.476.

695. Mann, T.; Eggers, K.; Rippke, F.; Tesch, M.; Buerger, A.; Darvin, M.E.; Schanzer, S.; Meinke, M.C.; Lademann, J.; Kolbe, L. High-energy visible light at ambient doses and intensities induces oxidative stress of skin-Protective effects of the antioxidant and Nrf2 inducer Licochalcone A in vitro and in vivo. *Photodermatol Photoimmunol Photomed* **2020**, *36*(2), 135-144, doi:10.1111/phpp.12523.

696. Randhawa, M.; Seo, I.; Liebel, F.; Southall, M.D.; Kollias, N.; Ruvolo, E. Visible Light Induces Melanogenesis in Human Skin through a Photoadaptive Response. *PLoS One* **2015**, *10*(6), e0130949, doi:10.1371/journal.pone.0130949.

697. Darvin, M.E.; Haag, S.F.; Lademann, J.; Zastrow, L.; Sterry, W.; Meinke, M.C. Formation of free radicals in human skin during irradiation with infrared light. *J Invest Dermatol* **2010**, *130*(2), 629-631, doi:10.1038/jid.2009.283.

698. Schieke, S.; Stege, H.; Kurten, V.; Grether-Beck, S.; Sies, H.; Krutmann, J. Infrared-A radiation-induced matrix metalloproteinase 1 expression is mediated through extracellular signal-regulated kinase 1/2 activation in human dermal fibroblasts. *J Invest Dermatol* **2002**, *119*(6), 1323-1329, doi:10.1046/j.1523-1747.2002.19630.x.

699. Schroeder, P.; Lademann, J.; Darvin, M.E.; Stege, H.; Marks, C.; Bruhnke, S.; Krutmann, J. Infrared radiation-induced matrix metalloproteinase in human skin: implications for protection. *J Invest Dermatol* **2008**, *128*(10), 2491-2497, doi:10.1038/jid.2008.116.

700. Barolet, D.; Christiaens, F.; Hamblin, M.R. Infrared and skin: Friend or foe. *J Photochem Photobiol B* **2016**, *155*78-85, doi:10.1016/j.jphotobiol.2015.12.014.

701. Chauhan, A.; Gretz, N. Role of Visible Light on Skin Melanocytes: A Systematic Review. *Photochem Photobiol* **2021**, *97*(5), 911-915, doi:10.1111/php.13454.

702. Jantschitsch, C.; Majewski, S.; Maeda, A.; Schwarz, T.; Schwarz, A. Infrared radiation confers resistance to UV-induced apoptosis via reduction of DNA damage and upregulation of antiapoptotic proteins. *J Invest Dermatol* **2009**, *129*(5), 1271-1279, doi:10.1038/jid.2008.362.

703. Luo, C.; Weber, C.E.; Osen, W.; Bosserhoff, A.K.; Eichmuller, S.B. The role of microRNAs in melanoma. *Eur J Cell Biol* **2014**, *93*(1-2), 11-22, doi:10.1016/j.ejcb.2014.02.001.

704. Satzger, I.; Mattern, A.; Kuettler, U.; Weinspach, D.; Voelker, B.; Kapp, A.; Gutzmer, R. MicroRNA-15b represents an independent prognostic parameter and is correlated with tumor cell proliferation and apoptosis in malignant melanoma. *Int J Cancer* **2010**, *126*(11), 2553-2562, doi:10.1002/ijc.24960.

705. Nguyen, T.; Kuo, C.; Nicholl, M.B.; Sim, M.S.; Turner, R.R.; Morton, D.L.; Hoon, D.S. Downregulation of microRNA-29c is associated with hypermethylation of tumor-related genes and disease outcome in cutaneous melanoma. *Epigenetics* **2011**, *6*(3), 388-394, doi:10.4161/epi.6.3.14056.

Danksagung

Zunächst gebührt mein Dank Dr. Beate Volkmer und Dr. Rüdiger Greinert. Für eure langjährige Begleitung und die Möglichkeit, Teil dieses unglaublich tollen Teams im Labor für molekulare Zellbiologie gewesen sein zu dürfen, bin ich euch zutiefst dankbar. Vielen Dank für eure herausragende fachliche Expertise, euren unermüdlichen Einsatz und vor allem für eure einzigartige und warmherzige Art.

Prof. Dr. Udo Schumacher und Prof. Dr. Julia Kehr danke ich für die Übernahme der Betreuung und Begutachtung dieser Arbeit.

Ein großer Dank gilt Dr. Mouna Mhamdi-Ghodbani. Insbesondere für deine intensive Betreuung und Unterstützung als Mentorin, Teampartnerin, Leidensgenossin und stete Bezugsperson während meiner gesamten Promotionszeit möchte ich mich herzlich bedanken. Unsere hervorragende Zusammenarbeit und deine investierte Zeit in die Korrektur dieser Arbeit haben maßgeblich zum Erfolg meiner Promotion beigetragen.

Dr. Sarah Degenhardt möchte ich für den exzellenten wissenschaftlichen Austausch durch ihre fachliche Expertise im Bereich der dermalen Stammzellen und ihre hilfreichen Anregungen in zahlreichen Diskussionen danken. Bei Stefan Henning und Dr. I-Peng Chen möchte ich mich für die Hilfestellung bei den Bestrahlungs-, microRNA- und Genexpressionsuntersuchungen sowie für die wertvollen Ideen und Hinweise bei Fragestellungen jeglicher Art bedanken. Des Weiteren danke ich Dr. Marc Bender für seine Hilfe und Geduld bei statistischen Auswertungen sowie für die wertvollen Anregungen und interessanten Diskussionen. Stefanie Balk, Rebecca Keck, Sylke Engel-Haskiris, Maren Brunsen und Regina Börger-Hoppe danke ich für die hervorragende praktische Unterstützung im Labor und die große Hilfsbereitschaft in allen Situationen.

Meinen Kolleginnen und Kollegen möchte ich zudem recht herzlich für die außergewöhnlich herzliche, freundliche und angenehme Arbeitsatmosphäre, die ermutigenden Gespräche und ihre moralische Unterstützung danken. Ihr alle habt mir nicht nur geholfen, die Herausforderungen meiner Promotion erfolgreich zu bewältigen, sondern habt auch dazu beigetragen, dass ich als Wissenschaftlerin und als Person gewachsen bin.

Ein besonderer Dank gebührt meiner Partnerin Yasmin für den starken emotionalen Rückhalt und ein immer offenes Ohr. Ohne deine verständnisvolle Unterstützung und unendliche Geduld wäre diese Dissertation nicht möglich gewesen.

Abschließend möchte ich mich bei meiner Familie bedanken. Meinen Schwestern Janine und Sarah danke ich für die Korrektur der schriftlichen Arbeit und für die tatkräftige Unterstützung und Ermutigung während meiner gesamten Promotionszeit. Vor allem danke ich meinen Eltern Regina und Hubert sowie meinen Großeltern Hannelore und Dieter, die mir meinen Werdegang durch ihre Unterstützung und ihren steten Rückhalt ermöglicht haben.

Declaration on Oath / Eidesstattliche Versicherung

I hereby declare, on oath, that I have written the present dissertation by my own and have not used other than the acknowledged resources and aids. I declare that the bound copy of the dissertation and the dissertation submitted in electronic form and the printed bound copy of the dissertation submitted to the Academic Office of the Department of Biology for archiving are identical.

Hiermit erkläre ich an Eides statt, dass ich die vorliegende Dissertationsschrift selbst verfasst und keine anderen als die angegebenen Quellen und Hilfsmittel benutzt habe. Ich versichere, dass das gebundene Exemplar der Dissertation und das in elektronischer Form eingereichte Dissertationsexemplar und das bei dem Studienbüro des Fachbereichs Biologie zur Archivierung eingereichte gedruckte gebundene Exemplar der Dissertationsschrift identisch sind.

Hamburg, March 19, 2024

Christin Starzonek